

# **Application of a site-specific *in situ* approach to keloid disease research**

A thesis submitted to the University of Manchester  
for the degree of Doctor of Philosophy in the Faculty  
of Biology, Medicine and Health

2016

**Natalie Jumper**

School of Biological Sciences

## Table of Contents

List of figures.....	6
List of Tables .....	11
Abstract.....	13
Declaration.....	14
Copyright statement .....	15
Acknowledgments.....	16
Abbreviations.....	17
Nomenclature .....	21
The Author .....	22
<b>CHAPTER 1 INTRODUCTION .....</b>	<b>27</b>
1.1 TOPIC BACKGROUND .....	28
1.2 RESEARCH AIMS, SPECIFIC QUESTIONS TO ADDRESS AND HYPOTHESES TO PURSUE .....	30
1.3 EXPERIMENTAL DESIGN .....	33
1.4 LAYOUT OF THESIS AND SUMMARY OF ORIGINAL CONTRIBUTIONS OF THE RESEARCH .....	35
REFERENCES.....	40
<b>CHAPTER 2 LITERATURE REVIEW .....</b>	<b>42</b>
2.1 INTRODUCTION .....	43
2.2 THE STRUCTURE OF HUMAN SKIN .....	44
2.2.1 Epidermis.....	45
2.2.2 Basement Membrane Zone (BMZ).....	47
2.2.3 Dermis.....	48
2.2.4 Hypodermis .....	49
2.3 ADULT CUTANEOUS WOUND HEALING.....	50
2.3.1 Phase I: Haemostasis (Day 1) .....	50
2.3.2 Phase II: Inflammation (Days 1-7) .....	51
2.3.3 Phase III: Proliferation (Days 3-14).....	53
2.3.4 Phase IV: Remodelling and maturation (Day 21 onwards) .....	55
2.4 OUTCOMES OF THE WOUND HEALING PROCESS .....	57
2.4.1 Acute wound healing.....	57
2.4.2 Chronic wound healing.....	57
2.4.3 Scarless wound healing vs fibrosis.....	58

2.5 SKIN SCARRING AND CLASSIFICATION.....	59
2.5.1 Normal skin scarring .....	60
2.5.2 Abnormal skin scarring: atrophic, stretch and hypertrophic .....	60
2.5.3 Hypertrophic scarring vs keloid scars .....	61
2.6 KELOID DISEASE (KD).....	63
2.6.1 Aetiology, epidemiology and clinical presentation .....	64
2.6.2 Histopathogenesis and differential diagnoses.....	65
2.6.3 Pathophysiology.....	74
2.6.4 Treatment and management .....	77
2.7 SITE-SPECIFIC KELOID DISEASE .....	81
2.8 EPITHELIAL-MESENCHYMAL INTERACTIONS (EMI).....	82
2.8.1 Normal skin and wound healing.....	83
2.8.2 Keloid EMI .....	84
2.8.3 Keloid epithelial-mesenchymal transition (EMT) .....	86
2.9. TRADITIONAL EXPERIMENTAL METHODOLOGIES IN KD RESEARCH .....	87
2.10 LASER CAPTURE MICRODISSECTION (LCM) .....	89
2.10.1 Application of LCM to fibrosis, skin and wound healing .....	92
2.10.2 Application to keloid scarring .....	94
2.11 SUMMARY.....	95
REFERENCES.....	96
<b>CHAPTER 3 METHODS .....</b>	<b>115</b>
3.1 AUTHOR CONTRIBUTIONS.....	116
3. 2 ETHICAL APPROVAL .....	116
3.3 PATIENT DATA AND TISSUE COLLECTION .....	116
3.4 LASER CAPTURE MICRODISSECTION (LCM) .....	117
3.4.1 Cryosection and staining .....	117
3.4.2 Laser Microdissection .....	118
3.4.3 Laser Microdissection Pressure Catapulting .....	118
3.5 GENE EXPRESSION EXPERIMENTS .....	121
3.5.1 mRNA extraction from tissue, cells and laser captured material.....	121
3.5.2 Measurement of RNA concentration and integrity.....	123
3.5.3 cDNA synthesis .....	125
3.5.4 Primer design and quantitative real-time polymerase chain reaction (qRT-PCR) .....	126
3.5.5 RNA amplification and purification .....	127
3.5.6 Microarray .....	128
3.6 HISTOCHEMISTRY & IMMUNOPATHOLOGY .....	129

3.6.1 Paraffin embedding of formalin-fixed tissue (FFPE) .....	129
3.6.2 De-waxing and rehydration of FFPE tissue sections .....	129
3.6.3 Haematoxylin and eosin (H&E) staining .....	130
3.6.4 Herovici staining.....	130
3.6.5 Peroxidase immunohistochemistry (IHC) protocol.....	130
3.6.6 Immunofluorescence protocol.....	131
3.6.7 Immunocytochemistry protocol.....	132
3.6.8 Rapid staining LCM protocol .....	132
3.6.9 Wide-field microscopy and image capture .....	132
3.7 CELL CULTURE METHODOLOGY .....	132
3.7.1 Establishment of primary keloid and normal skin keratinocytes .....	133
3.7.2 Establishment of primary keloid and normal skin fibroblasts.....	133
3.7.3 Cryopreservation of cultured cells .....	134
3.7.4 Revival of cryopreserved cells.....	134
3.7.5 Estimation of cell viability and cell number – trypan blue dye exclusion method.....	135
3.7.6 MTT cell viability colorimetric assay.....	135
3.8 SPECIALISED CULTURE EXPERIMENTS .....	136
3.8.1 Reconstitution of all-trans retinoic acid (atRA) & all-trans retinol (vitamin A) .....	137
3.8.2 Keratinocyte transfection .....	138
3.8.3 Immunocytochemistry.....	139
3.8.4 Dual Luciferase assay and analysis.....	139
3.8.5 Conditioned medium experiments.....	143
3.8.6 Treatment of cultured cells with neuregulin-1 .....	143
3.8.7 ErbB2 siRNA transfection studies .....	144
3.8.8 In vitro scratch wound migration assay (scratch assay) .....	145
3.9 SPECIALISED PROTEIN EXPRESSION EXPERIMENTS .....	145
3.9.1 Western blot.....	145
3.9.2 High-throughput in-cell western blotting and quantification .....	146
3.9.3 Co-immunoprecipitation .....	148
3.10 STATISTICS AND ANALYSIS .....	148
REFERENCES.....	150
<b>CHAPTER 4 COMBINED LASER CAPTURE MICRODISSECTION (LCM) AND WHOLE GENOME MICROARRAY PROFILING OF EPIDERMIS VS DERMIS OF SITE-SPECIFIC KELOID DISEASE COMPARED WITH WHOLE KELOID TISSUE BIOPSY AND MONOLAYER CULTURE PROVIDE NOVEL TARGETS WITH POTENTIAL CLINICAL IMPLICATIONS.....</b>	<b>152</b>
Abstract.....	154
Introduction .....	155



Materials and Methods.....	158
Results & Discussion .....	161
Conclusions and perspectives .....	190
References .....	193
SUPPLEMENTARY MATERIAL TO CHAPTER 4.....	203
<b>CHAPTER 5 THE ALDO-KETO REDUCTASE AKR1B10 IS UP-REGULATED IN KELOID EPIDERMIS, IMPLICATING RETINOIC ACID PATHWAY DYSREGULATION IN THE PATHOGENESIS OF KELOID DISEASE .....</b>	<b>244</b>
Published paper .....	1500-1512
Supplementary Material to Chapter 5 .....	245
<b>CHAPTER 6 A ROLE FOR NEUREGULIN-1 (NRG1) IN PROMOTING KELOID FIBROBLAST MIGRATION VIA ERBB2-MEDIATED SIGNALING .....</b>	<b>276</b>
Abstract.....	278
Introduction .....	279
Methods.....	280
Results.....	284
Discussion .....	296
References .....	301
SUPPLEMENTARY MATERIAL TO CHAPTER 6.....	305
<b>Chapter 7 Discussion.....</b>	<b>319</b>
7.1 DISCUSSION LAYOUT .....	320
7.2 CONTRIBUTIONS OF THIS THESIS TO KELOID DISEASE RESEARCH.....	320
7.2.1 <i>The challenges</i> .....	320
7.2.2 <i>Aims and specific questions addressed</i> .....	321
7.2.3 <i>General discussion</i> .....	324
7.3 THESIS STRENGTHS AND LIMITATIONS .....	334
7.4 FUTURE WORK .....	335
7.5 CONCLUDING REMARKS.....	340
REFERENCES.....	341
<b>FUNCTIONAL HISTOPATHOLOGY OF KELOID DISEASE .....</b>	<b>1033-1057</b>

## List of figures

### Chapter 1

- Figure 1.1: Schematic diagram of distinct keloid regions and pictures **29**
- Figure 1.2: Flow chart of experimental design of PhD project **34**

### Chapter 2

- Figure 2.1: Schematic diagram of the structure of human skin **45**
- Figure 2.2: Schematic representation of epidermal strata **46**
- Figure 2.3: Phases of wound healing and potential outcomes **56**
- Figure 2.4: Signaling pathways & molecules known to be dysregulated in keloid disease **77**
- Figure 2.5: Schematic diagram representing laser capture microdissection (LCM) **92**

### Chapter 3

- Figure 3.1: Flow of Laser Capture Microdissection (LCM) process from normal skin and site-specific keloid biopsy to microarray **120**
- Figure 3.2 Representation of electropherograms to determine RIN **125**
- Figure 3.3: Reagent combinations and experimental workflow for keratinocyte transfection and dual luciferase assay **142**

### Chapter 4

- Figure 1: Experimental approaches for the comparison of site-specific keloid disease with normal skin **157**
- Figure 2: Comparison of *in situ* KD expression to whole tissue biopsy and monolayer culture expression **165**

Figure 3:	Site-specific contribution to differential gene expression in KD	<b>168</b>
Figure 4:	Gene enrichment analysis of <i>in situ</i> site-specific KD	<b>171</b>
Figure 5:	<i>In situ</i> expression contributing to epithelial-mesenchymal transition (EMT) and collagen production in KD	<b>177</b>
Figure 6:	Cytokine relationship with potential inflammatory effects in keloid disease	<b>183</b>
Figure 7:	qRT-PCR validation of candidate genes	<b>189</b>
Figure S1:	qRT-PCR graphs showing differences in the degree of expression between LCM keloid and NS dermis and monolayer keloid and NS fibroblasts	<b>209</b>
Figure S2:	qRT-PCR graphs showing the <i>in situ</i> (LCM) contribution of both epidermis and dermis from keloid centre, margin and extralesional sites as well as normal skin	<b>210</b>
Figure S3a:	Top upregulated genes in keloid vs NS epidermis	<b>211</b>
Figure S3b:	Mean intensity and range values for selected genes	<b>212</b>
Figure S4:	Top downregulated genes in keloid vs NS epidermis	<b>213</b>
Figure S5:	Top 100 upregulated genes in keloid centre vs normal skin epidermis	<b>215</b>
Figure S6:	Top 50 downregulated genes in keloid centre vs normal skin epidermis	<b>217</b>
Figure S7:	Top 100 upregulated genes in keloid margin vs normal skin epidermis	<b>219</b>
Figure S8:	Top 50 downregulated genes in keloid margin vs normal skin epidermis	<b>222</b>
Figure S9:	Top 100 upregulated genes in keloid extralesional vs normal skin epidermis	<b>224</b>
Figure S10:	Top 50 downregulated genes in keloid extralesional vs normal skin epidermis	<b>227</b>

Figure S11: Top 100 upregulated genes in keloid centre vs normal skin dermis	<b>229</b>
Figure S12: Top 50 downregulated genes in keloid centre vs normal skin dermis	<b>232</b>
Figure S13: Top 100 upregulated genes in keloid margin vs normal skin dermis	<b>234</b>
Figure S14: Top 50 downregulated genes in keloid margin vs normal skin dermis	<b>237</b>
Figure S15: Top 100 upregulated genes in keloid extralesional vs normal skin dermis	<b>239</b>
Figure S16: Top 50 downregulated genes in keloid extralesional vs normal skin dermis	<b>242</b>
 <b>Chapter 5</b>	
Figure 1: AKR1B10 overexpression in keloid versus normal skin	<b>3</b>
Figure 2: Keloid tissue retinoic acid pathway dysregulation	<b>5</b>
Figure 3: AKR1B10 overexpression in normal skin keratinocytes	<b>6</b>
Figure 4: Effect of conditioned media on keloid fibroblasts and normal skin fibroblasts	<b>8</b>
Figure S1: qRT-PCR validation of relevant genes from the RA pathway found to be dysregulated in microarray data	<b>245</b>
Figure S2: Correlation plot showing negative correlation of AKR1B10 to analysis module	<b>246</b>
Figure S3: qRT-PCR for vimentin in AKR1B10-transfected vs non-transfected keratinocytes	<b>247</b>
Figure S4: Western blot of keratin 14 in transfected and non-transfected samples	<b>248</b>
Figure S5: Collagen I & III gene expression	<b>249</b>

Figure S6:	In-cell western results for each keloid and normal skin fibroblast patient for collagen I & III	<b>250</b>
Figure S7:	Quantitative data graphs for in-cell western performed on keloid fibroblasts	<b>251</b>
Figure S8:	Flow chart depicting summary in chronological order of experimental process	<b>252</b>
 <b>Chapter 6</b>		
Figure 1:	Neuregulin-1 (NRG1) and ErbB2 gene expression for <i>in situ</i> keloid tissue and keloid fibroblasts (KF) compared with normal skin	<b>286</b>
Figure 2:	Neuregulin-1 (NRG1) and ErbB2 protein expression in keloid versus normal skin	<b>288</b>
Figure 3:	Co-immunoprecipitation of total keloid and normal skin protein lysate	<b>290</b>
Figure 4:	Fibroblast ( <i>n</i> =5) treatment with recombinant human neuregulin-1 (rhNRG1)	<b>293</b>
Figure 5:	ErbB2 siRNA-transfected keloid fibroblasts	<b>295</b>
Figure S1:	Western blot for ErbB3 and ErbB4 in fibroblasts	<b>313</b>
Figure S2:	qRT-PCR gene expression of fibroblast growth factor 7 (FGF7) in keloid fibroblasts	<b>313</b>
Figure S3:	qRT-PCR gene expression of collagen I, collagen III, and fibronectin in keloid fibroblasts after NRG1 treatment	<b>314</b>
Figure S4:	qRT-PCR gene expression of IL-6 in keloid fibroblasts after NRG1 treatment	<b>314</b>
Figure S5:	qRT-PCR gene expression of collagen I, collagen III and fibronectin in keloid fibroblasts treated with siRNA	<b>315</b>
Figure S6:	qRT-PCR gene expression of TGF $\beta$ 1 in keloid fibroblasts treated with siRNA	<b>315</b>

Figure S7: Schematic diagram representing possible ErbB2 signaling permutations with NRG1 ligand	<b>316</b>
Figure S8: Conceptual illustration of proposed mechanism underlying keloid margin dermis migration	<b>317</b>
Figure S9: qRT-PCR gene expression of CTGF in keloid and normal skin fibroblasts treated with NRG1	<b>318</b>
Figure S10: qRT-PCR gene expression of CTGF in keloid fibroblasts following NRG1 treatment at a range of concentrations	<b>318</b>
 <b>Chapter 7</b>	
Figure 7.1: Proposed future work arising from thesis	<b>339</b>

## List of Tables

### Chapter 2

Table 2.1: Summary of the ECM molecules previously investigated in keloid disease tissue	<b>67</b>
Table 2.2: Bux S, Madaree A. <i>Keloids show regional distribution of proliferative and degenerate connective tissue elements</i> . Cells Tissues Organs. 2010; 191: 213-34	<b>69</b>
Table 2.3: Summary of the features of skin-related fibrotic disorders in common with and different from KD and the stains most commonly used in their diagnosis	<b>72</b>
Table 2.4: Summary of the characteristic features of keloid disease and their frequency reported in the literature	<b>73</b>

### Chapter 4

Table 1: Number of significant differentially expressed genes within each comparative microarray group (filtered for fold change > 2 and p-value < 0.05)	<b>163</b>
Table 2: Dysregulation of cytokines in site-specific KD microarray relating to IL-13, IL-37 and IL-17	<b>185</b>
Table S1: Demographic data for the samples used in this study	<b>203</b>
Table S2: Expanded names for each of the gene symbols used throughout the manuscript text and figures	<b>205</b>
Table S3: Details of primers used for qRT-PCR in this study	<b>208</b>

### Chapter 5

Table S1: Microarray expression of genes relevant to this study	<b>253</b>
Table S2: Demographic data of samples used in this study	<b>255</b>

Table S3:	Details of primers used for qRT-PCR	<b>257</b>
Table S4:	Concentration, incubation parameters and detection method of primary and secondary antibodies used in this study for immunohistochemistry	<b>259</b>
Table S4b:	Concentration, incubation parameters and detection method of primary and secondary antibodies used in this study for western blotting	<b>260</b>
Table S4c:	Concentration, incubation parameters and detection method of primary and secondary antibodies used in this study for in-cell western	<b>261</b>
 <b>Chapter 6</b>		
Table S1:	Microarray expression of genes relevant to this study	<b>307</b>
Table S2:	Demographic data of samples used in this study	<b>308</b>
Table S3:	Details of primers used for qRT-PCR in this study	<b>310</b>
Table S4:	Concentration, incubation parameters and detection method of primary and secondary antibodies used in this study for co-immunoprecipitation and western blot	<b>311</b>
Table S5:	Concentration, incubation parameters and detection method of primary and secondary antibodies used in this study for immunohistochemistry	<b>312</b>



## Abstract

Keloid disease (KD) is a cutaneous fibroproliferative tumour characterised by heterogeneity, locally aggressive invasion and therapeutic resistance. Clinical, histological and molecular differences between the keloid scar centre and margin as well as recent evidence of the importance of epithelial-mesenchymal interactions (EMI) in KD pathobiology contribute to the complexity and diversity of KD, which coupled with the lack of a validated animal model have hindered research and effective management. Despite significant progress in the field of KD research, reliance on conventional monolayer cell culture and whole tissue analysis methods have failed to fully reflect the natural architecture, pathology and complexity of KD *in vivo*. In order to address these challenges, a site-specific *in situ* approach was therefore employed here for the first time in KD research.

The first aim of this work was to compare the value of this contemporary approach with traditional methods of tissue dissection. The second aim was to compare the genomic expression between well-defined, distinct keloid sites and normal skin (NS). The third aim was to develop and explore hypotheses arising from this site-specific gene expression profiling approach, so as to enhance understanding of KD pathobiology as a basis for improved diagnostic and therapeutic strategies in future KD management. The fourth aim was to probe these hypotheses with relevant functional *in vitro* studies.

The current site-specific *in situ* approach was achieved through a combination of laser capture microdissection and whole genome microarray, allowing separation of epidermis from dermis for keloid centre, margin and extralesional sites compared with NS. This *in situ* approach yielded selective, accurate and sensitive data, exposing genes that were overlooked with alternative methods of dissection.

Identification of significant upregulation of the aldo-keto reductase enzyme AKR1B10 in all three sites of the keloid epidermis (KE) *in situ*, implicated dysregulation of the retinoic acid (RA) pathway in KD pathogenesis. This hypothesis was supported by showing that induced AKR1B10 overexpression in NS keratinocytes reproduced the keloid RA pathway expression pattern. Moreover, co-transfection with a luciferase reporter plasmid revealed reduced RA response element activity. Paracrine signals released by AKR1B10-overexpressing keratinocytes into conditioned medium resulted in TGF $\beta$ 1 and collagen upregulation in keloid fibroblasts, suggesting the disturbed RA metabolism exerts a pro-fibrotic effect through pathological EMI, thus further supporting the hypothesis of RA deficiency in KE. Gene expression profiling further revealed an upregulation of NRG1 and ErbB2 in keloid margin dermis. Exogenous NRG1 led to enhanced keloid fibroblast migration with increased Src and PTK2 expression, which were attenuated with ErbB2 siRNA studies. Together with the observed failure to recover this expression with NRG1 treatment, suggested the novel KD pathobiology hypothesis that NRG1/ErbB2/Src/PTK2 signaling plays a role in migration at the keloid margin. In addition to these hypotheses, LCM methodology with comprehensive analysis of the data permitted the development of additional novel working hypotheses that will inform future KD research, including inflammatory gene dysregulation and cancer-like stem cells that may contribute to the therapeutic resistance characteristic of KD.

**Declaration**

No portion of the work referred to in this thesis has been submitted in support of an application for another degree or qualification at this or any other university or institute of learning.

## Copyright statement

i) The author of this thesis (including any appendices and/or schedules to this thesis) owns certain copyright or related rights in it (the “Copyright”) and s/he has given The University of Manchester certain rights to use such Copyright, including for administrative purposes.

ii) Copies of this thesis, either in full or in extracts and whether in hard or electronic copy, may be made only in accordance with the Copyright, Designs and Patents Act 1988 (as amended) and regulations issued under it or, where appropriate, in accordance with licensing agreements which the University has from time to time. This page must form part of any such copies made.

iii) The ownership of certain Copyright, patents, designs, trademarks and other intellectual property (the “Intellectual Property”) and any reproductions of copyright works in the thesis, for example graphs and tables (“Reproductions”), which may be described in this thesis, may not be owned by the author and may be owned by third parties. Such Intellectual Property and Reproductions cannot and must not be made available for use without the prior written permission of the owner(s) of the relevant Intellectual Property and/or Reproductions.

iv) Further information on the conditions under which disclosure, publication and commercialisation of this thesis, the Copyright and any Intellectual Property and/or Reproductions described in it may take place is available in the University IP Policy (see <http://documents.manchester.ac.uk/display.aspx?DocID=24420>), in any relevant Thesis restriction declarations deposited in the University Library, The University Library’s regulations (see <http://www.manchester.ac.uk/library/aboutus/regulations>) and in The University’s policy on Presentation of Theses.

**Acknowledgments**

I would like to thank my supervisory panel, Dr. Ardeshir Bayat and Professor Ralf Paus for all of their guidance, support and advice throughout my PhD. I am grateful to them for the opportunity to work in a field of research about which I am passionate. I especially thank my advisor Dr. Rachel Watson for all her help, guidance and advice over the last four years. I would like to thank my friends and colleagues in the Plastic and Reconstructive Surgery Research group for their knowledge, support, advice and friendship, in particular: Dr. Anil Sebastian, Dr. Simon Barr, Dr. Gary Sidgwick, Dr. Sameer Farhatullah and Dr. Barbara Shih. I extend my thanks also to GlaxoSmithKline for the sponsorship of my research and to Andy Blanchard and Adam Taylor especially, who provided me with technical support, analysis assistance and advice throughout this PhD. I thank Ross Haggart, Epistem and Dr Edward Mckenzie for their contributing their expertise and also I extend my thanks to the surgeons Dr. Yaron Har-Shai, Dr. Guyan Arcscott, Dr. Young and of course all of the patients who donated their tissue to research and without whom this project would not have been possible.

My eternal gratitude goes to my family and friends. First of all, I thank my mother for her unending love, support, patience and invaluable words of wisdom. I thank my sister Elaina for donating her formatting skills and with my sister Aisling for their support and all of my friends for their ready ears and steady patience. Finally, yet most importantly, I thank my darling Tom, whose unfailing love, encouragement, support and tolerance cannot be quantified – I am forever grateful.

**Abbreviations**

ACKR3	atypical chemokine receptor 3
ADAM	a disintegrin and metalloproteinase
ADAMTS	a disintegrin and metalloproteinase with thrombospondin motifs
AD-MSC	adipose-derived mesenchymal stem cells
ADP	adenosine diphosphate
AKR1B	aldo-keto reductase family 1, member
AKR1B10	aldo-keto reductase family 1, member B10
ALDH	alcohol dehydrogenase
ALDH1A1	aldehyde dehydrogenase 1 family member A1
ANGPT	angiopoietin
ANXA	annexin
AP-1	activating protein 1
ASPN	asporin
ATF3	activating transcription factor 3
ATM	ataxia telangiectasia mutated
ATP	adenosine triphosphate
atRA	all-trans retinoic acid
AVEN	apoptosis and caspase activation inhibitor
BMP2	bone morphogenetic protein 2
BMZ	basement membrane zone
BRD4	bromodomain containing 4
BSA	bovine serum albumin
CCAR1	cell division cycle and apoptosis regulator protein 1
CCN	Cyr61, CTGF, Nov (family of matricellular proteins)
CD36	cluster of differentiation 36
cDNA	complementary deoxyribonucleic acid
CEACAM	carcinoembryonic antigen-related cell adhesion molecule
CLDN	claudin
CNTF	ciliary neurotrophic factor
COMP	cartilage oligomeric protein
CRABP	cellular retinoic acid binding protein
CREB	cAMP response element binding
CTAP	connective tissue activating protein
CTGF	and connective tissue growth factor
CTHRC1	collagen triple helix repeat containing 1
CXCR	chemokine (C-X-C motif) receptor
DAB2	Dab, mitogen-responsive phosphoprotein, homolog 2 (drosophila)
DACH1	dachshund family transcription factor 1
DAPI	4',6-diamidino-2-phenylindole
DEJ	dermo-epidermal junction
DFSP	dermatofibrosarcoma protuberans
DMEM	Dulbecco's modified essential medium
DMSO	dimethyl sulfoxide
DNA/RNA	deoxy/ribonucleic acid

ECM	extracellular matrix
EGF	epidermal growth factor
EIF3E	eukaryotic translation initiation factor 3 subunit E
EMI	Epithelial-mesenchymal interactions
EMT	epithelial-mesenchymal transition
EOMES	eomesodermin
EPHB4	ephrin (EPH) receptor B4
ErbB	epidermal growth factor receptor family
FBN1	fibrillin 1
FBS	Foetal bovine serum
FFPE	fresh frozen paraffin embedded
FGF	fibroblast growth factor
FLT3	fms related tyrosine kinase 3
FN1	fibronectin 1
FOXF2	forkhead box F2
GM-CSF	granulocyte macrophage colony-stimulating factor
GNB1	G protein subunit beta 1
H&E	haematoxylin and eosin
HA	hyaluronan
HIF-1 $\alpha$	hypoxia-inducible factor-1 alpha
HLA	human leukocyte antigen
HOXA13	homeobox A13
IFN	interferon
IGFBP4	insulin-like growth factor binding protein 4
IL	interleukin
ILC	innate lymphoid cell
INHBA	inhibin beta A
IRAK4	interleukin 1 receptor associated kinase 4
IRF7	interferon regulatory factor 7
JAG	jagged
JAK	janus kinase
K	keratin
KALT	keloid-associated lymphoid tissue
Kd	keloid dermis
KD	keloid disease
KE	keloid epidermis
KF	keloid fibroblasts
KGF	keratinocyte growth factor
KK	keloid keratinocytes
KLF6	kruppel-like factor
KMD	keloid margin dermis
KMT2A	lysine methyltransferase 2A
LCM	laser capture microdissection
LDH	lactate dehydrogenase
LIMS2	LIM zinc finger domain containing 2
LMPC	laser microdissection and pressure catapulting
MAPK/ERK	mitogen-activated protein kinase
MEN1	menin1

miRNA	micro ribonucleic acid
MMP	matrix metalloproteinase
mRNA	messenger ribonucleic acid
MTT	3-[4, 5-dimethylthiazol-2-yl]-2, 5-diphenyltetrazolium bromide
MUCL1	mucin-like 1
MYC	c-Myc
MYOCD	myocardin
NAP-2	neutrophil activating protein
NBT/BCIP	nitro blue tetrazolium/S-bromo-4-chloroindoxyl phosphate
NF- $\kappa$ B	nuclear factor kappa B
NHEK	normal human epidermal keratinocytes
NOTCH	notch
NRG1	neuregulin-1
NS	normal skin
NSF	normal skin fibroblasts
NSK	normal skin keratinocytes
OCT	optimum cutting temperature
ORMDL3	orosomuroid like 3
OSM	oncostatin M
PAX8	paired box 8
PD	papillary dermis
PDGF	platelet-derived growth factor
PEN	polyethylene naphthalate
PI3K	phosphoinositide 3-kinase
PKNOX1	PBX/knotted 1 homeobox 1
PRRX1	paired related homeobox 1
PTEN	phosphatase and tensin homolog
PXR	pregnane X receptor
qRT-PCR	quantitative real-time polymerase chain reaction
RA	retinoic acid
RD	reticular dermis
RIPA	radioimmunoprecipitation assay buffer
RORc	retinoic acid-related orphan receptor c
RXR	retinoid X receptor
S100A8	S100 calcium-binding protein A8
SERPINE1/PAI-1	serpin peptidase inhibitor. Clade E (plasminogen activator inhibitor 1)
SFKM	serum-free keratinocyte medium
SMO	smoothened
SNAI1	snail family zinc finger 1
SNAI2	snail family transcriptional repressor 2
SOCS	suppressor of cytokine signalling
SOX9	SRY (sex-determining region Y)-box 9
SPHK1	sphingosine kinase 1
STAT	signal transducer and activator of transcription
TBS	tris buffered solution
TGF $\beta$	transforming growth factor beta
TGM2	transglutaminase 2
TIMP3	tissue inhibitor of metalloproteinases-3

TLE1	transducin like enhancer of split 1
TLR	toll-like receptor
TNF	tumour necrosis factor
TNFR	tumour necrosis factor receptor
TP53	tumor protein p53
tPA	tissue plasminogen activator
TSPYL5	testis-specific protein Y encoded like 5
TUBB3	Tubulin $\beta$ 3, class III
UGT3A2	UDP glycosyltransferase family 3 member A2
uPA	urokinase plasminogen activator
UV	ultraviolet
VEGF	vascular endothelial growth factor
WDR66	WD repeat domain 66
WISP1	Wnt 1 inducible signaling pathway protein 1
Wnt	wingless-type MMTV integration site
ZEB	zinc finger E-box-binding proteins
$\alpha$ -SMA/ACTA2	alpha smooth muscle actin/actin, alpha 2, smooth muscle, aorta
$\Delta$ CT	difference in threshold cycle
2/3-D	2/3-dimensional



**Nomenclature**

°C	degrees celsius
µg	micrograms
µl	microlitre
µM	micromolar
hrs	hours
M	molar
mg	milligrams
min	minutes
ml	millilitre
mm	millimetre
mnths	months
ng	nanograms
nm	nanometre
pg	picograms
RPM	revolutions per minute
	standard error of the
SEM	mean
U	unit
v/v	volume per volume

## The Author

**Ms. Natalie Jumper** is currently a member of the Plastic and Reconstructive Surgery Research group at the University of Manchester. She graduated with a degree in Medicine (MB BCh BAO) from the National University of Ireland, Galway in 2007 before specialising in surgery and completing her MRCS exams in 2010 with the Royal College of Surgeons in Dublin. After completing a year of specialty training in plastic surgery in St. James's Hospital in Dublin she opted to undertake this PhD at the University of Manchester. Following completion she will continue her career in Medicine, specialising in plastic surgery, with a focus on wound healing disorders and keloid disease.

## Publications resulting from this work

- **Jumper N, Hodgkinson T, Arscott G, Har-Shai Y, Paus R, Bayat A. The aldol-keto reductase AKR1B10 is upregulated in keloid epidermis, implicating retinoic acid pathway dysregulation in the pathogenesis of keloid disease. *The Journal of Investigative Dermatology*. 2016 (in press). Impact factor 7.216.**
- **Jumper N, Paus R, Bayat A. Functional histopathology of keloid disease. *Histol Histopathol*. 2015; 30: 1033-57. Impact factor 2.096.**

## Journal articles under review at the time of thesis submission

- **Natalie Jumper, Tom Hodgkinson, Ralf Paus, Ardeshir Bayat. A role for neuregulin-1 (NRG1) in promoting keloid fibroblast migration via ErbB2-mediated signaling. Submitted to *Acta Dermato-Venereologica* 2016.**

### Journal articles under preparation for submission

- **Jumper N**, Hodgkinson T, Paus R, Bayat A. **Combined laser capture microdissection (LCM) and whole genome microarray profiling of epidermis versus dermis of site-specific keloid disease compared with whole keloid tissue biopsy and monolayer culture provide novel targets with potential clinical implications.** For submission to PLOSOne 2016.

### Published abstracts

- Laser capture microdissection and microarray analysis of acute sequential human cutaneous wounds enables dermal/epidermal profiling of chemokine expression and innate lymphoid cell localisation (2015) T. Hodgkinson, **N. Jumper**, M. Coles, A. Bayat. 7<sup>th</sup> Joint Meeting of the European Tissue Repair Society (ETRS) & the Wound Healing Society (WHS). **Wound Repair Regeneration**, 23:A1-A37. doi: 10.1111/wrr.12342
- An innovative approach to dissecting keloid disease leading to identification of the retinoic acid pathway as a potential therapeutic target (2015) **N. Jumper**, Y. Har-Shai, G. Arscott, R. Paus, A. Bayat. 7<sup>th</sup> Joint Meeting of the European Tissue Repair Society (ETRS) & the Wound Healing Society (WHS). **Wound Repair Regeneration**, 23:A1-A37. doi: 10.1111/wrr.12342
- Laser capture microdissection and microarray analysis of acute sequential human cutaneous wounds enables dermal/epidermal profiling of chemokine expression and innate lymphoid cell localisation (2015) Tom Hodgkinson, **N. Jumper**, Mark Coles, A. Bayat. 7<sup>th</sup> Joint Meeting of the European Tissue Repair Society (ETRS) & the Wound Healing Society (WHS). **Wound Repair Regeneration**, 23:A1-A37. doi: 10.1111/wrr.12342

- An innovative approach to dissecting keloid disease leading to identification of the retinoic acid pathway as a potential therapeutic target (2015) **N. Jumper**, Y. Har-Shai, G. Arscott, R. Paus, A. Bayat. 25<sup>th</sup> Annual Meeting of the Wound Healing Society SAWC-Spring/WHS Joint Meeting. **Wound repair and Regeneration**, 23:A14-A48. Doi 10.1111/wrr.12291 **AND** PRSGO.
- Comparative analysis of proteomic and whole genome microarray datasets in both keloid and normal skin tissue and fibroblasts reveals previously unknown novel targets and pathways in keloid disease (2015) G.P Sidgwick, **N. Jumper**, A. Bayat. 25<sup>th</sup> Annual Meeting of the Wound Healing Society SAWC-Spring/WHS Joint Meeting. **Wound repair and Regeneration**, 23:A14-A48. Doi 10.1111/wrr.12291
- The novel application of laser capture microdissection to site-specific keloid disease (2014) **N. Jumper**, Y. Har-Shai, G. Arscott, R. Paus, A. Bayat. 24<sup>th</sup> Annual Meeting of the European Tissue Repair Society. **Wound Repair Regeneration**, 22:A73-A100. doi: 10.1111/wrr.
- Novel application of laser capture microdissection to elucidate the role of epithelial-mesenchymal interactions in site-specific keloid tissue by whole genome expression profiling and immunohistochemistry (2014) N. Jumper, R. Paus, A. Bayat. 24<sup>th</sup> Annual Meeting of the Wound Healing Society SAWC-Spring/WHS Joint Meeting. **Wound repair and Regeneration**, 22: A27-A72. doi: 10.1111/wrr.12155

#### Oral presentations

- **Invited Keynote**- An innovative approach to dissecting keloid disease leading to identification of the retinoic acid pathway as a potential therapeutic target (2015) **N. Jumper**, Y. Har-Shai, G. Arscott, R. Paus, A. Bayat – 7<sup>th</sup> Joint Meeting of the European Tissue Repair Society (ETRS) with the Wound Healing Society (WHS), Copenhagen, Denmark *From bed to Bench*.

- An innovative approach to dissecting keloid disease leading to identification of the retinoic acid pathway as a potential therapeutic target (2015) **N. Jumper**, Y. Har-Shai, G. Arscott, R. Paus, A. Bayat – Irish Association of Plastic Surgeons, Galway, Ireland.
- An innovative approach to dissecting keloid disease leading to identification of the retinoic acid pathway as a potential therapeutic target (2015) **N. Jumper**, Y. Har-Shai, G. Arscott, R. Paus, A. Bayat - Wound Healing Society World Congress, San Antonio TX, USA.
- The novel application of laser capture microdissection to site-specific keloid disease (2014) **N. Jumper**, Y. Har-Shai, G. Arscott, R. Paus, A. Bayat – European Tissue Repair Society Annual Congress, Edinburgh, Scotland.
- Novel application of laser capture microdissection to elucidate the role of epithelial-mesenchymal interactions in site-specific keloid tissue by whole genome expression profiling and immunohistochemistry (2014) **N. Jumper**, R. Paus, A. Bayat – Wound Healing Society World Congress, Orlando FL, USA.

### Poster presentations

- Analysis of site-specific keloid disease tissue and cell gene expression using laser capture microdissection and functional evaluation of target genes in cell and novel *ex vivo* keloid models (2014) **N. Jumper**, R. Paus, A. Bayat – Inflammation & Repair Postgraduate Poster Event, University of Manchester.
- Analysis of differential gene expression in site-specific keloid disease tissue using laser capture microdissection (LCM) (2012) **N. Jumper**, R. Paus, A. Bayat – CRAFT (Creative Advances in Fibrosis Therapy) Symposium, Stevenage, UK.

- Functional evaluation of differentially expressed biomarkers using a novel *ex vivo* organotypic keloid model (2012) N. **Jumper**, R. Paus, A. Bayat – CRAFT (Creative Advances in Fibrosis Therapy) Symposium, GSK, Stevenage, UK.

## Awards

- **Oral Presentation** (2015) **3<sup>rd</sup> place** – European Tissue Repair Society for “Laser capture microdissection and microarray analysis of acute sequential human cutaneous wounds enables dermal/epidermal profiling of chemokine expression and innate lymphoid cell localisation”. Tom Hodgkinson, **N. Jumper**, Mark Coles, A. Bayat.
- **Poster Presentation** (2015) **Winner** – 2015 Mancunian Skin Club Annual International Workshop for “An innovative approach to dissecting keloid disease leading to identification of the retinoic acid pathway as a potential therapeutic target”. **N. Jumper**, Y. Har-Shai, G. Arscott, R. Paus, A. Bayat.  
Awarded £500.
- **Oral Presentation** (2015) **Winner** – Irish Association of Plastic Surgeons for “An innovative approach to dissecting keloid disease leading to identification of the retinoic acid pathway as a potential therapeutic target”. **N. Jumper**, Y. Har-Shai, G. Arscott, R. Paus, A. Bayat.  
Awarded €250 and the Gerry Edwards Memorial Medal.
- **Young Investigator Award** (2015) **Winner** – World Congress of Wound Healing Society for oral presentation “An innovative approach to dissecting keloid disease leading to identification of the retinoic acid pathway as a potential therapeutic target”. **N. Jumper**, Y. Har-Shai, G. Arscott, R. Paus, A. Bayat.  
Awarded \$1000 dollars and invitation to present at 2015 ETRS conference, Copenhagen.

# Chapter 1

---

## Introduction

## 1.1 Topic background

Keloid disease (KD) is a benign cutaneous fibroproliferative tumour of unknown aetiopathogenesis that is characterised by heterogeneity, locally aggressive invasion and high recurrence rates following treatment [1, 2]. Unique to humans and with a higher preponderance in genetically susceptible individuals, KD represents an aberration of the normal wound healing process following injury to the skin [3, 4]. The clinical, histological and molecular heterogeneity between and within keloid scars has resulted in poorly understood pathogenesis, difficult diagnosis and ineffective management [5, 6]. In an effort to overcome this, more recent studies have divided keloid scars into component parts based on the macroscopic differences between the pale, shrunken centre and raised erythematous margin [7, 8]. This strategy has revealed a hyper-cellular advancing edge in the keloid margin dermis accompanied by evidence of increased collagen production, cell proliferation and reduced apoptosis when compared with the keloid centre [8, 9]. Additional divergence in phenotype and expression between superficial and deep fibroblasts within the keloid scar present an overall picture of a complex and diverse disease [10]. This lesional variation is further compounded by involvement of the keloid epidermis [11]. Until quite recently, KD was considered a dermal disorder with the fibroblasts at the centre of its formation [12], however, evidence of the significance of epithelial-mesenchymal interactions in the development and maintenance of KD has brought the role of the epidermis to the fore [13, 14]. Only by separating the keloid scar into distinct regions and scrutinising the contribution of each of those regions to its pathogenesis will we be able to not only understand underlying mechanisms but also appropriately target the active site of disease **(Figure 1.1)**.

The lack of a validated animal model for KD has resulted in reliance on traditional methods of investigation to examine of these specific keloid sites [15, 16]. Although whole tissue biopsies



from keloid centre and margin have exposed expression differences between these component parts, dilution by multiple transcriptomes reduces the sensitivity and neglects significant but low amplitude signaling [17]. Monolayer cell culture and co-culture techniques are experimentally facile and reproducible but fail to fully recapitulate the 3D architecture of the tissue and with increasing passage lose pathology-associated expression [8, 18]. Therefore, a major challenge facing KD research is the capacity to examine specific sites and their relationships while maintaining the natural structure and pathology inherent in the *in situ* tissue.

Laser capture microdissection (LCM) is a technique used to isolate single cells or cell subpopulations from within a tissue and has been used to dissect defined regions from within heterogeneous tissues, including both dermatological conditions and other areas of fibrosis [19-21]. The capacity to overcome heterogeneity while maintaining the architecture and pathology of the tissue makes LCM an ideal platform for application to KD. Only through the capture of *in situ* signaling from within the site-specific dynamic microenvironment of the keloid scar will the underlying pathobiology be elucidated and the key to keloid management be unlocked.

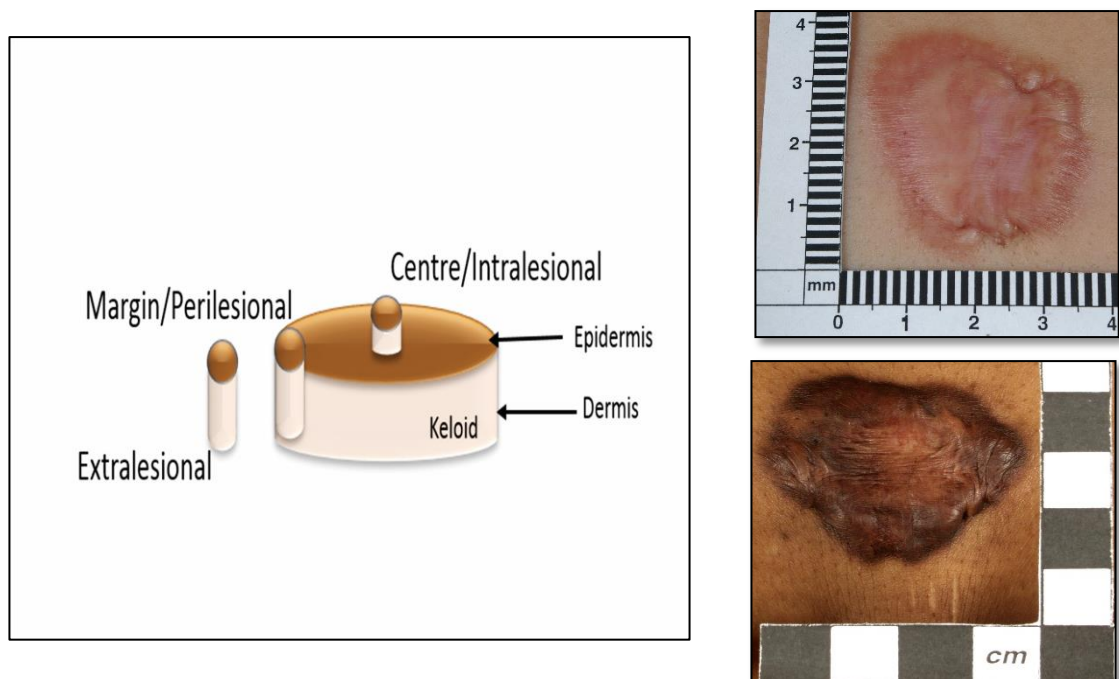


**Figure 1.1** Schematic diagram of distinct keloid regions and keloid photographs.

## 1.2 Research aims, specific questions to address and hypotheses to pursue

The overall objective of this thesis was to address the challenges facing KD research by asking specific questions for each of four research aims.

The first aim of this work was to compare the value of a site-specific *in situ* approach to KD research with traditional methods of tissue dissection. The second aim of the project was to compare the genomic expression between well-defined distinct keloid sites and normal skin. The third aim was to develop and explore hypotheses arising from this site-specific gene expression profiling approach so to enhance our understanding of KD pathobiology and promote new strategies for diagnosis and management. These aims formed the basis of **Chapter 4** where the following questions were addressed:

*Is a site-specific in situ approach the optimal strategy to investigate the pathogenesis of keloid disease and identify potentially significant differential gene expression?*

*Is there differential gene expression between different sites within the keloid epidermis and dermis?*

*Do the differentially expressed genes (DEG) and expression patterns identified between keloid sites within the epidermis and dermis offer new insight to KD pathobiology from which novel hypotheses can be developed?*

**a)** Application of combined laser capture microdissection and whole genome microarray to keloid centre, margin and extralesional epidermis and dermis as well as normal skin epidermis and dermis.

**b)** Evaluation of this site-specific *in situ* approach compared with alternative established methods of experimental investigation, including whole tissue biopsy and monolayer cell culture techniques.

**c)** Analysis and enrichment of the microarray data to detect expression patterns and differentially expressed genes within keloid sites and between keloid sites and normal skin.

**d)** Cultivation of progressive theories through identification of novel or underexplored concepts in keloid pathogenesis that will drive further research.

**e)** Development of detailed hypotheses that will be pursued with *in vitro* functional studies to elucidate possible mechanisms underlying keloid pathogenesis.

The fourth aim of this thesis was to probe the hypotheses arising out of the data analysis with relevant functional *in vitro* studies. Two major hypotheses arose from this site-specific gene expression profiling approach and were explored in further detail.

**Chapter 5: Hypothesis 1: Upregulation of AKR1B10 in keloid epidermis *in situ* implicates dysregulated retinoic acid metabolism in the pathogenesis of keloid disease**

**a)** Validation of aldo-keto reductase enzyme AKR1B10 upregulation in keloid compared with normal skin epidermis *in situ* and identification of other related relevant classical retinoic acid (RA) synthesis molecules that may also be dysregulated.

**b)** Determination of the effect of induced AKR1B10 overexpression in normal skin keratinocytes on the RA synthesis pathway expression.

**c)** Elucidation of the expression profile of AKR1B10-overexpressing keratinocytes in relation to keloid disease.

**d)** Investigation of the effect of AKR1B10 overexpression on RAR transactivation in the nucleus.

**e)** Assessment of the paracrine effects of AKR1B10-overexpressing keratinocytes on keloid and normal skin fibroblasts with regard to pro-fibrotic gene and protein expression.

**f)** Evaluation of RA treatment on TGF $\beta$ 1 and collagen expression in keloid fibroblasts.

**Chapter 6: Hypothesis II: Neuregulin-1 (NRG1) upregulation in keloid margin dermis promotes keloid fibroblast migration through ErbB2 mediated signaling**

**a)** Validation of NRG1 and ErbB2 upregulation as well as ErbB3 and ErbB4 downregulation in keloid dermis *in situ* and keloid fibroblasts compared with normal skin.

**b)** Evaluation of the dimerisation status of the ErbB family of tyrosine kinase receptors in keloid vs normal skin fibroblasts.

**c)** Investigation of the effect of NRG1 on the pro-fibrotic expression profile and migration of keloid and normal skin fibroblasts.

**d)** Determination of the dependence of the effects of NRG1 on ErbB2 expression.

### **1.3 Experimental design**

The experimental design of the research conducted for this thesis, along with the main project aims, is illustrated in **Figure 1.2**. The detailed materials and methods are provided in **Chapter 3** and each results chapter (**Chapters 4, 5 & 6**) contains a brief description of the specific methodologies relevant to that piece of work.

	Chapter 4	Chapter 4	Chapter 5	Chapter 5	Chapter 6	Chapter 6
	Application of site-specific <i>in situ</i> approach	Data analysis	AKR1B10 upregulation implicates retinoic acid (RA) in KD	Effect of induced AKR1B10 overexpression	Effect of NRG1 on pro-fibrotic profile expression & migration of fibroblasts	Dependence of NRG1 effects on ErbB2 signaling
<b>Project Aim</b>	To compare site-specific <i>in situ</i> approach (LCM) with monolayer & whole tissue methods of dissection	To compare expression between keloid sites & normal skin. To develop hypotheses arising from this novel approach	To validate the AKR1B10 upregulation and probe the hypothesis of RA deficiency in keloid epidermis	To determine the effect of AKR1B10 overexpression on RA pathway expression, secretory profile and nuclear transactivation	To validate NRG1 upregulation in KD & probe the hypothesis of NRG1 effects on keloid fibroblast (KF) migration	To validate ErbB expression in KD & to determine the hypothesised dependence of NRG1 effects on ErbB2
<b>Experiments</b>	8µm cryosections of whole tissue biopsies from centre, margin and adjacent lesional keloid tissue & NS	Quantile normalisation of data & filter criteria applied (fold change > 2, p-value < 0.05)	qRT-PCR and histochemistry for AKR1B10 in site-specific keloid and NS tissue	Forward transfection of NSK with AKR1B10, confirmed with qRT-PCR, western blot & immunocytochemistry	qRT-PCR & immunofluorescence for NRG1 in keloid tissue and KF vs NS	qRT-PCR & histochemistry for ErbB2 in keloid tissue and KF vs NS
	Cresyl violet rapid staining protocol & laser capture microdissection (LCM) of epidermis & dermis for each site	Enrichment analysis using Ingenuity pathway Analysis (IPA)	Further analysis of microarray data, qRT-PCR validation of RA pathway members identified as dysregulated	qRT-PCR of transfected NSK for RA pathway molecules dysregulated in microarray	Western blot for NRG1 in KF vs NS fibroblasts (NSF)	Combined immunofluorescence for NRG1 & ErbB2 in keloid tissue vs NS
	Extraction of primary keratinocytes and fibroblasts from keloid and normal skin	Validation of candidate genes using qRT-PCR	Combined immunofluorescence for AKR1B10 & CRABP2	qRT-PCR of transfected NSKs for epidermal homeostasis, proliferation and activation markers	Exogenous administration of NRG1 to KF & NSF	qRT-PCR for ErbB3 & ErbB4 in keloid tissue and KF vs NSF
	RNA extraction from whole tissue, monolayer cell culture & LCM. Amplification, purification and microarray		qRT-PCR for TGFβ1 & collagen following exogenous 1µM all-trans RA to KF	Double transfection of NSK with AKR1B10 and luciferase reporter assay for nuclear RA activity	qRT-PCR for TGFβ, IL-6, IL-8, CTGF, FN, collagen, FGF7 following NRG1 treatment	Western blot and co-immunoprecipitation for ErbB in KF vs NSF
		In-cell western blotting (ICW) for TGFβ1 and collagen I in KF following exogenous atRA	Fibroblast conditioned medium experiments with transfected/non-transfected keratinocyte medium	<i>In vitro</i> scratch assay to measure KF & NSF migration with/without NRG1 treatment	ErbB2 siRNA transfection studies in KF with qRT-PCR for TGFβ, IL, collagen, FGF7, Src, PTK2, STAT3	
			qRT-PCR & ICW for TGFβ1 & collagen expression of KF treated with conditioned medium	qRT-PCR for Src, PTK2 & STAT3 in KF & NSF following NRG1 treatment	In vitro scratch assay & MTT in KF following ErbB2 siRNA	
				MTT assay to measure proliferation & viability following NRG1 treatment	In vitro scratch assay & qRT-PCR in KF following ErbB2 siRNA combined with exogenous NRG1	

Figure 1.2 Flow chart of the key aims experimental design of the project.

#### **1.4 Layout of thesis and summary of original contributions of the research**

This thesis is displayed in the “alternative format” such that the results chapters are presented in the style of research papers that have been published, submitted or prepared for submission to peer-reviewed scientific journals. This method has been approved by the Faculty of Medical and Human Sciences in the University of Manchester.

All of the work in this thesis is entirely original and has employed the use of a wide range of investigative techniques and novel strategies to enhance the understanding of keloid pathobiology, provide a basis for future work and contribute to potential diagnostic and therapeutic approaches in the management of keloid disease (KD). The first results chapter (**Chapter 4**) provides extensive analysis of the microarray data from which two concrete hypotheses were developed and then explored in detail using functional *in vitro* studies, forming the subsequent two results chapters (**Chapters 5 & 6**).

##### *Chapter 1*

This chapter provides a brief introduction to the topic background and summarises the research aims accompanied by the experimental design.

##### *Chapter 2*

This chapter presents an in-depth literature review to allow interpretation of the current research in the context of the available literature. This overall review details the structure of normal skin and the normal wound healing process as well as describing the potential outcomes of abnormal wound healing, at the extreme end of which is KD. A general overview of KD with additional insight into current literature on site-specific disease, epithelial-mesenchymal

interactions and current methods of investigation are detailed. Much of the description of keloid histology is adapted from the publication of a review article written during the course of this thesis and included at the end of the entire thesis. This paper is referenced below. The technique of laser capture microdissection and its place in relevant research to date is also explored in the literature review.

- **Jumper N**, Paus R Bayat A. Functional histopathology of keloid disease. *Histol Histopathol* 2015; 30: 1033-1057.

### *Chapter 3*

This chapter encompasses the detailed descriptions of the materials and methods employed throughout the thesis, yet are only briefly described in each chapter-specific methodology section.

### *Chapter 4*

This chapter reports the analysis of the site-specific *in situ* approach to KD. It has been formatted for submission to PLOS One journal and appears in this thesis as per the formatting requirements of the journal. Original contributions and achievements arising from this chapter are detailed below:

- **Jumper N**, Hodgkinson T, Paus R, Bayat A. Combined laser capture microdissection (LCM) and whole genome microarray profiling of epidermis versus dermis of site-specific keloid disease compared with whole keloid tissue biopsy and monolayer culture provide novel targets with potential clinical implications. For submission to PLOSOne 2016.



a) Through the combination of laser capture microdissection and whole genome microarray a site-specific *in situ* approach, novel in its application to KD, proved a robust method of investigation into KD pathobiology. The broader scope of overall expression, increased sensitivity and improved accuracy compared with whole tissue and monolayer techniques, validated employment of this strategy in addressing the challenges facing KD.

b) This unique approach to dissecting KD allowed the allocation of specific signals to defined regions within the keloid scar. It also resulted in the identification of several significant differentially expressed genes that may foster progressive theories in the understanding of keloid pathobiology and form the basis of future work. Analysis revealed expression patterns associated with epithelial-mesenchymal transition (WDR66, BMP2, CLDN4, CLDN23), collagen deposition (ADAMTS2, ADAMTS14), inflammation (IL-37, IL-13RA), cancer-like stem cells (ALDH1A1, NOTCH4) and therapeutic resistance (AKR1B10, ALDH1A1, NOTCH4, TUBB3) that have not previously been associated with KD.

## Chapter 5

This chapter encompasses the published results from investigation into the role of AKR1B10, which was identified as upregulated in the microarray data from **Chapter 4**. It appears in the publication format of the Journal of Investigative Dermatology, in which it was published. The paper is referenced as detailed below and the original contributions and achievements of this work described underneath.

- **Jumper N**, Hodgkinson T, Arscott G, Har-Shai Y, Paus R Bayat A. The aldo-keto reductase AKR1B10 is upregulated in keloid epidermis, implicating retinoic acid pathway dysregulation in the pathogenesis of keloid disease. *J Invest Dermatol* 2016 Jul;136(7):1500-12. doi: 10.1016/j.jid.2016.03.022. Epub 2016 Mar 26.

a) AKR1B10 was validated as upregulated in keloid epidermis *in situ* and in combination with the upregulation of ALDH1A1, CRABP2 and downregulation of CYP26B1 and CRABP1, indicated dysregulation of the retinoic acid (RA) pathway in KD. This comprehensive study represents the first molecular exploration of the RA biosynthesis pathway in KD and given the pleiotropic effects of RA, may have significant mechanistic and therapeutic implications.

b) When normal skin keratinocytes were induced to overexpress AKR1B10 this recapitulated the keloid epidermal RA expression and demonstrated reduced RA transactivation, supporting the hypothesis that keloid epidermis is deficient in RA.

c) Treatment of keloid and normal skin fibroblasts with conditioned medium from AKR1B10-overexpressing keratinocytes resulted in the increased expression of pro-fibrotic factors including TGF $\beta$ 1, collagen I and collagen III, which are known to be upregulated in KD. This paracrine effect lends support to the significance of pathological epithelial-mesenchymal interactions in KD and highlights the role of the epidermis in keloid pathobiology.

d) Treatment of keloid fibroblasts with all-*trans* RA did not completely abrogate these pro-fibrotic effects, emphasising the potential importance of this work in identifying defined targets whose manipulation is subject to less extensive homeostatic effects than master modulators such as RA.

## Chapter 6

This chapter investigates the role of neuregulin-1 (NRG1) in KD following identification of its upregulation in microarray data from **chapter 4**. This work has been submitted to the *Acta Dermato-Venereologica* and appears in this thesis as per the formatting requirements for the journal. The original contributions and achievements of this work are outlined below:

- **Natalie Jumper**, Tom Hodgkinson, Ralf Paus, Ardeshir Bayat. A role for neuregulin-1 (NRG1) in promoting keloid fibroblast migration via ErbB2-mediated signaling.

Submitted to *Acta Dermato-Venereologica* 2016

a) Upregulation of NRG1 was shown to induce pro-fibrotic expression and migration in keloid and normal skin fibroblasts *in vitro*. The knockdown of ErbB2 attenuated these effects in keloid fibroblasts and the failure to recover migration or Src/PTK2 expression with further NRG1 administration, demonstrated the dependence of this response on ErbB2 signaling.

b) The dimerisation status of ErbB2 revealed keloid fibroblasts expressed higher levels of ErbB2/ErbB2 and ErbB2/ErbB3 than normal skin fibroblasts, supporting the hypothesis of maximal signaling via NRG1 binding.

c) Identification of NRG1-induced upregulation of Src and PTK2 via ErbB2-mediated signaling, exposes a role for this mechanism in keloid migration at the margin dermis not previously investigated. This finding may be significant in contributing to invasion of keloid into normal skin, a hallmark of the disease.

### *Chapter 7*

This chapter brings the thesis together and incorporates all of the findings into a general discussion, shedding light on interpretation of results, strengths and weaknesses of the current work and possible topics for future studies arising from this research.

Overall, the findings from this research offer new insight into the mechanisms underlying keloid pathobiology and present compelling concepts for processes contributing to the formation and maintenance of KD. As a result of the novel application and robust performance of this *in situ* approach to KD, there may be potential diagnostic and therapeutic implications through molecular targeting. Further studies built on the work of this research may yield promising advancements in the management of the complex disorder that is KD.

## References

1. Bella H, Heise M, Yagi KI, Black G, McGrouther DA, Bayat A. A clinical characterization of familial keloid disease in unique African tribes reveals distinct keloid phenotypes. *Plast Reconstr Surg*. 2011;127: 689-702.
2. Andrews JP, Marttala J, Macarak E, Rosenbloom J, Uitto J. Keloids: The paradigm of skin fibrosis - Pathomechanisms and treatment. *Matrix Biol*. 2016
3. Hunasgi S, Koneru A, Vanishree M, Shamala R. Keloid: A case report and review of pathophysiology and differences between keloid and hypertrophic scars. *Journal of Oral and Maxillofacial Pathology*. 2013;17: 116.
4. Butzelaar L, Ulrich M, van der Molen AM, Niessen F, Beelen R. Currently known risk factors for hypertrophic skin scarring: A review. *Journal of Plastic, Reconstructive & Aesthetic Surgery*. 2015.
5. Arno AI, Gauglitz GG, Barret JP, Jeschke MG. Up-to-date approach to manage keloids and hypertrophic scars: a useful guide. *Burns*. 2014;40: 1255-66.
6. Trace AP, Enos CW, Mantel A, Harvey VM. Keloids and Hypertrophic Scars: A Spectrum of Clinical Challenges. *Am J Clin Dermatol*. 2016;17: 201-23
7. Seifert O, Bayat A, Geffers R, Dienus K, Buer J, Lofgren S, et al. Identification of unique gene expression patterns within different lesional sites of keloids. *Wound repair and regeneration : official publication of the Wound Healing Society [and] the European Tissue Repair Society*. 2008;16: 254-65.
8. Syed F, Ahmadi E, Iqbal SA, Singh S, McGrouther DA, Bayat A. Fibroblasts from the growing margin of keloid scars produce higher levels of collagen I and III compared with intralesional and extralesional sites: clinical implications for lesional site-directed therapy. *Br J Dermatol*. 2011;164: 83-96.
9. Luo S, Benathan M, Raffoul W, Panizzon RG, Egloff DV. Abnormal balance between proliferation and apoptotic cell death in fibroblasts derived from keloid lesions. *Plast Reconstr Surg*. 2001;107: 87-96.
10. Supp DM, Hahn JM, Glaser K, McFarland KL, Boyce ST. Deep and superficial keloid fibroblasts contribute differentially to tissue phenotype in a novel in vivo model of keloid scar. *Plast Reconstr Surg*. 2012;129: 1259-71.
11. Hahn JM, Glaser K, McFarland KL, Aronow BJ, Boyce ST, Supp DM. Keloid-derived keratinocytes exhibit an abnormal gene expression profile consistent with a distinct causal role in keloid pathology. *Wound repair and regeneration : official publication of the Wound Healing Society [and] the European Tissue Repair Society*. 2013;21: 530-44.
12. Datubo-Brown DD. Keloids: a review of the literature. *British journal of plastic surgery*. 1990;43: 70-7.
13. Lim IJ, Phan TT, Bay BH, Qi R, Huynh H, Tan WT, et al. Fibroblasts cocultured with keloid keratinocytes: normal fibroblasts secrete collagen in a keloidlike manner. *American journal of physiology Cell physiology*. 2002;283: C212-22.
14. Do DV, Ong CT, Khoo YT, Carbone A, Lim CP, Wang S, et al. Interleukin-18 system plays an important role in keloid pathogenesis via epithelial-mesenchymal interactions. *Br J Dermatol*. 2012;166: 1275-88.
15. Marttala J, Andrews JP, Rosenbloom J, Uitto J. Keloids: Animal models and pathologic equivalents to study tissue fibrosis. *Matrix Biology*. 2016;51: 47-54.
16. Williams FN, Herndon DN, Branski LK. Where we stand with human hypertrophic and keloid scar models. *Exp Dermatol*. 2014;23: 811-2.
17. Lovendorf MB, Mitsui H, Zibert JR, Ropke MA, Hafner M, Dyring-Andersen B, et al. Laser capture microdissection followed by next-generation sequencing identifies disease-related microRNAs in psoriatic skin that reflect systemic microRNA changes in psoriasis. *Exp Dermatol*. 2015;24: 187-93.

18. Mabry KM, Payne SZ, Anseth KS. Microarray analyses to quantify advantages of 2D and 3D hydrogel culture systems in maintaining the native valvular interstitial cell phenotype. *Biomaterials*. 2016;74: 31-41.
19. Datta S, Malhotra L, Dickerson R, Chaffee S, Sen CK, Roy S. Laser capture microdissection: Big data from small samples. *Histol Histopathol*. 2015;30: 1255-69.
20. Marmai C, Sutherland RE, Kim KK, Dolganov GM, Fang X, Kim SS, et al. Alveolar epithelial cells express mesenchymal proteins in patients with idiopathic pulmonary fibrosis. *Am J Physiol Lung Cell Mol Physiol*. 2011;301: L71-8.
21. Quan C, Cho MK, Shao Y, Miannecki LE, Liao E, Perry D, et al. Dermal fibroblast expression of stromal cell-derived factor-1 (SDF-1) promotes epidermal keratinocyte proliferation in normal and diseased skin. *Protein Cell*. 2015;6: 890-903.

# Chapter 2

---

## Literature review

## 2.1 Introduction

Keloid disease (KD) is a fibroproliferative cutaneous tumour characterised by clinical, behavioural and histological heterogeneity. The associated aesthetic distress and frequent physical disability leaves those affected in search of both a cosmetic and functional cure. Unfortunately, the lack of any one effective treatment, despite an abundance of available therapies, has resulted in both patient and clinician frustration.

A keloid scar begins like any other injury, with the process of wound healing. It is within these four integrated phases, conducted under the fine-tuned orchestration of numerous cytokines, chemokines and growth factors that there are several potential points of dysregulation, which underlie the pathogenesis of this fibroproliferative disease. As such, this first chapter discusses the structure of human skin, the phases of wound healing and potential outcomes of the wound healing process, including scarring. Although valuable progress has been made in this field, research into KD is hindered by a number of factors. Inter-patient, inter-lesional and intralesional heterogeneity hamper any attempt to establish a biomarker that could represent a diagnostic or therapeutic target. This chapter reviews KD in detail and addresses these discrepancies by discussing the site-specific nature of KD and the role of epithelial-mesenchymal interactions. Lack of a validated animal model and paucity of available tissue for experimentation, secondary to high rates of recurrence following excision, have led to reliance on 2D monolayer culture or whole tissue biopsy techniques. In this chapter, these methods and an alternative investigative technique, laser capture microdissection (LCM), are discussed.

Two of the major challenges in understanding keloid pathogenesis include overcoming the heterogeneity within the scar and capturing a complete picture of gene expression from within the natural architecture of the tissue. In this thesis, these challenges are addressed using a site-specific

*in situ* approach to KD, achieved through a combination of LCM and whole genome microarray.

This chapter explores that approach in the context of the existing literature.

## 2.2 The structure of human skin

The skin is a large, multi-functional organ that can adapt to the surrounding environment by serving as an interface between the body and the outside world. On the most basic level, the skin acts as a physical barrier giving protection from external stressors, including mechanical and chemical insults, radiation and pathogenic microorganisms. Its role in homeostasis comprises immune control, synthesis of vitamin D and heat regulation through vasoconstriction/vasodilation and perspiration. An essential function of the skin is sensory perception (the detection of pressure, temperature and vibration), which through prevention or limitation of injury reduces the morbidity associated with breaching the skin barrier [1, 2].

Human skin varies in texture, colour and thickness throughout the body [3]. The two patterns of skin, hairy and glabrous, are divided into four distinct layers (**Figure 2.1**). Most superficial is the stratified epidermis, which is composed predominantly of keratinocytes and to a lesser extent pigment-producing melanocytes, sensory Merkel cells and immune-related Langerhans cells. Beneath the epidermis is the basement membrane zone, which anchors it to the underlying dermis and facilitates communication between these layers. The dermis is rich in extracellular matrix (ECM) and contains the pilosebaceous units, nerves and blood vessels. The deepest layer is the hypodermis or subcutaneous adipose tissue layer, responsible for conserving body heat and acting as a shock absorber against external injury [4-6]. Whilst all four of these layers have different morphology and functions, they act in synergy to protect the body and act as an interface with the surrounding environment.



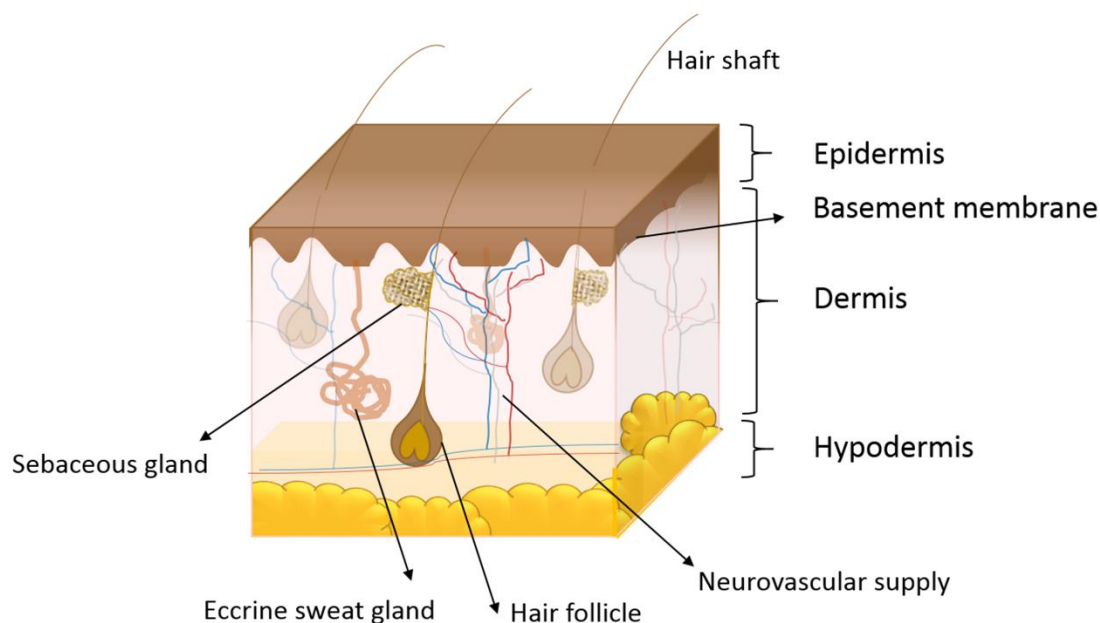


**Figure 2.1 Schematic diagram of the structure of human skin.**

### 2.2.1 Epidermis

The epidermis is a stratified squamous epithelium consisting of four layers of cells generated through a process of continuous keratinocyte differentiation. The layers comprise the *stratum basale/germinativum* (the deepest layer), *stratum spinosum*, *stratum granulosum* and the most superficial, the *stratum corneum* [7, 8]. In areas of thicker glabrous skin the *stratum lucidum*, located between the *granulosum* and *corneum*, is rich in protein-bound lipids. The *stratum basale*, composed of columnar cells, borders the basement membrane and interacts with it through hemidesmosomes, while keratinocytes within the *stratum spinosum* are bound to each other by desmosomes [8]. The *stratum corneum* is the most differentiated layer, consisting of anucleate cells, and is of varying thickness, serving as the primary protective barrier [4]. These cells eventually slough off, in a process known as desquamation resulting in periodic recycling, and are routinely

replaced with differentiating cells moving up from the *stratum basale* [9]. This continuous turnover of cells allows those most superficial cells, those most likely to be damaged from UV radiation or injury, to be discarded.

The epithelium is an avascular layer requiring nourishment to be diffused up from the dermis. It is composed largely of keratinocytes (~95%), which can be identified as either active or in the midst of their several stages off differentiation, based on the coordinated expression of proteins known as cytokeratins [10]. The basal keratinocytes express Keratin 5 and Keratin 14 (K5, K14) while those set on the path of differentiation express K1 and K10 [7, 11]. As these suprabasal keratinocytes move toward the *stratum corneum*, in addition to K1 and K10, they express involucrin, filaggrin and loricrin [12] (**Figure 2.2**).

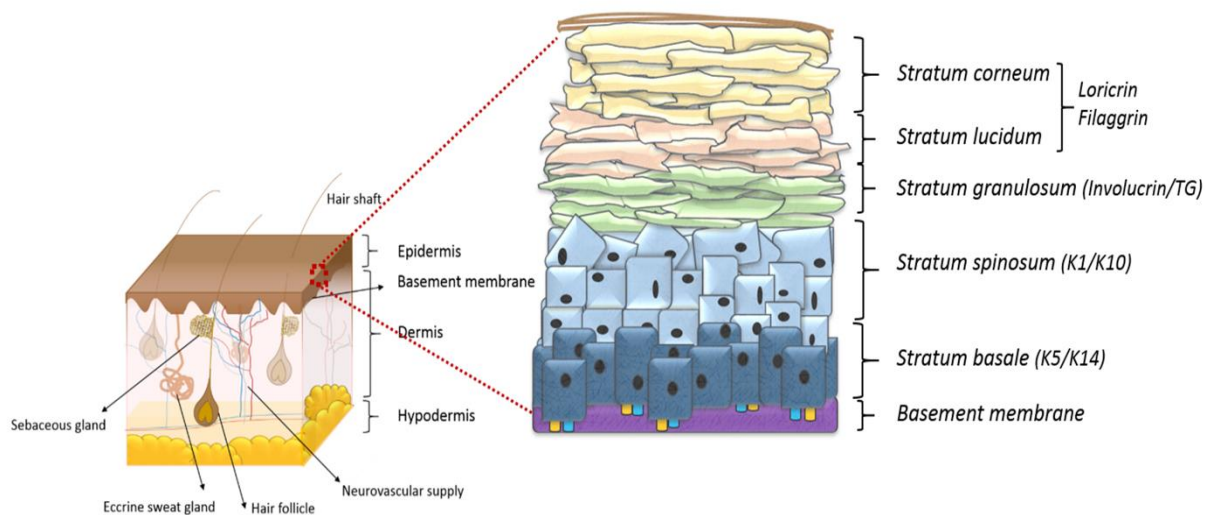


**Figure 2.2** Schematic representation of epidermal strata.

Other cells also populate the epidermis; melanocytes, Langerhans cells, lymphocytes and Merkel cells [10]. Each of these cells has a specialised role in the functioning of the epidermal layer. The melanocytes are derived from the neural crest and along with the basal keratinocytes form epidermal melanin units, are responsible for pigmentation of the skin through keratinocyte interaction [13]. Langerhans cells are basement membrane-derived cells that are related to the monocyte-macrophage-histiocyte lineage and have an antigen presenting capacity that enable them to contribute to the immune function of the skin [8]. The Merkel cells are primarily located in the basal layer and the bulge of hair follicles, performing a type I mechanoreceptor function [14].

In addition to these specialised cells there are different stem cell populations within the epidermis, responsible for the repair and maintenance of the skin during physiological (hair follicle homeostasis) and pathological (wound healing) conditions [15]. Some of these stem cells are resident, as in the hair follicle bulge or sebaceous gland, while others are either recruited or arise from transient plasticity, a process largely attributed to the niche microenvironment [16, 17]. In the epidermis, it is thought that rare stem cells give rise to keratinocyte progenitors (transit amplifying cells) and that these cells are responsible for the short-term maintenance of the skin, eventually differentiating in a hierarchical manner [18]. However, it is possible that these epidermal stem cells are also a source of skin pathology, including tumorigenesis [19].

### **2.2.2 Basement Membrane Zone (BMZ)**

As well as being a physical boundary anchoring the epidermis and dermis, the basement membrane zone (BMZ), or dermo-epidermal junction (DEJ), acts as a diffusion barrier and reservoir for a plethora of cytokines and growth factors [2, 7]. Composed of an upper *lamina basale*, itself consisting of the *lamina lucida* and *densa*, and lower *lamina reticularis* [4], the basement membrane

communicates with the epidermis via hemidesmosomes and with the dermis below through anchoring fibrils, themselves made of collagen VII [20].

Formed by contributions from both epidermal and dermal cells, the DEJ binds these layers together through a combination of structural and bridging proteins. Collagen IV and members of the laminin family (principally laminin 5, which is keratinocyte-produced) provide the mechanical stability and adhesiveness, through integrin binding, necessary to maintain the architecture of the skin [21]. Several bridging proteins, including nidogens, perlecan, fibronectins and other ECM molecules are responsible for holding the scaffold together [2, 22].

In full thickness skin injuries, the DEJ requires reconstruction by properly functioning keratinocytes and fibroblasts working in unison. This has been demonstrated using reconstructed *ex vivo* skin models, where the *de novo* morphogenesis of the basement membrane can be temporally analysed [23].

### **2.2.3 Dermis**

The dermis functions to provide structural support, act as a shock absorber, regulate temperature and nourish the epidermis. The thickness of the dermis varies depending on anatomical location and is considered in two parts, the superficial papillary dermis and deeper reticular dermis [20].

The papillary dermis communicates with the epidermis via the BMZ, where bi-directional projections from epidermis to dermis (Rete ridges) and dermis to epidermis (papillae) result in increased interface area [8]. As the dermal layer is in close contact with the epidermis, the papillary

dermis is rich in vasculature and specialised sensory receptors. The reticular dermis is thicker than the papillary layer and is essentially connective tissue populated by fibroblasts, the most abundant cell in the dermis [7].

The fibroblasts are the major cell type responsible for ECM production, creating structural support in the form of collagen (provides strength), elastin (provides elasticity and aids load-bearing) proteoglycans, glycosaminoglycans, glycoproteins and interposed loose connective tissue [4]. Although the fibroblast is considered the principal cell in the dermis, there are several other cells present, including macrophages, lymphocytes, monocytes, mast cells, myofibroblasts and pericytes among others [10].

#### **2.2.4 Hypodermis**

The hypodermis lies deep to the dermis and is also known as the subcutaneous tissue. This layer is composed largely of adipose tissue, connective tissue and elastin. In addition to attaching the skin to the underlying fascia, the hypodermis provides insulation and acts as a shock absorber against external insults as well as an important site of hormone conversion [7]. The main cell types in the subcutaneous tissue are fibroblasts, adipocytes and immune cells. This layer has attracted a lot of attention in recent years as a source of progenitor and stem cells (AD-MSC: adipose-derived mesenchymal stem cells), which are thought to contribute to the wound healing and tissue homeostasis processes [24-26].

Injury to the skin at varying depths interrupts some or all of these four layers, setting in motion the process of wound healing described below.

### 2.3 Adult cutaneous wound healing

When the skin is breached it sets in motion a healing process critical for the restoration of tissue integrity and function, ensuring the prevention of fluid loss, electrolyte imbalance and infection. This process (**Figure 2.3**) is a finely honed symphony of cellular communication, connective tissue deposition, re-epithelialization and angiogenesis, occurring as four overlapping phases orchestrated by a plethora of cytokines, chemokines and growth factors [27]. These four phases are briefly discussed below and, although a highly organised and dynamic process, the possibility of dysregulation exists at each phase, which may alter the fate of the wound.

#### 2.3.1 Phase I: Haemostasis (Day 1)

Haemostasis is the formation of a clot to limit local blood loss and is mediated on a cellular level principally by platelets. Two concurrent pathways lead to the formation of a fibrin clot following the sub-endothelial exposure of collagen and tissue factor [28]. Once formed, this “provisional wound matrix” acts as a scaffold for incoming cells, including neutrophils, monocytes, endothelial cells and fibroblasts, as well as growth factors, including TGF $\beta$  and PDGF [29]. The activated platelets stimulate further aggregation, increase their surface receptors (GPVI,  $\alpha$ 2 $\beta$ 1 and GPIb-V-IX,  $\alpha$ IIb $\beta$ 3) and de-granulate from their  $\alpha$  granules (releasing adhesive proteins, growth factors, cytokines, clotting factors and proteases) and dense granules (exocytosis of ADP, ATP, histamine, serotonin and calcium), thereby stimulating fibroblasts to lay down early ECM [30]. Many of the mediators released are pro-inflammatory (IL-1 $\alpha$ , IL-1 $\beta$ , IL-6 and TNF- $\alpha$ ), creating an overlap with the next stage of wound healing by initiating the inflammatory process [31]. Fibrinolysis begins shortly after clot formation and is mediated by plasmin, formed from the cleavage of plasminogen by activators released by platelets. Fibrinolysis is necessary in order to allow granulation tissue to form.

SERPINE1/PAI-1(plasminogen activator inhibitor) is a potent inhibitor of the plasminogen activators (tPA and uPA) and is used to protect the ECM from degradation during the fibrinolysis process. In cases of PAI-1 excess, however, inadequate removal of the clot may lead to sustained fibroblastic secretion of collagen and result in fibrosis. This may be a point of consideration in excess scar formation [32].

### **2.3.2 Phase II: Inflammation (Days 1-7)**

The inflammatory phase can be divided into early and late stages. Within the first twenty-four hours the wound becomes flooded with polymorphonuclear (PMN) cells/ neutrophils, chemo-attracted to the site by ECM (extracellular matrix) fragments, complement factors (C3a or C5a), bacteria (formyl methionyl peptide) and chemokines (TGF $\beta$ , GRO $\alpha$ , platelet factor 4) [33]. The blood clot platelets release CTAP-III, a chemokine that is proteolytically converted into NAP-2 by neutrophils. NAP-2 is a first-line mediator that acts via CXCR-2 to attract neutrophils to the site of injury within minutes [34]. Neutrophil influx, achieved through margination and diapedesis (trans-epithelial migration), is essential for the removal of bacteria and cellular debris, which it accomplishes by phagocytosis and the release of protease enzymes. Neutrophils themselves are a source of pro-inflammatory cytokines, among which are IL-1, IL-6 and TNF $\alpha$ , which is responsible for matrix metalloproteinase (MMP) activation [30]. Generally, these cells disappear from the wound within 48 hours, either as a result of eschar sloughing or apoptosis.

The later stage of inflammation is heralded by the arrival of monocytes, which are stimulated within the ECM to metamorphose into macrophages, considered the conductors of wound healing. These cells are attracted to the wound site by pro-inflammatory cytokines, growth factors and bacterial lipopolysaccharides (LPS) [35]. Macrophages are multi-functional in that they are responsible for

pro-inflammatory cytokine release, phagocytosis, the release of MMPs, nitric oxide and proteinase uPA, which is necessary for fibrinolysis [36]. Additionally, they stimulate angiogenesis (VEGF, FGF, TGF $\beta$ ), re-epithelialisation (FGF, TGF $\beta$ , IGF, KGF), and collagen production via the attraction of fibroblasts, thus fostering the link between the inflammatory and proliferative phases [30, 35].

Similar to macrophages, T lymphocytes, under the influence of IL-1, arrive even later in the inflammatory phase, overlapping with both proliferation and remodelling. Mediated in part through toll-like receptors (TLR) the precise role of these lymphocytes is unclear in wound healing but knockout mice have shown that impairment of the T lymphocyte response interrupts the normal wound healing process [37]. Other cells that take part in the inflammatory process include pericytes, fibrocytes, lymphocytes and mast cells. Pericytes have been implicated in the haemostatic and inflammatory phases of wound healing, interacting with platelets, endothelial cells, macrophages and T-cells. It has been described that pericytes contribute to fibrosis through acquiring a fibroblast-like phenotype that then differentiate into myofibroblasts, thereby contributing to ECM deposition [38]. Fibrocytes, also associated with fibrosis, are bone marrow-derived mesenchymal progenitors that play an early role in the wound healing process as antigen-presenting cells [39]. Mast cells contribute to initial vasodilation allowing the clinical signs of inflammation to become evident: rubor, calor, tumor, and dolor. These cells also modulate proteolytic activity and are involved in the fine-tuning of angiogenesis [40].

Protracted inflammation is detrimental to tissue repair, leading to chronic wounds and excess scarring [33, 41]. For this reason there are checkpoint controllers of inflammation, mediated by specialised pro-resolving lipid mediators (SPM) including lipoxins, formed by platelets and leukocytes [42].



### 2.3.3 Phase III: Proliferation (Days 3-14)

The proliferative phase is marked by the formation of granulation tissue, a highly vascular connective tissue that replaces the fibrin clot, by re-epithelialisation, neo-angiogenesis and new ECM deposition [31]. Keratinocytes at the wound edge and under the influence of EGF, TNF $\alpha$  and KGF “shuffle” across the fibrin clot along an IL-1 established chemotactic gradient [43]. These keratinocytes, also sourced from the hair follicle bulge, undergo morphological changes and migrate via lamellopodal crawling, once the anchoring hemidesmosomes are dissolved by elastase and collagenase [31]. This migration occurs on specific tracks of ECM, requiring laminin 5, uPA and matrix metalloproteinases to degrade and  $\beta$ 1 integrins to interact with the tissue [44].

In addition to keratinocytes, the predominant cells proliferating during this phase are the fibroblasts and endothelial cells. Stimulated by the wound micro-environment (hypoxia, increased lactate) and growth factors (VEGF, bFGF, TGF $\beta$ ) released from platelets and keratinocytes, damaged vessels are replaced by “sprouts” from intact capillaries [45]. These sprouts orientate themselves using integrins, particularly  $\alpha$ 5 $\beta$ 3, and secrete MMPs to degrade tissue, allowing navigation of the ECM [31]. The pro-angiogenic anti-hypoxic effects of VEGF are mediated through HIF-1 $\alpha$  (hypoxia inducible factor) expression, which further induces VEGF and endothelial nitric oxide synthase (eNOS) expression [46]. Hypoxia has been investigated as an aetiological factor for KD, supported by findings of decreased central vascular density compounded by microvascular occlusion and invasive capacity [47-49].

Fibroblasts are elongated, spindle cells, defined by their ability to secrete ECM. Although these cells share a common name within a variety of mesenchymal tissues of the body (hepatic, renal, cardiac etc.), they have been shown to differ not only between organs but also within a single tissue [50]. This fibroblast heterogeneity has been shown to result in differences with regard to

morphology, proliferation, collagen synthesis and response to stimuli [51]. Keloid fibroblasts differ not only from normal skin fibroblasts in morphology, gene expression and collagen gel contraction but also within the keloid lesion itself the fibroblasts from the centre and margin differ with regard to proliferation, cell cycle phase, apoptotic factor expression and collagen production [52-55]. Interestingly, a recent study identified a distinct, local resident cutaneous fibroblast lineage expressing CD26/DPP4 as responsible for fibrosis during wound healing [56]. It would be interesting to explore the role of these fibroblasts in keloid disease.

The provisional ECM, consisting of mostly fibronectin and hyaluronan, is replaced by a more established ECM, largely consisting of collagen. Fibroblasts, the major source of collagen, arrive at the wound site in response to PDGF, EGF, CTGF, TGF $\beta$  and numerous other cytokines and growth factors [31, 57]. Some of these fibroblasts, sourced from the local wound site or mesenchymal stem cell (MSC) population, undergo morphological conformation under the influence of TGF $\beta$  to become myofibroblasts expressing *de novo*  $\alpha$ SMA [58]. In response to CTGF, PDGF, hyaluronic acid and Wnt activation, these myofibroblasts may also arise from pericytes, adipose/mesenchymal stem cells, endothelial/epithelial cells and fibrocytes [59]. Myofibroblasts significantly contribute to wound closure through contractile forces generated by actin microfilaments, which has been witnessed *in vitro* in a populated collagen gel [60, 61].

The communication between keratinocytes and fibroblasts in this phase is crucial for the maintenance of balanced ECM production. Dysregulation of these epithelial-mesenchymal interactions has come to light as a major factor in delayed wound healing and excess scar formation.

#### **2.3.4 Phase IV: Remodelling and maturation (Day 21 onwards)**

This phase of wound healing, in contrast to the relatively short preceding phases, can last for months to years. The ultimate role of this phase is to increase the tensile strength within the wound, decrease the thickness of the newly formed tissue and promote terminal differentiation of the epidermis, thereby restoring a functional barrier [62]. The interplay of collagen deposition with MMP and TIMP (tissue inhibitors of metalloproteinase) activity dominates this phase [63]. The myofibroblasts, stimulated into existence by PDGF, TGF $\beta$  and mechanical loading, begin to contract the wound [59, 64]. These cells also support the fibroblasts in their production of collagen. Remodelling is dependent on the gradual conversion of early collagen III to the higher tensile collagen I, which only produces a final comparative strength of 80% versus pre-wounded skin [65]. The process of apoptosis is essential for the completion of a mature scar, which is hypo-cellular, hypo-vascular and dominated by collagen I fibrils. The failure of myofibroblasts at this stage to undergo apoptosis is likely to be instrumental in the formation of excess scarring [66].

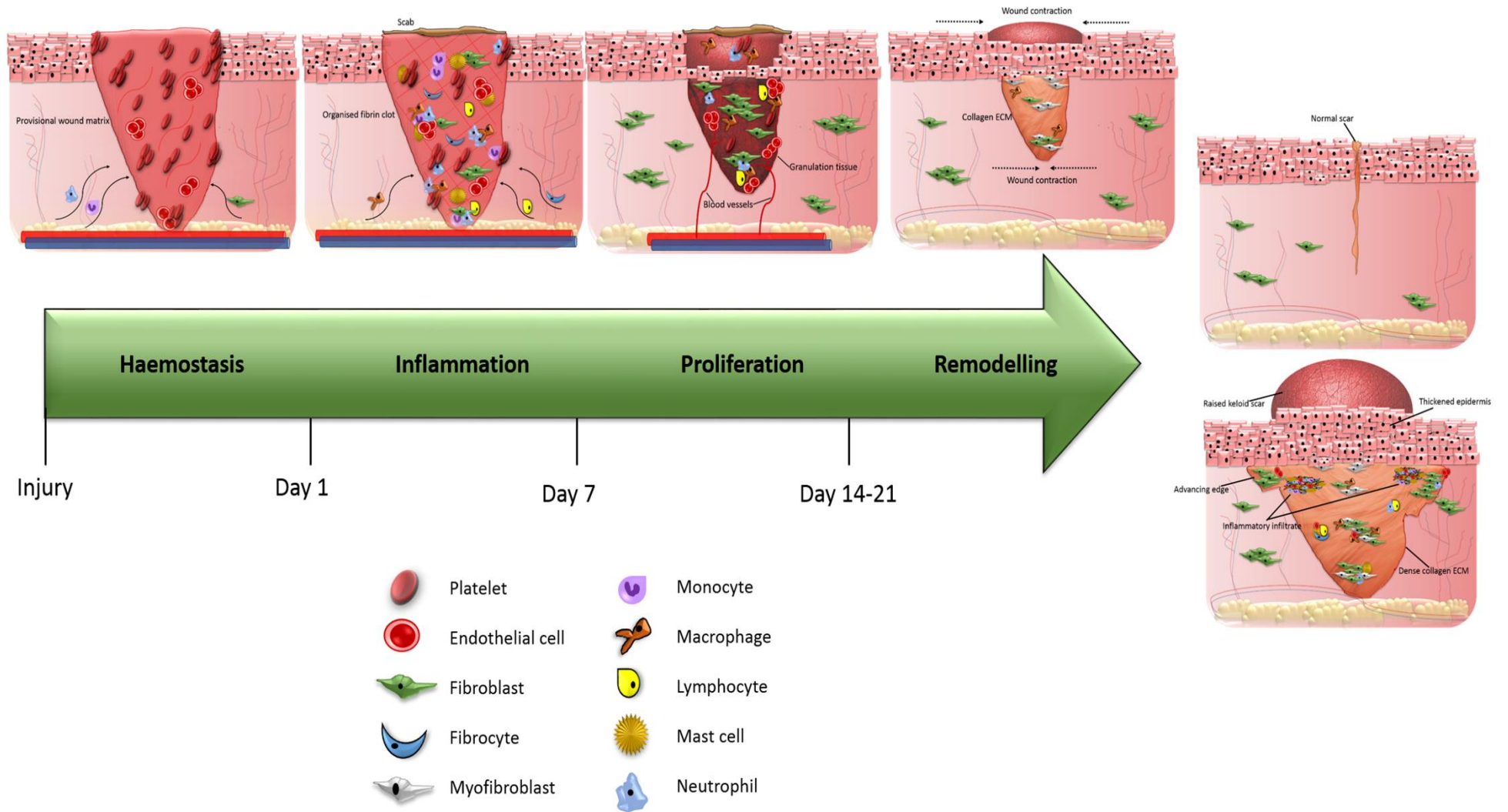


Figure 2.3 Phases of wound healing and potential outcomes.

## **2.4 Outcomes of the wound healing process**

The process of wound healing is affected by both internal and external factors including genetics, gender, age, mechanism of injury, contamination, nutrition status, co-morbidities and treatment. These factors can affect the mechanisms underlying the four phases of the wound healing and change the efficiency of this process. Therefore the outcome may vary from an acute wound healed with no scar (exceptional) or minimal scar to abnormal scar formation, which results in varying degrees of fibrosis. Epidermal appendages are not re-formed during the healing process and therefore the scar appears as a hairless area [27]. In addition to fibrotic scars, a presence of a chronic wound also represents abnormal wound healing. These outcomes are discussed in more detail below.

### **2.4.1 Acute wound healing**

Acute wound healing follows an orderly and predictable timeline through the four overlapping phases of haemostasis, inflammation, proliferation and remodelling, described above. The inflammatory phase is often described as that most indicative of acute versus chronic wound healing [67]. In an acute wound the inflammation is evidenced by the clinical signs and cardinal symptoms of pain, swelling and redness. For a wound to be acute, this inflammatory phase should not last longer than 2 weeks, at which point it becomes pathologic inflammation and may lose the clinically associated cardinal signs [68]. A prolonged inflammatory phase and failure of wound closure results in a chronic wound.

### **2.4.2 Chronic wound healing**

A chronic wound is defined as one in which the epidermis remains interrupted for more than 42 days or where it is recurrently interrupted [68]. There are various factors, local and systemic, that can impair the streamlined flow of the phases of wound healing and result either in a delayed or non-healing wound. Those wounds that heal by secondary intention, including

trauma, burns and infected wounds are particularly subject to chronicity. Local factors affecting wound healing, such as oxygen and perfusion, tension on wound edges, foreign body presence and infection should be as tightly controlled as possible from the outset [69]. Systemic factors that affect wound healing include age, nutrition status, chronic disease (peripheral vascular disease and diabetes), medications and many more [25, 69]. The chronic wounds resulting from alterations in local factors or presence of systemic factors present a huge clinical and economic burden [70].

Neutrophilia has been proposed as the major factor in chronic wound healing and can be used as a biological marker in addition to reactive oxygen species (ROS) [71]. The destruction of growth factors by elastase and collagenase, released by neutrophils, impairs the communication required for the smooth transition from open wound to healed scar and can contribute to cellular senescence.

Not only is healing of these wounds essential from a homeostatic point of view, but also the patients are affected by the associated poor cosmesis. Several therapeutic options have been proposed in an effort to turn a chronic wound into an acute wound, thus returning to the normal healing process. Hyperbaric oxygen, whirlpool hydrostatic therapy, negative pressure dressings and adjuncts such as bioengineered substitutes and electrostimulation have all been researched and trialled with varying results [70, 72]. As yet there is no one clear treatment for chronic wounds. The importance of preventative measures and optimisation of underlying conditions is crucial.

### **2.4.3 Scarless wound healing vs fibrosis**

There has been significant attention paid to foetal wound healing in the hopes of ameliorating the scarring that results from trauma to the adult skin. Much of the research to date has been conducted on animals, given the ethical implications of studying human foetuses. However, it

appears that scarring in humans begins around the 24<sup>th</sup> gestational week, depending also on the extent of injury [73]. Prior to this, foetal skin has a regenerative capacity that not only leads to scarless healing but also retention of adnexal structures [73]. The major differences noted in foetal healing to date concern tensile strength, ECM components, differential gene expression, inflammatory mediators and stem cell function [25, 74]. The healing matrix contains higher collagen III to collagen I and TGF $\beta$ 3 to TGF $\beta$ 1/2 ratios with increased hyaluronan content and MMP activity [75]. Production of PDGF and pro-inflammatory cytokines (especially IL-1 and TNF $\alpha$ ) is reduced compared to that of adult healing [75, 76]. Additionally, the myofibroblasts that persist for a number of weeks in adult wounds disappear much earlier in foetuses. Recent interest in foetal skin stem cells and homeobox genes, transcription factors regulating foetal development and micro-RNAs add another dimension to the complexities distinguishing foetal from adult regeneration [74, 77, 78].

The other end of the spectrum to scarless regeneration is excessive wound healing and fibrosis, leading to hypertrophic or keloid scar formation. Fibrosis is characterised by cellular heterogeneity resulting in the deposition of excess ECM within various tissues, which often results in organ failure, emphasising fibrosis as a crucial therapeutic target from both medical and economical perspectives [79]. To this end, identifying the relevant molecules responsible for the spatiotemporal modulation of both inflammation and ECM deposition is necessary in understanding the pathogenesis of fibrosis. By identifying the differences between foetal and adult wound healing we may be able to abrogate the fibrotic response and control the formation of hypertrophic and keloid scars.

## **2.5 Skin scarring and classification**

Scarring is the end point of the process of wound healing in mammals [80]. Prolonged inflammation is considered to be one of the most significant factors contributing to the severity

of scar formation. Numerous other factors, including genetics, age, depth and location of the original wound, tension and stretch, infection and nutritional status, also contribute to the discrepancy in clinical observations of scarring [81]. This wide variation in scar morphology forms a spectrum that spreads from depressed, stretched or flattened scars to raised or even bulky scar and keloid formation. The International Advisory Panel on Scar Management has established a cutaneous scar classification that ranges from mature through immature, linear hypertrophic, widespread hypertrophic to minor and major keloid scars [82]. Several scales and grading systems exist for the assessment and quantification of scars, the mostly widely used being the Vancouver Scar Scale and patient observer scar assessment scale (POSAS) [82, 83]. These grading systems measure a variety of parameters including pigmentation, vascularity, thickness, height or depression, pliability and patient symptoms. The purpose of these classification and grading systems is to provide a framework for management that is evidence-based. The different types of scars are discussed in detail below.

### **2.5.1 Normal skin scarring**

Immature and mature scars are those that are proceeding along the normal course of events in the healing process but represent different time points along that course. While these scars usually become a fine line that is minimally disfiguring and not functionally impairing, the immature scars have the potential to become hypertrophic [82].

### **2.5.2 Abnormal skin scarring: atrophic, stretch and hypertrophic**

Atrophic scars are those that have a pitted or indented appearance and frequently result from acne or varicella zoster pox. Histologically these scars have a thin epidermis and broad interfibrillar spaces in the dermis [84]. Stretched scars or *striae* result from tension on the wound, frequently occurring in the vicinity of joints. These scars, whilst often cosmetically apparent, do not cause the disfigurement or physical disability that is known to be associated



with excessive scar formation, such as hypertrophic or keloid scars [25]. These entities represent the far end of the fibrotic spectrum in skin scarring [82, 85]. Hypertrophic scars are raised, erythematous and pruritic scars that are often confused with keloid scars and for which there is no known diagnostic differential biomarker [86, 87].

### **2.5.3 Hypertrophic scarring vs keloid scars**

Over the years there has been significant conflict and debate regarding the relationship between hypertrophic scars and keloid scars, whether they are two points along a continuum or whether they represent separate entities. Due to the heterogenous nature of keloid scars, both from a clinical and histopathological standpoint, it is often difficult to distinguish them from hypertrophic scars. This inability to clearly differentiate the two has resulted in many clinicians and researchers believing they are part of the same pathological process [83, 86, 88]. However, the more recent, and greater number of, studies favour these two forms of aberrant wound healing as being distinct processes with independent clinical signs and pathological hallmarks. Keloid scars extend beyond the margins of the original wound to invade the surrounding normal skin (NS) whereas hypertrophic scars remain confined to the boundaries of the initial injury but push them out by expansion. Hypertrophic scars tend to regress with time and do not usually recur after excision (10%) but are more associated with contractures than their counterparts, evidenced by a higher rate of fibrin matrix gel contraction [89-91]. Keloid scars, however, have very high rates of recurrence (45-100%) following excision[91]. Keloid scars are also more likely to be erythematous and pruritic than are hypertrophic scars but both can present with these symptoms, and indeed it happens that there may be a mixture of the two processes occurring within the one wound.

Further differentiation can be made using light microscopy, electron microscopy and immunohistochemistry of histological specimens. Although there is conflicting information

within the literature there is a common thread with regard to certain aspects of the morphology, including collagen deposition, vasculature, immune cell infiltrate and  $\alpha$ -SMA staining [92]. While infrequently observed in keloid, distinct nodules of collagen with a high cellular density and organised fibres lying parallel to skin tension lines, appear to be more representative of hypertrophic scars and are commonly compared with those seen in Dupuytren's disease [89]. Keloid scars show thick bundles of hyalinised collagen that lie haphazardly and are often fragmented. The appearance of both hyalinised collagen and nodules within the same keloid sample has led to support for these two scar types being successive forms of fibroproliferation with varying degrees of inflammation [86]. Keloid tissue also contains a prominent horizontal fibrous band in the upper reticular dermis and an advancing edge beneath the epidermis, indicative of the invasion characteristic of keloid disease [93, 94]. While both keloid and hypertrophic scars show evidence of microvascular occlusion, the former is characterised by subepidermal disarrayed aggregates and the latter vertical blood vessels arranged around the collagen nodules [95]. The overexpression of VEGF in keloids is thought to drive the angiogenic process, compounded by hypoxia, propagating the extracellular matrix deposition [96, 97]. Although scattered mast cells have been identified in both scar types, keloid specimens demonstrate a higher immune cell infiltrate and the fibroblasts are more resistant to FAS-mediated apoptosis, which may explain the overabundance of extracellular matrix in these lesions [89].

The majority of discord is with respect to myofibroblasts ( $\alpha$ SMA staining) and epidermal thickness. There has been much controversy over whether there are myofibroblasts in KD [98] and whether there is  $\alpha$ SMA positive staining [99]. It has been suggested that  $\alpha$ SMA be used as a differentiation marker between keloid and hypertrophic scars [100], however it has been shown that keloid scars do express  $\alpha$ SMA [101] and due to the variability in expression in both forms of scarring (45% of keloid and 70% hypertrophic [93]) this cannot be a reliable method of

distinction [93]. The majority of studies describe hypertrophic scars as having a flattened epidermis with basal cell disarray [102]. There is a relatively inconsistent description, on the other hand, of keloid epidermis as either being of normal thickness with flattening of rete ridges or a thicker epidermal layer with basal cell vacuolar change [103]. The epidermis in keloid scars is increasingly thought to be of importance based on epithelial-mesenchymal interaction studies [104, 105].

Much of the confusion between keloid and hypertrophic scars can be explained by differences in genetic background, the presence of mixed lesions, different criteria for scar definitions and interobserver variability [103]. Overall, the most distinguishing features apply to keloid and include an invading edge beneath the epidermis, a horizontal fibrous band within the upper dermis and although controversial, “keloidal collagen”, which is not always present (55% of cases in Lee *et al*) [106]. The different management strategies for hypertrophic and keloid scar drives the continued research into distinguishing these entities. Only through identification of the underlying molecular mechanisms will we be able to accurately diagnose and effectively treat these conditions.

## **2.6 Keloid disease (KD)**

The exact historical background is somewhat murky but reported *ad nauseum* is that “cheloide” or keloid was a term first coined in 1806 by a french dermatologist, Baron Alibert, but was originally described as far back as 1700 BC in the ancient Egyptian Smith papyrus. The Greek word “cheloide” denotes a ‘claw-like’ scarring that arises from wounding of the skin, be it intentional or traumatic [107-109]. Many tribes throughout history have exploited this form of aberrant healing as a means of ritualistic marking or decoration. Although still purposely inflicted by some today, the majority arise as a result of injury, either significant or minor. A keloid is a benign cutaneous fibroproliferative tumour that behaves with the local aggression of

a cancer but does not metastasise [110-112]. This local invasion creates a symptomatic, disfiguring bulky mass that has clinical, psychosocial and economic implications.

### **2.6.1 Aetiology, epidemiology and clinical presentation**

Rare at extremes of age, with the highest incidence in the 10-30 year age group [88], the most striking epidemiological feature of KD is the higher preponderance in dark-skinned individuals. Incidence rates in the Black/Hispanic population are reported to be 4.5-16% [88, 93, 113] compared with rates of <1% in UK Caucasians [88]. The variable prevalence amongst different ethnicities in addition to increased frequency in certain families and concordance within identical twins, indicates a strong genetic component in the aetiology of keloid scarring. Despite the identification of susceptibility loci on specific chromosomes and association with HLA-DRB1\*15 status, as well as select others [114, 115], the genetic expression alone does not explain why, even in predisposed individuals, not all traumas lead to excessive scarring. The knowledge that tension drives fibroblast proliferation and collagen synthesis [116] has led to the postulation that KD is a mechanosensory disorder, supported by the predominance of these scars in areas of high tension, including the anterior chest and shoulder [117, 118]. Other theories put forward concerning influence of the local environment on keloid formation include hypoxia and pilosebaceous unit distribution, which is associated with increased sebum production [47, 115, 119, 120]. More recently, based on elevated levels of immunoglobulins, mast cells and lymphocytes as well as description of a keloid-associated lymphoid tissue (KALT), the role of immune responses have come to the fore as culprits in keloid formation [121, 122]. Hormonal factors have also been considered, as occurrence is increased at sites of higher testosterone metabolism, particularly peri-pubertally [123, 124]. The fact that no one theory has been proven to be solely responsible indicates a multifactorial aetiology for keloids, with one commonality: requirement for a precipitant. Although there have been reports of spontaneous keloid formation, it is more likely that a minor trauma has gone unnoticed in these

cases. A Jamaican study including 211 people with 369 scars recorded every single case as having had a history of trauma, however minor [125].

There are certain clinical criteria considered to be pathognomonic of keloid disease. This scar grows beyond the boundaries of the original wound, does not regress with time, is likely to recur following excision and should be present for at least a year [93, 112, 125, 126]. Keloid scars vary widely in their clinical appearance with many taking on the traditional “claw-like” appearance and others resembling a butterfly lesion, nodule or polypoid mass [113]. Commonly, the centre is pale soft and involuted compared with the raised, erythematous margin, resulting in the hypothesis that this active margin is the leading edge of invasion [127, 128]. Keloid tissue is typically firm and well-demarcated, with or without telangiectasia. Although keloid scars can cause contracture and produce symptoms of pruritis and pain, the majority of patients presenting with these scars are concerned with cosmesis rather than debilitation. The appearance can be severely disfiguring leading to psychosocial issues that affect quality of life.

### **2.6.2 Histopathogenesis and differential diagnoses**

Throughout the course of this PhD a review on the histopathology of keloid disease was published (enclosed at end of thesis). This section of the literature review contains portions from that publication [94].

It is now generally accepted that keloid scars contain thick hyalinised eosinophilic collagen, arranged in whorls or nodules, associated with a mucinous extracellular matrix and fibroblastic cells [98, 129]. Lee *et al* in 2004 referred to this haphazard collagen pattern as “keloidal collagen”, identifying it as a histologic hallmark of KD, albeit with a low sensitivity (55%) [93]. Their group also identified three other statistically significant features of keloid scars when

compared with hypertrophic scars: lack of flattening of the overlying epidermis, absence of prominent vertically oriented blood vessels and the presence of a tongue-like advancing edge, which extends through the upper reticular dermis [93]. Collagen I and collagen III are the most abundant fibrillar collagens in fibrotic tissue and it has been shown that the ratio of these collagens is altered in KD [53, 94]. In addition to excess collagen, several other components of the ECM have been shown to be disorganised in KD, as indicated in **Table 2.1**. It is not the absolute presence or absence of these proteins within the tissue but their respective ratios to each other and persistence over time that aid in the diagnosis of keloid scarring. Bux *et al* studied the histology of keloid samples using microscopy and divided the tissue into six regional zones (**Table 2.2**). Addressing the issue of cellular composition, they found there was marked cellular proliferation in some areas but that most of the fibroblasts were necrotic, likely as a result of ischemia [129].

**Table 2.1 Summary of the ECM molecules previously investigated in keloid disease tissue.**

ECM molecule	Location within keloid tissue	ID technique	Ref
<b>Collagen I</b>	Abundant expression throughout dermis	Masson's trichome	[130]
	↑ thicker bundles at margin, especially RD	Herovici	[53]
<b>Collagen III</b>	Thinner vs collagen I, ↑ in keloid margin PD	Herovici	[53]
	Strongly ↑ in keloid vs NS	IHC	[131]
<b>Collagen IV</b>	Along BMZ and ↑ proximal to small blood vessels	IHC	[131]
<b>Collagen VI</b>	Co-localised with col I proximal to small blood vessels, Also ↑ papillary dermis	IHC	[132]
<b>Fibronectin</b>	↑ at dermo-epidermal junction		
	Co-localised with cells in deep dermis between collagen bundles	IHC	[133]
	Intense localisation with fibroblasts upper RD	IHC	[134]
	Diffuse positivity in keloid tissue	IHC	[135-137]
<b>Hyaluronan (HA)</b>	Gross HA stain in upper layers epidermis		
	PD- mesh-like staining, RD- Intense staining	HABP	[138]
	↑ Intercellular in spinous & granular layers	HABP	[139]
	↓ HA in keloid dermis		
	↓ intensity stain in PD	HABP	[140]
<b>Elastin</b>	↓ superficial dermis	IHC	[141]
	↑ deep dermis, parallel to collagen	Histomorphometric	
	↓ elastic fibres all scar types	Verhoeff van Giesson	[142]
	↓ elastic fibres, due to impaired fibrillin-1	IHC	[143]
	↑ elastin deep dermis, node structure	Multiphoton microscopy	[144]

	↓ superficial and deep dermis	IHC	[141]
	Thin fibres, no candelabra pattern	Histomorphometric	
<b>Fibrillin</b>	Altered distribution, thick irregular bundles	IHC	[143]
	Altered fibrillin distribution, related to TGFβ	IHC	[145]
<b>Tenascin</b>	Diffusely expressed in dermis	IHC	[146]
	Associated with ↑ collagen bundles in RD		
<b>Dermatopontin</b>	↓ stain compared with NS	IHC	[147]
<b>Decorin</b>	Indistinguishable from NS, strong stain in dermis, weaker in epidermis	IHC	[147- 149]
<b>Biglycan</b>	↑ in nodular areas of keloid	IHC	[148]
	Indistinguishable from NS	IHC	[149]
<b>Periostin</b>	↑ in epidermis and dermis vs NS counterpart	IHC	[97]
	Co-localisation with CD31		
	↑ especially in acellular node region of deep dermis	IHC	[150]
<b>Versican</b>	Intense deposition in keloid but not NS	IHC	[151]

IHC, immunohistochemistry; NS, normal skin; PD, papillary dermis; RD, reticular dermis

Characterised by the overproduction of collagen, the fibroblast has always been considered the culprit in KD and that keloid fibroblasts (KF) may have an epigenetically distinct phenotype [152, 153]. This was postulated on the basis that fibroblasts from the keloid nodule resisted down-regulation in response to hydrocortisone, whereas superficial dermal KF and NS fibroblasts (NSF) did not [152]. It has since been shown that KF from both papillary and reticular dermis as well as centre and margin keloid dermis, behave differently, lending credence to this hypothesis [53, 154]. It is during the proliferative and remodelling phases that the imbalance in ECM synthesis and degradation results in excess deposition of collagen and other ECM components. Fibroblasts are also known to affect the inflammatory phase by behaving as immune modulators



[155]. This prolonged inflammation, in addition to the failure of myofibroblastic apoptosis/senescence, contributes to excessive scar formation [156]. In the normal wound healing process fibroblasts and myofibroblasts have a synergy that creates a seemingly seamless transition from one phase to the next, producing adequate ECM and the correct level of tension for wound closure. The presence of myofibroblasts in keloid was, for a time, under debate, as was the presence of  $\alpha$ SMA staining [98-100]. In much of the literature myofibroblasts are considered to be the major source of collagen synthesis and the failure of their apoptosis contributory to fibrosis [157, 158]. While myofibroblasts undoubtedly contribute to keloid collagen and ECM, it is likely that this is in concert with several other cell populations present in keloid scars and known to produce ECM, including macrophages, fibroblasts and fibrocytes [159-161].

**Table 2.2 Bux S, Madaree A. Keloids show regional distribution of proliferative and degenerate connective tissue elements. Cells Tissues Organs. 2010;191: 213-34.**

No. Regions	Sub-regions
1 Zone hyalinising collagen bundles	a. Isolated b. Aggregated
2 Fine fibrous areas	a. Fine fibrous cellular areas b. Fine fibrous less cellular areas c. Wavy fine fibrous areas d. Fibrous tubular areas
3 Area of inflammation	a. Severe inflammation b. Moderate inflammation c. Mild inflammation
4 Zone dense regular connective tissue	a. Eosinophilic b. Pale
5 Nodular fibrous area	a. Nodular fine fibrous cellular areas b. Nodular fine fibrous tubular areas
6 Area of angiogenesis	

KD is characterised by histological heterogeneity, resulting in mixed reports in the literature as well as varied responses to therapy. Many of the histological findings from keloid scar tissue sections endorse the aetiological hypotheses put forward for KD. The persistence of

macrophages, lymphocytes, mast cells and fibrocytes as well as the description of keloid-associated lymphoid tissue (KALT) support prolonged inflammation and an immune role in keloid pathogenesis [121]. Macrophages and fibrocytes have been shown to regulate ECM production and the continued presence of mast cells may contribute to symptoms of pruritis associated with KD [68, 162]. The contribution of hypoxia to KD has previously been investigated [48, 97, 163] but support for this theory from a histological standpoint has been tenuous. While some studies on keloid vasculature favoured hyper-vascularity with long and dilated vessels [164, 165], the majority of studies identified reduced central keloid blood supply with microvascular luminal occlusion [47, 48, 166, 167]. It was postulated and seems likely that in areas of increased vascularity (ie the margin) the rate of growth exceeds the vascularity, resulting in persistent ischemia despite histological signs of increased vessels [165]. It has also been suggested that this hypoxic state is aggravated by hypertension in keloid patients [168, 169]. The structure of keloid collagen has been described as tendon-like, leading to the hypothesis this thickness is secondary to mechanical loading [170]. Increased mechanical stress as an aetiological factor in keloid pathogenesis is supported by studies showing the effect of stress on both keloid morphology [171] as well as increased expression of tension-related genes, ECM synthesis and cell spreading [172].

Many of the histological features of KD can also be found in other cutaneous fibroses [173]. As there is no one biomarker for KD, there is a significant reliance on both clinical appearance and histopathology for differential diagnosis and thus appropriate management. **Table 2.3** presents a summary of the other conditions that may be confused with KD and how they might be distinguished. Hypertrophic scarring is the condition most commonly confused with KD and is discussed in **section 2.5.3** of this chapter. In contrast to keloid scars, dermatofibroma typically has sparing of the papillary dermis and dermatofibrosarcoma protuberans (DFSP) is discernible by a characteristic storiform pattern of spindled cells surrounded by fibrous stroma [174, 175].

Morphea or cutaneous scleroderma has also been misdiagnosed as keloid scarring, made more difficult by the existence of a keloid variant within this condition. As another form of fibrosis, the presence of myofibroblasts in morphea has led to the use of these cells as a way to determine the stage of differentiation along a hypothetical continuum from morpheiform nodule to hypertrophic scar and finally keloid [176]. Due to the impact of systemic sclerosis as well as the risk of metastasis associated with DFSP, it is essential to make the correct diagnosis and ensure the appropriate therapy is instituted. In clarifying the “pathognomonic” features of KD (**Table 2.4**) this distinction can prevent misdiagnosis of more sinister conditions.

**Table 2.3 Summary of the features of skin-related fibrotic disorders in common with and different from KD and the stains most commonly used in their diagnosis.**

<b>Condition</b>	<b>Histological features in common with KD</b>	<b>Histological features different from KD</b>	<b>Stain</b>
Hypertrophic scar	Raised scar	Non-flattened epidermis	
	Thickened collagen	Organised collagen fibres	H&E
	Nodules	No recurrence	$\alpha$ SMA
	Increased cellularity		
DFSP	Slow-growing	Increased nodularity	Vimentin, $\alpha$ SMA
	Raised, pigmented skin	Honeycomb pattern	CD34+, XVIIIa-
	Recurrence	Non-polarizing collagen	S100-
Dermatofibroma	Thickened epidermis	Scaly lesions	
	Hyperkeratosis	No recurrence	XVIII+
	Hyalinised collagen	Reduced cellularity	CD34-
		Grenz zone	
Scleroderma/ morphea	Pigmented	Reduced cellularity	CD34-
	Lack of adnexal appendages	Collagen arranged parallel	CD1a, CD3, CD8,
	Nodules	Systemic features	CD20+ CD25, CD57+

DFSP, dermatofibrosarcoma protuberans; H&E, haematoxylin & eosin;  $\alpha$ SMA, alpha smooth muscle actin

**Table 2.4 Summary of the characteristic features of keloid disease and their frequency reported in the literature.**

Ref	n	Epidermis	Advancing edge	Collagen	Cellularity	Horizontal fibrous band	Inflammation	aSMA(+)	Vascularity
[103]	15	10/15 samples have rete ridges	-	15/15 samples show haphazard collagen	10/15 samples increased cellularity	14/15 samples have a band	-	5/15 positive	Sub-epidermal evidence of vascularity
[129]	58	-	-	Thick bundles of collagen identified	Between collagen bundles. Fibroblastic Immune	-	Chronic inflammation present	-	Impaired angiogenesis
[137]	26	Flattened epidermis, Adnexae displaced		25/26 samples with thick Hyalinised & Haphazard collagen	24/26 Diffuse cellularity, myofibroblasts	-	Persistent immune cell infiltrate	21/26 positive stain	-
[93]	40	37/40 flattened epidermis identified	Present in 14/14 marginal sections	24/40 Thick hyalinised bundles	33/40 samples increased cellularity	Identified in 10/40 samples	39/40 samples had increased lymphocytes 8/40 had a sinus tract/ruptured follicle	18/40 (>10%+)	Blood vessels in disarray
[177]	10	Thickened epidermis identified	Lined with BM	-	-	-	-	-	-
[94]	13	Thickened & flattened 11/13 Thickened not flattened 2/13 Hyperkeratotic 12/13	Identified in 3/13 samples	Whorls, thickened Haphazard 11/13 Nodule 1/13 Fine, organised 1/13 Obliteration PD-RD 11/13	Diffuse cellularity in 13/13 samples, including between collagen bundles	5/13 samples, Present in upper dermis	10/13 samples had inflammation, most commonly sub-epidermal	-	10/13 occlusion of vessels between collagen fibres, Neoangiogenesis evident in deeper dermis

BM, basement membrane; PD, papillary dermis; RD, reticular dermis

### 2.6.3 Pathophysiology

To date, a number of signaling pathways have been implicated in the pathogenesis of KD, not least of which is the inexhaustible investigation into the role of transforming growth factor beta (TGF $\beta$ ). TGF $\beta$  is a pleiotropic growth factor considered to be the master regulator of fibrosis and its effects on collagen deposition, cell proliferation, immune modulation, apoptosis, differentiation and several other processes have been well established in KD [178-180]. The TGF $\beta$  ligand superfamily interacts primarily with TGF $\beta$ RI and TGF $\beta$ RII, serine/threonine kinase receptors that are responsible for the phosphorylation and subsequent activation of Smad in a well described but complicated canonical signaling pathway [181]. TGF $\beta$ 1 and TGF $\beta$ 2 isoforms, those believed to promote fibrosis, have been shown to be upregulated in KD along with TGF $\beta$ RI and TGF $\beta$ RII, which may indicate the presence of a positive autocrine feedback loop [182-184]. The identification of an altered Smad2/Smad3 ratio, up-regulation of Smad4 and down-regulation of inhibitory Smad6 and Smad7, suggest failure of an inhibitory feedback mechanism leading to exponential fibrosis [178, 185]. Although TGF $\beta$  represents an attractive therapeutic target, its regulation of so many key biological responses makes it a risky one. To this end, other members of the TGF $\beta$  canonical pathway have been explored as therapeutic targets [186-188].

Also dysregulated in KD is the MAPK/ERK signaling cascade, known to influence migration, proliferation and apoptosis [189]. The activation of this cascade in response to mechanical strain mediates the effects of TGF $\beta$  and in synergy with PI3K signaling in KD, increases the production of collagen [190-193]. The Akt/PI3K/mTOR pathway regulates numerous critical cell processes and is a key player in tumorigenesis, where in the presence of PI3K with optimal environmental conditions, mTOR mediates cell cycle progression [194]. Akt/PI3K/mTOR is a mechanism for TGF $\beta$  and HIF1 $\alpha$  activation [195] and in KD has been associated with ECM overproduction, cell proliferation and invasion, making it an attractive therapeutic target [196, 197]. Similarly, insulin-like growth factor-I receptor (IGF-IR), a protein tyrosine kinase receptor modulated by

IGF binding proteins (IGFBP), interacts with IGF to promote proliferation and invasion of KF through interaction with MAPK and PI3K signaling cascades [184, 198-200].

Further shown to work in concert with TGF $\beta$  is the Wnt/ $\beta$ -catenin signaling pathway, which is associated with fibroblast proliferation, migration and epithelial-mesenchymal transition (EMT) [193, 201-203]. KF have been shown to be more susceptible to Wnt3a treatment, resulting in increased fibroblast proliferation and fibronectin expression [204]. Additionally, Wnt5a, a non-canonical protein, is upregulated in KF compared with NSF [205] and given the association of Wnt5a with inflammation in psoriasis, atherosclerosis, lichen planus and rheumatoid arthritis, it may play a similar role in inflammation in KD [206, 207]. The Wnt signaling pathway is frequently investigated in partnership with Notch signaling, as both of these cascades determine cell fate by directing stem cell maintenance, proliferation and differentiation [208, 209]. Notch is overexpressed in keloid tissue where it is associated with inflammatory infiltrate. This in addition to its association with EMT may link Notch and Wnt dysregulation in KD [210]. Indeed, inhibition of the Notch ligand, JAG-1, with associated blockade of Notch signaling was recently shown to abrogate cell attachment, spreading, proliferation and migration of KF [211]. Also implicated in inflammation is TNF- $\alpha$ /NF- $\kappa$ B signaling. This pathway is involved in the regulation of apoptosis, implicated in EMT and responsible for the transcription of a number of pro-inflammatory genes, including among many, the interleukins [111, 193]. Several studies have identified upregulation of TNF- $\alpha$ , IL-6, IL-8, IL-13 and IL-1 responsive genes in keloid tissue and fibroblasts [212-216]. The expression of these molecules may contribute to the prolonged inflammation and associated inflammatory infiltrate seen in keloid histology [121]. IL-6 is thought to affect keloid pathogenesis through its interaction with JAK/STAT3 signaling, which in turn affects ECM production, cell proliferation and may promote oncogenesis [217]. STAT3 siRNA decreased collagen production, proliferation and migration in KF compared with NSF [218].

In addition to the above major signaling pathways involved in KD, there are several other mechanisms and molecules that are implicated. Integrin expression, upregulated in KF, is thought to mediate the effects of mechanical loading through modulation of TGF $\beta$  activation and thereby collagen production [118, 219]. TGF $\beta$  also induces CTGF expression in KF [220, 221] and influences matrix metalloproteinase activity, which is an essential component of the remodelling process [222, 223]. Most recently, attention has been focused on micro RNAs in KD. These miRNAs are involved in post-transcriptional regulation of gene expression and may participate in signaling pathways related to keloid pathophysiology [224, 225]. miR-199a-5p has been implicated in KF proliferation and both miR-196a and miR-29a associated with collagen deposition [226, 227]. Involved in crucial processes such as TGF $\beta$  signaling, ECM deposition, proliferation, differentiation and EMT, miRNAs are currently regarded as potential novel therapeutic targets for fibrosis, where to date there is no effective treatment [228].

The dysregulation of cytokines, chemokines, growth factors and transcription factors that populate the signaling mechanisms underlying keloid pathophysiology (**Figure 2.4**), represents a dynamic microenvironment engaged in continuous crosstalk. These molecules and pathways also serve as potential therapeutic targets in the search for an effective treatment for KD.





**Figure 2. 4 Signaling pathways & molecules known to be dysregulated in KD.**

#### 2.6.4 Treatment and management

As with any condition for which there is no effective treatment, prevention is better than cure. Meticulous surgical technique with the studious avoidance of infection and post-operative friction or tension is paramount. Once there is an established keloid scar, management is far more difficult. Therapy must be tailored on the characteristics of the scar including number, size, site and duration. It must first be established if the therapeutic goal is cosmesis or whether symptomatic and functional aspects need to be addressed. Most of these therapies can be used alone (monotherapy) or in combination to attenuate recurrence rates and treat refractory keloid scars.

Traditionally, KD has been treated with non-targeted therapies. First line management should be the least invasive treatment and appropriate to the patient. Physical therapies include camouflage makeup, massage, hydrotherapy, physiotherapy and pressure therapy that may be in the form of customised garments, magnets, silicone gel sheeting or pressure clips/buttons. While recommended regimens for duration and amount of pressure are undefined, the aesthetic effects, side-effects and length of time required for wear result in poor patient compliance [85]. Pressure therapy may be used in combination with corticosteroids and most recently has shown beneficial outcome as an adjuvant therapy for surgical excision [229, 230].

Second-line and the most commonly used treatment worldwide is corticosteroid injection (HCA, hydrocortisone acetate; TAC, triamcinolone acetonide being the most used). Dosage and duration are undefined but it has been postulated to reduce inflammation, modulate TGF $\beta$  and enhance collagen degradation [85]. Complications include hypopigmentation, telangectasia and variable recurrence rates but these factors are abrogated by using steroid injections as adjuvant or even part of multimodal combination therapy regimes [178, 231-233]. Often considered second-line and frequently used in conjunction with steroid injections, is cryotherapy, which can be external/contact or intralesional. The ischaemic necrosis following physical and vascular phases, is thought to reduce recurrence rates by differentiating abnormal KF back toward a normal phenotype [234]. Intralesional cryotherapy has been shown to be superior to contact, resulting in increased scar flattening, less pain, fewer sessions and fewer degrees of hypopigmentation [235]. Further second-line therapies are laser therapy (pulsed-dye, Nd:YAG, CO<sub>2</sub> etc) and photodynamic therapy [236, 237]. Ablative lasers may be used for debulking and require an adjuvant therapy to reduce recurrence rates [238]. The true efficacy of these treatments is difficult to assess given the number of lasers available, the undefined regimes and lack of reproducible outcomes [85].

There are now several further agents that have been used to treat KD in the hopes of controlling the fibroproliferation. Retinoids are compounds used in the treatment of several skin disorders and are largely postulated to abrogate fibrosis through immune regulation and alteration of ECM, cell proliferation and differentiation [239, 240]. Despite several applications to KD in the past with some success, there are limited experimental studies on retinoic acid in KD and no recent trials regarding its efficacy [241-244]. Immunomodulators have become more common, including the calcineurin inhibitor tacrolimus (FK-506), imiquimod 5%, a Toll-like receptor antagonist that stimulates interferon and TNF- $\alpha$ , IFN- $\alpha$ 2b, which reduces collagen and cell proliferation and an anti-inflammatory onion extract (extractum cepae)[85, 245, 246]. Injection of alternative agents including botulinum toxin A, postulated to be effective through downregulation of TGF $\beta$  and CTGF expression and verapamil, a calcium channel blocker shown to increase decorin and provide beneficial adjuvant treatment, are also widely used [85, 245, 247]. As with most of the therapies available for KD, there are mixed reports in the literature with regard to the efficacy of these agents [248, 249], which led to the employment of chemotherapeutic agents to manage this fibroproliferative tumour.

Most of the chemotherapeutic drugs used for keloid are antitumour/antimetabolite or steroid and include 5-Fluorouracil (5-FU), mitomycin C, bleomycin and those less common such as vincristine. 5-FU is one of the most tested and best tolerated of these drugs, mitomycin C is a topical antibiotic that is thought to delay rather than reverse fibrosis with little efficacy against recurrence and bleomycin, also an antibiotic with antitumour effects but for which there are mixed reports, also carries risks of organ fibrosis [250]. Given the local and systemic toxicity of these drugs they must be dosed very cautiously, side-effects monitored, contraindications taken into account and be used in refractory cases [85]. Chemotherapeutics are frequently used in combination therapies and have also shown evidence of resistance, further complicating the

management of KD [251]. Some of this drug resistance is attributable to a stem-cell like population within the keloid lesion [252].

Although surgical excision is associated with recurrence rates of 45-100%, it is frequently performed as a last ditch effort to manage keloid expansion and debulk the tumour [107, 253]. When surgery is performed it is recommended to perform intra-marginal fusiform excision at a 308° angle with skin tension lines and closure with minimal tension and no undermining [245]. The combination of surgery with adjuvant therapies frequently treats the keloid scar initially but with varying rates of recurrence. These adjuvant therapies include steroid injection, alone or in combination with 5-Fluorouracil [108, 254], radiotherapy, most recently recommended in the form of high-dose-rate brachytherapy [255], pressure therapy using magnets or silicone gel sheeting [229], laser ablation and many others. A recent meta-analysis identified equal rates of recurrence following surgery for both triamcinolone and radiotherapy, at 15.4% and 14% respectively [256].

In addition to the above therapies many naturally based compounds have been attempted in the management of KD (green tea, aloe vera, plant extract) [257]. These alternative therapies have the benefit of limited side-effects when compared with chemical therapies and many do not affect NSF, giving them a specificity boasted by few other treatments [219]. With more and more molecules identified as up and down regulated in KD, there is increased potential for the development of targeted therapies [178]. Many agents are proposed to date but very few have sufficient studies to determine their fate in the clinical setting [258]. The transient success and subsequent failure of recombinant TGF $\beta$ 3 (Justiva) highlights the complexities faced with targeted therapies but also the potential that lies in identification of potential biomarkers [85]. The recent identification of CD26+ fibroblasts as responsible for the cultivation of skin fibrosis may have clinical implications for KD, although this remains to be investigated [56]. Finally, an

emerging area in keloid management is the use of stem cell therapy, which although shown to modulate inflammation and downregulate fibrosis, is still in the very nascent stages of research [26, 259, 260].

Overall, the levels of evidence for these therapies are poor and inconsistent [261, 262]. A recent survey on current practice with regard to management of KD highlights the overabundance of therapies available and the variability with which physicians treat this condition [263]. There is no absolutely effective treatment for KD and only by understanding keloid formation on a molecular level will we be able to alleviate the afflicted with not only confidence but on a more enduring basis.

## **2.7 Site-specific keloid disease**

KD is characterised by heterogeneity between patients, between lesions and even within the lesion itself. This heterogeneity is evident clinically, histologically and on a molecular level. Macroscopically, keloid scars are represented by a number of morphologies but frequently within a scar the “older” centre is pale, soft and shrunken when compared with a raised, aggressive and erythematous margin [264]. These clinically evident differences led to researchers investigating the histological and molecular differences between the centre (intralesional), margin/periphery (perilesional) and rarely, extralesional (adjacent normal) skin [265].

Histologically, the keloid centre and margin show increased inflammatory infiltrate over extralesional tissue [121]. When centre and margin were compared, there were differences with regard to cellularity, fatty acid composition, vascularity and collagen production, with the majority favouring a growing, active margin [53, 264, 266-268]. The altered collagen I/III ratio, found in one study to be elevated in margin tissue and fibroblast culture only, seems to

contradict the demonstration of increased TGF $\beta$ R1 and Smad2/3 in keloid central fibroblasts in another study, where margin and NSF TGF $\beta$  expression were equivocal [269]. This discrepancy may be attributable to the use of *in vitro* experiments in the latter study, which have been shown to alter cellular expression and signaling with increasing passage number [53].

The morphology of the fibroblasts within the keloid tissue has been shown to differ under light and electron microscopy [270]. Further examination of these *in vitro* differences identified behavioural variation between centre and margin but also superficial and deep KF, leading to the postulation that several distinct subpopulations of fibroblasts occupy the keloid dermis [54, 153, 270]. Although there is some inconsistency with regard to which site, centre or margin, exhibits more proliferation and apoptosis, the general consensus supports a disturbed balance between these two processes [271, 272]. While both sets of fibroblasts were refractory to FAS-mediated apoptosis, when cell cycles of centre and margin fibroblasts were compared, those in the centre were arrested at G<sub>0</sub>-G<sub>1</sub> phase with increased p53 expression, while those at the periphery were in the proliferative phases (G<sub>2</sub>-S) [273]. Similarly, reported by Seifert *et al*, there was mRNA upregulation of apoptotic genes (ADAM-12, ANXA-1 and CCAR-1) and degradation promoters (MMP19 and MMP3) in fibroblasts from the keloid centre but upregulation of apoptotic inhibitors within the margin (AVEN and INHBA) [52]. Engineered skin substitutes were used to look at differences between superficial and deep keloid fibroblasts, concluding that different keloid phenotypes may result from different contributions of these distinct fibroblasts [154]. It has been suggested that the fibroblastic differences within keloid arise as a result of hypoxic gradients within the tissue, a theory which is supported by those more recent studies identifying perfusion differences between centre and margin [165].

## **2.8 Epithelial-mesenchymal interactions (EMI)**

Epithelial-mesenchymal interactions represent an essential means of communication between two developmentally, structurally and functionally distinct tissues, which in the case of the skin

are the epidermis and dermis [274]. These reciprocal interactions are mediated through several signaling pathways and molecules.

### **2.8.1 Normal skin and wound healing**

Examples of epithelial-mesenchymal interactions in NS include hair follicle morphogenesis and cycling, basement membrane formation, epidermal stem cell production, skin pathologies and tissue regeneration and repair [275, 276]. Although the importance of EMI in NS function and wound healing was acknowledged long ago, to properly investigate this process required the ability to successfully culture primary keratinocytes *in vitro*, which was first achieved by Rheinwald and Green in the 1970's [277]. It was demonstrated that keratinocytes grew faster when cultured with fibroblast feeder layers and that when cultured at an air-liquid interface, the epidermis became stratified [278, 279]. It has since become apparent that double paracrine signaling with fibroblasts, involving factors such as FGF, IL-6 and GM-CSF, is responsible for epidermal phenotypes necessary for different functions, including wound healing [280].

In wound healing, the epidermis and dermis must work together to reconstitute a break in the cutaneous barrier as efficiently as possible and restore skin function. This involves re-formation of the basement membrane, re-epithelialisation, modulation of inflammation, contraction of the wound and remodelling. Both keratinocytes (TGF- $\alpha$ , EGF, PDGF) and fibroblasts (FGF7, IL-6, GM-CSF) release a number of growth factors that have autocrine or paracrine effects, resulting in proliferation, differentiation, migration, angiogenesis, lymphangiogenesis and contraction [281]. Co-culture studies demonstrate the crucial role of keratinocytes on mesenchymal TGF $\beta$  expression, as well as NF- $\kappa$ B and Wnt among others [280]. The close proximity of epidermal and dermal cells also upregulates  $\alpha$ -SMA in fibroblasts, contributing to contraction necessary for healing. Failure of these processes results in delayed wound healing or fibrosis, which contribute to morbidity and mortality [282].

A recent study looking at the role of EMI in fibrosis, as it pertains to TGF $\beta$ , indicated a positive feedback loop between integrins and TGF $\beta$  that is activated following injury to the epithelium [282]. When considered from a scarring perspective, interruption to EMI cause delayed epithelialisation, resulting in a failure of the stop signal to fibroblasts accumulating ECM. The regulation of matrix metalloproteinases (MMP) and thus ECM turnover, by EMI is thought to contribute to hypertrophic scarring. The release of MMP-1, IL-1 $\beta$  and EGF by keratinocytes are implicated in fibroblast MMP expression [283].

Given the significance of EMI in the maintenance of homeostasis and wound healing as well as the role they play in cutaneous tumorigenesis [284], it stood to reason that deregulated EMI may be involved in the pathogenesis of KD.

### **2.8.2 Keloid EMI**

Much of the original research on KD refers to it as a dermal disorder and the fibroblasts as the culprits of its formation. However, a thickened and activated epidermis as well as observations of the benefits of early skin grafting on scar formation has shifted some of the focus to the epidermis. Investigation of EMI in KD has supported these observations and highlighted the role of the epidermis in the pathogenesis of this fibrotic scar.

Both early conditioned medium experiments and co-culture studies have shown that keloid keratinocytes (KK) co-cultured with KF have a higher proliferation rate than KF cultured with NS keratinocytes (NSK). Even the NSF displayed not only increased proliferation but also increased collagen secretion when cultured with KK versus NSK [285, 286]. In addition to proliferation and collagen, co-culture with KK has been shown to result in decreased apoptosis, upregulation of TGF $\beta$ -1 and CTGF and increased  $\alpha$ -SMA expression, supporting the theory that KK are the puppet masters driving keloid growth through their regulation of KF [221, 287, 288]. It is even thought that as well as local paracrine effects, keratinocytes have far-reaching effects on the immune



system. Not only TGF $\beta$  itself but also other elements of the cascade including TGF $\beta$  receptors and Smad2 and Smad3 are implicated in regulation by EMI [289]. It was even demonstrated that where KK increased the expression of T $\beta$ R1 and Smad2 in KF, NK has the opposite effect, an observation which may have clinical implications [290]. Complementary to the KK effect, co-culture with KF vs NSF has been shown to stimulate expression of more TGF $\beta$  ligands [290].

Aside from TGF $\beta$ , EMI in KD also involve abnormal regulation of the insulin-like growth factor (IGF) family, particularly the downregulation of IGFBP-3, which is thought to affect proliferation and apoptosis and may even affect invasion [291]. Both VEGF, which was found to have a pro-angiogenic effect [292] and IL-18, postulated to play a role in collagen regulation, are affected following KK/KF co-culture, thus suggesting a role for PI3K/mTOR in EMI in KD [105]. The JAK/STAT signaling pathway dysregulation identified in a recent study proposes that there may be negative feedback regulation in EMI, which may serve as a therapeutic target [293]. Also associated with keloid pathogenesis through keratinocyte-fibroblast interactions are IL-8, ANG, OSM and GM-CSF [293]. Given this evidence of KK involvement in keloid pathogenesis, there are relatively few studies focussed in the expression patterns of the keloid epidermis alone [104].

Many methods have been employed to study keloid EMI, including the feeder layer co-culture system, two-chamber co-culture, organ culture and organotypic culture models but recapitulating the full 3D architecture of the skin in the laboratory is rudimentary compared with the natural *in vivo* environment. As such, a full understanding of these reciprocal interactions is not yet elucidated and the search for a method to dissect these signals from within natural tissue surroundings is ongoing.

### 2.8.3 Keloid epithelial-mesenchymal transition (EMT)

Epithelial-mesenchymal transition is when an epithelial/epidermal cell undergoes biochemical changes allowing it to take on the phenotype and expression profile of a mesenchymal/dermal cell. This alteration is accompanied by enhanced migration, invasion, resistance to apoptosis and ECM production [294]. Some cells are able to move back and forth between epithelial and mesenchymal states via EMT and mesenchymal-epithelial transition (MET). There are three types of EMT: type 1 is associated with development, type 2 associated with inflammation and fibrosis and type 3 associated with neoplasia [294]. It is type 2 and 3 EMT that may play a role in KD.

Many of the markers classically associated with EMT in inflammation and fibrosis are also dysregulated in KD. Downregulation of E-cadherin and loss of polarisation with simultaneous upregulation of FSP-1,  $\alpha$ -SMA, vimentin, fibronectin, MMPs and many others, are typical of a cell undergoing transition [295]. EMT is driven by a host of transcription factors including ZEB, SNAIL, TWIST and miRNA among others [296]. A role for aberrant EMT in fibrosis has been demonstrated in renal, pulmonary hepatic and scleroderma studies and given the importance of TGF $\beta$  in this process it is not surprising that EMT has been considered in KD pathogenesis [297]. Another source of myofibroblasts that may contribute to these fibrotic conditions is endothelial cells (EndoMT), although this remains controversial [298, 299]. The EMT and MET processes are multi-step dynamic phenomena that may have intermediary stages, referred to as “partial EMT” [297, 300]. In addition to propagation of fibrosis, EMT is implicated in therapeutic resistance and is thought to be due to the acquisition of stem cell-like properties, as well as increased heterogeneity [301].

Due to the overlap of signaling pathways involved in EMT and KD as well as the evidence for EMT in fibrosis and tumorigenesis, it is now thought to be significant in KD but the evidence thus far remains limited [296, 301]. A recent microarray study on KK expression identified features

indicative of EMT, with decreased adhesion, increased motility and reduced differentiation [104]. This is supported by another study suggesting the EMT in KD is mediated through overexpression of TGF $\beta$ /Smad3 signaling with aberrant expression of FGFR2 and p63 [302]. Further evidence for EMT in KD lies in the presence of HIF-1 $\alpha$  overexpression and hypoxic environment, such that when HIF-1 $\alpha$  was knocked down the EMT process was inhibited [48]. Hypoxia has long been implicated in keloid pathogenesis and its contribution to EMT may indicate these two processes are linked in keloid scarring.

The evidence for EMT in KD to date is indicative rather than confirmative. Over the last 20 years, the shifted focus to keloid epidermis and the effects of its interactions with the dermis, have paved the way for EMT hypotheses in KD. EndoMT, partial EMT and their associated therapeutic resistance are likely candidates underlying keloid scar formation, however, more in-depth research is required before these processes can be considered causal in KD.

## **2.9. Traditional experimental methodologies in KD research**

Uniquely afflicting humans, there is no validated and accepted animal model for KD, despite significant efforts to identify one. Some focus was originally concentrated on equine models, as they form exuberant granulation tissue (EGT) on their limbs, which resembles keloid scars [303]. Failing to find any other animal with naturally occurring keloid, research turned its focus to implanting human scar tissue in animals and inducing scarring in site-specific areas. Over the years the majority of the work has been carried out using athymic mice, into which keloid tissue fragments are implanted subcutaneously, or immune-privileged sites such as the cheeks of hamsters [304, 305]. Although in most cases the implants maintained their viability and morphology, the invariable outcome was regression, albeit at different time points [306, 307]. As an alternative to implantation it has been attempted to induce hypertrophic and keloid scars in animals. Rabbit ears have been used for both grafting of human skin [308] and as a primary model [309, 310]. In the latter case it is necessary to incise down to the perichondrium to

achieve approximation to human scarring, which may result in chondrocytes confounding the reaction [311]. In both cases the scars are short-lived, limiting their usefulness as a model.

In recent years attention has been diverted back to porcine models for fibroproliferative scarring. While the porcine wound shows similar inflammatory infiltrate, collagen nodules and myofibroblasts, the macroscopic appearance is less pronounced and TGF $\beta$  distribution less abundant [312, 313]. Regardless of the degree of similarity, none of these animal models can fully replicate the *in vivo* human environment [314]. Limitations including scar tissue regression, animal maintenance/handling and the incomplete genome chip of animal models, has diverted the focus away from animals somewhat over the years [315]. The drive toward replacement, reduction and refinement of animal models together with the question of whether the yielded data can be sufficiently translated into humans has necessitated alternative methods of keloid research [316]. These models comprise 2D monolayer culture, histotypic culture including spheroids, organ explant culture, co-culture models, including two-chamber and organotypic and most recently this is in the form of plasma/fibrin-based skin-equivalent models in mice [317].

Whole tissue biopsy or *ex vivo* organ culture has the advantage of being the natural 3D architecture of the skin comprised of the full complement of cells, tissues and adnexal structures that retain their pathologic state. Unfortunately, despite a recent study showing survival of these explants for a number of weeks, there are several other drawbacks [318, 319]. Organ explant models require human subject participation, the dearth of available tissue and variations in samples engenders a lack of reproducibility and in a heterogeneous tissue like KD there can be averaging out of signals, ultimately restricting this model as the best form to study keloid scars [314, 320, 321]. 2D monolayer culture studies are beneficial as they are convenient, technically facile, have little inter-sample variability, are reproducible, allow for environmental

control including addition of exogenous factors or knockdown of specific genes and allow good maintenance of cell viability. However, this method falls significantly short of mimicking the true *in vivo* microenvironment due to the synthetic static platform in addition to undefined medium condition (FBS) which may alter the magnitudes of expression [322]. Furthermore, cell culture monolayer has been shown to alter cell phenotype and with increasing passage number alter expression [53, 322].

In an effort to address some of these shortcomings, 3D models including spheroids, co-culture and organotypic cultures are used in KD research [323, 324]. These models retain the reproducibility, technical ease and ability to control external factors associated with 2D monolayer but also incorporate the architectural and multi-cellular aspects of organ explant culture. Unfortunately, while 3D systems are useful in terms of examining cell-cell and cell-matrix interactions and superior to 2D models especially given the importance of EMI, they are still reliant on synthetic environments and lack the components of skin (blood vessels, other cells and interstitial factors) that contribute to cutaneous fibrosis [90, 325].

Therefore, despite a wide range of available methods to investigate KD, there is still no ideal platform to capture the molecular signals from within the natural 3D architecture of the tissue without disturbing the pathology. Without a means to achieve therapeutic testing there is still an impediment to optimal keloid research, however, LCM represents an excellent platform to address the limitations.

### **2.10 Laser capture microdissection (LCM)**

Laser microdissection is a technique employed to isolate single cells or cell subpopulations from frozen, embedded or fresh tissue through the use of a microscope coupled to a high-precision laser [326]. These laser microdissection platforms have been given numerous synonyms in the literature but they fall into two general categories: UV (ultraviolet) cutting microdissection, also

known as laser microdissection and pressure catapulting (LMPC) and the infra-red laser capture microdissection (LCM) [327]. These devices are now available in both automated (robotic) and manual platforms. The original version is that developed by Emmert-Buck *et al*, and incorporates an inverted light microscope and infra-red laser [328]. In this model a downward-facing cap covered in a thermoplastic polymer film comes into direct contact with the visualised cells of interest and is rapidly melted and cooled by the laser, fusing the two. When the cap is lifted it overcomes the necessary forces to raise the desired specimen with it [329]. Although the IR laser can accommodate plain glass slides and has been shown not to affect downstream molecular analysis [329], it lacks the precision (7.5  $\mu\text{m}$  smallest diameter) and speed of the UV laser. The other significant limitation lies in the contact between the cap and the tissue (polymer-cell composite), where the dissected specimen may be contaminated by adherence of undesired cells to the polymer film, resulting in altered data [326, 330]. The UV (337nm or 355nm solid state laser) system differs in that it allows the user to select a desired area with a laser diameter of down to  $<1\mu\text{m}$ , which is then cut out and collected via gravity, catapult or capture (**Figure 2.5**). Due to the non-contact nature of the former two there is also less risk of contamination by adjacent cells, which may be ablated if so wished. This system is often preferred for thicker sections and proteomic applications, but for optimal output does require special polyethylene naphthalate (PEN) or polyethylene terephthalate (PET) slides [331]. There is some concern that the UV may cause damage to the cells within range of the laser, jeopardising the final molecular signal, particularly if the sample size is small (perimeter contributing to  $>10\%$  of overall area) [329].

Laser microdissection enables the acquisition of target cells or histological strata from complex tissue sections with accuracy and speed but without corrupting the nucleic acids and proteins within. Prior to the advent of this technology researchers relied on gross dissection of frozen sections, manual dissection and negative selection, using irradiation on unmarked cells [327].

These methods were not only time-consuming and operator-dependent, requiring both skill and dexterity, but were also frequently inaccurate [332, 333]. LCM can be combined with protein or gene-based studies thereby rapidly expanding the potential to research heterogeneous tissues, previously difficult to achieve. Protein studies require significantly more material than genomics for downstream applications, therefore, genomic studies can be performed on samples down to single cells [334]. One of the biggest drawbacks of using LCM is the limitation of morphological distinction without coverslips or using frozen sections. The user must also be able to recognise the histological characteristics in order to select the area of interest, which may require an expert pathologist or, technologist or cytologist. While simple stains differentiate basic histology, the use of immunostaining to detect specific molecules precludes expression dynamics due to antibody binding to the protein of interest. Finally, LCM can be time consuming and in the case of genomics the risk of RNA degradation requires the capture to be completed within one hour of staining [335]. Newer techniques such as expression microdissection (xMD) are now becoming available to researchers that will eliminate the subjectivity of individual operators and eliminate the need for amplification [336].

The ability to select a homogenous sample or even a single cell from a mixed tissue section means that specific molecular signaling can be attributed more accurately to the appropriate cells. To date LCM is the only method available that can separate cell subpopulations from tissue or monolayer without disturbing the cell's molecular state [327].

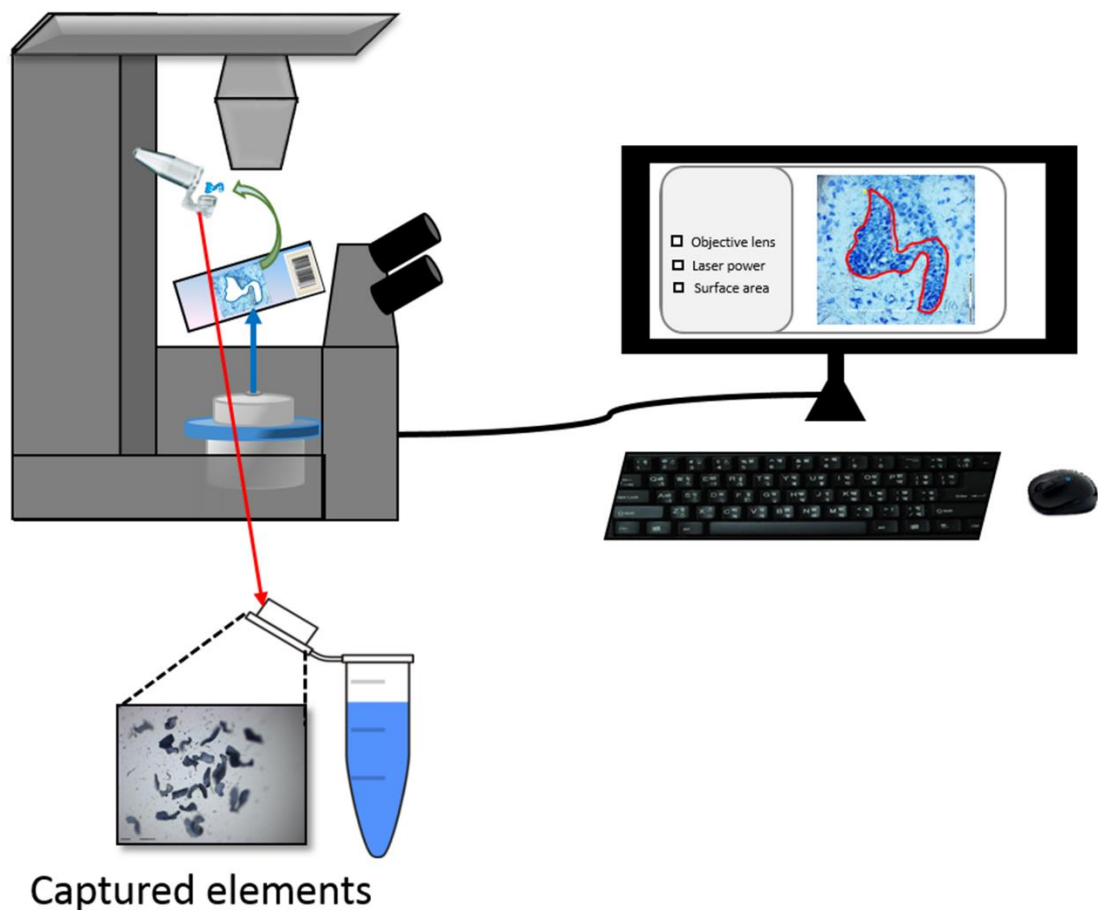


**Figure 2.5 Schematic diagram representing laser capture microdissection (LCM).**

### **2.10.1 Application of LCM to fibrosis, skin and wound healing**

In the literature to date, LCM has played a limited role in illuminating the pathogenesis of skin fibrosis. However, this technique has been applied to fibrosis of other organs and to alternative conditions of the skin. This is likely due to the fact that fibrosis of the internal organs is associated with a much higher risk of significant, even in some cases life-threatening, complications. LCM has been pivotal in both liver fibrosis, where hepatic stellate cells (HSC) are the main culprits, and idiopathic pulmonary fibrosis (IPF), a condition with a startlingly poor prognosis [337, 338], as it provides a solution to the difficulty in isolating these cells from the melee of parenchymal constituents. Prior to its advent, whole tissue samples were analysed



with IHC and ISH, which was impractical and resulted in “averaging out” of cellular signals [339, 340]. The definitive procurement of compartments (i.e. fibroblastic foci) within a tissue section has highlighted the importance of EMI in the lung [341] and supported the theories for EMT in both renal and pulmonary fibrosis [342, 343]. LCM is only now coming to the fore in other areas of fibrosis including corneal, retroperitoneal and cardiac. Most studies have concentrated on myocardial infarction models, some looking at p21 as a marker of perceived hyperoxia, indicating a phenotypic switch from fibroblasts to myofibroblasts [344, 345]. LCM has been pivotal in this field for the histological separation of infarcted, peri-infarct and non-infarcted areas, often separated by only millimetres. The infarct boundary may be the key to understanding fibrosis as the peri-infarct region undergoes healing, but without loss of function [344].

Similar to fibrosis, LCM has, until recently, been focussed on the skin conditions that pose the most risk to patients, namely the carcinomas. Malignant melanomas are characterised by significant intra-tumoural heterogeneity [346, 347], which has meant that analysis of tumour bulk may not reflect the presence of mutated cells due to drowning out of the molecular signal [321]. Not only has LCM aided the isolation of these sparse melanocytes but also contributed to identifying the clonal genetic relationship between an assumed primary and its metastasis [348]. Basal cell carcinoma (BCC) [349, 350], squamous cell carcinoma (SCC) [351] and benign conditions including psoriasis [352, 353], SLE [354] and neurofibromatosis [355] have benefitted from the precision and accuracy of this new technique. More recently LCM has allowed a breakthrough in accessing the stem cells sequestered in the hair follicle bulge, whose multipotency may be the key to halting cancer progression and aberrant wound healing [356].

Relatively few studies have alluded to the potential benefit of this technique in human wound healing, especially given recent advances in high through-put technologies [357, 358]. LCM can

be used to isolate specific cells from different histological strata as exemplified in research on keratinocytes in burn wounds [359], localisation of CCN proteins to interfollicular epidermal and dermal layers [360] and even within the epidermis itself, genomic mapping of keratinocyte layers [361]. The modulation of TLR4 in acute wound healing in mice was achieved using LCM, showing its upregulation in early healing where it regulates wound inflammation and affects wound closure [362]. LMPC has been used to examine the proteomic profile of chronic wounds as well as the associated biofilm in porcine models, identifying a role for miRNA in this process [363, 364]. In humans, chronic wounds are highly heterogeneous. A similar study used LCM to dissect out blood vessels from within 3mm punch biopsy sections but of human chronic wounds, describing a method applicable to a wide range of disease settings and with translational implications [365].

### **2.10.2 Application to keloid scarring**

Following a thorough search of the literature, the use of LCM has not been described in relation to KD, however, it has been employed in the investigation of hypertrophic scarring in animals. A recent study using Duroc pigs to look at collagen mRNA expression, highlighted the heterogeneity of fibroproliferative scars and favoured the use of LCM in the dissection of skin into its constituent parts [315]. Similarly, LCM would provide an excellent platform to overcome the histological heterogeneity through the isolation of specific sites described in keloid scars. To date, there are no comprehensive studies combining both site-specific and *in situ* approaches to KD and LCM, with its precision, accuracy and previous evidence of success, would allow the dissection of keloid sites without risk of signal dilution or alteration of expression seen with traditional methods. This technique offers access to analyse expression patterns of distinct regional components from within the natural architecture of keloid tissue maintained in its pathological state. Therefore, LCM application to KD would be a unique opportunity to

investigate heretofore undetected or overlooked genes and pathways significant to not only understanding the pathogenesis but also aiding diagnosis and management.

### **2.11 Summary**

Keloid scars are cutaneous fibroproliferative tumours that represent the extreme end of the abnormal wound healing spectrum. In order to put the histological and molecular aberrations of KD into context, this literature review has described the structure of the normal skin and normal wound healing process as well as the range of potential outcomes, from scarless healing to hypertrophic or keloid scar formation. This review describes keloid as a tumour-like bulky mass that is characterised by excess ECM, aggressive local invasion and multi-layered heterogeneity. Keloid lesions are known to differ between centre and margin on clinical, microscopic and molecular levels, resulting in diagnostic dilemmas and therapeutic resistance. The contribution of epithelial-mesenchymal interactions to keloid pathology compounded by these site-specific variations represents a significant challenge in the elucidation of significant underlying mechanisms. Lack of a validated animal model for KD has led to reliance on alternative methods of investigation, including whole tissue and monolayer cell culture. These current techniques fall considerably short of representing the complex, heterogeneous microenvironment that exists in keloid scars, as described in this chapter. Therefore, the advent of specialised systems like LCM, provide an ideal platform to address these challenges facing KD research and overcome the limitations of heterogeneity and traditional dissection. The application of this contemporary approach to KD paves the way for potentially promising results.

## References

1. Lee V, Singh G, Trasatti JP, Bjornsson C, Xu X, Tran TN, et al. Design and fabrication of human skin by three-dimensional bioprinting. *Tissue Eng Part C Methods*. 2014;20: 473-84.
2. Breitzkreutz D, Koxholt I, Thiemann K, Nischt R. Skin basement membrane: the foundation of epidermal integrity—BM functions and diverse roles of bridging molecules nidogen and perlecan. *BioMed research international*. 2013;2013.
3. Sanford JA, Gallo RL. Functions of the skin microbiota in health and disease. *Semin Immunol*. 2013;25: 370-7.
4. Menon GK. Skin Basics; Structure and Function. *Lipids and Skin Health*: Springer; 2015. p. 9-23.
5. Walters KA, Roberts MS. The structure and function of skin. *Drugs and the pharmaceutical Sciences*. 2002;119: 1-40.
6. Burns T. *Rook's textbook of dermatology*. 2004.
7. James WD, Berger T, Elston D. *Andrews' diseases of the skin: clinical dermatology*: Elsevier Health Sciences; 2015.
8. Kusuma S, Vuthoori RK, Piliang M, Zins JE. *Skin anatomy and Physiology*. *Plastic and Reconstructive Surgery*: Springer; 2010. p. 161-71.
9. Matsui T, Amagai M. Dissecting the formation, structure and barrier function of the stratum corneum. *Int Immunol*. 2015;27: 269-80.
10. Baroni A, Buommino E, De Gregorio V, Ruocco E, Ruocco V, Wolf R. Structure and function of the epidermis related to barrier properties. *Clin Dermatol*. 2012;30: 257-62.
11. Wang F, Zieman A, Coulombe PA. Skin Keratins. *Methods Enzymol*. 2016;568: 303-50.
12. Boer M, Duchnik E, Maleszka R, Marchlewicz M. Structural and biophysical characteristics of human skin in maintaining proper epidermal barrier function. *Postepy Dermatol Alergol*. 2016;33: 1-5.
13. Costin G-E, Hearing VJ. Human skin pigmentation: melanocytes modulate skin color in response to stress. *The FASEB Journal*. 2007;21: 976-94.
14. Nakatani M, Maksimovic S, Baba Y, Lumpkin EA. Mechanotransduction in epidermal Merkel cells. *Pflugers Arch*. 2015;467: 101-8.
15. Beck B, Blanpain C. Mechanisms regulating epidermal stem cells. *The EMBO journal*. 2012;31: 2067-75.
16. Blanpain C, Fuchs E. Plasticity of epithelial stem cells in tissue regeneration. *Science*. 2014;344: 1242281.
17. Arwert EN, Hoste E, Watt FM. Epithelial stem cells, wound healing and cancer. *Nature Reviews Cancer*. 2012;12: 170-80.
18. Martin MT, Vulin A, Hendry JH. Human epidermal stem cells: Role in adverse skin reactions and carcinogenesis from radiation. *Mutation Research/Reviews in Mutation Research*. 2016.
19. Hsu Y-C, Li L, Fuchs E. Emerging interactions between skin stem cells and their niches. *Nature medicine*. 2014;20: 847-56.
20. Mikesch LM, Aramadhaka LR, Moskaluk C, Zigrino P, Mauch C, Fox JW. Proteomic anatomy of human skin. *J Proteomics*. 2013;84: 190-200.
21. Nguyen BP, Ryan MC, Gil SG, Carter WG. Deposition of laminin 5 in epidermal wounds regulates integrin signaling and adhesion. *Curr Opin Cell Biol*. 2000;12: 554-62.
22. Kalluri R. Basement membranes: structure, assembly and role in tumour angiogenesis. *Nature Reviews Cancer*. 2003;3: 422-33.
23. Marionnet C, Pierrard C, Vioux-Chagnoleau C, Sok J, Asselineau D, Bernerd F. Interactions between fibroblasts and keratinocytes in morphogenesis of dermal epidermal junction in a model of reconstructed skin. *The Journal of investigative dermatology*. 2006;126: 971-9.

24. Hassan WU, Greiser U, Wang W. Role of adipose-derived stem cells in wound healing. *Wound Repair and Regeneration*. 2014;22: 313-25.
25. Eming SA, Martin P, Tomic-Canic M. Wound repair and regeneration: mechanisms, signaling, and translation. *Sci Transl Med*. 2014;6: 265sr6.
26. Duscher D, Barrera J, Wong VW, Maan ZN, Whittam AJ, Januszyk M, et al. Stem Cells in Wound Healing: The Future of Regenerative Medicine? A Mini-Review. *Gerontology*. 2016;62: 216-25.
27. Zielins ER, Atashroo DA, Maan ZN, Duscher D, Walmsley GG, Hu M, et al. Wound healing: an update. *Regen Med*. 2014;9: 817-30.
28. Furie B, Furie BC. Mechanisms of thrombus formation. *N Engl J Med*. 2008;359: 938-49.
29. Bielefeld KA, Amini-Nik S, Alman BA. Cutaneous wound healing: recruiting developmental pathways for regeneration. *Cellular and Molecular Life Sciences*. 2013;70: 2059-81.
30. Golebiewska EM, Poole AW. Platelet secretion: From haemostasis to wound healing and beyond. *Blood Rev*. 2015;29: 153-62.
31. Reinke J, Sorg H. Wound repair and regeneration. *European Surgical Research*. 2012;49: 35-43.
32. Ghosh AK, Vaughan DE. PAI-1 in tissue fibrosis. *Journal of cellular physiology*. 2012;227: 493-507.
33. Eming SA, Krieg T, Davidson JM. Inflammation in wound repair: molecular and cellular mechanisms. *The Journal of investigative dermatology*. 2007;127: 514-25.
34. Brandt E, Petersen F, Ludwig A, Ehlert JE, Bock L, Flad HD. The beta-thromboglobulins and platelet factor 4: blood platelet-derived CXC chemokines with divergent roles in early neutrophil regulation. *J Leukoc Biol*. 2000;67: 471-8.
35. Brancato SK, Albina JE. Wound macrophages as key regulators of repair: origin, phenotype, and function. *Am J Pathol*. 2011;178: 19-25.
36. Wynn TA, Vannella KM. Macrophages in Tissue Repair, Regeneration, and Fibrosis. *Immunity*. 2016;44: 450-62.
37. Portou MJ, Baker D, Abraham D, Tsui J. The innate immune system, toll-like receptors and dermal wound healing: A review. *Vascul Pharmacol*. 2015;71: 31-6.
38. Bodnar RJ, Satish L, Yates CC, Wells A. Pericytes: A newly recognized player in wound healing. *Wound Repair and Regeneration*. 2016.
39. Blakaj A, Bucala R. Fibrocytes in health and disease. *Fibrogenesis Tissue Repair*. 2012;5: S6.
40. Wulff BC, Wilgus TA. Mast cell activity in the healing wound: more than meets the eye? *Experimental dermatology*. 2013;22: 507-10.
41. Martin P, Nunan R. Cellular and molecular mechanisms of repair in acute and chronic wound healing. *British Journal of Dermatology*. 2015;173: 370-8.
42. Herrera BS, Kantarci A, Zarroug A, Hasturk H, Leung KP, Van Dyke TE. LXA 4 actions direct fibroblast function and wound closure. *Biochem Biophys Res Commun*. 2015;464: 1072-7.
43. Broughton G, 2nd, Janis JE, Attinger CE. The basic science of wound healing. *Plast Reconstr Surg*. 2006;117: 12S-34S.
44. Frank DE, Carter WG. Laminin 5 deposition regulates keratinocyte polarization and persistent migration. *J Cell Sci*. 2004;117: 1351-63.
45. Young A, McNaught C-E. The physiology of wound healing. *Surgery (Oxford)*. 2011;29: 475-9.
46. Yip WL. Influence of oxygen on wound healing. *Int Wound J*. 2015;12: 620-4.
47. Zhang Z, Nie F, Kang C, Chen B, Qin Z, Ma J, et al. Increased periostin expression affects the proliferation, collagen synthesis, migration and invasion of keloid fibroblasts under hypoxic conditions. *Int J Mol Med*. 2014;34: 253-61.
48. Ma X, Chen J, Xu B, Long X, Qin H, Zhao RC, et al. Keloid-derived keratinocytes acquire a fibroblast-like appearance and an enhanced invasive capacity in a hypoxic microenvironment in vitro. *Int J Mol Med*. 2015;35: 1246-56.

49. Beer TW, Baldwin HC, Goddard JR, Gallagher PJ, Wright DH. Angiogenesis in pathological and surgical scars. *Hum Pathol.* 1998;29: 1273-8.
50. Jelaska A, Strehlow D, Korn JH, editors. *Fibroblast heterogeneity in physiological conditions and fibrotic disease.* Springer seminars in immunopathology; 2000: Springer.
51. Sempowski GD, Borrello MA, Blieden TM, Barth RK, Phipps RP. Fibroblast heterogeneity in the healing wound. *Wound Repair and Regeneration.* 1995;3: 120-31.
52. Seifert O, Bayat A, Geffers R, Dienus K, Buer J, Lofgren S, et al. Identification of unique gene expression patterns within different lesional sites of keloids. *Wound repair and regeneration : official publication of the Wound Healing Society [and] the European Tissue Repair Society.* 2008;16: 254-65.
53. Syed F, Ahmadi E, Iqbal SA, Singh S, McGrouther DA, Bayat A. Fibroblasts from the growing margin of keloid scars produce higher levels of collagen I and III compared with intralesional and extralesional sites: clinical implications for lesional site-directed therapy. *Br J Dermatol.* 2011;164: 83-96.
54. Tucci-Viegas VM, Hochman B, Franca JP, Ferreira LM. Keloid explant culture: a model for keloid fibroblasts isolation and cultivation based on the biological differences of its specific regions. *Int Wound J.* 2010;7: 339-48.
55. Witt E, Maliri A, McGrouther DA, Bayat A. RAC activity in keloid disease: comparative analysis of fibroblasts from margin of keloid to its surrounding normal skin. *Eplasty.* 2008;8: e19.
56. Rinkevich Y, Walmsley GG, Hu MS, Maan ZN, Newman AM, Drukker M, et al. Skin fibrosis. Identification and isolation of a dermal lineage with intrinsic fibrogenic potential. *Science.* 2015;348: aaa2151.
57. Pakyari M, Farrokhi A, Maharlooei MK, Ghahary A. Critical role of transforming growth factor beta in different phases of wound healing. *Advances in wound care.* 2013;2: 215-24.
58. Wight TN, Potter-Perigo S. The extracellular matrix: an active or passive player in fibrosis? *Am J Physiol Gastrointest Liver Physiol.* 2011;301: G950-5.
59. Hinz B. Myofibroblasts. *Exp Eye Res.* 2016;142: 56-70.
60. Fujiwara T, Kubo T, Kanazawa S, Shingaki K, Taniguchi M, Matsuzaki S, et al. Direct contact of fibroblasts with neuronal processes promotes differentiation to myofibroblasts and induces contraction of collagen matrix in vitro. *Wound repair and regeneration : official publication of the Wound Healing Society [and] the European Tissue Repair Society.* 2013;21: 588-94.
61. Arora PD, McCulloch CA. Dependence of collagen remodelling on alpha-smooth muscle actin expression by fibroblasts. *J Cell Physiol.* 1994;159: 161-75.
62. Carlson MA, Longaker MT. The fibroblast-populated collagen matrix as a model of wound healing: A review of the evidence. *Wound Repair and Regeneration.* 2004;12: 134-47.
63. Behm B, Babilas P, Landthaler M, Schreml S. Cytokines, chemokines and growth factors in wound healing. *Journal of the European Academy of Dermatology and Venereology.* 2012;26: 812-20.
64. Ehrlich HP, Hunt TK. Collagen Organization Critical Role in Wound Contraction. *Adv Wound Care (New Rochelle).* 2012;1: 3-9.
65. Xue M, Jackson CJ. Extracellular matrix reorganization during wound healing and its impact on abnormal scarring. *Advances in wound care.* 2015;4: 119-36.
66. Van De Water L, Varney S, Tomasek JJ. Mechanoregulation of the Myofibroblast in Wound Contraction, Scarring, and Fibrosis: Opportunities for New Therapeutic Intervention. *Adv Wound Care (New Rochelle).* 2013;2: 122-41.
67. Martin P, Nunan R. Cellular and molecular mechanisms of repair in acute and chronic wound healing. *Br J Dermatol.* 2015;173: 370-8.
68. Greaves NS, Ashcroft KJ, Baguneid M, Bayat A. Current understanding of molecular and cellular mechanisms in fibroplasia and angiogenesis during acute wound healing. *Journal of dermatological science.* 2013;72: 206-17.

69. Morton LM, Phillips TJ. Wound healing and treating wounds: Differential diagnosis and evaluation of chronic wounds. *Journal of the American Academy of Dermatology*. 2016;74: 589-605.
70. Powers JG, Higham C, Broussard K, Phillips TJ. Wound healing and treating wounds: Chronic wound care and management. *Journal of the American Academy of Dermatology*. 2016;74: 607-25.
71. Diegelmann RF, Evans MC. Wound healing: an overview of acute, fibrotic and delayed healing. *Front Biosci*. 2004;9: 283-9.
72. Enoch S, Leaper DJ. Basic science of wound healing. *Surgery (Oxford)*. 2008;26: 31-7.
73. Larson BJ, Longaker MT, Lorenz HP. Scarless fetal wound healing: a basic science review. *Plast Reconstr Surg*. 2010;126: 1172-80.
74. Leavitt T, Hu MS, Marshall CD, Barnes LA, Lorenz HP, Longaker MT. Scarless wound healing: finding the right cells and signals. *Cell Tissue Res*. 2016.
75. Walmsley GG, Maan ZN, Wong VW, Duscher D, Hu MS, Zielins ER, et al. Scarless wound healing: chasing the holy grail. *Plast Reconstr Surg*. 2015;135: 907-17.
76. Namazi MR, Fallahzadeh MK, Schwartz RA. Strategies for prevention of scars: what can we learn from fetal skin? *Int J Dermatol*. 2011;50: 85-93.
77. Bullard KM, Longaker MT, Lorenz HP. Fetal wound healing: current biology. *World J Surg*. 2003;27: 54-61.
78. Hu MS, Rennert RC, McArdle A, Chung MT, Walmsley GG, Longaker MT, et al. The Role of Stem Cells During Scarless Skin Wound Healing. *Adv Wound Care (New Rochelle)*. 2014;3: 304-14.
79. Rosenbloom J, Mendoza FA, Jimenez SA. Strategies for anti-fibrotic therapies. *Biochim Biophys Acta*. 2013;1832: 1088-103.
80. Reinke JM, Sorg H. Wound repair and regeneration. *European surgical research Europäische chirurgische Forschung Recherches chirurgicales europeennes*. 2012;49: 35-43.
81. Butzelaar L, Ulrich MM, Mink van der Molen AB, Niessen FB, Beelen RH. Currently known risk factors for hypertrophic skin scarring: A review. *Journal of plastic, reconstructive & aesthetic surgery : JPRAS*. 2016;69: 163-9.
82. Gold MH, McGuire M, Mustoe TA, Pusic A, Sachdev M, Waibel J, et al. Updated international clinical recommendations on scar management: part 2—algorithms for scar prevention and treatment. *Dermatologic Surgery*. 2014;40: 825-31.
83. Mustoe TA, Cooter RD, Gold MH, Hobbs FD, Ramelet AA, Shakespeare PG, et al. International clinical recommendations on scar management. *Plastic and Reconstructive Surgery*. 2002;110: 560-71.
84. Trelles MA, Martinez-Carpio PA. Clinical and histological results in the treatment of atrophic and hypertrophic scars using a combined method of radiofrequency, ultrasound, and transepidermal drug delivery. *Int J Dermatol*. 2016.
85. Gauglitz GG. Management of keloids and hypertrophic scars: current and emerging options. *Clin Cosmet Investig Dermatol*. 2013;6.
86. Huang C, Akaishi S, Hyakusoku H, Ogawa R. Are keloid and hypertrophic scar different forms of the same disorder? A fibroproliferative skin disorder hypothesis based on keloid findings. *International wound journal*. 2014;11: 517-22.
87. Trace AP, Enos CW, Mantel A, Harvey VM. Keloids and Hypertrophic Scars: A Spectrum of Clinical Challenges. *Am J Clin Dermatol*. 2016.
88. Seifert O, Mrowietz U. Keloid scarring: bench and bedside. *Arch Dermatol Res*. 2009;301: 259-72.
89. Atiyeh BS, Costagliola M, Hayek SN. Keloid or hypertrophic scar: the controversy: review of the literature. *Ann Plast Surg*. 2005;54: 676-80.
90. van den Broek LJ, Limandjaja GC, Niessen FB, Gibbs S. Human hypertrophic and keloid scar models: principles, limitations and future challenges from a tissue engineering perspective. *Exp Dermatol*. 2014;23: 382-6.

91. Verhaegen PD, van Zuijlen PP, Pennings NM, van Marle J, Niessen FB, van der Horst CM, et al. Differences in collagen architecture between keloid, hypertrophic scar, normotrophic scar, and normal skin: An objective histopathological analysis. *Wound repair and regeneration : official publication of the Wound Healing Society [and] the European Tissue Repair Society*. 2009;17: 649-56.
92. Munteanu AD, Bedereag SI, NiTescu C, Florescu IP. Anatomopathological findings in scars: comparative study between different specimens. *Rom J Morphol Embryol*. 2015;56: 283-8.
93. Lee JY, Yang CC, Chao SC, Wong TW. Histopathological differential diagnosis of keloid and hypertrophic scar. *Am J Dermatopathol*. 2004;26: 379-84.
94. Jumper N, Paus R, Bayat A. Functional histopathology of keloid disease. *Histol Histopathol*. 2015;30: 1033-57.
95. Meshref S, Mufti S. Keloid and hypertrophic scars: Comparative histopathological and immunohistochemical study. *Medical Science*. 2010;17.
96. Mogili NS, Krishnaswamy VR, Jayaraman M, Rajaram R, Venkatraman A, Korrapati PS. Altered angiogenic balance in keloids: a key to therapeutic intervention. *Transl Res*. 2012;159: 182-9.
97. Zhang Z, Nie F, Chen X, Qin Z, Kang C, Chen B, et al. Upregulated periostin promotes angiogenesis in keloids through activation of the ERK 1/2 and focal adhesion kinase pathways, as well as the upregulated expression of VEGF and angiopoietin1. *Mol Med Rep*. 2015;11: 857-64.
98. Matsuoka LY, Uitto J, Wortsman J, Abergel RP, Dietrich J. Ultrastructural characteristics of keloid fibroblasts. *Am J Dermatopathol*. 1988;10: 505-8.
99. Sarrazy V, Billet F, Micallef L, Coulomb B, Desmoulière A. Mechanisms of pathological scarring: role of myofibroblasts and current developments. *Wound Repair and Regeneration*. 2011;19: s10-s5.
100. Ehrlich HP, Desmouliere A, Diegelmann RF, Cohen I, Compton CC, Garner WL, et al. Morphological and immunochemical differences between keloid and hypertrophic scar. *The American journal of pathology*. 1994;145: 105.
101. Lee CH, Hong CH, Chen YT, Chen YC, Shen MR. TGF-beta1 increases cell rigidity by enhancing expression of smooth muscle actin: keloid-derived fibroblasts as a model for cellular mechanics. *Journal of dermatological science*. 2012;67: 173-80.
102. Suarez E, Syed F, Alonso-Rasgado T, Bayat A. Identification of biomarkers involved in differential profiling of hypertrophic and keloid scars versus normal skin. *Arch Dermatol Res*. 2015;307: 115-33.
103. Moshref SS MS. Keloid and Hypertrophic scars: Comparative Histopathological and Immunohistochemical Study. *JKAU*. 2010;17: 3-22.
104. Hahn JM, Glaser K, McFarland KL, Aronow BJ, Boyce ST, Supp DM. Keloid-derived keratinocytes exhibit an abnormal gene expression profile consistent with a distinct causal role in keloid pathology. *Wound repair and regeneration : official publication of the Wound Healing Society [and] the European Tissue Repair Society*. 2013;21: 530-44.
105. Do DV, Ong CT, Khoo YT, Carbone A, Lim CP, Wang S, et al. Interleukin-18 system plays an important role in keloid pathogenesis via epithelial-mesenchymal interactions. *Br J Dermatol*. 2012;166: 1275-88.
106. Lee JY-Y, Yang C-C, Chao S-C, Wong T-W. Histopathological differential diagnosis of keloid and hypertrophic scar. *The American journal of dermatopathology*. 2004;26: 379-84.
107. Butler PD, Longaker MT, Yang GP. Current progress in keloid research and treatment. *J Am Coll Surg*. 2008;206: 731-41.
108. Shah VV, Aldahan AS, Mlacker S, Alsaidan M, Samarkandy S, Nouri K. 5-Fluorouracil in the Treatment of Keloids and Hypertrophic Scars: A Comprehensive Review of the Literature. *Dermatol Ther (Heidelb)*. 2016.



109. Hunasgi S, Koneru A, Vanishree M, Shamala R. Keloid: A case report and review of pathophysiology and differences between keloid and hypertrophic scars. *Journal of Oral and Maxillofacial Pathology*. 2013;17: 116.
110. Naylor MC, Lazar DA, Zamora IJ, Mushin OP, Yu L, Brissett AE, et al. Increased in vitro differentiation of fibrocytes from keloid patients is inhibited by serum amyloid P. *Wound repair and regeneration : official publication of the Wound Healing Society [and] the European Tissue Repair Society*. 2012;20: 277-83.
111. Dong X, Mao S, Wen H. Upregulation of proinflammatory genes in skin lesions may be the cause of keloid formation (Review). *Biomed Rep*. 2013;1: 833-6.
112. Niessen FB, Spauwen PH, Schalkwijk J, Kon M. On the nature of hypertrophic scars and keloids: a review. *Plastic and Reconstructive Surgery*. 1999;104: 1435-58.
113. Bayat A, Arscott G, Ollier W, Ferguson M, Mc Grouther D. Description of site-specific morphology of keloid phenotypes in an Afrocaribbean population. *British journal of plastic surgery*. 2004;57: 122-33.
114. Gauglitz GG, Korting HC, Pavicic T, Ruzicka T, Jeschke MG. Hypertrophic scarring and keloids: pathomechanisms and current and emerging treatment strategies. *Molecular medicine*. 2011;17: 113-25.
115. Song C. Hypertrophic scars and keloids in surgery: current concepts. *Ann Plast Surg*. 2014;73 Suppl 1: S108-18.
116. Akaishi S, Akimoto M, Ogawa R, Hyakusoku H. The relationship between keloid growth pattern and stretching tension: visual analysis using the finite element method. *Ann Plast Surg*. 2008;60: 445-51.
117. Ogawa R. Keloid and hypertrophic scarring may result from a mechanoreceptor or mechanosensitive nociceptor disorder. *Med Hypotheses*. 2008;71: 493-500.
118. Suarez E, Syed F, Alonso-Rasgado T, Mandal P, Bayat A. Up-regulation of tension-related proteins in keloids: knockdown of Hsp27,  $\alpha 2\beta 1$ -integrin, and PAI-2 shows convincing reduction of extracellular matrix production. *Plastic and reconstructive surgery*. 2013;131: 158e-73e.
119. Fong EP, Bay BH. Keloids - the sebum hypothesis revisited. *Med Hypotheses*. 2002;58: 264-9.
120. Ma X, Chen J, Xu B, Long X, Qin H, Zhao RC, et al. Keloid-derived keratinocytes acquire a fibroblast-like appearance and an enhanced invasive capacity in a hypoxic microenvironment in vitro. *International journal of molecular medicine*. 2015;35: 1246-56.
121. Bagabir R, Byers RJ, Chaudhry IH, Muller W, Paus R, Bayat A. Site-specific immunophenotyping of keloid disease demonstrates immune upregulation and the presence of lymphoid aggregates. *Br J Dermatol*. 2012;167: 1053-66.
122. Jiao H, Fan J, Cai J, Pan B, Yan L, Dong P, et al. Analysis of Characteristics Similar to Autoimmune Disease in Keloid Patients. *Aesthetic Plast Surg*. 2015;39: 818-25.
123. Al-Attar A, Mess S, Thomassen JM, Kauffman CL, Davison SP. Keloid pathogenesis and treatment. *Plastic and Reconstructive Surgery*. 2006;117: 286-300.
124. Schierle HP, Scholz D, Lemperle G. Elevated levels of testosterone receptors in keloid tissue: an experimental investigation. *Plast Reconstr Surg*. 1997;100: 390-5; discussion 6.
125. Bayat A, Arscott G, Ollier WE, McGrouther DA, Ferguson MW. Keloid disease: clinical relevance of single versus multiple site scars. *British journal of plastic surgery*. 2005;58: 28-37.
126. Kakar AK, Shahzad M, Haroon TS. Keloids: Clinical features and management. Part II. *Journal of Pakistan Association of Dermatologists*. 2006;16: 163-72.
127. Bond JE, Bergeron A, Thurlow P, Selim MA, Bowers EV, Kuang A, et al. Angiotensin-II mediates nonmuscle myosin II activation and expression and contributes to human keloid disease progression. *Mol Med*. 2011;17: 1196-203.

128. Shih B, McGrouther DA, Bayat A. Identification of novel keloid biomarkers through profiling of tissue biopsies versus cell cultures in keloid margin specimens compared to adjacent normal skin. *Eplasty*. 2010;10: e24.
129. Bux S, Madaree A. Keloids show regional distribution of proliferative and degenerate connective tissue elements. *Cells Tissues Organs*. 2009;191: 213-34.
130. Kauh YC, Rouda S, Mondragon G, Tokarek R, diLeonardo M, Tuan RS, et al. Major suppression of pro-alpha1(I) type I collagen gene expression in the dermis after keloid excision and immediate intrawound injection of triamcinolone acetonide. *Journal of the American Academy of Dermatology*. 1997;37: 586-9.
131. Naitoh M, Hosokawa N, Kubota H, Tanaka T, Shirane H, Sawada M, et al. Upregulation of HSP47 and collagen type III in the dermal fibrotic disease, keloid. *Biochem Biophys Res Commun*. 2001;280: 1316-22.
132. Peltonen J, Hsiao LL, Jaakkola S, Sollberg S, Aumailley M, Timpl R, et al. Activation of collagen gene expression in keloids: co-localization of type I and VI collagen and transforming growth factor-beta 1 mRNA. *The Journal of investigative dermatology*. 1991;97: 240-8.
133. Sible JC, Eriksson E, Smith SP, Smith N. Fibronectin gene expression differs in normal and abnormal human wound healing. *Wound repair and regeneration : official publication of the Wound Healing Society [and] the European Tissue Repair Society*. 1994;2: 3-19.
134. Kischer CW, Hendrix MJ. Fibronectin (FN) in hypertrophic scars and keloids. *Cell Tissue Res*. 1983;231: 29-37.
135. Knaggs HE, Layton AM, Morris C, Wood EJ, Holland DB, Cunliffe WJ. Investigation of the expression of the extracellular matrix glycoproteins tenascin and fibronectin during acne vulgaris. *Br J Dermatol*. 1994;130: 576-82.
136. Liang CJ, Yen YH, Hung LY, Wang SH, Pu CM, Chien HF, et al. Thalidomide inhibits fibronectin production in TGF-beta1-treated normal and keloid fibroblasts via inhibition of the p38/Smad3 pathway. *Biochemical pharmacology*. 2013;85: 1594-602.
137. Santucci M, Borgognoni L, Reali UM, Gabbiani G. Keloids and hypertrophic scars of Caucasians show distinctive morphologic and immunophenotypic profiles. *Virchows Arch*. 2001;438: 457-63.
138. Bertheim U, Hellstrom S. The distribution of hyaluronan in human skin and mature, hypertrophic and keloid scars. *British journal of plastic surgery*. 1994;47: 483-9.
139. Meyer LJ, Russell SB, Russell JD, Trupin JS, Egbert BM, Shuster S, et al. Reduced hyaluronan in keloid tissue and cultured keloid fibroblasts. *The Journal of investigative dermatology*. 2000;114: 953-9.
140. Tan KT, McGrouther DA, Day AJ, Milner CM, Bayat A. Characterization of hyaluronan and TSG-6 in skin scarring: differential distribution in keloid scars, normal scars and unscarred skin. *J Eur Acad Dermatol Venereol*. 2011;25: 317-27.
141. Amadeu TP, Braune AS, Porto LC, Desmouliere A, Costa AM. Fibrillin-1 and elastin are differentially expressed in hypertrophic scars and keloids. *Wound repair and regeneration : official publication of the Wound Healing Society [and] the European Tissue Repair Society*. 2004;12: 169-74.
142. Kamath NV, Ormsby A, Bergfeld WF, House NS. A light microscopic and immunohistochemical evaluation of scars. *Journal of cutaneous pathology*. 2002;29: 27-32.
143. Ikeda M, Naitoh M, Kubota H, Ishiko T, Yoshikawa K, Yamawaki S, et al. Elastic fiber assembly is disrupted by excessive accumulation of chondroitin sulfate in the human dermal fibrotic disease, keloid. *Biochem Biophys Res Commun*. 2009;390: 1221-8.
144. Chen J, Zhuo S, Jiang X, Zhu X, Zheng L, Xie S, et al. Multiphoton microscopy study of the morphological and quantity changes of collagen and elastic fiber components in keloid disease. *J Biomed Opt*. 2011;16: 051305.
145. Nie FF, Wang Q, Qin ZL. [The expression of fibrillin 1 in pathologic scars and its significance]. *Zhonghua Zheng Xing Wai Ke Za Zhi*. 2008;24: 339-42.

146. Dalkowski A, Schuppan D, Orfanos CE, Zouboulis CC. Increased expression of tenascin C by keloids in vivo and in vitro. *Br J Dermatol*. 1999;141: 50-6.
147. Catherino WH, Leppert PC, Stenmark MH, Payson M, Potlog-Nahari C, Nieman LK, et al. Reduced dermatopontin expression is a molecular link between uterine leiomyomas and keloids. *Genes, chromosomes & cancer*. 2004;40: 204-17.
148. Hunzelmann N, Anders S, Sollberg S, Schonherr E, Krieg T. Co-ordinate induction of collagen type I and biglycan expression in keloids. *Br J Dermatol*. 1996;135: 394-9.
149. Tan EM, Hoffren J, Rouda S, Greenbaum S, Fox JWt, Moore JH, Jr., et al. Decorin, versican, and biglycan gene expression by keloid and normal dermal fibroblasts: differential regulation by basic fibroblast growth factor. *Exp Cell Res*. 1993;209: 200-7.
150. Zhou HM, Wang J, Elliott C, Wen W, Hamilton DW, Conway SJ. Spatiotemporal expression of periostin during skin development and incisional wound healing: lessons for human fibrotic scar formation. *J Cell Commun Signal*. 2010;4: 99-107.
151. Yagi Y, Muroga E, Naitoh M, Isogai Z, Matsui S, Ikehara S, et al. An Ex Vivo Model Employing Keloid-Derived Cell-Seeded Collagen Sponges for Therapy Development. *The Journal of investigative dermatology*. 2012.
152. Russell JD, Russell SB, Trupin KM. Fibroblast heterogeneity in glucocorticoid regulation of collagen metabolism: genetic or epigenetic? *In Vitro*. 1982;18: 557-64.
153. Sorrell JM, Caplan AI. Fibroblast heterogeneity: more than skin deep. *J Cell Sci*. 2004;117: 667-75.
154. Supp DM, Hahn JM, Glaser K, McFarland KL, Boyce ST. Deep and superficial keloid fibroblasts contribute differentially to tissue phenotype in a novel in vivo model of keloid scar. *Plast Reconstr Surg*. 2012;129: 1259-71.
155. Silzle T, Randolph GJ, Kreutz M, Kunz-Schughart LA. The fibroblast: sentinel cell and local immune modulator in tumor tissue. *Int J Cancer*. 2004;108: 173-80.
156. Czubryt MP. Common threads in cardiac fibrosis, infarct scar formation, and wound healing. *Fibrogenesis Tissue Repair*. 2012;5: 19.
157. Kisseleva T, Brenner DA. Mechanisms of fibrogenesis. *Exp Biol Med (Maywood)*. 2008;233: 109-22.
158. Darby IA, Zakuan N, Billet F, Desmouliere A. The myofibroblast, a key cell in normal and pathological tissue repair. *Cell Mol Life Sci*. 2016;73: 1145-57.
159. Mantovani A, Biswas SK, Galdiero MR, Sica A, Locati M. Macrophage plasticity and polarization in tissue repair and remodelling. *The Journal of pathology*. 2013;229: 176-85.
160. Christmann RB. Another Piece in the Fibrotic Puzzle: TSLP as a Novel Ligand for Fibrocyte Activation. *Journal of Investigative Dermatology*. 2016;136: 360-2.
161. Shin JU, Lee WJ, Tran T-N, Jung I, Lee JH. Hsp70 Knockdown by siRNA Decreased Collagen Production in Keloid Fibroblasts. *Yonsei medical journal*. 2015;56: 1619-26.
162. Eishi K, Bae SJ, Ogawa F, Hamasaki Y, Shimizu K, Katayama I. Silicone gel sheets relieve pain and pruritus with clinical improvement of keloid: possible target of mast cells. *Journal of dermatological treatment*. 2003;14: 248-52.
163. Zhang Q, Wu Y, Chau CH, Ann DK, Bertolami CN, Le AD. Crosstalk of hypoxia-mediated signaling pathways in upregulating plasminogen activator inhibitor-1 expression in keloid fibroblasts. *J Cell Physiol*. 2004;199: 89-97.
164. Amadeu T, Braune A, Mandarim-de-Lacerda C, Porto LC, Desmouliere A, Costa A. Vascularization pattern in hypertrophic scars and keloids: a stereological analysis. *Pathol Res Pract*. 2003;199: 469-73.
165. Liu Q, Wang X, Jia Y, Long X, Yu N, Wang Y, et al. Increased blood flow in keloids and adjacent skin revealed by laser speckle contrast imaging. *Lasers Surg Med*. 2016;48: 360-4.
166. Ueda K, Yasuda Y, Furuya E, Oba S. Inadequate blood supply persists in keloids. *Scand J Plast Reconstr Surg Hand Surg*. 2004;38: 267-71.

167. Kurokawa N, Ueda K, Tsuji M. Study of microvascular structure in keloid and hypertrophic scars: density of microvessels and the efficacy of three-dimensional vascular imaging. *J Plast Surg Hand Surg.* 2010;44: 272-7.
168. Arima J, Huang C, Rosner B, Akaishi S, Ogawa R. Hypertension: a systemic key to understanding local keloid severity. *Wound repair and regeneration : official publication of the Wound Healing Society [and] the European Tissue Repair Society.* 2015;23: 213-21.
169. Huang C, Ogawa R. The link between hypertension and pathological scarring: does hypertension cause or promote keloid and hypertrophic scar pathogenesis? *Wound repair and regeneration : official publication of the Wound Healing Society [and] the European Tissue Repair Society.* 2014;22: 462-6.
170. Bux S, Madaree A. Involvement of upper torso stress amplification, tissue compression and distortion in the pathogenesis of keloids. *Medical hypotheses.* 2012;78: 356-63.
171. Nagasao T, Aramaki-Hattori N, Shimizu Y, Yoshitatsu S, Takano N, Kishi K. Transformation of keloids is determined by stress occurrence patterns on peri-keloid regions in response to body movement. *Med Hypotheses.* 2013;81: 136-41.
172. Suarez E, Syed F, Rasgado TA, Walmsley A, Mandal P, Bayat A. Skin equivalent tensional force alters keloid fibroblast behavior and phenotype. *Wound repair and regeneration : official publication of the Wound Healing Society [and] the European Tissue Repair Society.* 2014;22: 557-68.
173. Ogawa R, Akaishi S, Hyakusoku H. Differential and exclusive diagnosis of diseases that resemble keloids and hypertrophic scars. *Ann Plast Surg.* 2009;62: 660-4.
174. Sabater-Marco V, Pérez-Vallés A, Berzal-Cantalejo F, Rodriguez-Serna M, Martinez-Diaz F, Martorell-Cebollada M. Sclerosing dermatofibrosarcoma protuberans (DFSP): an unusual variant with focus on the histopathologic differential diagnosis. *International journal of dermatology.* 2006;45: 59-62.
175. Luzar B, Calonje E. Cutaneous fibrohistiocytic tumours—an update. *Histopathology.* 2010;56: 148-65.
176. Barzilai A, Lyakhovitsky A, Horowitz A, Trau H. Keloid-like scleroderma. *The American journal of dermatopathology.* 2003;25: 327-30.
177. Ong C, Khoo Y, Mukhopadhyay A, Masilamani J, Do D, Lim I, et al. Comparative proteomic analysis between normal skin and keloid scar. *British Journal of Dermatology.* 2010;162: 1302-15.
178. Andrews JP, Marttala J, Macarak E, Rosenbloom J, Uitto J. Keloids: The paradigm of skin fibrosis - Pathomechanisms and treatment. *Matrix Biol.* 2016.
179. Zhou P, Shi L, Li Q, Lu D. Overexpression of RACK1 inhibits collagen synthesis in keloid fibroblasts via inhibition of transforming growth factor- $\beta$ 1/Smad signaling pathway. *International journal of clinical and experimental medicine.* 2015;8: 15262.
180. Chodon T, Sugihara T, Igawa HH, Funayama E, Furukawa H. Keloid-derived fibroblasts are refractory to Fas-mediated apoptosis and neutralization of autocrine transforming growth factor- $\beta$ 1 can abrogate this resistance. *The American journal of pathology.* 2000;157: 1661-9.
181. Meng XM, Nikolic-Paterson DJ, Lan HY. TGF-beta: the master regulator of fibrosis. *Nat Rev Nephrol.* 2016.
182. Jagadeesan J, Bayat A. Transforming growth factor beta (TGFbeta) and keloid disease. *Int J Surg.* 2007;5: 278-85.
183. Tang B, Zhu B, Liang Y, Bi L, Hu Z, Chen B, et al. Asiaticoside suppresses collagen expression and TGF-beta/Smad signaling through inducing Smad7 and inhibiting TGF-betaRI and TGF-betaRII in keloid fibroblasts. *Arch Dermatol Res.* 2011;303: 563-72.
184. Smith JC, Boone BE, Opalenik SR, Williams SM, Russell SB. Gene profiling of keloid fibroblasts shows altered expression in multiple fibrosis-associated pathways. *The Journal of investigative dermatology.* 2008;128: 1298-310.

185. Yu H, Bock O, Bayat A, Ferguson MW, Mrowietz U. Decreased expression of inhibitory SMAD6 and SMAD7 in keloid scarring. *Journal of plastic, reconstructive & aesthetic surgery : JPRAS*. 2006;59: 221-9.
186. Kim WS, Lee JS, Bae GY, Kim JJ, Chin YW, Bahk YY, et al. Extract of *Aneilema keisak* inhibits transforming growth factor-beta-dependent signalling by inducing Smad2 downregulation in keloid fibroblasts. *Exp Dermatol*. 2013;22: 69-71.
187. Wu CS, Wu PH, Fang AH, Lan CC. FK506 inhibits the enhancing effects of transforming growth factor (TGF)-beta1 on collagen expression and TGF-beta/Smad signalling in keloid fibroblasts: implication for new therapeutic approach. *Br J Dermatol*. 2012;167: 532-41.
188. Fan DL, Zhao WJ, Wang YX, Han SY, Guo S. Oxymatrine inhibits collagen synthesis in keloid fibroblasts via inhibition of transforming growth factor-beta1/Smad signaling pathway. *Int J Dermatol*. 2012;51: 463-72.
189. Huang C, Akaishi S, Ogawa R. Mechanosignaling pathways in cutaneous scarring. *Arch Dermatol Res*. 2012;304: 589-97.
190. Wang Z, Fong KD, Phan TT, Lim IJ, Longaker MT, Yang GP. Increased transcriptional response to mechanical strain in keloid fibroblasts due to increased focal adhesion complex formation. *J Cell Physiol*. 2006;206: 510-7.
191. Lim IJ, Phan TT, Tan EK, Nguyen TT, Tran E, Longaker MT, et al. Synchronous activation of ERK and phosphatidylinositol 3-kinase pathways is required for collagen and extracellular matrix production in keloids. *The Journal of biological chemistry*. 2003;278: 40851-8.
192. Song R, Li G, Li S, Aspidin PB, a novel natural anti-fibrotic compound, inhibited fibrogenesis in TGF-beta1-stimulated keloid fibroblasts via PI-3K/Akt and Smad signaling pathways. *Chem Biol Interact*. 2015;238: 66-73.
193. Huang C, Ogawa R. Fibroproliferative disorders and their mechanobiology. *Connect Tissue Res*. 2012;53: 187-96.
194. Morgensztern D, McLeod HL. PI3K/Akt/mTOR pathway as a target for cancer therapy. *Anticancer Drugs*. 2005;16: 797-803.
195. Ong CT, Khoo YT, Mukhopadhyay A, Do DV, Lim IJ, Aalami O, et al. mTOR as a potential therapeutic target for treatment of keloids and excessive scars. *Exp Dermatol*. 2007;16: 394-404.
196. Syed F, Sherris D, Paus R, Varmeh S, Singh S, Pandolfi PP, et al. Keloid disease can be inhibited by antagonizing excessive mTOR signaling with a novel dual TORC1/2 inhibitor. *Am J Pathol*. 2012;181: 1642-58.
197. Syed F, Sanganee HJ, Singh S, Bahl A, Bayat A. Potent dual inhibitors of TORC1 and TORC2 complexes (KU-0063794 and KU-0068650) demonstrate in vitro and ex vivo anti-keloid scar activity. *The Journal of investigative dermatology*. 2013;133: 1340-50.
198. Yoshimoto H, Ishihara H, Ohtsuru A, Akino K, Murakami R, Kuroda H, et al. Overexpression of insulin-like growth factor-1 (IGF-I) receptor and the invasiveness of cultured keloid fibroblasts. *Am J Pathol*. 1999;154: 883-9.
199. Phan TT, Lim IJ, Bay BH, Qi R, Longaker MT, Lee ST, et al. Role of IGF system of mitogens in the induction of fibroblast proliferation by keloid-derived keratinocytes in vitro. *Am J Physiol Cell Physiol*. 2003;284: C860-9.
200. Ohtsuru A, Yoshimoto H, Ishihara H, Namba H, Yamashita S. Insulin-like growth factor-I (IGF-I)/IGF-I receptor axis and increased invasion activity of fibroblasts in keloid. *Endocr J*. 2000;47 Suppl: S41-4.
201. Sato M. Upregulation of the Wnt/beta-catenin pathway induced by transforming growth factor-beta in hypertrophic scars and keloids. *Acta Derm Venereol*. 2006;86: 300-7.
202. Hamburg-Shields E, DiNuoscio GJ, Mullin NK, Lafyatis R, Atit RP. Sustained beta-catenin activity in dermal fibroblasts promotes fibrosis by up-regulating expression of extracellular matrix protein-coding genes. *J Pathol*. 2015;235: 686-97.
203. Lee WJ, Park JH, Shin JU, Noh H, Lew DH, Yang WI, et al. Endothelial-to-mesenchymal transition induced by Wnt 3a in keloid pathogenesis. *Wound Repair and Regeneration*. 2015;23: 435-42.

204. Chua AW, Gan SU, Ting Y, Fu Z, Lim CK, Song C, et al. Keloid fibroblasts are more sensitive to Wnt3a treatment in terms of elevated cellular growth and fibronectin expression. *Journal of dermatological science*. 2011;64: 199-209.
205. Igota S, Tosa M, Murakami M, Egawa S, Shimizu H, Hyakusoku H, et al. Identification and characterization of Wnt signaling pathway in keloid pathogenesis. *Int J Med Sci*. 2013;10: 344-54.
206. Bhatt PM, Malgor R. Wnt5a: a player in the pathogenesis of atherosclerosis and other inflammatory disorders. *Atherosclerosis*. 2014;237: 155-62.
207. Zhang Y, Zhang D, Tu C, Zhou P, Zheng Y, Peng Z, et al. Wnt5a is involved in the pathogenesis of cutaneous lichen planus. *Clin Exp Dermatol*. 2015;40: 659-64.
208. Kim JE, Bang SH, Choi JH, Kim CD, Won CH, Lee MW, et al. Interaction of Wnt5a with Notch1 is Critical for the Pathogenesis of Psoriasis. *Ann Dermatol*. 2016;28: 45-54.
209. Xing Y, Chen X, Cao Y, Huang J, Xie X, Wei Y. Expression of Wnt and Notch signaling pathways in inflammatory bowel disease treated with mesenchymal stem cell transplantation: evaluation in a rat model. *Stem Cell Res Ther*. 2015;6: 101.
210. Kim JE, Lee JH, Jeong KH, Kim GM, Kang H. Notch intracellular domain expression in various skin fibroproliferative diseases. *Ann Dermatol*. 2014;26: 332-7.
211. Syed F, Bayat A. Notch signaling pathway in keloid disease: Enhanced fibroblast activity in a Jagged-1 peptide-dependent manner in lesional vs. extralesional fibroblasts. *Wound repair and regeneration : official publication of the Wound Healing Society [and] the European Tissue Repair Society*. 2012;20: 688-706.
212. Zhu G, Cai J, Zhang J, Zhao Y, Xu B. Abnormal nuclear factor (NF)-kappaB signal pathway and aspirin inhibits tumor necrosis factor alpha-induced NF-kappaB activation in keloid fibroblasts. *Dermatol Surg*. 2007;33: 697-708.
213. Ghazizadeh M, Tosa M, Shimizu H, Hyakusoku H, Kawanami O. Functional implications of the IL-6 signaling pathway in keloid pathogenesis. *Journal of investigative Dermatology*. 2007;127: 98-105.
214. Uitto J. IL-6 signaling pathway in keloids: a target for pharmacologic intervention? *Journal of Investigative Dermatology*. 2007;127: 6-8.
215. Yeh FL, Shen HD, Tai HY. Decreased production of MCP-1 and MMP-2 by keloid-derived fibroblasts. *Burns*. 2009;35: 348-51.
216. Oriente A, Fedarko NS, Pacocha SE, Huang SK, Lichtenstein LM, Essayan DM. Interleukin-13 modulates collagen homeostasis in human skin and keloid fibroblasts. *J Pharmacol Exp Ther*. 2000;292: 988-94.
217. Ray S, Ju X, Sun H, Finnerty CC, Herndon DN, Brasier AR. The IL-6 trans-signaling-STAT3 pathway mediates ECM and cellular proliferation in fibroblasts from hypertrophic scar. *Journal of Investigative Dermatology*. 2013;133: 1212-20.
218. Lim CP, Phan TT, Lim IJ, Cao X. Stat3 contributes to keloid pathogenesis via promoting collagen production, cell proliferation and migration. *Oncogene*. 2006;25: 5416-25.
219. Unahabhokha T, Sucontphunt A, Nimmannit U, Chanvorachote P, Yongsanguanchai N, Pongrakhananon V. Molecular signalings in keloid disease and current therapeutic approaches from natural based compounds. *Pharm Biol*. 2015;53: 457-63.
220. Mun JH, Kim YM, Kim BS, Kim JH, Kim MB, Ko HC. Simvastatin inhibits transforming growth factor-beta1-induced expression of type I collagen, CTGF, and alpha-SMA in keloid fibroblasts. *Wound repair and regeneration : official publication of the Wound Healing Society [and] the European Tissue Repair Society*. 2014;22: 125-33.
221. Khoo YT, Ong CT, Mukhopadhyay A, Han HC, Do DV, Lim IJ, et al. Upregulation of secretory connective tissue growth factor (CTGF) in keratinocyte-fibroblast coculture contributes to keloid pathogenesis. *J Cell Physiol*. 2006;208: 336-43.
222. Fujiwara M, Muragaki Y, Ooshima A. Keloid-derived fibroblasts show increased secretion of factors involved in collagen turnover and depend on matrix metalloproteinase for migration. *Br J Dermatol*. 2005;153: 295-300.

223. Li H, Nahas Z, Feng F, Elisseeff JH, Boahene K. Tissue engineering for in vitro analysis of matrix metalloproteinases in the pathogenesis of keloid lesions. *JAMA Facial Plast Surg.* 2013;15: 448-56.
224. Yu X, Li Z, Chan MT, Wu WK. microRNA deregulation in keloids: an opportunity for clinical intervention? *Cell Prolif.* 2015;48: 626-30.
225. Luan Y, Liu Y, Liu C, Lin Q, He F, Dong X, et al. Serum miRNAs signature plays an important role in keloid disease. *Curr Mol Med.* 2016.
226. Wu ZY, Lu L, Liang J, Guo XR, Zhang PH, Luo SJ. Keloid microRNA expression analysis and the influence of miR-199a-5p on the proliferation of keloid fibroblasts. *Genet Mol Res.* 2014;13: 2727-38.
227. Zhang GY, Wu LC, Liao T, Chen GC, Chen YH, Zhao YX, et al. A novel regulatory function for miR-29a in keloid fibrogenesis. *Clin Exp Dermatol.* 2015.
228. Babalola O, Mamalis A, Lev-Tov H, Jagdeo J. The role of microRNAs in skin fibrosis. *Arch Dermatol Res.* 2013;305: 763-76.
229. Park TH, Rah DK. Successful eradication of helical rim keloids with surgical excision followed by pressure therapy using a combination of magnets and silicone gel sheeting. *Int Wound J.* 2015.
230. Tanaydin V, Beugels J, Piatkowski A, Colla C, van den Kerckhove E, Hugenholtz GC, et al. Efficacy of custom-made pressure clips for ear keloid treatment after surgical excision. *Journal of plastic, reconstructive & aesthetic surgery : JPRAS.* 2016;69: 115-21.
231. De Sousa RF, Chakravarty B, Sharma A, Parwaz MA, Malik A. Efficacy of triple therapy in auricular keloids. *J Cutan Aesthet Surg.* 2014;7: 98-102.
232. Camacho-Martinez FM, Rey ER, Serrano FC, Wagner A. Results of a combination of bleomycin and triamcinolone acetonide in the treatment of keloids and hypertrophic scars. *An Bras Dermatol.* 2013;88: 387-94.
233. Martin MS, Collawn SS. Combination treatment of CO2 fractional laser, pulsed dye laser, and triamcinolone acetonide injection for refractory keloid scars on the upper back. *J Cosmet Laser Ther.* 2013;15: 166-70.
234. van Leeuwen MC, Bulstra AE, Ket JC, Ritt MJ, van Leeuwen PA, Niessen FB. Intralesional Cryotherapy for the Treatment of Keloid Scars: Evaluating Effectiveness. *Plast Reconstr Surg Glob Open.* 2015;3: e437.
235. Abdel-Meguid AM, Weshahy AH, Sayed DS, Refaiy AE, Awad SM. Intralesional vs. contact cryosurgery in treatment of keloids: a clinical and immunohistochemical study. *Int J Dermatol.* 2015;54: 468-75.
236. Mendoza-Garcia J, Sebastian A, Alonso-Rasgado T, Bayat A. Ex vivo evaluation of the effect of photodynamic therapy on skin scars and striae distensae. *Photodermatol Photoimmunol Photomed.* 2015;31: 239-51.
237. Al-Mohamady AE, Ibrahim SM, Muhammad MM. Pulsed dye laser versus long-pulsed Nd:YAG laser in the treatment of hypertrophic scars and keloid: A comparative randomized split-scar trial. *J Cosmet Laser Ther.* 2016: 1-5.
238. Poetschke J, Gauglitz GG. Current options for the treatment of pathological scarring. *J Dtsch Dermatol Ges.* 2016;14: 467-77.
239. Bidad K, Salehi E, Oraei M, Saboor-Yaraghi AA, Nicknam MH. Effect of all-trans retinoic acid (ATRA) on viability, proliferation, activation and lineage-specific transcription factors of CD4+ T cells. *Iran J Allergy Asthma Immunol.* 2011;10: 243-9.
240. Tabata C, Kadokawa Y, Tabata R, Takahashi M, Okoshi K, Sakai Y, et al. All-trans-retinoic acid prevents radiation- or bleomycin-induced pulmonary fibrosis. *Am J Respir Crit Care Med.* 2006;174: 1352-60.
241. Chike-Obi CJ, Cole PD, Brissett AE, editors. *Keloids: pathogenesis, clinical features, and management. Seminars in plastic surgery;* 2009.
242. Abergel RP, Meeker CA, Oikarinen H, Oikarinen AI, Uitto J. Retinoid modulation of connective tissue metabolism in keloid fibroblast cultures. *Archives of dermatology.* 1985;121: 632-5.

243. Uchida G, Yoshimura K, Kitano Y, Okazaki M, Harii K. Tretinoin reverses upregulation of matrix metalloproteinase-13 in human keloid-derived fibroblasts. *Exp Dermatol*. 2003;12 Suppl 2: 35-42.
244. Panabiere-Castaings MH. Retinoic acid in the treatment of keloids. *The Journal of dermatologic surgery and oncology*. 1988;14: 1275-6.
245. Arno AI, Gauglitz GG, Barret JP, Jeschke MG. Up-to-date approach to manage keloids and hypertrophic scars: a useful guide. *Burns*. 2014;40: 1255-66.
246. Wong VW, You F, Januszyk M, Kuang AA. Tacrolimus fails to regulate collagen expression in dermal fibroblasts. *J Surg Res*. 2013;184: 678-90.
247. Trislina Perdanasari A, Lazzeri D, Su W, Xi W, Zheng Z, Ke L, et al. Recent developments in the use of intralesional injections keloid treatment. *Arch Plast Surg*. 2014;41: 620-9.
248. Danielsen PL, Rea SM, Wood FM, Fear MW, Viola HM, Hool LC, et al. Verapamil is Less Effective than Triamcinolone for Prevention of Keloid Scar Recurrence After Excision in a Randomized Controlled Trial. *Acta Derm Venereol*. 2016.
249. Ahuja RB, Chatterjee P. Comparative efficacy of intralesional verapamil hydrochloride and triamcinolone acetonide in hypertrophic scars and keloids. *Burns*. 2014;40: 583-8.
250. Jones CD, Guiot L, Samy M, Gorman M, Tehrani H. The Use of Chemotherapeutics for the Treatment of Keloid Scars. *Dermatol Reports*. 2015;7: 5880.
251. Song N, Wu X, Gao Z, Zhou G, Zhang WJ, Liu W. Enhanced expression of membrane transporter and drug resistance in keloid fibroblasts. *Hum Pathol*. 2012;43: 2024-32.
252. Qu M, Song N, Chai G, Wu X, Liu W. Pathological niche environment transforms dermal stem cells to keloid stem cells: a hypothesis of keloid formation and development. *Med Hypotheses*. 2013;81: 807-12.
253. Ogawa R. The most current algorithms for the treatment and prevention of hypertrophic scars and keloids. *Plastic and Reconstructive Surgery*. 2010;125: 557-68.
254. Shin JY, Kim JS. Could 5-Fluorouracil or Triamcinolone Be an Effective Treatment Option for Keloid After Surgical Excision? A Meta-Analysis. *J Oral Maxillofac Surg*. 2016;74: 1055-60.
255. van Leeuwen MC, Stokmans SC, Bulstra AE, Meijer OW, Heymans MW, Ket JC, et al. Surgical Excision with Adjuvant Irradiation for Treatment of Keloid Scars: A Systematic Review. *Plast Reconstr Surg Glob Open*. 2015;3: e440.
256. Shin JY, Lee JW, Roh SG, Lee NH, Yang KM. A Comparison of the Effectiveness of Triamcinolone and Radiation Therapy for Ear Keloids after Surgical Excision: A Systematic Review and Meta-Analysis. *Plast Reconstr Surg*. 2016;137: 1718-25.
257. Sidgwick GP, McGeorge D, Bayat A. A comprehensive evidence-based review on the role of topicals and dressings in the management of skin scarring. *Arch Dermatol Res*. 2015;307: 461-77.
258. Arno AI, Gauglitz GG, Barret JP, Jeschke MG. New molecular medicine-based scar management strategies. *Burns*. 2014;40: 539-51.
259. Kirby GT, Mills SJ, Cowin AJ, Smith LE. Stem Cells for Cutaneous Wound Healing. *Biomed Res Int*. 2015;2015: 285869.
260. Seo BF, Jung SN. The Immunomodulatory Effects of Mesenchymal Stem Cells in Prevention or Treatment of Excessive Scars. *Stem Cells Int*. 2016;2016: 6937976.
261. Shaarawy E, Hegazy RA, Abdel Hay RM. Intralesional botulinum toxin type A equally effective and better tolerated than intralesional steroid in the treatment of keloids: a randomized controlled trial. *J Cosmet Dermatol*. 2015;14: 161-6.
262. Durani P, Bayat A. Levels of evidence for the treatment of keloid disease. *Journal of Plastic, Reconstructive & Aesthetic Surgery*. 2008;61: 4-17.
263. Lumenta DB, Siepmann E, Kamolz LP. Internet-based survey on current practice for evaluation, prevention, and treatment of scars, hypertrophic scars, and keloids. *Wound repair and regeneration : official publication of the Wound Healing Society [and] the European Tissue Repair Society*. 2014;22: 483-91.



264. Ladin DA, Hou Z, Patel D, McPhail M, Olson JC, Saed GM, et al. p53 and apoptosis alterations in keloids and keloid fibroblasts. *Wound repair and regeneration*. 1998;6: 28-37.
265. Hollywood KA, Maatje M, Shadi IT, Henderson A, McGrouther DA, Goodacre R, et al. Phenotypic profiling of keloid scars using FT-IR microspectroscopy reveals a unique spectral signature. *Arch Dermatol Res*. 2010;302: 705-15.
266. Louw L, van der Westhuizen JP, Duyvene de Wit L, Edwards G. Keloids: peripheral and central differences in cell morphology and fatty acid compositions of lipids. *Adv Exp Med Biol*. 1997;407: 515-20.
267. Touchi R, Ueda K, Kurokawa N, Tsuji M. Central regions of keloids are severely ischaemic. *Journal of plastic, reconstructive & aesthetic surgery : JPRAS*. 2016;69: e35-41.
268. Ashcroft KJ, Syed F, Bayat A. Site-specific keloid fibroblasts alter the behaviour of normal skin and normal scar fibroblasts through paracrine signalling. *PLoS One*. 2013;8: e75600.
269. Tsujita-Kyutoku M, Uehara N, Matsuoka Y, Kyutoku S, Ogawa Y, Tsubura A. Comparison of transforming growth factor-beta/Smad signaling between normal dermal fibroblasts and fibroblasts derived from central and peripheral areas of keloid lesions. *In Vivo*. 2005;19: 959-63.
270. Luo S, Benathan M, Raffoul W, Panizzon RG, Egloff DV. Abnormal balance between proliferation and apoptotic cell death in fibroblasts derived from keloid lesions. *Plast Reconstr Surg*. 2001;107: 87-96.
271. Javad F, Day PJ. Protein profiling of keloidal scar tissue. *Arch Dermatol Res*. 2012;304: 533-40.
272. Giugliano G, Pasquali D, Notaro A, Brongo S, Nicoletti G, D'Andrea F, et al. Verapamil inhibits interleukin-6 and vascular endothelial growth factor production in primary cultures of keloid fibroblasts. *British journal of plastic surgery*. 2003;56: 804-9.
273. Lu F, Gao J, Ogawa R, Hyakusoku H, Ou C. Biological differences between fibroblasts derived from peripheral and central areas of keloid tissues. *Plast Reconstr Surg*. 2007;120: 625-30.
274. Kratochwil K. *Epithelial-Mesenchymal Interactions*. eLS. 2013.
275. Sennett R, Rendl M. Mesenchymal-epithelial interactions during hair follicle morphogenesis and cycling. *Semin Cell Dev Biol*. 2012;23: 917-27.
276. Ohyama M, Veraitch O. Strategies to enhance epithelial-mesenchymal interactions for human hair follicle bioengineering. *Journal of dermatological science*. 2013;70: 78-87.
277. Rheinwald JG, Green H. Formation of a keratinizing epithelium in culture by a cloned cell line derived from a teratoma. *Cell*. 1975;6: 317-30.
278. Rheinwald JG, Green H. Epidermal growth factor and the multiplication of cultured human epidermal keratinocytes. *Nature*. 1977;265: 421-4.
279. Bell E, Sher S, Hull B, Merrill C, Rosen S, Chamson A, et al. The reconstitution of living skin. *Journal of investigative dermatology*. 1983;81.
280. Werner S, Krieg T, Smola H. Keratinocyte-fibroblast interactions in wound healing. *The Journal of investigative dermatology*. 2007;127: 998-1008.
281. Wong T, McGrath JA, Navsaria H. The role of fibroblasts in tissue engineering and regeneration. *Br J Dermatol*. 2007;156: 1149-55.
282. Sheppard D. Epithelial-mesenchymal interactions in fibrosis and repair. Transforming growth factor-beta activation by epithelial cells and fibroblasts. *Ann Am Thorac Soc*. 2015;12 Suppl 1: S21-3.
283. Ghahary A, Ghaffari A. Role of keratinocyte-fibroblast cross-talk in development of hypertrophic scar. *Wound repair and regeneration : official publication of the Wound Healing Society [and] the European Tissue Repair Society*. 2007;15 Suppl 1: S46-53.
284. Lacina L, Smetana K, Jr., Dvorankova B, Pytlík R, Kideryova L, Kucerova L, et al. Stromal fibroblasts from basal cell carcinoma affect phenotype of normal keratinocytes. *Br J Dermatol*. 2007;156: 819-29.

285. Lim IJ, Phan T-T, Bay B-H, Qi R, Huynh H, Tan WT-L, et al. Fibroblasts cocultured with keloid keratinocytes: normal fibroblasts secrete collagen in a keloidlike manner. *American Journal of Physiology-Cell Physiology*. 2002;283: C212-C22.
286. Lim IJ, Phan T-T, Song C, Tan W, Longaker MT. Investigation of the influence of keloid-derived keratinocytes on fibroblast growth and proliferation in vitro. *Plastic and reconstructive surgery*. 2001;107: 797-808.
287. Mukhopadhyay A, Tan E, Khoo Y, Chan S, Lim I, Phan T. Conditioned medium from keloid keratinocyte/keloid fibroblast coculture induces contraction of fibroblast-populated collagen lattices. *British Journal of Dermatology*. 2005;152: 639-45.
288. Funayama E, Chodon T, Oyama A, Sugihara T. Keratinocytes promote proliferation and inhibit apoptosis of the underlying fibroblasts: an important role in the pathogenesis of keloid. *The Journal of investigative dermatology*. 2003;121: 1326-31.
289. Phan TT, Lim IJ, Aalami O, Lorget F, Khoo A, Tan EK, et al. Smad3 signalling plays an important role in keloid pathogenesis via epithelial-mesenchymal interactions. *J Pathol*. 2005;207: 232-42.
290. Xia W, Phan TT, Lim IJ, Longaker MT, Yang GP. Complex epithelial-mesenchymal interactions modulate transforming growth factor-beta expression in keloid-derived cells. *Wound repair and regeneration : official publication of the Wound Healing Society [and] the European Tissue Repair Society*. 2004;12: 546-56.
291. Phan T-T, Lim IJ, Bay BH, Qi R, Longaker MT, Lee S-T, et al. Role of IGF system of mitogens in the induction of fibroblast proliferation by keloid-derived keratinocytes in vitro. *American Journal of Physiology-Cell Physiology*. 2003;284: C860-C9.
292. Ong CT, Khoo YT, Tan EK, Mukhopadhyay A, Do DV, Han HC, et al. Epithelial-mesenchymal interactions in keloid pathogenesis modulate vascular endothelial growth factor expression and secretion. *J Pathol*. 2007;211: 95-108.
293. Lim CP, Phan TT, Lim IJ, Cao X. Cytokine profiling and Stat3 phosphorylation in epithelial-mesenchymal interactions between keloid keratinocytes and fibroblasts. *The Journal of investigative dermatology*. 2009;129: 851-61.
294. Kalluri R, Weinberg RA. The basics of epithelial-mesenchymal transition. *The Journal of clinical investigation*. 2009;119: 1420-8.
295. Kalluri R, Neilson EG. Epithelial-mesenchymal transition and its implications for fibrosis. *The Journal of clinical investigation*. 2003;112: 1776-84.
296. Lamouille S, Xu J, Derynck R. Molecular mechanisms of epithelial-mesenchymal transition. *Nature reviews Molecular cell biology*. 2014;15: 178.
297. Nikitorowicz-Buniak J, Denton CP, Abraham D, Stratton R. Partially Evoked Epithelial-Mesenchymal Transition (EMT) Is Associated with Increased TGFbeta Signaling within Lesional Scleroderma Skin. *PLoS One*. 2015;10: e0134092.
298. Piera-Velazquez S, Mendoza FA, Jimenez SA. Endothelial to Mesenchymal Transition (EndoMT) in the Pathogenesis of Human Fibrotic Diseases. *J Clin Med*. 2016;5.
299. Sanchez-Duffhues G, Orlova V, Ten Dijke P. In Brief: Endothelial-to-mesenchymal transition. *J Pathol*. 2016;238: 378-80.
300. Grigore AD, Jolly MK, Jia D, Farach-Carson MC, Levine H. Tumor Budding: The Name is EMT. Partial EMT. *J Clin Med*. 2016;5.
301. Smith BN, Bhowmick NA. Role of EMT in Metastasis and Therapy Resistance. *J Clin Med*. 2016;5.
302. Yan L, Cao R, Wang L, Liu Y, Pan B, Yin Y, et al. Epithelial-mesenchymal transition in keloid tissues and TGF-beta1-induced hair follicle outer root sheath keratinocytes. *Wound repair and regeneration : official publication of the Wound Healing Society [and] the European Tissue Repair Society*. 2015;23: 601-10.
303. Miragliotta V, Pirone A, Donadio E, Abramo F, Ricciardi MP, Theoret CL. Osteopontin expression in healing wounds of horses and in human keloids. *Equine Vet J*. 2016;48: 72-7.

304. Hochman B, Vilas Bôas FC, Mariano M, Ferreira LM. Keloid heterograft in the hamster (*Mesocricetus auratus*) cheek pouch. *Acta Cirurgica Brasileira*. 2005;20: 200-12.
305. Philandrianos C, Bertrand B, Andrac-Meyer L, Magalon G, Casanova D, Kerfant N, et al. Treatment of keloid scars with a 1210-nm diode laser in an animal model. *Lasers Surg Med*. 2015;47: 798-806.
306. Shetlar MR, Shetlar CL, Hendricks L, Kischer CW. The use of athymic nude mice for the study of human keloids. *Proc Soc Exp Biol Med*. 1985;179: 549-52.
307. Wang H, Luo S. Establishment of an animal model for human keloid scars using tissue engineering method. *J Burn Care Res*. 2013;34: 439-46.
308. Yang DY, Li SR, Li G, Liu JY, Wang ZX, Wu JL, et al. [Establishment of an animal model of human hyperplastic scar in nude mice]. *Zhonghua Shao Shang Za Zhi*. 2004;20: 82-4.
309. Xiang J, Wang ZY, Jia SX, Jin SW, Lu SL, Liao ZJ. [Establishment of an animal model with hypertrophic scar]. *Zhonghua Shao Shang Za Zhi*. 2004;20: 281-3.
310. Lee JP, Jalili RB, Tredget EE, Demare JR, Ghahary A. Antifibrogenic effects of liposome-encapsulated IFN-alpha2b cream on skin wounds in a fibrotic rabbit ear model. *J Interferon Cytokine Res*. 2005;25: 627-31.
311. Ramos ML, Gragnani A, Ferreira LM. Is there an ideal animal model to study hypertrophic scarring? *J Burn Care Res*. 2008;29: 363-8.
312. Zhu KQ, Engrav LH, Gibran NS, Cole JK, Matsumura H, Piepkorn M, et al. The female, red Duroc pig as an animal model of hypertrophic scarring and the potential role of the cones of skin. *Burns*. 2003;29: 649-64.
313. Harunari N, Zhu KQ, Armendariz RT, Deubner H, Muangman P, Carrougher GJ, et al. Histology of the thick scar on the female, red Duroc pig: final similarities to human hypertrophic scar. *Burns*. 2006;32: 669-77.
314. Williams FN, Herndon DN, Branski LK. Where we stand with human hypertrophic and keloid scar models. *Exp Dermatol*. 2014;23: 811-2.
315. Zhu KQ, Carrougher GJ, Couture OP, Tuggle CK, Gibran NS, Engrav LH. Expression of collagen genes in the cones of skin in the Duroc/Yorkshire porcine model of fibroproliferative scarring. *J Burn Care Res*. 2008;29: 815-27.
316. Marttala J, Andrews JP, Rosenbloom J, Uitto J. Keloids: Animal models and pathologic equivalents to study tissue fibrosis. *Matrix Biology*. 2016;51: 47-54.
317. Lee YS, Hsu T, Chiu WC, Sarkozy H, Kulber DA, Choi A, et al. Keloid-derived, plasma/fibrin-based skin equivalents generate de novo dermal and epidermal pathology of keloid fibrosis in a mouse model. *Wound repair and regeneration : official publication of the Wound Healing Society [and] the European Tissue Repair Society*. 2016;24: 302-16.
318. Bagabir R, Syed F, Paus R, Bayat A. Long-term organ culture of keloid disease tissue. *Exp Dermatol*. 2012;21: 376-81.
319. Duong HS, Zhang Q, Kobi A, Le A, Messadi DV. Assessment of morphological and immunohistological alterations in long-term keloid skin explants. *Cells Tissues Organs*. 2005;181: 89-102.
320. El-Serag HB, Nurgalieva ZZ, Mistretta TA, Finegold MJ, Souza R, Hilsenbeck S, et al. Gene expression in Barrett's esophagus: laser capture versus whole tissue. *Scand J Gastroenterol*. 2009;44: 787-95.
321. Yazdi AS, Ghoreschi K, Sander CA, Rocken M. Activation of the mitogen-activated protein kinase pathway in malignant melanoma can occur independently of the BRAF T1799A mutation. *Eur J Dermatol*. 2010;20: 575-9.
322. Mabry KM, Payne SZ, Anseth KS. Microarray analyses to quantify advantages of 2D and 3D hydrogel culture systems in maintaining the native valvular interstitial cell phenotype. *Biomaterials*. 2016;74: 31-41.
323. Lee WJ, Choi IK, Lee JH, Kim YO, Yun CO. A novel three-dimensional model system for keloid study: organotypic multicellular scar model. *Wound repair and regeneration : official publication of the Wound Healing Society [and] the European Tissue Repair Society*. 2013;21: 155-65.

324. Butler PD, Ly DP, Longaker MT, Yang GP. Use of organotypic coculture to study keloid biology. *Am J Surg*. 2008;195: 144-8.
325. Baker BM, Chen CS. Deconstructing the third dimension: how 3D culture microenvironments alter cellular cues. *J Cell Sci*. 2012;125: 3015-24.
326. Datta S, Malhotra L, Dickerson R, Chaffee S, Sen CK, Roy S. Laser capture microdissection: Big data from small samples. *Histol Histopathol*. 2015;30: 1255-69.
327. Jensen E. Laser-Capture Microdissection. *The Anatomical Record*. 2013;296: 1683-7.
328. Emmert-Buck MR, Bonner RF, Smith PD, Chuaqui RF, Zhuang Z, Goldstein SR, et al. Laser capture microdissection. *Science*. 1996;274: 998-1001.
329. Murray GI. An overview of laser microdissection technologies. *Acta Histochem*. 2007;109: 171-6.
330. Shibata D, Hawes D, Li ZH, Hernandez AM, Spruck CH, Nichols PW. Specific genetic analysis of microscopic tissue after selective ultraviolet radiation fractionation and the polymerase chain reaction. *The American journal of pathology*. 1992;141: 539-43.
331. Liu H, McDowell TL, Hanson NE, Tang X, Fujimoto J, Rodriguez-Canales J. Laser capture microdissection for the investigative pathologist. *Vet Pathol*. 2014;51: 257-69.
332. Agar NS, Halliday GM, Barnetson RS, Jones AM. A novel technique for the examination of skin biopsies by laser capture microdissection. *J Cutan Pathol*. 2003;30: 265-70.
333. Sirivatanauksorn Y, Drury R, Crnogorac-Jurcevic T, Sirivatanauksorn V, Lemoine NR. Laser-assisted microdissection: applications in molecular pathology. *The Journal of pathology*. 1999;189: 150-4.
334. Morrison JA, Box AC, McKinney MC, McLennan R, Kulesa PM. Quantitative single cell gene expression profiling in the avian embryo. *Developmental Dynamics*. 2015;244: 774-84.
335. Clément-Ziza M, Munnich A, Lyonnet S, Jaubert F, Besmond C. Stabilization of RNA during laser capture microdissection by performing experiments under argon atmosphere or using ethanol as a solvent in staining solutions. *Rna*. 2008;14: 2698-704.
336. Rosenberg AZ, Armani MD, Fetsch PA, Xi L, Pham TT, Raffeld M, et al. High-Throughput Microdissection for Next-Generation Sequencing. *PloS one*. 2016;11: e0151775.
337. Adkins JM, Collard HR. Idiopathic pulmonary fibrosis. *Semin Respir Crit Care Med*. 2012;33: 433-9.
338. Crystal RG, Bitterman PB, Mossman B, Schwarz MI, Sheppard D, Almasly L, et al. Future research directions in idiopathic pulmonary fibrosis: summary of a National Heart, Lung, and Blood Institute working group. *Am J Respir Crit Care Med*. 2002;166: 236-46.
339. Betsuyaku T, Griffin GL, Watson MA, Senior RM. Laser capture microdissection and real-time reverse transcriptase/ polymerase chain reaction of bronchiolar epithelium after bleomycin. *Am J Respir Cell Mol Biol*. 2001;25: 278-84.
340. Betsuyaku T, Senior RM. Laser capture microdissection and mRNA characterization of mouse airway epithelium: methodological considerations. *Micron*. 2004;35: 229-34.
341. Kelly MM, Leigh R, Gilpin SE, Cheng E, Martin GE, Radford K, et al. Cell-specific gene expression in patients with usual interstitial pneumonia. *Am J Respir Crit Care Med*. 2006;174: 557-65.
342. Marmai C, Sutherland RE, Kim KK, Dolganov GM, Fang X, Kim SS, et al. Alveolar epithelial cells express mesenchymal proteins in patients with idiopathic pulmonary fibrosis. *American journal of physiology Lung cellular and molecular physiology*. 2011;301: L71-8.
343. Wilkinson R, Wang X, Kassianos AJ, Zuryn S, Roper KE, Osborne A, et al. Laser capture microdissection and multiplex-tandem PCR analysis of proximal tubular epithelial cell signaling in human kidney disease. *PloS one*. 2014;9: e87345.
344. Kuhn DE, Roy S, Radtke J, Khanna S, Sen CK. Laser microdissection and capture of pure cardiomyocytes and fibroblasts from infarcted heart regions: perceived hyperoxia induces p21 in peri-infarct myocytes. *Am J Physiol Heart Circ Physiol*. 2007;292: H1245-53.
345. Roy S, Khanna S, Rink T, Radtke J, Williams WT, Biswas S, et al. P21waf1/cip1/sdi1 as a central regulator of inducible smooth muscle actin expression and differentiation of cardiac fibroblasts to myofibroblasts. *Mol Biol Cell*. 2007;18: 4837-46.

346. Katona TM, Jones TD, Wang M, Eble JN, Billings SD, Cheng L. Genetically heterogeneous and clonally unrelated metastases may arise in patients with cutaneous melanoma. *Am J Surg Pathol.* 2007;31: 1029-37.
347. Sha J, Gastman BR, Morris N, Mesinkovska NA, Baron ED, Cooper KD, et al. The Response of microRNAs to Solar UVR in Skin-Resident Melanocytes Differs between Melanoma Patients and Healthy Persons. *PLoS One.* 2016;11: e0154915.
348. Bahrami S, Cheng L, Wang M, Jones TD, Malone JC, Billings SD. Clonal relationships between epidermotropic metastatic melanomas and their primary lesions: a loss of heterozygosity and X-chromosome inactivation-based analysis. *Mod Pathol.* 2007;20: 821-7.
349. Asplund A, Gry Bjorklund M, Sundquist C, Stromberg S, Edlund K, Ostman A, et al. Expression profiling of microdissected cell populations selected from basal cells in normal epidermis and basal cell carcinoma. *Br J Dermatol.* 2008;158: 527-38.
350. Quan C, Cho MK, Shao Y, Miannecki LE, Liao E, Perry D, et al. Dermal fibroblast expression of stromal cell-derived factor-1 (SDF-1) promotes epidermal keratinocyte proliferation in normal and diseased skin. *Protein Cell.* 2015;6: 890-903.
351. Pedersen TX, Leethanakul C, Patel V, Mitola D, Lund LR, Dano K, et al. Laser capture microdissection-based in vivo genomic profiling of wound keratinocytes identifies similarities and differences to squamous cell carcinoma. *Oncogene.* 2003;22: 3964-76.
352. Mitsui H, Suarez-Farinas M, Belkin DA, Levenkova N, Fuentes-Duculan J, Coats I, et al. Combined use of laser capture microdissection and cDNA microarray analysis identifies locally expressed disease-related genes in focal regions of psoriasis vulgaris skin lesions. *The Journal of investigative dermatology.* 2012;132: 1615-26.
353. Lovendorf MB, Mitsui H, Zibert JR, Ropke MA, Hafner M, Dyring-Andersen B, et al. Laser capture microdissection followed by next-generation sequencing identifies disease-related microRNAs in psoriatic skin that reflect systemic microRNA changes in psoriasis. *Exp Dermatol.* 2015;24: 187-93.
354. Carneiro JR, Fuzii HT, Kayser C, Alberto FL, Soares FA, Sato EI, et al. IL-2, IL-5, TNF-alpha and IFN-gamma mRNA expression in epidermal keratinocytes of systemic lupus erythematosus skin lesions. *Clinics (Sao Paulo).* 2011;66: 77-82.
355. Brems H, Park C, Maertens O, Pemov A, Messiaen L, Upadhyaya M, et al. Glomus tumors in neurofibromatosis type 1: genetic, functional, and clinical evidence of a novel association. *Cancer Res.* 2009;69: 7393-401.
356. Harries MJ, Meyer K, Chaudhry I, J EK, Poblet E, Griffiths CE, et al. Lichen planopilaris is characterized by immune privilege collapse of the hair follicle's epithelial stem cell niche. *J Pathol.* 2013;231: 236-47.
357. Feghali-Bostwick CA. Genetics and proteomics in scleroderma. *Curr Rheumatol Rep.* 2005;7: 129-34.
358. Engrav LH, Garner WL, Tredget EE. Hypertrophic scar, wound contraction and hyper-pigmentation. *J Burn Care Res.* 2007;28: 593-7.
359. Nanney LB, Caldwell RL, Pollins AC, Cardwell NL, Opalenik SR, Davidson JM. Novel approaches for understanding the mechanisms of wound repair. *The journal of investigative dermatology Symposium proceedings / the Society for Investigative Dermatology, Inc [and] European Society for Dermatological Research.* 2006;11: 132-9.
360. Rittie L, Perbal B, Castellot JJ, Jr., Orringer JS, Voorhees JJ, Fisher GJ. Spatial-temporal modulation of CCN proteins during wound healing in human skin in vivo. *J Cell Commun Signal.* 2011;5: 69-80.
361. Gulati N, Krueger JG, Suarez-Farinas M, Mitsui H. Creation of differentiation-specific genomic maps of human epidermis through laser capture microdissection. *The Journal of investigative dermatology.* 2013;133: 2640-2.
362. Chen L, Guo S, Ranzer MJ, DiPietro LA. Toll-like receptor 4 has an essential role in early skin wound healing. *Journal of Investigative Dermatology.* 2013;133: 258-67.

363. Shapiro JP, Biswas S, Merchant AS, Satoskar A, Taslim C, Lin S, et al. A quantitative proteomic workflow for characterization of frozen clinical biopsies: laser capture microdissection coupled with label-free mass spectrometry. *J Proteomics*. 2012;77: 433-40.
364. Roy S, Elgharably H, Sinha M, Ganesh K, Chaney S, Mann E, et al. Mixed-species biofilm compromises wound healing by disrupting epidermal barrier function. *J Pathol*. 2014;233: 331-43.
365. Roy S, Patel D, Khanna S, Gordillo GM, Biswas S, Friedman A, et al. Transcriptome-wide analysis of blood vessels laser captured from human skin and chronic wound-edge tissue. *Proc Natl Acad Sci U S A*. 2007;104: 14472-7.

# Chapter 3

---

## Methods

### 3.1 Author contributions

All of the experiments performed during the course of this PhD were designed and executed by the author, Natalie Jumper, unless otherwise stated. Although the relevant experiments are described in brief in the appropriate results chapter, this chapter contains a more detailed explanation of the methods used in the realisation of this research.

### 3.2 Ethical approval

Both normal skin and keloid tissue were acquired after obtaining full verbal and written consent from patients in line with the North West Research Ethics Committee (Ref. 11/NW/0683) and Declaration of Helsinki protocols. All harvested tissue was stored, used and disposed of in accordance with the Human Tissue Act (HTA) 2004. All samples were anonymised with a unique identifying number and recorded in a sample-tracking database for HTA records.

### 3.3 Patient data and tissue collection

A scar was considered to be keloid if it fulfilled the following criteria: growth beyond the boundaries of the original wound, failure to regress with time, present for at least one year and likely to recur with excision/unresponsive to treatment. Keloid biopsies were harvested from the centre of the lesion (intralesional), the margin (perilesional) and the adjacent normal skin (extralesional) (**Figure 3.1**). These biopsies were halved and immediately stored in either 10% (v/v) formalin buffer solution (Sigma-Aldrich, UK) for 24 hours at 4°C before processing or incubated in RNA stabilisation solution (RNAlater®, ThermoFisher Scientific, UK) for 24 hours before embedding in optimum cutting temperature (OCT) embedding matrix (CellPath, UK) and storage at -80°C. Only those samples that were frozen were used for the laser capture microdissection. In cases where the keloid tissue was fully excised it was collected in fully supplemented Dulbecco's Modified Essential Medium (DMEM) (Sigma-Aldrich, UK) so that the



final concentrations were: 10% (v/v) fetal bovine serum (FBS), L-glutamine (10 $\mu$ M) and penicillin (100 $\mu$ g/ml)/streptomycin (100 U/ml) (Sigma-Aldrich, UK). This tissue was processed for cell culture within 12 hours wherever possible. Normal skin samples were harvested following routine elective surgery and all biopsies and tissue were treated as for keloid.

### **3.4 Laser Capture Microdissection (LCM)**

#### **3.4.1 Cryosection and staining**

Following 24 hours in RNA stabilisation solution (RNA $later^{\circ}$ , ThermoFisher Scientific, UK) tissue samples were embedded in OCT (CellPath, UK) using a cryomould in an RNase-free class II safety cabinet. The specimens were then stored at -80°C until ready to be sectioned in the cryostat (Leica CM3050S). Mounted on an OCT-laden chuck, the tissue was sectioned onto nuclease free polyethylene naphthalate (PEN) membrane slides (Carl Zeiss) at 8 $\mu$ m thickness. These slides were kept on dry ice until safely stored at -80°C. In order to preserve the RNA integrity the slides were stained immediately prior to capture using cresyl violet (Ambion, ThermoFisher Scientific, UK) in an RNase-free class II safety cabinet [1]. The slides were taken from frozen and placed into successive slide chambers using the following rapid staining protocol and kit (LCM staining kit, ThermoFisher Scientific):

1. 95% (v/v) ethanol (40 seconds)
2. 75% (v/v) ethanol (30 seconds)
3. 50% (v/v) ethanol (30 seconds)
4. 1 minute in 300 $\mu$ l cresyl violet (Ambion, UK)
5. 50%(v/v) ethanol (30 seconds)
6. 75% (v/v) ethanol (30 seconds)
7. 95% (v/v) ethanol (30 seconds)
8. 100% ethanol twice for one minute each.

### 3.4.2 Laser Microdissection (*Figure 3.1*)

Laser microdissection is a technique employed to isolate single cells or cell subpopulations from within frozen, embedded or fresh tissue through the use of a microscope coupled to a high-precision laser. As previously discussed in the literature review, there are two main types of laser microdissection. For work on this project the Carl Zeiss P.A.L.M MicroBeam LCM 4.2 (Carl Zeiss, Germany) fitted with an inverse microscope Axiovert 200 resp. 200M, was used [2]. This consists of a frequency tripled solid-state laser (FTSS) ( $\lambda=355\text{nm}$ ) accompanied by an epifluorescent path into a microscope and focussed through an objective. Depending on the objective the laser focus can be narrowed to less than  $1\mu\text{m}$ , allowing for precision cutting of the specimen and ultra-selectivity from within a heterogeneous environment. The slide is placed on a motorised computer-controlled stage facilitating flexibility and rapidity of movement. The tissue section, adherent to the  $1.35\mu\text{m}$  PEN membrane on the slide (avoids static and protects specimen from UV damage) (Carl, Zeiss), is viewed under the microscope or on screen and the required area for harvest chosen. This selected trajectory, or *element*, is cut out and separated from the sample. The Zeiss P.A.L.M. uses “catapult” technology for the acquisition of desired cells, a technique known as Laser Micro-dissection Pressure Catapulting (LMPC). This catapulting is thought to be initially driven by linear absorption (thermal ablation) and then mediated by plasma formation through focussed UV-A pulses [3]. The nonlinear absorption (plasma formation) accelerates the specimen, against inertia and hydrodynamic drag, to speeds of up to  $300\text{m/s}$  within 200 nanoseconds whereupon it is slowed by air friction and captured in a microfuge tube cap in what is a non-contact system, avoiding contamination by adjacent cells.

### 3.4.3 Laser Microdissection Pressure Catapulting

The slide was mounted onto the movable stage and the caps loaded into the cap holder ready for use. Using both the microscope and the computer software (P.A.L.M. RoboSoftware, Carl Zeiss) the desired tissue section areas were highlighted by either free hand drawing or

employing available fixed shapes (circle or square) and the RoboLPC selection made from the menu. This functions to automatically cut out and subsequently catapult the selected elements sequentially into the chosen microfuge tube cap. Images were taken both before and after each element was cut and catapulted. To further confirm the capture of each specimen the tube cap can be checked afterwards and the individual elements seen and counted if so wished.

The captured elements were mixed with 350µl lysis buffer, RLT (Qiagen, UK) mixed with 2-mercaptoethanol (Sigma-Aldrich, UK) in a ratio of 100:1, and the microtube briefly vortexed and inverted to immerse the elements in the cap (30 minutes) (**Figure 3.1**). This was then either stored at -80°C or immediately RNA extracted. Collection times were limited to a maximum of 60-90 minutes, as studies suggest RNA degradation starts after this point [4].

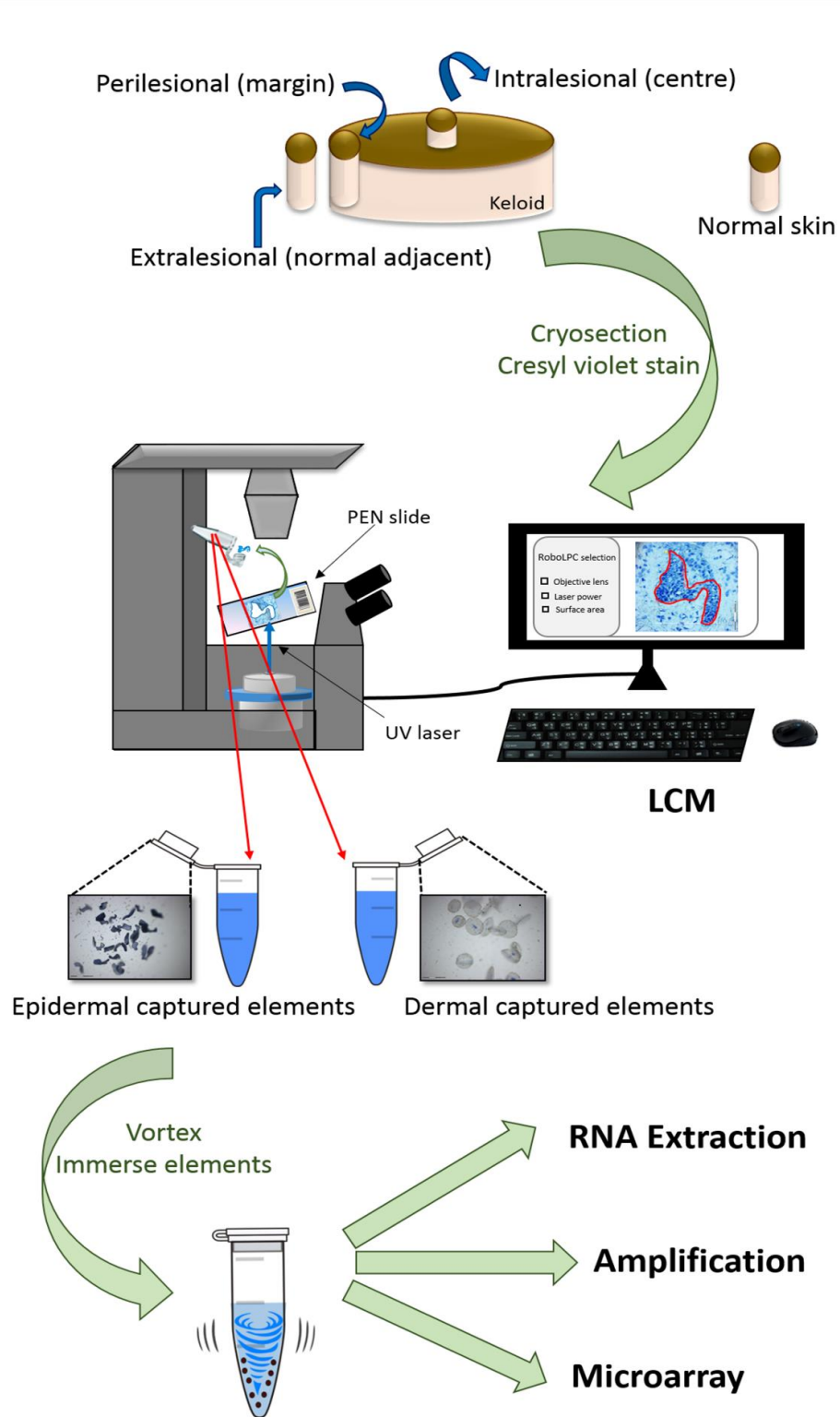


**Figure 3.1 Flow of Laser Capture Microdissection (LCM) process from normal skin and site-specific keloid biopsy to microarray.**

### 3.5 Gene expression experiments

#### 3.5.1 mRNA extraction from tissue, cells and laser captured material

##### Tissue

This took place in an RNase-free class II safety cabinet. The tissue sample was put in a 2ml round bottom Eppendorf containing trizol (ThermoFisher Scientific, UK) with a sterile ball bearing and homogenised in a Qiagen tissue lyser for three four-minute cycles of 30 oscillations per second. Chloroform, at 0.2ml per 1ml of trizol, was added to the tube and shaken vigorously for 15 seconds before centrifugation at  $>10,000 \times g$  for 15 minutes. The upper aqueous layer, which contains the RNA, was pipetted off the surface and transferred to a new Eppendorf. An equal volume (1:1) of 70% (v/v) ethanol was added to the RNA and mixed using a pipette. This mixture was then transferred to an RNeasy mini spin column (RNeasy Mini kit, Qiagen, UK) and centrifuged at  $>10,000 \times g$  for 30 seconds. Elute was discarded from the collection tube, 700 $\mu$ l of buffer RW1 added to the spin column and centrifugation repeated. Following this a new collection tube was used for three cycles of 500 $\mu$ l buffer RPE at  $> 10,000 \times g$  for 30 seconds, 30 seconds and two minutes respectively. A one-minute dry cycle spin was conducted and the spin column transferred to a new tube for the collection of the RNA yield. 30 $\mu$ l of RNase-free water was added directly to the silica gel membrane and then centrifuged for one minute at  $>10,000 \times g$ . The yield was then quantified using a NanoDrop spectrophotometer (ThermoScientific, UK).

##### Monolayer cells

Either an RNeasy mini kit (Qiagen, UK) or an RNeasy micro kit (Qiagen, UK) was used depending on the expected RNA yield. The cells were trypsinised, pelleted and then re-suspended in lysis buffer (RLT: 2-mercaptoethanol, 100:1). The volume was dependent on number of cells present. An equal volume (1:1) of 70% (v/v) ethanol was added to each tube and mixed thoroughly by pipetting up and down. The mixture was then added to a Qiagen spin column and centrifuged at  $> 10,000 \times g$  for 30 seconds. The flow-through was discarded, 350 $\mu$ l of buffer RW1 added and

centrifugation repeated. An intervening DNase step was performed with 80µl incubation over 15 minutes at room temperature. A further 350µl of RW1 was added and centrifugation repeated. Following this a new collection tube was used for three cycles of 500µl buffer RPE at > 10,000 x g for 30 seconds, 30 seconds and two minutes respectively. A one minute dry cycle spin was conducted and the spin column transferred to a new tube for the collection of the RNA yield. 30µl of RNase-free water was added directly to the silica gel membrane and then centrifuged for one minute at >10,000 x g. The yield was the quantified using a NanoDrop spectrophotometer (ThermoScientific, UK).

In some cases trizol was used to extract RNA from monolayer cells. In this case the Trizol (ThermoFisher Scientific, UK) was applied directly to the cells and left to incubate at room temperature for 5 minutes prior to using a cell scraper to remove the cells and collect in a microtube. Chloroform was added to the tube and the procedure continued as is described above for tissue.

#### Laser captured elements

Due to the predicted low yield, the RNeasy Micro kit (Qiagen, UK) was used and performed as previously described [5].

An equal (1:1) volume of 70% (v/v) ethanol was added to the lysis buffer and mixed well by pipetting. This 700µl mixture was then transferred to a mini-column and centrifuged at >10,000 x g for 30 seconds. Elute was then discarded and 350µl of buffer RW1 added to the spin column and centrifugation repeated. Following transfer to a new collection tube an intervening DNase step was performed with 80µl incubation over 15 minutes at room temperature. A further 350µl of RW1 was added and centrifugation repeated. One wash with 500µl buffer RPE followed by a wash with 500µl freshly made 80% ethanol were conducted with centrifugations of 30 seconds and two minutes respectively, using a new collection tube each time. Following a dry spin of

one minute, 15µl of RNase-free water was added to the silica-gel membrane of the spin column in order to elute the bound RNA. This was collected in a new Eppendorf and the yielded RNA kept on ice whilst performing quantification using NanoDrop spectrophotometer (ThermoScientific, UK).

### **3.5.2 Measurement of RNA concentration and integrity**

#### Concentration

The concentration of extracted RNA was measured using the ThermoScientific NanoDrop 2000 UV-vis microvolume spectrophotometer. This is used to ascertain the concentration and purity ratios (260/280 and 260/230) of nucleic acids and protein. Using a modified Beer Lambert equation ( $c = (A \cdot \epsilon) / b$ ) the NanoDrop requires minimal volumes of RNA for analysis (1-1.5µl). I used the NanoDrop 2000 to quantify all of my RNA samples, although the accuracy of the concentration of RNA below 20ng/µl is questionable and therefore less relevant in cases of laser captured material. Gauging the concentration allowed selection of the appropriate lab chip for the integrity assessment on the Agilent Bioanalyser. The extraction protocol was altered to improve the purity ratios, known to be affected by other molecules absorbed at the 260nm wavelength including residual salts (phenol, guanidine), carbohydrates and protein. Acceptable values for RNA purity ratios included:

260/280: 1.8 - 2.0

260/230: 1.8 - 2.2

#### Integrity

All of the samples were further analysed using the Agilent 2100 Bioanalyser to measure the integrity of the RNA. Based on the principles of electrophoresis and flow cytometry the charged biomolecules (in this case RNA) are driven through a gel-dye complex, past a laser detector and

along a voltage gradient, thereby being separated by size. Using an external standard (ladder) for comparison and a marker to compensate for drift effect, 1 $\mu$ l of each sample was heat denatured at 70°C for two minutes, pipetted into a well-based chip and loaded into the machine. The RNA 600 Nano Labchip kit (Agilent Technologies, UK) was used for concentrations of 5ng/ $\mu$ l or greater and the Pico Labchip (Agilent Technologies, UK) for concentrations down to 200pg/ $\mu$ l. The data for total eukaryote RNA is presented as an electropherogram with two distinct ribosomal peaks, the 18s and 28s.

RIN (RNA Integrity number): This number reflects the level of RNA degradation of a given sample. It takes the entire electrophoretic trace into account and gives a number between 1 and 10, based on how intact the RNA is. This number is used for comparative purposes, extraction process or sample preservation methods, quantitative assessment for downstream analysis, be it microarray or qRT-PCR, and confers reproducibility.

One of the difficulties encountered in LCM is maintenance of the RNA integrity of each sample throughout the entire process. For this PhD, each step of the LCM procedure (preservation method, staining method, LCM protocol and extraction method) was optimised using the RIN. Although a higher RIN (~ 7-8) is considered desirable for downstream genomic studies, it cannot predict the usefulness of the sample for gene expression data. The bioanalyser is unable to differentiate ribosomal RNA from other RNA and therefore the quality index may be underestimated. Several studies have used FFPE samples, well known to be highly degraded, and yielded good quality data from RIN as low as 1.4 [6-8]. Although the RIN of the samples used in this project ranged from 2 to 8.6 for the laser-captured samples, of which some are represented in **Figure 3.2**, those with the higher RIN from these samples were chosen for microarray. This is compared with cell culture or whole tissue samples, which consistently had RIN of 8-10.



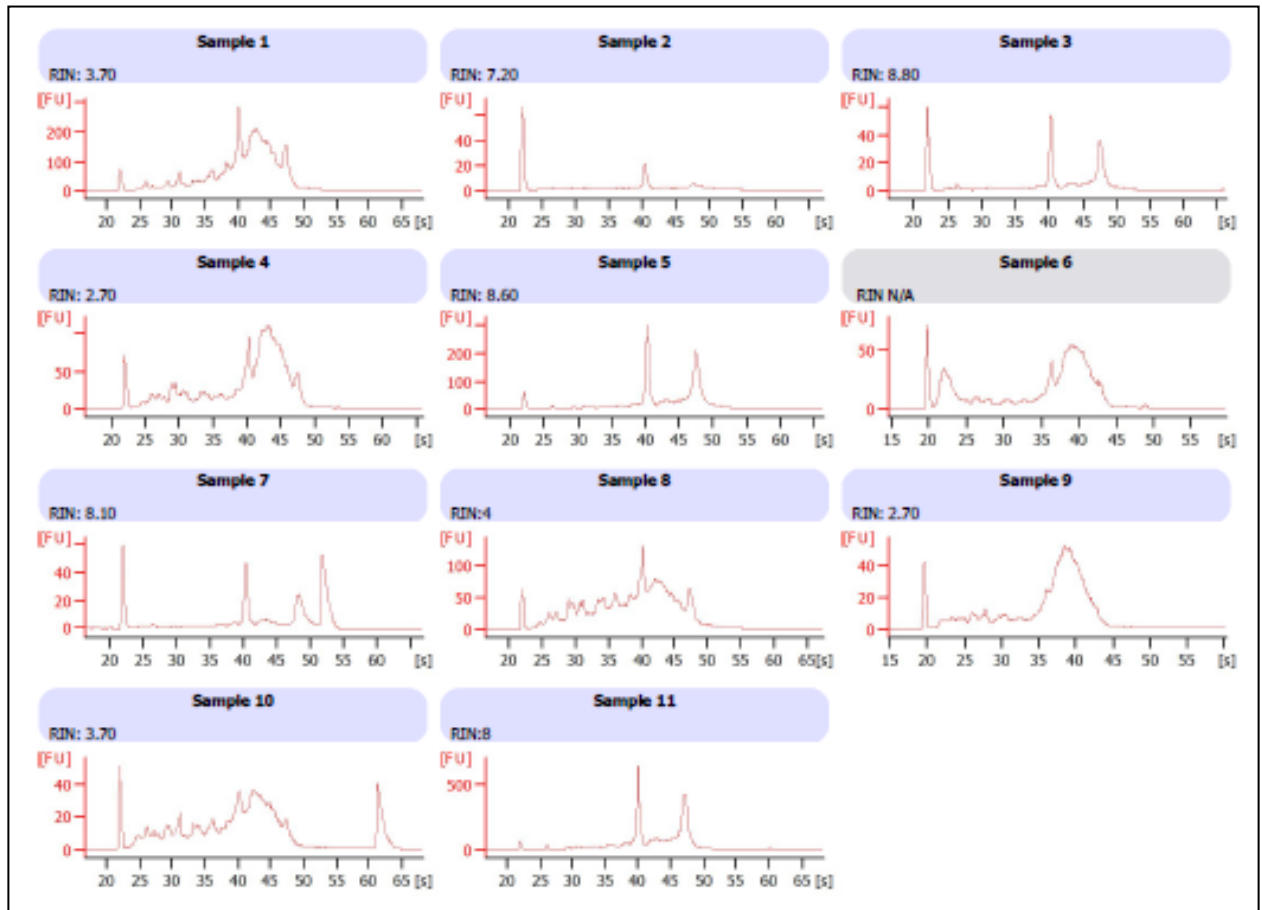


**Figure 3.2** Representation electropherograms for laser-captured samples showing the range of quality between intact and degraded samples.

### 3.5.3 cDNA synthesis

Total RNA concentration was estimated and normalised for all samples and cDNA synthesis was performed using qScript™ cDNA SuperMix (Quanta Biosciences, MD, UK), according to the manufacturer's protocol and as previously described [6]. Briefly, 16µl normalised RNA was added to 4µl qScript™ to give a total of 20µl for each reaction. The 96-well plate was centrifuged to collect the reaction mix at the bottom and the incubated: 5 minutes at 25°C, 60 minutes at 42°C and 5 minutes at 85°C. Synthesised cDNA was stored at 4°C until quantitative real-time polymerase chain reaction was performed.

### 3.5.4 Primer design and quantitative real-time polymerase chain reaction (qRT-PCR)

Specific primers for targeted analysis were designed for each gene. The primer sequences for each gene used are detailed in the supplementary data of the results chapter in which the analysis was conducted. The sequences for all genes were sourced from the National Centre for Biotechnology Information (NCBI: <http://www.ncbi.nlm.nih.gov/>). The FASTA sequence was then imported into the Roche Universal Probe Library Assay Design Centre (<https://lifescience.roche.com/>) to design the specific primer sequences. The criteria to select the most appropriate primer included: approximately 50% GC content, melting temperature 58-60°C and 15-30 base pairs in length. Final versions of the primer sets were submitted to Sigma-Aldrich.

Quantitative polymerase chain reactions were done in real time using the LightCycler®480 II platform (Roche Diagnostics, UK), as previously described [9]. Each reaction was carried out in a 96-well plate with a final volume of 10µl containing 4µl diluted normalised cDNA, 5µl LightCycler®480 probes master mix (Roche, UK), 0.2µM forward and reverse primers, 0.1µl probe from Roche Universal Probe Library and 0.5µl nuclease-free water (Qiagen, UK). Each reaction was performed in triplicate and 2 housekeeping genes were used to allow relative quantification (GAPDH and RPL32). The cycle initiated at 95°C for 10 minutes to activate the Hot-Start Taq polymerase and then each of the 40 amplification cycles consisted of a 10 second denaturation step at 95°C followed by a 30 second annealing and elongations step at 60°C and finally a cooling step at 40°C. The fluorescence intensity was recorded prior to the cooling step. The amplified targets were analysed using the LightCycler®480 II software (1.5.0 SP3, Roche, UK).

### 3.5.5 RNA amplification and purification

Laser capture microdissection produces very small quantities of RNA so in order to have sufficient samples for microarray, whole transcriptome amplification was performed. The instructions from Ovation® Pico WTA system v2 kit (NuGen Technologies) were adhered to exactly for RNA amplification and cDNA synthesis. In brief, samples were diluted to ensure concentrations were between 500pg and 50ng using RNase-free water (NuGen, UK). For primer annealing, 5µl of RNA from each sample was heated to 65°C for two minutes. Then for first strand cDNA synthesis the sample was added to the first strand buffer and enzyme mix (mixture of random and oligodT primers) before placing in a pre-cooled thermal cycler and put through: 4°C – 2min, 25°C – 30min, 42°C – 15min, 70°C – 15min and returned to 4°C. The resulting sample was mixed with second strand buffer and enzyme mix (cDNA) to synthesise the second strand and placed in a thermal cycler: 4°C – 1min, 25°C – 10min, 50°C – 30min, 80°C – 20min and returned to 4°C. The resultant cDNA clean-up was then performed using a bead purification process (Agencourt® RNAClean® XP Purification Beads) prior to amplification. This was achieved using a magnet block and several 70% ethanol washes. The SPIA™ (single primer isothermal amplification) step elutes the cDNA from the beads using a DNA polymerase and RNase H in an isothermal assay put through thermal cycling: 4°C – 1min, 47°C – 75min, 95°C – 5min, return to 4°C.

The final 100µl volume was then purified using QIAquick PCR purification kit (Qiagen, UK) according to manufacturer's instructions. Briefly, 500µl buffer PB was added to the entire 100µl SPIA elute, vortexed and centrifuged before placing in a QIAquick spin column. Half of the mix was placed into the column and centrifuged for 1 minute at 17,900 X g, the flow-through discarded and the second half treated the same. 700µl of freshly made 80% ethanol was added to the column and centrifuged at 17,900 X g for 1 minute before discarding the flow-through. This was repeated and then the column centrifuged for 2 minutes at 17,900 X g. The column

was added to a new Eppendorf and 30µl room temperature nuclease-free water dispensed onto the membrane. It was left to stand for 5 minutes and then centrifuged for 1 minute at 17,900 X g. The resultant elute was measured with NanoDrop (ThermoScientific, UK) using ssDNA setting. All of the RNA was successfully amplified with acceptable purity ratios. This was then stored at -20°C.

### 3.5.6 Microarray

This was done using SureTag DNA Labeling Kit, which forms part of Agilent Whole Genome (8 x 60K) Oligo Microarrays (Agilent Technologies, UK) containing 50,599 probes and is a one-colour microarray-based gene expression analysis. The successful combination of these protocols has been previously demonstrated [10-12].

Each sample was diluted to contain 1.8µg of cDNA in a final volume of 26µl. 5µl of random primer was added to the sample and incubated for 5 minutes at 95°C. They were then placed immediately in ice for 5 minutes and spun down in a centrifuge at 6000 x g for 1 minute. The cyanine 3 labeling master mix was prepared by mixing the sample with appropriate volumes of reaction buffer (10µl per reaction), 10 x dNTPs (5µl per reaction), cyanine 3-dUTP (3µl per reaction) and Exo (-) Klenow (1µl per reaction). This mix was then incubated at 37°C for 2 hours after which the samples were transferred to 65°C for 10 minutes to inactivate the enzyme. Samples were incubated on ice for 3 minutes and then centrifuged at 6000 x g for 1 minute.

The cDNA was purified following Cy3 labeling. 430µl of 1xTE (pH 8.0) was added to each sample in a purification column and spun for 10 minutes at 14,000 x g at room temperature. The flow-through was discarded and a further 480µl of 1xTE added and again centrifuged at 14,000 x g for 10 minutes. The flow-through was discarded and the tube inverted into an Eppendorf and spun for 1 minute at 1,000 x g. The labelled cDNA sample was concentrated to dryness using a vacuum concentrator and re-suspended in 21.5µl of 1xTE buffer. At this stage 1.5µl was placed in the NanoDrop (ThermoScientific, UK) to calculate the degree of labeling.

The labelled cDNA was prepared for hybridization by adding 10 x Gene Expression Blocking Agent (5µl per reaction) and 2 x Hi-RPM Hybridisation Buffer (25µl per reaction) then incubating at 95°C for 3 minutes before placing on ice. The samples were centrifuged briefly and 40µl of each sample was loaded onto a window of the 8-sample slide (SurePrint G3 Human GE 8x60K V2). The slides were hybridised at 65°C for 17 hours at 20 RPM before undergoing wash steps and storage in a cool dry ozone-free light-protected place. The slides were then scanned (Agilent DNA Microarray Scanner G2505c) and the data analysed following quantile normalisation. Analysis is described in detail in **chapter 4**.

### **3.6 Histochemistry & Immunopathology**

#### **3.6.1 Paraffin embedding of formalin-fixed tissue (FFPE)**

This was performed using a Leica automated tissue processor (Leica 1020, Leica Biosystems, UK) under the following conditions: 70% ethanol for 2hrs, 90% ethanol 2hrs, 5 further steps 100% ethanol each for 2hrs, 3 xylene steps for 1hr each and two final immersion steps in wax at 2hrs each. The tissue was then embedded in paraffin blocks and stored at room temperature. Prior to sectioning (microtome: Leica, UK) the blocks were cooled. 5µm sections were cut, placed in a 52°C water bath and collected on electrostatically charged Superfrost Plus slides (ThermoFisher Scientific, UK). Slides were dried on a rack at 65°C then placed onto a hot plate at 60°C overnight to fix the sections to the slides. Slides were then stored at room temperature until use.

#### **3.6.2 De-waxing and rehydration of FFPE tissue sections**

Slides were de-waxed with two ten-minute cycles of heated xylene followed by a further two five-minute room temperature xylene incubations. The slides were hydrated through sequential steps of an ethanol gradient (100% x 3, 95%, 90%, 80%, 70% and 50% (v/v) ethanol) and two changes of distilled water prior to staining/antigen retrieval.

### **3.6.3 Haematoxylin and eosin (H&E) staining**

Haematoxylin and eosin (H&E) staining highlights the contrast between the nuclei, stained purple with haematoxylin (Sigma-Aldrich, UK) and the cytoplasm/connective tissue counterstained pink with eosin (Sigma-Aldrich, UK), which binds to positively charged proteins. Harris haematoxylin, a progressive stain, was used in this staining protocol. Sections were de-waxed and rehydrated as described. The slides were immersed in filtered haematoxylin for four minutes, rinsed with running water to remove excess stain and then submerged for one minute in filtered eosin to counter stain and then again rinsed in distilled water. The slides were then dehydrated using an incremental ethanol gradient of 70%, 85%, 90% and absolute (v/v) solutions. Two final ten-minute steps of xylene were followed by mounting with non-aqueous Shandon Consul-Mount (ThermoScientific, UK) and glass cover slips (22 x 64mm) for microscopic analysis.

### **3.6.4 Herovici staining**

This stain differentiates collagen I (red-stained) from collagen III (blue-stained) as well as selectively stained nuclei. De-waxed and hydrated slides were incubated in a solution containing ferric chloride and haematoxylin for 15 minutes then washed for 1 minute in running water. Slides were then incubated in a solution containing van Gieson (Sigma-Aldrich, UK) and methyl blue for 5 minutes before dipping in 1% acetic acid. Slides were dehydrated in 3 sets of 100% ethanol followed by 4 x 5 minute xylene steps and then mounted.

### **3.6.5 Peroxidase immunohistochemistry (IHC) protocol**

This was performed as previously described [13]. Slides were de-waxed and hydrated prior to antigen retrieval. Antigen retrieval was performed as indicated for each antibody, which are separately discussed in the results chapter in which they feature, along with the associated incubation parameter details. The predominant antigen retrieval method was citrate pH 6.0 in

a heated water bath, either 1 hour at 65°C or 20 minutes at 90°C. Following this the slides were washed in TBS (Tris buffered solution) before blocking. For immunohistochemistry the Novolink® polymer detection kit (Leica Biosystems, UK) was used from this point forward. This included endogenous peroxidase block 30 minutes, protein block 45 minutes, primary antibody (diluent 1% BSA or Odyssey® (LI-COR, UK) blocking buffer) incubation 1hour at room temperature or overnight at 4°C, post primary block 30 minutes and Novolink® polymer incubation 30 minutes. Prior to the primary antibody TBS was used for washes and afterward TBS with 0.1% Tween®20 (ThermoFisher Scientific, UK). After this, sections were incubated with Vector® NovaRED™ substrate kit (Vector, CA, USA), which allowed differentiation from melanin staining in pigmented skin. Sections were counterstained with haematoxylin (Sigma-Aldrich, UK), rinsed in water and placed on a heat block at 55°C for 10 minutes to dry. They were then dipped in xylene twice for 2 minutes each and cover-slipped.

### **3.6.6 Immunofluorescence protocol**

Slides were de-waxed and hydrated prior to antigen retrieval. Similar to IHC the antibody-specific retrieval method and incubation parameters are detailed in the results chapter in which they feature. For immunofluorescence staining, protein block using either Odyssey® blocking buffer (LI-COR, UK) or 10%human/10% donkey serum (Sigma-Aldrich, UK) was done at room temperature for 1 hour following antigen retrieval. The primary antibodies were treated the same as above as were the wash steps. All steps involving secondary antibody were conducted in darkness. Sections were incubated in Alexa Fluor®-conjugated secondary antibodies (ThermoFisher Scientific, UK) for one hour at room temperature. 4',6-diamidino-2-phenylindole (DAPI; ThermoFisher Scientific, UK) 1/500 was applied for 15 minutes before washing and mounting using hard-set Prolong® Gold reagent (ThermoFisher Scientific, UK).

### **3.6.7 Immunocytochemistry protocol**

This is discussed in the specialised culture experiments (**section 3.8.3**).

### **3.6.8 Rapid staining LCM protocol**

This is discussed under laser capture microdissection (**section 3.4.1**).

### **3.6.9 Wide-field microscopy and image capture**

All histology was imaged using either a phase contrast microscope (Olympus BX51, Olympus, UK) analysed by MetaVue Software (Molecular Devices) and ImageJ (Fiji, 1.47t, NIH, USA) or scanned using a digital slide scanner (Panoramic 250 Flash III (3DHISTECH, Hungary)).

## **3.7 Cell culture methodology**

All tissue culture methods and techniques were conducted in a class II safety cabinet. Tissue was collected and transported at 4°C in sterile 50ml tubes (Falcon, UK) containing DMEM supplemented with heat-inactivated filtered FBS, L-glutamine and penicillin/streptomycin (referred to in methods as complete DMEM). Complete serum-free keratinocyte medium (SFKM) was used to maintain keratinocytes following dispase incubation. Complete SFKM (ThermoFisher Scientific, UK) was supplemented with Human Keratinocyte Growth Supplements (HKGS; ThermoFisher Scientific, UK), which consisted of: bovine insulin (5µg/ml), bovine transferrin (5µg/ml), human epidermal growth factor (0.2ng/ml), hydrocortisone (0.18µg/ml), bovine pituitary extract (0.2% v/v) and gentamicin (100U/ml). It was processed immediately on arrival at the laboratory. The methods detailed here represent the optimised protocols to yield maximal viable cell culture.



### 3.7.1 Establishment of primary keloid and normal skin keratinocytes

Tissue samples were washed first in PBS containing penicillin/streptomycin (Sigma-Aldrich, UK) then cut into narrow strips approximately 1mm wide and 2cm long. This tissue was placed in a sterile falcon tube containing Dispase II ( $2.4\text{Uml}^{-1}$ ; Roche Diagnostics, UK) and incubated overnight in a  $37^{\circ}\text{C}$  water bath. Following incubation the epidermis was carefully separated from the dermis using a sterile scalpel and forceps. The epidermal strips were diced and carefully placed in TrypLE™Express (ThermoFisher Scientific, UK) with complete SFKM for one hour in the water bath, with intermittent vigorous shaking to release the cells until the suspension was murky. Trypsin neutralising solution (ThermoFisher Scientific, UK), equal in amount to the trypsin, was added and the cell-solution mixture and centrifuged at 1300 rpm for 8 minutes. The supernatant was discarded and the cells re-suspended in complete defined SFKM using gentle, repeated pipetting to ensure a homogenised cell suspension. This was then seeded into T25 collagen1-coated or CellBind (Corning, UK) culture flasks containing 4mls of complete SFKM. The flasks were then incubated (temperature  $37^{\circ}\text{C}$ ,  $\text{CO}_2$  5% and 95% humidity) undisturbed for 48 hours. Following this the cell culture media was changed every 48 hours until 70-80% confluent. Only keratinocytes from passage 1-4 were used in all experiments. All references to keratinocytes from this point forward refer to primary human keratinocytes

### 3.7.2 Establishment of primary keloid and normal skin fibroblasts

Following removal of the epidermis the remaining dermal portion of the skin was minced into pieces approximately  $1\text{mm}^3$  in size. As previously described [14, 15], these were transferred to a sterile falcon tube containing Collagenase A ( $2.5\text{mg/ml}$ ; Roche Diagnostics, UK) and complete DMEM, which was left to incubate in the water bath at  $37^{\circ}\text{C}$  for approx. three hours. Alternatively the original tissue sample was halved, one portion used for the extraction of keratinocytes and the other for fibroblasts. In this case the  $1\text{mm}^3$  fragments were either incubated for 3-4 hours in the  $37^{\circ}\text{C}$  water bath or left overnight at  $4^{\circ}$  and re-warmed the next

morning for one hour in the water bath. Following this the tissue was vigorously pipetted to release the cells and subsequently centrifuged at 1800 rpm for 10 minutes. The supernatant was then discarded and the cells re-suspended in complete DMEM and seeded into T25 flasks containing 5mls of sterile medium. The cell culture medium was changed every 48-72 hours until the cells reached 80% confluence (temperature 37°C, CO<sub>2</sub> 5% and 95% humidity). All fibroblasts from this point forward refer to primary human fibroblasts.

### **3.7.3 Cryopreservation of cultured cells**

Cells were washed in phosphate buffered saline (PBS; Sigma-Aldrich, UK), trypsinised, pelleted and re-suspended in 1ml of cryopreservation medium. For keratinocytes the cryopreservation medium contained: 70% complete SFKM, 20% FBS and 10% dimethyl sulfoxide (DMSO: Sigma-Aldrich, UK). For fibroblasts the cryopreservation medium contained: 80% FBS, 10% complete DMEM and 10% DMSO. The cryovials were placed in a freezing container (Nalgene®, Sigma-Aldrich, UK) filled with isopropyl alcohol and stored at -80°C for 24 hours to facilitate controlled cooling of the cells and prevent ice crystal formation. Following this, the vials were transferred to the liquid nitrogen container until required.

### **3.7.4 Revival of cryopreserved cells**

The cryovial was retrieved from the liquid nitrogen and immediately placed in a 37°C water bath until the pellet was freed from the bottom of the vial. With speed, the vial was emptied into a sterile 15ml tube and the appropriate medium added drop-wise until the pellet was dissolved. The cells were then centrifuged (fibroblasts at 1800rpm, keratinocytes at 1200rpm) for ten minutes and the supernatant discarded. This is important so as to rid the cell environment of DMSO, a chemical toxic to their viability. The cells were re-suspended in the appropriate medium and then added to sterile or collagen-coated T25 flasks (already containing sterile

complete medium) and stored in the incubator (temperature 37°C, CO<sub>2</sub> 5% and 95% humidity).

There is an expected cell loss of approximately 20% following thawing.

### 3.7.5 Estimation of cell viability and cell number – trypan blue dye exclusion method

This method uses a blue dye that cannot cross an intact cell membrane, relying on the principle that a dead cell has a disrupted membrane thereby staining blue. 10µl of trypan blue dye was thoroughly mixed with 90µl of cell suspension in a sterile Eppendorf tube. This solution was then loaded into an improved Neubauer counting chamber. Viable cells were counted using an inverted microscope, with all 25 squares of both chambers counted. To estimate viable cell number the following calculation was used:

$$\text{Number cells per ml} = \frac{\text{Number cells counted} \times 25 \times 10^4}{\text{Number squares counted}} \times \text{original dilution}$$

Where the number of squares counted = 25 and the total number of squares = 25.

For some experiments an alternative method of cell counting was employed. In these cases the handheld automatic cell counter (Scepter 2.0, Merck Millipore, MA USA) was used.

### 3.7.6 MTT cell viability colorimetric assay

The MTT proliferation assay kit (Roche, UK) is based on the principle that the yellow tetrazolium salt (3-[4, 5-dimethylthiazol-2-yl]-2, 5-diphenyltetrazolium bromide) is cleaved to insoluble purple formazan crystals by metabolically active cells. These formazan crystals are solubilised and the resultant coloured solution can be quantified using a spectrophotometer to measure absorbance. In the case of fibroblasts, the cells were maintained in synchronisation medium (serum-free complete DMEM) for up to 16 hours prior to performing the assay, as previously described [16].

To perform the assay the cells were pelleted and re-suspended in 5mls of medium. The required number of cells (number of wells x number of time points x 5,000 cells per well) was added to a 15ml tube. The remainder was made up with complete media, on the basis that 200µl needed per well in a 96-well plate. Once complete, the plates were kept in the incubator until the appropriate time point (24hrs, 48hrs, 72hrs, 96hrs, 1week and 2weeks). Prior to each assay the medium from the wells was aspirated and kept for an LDH assay. This was stored at -80°C.

After aspiration of the 200µl medium in each well it was replaced with 100µl fresh complete medium (containing 10% (v/v) FBS in the case of fibroblasts) and 10µl of MTT reagent. The plate was then incubated for 4 hours (temperature 37°C, CO<sub>2</sub> 5% and 95% humidity) after which time 100µl solubilisation reagent was added to the wells and the plate left to incubate overnight (temperature 37°C, CO<sub>2</sub> 5% and 95% humidity). The next day 100µl of the reaction mix was transferred to wells in a new 96-well plate to read the absorbance on a spectrophotometer at 550nm wavelength, with a background reference of 690nm (FLUOstar Optima, BMG Labtech). All samples were prepared in triplicate.

In the case of keloid and normal skin fibroblasts treated with siRNA and/or rhNRG1, 5 x 10<sup>3</sup> cells were seeded into 96-well plate. The next day cells were transfected with either ErbB2 or control siRNA (**section 3.8.7**) in serum-free Opti-MEM® (ThermoFisher Scientific, UK). This medium was replaced 24 hours later with 50ng/ml rhNRG1 in serum-free Opti-MEM®. This was replaced with fresh rhNRG1 each day until harvested at the appropriate time-point for MTT.

### **3.8 Specialised culture experiments**

The methods presented here are the optimised protocols used to yield the results in the following chapters. This optimisation was performed by the author, Natalie Jumper.

### 3.8.1 Reconstitution of all-trans retinoic acid (atRA) & all-trans retinol (vitamin A)

For all experiments involving atRA and retinol the frozen aliquots from the following calculations were used and were kept in the dark:

atRA (Sigma-Aldrich 100mg) Molecular weight 300.4

*Stock solution*

100mg dissolved in 5ml 100% DMSO

$100/5 \times 300.4 = 0.0666M = 66,600\mu M$  (stored in aliquots at  $-20^{\circ}C$  light protected)

*Working solution 1 $\mu M$*

$10,000 \times 1,000/66,600 = 150.15\mu l$  aliquots

Therefore, 150.15 $\mu l$  atRA stock dissolved in 849.85 $\mu l$  culture medium = 10,000 $\mu M$

Using a dilution factor of 10, 10,000 $\mu M$  diluted four times to get 1 $\mu M$ .

atRA was made fresh from stock each time and always kept protected from light.

Retinol (Sigma-Aldrich 100mg) Molecular weight 286.5

*Stock solution*

100mg dissolved in 5ml 100% DMSO

$100/5 \times 286.5 = 0.0698M = 69,800\mu M$  (stored at  $-70^{\circ}C$  in light protected aliquots)

*Working solution 10 $\mu M$*

$10,000 \times 1,000/69,800 = 143.3\mu l$  aliquots

143.3 $\mu l$  stock dissolved in 856.7 $\mu l$  culture medium = 10,000 $\mu M$

Using a dilution factor of 10, 10,000 $\mu$ M diluted 3 times to get 10 $\mu$ M

Retinol was made fresh from stock each time and always kept protected from light.

### 3.8.2 Keratinocyte transfection

In advance the AKR1B10-containing plasmid (Origene TrueClone<sup>®</sup>, USA) was transformed into a DH5a E. coli strain to scale up and the purified DNA NanoDrop-checked (ThermoScientific, UK) for purity and gel-checked (performed by Protein Expression Research Facility, University of Manchester). Transfection was performed as per manufacturer's instructions (forward transfection) and has been previously applied in the literature [17, 18]. The day prior to transfection primary normal skin keratinocytes were seeded in complete SFKM at  $1 \times 10^6$  cells per well in a collagen-coated 6-well plate. This achieved a confluency of 80-90%, which is ideal for transfection using Turbofectin 8.0 (Origene, USA). Following an optimisation step, 3 $\mu$ g of the AKR1B10 cloned into pCMV6-XL5 vector (Origene TrueClone<sup>®</sup>, USA) was used per well. The Turbofectin 8.0 was added in a ratio of 1:2, at 6 $\mu$ l per well of a 6-well plate. To 100 $\mu$ l of serum-free Opti-MEM<sup>®</sup> (ThermoFisher Scientific, UK) 6 $\mu$ l of transfection reagent (Turbofectin 8.0) was added and incubated at room temperature for 5 minutes. The plasmid was then added and gently pipette-mixed before incubating at room temperature for 20 minutes. The medium in the 6-well plate was replaced with fresh complete SFKM and the transfection mixture added dropwise. The plate was gently rocked then left in the incubator (temperature 37°C, CO<sub>2</sub> 5% and 95% humidity) for 24 hours. For those keratinocytes used to determine the effect of AKR1B10 overexpression on the RA pathway and downstream conditioned media experiments, the medium was replaced with fresh complete SFKM at 24 hours for a further 24 hours. These cells were then harvested, under dimmed light, for western blot and qRT-PCR. Successful transfection was confirmed with western blot, qRT-PCR and immunocytochemistry (**Figure 3.2**).

### 3.8.3 Immunocytochemistry

For immunocytochemistry experiments,  $2.5 \times 10^4$  normal skin keratinocytes were seeded onto collagen-coated 24 well plates with coverslips placed in the bottom. Half of these keratinocytes for each patient were transfected with AKR1B10 as above and incubated for 24 hours. The medium was then removed and the cells washed with PBS prior to fixation with 4% formaldehyde for 30 minutes at room temperature. Cells were then permeabilised with 0.1% Triton X-100 (Sigma-Aldrich, UK) in PBS for 15 minutes and blocked in 10% human/10% donkey serum (Sigma-Aldrich, UK) in PBS for 1 hour at room temperature. The primary antibody was diluted in Odyssey® blocking buffer (LI-COR, UK) and left overnight at 4°C. The next day following washes the cells were incubated in Alexa Fluor®-conjugated secondary antibody (ThermoFisher Scientific, UK) for 1 hour at room temperature and then DAPI (ThermoFisher Scientific, UK) for 10 minutes. The coverslips were then reverse mounted onto slides and dried before storing in the dark at 4°C. Antibody-specific antigen retrieval and incubation parameters are detailed in the results chapter in which they feature. Images were captured using an Olympus IX71 inverted system microscope.

### 3.8.4 Dual Luciferase assay and analysis (*Figure 3.3*)

This protocol was optimised following a number of experimental combinations. The presented protocol here is based on the method with combined optimal GFP reading, qRT-PCR and western blot confirmation of transfection. Similar to the forward transfection, primary normal skin keratinocytes were seeded at  $5 \times 10^4$  cells per well of a 96-well opaque collagen-coated white plate (Corning, UK) the day before transfection. A clear 96-well plate was seeded simultaneously to allow assessment of cell confluence and viability following transfection.

The following day the transfection mixture was prepared as above. Per well of a 96 well plate 0.3µl of transfection reagent (Turbofectin 8.0 (Origene, USA)) was added to 5µl of Opti-MEM® and incubated for 5 minutes. 150ng/well of AKR1B10 plasmid (Origene TrueClone®, USA) was

added to this and incubated at room temperature for a further 20 minutes. The mixture was added to freshly replaced 150µl complete SFKM in half of the wells for each patient. This was incubated (temperature 37°C, CO<sub>2</sub> 5% and 95% humidity) for 24 hours. At 24 hours the medium was replaced with 125µl fresh complete SFKM and the RARE Cignal dual luciferase reporter (SABioscience, Qiagen, UK) transfected using Attractene transfection reagent (Qiagen, UK) as per manufacturer's instructions. For each patient half of the wells were AKR1B10 positive and half negative. Of these each had RARE reporter transfected into 4 wells, negative control into 2 wells and positive control into one well. Per well 25µl of Opti-MEM® was added to 0.6µl of Attractene and this was incubated for 5 minutes. 1µl of RARE reporter/negative control/positive control was then added and incubated for 20 minutes before being added to the appropriate well of the 96-well plate. This was incubated (temperature 37°C, CO<sub>2</sub> 5% and 95% humidity) for 6 hours and then the medium removed and replaced with 150µl fresh complete SFKM. After 24 hours the positive control well in the clear 96-well plate was checked for constitutive GFP fluorescence in the FITC channel of a phase contrast microscope (Olympus IX51 microscope; Olympus, UK). This confirmed transfection was successful and the luciferase activity measured. Additional controls included non-transfected (with either plasmid) cells and empty wells.

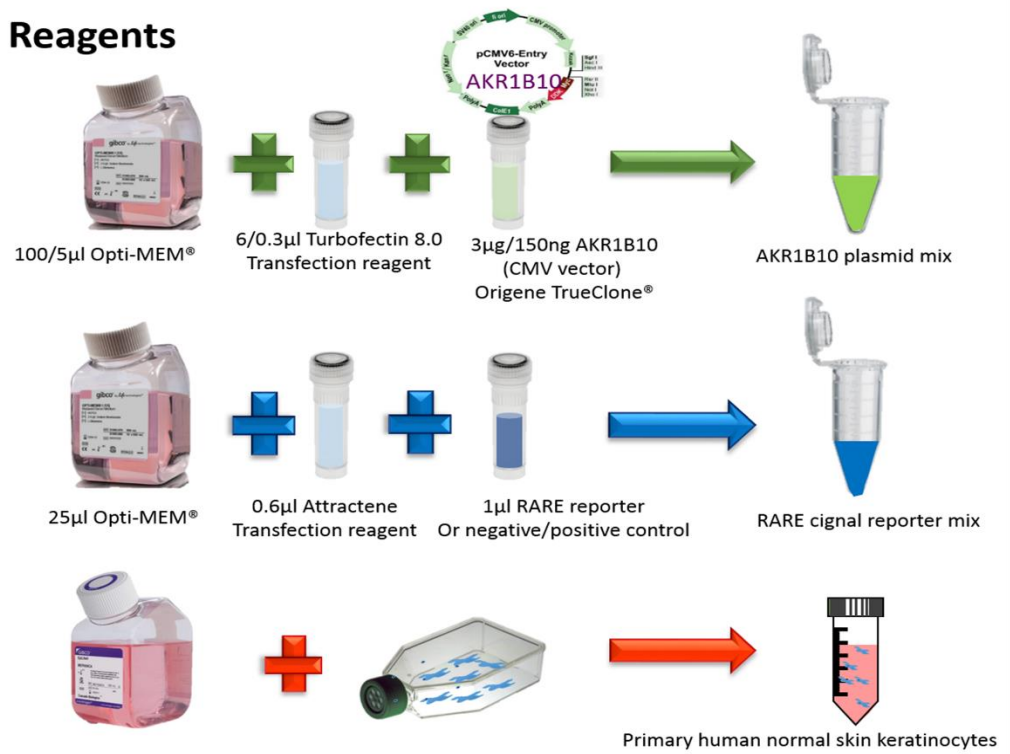
The medium was replaced with 75µl of SFKM and the Dual-Glo® Luciferase Assay System (Promega, UK) used to measure luciferase *firefly* and *Renilla* activity. An equal volume (75µl) of Dual-Glo® Reagent was added to each well and left for 15 minutes to allow cell lysis. The *firefly* luminescence was then measured. (FLUOstar Optima, BMG Labtech)). Immediately afterwards 75µl of Dual-Glo® Stop&Glo® was added to each well and left for 15 minutes before reading *Renilla* luminescence.

For analysis the *firefly* reading was divided by *Renilla* readings to normalise for cell number. This was done for both RARE reporter cells and also the negative controls. The relative luciferase activity (RLA) was then measured by dividing the normalised RARE reporter value by the corresponding negative control to give a fold change increase over control.

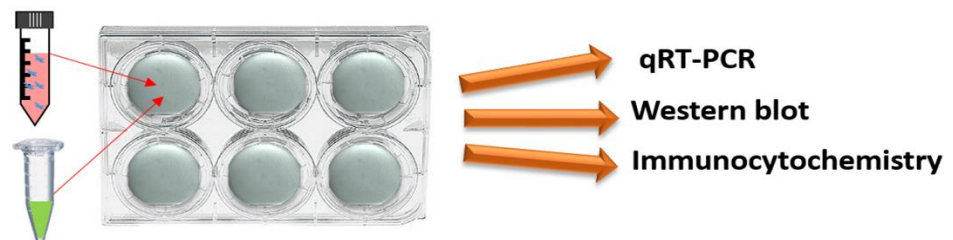


This assay was repeated on both transfected and non-transfected cells, which were then treated either 10 $\mu$ M all-*trans* retinol or 1 $\mu$ M all-*trans* retinoic acid in the place of complete SFKM for 24 hours before reading luminescence.

## Reagents



## AKR1B10 keratinocyte transfection



## Dual Luciferase assay

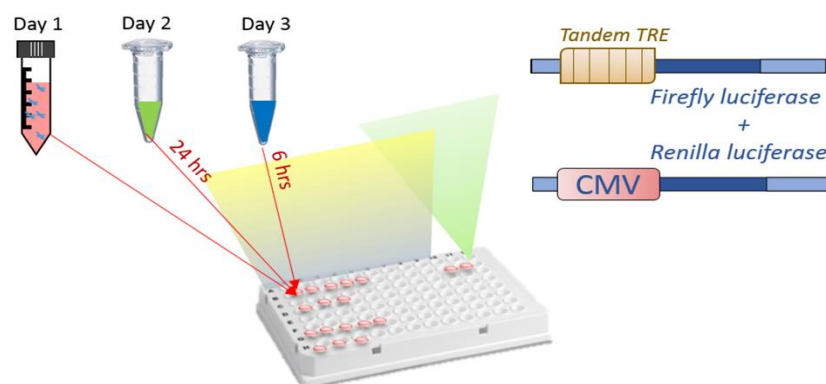


Figure 3.3 Reagent combinations and experimental workflow for keratinocyte transfection and dual luciferase assay.

### 3.8.5 Conditioned medium experiments

Normal skin keratinocytes were seeded into 6-well plates and forward transfected as described above. Both keloid and normal skin fibroblasts ( $3 \times 10^5$ ) were seeded into 6-well plates in complete DMEM containing 2% FBS (to synchronise cells). The concentration seeded was to achieve ~60% confluence the next day for the addition of conditioned medium. The medium was collected from transfected and non-transfected keratinocytes and placed directly onto fibroblasts. The keratinocyte medium was replaced with fresh complete SFKM and all cells were incubated for 24 hours (temperature 37°C, CO<sub>2</sub> 5% and 95% humidity). At 24hrs the medium was removed from all fibroblasts and replaced with the medium from keratinocytes, as before. This was left for a further 24 hours. The keratinocytes were harvested for qRT-PCR and western blot to ensure successful transfection. After a total of 48 hours the fibroblasts were harvested using Trizol (ThermoFisher Scientific, UK) for RNA extraction and qRT-PCR or radioimmunoprecipitation assay buffer (RIPA buffer: Sigma-Aldrich, UK) supplemented with protease and phosphatase inhibitors cocktail (Halt™ Inhibitor Cocktail 100X, ThermoScientific, UK) for protein extraction and western blot.

### 3.8.6 Treatment of cultured cells with neuregulin-1

The appropriate concentration for addition to cultured cells was determined through literature review [19] and optimisation. Lyophilised recombinant human neuregulin-1-β1 (rhNRG1) was purchased from PeproTech, USA. This was reconstituted in water to a 0.1mg/ml concentration and stored at 4°C and used within a week or at -20°C as advised. Cells were seeded into 6-well plates in complete DMEM and then serum-starved for 24 hours. Test concentrations of 20ng/ml, 50ng/ml and 100ng/ml were added to serum-starved fibroblasts for 6, 12, 24 or 72 hours and the cells harvested for RNA extraction using Trizol (ThermoFisher Scientific, UK). The rhNRG1 was diluted in fresh serum-free medium each time. For final experiments a concentration of 50ng/ml was chosen for 24 hours.

NSF and KF were seeded into 6-well plates in complete DMEM. Once ~80% confluent, cells were serum-starved for 24 hours before adding 50ng/ml rhNRG1 for 24 hours. Control cells were treated with serum-free medium for a total of 48 hours. rhNRG1 treatment for MTT (**section 3.7.6**) and migration assays (**section 3.8.8**) are discussed in the relevant parts of this chapter.

### **3.8.7 ErbB2 siRNA transfection studies**

ErbB2 siRNA gene knockdown was performed using validated Ambion® *Silencer*® Select s613 (5nmol) and *Silencer*® Select Negative Control No. 1 (5nmol) purchased from ThermoFisher Scientific, UK, according to manufacturer's directions and as previously described in the literature [20-22]. The ErbB2 siRNA was reconstituted using nuclease-free water to a concentration of 50µM and stored at -20°C. The negative control siRNA was reconstituted for a final concentration of 100µM stored at -20°C and a working stock of 10µM using nuclease-free water further diluted on the day of transfection.

The siRNA were introduced to keloid fibroblasts (KF) using Lipofectamine® RNAiMAX (ThermoFisher Scientific, UK) in serum-free and antibiotic-free Opti-MEM® (ThermoFisher Scientific, UK). KF were seeded in 6-well plates at  $2.5 \times 10^5$ . Once 60-80% confluent, for one well of a 6-well plate: diluted siRNA (final concentration in 150µl Opti-MEM) was added to diluted Lipofectamine® RNAiMAX (7.5µl in 150µl Opti-MEM) and incubated at room temperature for five minutes. The mixture was then added to the well so that final well volume was 2.5ml, and the plate gently rocked to ensure homogenisation. This was incubated at: temperature 37°C, CO<sub>2</sub> 5% and 95% humidity.

Optimisation was carried out to establish the most effective concentration and time point. Final concentrations of 2.5nM, 5nM, 10nM, 15nM, 20nM and 30nM were tested over 24, 48 and 72 hours. At each time point the KF were harvested using Trizol (ThermoFisher Scientific, UK) for RNA extraction or RIPA buffer (Sigma-Aldrich, UK) supplemented with protease and phosphatase inhibitors cocktail (Halt™ Inhibitor Cocktail 100X, ThermoScientific, UK) for western

blot. For all experiments following optimisation a final concentration of 5nM for 48 hours was used as this was determined to result in the most efficient reduction in expression.

### **3.8.8 In vitro scratch wound migration assay (scratch assay)**

This was performed as has been previously described in the literature [23-27]. Keloid and normal skin fibroblasts were seeded at  $3 \times 10^5$  per well of a 6-well plate to achieve ~90% confluency. NSF were either treated with 50ng/ml rhNRG1 or control (serum-free) complete DMEM. KF were treated with 50ng/ml rhNRG1 alone, 5nM ErbB2 siRNA alone, 5nM negative control siRNA alone or combined ErbB2 siRNA with 50ng/ml rhNRG1. A scratch wound was introduced using a 10 $\mu$ l pipette tip and non-adherent cells washed off. At time 0 and at 48 hours fibroblasts were fixed with 4% formaldehyde for 30 minutes, permeabilised with 0.1% triton X-100 (Sigma-Aldrich, UK) and treated with F-actin using 1:250 rhodamine isothiocyanate (Sigma-Aldrich, UK) and 1:500 DAPI. Three non-overlapping fields were captured using an inverted Olympus IX71. The number of cells migrated into the wound site were counted and presented as mean  $\pm$  SEM. This was done in duplicate with six scratches per well, giving a total of 54 measurements per experimental condition for each of keloid and normal skin fibroblasts.

## **3.9 Specialised protein expression experiments**

### **3.9.1 Western blot**

Cells were washed with cold phosphate buffered saline (PBS; Sigma-Aldrich) and then either trypsinised, pelleted and re-suspended in radioimmunoprecipitation assay buffer (RIPA, Sigma-Aldrich) or the RIPA added directly to the cells over ice and then scraped and collected. The RIPA volume depended on number of cells and was supplemented with protease and phosphatase inhibitors cocktail (Halt™ Inhibitor Cocktail 100X, ThermoScientific, UK). The protein was then extracted using 5 freeze-thaw cycles including a 1.5 minute lysis step. The

concentration was determined using the bicinchoninic acid protein assay reagent kit (BCA; ThermoScientific, UK) and was plotted against a standard curve using bovine serum albumin (BSA).

An equal amount of protein (30µg) was denatured (NuPage sample buffer; ThermoScientific and 95°C heating x 5 minutes) and resolved on 4-12% Bis-Tris gels (ThermoFisher Scientific, UK) and electrophoresed according to the manufacturer's instructions. The protein was blotted onto polyvinylidene difluoride membranes (PVDF; ThermoFisher Scientific) using iBlot Dry Blotting System (Life Technologies/ThermoFisher Scientific). Following transfer the PVDF membranes were incubated at room temperature for 1 hour in Odyssey® blocking buffer (LI-COR Biosciences, UK). Each membrane was then incubated in its respective primary antibody diluted in blocking buffer and rocked overnight at 4°C. The next day the membranes were washed in 3 x 1% Tween®20 (ThermoFisher Scientific, UK) PBS and a plain PBS for 5 minutes each before incubating in respective alkaline-phosphatase conjugated secondary antibodies (prepared using blocking buffer) at room temperature for 1 hour.

Following washes the membrane was developed using one-step nitro blue tetrazolium/5-bromo-4-chloroindoxyl phosphate (NBT/BCIP; ThermoScientific). Each sample was blotted with its corresponding internal control (β-actin) each time. To analyse the blots the percentage of band intensity was calculated by Image J (Fiji, 1.47t, NIH, USA). The band intensity for each target was divided by its own control and then compared with other samples using fold change. All antibody-specific incubation parameters are detailed in the results chapter in which they feature.

### **3.9.2 High-throughput in-cell western blotting and quantification**

This was performed as previously described [9, 14, 15]. Both normal skin and keloid fibroblasts were seeded at  $1 \times 10^4$  into a black opaque clear-bottom 96-well plate in 2%FBS DMEM the day

before conditioned medium addition. Medium from both AKR1B10 transfected and non-transfected (6-well plates) keratinocytes was taken immediately after the first 24 hour incubation and added to a row each of the same fibroblast patient. This was repeated at 24 hours (48hour transfected). At 48 hours the plate was fixed for in-cell western blotting.

The medium was removed and 150µl 4% formaldehyde (Sigma-Aldrich, UK) was added to each well for 20 minutes at room temperature. The cells were then permeabilised using 200µl of 0.1% Triton X-100 (Sigma-Aldrich, UK) for 5 washes at 5 minutes each and subsequently blocked by adding 150µL Odyssey® (LI-COR, UK) for 1.5 hours at room temperature with moderate shaking. 50µl of primary antibody was added to each well and 50µl of blocking buffer to control wells. The plate was incubated at 4°C overnight and the next day washed with 1% Tween®20 (ThermoFisher Scientific) PBS 5 times. All rabbit primary antibodies were stained with IRDye® 800CW goat anti-rabbit secondary antibody (1/800) (LI-COR, UK) and the mouse with IRDye® 800CW goat anti-mouse (1/800). In addition, CellTag™ 700 (LI-COR, UK) stain was used to normalise for cell number. This was added to the diluted secondary antibody at 1/500 blocking buffer and the plate left at room temperature for 1 hour. The plate was protected from light from this point forward. Following a further wash with 0.1% Tween®20 PBS the plate was dried and scanned immediately. In-cell western was also completed for fibroblasts that had been treated with 1µM all-*trans* retinoic acid (atRA) (Sigma-Aldrich, UK) for 24 hours prior to fixation. For analysis the expression of each protein marker was normalised against the CellTag™ reading in the 700 channel (800/700nm ratio). The plate was imaged using an Odyssey infrared scanner (LI-COR) and the data acquired with Odyssey software, exported and analysed in Excel (Microsoft, UK). The expression was then compared for those fibroblasts treated with AKR1B10-overexpressing keratinocyte medium, non-transfected keratinocyte medium or retinoic acid. All antibody-specific concentrations are in the supplementary data of the results chapter in which they feature.

### 3.9.3 Co-immunoprecipitation

The co-immunoprecipitation experiments were performed by Dr. Tom Hodgkinson assisted by the author, Natalie Jumper. To determine ErbB dimerisation, co-immunoprecipitation of ErbB receptor complexes was performed according to manufacturer's instructions (Pierce co-immunoprecipitation (Co-IP) kit, ThermoFisher Scientific, UK) similar to that published in the literature [28-30]. NSF and KF were lysed in Co-IP Lysis Buffer, cell debris pelleted and protein quantified using BCA assay kit (ThermoFisher Scientific, UK). 1 mg of each cell population lysate was pre-cleared by 1 hour incubation with non-specific agarose resin. This was then centrifuged at 1000 x g for 1 minute and saved for addition to immobilised antibody. For each receptor subunit, the primary antibody was covalently bound to an amine-reactive resin and incubated with cleared cell lysate over-night at 4°C. Non-bound protein was removed, specifically bound complex-resin washed and proteins eluted. Immunoprecipitate was subjected to western blot. Blots from each Co-IP reaction were probed with anti-ErbB2, 3 and 4 antibodies and developed using nitro blue tetrazolium/S-bromo-4-chloroindoxyl phosphate (NBT/BCIP, 34042, ThermoFisher Scientific, UK).

### 3.10 Statistics and analysis

All data are presented as mean  $\pm$  SEM (standard error of the mean) of at least three independent experiments unless otherwise stated. For qRT-PCR, gene expression levels were normalised against two internal reference genes and the  $\Delta\Delta C_T$  calculated. Using SPSS v22 (IBM) for two-group comparison the Student's *t* test used and for three or more group comparisons one way ANOVA was used for statistical analysis, where  $p < 0.05$  was considered significant. Following ANOVA, individual group significance was determined using Tukey post-hoc analysis.

For microarray, the data was quantile normalised [31, 32] and the initial analysis done in Array Studio v7.2 (Performed by Adam Taylor at GlaxoSmithKline). Enrichment was performed using Ingenuity Pathway Analysis (IPA) database (Ingenuity Systems; [www.ingenuity.com](http://www.ingenuity.com)), which was



performed by the author and is discussed in detail in results **chapter 4**. Criteria for gene selection were: fold change  $\geq 2$ , p-value  $< 0.05$   $\pm$  q-value  $< 0.05$ .

## References

1. Koliijn K, van Leenders GJ. Comparison of RNA extraction kits and histological stains for laser capture microdissected prostate tissue. *BMC research notes*. 2016;9: 1-6.
2. Vandewoestyne M, Goossens K, Burvenich C, Van Soom A, Peelman L, Deforce D. Laser capture microdissection: should an ultraviolet or infrared laser be used? *Anal Biochem*. 2013;439: 88-98.
3. Vogel A, Horneffer V, Lorenz K, Linz N, Hüttmann G, Gebert A. Principles of laser microdissection and catapulting of histologic specimens and live cells. *Methods in cell biology*. 2007;82: 153-205.
4. Clément-Ziza M, Munnich A, Lyonnet S, Jaubert F, Besmond C. Stabilization of RNA during laser capture microdissection by performing experiments under argon atmosphere or using ethanol as a solvent in staining solutions. *Rna*. 2008;14: 2698-704.
5. Harries MJ, Meyer K, Chaudhry I, J EK, Poblet E, Griffiths CE, et al. Lichen planopilaris is characterized by immune privilege collapse of the hair follicle's epithelial stem cell niche. *J Pathol*. 2013;231: 236-47.
6. Salmon CR, Silvério KG, de Oliveira Giorgetti AP, Sallum EA, Casati MZ, Nociti Jr FH. Gene expression analysis in microdissected samples from decalcified tissues. *Diagnostic Molecular Pathology*. 2012;21: 120-6.
7. Ribeiro-Silva A, Zhang H, Jeffrey SS. RNA extraction from ten year old formalin-fixed paraffin-embedded breast cancer samples: a comparison of column purification and magnetic bead-based technologies. *BMC molecular biology*. 2007;8: 1.
8. Madabusi LV, Latham GJ, Andruss BF. [1] RNA Extraction for Arrays. *Methods in enzymology*. 2006;411: 1-14.
9. Syed F, Ahmadi E, Iqbal SA, Singh S, McGrouther DA, Bayat A. Fibroblasts from the growing margin of keloid scars produce higher levels of collagen I and III compared with intralesional and extralesional sites: clinical implications for lesional site-directed therapy. *Br J Dermatol*. 2011;164: 83-96.
10. Kameda T, Shide K, Yamaji T, Kamiunten A, Sekine M, Hidaka T, et al. Gene expression profiling of loss of TET2 and/or JAK2V617F mutant hematopoietic stem cells from mouse models of myeloproliferative neoplasms. *Genomics data*. 2015;4: 102-8.
11. Masuda A, Katoh N, Nakabayashi K, Kato K, Sonoda K, Kitade M, et al. An improved method for isolation of epithelial and stromal cells from the human endometrium. *The Journal of reproduction and development*. 2016;62: 213.
12. Leguen I, Le Cam A, Montfort J, Peron S, Fautrel A. Transcriptomic Analysis of Trout Gill Ionocytes in Fresh Water and Sea Water Using Laser Capture Microdissection Combined with Microarray Analysis. *PLoS one*. 2015;10: e0139938.
13. Kyle DJ, Oikonomou A, Hill E, Bayat A. Development and functional evaluation of biomimetic silicone surfaces with hierarchical micro/nano-topographical features demonstrates favourable in vitro foreign body response of breast-derived fibroblasts. *Biomaterials*. 2015;52: 88-102.
14. Suarez E, Syed F, Alonso-Rasgado T, Bayat A. Identification of biomarkers involved in differential profiling of hypertrophic and keloid scars versus normal skin. *Arch Dermatol Res*. 2015;307: 115-33.
15. Ashcroft KJ, Syed F, Bayat A. Site-specific keloid fibroblasts alter the behaviour of normal skin and normal scar fibroblasts through paracrine signalling. *PLoS One*. 2013;8: e75600.
16. Hodgkinson T, Bayat A. In vitro and ex vivo analysis of hyaluronan supplementation of Integra(R) dermal template on human dermal fibroblasts and keratinocytes. *J Appl Biomater Funct Mater*. 2016;14: e9-e18.

17. Chinnathambi S, Wiechert S, TOMANEK-CHALKLEY A, Winter MC, Bickenbach JR. Treatment with the cancer drugs decitabine and doxorubicin induces human skin keratinocytes to express Oct4 and the OCT4 regulator mir-145. *The Journal of dermatology*. 2012;39: 617-24.
18. Ouazia D, Levros L-C, Rassart É, Desrosiers R. The protein I-isoaspartyl (d-aspartyl) methyltransferase protects against dopamine-induced apoptosis in neuroblastoma SH-SY5Y cells. *Neuroscience*. 2015;295: 139-50.
19. Kim JS, Choi IG, Lee BC, Park JB, Kim JH, Jeong JH, et al. Neuregulin induces CTGF expression in hypertrophic scarring fibroblasts. *Mol Cell Biochem*. 2012;365: 181-9.
20. Sebastian A, Iqbal SA, Colthurst J, Volk SW, Bayat A. Electrical Stimulation Enhances Epidermal Proliferation in Human Cutaneous Wounds by Modulating p53–SIVA1 Interaction. *Journal of Investigative Dermatology*. 2015;135: 1166-74.
21. Merry CR, McMahon S, Thompson CL, Miskimen KL, Harris LN, Khalil AM. Integrative transcriptome-wide analyses reveal critical HER2-regulated mRNAs and lincRNAs in HER2+ breast cancer. *Breast cancer research and treatment*. 2015;150: 321-34.
22. Montero-Conde C, Ruiz-Llorente S, Dominguez JM, Knauf JA, Viale A, Sherman EJ, et al. Relief of feedback inhibition of HER3 transcription by RAF and MEK inhibitors attenuates their antitumor effects in BRAF-mutant thyroid carcinomas. *Cancer discovery*. 2013;3: 520-33.
23. Skazik C, Amann PM, Heise R, Marquardt Y, Czaja K, Kim A, et al. Downregulation of STRA6 expression in epidermal keratinocytes leads to hyperproliferation-associated differentiation in both in vitro and in vivo skin models. *The Journal of investigative dermatology*. 2014;134: 1579-88.
24. Brogliato AR, Moor AN, Kesl SL, Guilherme RF, Georgii JL, Peters-Golden M, et al. Critical role of 5-lipoxygenase and heme oxygenase-1 in wound healing. *The Journal of investigative dermatology*. 2014;134: 1436-45.
25. Soong J, Chen Y, Shustef EM, Scott GA. Sema4D, the ligand for Plexin B1, suppresses c-Met activation and migration and promotes melanocyte survival and growth. *The Journal of investigative dermatology*. 2012;132: 1230-8.
26. Truzzi F, Marconi A, Lotti R, Dallaglio K, French LE, Hempstead BL, et al. Neurotrophins and their receptors stimulate melanoma cell proliferation and migration. *The Journal of investigative dermatology*. 2008;128: 2031-40.
27. Kroeze KL, Jurgens WJ, Doulabi BZ, van Milligen FJ, Scheper RJ, Gibbs S. Chemokine-mediated migration of skin-derived stem cells: predominant role for CCL5/RANTES. *The Journal of investigative dermatology*. 2009;129: 1569-81.
28. Adebisi A, Narayanan D, Jaggar JH. Caveolin-1 assembles type 1 inositol 1,4,5-trisphosphate receptors and canonical transient receptor potential 3 channels into a functional signaling complex in arterial smooth muscle cells. *The Journal of biological chemistry*. 2011;286: 4341-8.
29. Yin D, Yang X, Li H, Fan H, Zhang X, Feng Y, et al.  $\beta$ -Arrestin 2 Promotes Hepatocyte Apoptosis by Inhibiting Akt Protein. *Journal of Biological Chemistry*. 2016;291: 605-12.
30. Le LT-N, Cazares O, Mouw JK, Chatterjee S, Macias H, Moran A, et al. Loss of miR-203 regulates cell shape and matrix adhesion through ROBO1/Rac/FAK in response to stiffness. *The Journal of cell biology*. 2016;212: 707-19.
31. Bolstad BM, Irizarry RA, Åstrand M, Speed TP. A comparison of normalization methods for high density oligonucleotide array data based on variance and bias. *Bioinformatics*. 2003;19: 185-93.
32. Harris M, Taylor G, Harris M, Taylor G. *Medical statistics made easy* 3. ed: Martin Dunitz. 2014.

# Chapter 4

---

**Combined laser capture microdissection (LCM) and whole genome microarray profiling of epidermis vs dermis of site-specific keloid disease compared with whole keloid tissue biopsy and monolayer culture provide novel targets with potential clinical implications**

**Declaration:**

Natalie Jumper carried out all of the experimental work, interpretation of data, design and composition of the article and accompanying figures. Adam Taylor provided assistance with microarray data quality control assessment, normalisation and initial analysis but the significant majority of the microarray data analysis presented here, was performed by the first author, Natalie Jumper. Dr. Hodgkinson provided technical advice and along with the senior authors gave guidance and final approval of the paper. This paper is prepared in the format required for submission to PLOS One journal. To facilitate interpretation the core figures have been included within the article and the supplementary material at the end.

**Combined laser capture microdissection (LCM) and whole genome microarray profiling of epidermis vs dermis of site-specific keloid disease compared with whole keloid tissue biopsy and monolayer culture provide novel targets with potential clinical implications**

N. Jumper<sup>1</sup>, T. Hodgkinson<sup>1,2</sup>, R. Paus<sup>3,4</sup>, A. Bayat<sup>1,3</sup>

<sup>1</sup>*Plastic and Reconstructive Surgery Research, University of Manchester, Oxford Rd, M13 9PT*

<sup>2</sup>*Centre for Tissue Injury and Repair, Institute of Inflammation and Repair, University of Manchester, UK3*

<sup>3</sup>*Centre for Dermatology Research, Institute of Inflammation and Repair, University of Manchester, Manchester, UK*

<sup>4</sup>*Department of Dermatology, University of Münster, D-48149, Münster, Germany*

*Correspondence to: Dr. A. Bayat, Stopford building, University of Manchester, Oxford Rd, M13 9PT UK Email: [Ardeshir.Bayat@manchester.ac.uk](mailto:Ardeshir.Bayat@manchester.ac.uk)*

**Key words:** Laser capture microdissection, microarray, keloid,

**Abstract**

Keloid disease (KD) is a fibroproliferative cutaneous tumour characterised by heterogeneity, excess collagen deposition and aggressive local invasion. Lack of a validated animal model and resistance to a multitude of available therapies has resulted in difficult and ineffective clinical management of keloid scars. In order to address KD from a new perspective, we applied for the first time a site-specific *in situ* approach, through combined laser capture microdissection and whole genome array profiling. We aimed to analyse the utility of this approach compared with established methods of investigation, including whole tissue biopsy and monolayer cell culture techniques. This study was not designed to prove or disprove specific hypotheses but to approach KD from a hypothesis-free and compartment-specific angle, using state-of-the-art *in situ* gene expression profiling technology. We sought to characterise expression differences between keloid lesional sites and elucidate potential contributions of significantly dysregulated genes to mechanisms underlying keloid pathobiology, thus informing future explorative research into KD. Here, we highlight the advantages of our *in situ* strategy in generating expression data with improved sensitivity and accuracy over traditional methods. The *in situ* expression analysis supported an active role for the epidermis in the pathogenesis of KD, through identification of genes and upstream regulators implicated in epithelial-mesenchymal transition, inflammation and immune modulation. We describe dermal expression patterns crucial to collagen deposition that are associated with TGF $\beta$  but which have not previously been examined in KD. Additionally, this study supports the already proposed presence of a cancer-like stem cell population in keloid scars and explores the possible contribution of gene dysregulation to the therapeutic resistance complicating KD management. Through this innovative *in situ* gene profiling approach we provide better-defined gene signatures of distinct keloid regions thereby addressing KD heterogeneity, facilitating differential diagnosis with other cutaneous fibroses and highlighting key areas for prospective research.

## Abbreviations

DEG, differentially expressed genes; ECM, extracellular matrix; EMI, epithelial-mesenchymal interactions; EMT, epithelial-mesenchymal transition; IL, interleukin; KD, keloid; Kd, keloid dermis; KE, keloid epidermis; LCM, laser capture microdissection; MET, mesenchymal-epithelial transition; NS, normal skin; disease, TGF, transforming growth factor; 2D, 2-dimensional

## Introduction

Keloid disease (KD) is a fibroproliferative cutaneous tumour of ill-defined pathogenesis characterised by clinical, behavioural and histological heterogeneity [1]. KD research has been hindered by lack of a validated animal model, a paucity of tissue for experimentation secondary to high rates of recurrence following excision [2] and both inter-patient and inter-lesional heterogeneity [3] that has resulted in a number of available therapies but no gold standard effective treatment option for KD [4]. In an effort to overcome this, many recent studies have considered KD in terms of different sites within the lesion: intralesional (centre), perilesional (margin) and extralesional (adjacent normal skin) [5].

The evidence for site-specific KD is threefold. Macroscopically, the centre is often pale soft and shrunken when compared with the raised erythematous margin. Microscopically there are differences with respect to epidermal thickness, inflammatory infiltrate, collagen ratios and cellularity [6, 7]. Finally, on a molecular level, these sites have been shown to differ with regard to cell cycle phase and apoptotic factor expression [8]. While this site-specific approach has highlighted the diversity within KD, the use of whole tissue biopsy and monolayer culture fail to accurately reflect the *in situ* expression of this unique 3D microenvironment.

Therefore, in addition to site-specific, the second aspect of our approach was to examine *in situ* signalling. We achieved this by combining laser capture microdissection (LCM) and whole genome microarray (**Figure 1a**). To date, LCM has played a limited role in cutaneous wound

healing but given its success both in other areas of fibrosis as well as benign and malignant dermatological conditions [9-11], we felt it was an ideal platform for application to KD. This approach also allowed us to focus on individual expression in different regions of the keloid scar without the “averaging out” of signals consequential to whole tissue biopsy analysis or the altered expression that can result from the *in vitro* environment of monolayer cell culture [12].

The overall aim of this study was not to validate specific theories but to apply an innovative hypothesis-free and compartment-specific approach to KD. Thus, the first aim was to compare this combined LCM and microarray (*in situ*) approach to both whole tissue biopsy and monolayer culture methods of analysing gene expression (**Figure 1b**). The second aim was to enrich the data in terms of gene ontology, in an effort to explore the biological processes within different lesional sites of the keloid scar. Finally, we aimed to examine differentially expressed genes (DEG) from each site of both epidermis and dermis compared with *in situ* normal skin (NS), to identify pathways for potential diagnostic and therapeutic exploitation.

We show that our *in situ* approach most accurately reflects the *in vivo* environment without missing functionally important DEG through dilution and averaging out. These DEG indicate an activated epidermis with a potential for epithelial-mesenchymal transition (EMT) and expose dermal collagen-promoting molecules of which *TGFβ* is an integral component but which remain overlooked in KD. The sensitivity of this technique allowed us to unveil another piece of the complex inflammatory network contributing to KD, unravel some of the elements contributing to therapeutic resistance and strengthen the argument for a stem cell population in KD [13].



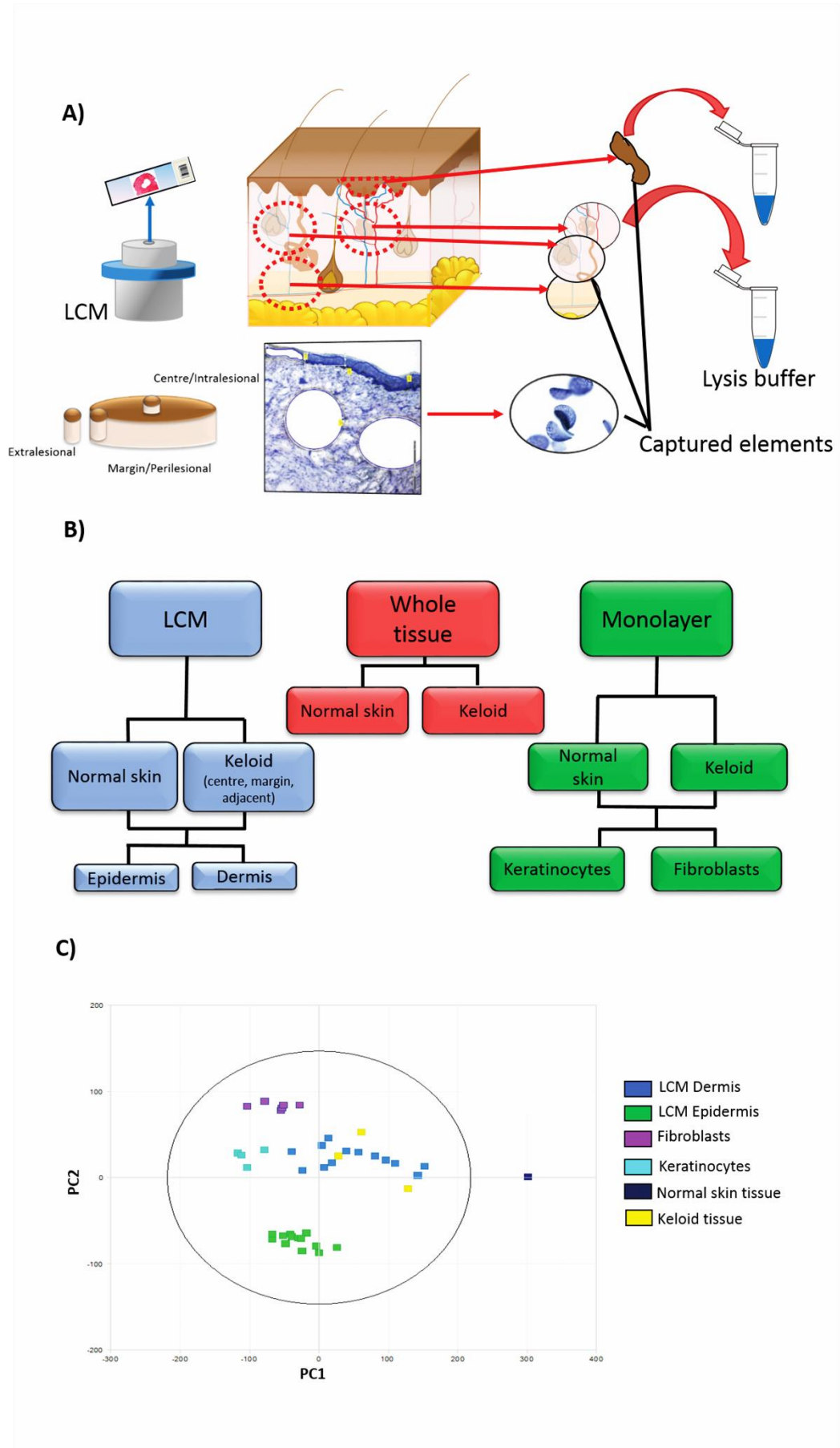


**Figure 1 Experimental approaches for the comparison of site-specific keloid disease with normal skin.** A) Schematic diagram demonstrating laser capture microdissection (LCM) of epidermis and dermis for each of the shown keloid biopsy sites, centre (intralesional), margin (perilesional) and keloid-adjacent normal skin (extralesional). LCM was performed for keloid sites and normal skin. As shown the elements (epidermis separate to dermis) were delineated, cut using UV laser and catapulted into the cap of an overhanging tube, where images confirmed their presence. This was then immersed in lysis buffer and stored at -80°C. B) The three methods of experimental technique used to compare keloid with normal skin: LCM, whole tissue biopsy and 2D monolayer cell culture. C) Principal component analysis (PCA) plot for the gene expression derived from experimental approaches described above. The epidermal and dermal samples are evident as separate clusters as are the laser captured material and the monolayer culture samples.

## Materials and Methods

### Study approval

Keloid and NS tissue were harvested at the time of surgery following full verbal and written consent in accordance with Declaration of Helsinki and North West Research Ethics Committee (Ref. 11/NW/0683). In total there were 8 of each NS and keloid tissue donors used for microarray, with additional samples included for supporting data (**Supplementary table S1**). The scar was considered to be keloid if it fulfilled the following criteria: growth beyond the boundaries of the original wound, failure to regress with time, present for at least on year and likely to recur with excision [14, 15].

### **Tissue processing**

Tissue biopsies were taken from keloid scar centre, margin and extralesional sites (**Figure 1a**). NS biopsies were from patients undergoing routine elective surgery. Biopsies were immediately preserved in either RNA stabilisation solution (RNA*later*<sup>®</sup>, Life technologies Ltd, Paisley, UK) or 10% (v/v) neutral buffered formalin (Sigma-Aldrich, UK). The RNA stabilised samples were OCT-embedded (CellPath, UK) and snap frozen before being stored at -80°C.

### **Laser capture microdissection**

Serial 8µm cryosections (Leica CM3050S) of OCT-embedded keloid and NS samples were cut onto specialised PEN membrane slides (Carl Zeiss, UK). To differentiate epidermis from dermis, whilst preserving tissue RNA integrity, a rapid staining protocol was performed (LCM Staining Kit, Ambion, Austin TX, USA) according to the manufacturer's instructions [16, 17]. Using a P.A.L.M. LCM microscope (Carl Zeiss MicroBeam 4.2) epidermis and dermis of each sample was laser cut and catapulted away from the slide into separate overhanging microtube caps (AdhesiveCap 200 Opaque, Carl Zeiss Microscopy Ltd, Cambridge, UK). At least three sequential sections from each patient were captured and pooled per sample. The captured tissue was mixed with lysis buffer (Buffer RLT with 1% 2-mercaptoethanol, RNeasy Micro Kit, Qiagen) and stored at -80°C until extraction according to manufacturer's instructions (RNeasy Micro Kit, Qiagen). Following extraction the samples were again stored at -80°C [18].

### **RNA amplification and microarray**

Extracted RNA was amplified using the Ovation<sup>®</sup> Pico WTA system v2 kit (NuGen Technologies) and purified with QIAquick PCR purification kit (Qiagen), according to manufacturer's instructions. Prior to microarray, RNA quantity was estimated using a microvolume spectrophotometer (ThermoScientific NanoDrop 2000 UV-vis). Agilent SureTag DNA Labeling

and hybridisation kit were used according to manufacturer's instructions and slides (SurePrint G3 Human GE 8x60K V2) scanned using an Agilent Microarray Scanner G2505c [19-21]. This is a one-colour array platform yielding intensity values for each sample.

### **Quantitative real-time polymerase chain reaction**

qRT-PCR was performed using the Lightcycler® 480 II platform (Roche Diagnostics, UK) as previously described [22]. A final reaction volume of 10µl contained normalised cDNA, LightCycler®480 probes master mix, forward and reverse primers, nuclease-free water (Qiagen, UK) and the associated probe from the Universal Probe Library (Roche, UK). Reactions were performed in triplicate with two house-keeping genes (RPL32 and GAPDH) for relative quantification. Amplified targets were analysed using the Lightcycler® II software (1.5.0 SP3, Roche, UK).

### **Cell culture**

Primary keratinocytes and fibroblasts were established as previously described [22, 23]. In brief, tissue was cut and incubated in Dispase II (10mg/ml; Roche Diagnostics, UK) at 37°C. The epidermis was stripped, diced and incubated in TrypLE™Express (ThermoFisher Scientific, UK) with serum-free keratinocyte medium (Epilife®, Invitrogen Life Technologies, ThermoFisher Scientific) for one hour before neutralising, centrifugation and dispersion into T25 flasks. The dermis was further incubated in collagenase before adding to complete DMEM and grown in flasks. Medium was changed every 48hrs until confluent. Passages 1-3 were used. Cells were lysed and RNA extracted using Qiagen RNeasy Micro Kit, according to manufacturer's instruction.

## Statistical analysis

Data was extracted from the raw files and initial microarray analysis performed using Array studio v7.2 (OmicSoft Corporation, USA) and the data quantile normalised. A linear model was then fitted to the  $\log_2$  transformed data for which both p-value and False Discovery Rate (FDR), controlled for using Benjamini-Hochberg method, were calculated for each group comparison [24]. Least squared means (LS means) and 95% confidence interval (where  $n > 1$ ) were outputted for each group. The data was then filtered using the following criteria: maximum median signal intensity  $> 8$  (leaving 46802 probe sets), p-value  $< 0.05$ , fold change  $> 2$  and for individual genes of interest, q-value  $< 0.05$  (**Supplementary Figure S3 & S4**). Lists of DEG were loaded into Ingenuity Pathway Analysis (IPA, Qiagen). A full table of expanded gene names for each symbol discussed below can be found in **Supplementary table S2**.

For qRT-PCR, expression was normalised against internal controls and  $\Delta\Delta C_T$  calculated. Statistical analysis was performed using Student's *t*-test and one way ANOVA with Tukey post-hoc correction (SPSS, IBM), where p-value  $< 0.05$  was considered significant [25]. Data are represented as mean  $\pm$  SEM.

## Results & Discussion

### Microarray analysis reveals variable differential gene expression based on experimental approach

Initial analysis was conducted to define site-specific gene expression, determine relationships between experimental approaches and establish networks based on correlation clustering. We compared gene expression for both epidermis and dermis between different sites within the keloid lesion, based on their expression difference over their NS epidermal and dermal counterpart. Additionally, we analysed whole tissue biopsy and monolayer culture (keratinocyte and fibroblast) expression for both KD and NS. The number of significant DEG within these comparative groups as well as their direction of change is shown in **Table 1**.

Principal component analysis (PCA) was used to assess technical variability in the microarray QC metrics; the expected 5% of samples (2/40) lay outside the 95% confidence interval but were from two separate donors and therefore not excluded. Following quantile normalisation [26], probe sets were filtered by calculating maximum group median and removed if minimum signal intensity was  $< 8$  (on  $\log_2$  scale), leaving 24,228 probes (approximately 40%). PCA was employed to ascertain relationships between sample groups and compare variability between replicate arrays and experimental conditions [27].

This plot indicated the most significant variability existed between different cell types, that is epidermis and dermis or keratinocyte and fibroblast, which fell into separate clusters (X-axis) but variability was also found between the *in situ* cell layer and its *in vitro* monolayer culture equivalent i.e. epidermis and keratinocyte (Y-axis) (**Figure 1c**). Some of this variability could be attributed to the differentiation state of keratinocytes. Additionally, while keratinocytes and fibroblasts constitute the major cell type in the epidermis and dermis respectively, the *in situ* tissue layer will comprise additional cells that contribute to expression. As expected, gene signatures of keratinocyte/epidermis and fibroblast/dermis differed but intriguingly, this analysis also indicated there was differential gene expression dependent on the experimental approach.

**Table 1. Number of significant differentially expressed genes within each comparative microarray group (filtered for fold change > 2 and p-value < 0.05).**

Harvest method	Comparison	Total sig. changes	Up	Down	FDR-corrected
LCM	<i>Keloid centre vs normal epidermis</i>	1165	591	574	18
LCM	<i>Keloid margin vs normal epidermis</i>	911	562	349	11
LCM	<i>Keloid extralesional vs normal epidermis</i>	1425	608	817	28
LCM	<i>Keloid centre vs normal dermis</i>	3640	1795	1845	1085
LCM	<i>Keloid margin vs normal dermis</i>	3818	1852	1966	882
LCM	<i>Keloid extralesional vs normal dermis</i>	3313	1549	1765	423
Monolayer	<i>Keloid vs normal keratinocytes*</i>	356	207	149	21
Monolayer	<i>Keloid vs normal fibroblasts</i>	247	146	101	3
Whole tissue	<i>Keloid vs normal skin*</i>	12527	7583	4944	9076

FDR, false discovery rate; LCM, laser capture microdissection \*the latter group has  $n = 1$

### **An *in situ* approach leads to improved accuracy and sensitivity of differential gene expression over monolayer culture and whole tissue biopsy dissection**

We compared differential gene expression of KD with NS samples from whole tissue biopsy, monolayer culture and *in situ* LCM, in order to determine both experimental approach most representative of the keloid microenvironment and also the method most likely to identify important or novel biomarkers/pathways.

This was achieved by first comparing the DEG produced by each approach to establish any overlap or disparity. As seen from Venn diagrams [28] (**Figure 2a & 2b**) only 0.2% and 0.5% of DEG were common to all three approaches in epidermis and dermis respectively. Given that whole tissue biopsy incorporates both epidermis and dermis, it's clear the *in situ* approach produces the highest number of DEG specific to either layer. This data was uploaded to Ingenuity Pathway Analysis (IPA) Software (Ingenuity® Systems, [www.ingenuity.com](http://www.ingenuity.com)), which organised the DEG into known canonical pathways, biological functions, upstream regulators

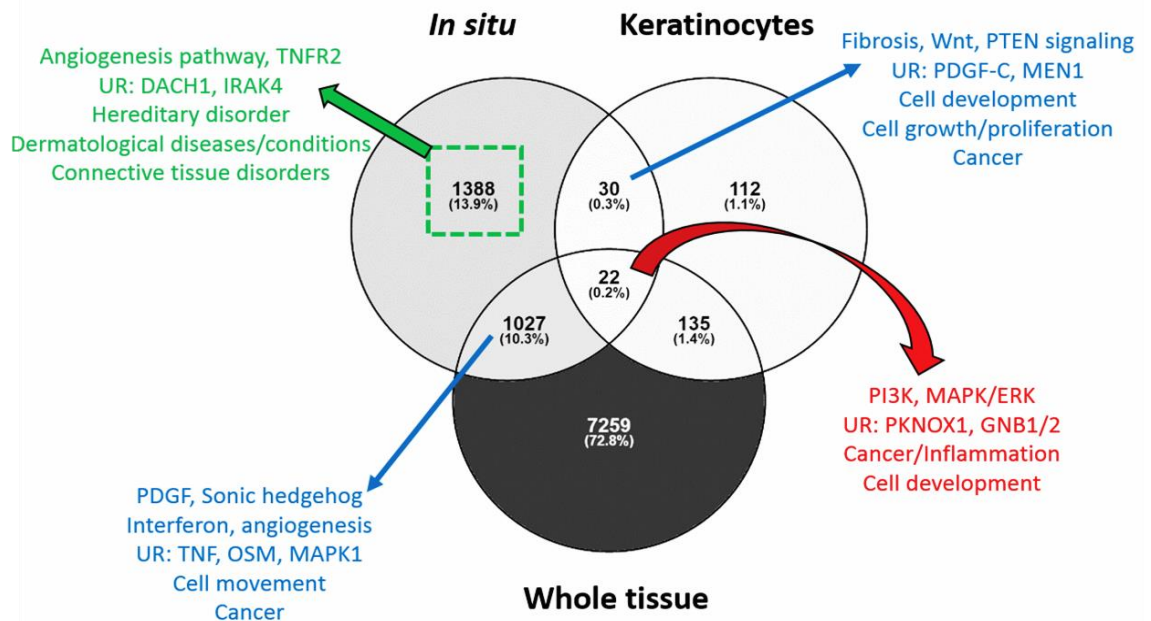
and interactive networks. For both epidermis and dermis, while all three groups captured the predominant epidermal (*PI3K*, *MAPK/ERK*) and dermal (*TGFβ*) expression, the *in situ* approach incorporated the essential elements of both whole tissue and monolayer expression, providing a more complete picture of overall expression. Also, there were a significant number of DEG in the *in situ* group alone that were not identified with monolayer or were averaged out in whole tissue analysis. This is due to the dilution effect of looking at whole tissue as transcriptomes from different cell types that are pooled together, which reduces the sensitivity.

In addition to comparing DEG between approaches, we examined the difference in degree of expression. For this, we compared expression between *in situ* dermis, captured by LCM and 2D *in vitro* cultured fibroblasts for genes known to be dysregulated in KD. Representative graphs are shown in **Figure 3a**, which demonstrate significantly increased expression of both *TGFβ1* and *CTGF* with *in vitro* monolayer fibroblasts compared with *in situ* tissue, for both KD and NS. This was also true for the rest of the genes analysed (**Supplementary Figure S1**). This might be somewhat expected considering 2D culture is a static physical environment, maintained with exogenous often undefined (foetal bovine serum) medium that lacks stimuli from other cell types and can alter cell morphology/polarity and phenotype [29]. These factors affect expression, with monolayer often resulting in higher-magnitude changes [12]. In this case, the overexpression seen with monolayer culture vs *in situ* approach falsely minimises the degree of gene upregulation in keloid compared with NS dermis.

Given the sensitivity and accuracy of degree of expression, we concluded our *in situ* LCM approach would be the most fruitful going forward.



a)



b)

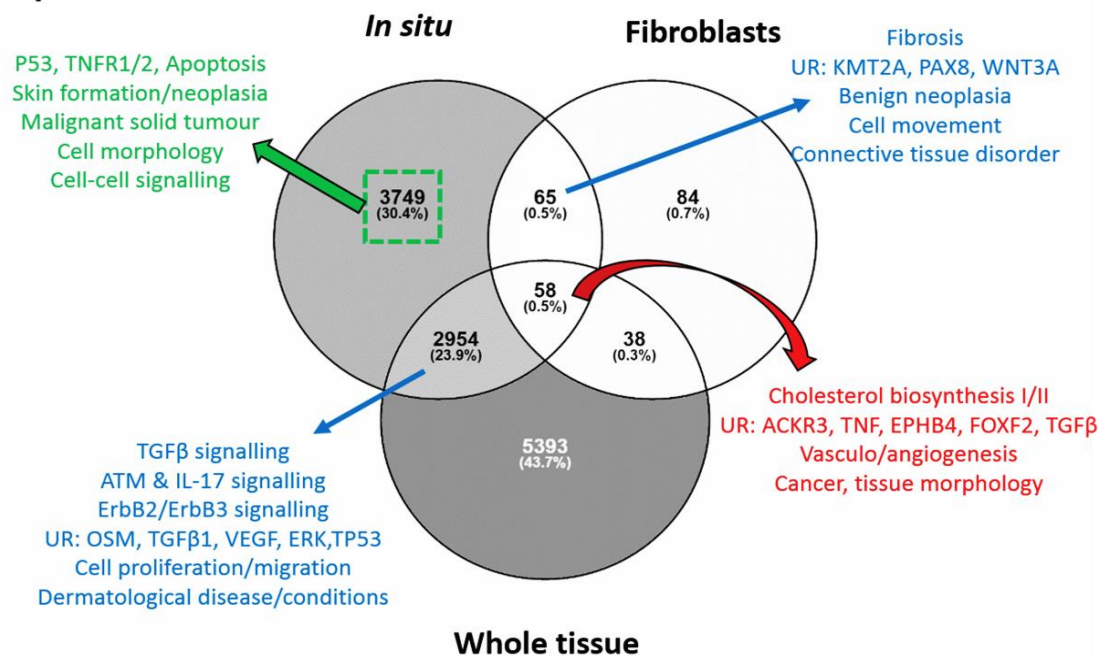


**Figure 2. Comparison of *in situ* KD expression to whole tissue biopsy and monolayer culture expression.**

(A) Venn diagram comparing *in situ* keloid epidermal expression to whole tissue and keratinocyte culture expression. The red arrow and text indicates where all 3 methods overlap and the results of enrichment using Ingenuity Pathway Analysis (IPA) for this group. The blue arrows and text indicate where either alternative method overlaps with *in situ* expression and the associated enrichment for that group. The green arrow and text indicates the enrichment analysis result for the 1388 genes that were identified in the *in situ* group alone. In total 1500 genes were differentially expressed between *in situ* LCM epidermis and keratinocyte culture methods and 8647 between *in situ* LCM epidermis and whole tissue.

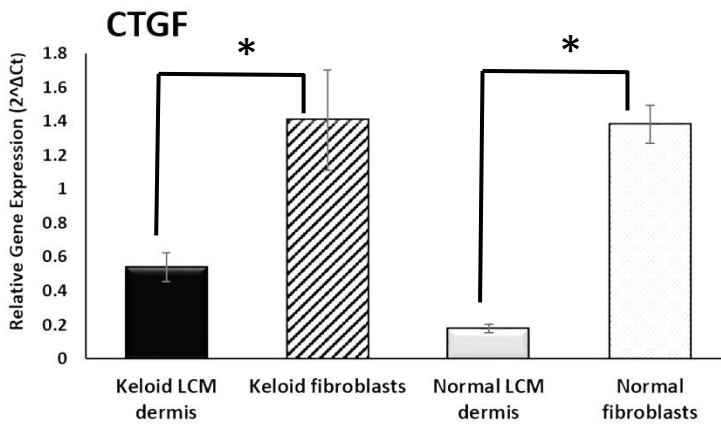
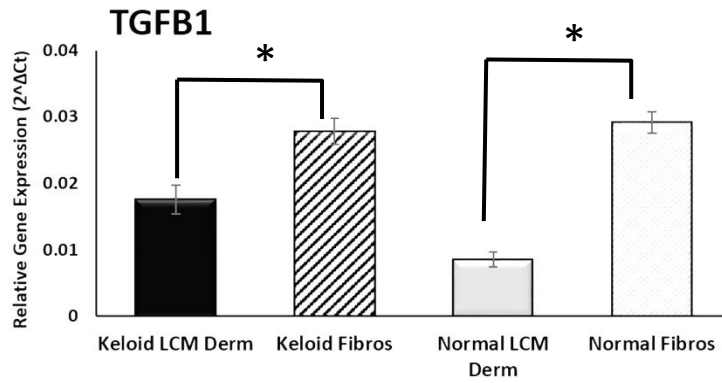
(B) Venn diagram comparing *in situ* keloid dermal expression to whole tissue and fibroblast culture expression. The red arrow and text indicates where all 3 methods overlap and the results of enrichment using IPA for this group. The blue arrows and text indicate where either alternative method overlaps with *in situ* expression and the associated enrichment for that group. The green arrow and text indicates the enrichment analysis result for the 3749 genes that were identified in the *in situ* group alone. In total 3,833 genes were differentially expressed between *in situ* LCM dermis and fibroblast culture methods and 9,142 between *in situ* LCM dermis and whole tissue.

ACKR3, atypical chemokine receptor 3; ATM, ataxia telangiectasia mutated; DACH1, dachshund family transcription factor 1; EGF, epidermal growth factor; EPHB4, ephrin (EPH) receptor B4; FOXF2, forkhead box F2; GNB, guanine nucleotide binding protein (G protein); IL, interleukin; IRAK4, interleukin-1 receptor associated kinase-4; KMT2A, lysine (K)-specific methyltransferase 2A; MAPK/ERK, mitogen-activated protein kinase; MEN1, menin; OSM, oncostatin M; PAX8, paired box 8; PDGF, platelet-derived growth factor; PI3K, phosphoinositide 3-kinase; PKNOX1, PBX/knotted 1 homeobox 1; PTEN, phosphatase and tensin homolog; TGF $\beta$ , transforming growth factor beta; TNF, tumour necrosis factor; TNFR2, tumour necrosis factor receptor 2; TP53, tumour protein 53; UR, upstream regulators; VEGF, vascular endothelial growth factor.

***In situ* dissection reveals keloid sites contribute disproportionately to differential gene expression**

Given the advantages of LCM *in situ* tissue capture, we then sought to use this technique to define the contribution of different sites within the keloid lesion to specific gene expression as well as distinguish epidermal from dermal signalling. To achieve this, we performed qRT-PCR for a number of genes known to be dysregulated in KD (**Supplementary figure S2**), of which two are represented in **Figure 3b**. We demonstrated that *TGFβ1* signalling is largely attributed the keloid centre as compared to the margin or extralesional dermis and identified IL-8 upregulation as localised largely to keloid centre epidermis. By examining the keloid as separate components we were able to attribute specific expression to key sites, with the precision necessary for therapeutic targeting.

a)



b)

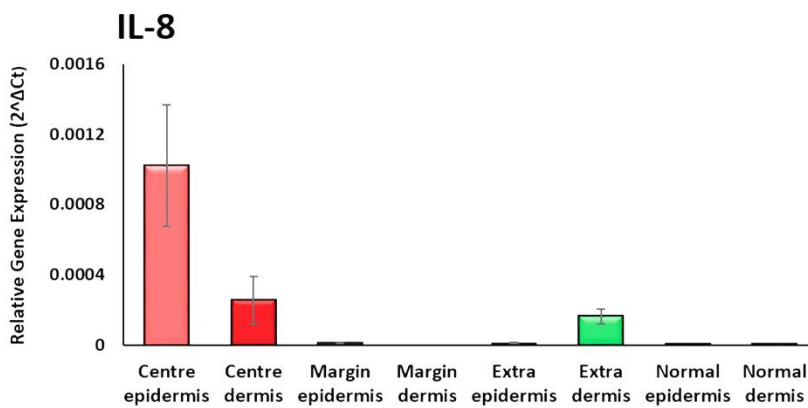
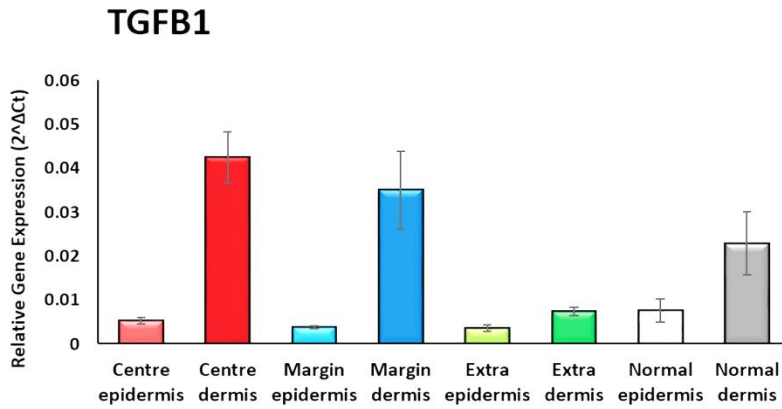


**Figure 3. Site-specific contribution to differential gene expression in KD.** (A) Comparison of gene expression between laser-captured dermal tissue (*in situ*) and fibroblasts for both keloid and normal skin. qRT-PCR graph for both *TGF $\beta$ 1* and *CTGF* (additional examples found in **Supplementary Figure S1**). All data are mean  $\pm$  SEM for at least three independent experiments. B) qRT-PCR for *TGF $\beta$ 1* and interleukin-8 (*IL-8*) showing relative contributions of different keloid sites to overall expression and comparison with normal skin (additional genes available in **Supplementary Figure S2**). Data are mean  $\pm$  SEM where \* p-value <0.05 using Student's *t* test and ANOVA with Tukey post hoc correction. CTGF, connective tissue growth factor; TGF $\beta$ , transforming growth factor beta.

### **Enrichment of the site-specific *in situ* keloid epidermis suggests an active role in the pathogenesis of keloid disease**

We employed LCM to look at the epidermis as a separate entity from the dermis, which highlighted a number of DEG that have previously been overlooked with alternative methods of dissection. Generally for the epidermis, the margin and centre shared more upregulated genes than either did with the extralesional tissue, however, the centre and extralesional sites had more downregulated genes in common than either did with the margin. To interpret the expression differences and similarities between epidermal sites, the data was uploaded to IPA (**Figure 4a**). The centre keloid epidermis (KE) alone was characterised by fibrosis, inflammation and apoptosis. When taken together with the margin KE, collagen turnover and inflammation were distinguished as key events. The upstream regulators *TGF $\beta$* , *PRRX1* and *DAB2* supported an EMT hypothesis. The identification of angiogenesis and cell-cell signalling networks as well as *VEGF* as an upstream regulator upheld the margin as the active site of keloid and emphasised the role of the epidermis in this process [7]. There were 232 DEG common to all three sites of the KE compared with NS epidermis (NSE). Interestingly, retinoate biosynthesis was revealed to

be the top canonical pathway in this group with key molecules including *IFN*, *TNF*, *HOXA13* and *MAPK1* proposed as upstream regulators.

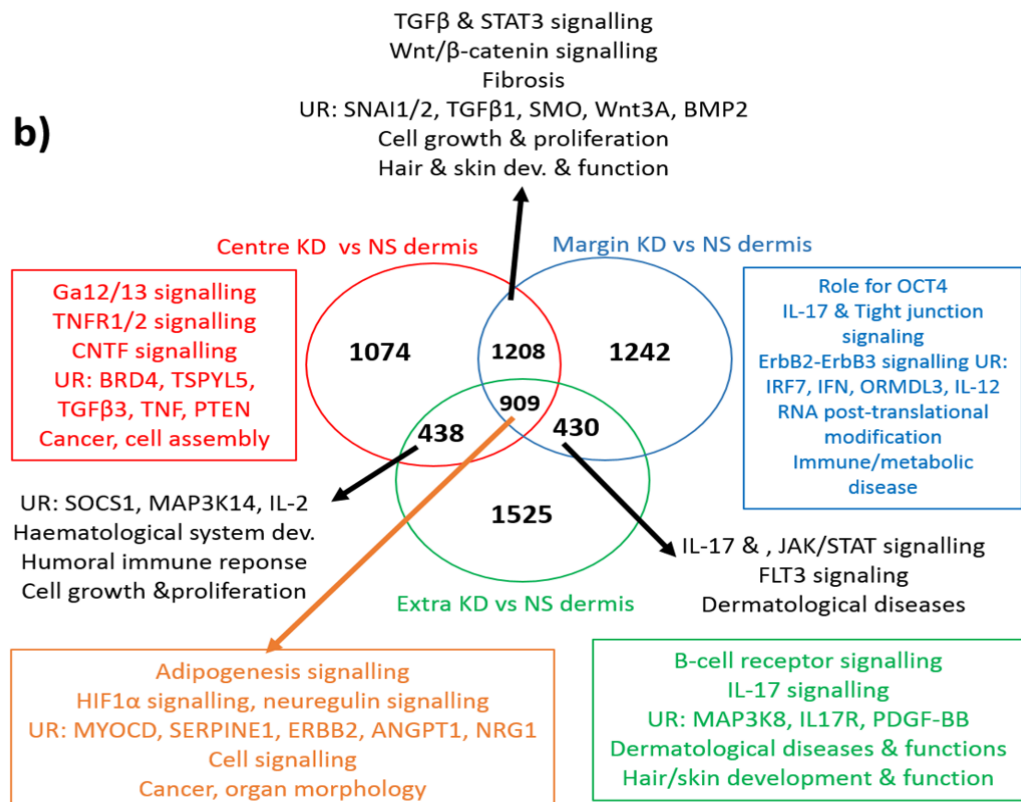
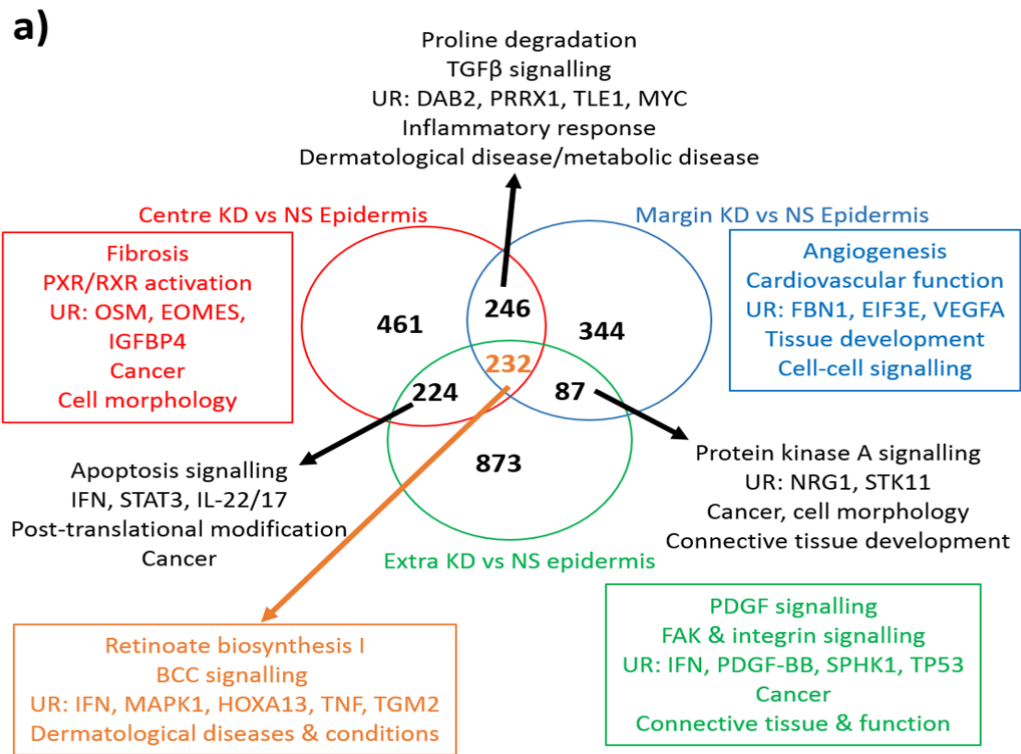


**Figure 4. Gene enrichment analysis of *in situ* site-specific keloid disease.** Venn diagram of keloid disease (KD) centre, margin and extralesional expression vs normal skin (NS), where A) refers to the epidermis and B) refers to the dermis. The red circle and text refer to the centre vs NS alone, the blue to margin vs NS and the green to extralesional keloid site alone vs NS. The black arrows and text refer to the enrichment results of where the expression of the indicated sites overlap. The orange arrow and text refers to the enrichment analysis of the indicated number of genes in common to all three keloid sites over NS. In both A) and B) enrichment analysis was performed with Ingenuity Pathway Analysis (IPA) and included canonical pathways, diseases & functions, networks and upstream regulators of interest.

ANGPT2, angiopoietin 2; BCO1, beta-carotene oxygenase 1; BMP2, bone morphogenetic protein 2; BRD4, bromodomain containing 4; DAB2, Dab, mitogen-responsive phosphoprotein, homolog 2 (drosophila); EGF, epidermal growth factor; EIF3E, eukaryotic translation initiation factor 3 subunit E; EOMES, eomesodermin; FBN1, fibrillin 1; FLT3, fms related tyrosine kinase 3; GSTP1, glutathione s-transferase pi 1; HIF, hypoxia-inducible factor; HOXA13, homeobox A13; IFN, interferon; IGFBP, insulin-like growth factor binding protein; IL, interleukin; IRF, interferon regulatory factor; JAK, janus kinase; MAPK, mitogen-activated protein kinase; MYC, c-Myc; MYOCD, myocardin; NRG1, neuregulin-1; OCT4, octamer-binding transcription factor 4; ORMDL3, orosomucoid like 3; OSM, oncostatin M; PDGF, platelet-derived growth factor; PTEN, phosphatase and tensin homolog; PXR, pregnane X receptor; PRRX1, paired related homeobox 1RXR, retinoid X receptor; SERPINE1(PAI-1), serpin peptidase inhibitor. Clade E (plasminogen activator inhibitor 1); SMO, smoothed; SNAI1, snail family zinc finger 1; SOCS, suppressor of cytokine signalling; SPHK, sphingosine kinase; STAT, signal transducer and activator of transcription; STK11, serine/threonine kinase 11; TGF, transforming growth factor; TGM2, transglutaminase 2; TLE1, transducin like enhancer of split 1; TNF(R), tumour necrosis factor (receptor); TP53, tumour protein 53; TSPYL5, testis-specific protein Y encoded like 5; UR, upstream regulators; VEGF, vascular endothelial growth factor.



### **Enrichment of the site-specific *in situ* keloid dermis supports the presence of epithelial-mesenchymal transition, immune modulation and keloid margin-related migration**

With regard to the keloid dermis (Kd), there was a significant increase in shared expression between centre and margin than with extralesional tissue, for both up and downregulated genes (**Figure 4b**). Compared with NS dermis (NSD), there were 1208 DEG common to centre and margin Kd, where *TGFβ* signalling was identified by IPA as a top canonical pathway, as might be expected in KD. The proposed upstream regulators in this group included *SNAI1*, *SNAI2*, *SMO*, *Wnt3A* and *BMP2*, which not only influence cell growth, proliferation and fibrosis but are also all involved in EMT [30-33]. When we examined all three sites of the Kd *in situ* together, we identified angiogenic factors (*HIF1α*, *ANGPT2*) and migration regulators (ErbB, *SERPINE1*) to be in common. Enrichment of the margin Kd highlighted migration regulators (ErbB & tight junction signalling), the potential existence of embryonic stem cells (*OCT4*) in keloid tissue [34] as well as immune response modulators (*IL-17*, *IL-12* & *IRF7* [35]) to be significant, much of which was shared at its overlap with extralesional dermis expression. These processes are consistent with the signature expected of an invading tumour margin [36].

### **The *in situ* keloid epidermis expresses an activated, pro-inflammatory profile with the potential for epithelial-mesenchymal transition**

In addition to expression overview and enrichment, we investigated the individual DEG of *in situ* sites for both KE and Kd compared with NS. A full list of the top 100 upregulated and 50 downregulated genes is available for each site in **Supplementary tables S5-S16**. Additionally, a detailed table of expanded genes for each of the symbols below can be found in **Supplementary Table S2**.

For the epidermis, the most significantly dysregulated genes were common to all three sites and indicated an activated, hyper-proliferative, pro-inflammatory and mesenchymally-poised

epithelium. Keratin 6 $\alpha$  and 6 $\beta$  were both significantly upregulated in all three epidermal sites, supporting the hyper-proliferation seen on keloid histology [1]. *K6* is induced in keratinocytes following injury where it is associated with migration through *Src* regulation [37, 38]. This activated epidermal expression [39] is reversible on wound closure and NSE (except the hair follicle) does not express *K6* [40]. Mucin-like 1 (*MUCL1*) was also significantly overexpressed in the *in situ* epidermis and has been associated with aggressive breast tumorigenesis and recurrence [41]. Interestingly, it was demonstrated that *MUCL1* may be required for proliferation of *ErbB2*-overexpressing breast cells [41] and this group have recently identified *ErbB2* overexpression in margin Kd (**chapter 6**). The inflammation-associated scavenger receptor *CD36* is also a marker of epidermal activation and not present in NS keratinocytes without specific stimuli [42]. It was found to disappear from hypertrophic scars with age whereas keloid scars maintained their *CD36* expression [43, 44], which is supported here by *CD36* upregulation in all 3 sites of the KE. The role of *CD36* in signal transduction suggests it may contribute to epithelial-mesenchymal signalling and it has been shown to affect the secretion of *TGF $\beta$ 1* [45], which is dysregulated in KD [46, 47].

The presence of EMT in KD is supported by our finding of *S100A8*, *WDR66* and *AKR1B10* overexpression in all 3 epidermal sites *in situ*. The knockdown of keratinocyte *S100A8*, recently shown to be upregulated in both keloid and hypertrophic scar epidermis, resulted in a failure to activate co-cultured fibroblasts and reduction in dermal fibrosis [48]. As a mediator of neutrophil migration [49, 50], *S100A8* is found in the suprabasal epidermis following injury, but gradually returns to baseline in a normally healed wound [51]. The role of *S100A8* in conversion of wounded keratinocytes to a migratory phenotype may represent a potential link to EMT and contribution to tumorigenesis [51]. Also implicated in EMT is the protein *WDR66*, which in oesophageal carcinoma has been shown to affect vimentin and occludin expression where its knockdown attenuated both cell proliferation and motility [52]. While we did not find altered vimentin expression, we did identify upregulation of fibronectin (*FN1*) ( $p = 0.06$ ) and  $\alpha$ -*SMA/ACTA2* ( $p = 0.033$ ) in the centre KE *in situ*. Our data also identified a significant upregulation

of *AKR1B10* (as well as *AKR1B1* and *AKR1B15*) in all three sites of the KE. This enzyme has a key role in the metabolism of retinoic acid (RA) and our recent study found the induced overexpression of *AKR1B10* in NS keratinocytes resulted in significant downregulation of E-cadherin [23]. Additionally, the treatment of keloid fibroblasts with *AKR1B10*-overexpressing keratinocyte medium resulted in upregulation of *TGFβ1*, Collagen I and collagen III, supporting a role for pathological epithelial-mesenchymal interactions (EMI) in keloid pathogenesis.

EMI encompass the essential cross-talk that governs the epidermal-dermal relationship in the skin and in addition to a multitude of essential organ development and physiologic processes, are essential for successful wound healing. Dysregulation of the processes involved in EMI (e.g. malfunction of negative feedback loops) can lead to abnormal wound healing and fibrosis or contribute to tumorigenesis [53, 54]. Previous exploration into the contribution of these EMI to KD have highlighted the significance of the epidermis in the formation and maintenance of this fibrotic scar [55, 56].

*BMP2*, a member of the *TGFβ* superfamily, was downregulated in our microarray data and has been shown to attenuate renal fibrosis, by reversing *TGFβ1*-induced EMT and cellular fibrotic markers [32]. Similarly, the loss of claudin-4 (*CLDN4*) and *CLDN23*, integral components of the tight junctions that maintain epithelial cell contacts [57] and downregulated here in KE *in situ*, are strongly implicated in EMT, potentially through E-cadherin modulation and thought to be negatively regulated by *TGFβ* [58-60]. We also identified significant upregulation of *NOTCH4* in all 3 epidermal sites and centre and margin Kd, which is linked with cancer stem cell activity and interestingly has very recently been associated with mesenchymal-epithelial transition (MET) [61, 62].

A role for EMT has previously been implicated in the pathogenesis of KD [63, 64]. EMT is a potentially reversible process whereby epithelial cells lose adhesion properties (downregulation E-cadherin, *CLDN4* and *CLDN23*) and gain migratory and invasive characteristics, transforming

into mesenchymal cells (upregulation *FN1* and *ACTA2*) [65]. Here, we present DEG that in combination support a role for EMT or at least “partial EMT” in KD (**Figure 5a**).

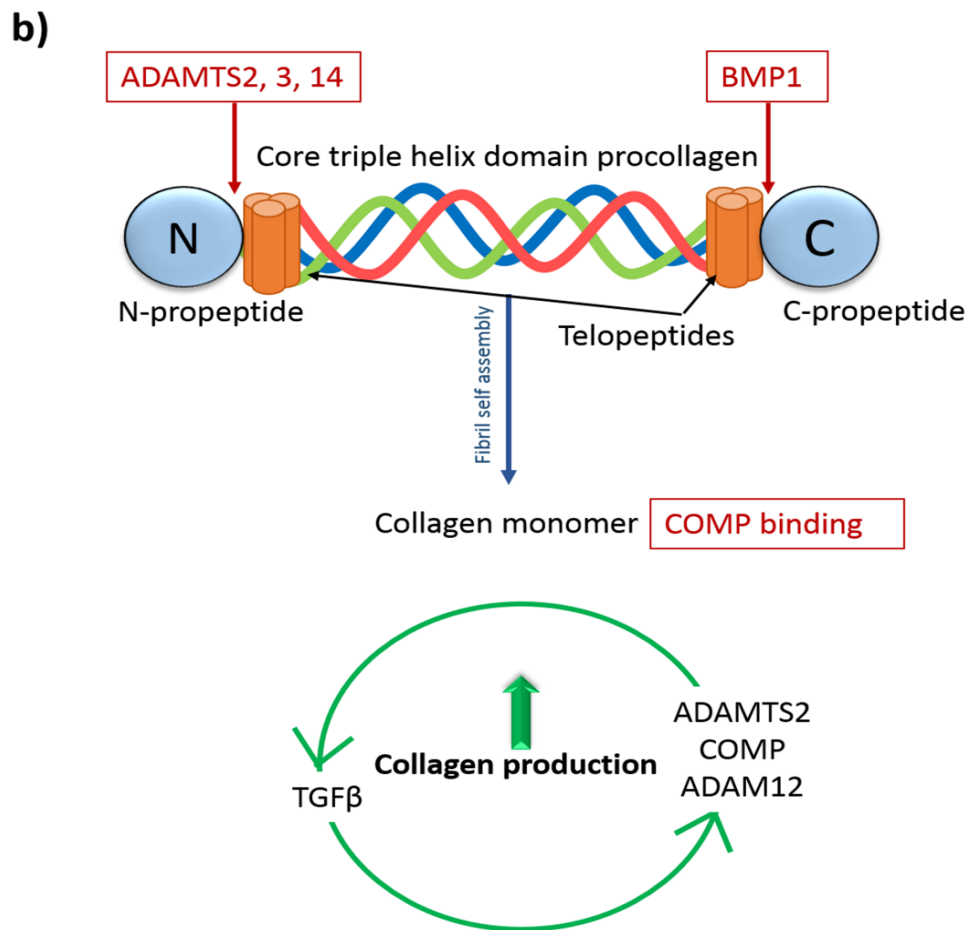
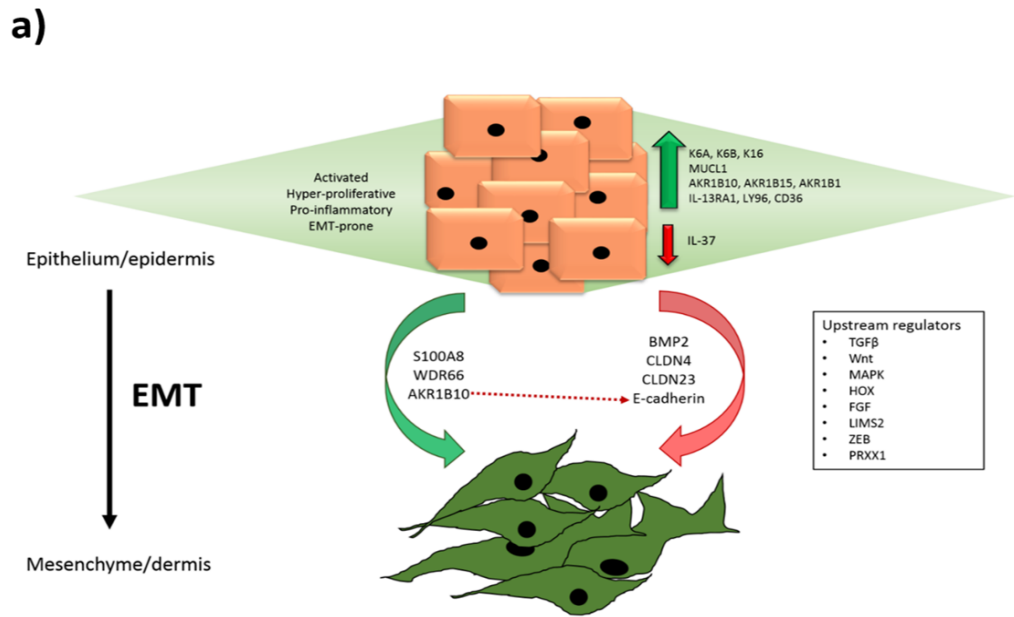


**Figure 5. *In situ* expression contributing to epithelial-mesenchymal transition (EMT) and collagen production in KD.** A) Schematic diagram of the differentially expressed genes (DEG) in KD that contribute to an activated, hyper-proliferative and inflammatory epidermis. Also depicted are DEG from our microarray data hypothesised to contribute to EMT through upregulation (green arrow) or downregulation (red arrow), which are described along with the upstream regulators identified on enrichment analysis of our microarray data and which have been previously implicated in the EMT process. B) Schematic diagram depicting where ADAMTS and BMP cleave the procollagen peptides to form tropocollagen and allow collagen fibril assembly necessary for collagen turnover (modified after [71]). Once a collagen monomer, it may bind COMP. Collagen production in KD may be increased by the potential existence of positive feedback loops between ADAMTS2/COMP/ADAM12 and TGF $\beta$ .

ADAM, a disintegrin and metalloproteinase; ADAMTS, a disintegrin and metalloproteinase with thrombospondin motifs; AKR1B10, aldo-keto reductase family 1, member 10; BMP, bone morphogenetic protein ; CLDN, claudin; COMP, cartilage oligomeric protein; FGF, fibroblast growth factor; HOX, homeotic gene subset; IL, interleukin; K, keratin; LIMS2, LIM zinc finger domain containing 2; MAPK, mitogen-activated protein kinase; MUCL1, mucin-like 1; S100A8, S100 calcium-binding protein A8; TGF $\beta$ , transforming growth factor beta; WDR66, WD repeat domain 66; ZEB, zinc finger E-box-binding proteins.

***In situ* keloid dermis expression reinforces the significance of TGF $\beta$  in KD pathogenesis through its regulation of the collagen network**

Collagen is the major structural protein of the ECM and fibrillar collagens (type I & III) are present in abundance in KD [1]. Fibroblasts are the most common producers of collagen and are subject to complex autocrine and paracrine cytokine signals to regulate its formation, of which TGF $\beta$  is crucial [66, 67]. In combination with these cytokines there are a number of enzymes and proteins that through cleavage or binding can affect collagen turnover [68].

Within the centre and margin Kd *in situ*, we identified dysregulation of a number of members of the ADAMTS family of enzymes, which are associated with tissue morphogenesis, remodelling, inflammation and angiogenesis [69]. Of these, *ADAMTS14* and *ADAMTS2* were the most significantly upregulated and are both pro-collagen N peptidases (pNP), responsible for the cleavage of type I and II pro-collagen necessary for fibril assembly and collagen biosynthesis (**Figure 5b**) [70, 71]. Interestingly, *BMP1*, responsible for the cleavage of the C-proteinase is also upregulated in centre and margin Kd (**Figure 5b**) [72]. The *ADAMTS* enzymes are associated with Dupuytren's disease [73], craniofacial fibrosis [74], Ehlers Danlos [75] and cancer [76, 77], with *ADAMTS2*-knockout mice demonstrating skin fragility [78] and reduced liver fibrosis *in vivo* [79]. More recently, studies have argued for *ADAMTS* involvement in a positive *TGFβ* feedback loop, whereby *ADAMTS2* is induced by but also targets *TGFβ* [80, 81]. To date the best described inhibitor of *ADAMTS* is *TIMP3* [70, 82, 83], which we found to be significantly downregulated in our microarray data in both centre ( $p = 0.026$ ) and margin ( $p = 0.037$ ) Kd. Interestingly, we identified upregulation of disintegrin and metalloproteinase *ADAM12*, the member of a family closely related to the *ADAMTS* group of proteins and which was also suggested to be involved in a positive feedback loop with *TGFβ*, resulting in continuous collagen production [84]. This proteinase is upregulated in several cancers and fibroses and was previously identified as upregulated in the keloid centre, where it was thought contribute to tissue remodelling [5, 85, 86]. Through its association with *TGFβ*, *ADAM12* has been implicated in EMT [87].

Also involved in collagen fibril assembly, is cartilage oligomeric matrix protein (*COMP*), which was significantly upregulated in both centre and margin Kd. *COMP* binds with affinity to collagens, especially collagen I, and has been previously identified in KD [88], where similar to *ADAMTS* it may be involved in a positive *TGFβ* feedback loop [89, 90]. Another member of the collagen matrix regulators and also previously investigated in KD is collagen triple helix repeat containing 1 (*CTHRC1*), which was demonstrated to decrease *TGFβ*-induced keloid fibroblast collagen I expression [91]. However, despite the seemingly contradictory descriptions of the negative effect of *CTHRC* on collagen I expression [92, 93], it has been widely correlated with

tissue invasion and migration, where its expression was induced by *TGFβ* [94, 95]. Here, we found *CTHRC1* significantly upregulated in centre and margin Kd *in situ*. This may represent the result of a feedback mechanism to counteract the expression of *TGFβ*, *ADAMTS* and *COMP* but without further investigation the mechanism underlying *CTHRC1* overexpression in keloid scars remains to be fully elucidated. In addition to *ADAMTS*, *ADAM12*, *COMP* and *CTHRC1*, we identified asporin (*ASPN*) and Wnt1-inducible-signaling pathway protein 1 (*WISP1*) as upregulated in both centre and margin Kd, which are also correlated with *TGFβ* expression. *ASPN*, a small leucine-rich proteoglycan thought to regulate tumour microenvironment, is known to bind *TGFβ* [96, 97] and has previously been found to be upregulated in the margin of KD [98]. The pro-proliferative *WISP1*, a member of the matricellular CCN family, was detected in Dupuytren's disease [99] and is strongly associated with liver [100] and lung fibrosis, where it was induced by *TGFβ1* [101] and implicated in EMT.

*TGFβ* is considered a master regulator in KD, involved in several positive and negative feedback loops that culminate in the net production of excess ECM through angiogenesis, proliferation, inflammation, differentiation processes and as indicated here, collagen deposition (**Figure 5b**) [102, 103]. *TGFβ* is also a major player in EMT, where it effects change at transcriptional and translational levels through both Smad and non-Smad pathway signalling [104-108]. While *TGFβ3* was significantly upregulated in the keloid centre and margin on microarray, *TGFβ1* was confirmed as upregulated in Kd compared with normal skin dermis using qRT-PCR (**Figure 3a**).

***In situ* expression indicates the potential contribution of IL-13, IL-17 and IL-37 to the inflammatory process underlying keloid disease**

The inflammatory phase of wound healing is a spatially and temporally precise process, essential to the supply of growth factor, chemokine and cytokine signalling necessary for repair. However, prolonged inflammation can result in impaired wound healing, leading to chronic wounds or excess scarring [109, 110]. KD is associated with an exaggerated inflammatory



response [6, 111]. Prolongation of the inflammatory phase with extended residency of these factors promotes proliferation, angiogenesis and increased deposition of ECM [112]. Interleukins are a group of secreted cytokines central to the inflammatory process that have an incompletely understood role in KD and may represent potential therapeutic targets.

*IL-13*, a potent fibrosis-promoting cytokine secreted by activated T<sub>H</sub>2 T-cells [113, 114], has been shown to increase collagen I & III production in keloid fibroblasts *in vitro* [115]. We found significant upregulation of *IL13RA1* in KE, epidermal and dermal upregulation of *IL-4R* and downregulation of *IL13RA2* in Kd *in situ* (**Table 2**). Together, *IL-13RA1* and *IL-4R* bind both *IL-13* and *IL-4* with high affinity to activate *JAK/STAT6* signalling (**Figure 6**) [116]. *IL-13RA2* is largely considered a high affinity decoy receptor thought to inhibit *IL-13* signalling *in vivo* and protect against fibrosis [117, 118]. Although this has been disputed [116], *IL-13* inhibition attenuated fibrosis and *IL-13RA2*-knockout mice have demonstrated enhanced *IL-13*-mediated responses *in vivo* [119-121]. Our current microarray findings, combined with previous evidence of KD containing an inflammatory niche populated by M2 macrophages [6], known to be *IL-13* recruited, supports an overexpression of *IL-13* in KD.

In addition to *IL-13* dysregulation, in all 3 KE sites compared with NS epidermis we identified loss of *IL-37*, a relatively new member of the interleukin-1 (*IL-1*) family, which described as anti-inflammatory has been shown to decrease the expression of *IL-6*, *IL-1 $\beta$* , *TNF $\alpha$*  and *IL-17* [122], all of which are associated with KD [13, 112]. It is thought *IL-37* is involved in a negative feedback loop to control excess inflammation, whereby *IL-37* induction by *TNF $\alpha$*  or toll-like receptors (TLR) results in suppression of *TNF $\alpha$*  and inhibition of pro-inflammatory cytokine release (**Figure 5**) [123]. While *IL-37* itself has not previously been investigated in KD, this finding is supported by altered expression of *IL-17*, *IL-1 $\beta$*  and *TNF $\alpha$*  in our microarray data.

*IL-17* signalling was dysregulated in common to both margin and extralesional Kd sites on enrichment analysis (**Figure 4b**). The pro-inflammatory *IL-17* is produced by a subset of activated CD4<sup>+</sup> T-cells, namely T<sub>H</sub>17 and a subset of innate lymphoid cells termed ILC3s, whose

differentiation and cytokine production is regulated by a complex interplay of molecules [124-126]. Studies have shown that *IL-6* and *TGFβ* initiate  $T_H17$  differentiation, *IL-23* in an autoregulatory feedback loop with *IL-1β* is responsible for the maintenance of *IL-17* and that *IL-2*, *IL-27*, *IL-4* and *IFNγ* are negative regulators [124, 127]. While we know KD shows an increased T-cell infiltrate in the dermis and that there is an inflammatory niche driven by the *IL-17/IL-6* axis, the complex interplay of this signalling mechanism remains incompletely understood [6, 13, 128]. Here, we identify an imbalance in inflammatory cytokine signalling, which alters between the three KE and Kd sites compares to NS (**Table 2**). Within the literature the association between these cytokines and their regulators/substrates is described with some variability and **Figure 6** depicts an interpretation of these relationships and how they may interact in KD. The *IL-17* environment is both cell-type and context-type dependent in contribution to neutrophil recruitment, angiogenesis and invasion [129, 130]. *IL-17* is known to be involved in other fibrotic conditions [131-133] and in KD it may be that *IL-17* expression differs between different sites within the keloid scar and that ongoing paracrine signalling produces the dynamic expression seen here.

The dysregulation of *IL13*, *IL-37* and *IL-17* in KD from our microarray data are likely interconnected (**Table 2**) and the mechanisms underlying modulation of KD by these interleukins requires further elucidation to determine their contribution to its pathogenesis and potential for therapeutic exploitation (**Figure 6**).

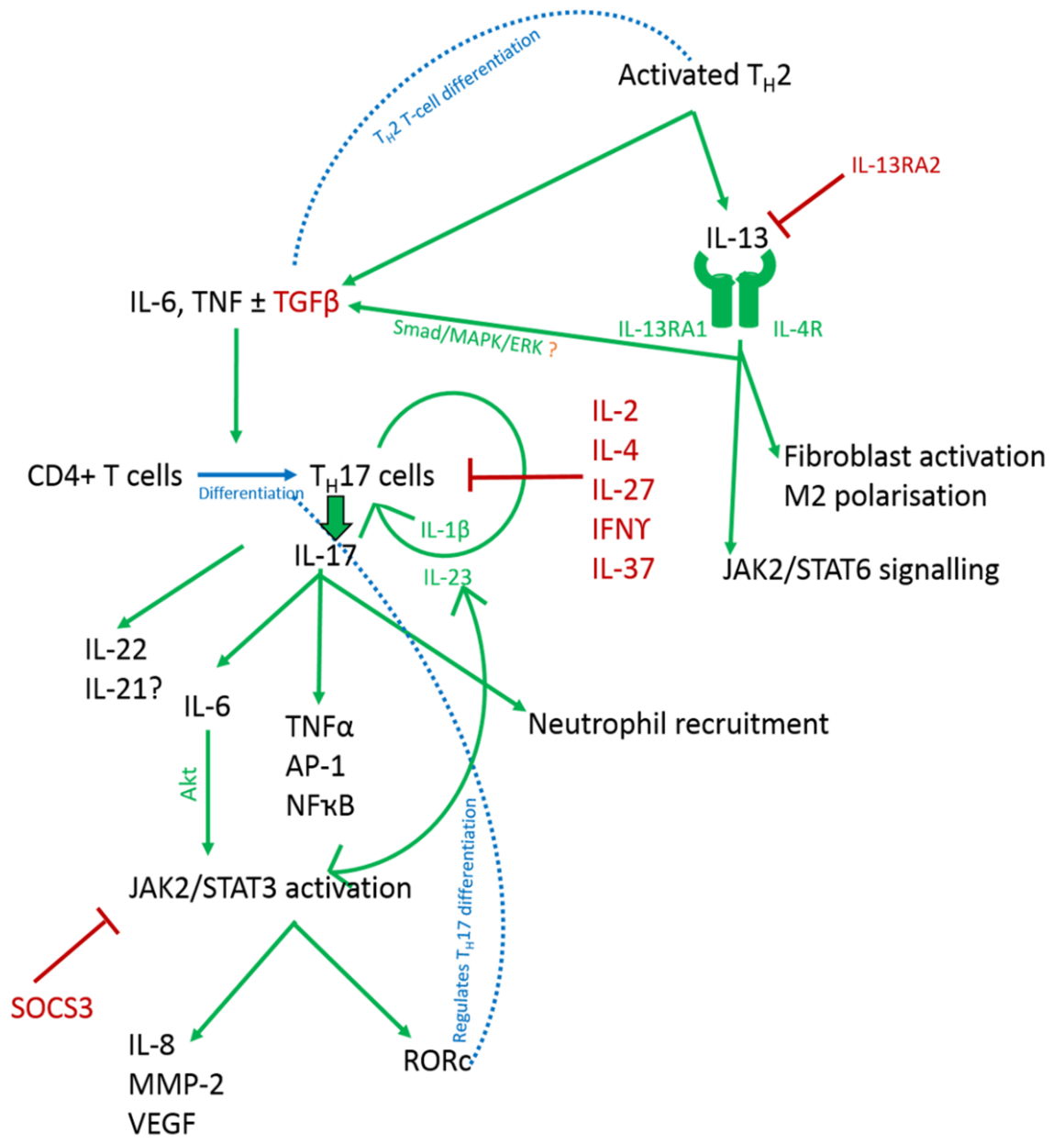


**Figure 6. Cytokine relationship with potential inflammatory effects in KD.** Schematic diagram of the possible relationships existing between a number of cytokines and growth factors identified as dysregulated in KD epidermis and dermis *in situ* in our microarray data. This figure should be correlated with Table 2 where the direction and fold change for each of these molecules can be found for each site within keloid epidermis and dermis.

AP-1, activating protein 1; IL, interleukin; INF, interferon; JAK, janus kinase; MMP, matrix metalloproteinase; NF $\kappa$ B, nuclear factor kappa B; ROR, retinoic acid-related orphan receptor c; STAT, signal transducer and activator of transcription; TGF $\beta$ , transforming growth factor beta; TNF, tumour necrosis factor.

**Table 2. Dysregulation of cytokines in site-specific KD microarray relating to IL-13, IL-37 and IL-17. All have p-value < 0.05. See Figure 6 for relationships.**

<b>Molecule</b>	<b>Keloid site</b>	<b>Centre: direction &amp; fold change</b>	<b>Margin: direction &amp; fold change</b>	<b>Extralesional: direction &amp; fold change</b>
<b>IL-13RA1</b>	<i>Epidermis</i>	↑ 8.45	↑ 4.8	↑ 3
<b>IL-13RA2</b>	<i>Dermis</i>	↓ 10.8	↓ 8.67	↓ 9.66
<b>IL-37</b>	<i>Epidermis</i>	↓ 6.51	↓ 4.85	↓ 10.66
<b>IL-17RA</b>	<i>Epidermis</i>	-	-	↓ 2.6
<b>IL-17RA</b>	<i>Dermis</i>	↓ 2.9	↓ 2.35	↑ 3.36
<b>IL-1β</b>	<i>Dermis</i>	-	↑ 3.83	↑ 4.61
<b>IL-23A</b>	<i>Dermis</i>	-	-	↑ 2.73
<b>IL-6R</b>	<i>Epidermis</i>	-	↑ 4.06	-
<b>IL-21R</b>	<i>Dermis</i>	-	↑ 2.64	↑ 2.01
<b>IL-2RA</b>	<i>Dermis</i>	-	↑ 2.95	-
<b>IL-4R</b>	<i>Epidermis</i>	↑ 2.31	-	-
<b>IL-4R</b>	<i>Dermis</i>	↑ 5.97	↑ 11.41	↓ 4.65
<b>IL-27</b>	<i>Dermis</i>	↑ 2.34	↑ 1.84	↑ 2.15
<b>STAT3</b>	<i>Dermis</i>	-	↓ 2.02	↓ 2.1
<b>SOCS3</b>	<i>Epidermis</i>	-	-	↑ 3.64
<b>SOCS3</b>	<i>Dermis</i>	↑ 4.32	↑ 5.68	↑ 5.69
<b>IL-8</b>	<i>Dermis</i>	-	-	↑ 12.27
<b>RORc</b>	<i>Dermis</i>	↓ 4.92	-	-

IL, interleukin; R, receptor; RA, receptor alpha; A, alpha; STAT, signal transducer and activator of transcription; SOCS, suppressor of cytokine signalling; ROR, retinoid-related orphan receptor

***In situ* analysis identifies loss of tumour suppression genes that combined with an expression profile promoting therapeutic resistance may account for currently ineffective keloid management**

The failure to switch on essential genes responsible for the attenuation of processes central to fibrosis can lead to exponential growth. The loss of expression of these genes can be as significant in the pathogenesis of KD as the overexpression of others. In this study, we identified a number of DEG previously associated with tumour suppression and drug resistance but not fully explored in KD.

Looking at the dermis, both *CEACAM1* and *SOX9* were found to be downregulated in keloid centre and margin compared with NSD. *CEACAM1*, a glycoprotein that mediates cell adhesion and immunity, is dysregulated in a number of cancers and considered a tumour suppressor gene [134-136]. Loss of *CEACAM1* has been implicated in the switch from superficial to pro-angiogenic, invasive tumour [137]. The concomitant downregulation of *SOX9* is likely to be linked given the correlation to *CEACAM1* in the literature to date [138-140].

We identified downregulation of *ATF3* in both centre and margin KE compared with NSE *in situ*. Although not previously investigated in KD, this CREB family protein is downregulated in a number of cancers [141] and considered an adaptive-response gene with tumour-suppressing effects that to date, demonstrate dual-role cell-type dependency [142, 143]. *ATF3* promotion of apoptosis, a key process in prevention of growth and invasion, may result from *KLF6* induction of *ATF3* [144] or through its activation of *p53* [145]. We found a significant downregulation of *KLF6* in the centre KE ( $p = 0.02$ ) and interestingly, *ATF3* has been shown to mediate apoptosis by anti-cancer therapies [146-148]. Also in KE *in situ*, *UGT3A2*, a member of the UDP-glycosyltransferase superfamily that plays a role in drug metabolism and which may affect detoxification of therapeutic drugs, was found to be strongly under-expressed [149, 150].

Our recent publication on the upregulation of *AKR1B10* in KE, where we hypothesised its ability to catalyse the reduction of carbonyls and xenobiotics may render keloid susceptible to

chemotherapeutic resistance and thus explain some of the difficulties associated with management of KD to date [23, 151]. Both *ALDH1A1* and the aforementioned upregulation of *NOTCH4* in KE are also associated with drug resistance [152, 153]. The upregulation of these molecules and multi-drug resistant nature of keloid scars may indicate the presence of a cancer stem cell-like population within the scar, which has been touched on but not fully explored in the literature [154, 155]. Tubulin  $\beta$ 3, class III (*TUBB3*), a cytoskeletal microtubule protein previously identified in solid tumours and extraocular fibrosis [156, 157], was also significantly upregulated in both centre and margin KE and Kd *in situ*. This molecule has been linked to both overexpression of *ErbB2* [158, 159], which we found upregulated in margin Kd ( $p = 0.0031$ ) and loss of *PTEN* [160, 161], which was also significantly downregulated in the margin Kd in our microarray data ( $p = 2.86 \times 10^{-5}$ ). *TUBB3* is associated with aggressive tumorigenesis in hypoxic environments [162], where it has been linked with chemoresistance, particularly taxanes [163-165]. This may be relevant to KD where there is evidence of a similarly hypoxic environment [63, 166, 167].

KD is notoriously difficult to manage in the clinical setting, with several available treatments but no one absolutely effective therapy [168-170]. Drug resistance has formed a major part of this failure [171]. In identifying DEG that may contribute to this seemingly multi-drug-resistant disease, it may be possible to tailor management by targeting these molecules with adjuvant therapies.

#### **Microarray data was validated through qRT-PCR of interesting targets**

We chose four candidate genes from each of the KE and Kd for qRT-PCR validation of the microarray findings. For the epidermis, the dysregulation of *AKR1B10* and associated *AKR1B1*, *AKR1B15* and *ALDH1A1* all related to the retinoic acid pathway and as such were previously validated [23]. Also in the KE, we wanted to validate genes representing different areas of interest including epidermal activation and inflammation (*CD36*), EMT (*WDR66* and *BMP2*) and

the possible existence of a cancer-like stem cell population (*NOTCH4*). As the most abundant protein in keloid ECM, collagen has long been investigated as a potential therapeutic target. Our identification of *ADAMTS14*, *ADAMTS2*, *COMP* and *ADAM12* represent significant alternative targets to *TGFβ* and as such were chosen for validation in the dermis. qRT-PCR for these genes not only reflected the microarray findings but also preserved the site-specific differences in expression, thus validating our data (**Figure 7**).



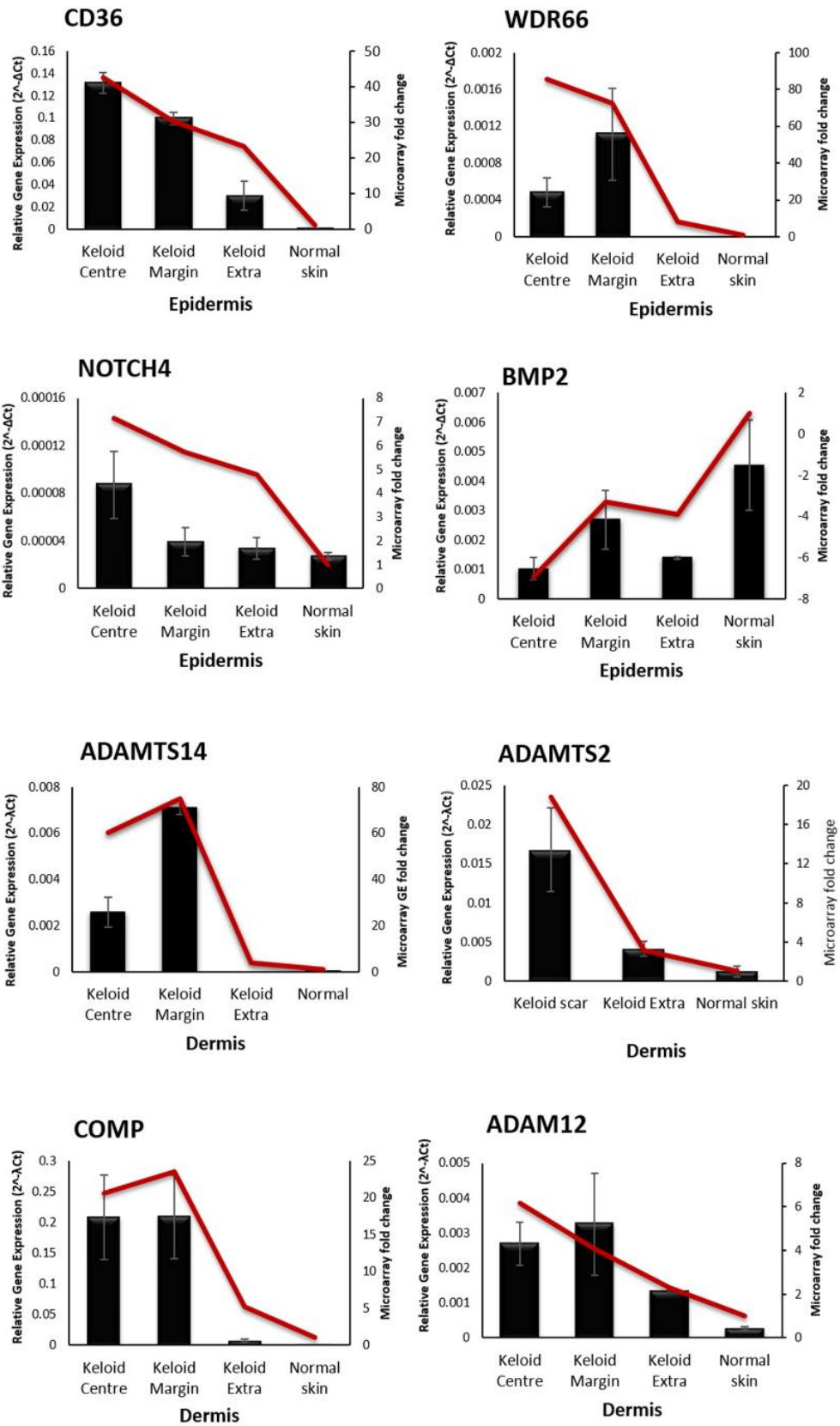


**Figure 7. qRT-PCR validation of candidate genes.** Four candidate genes were chosen from each of the epidermis and dermis for validation by qRT-PCR. The bar graphs represent the qRT-PCR data for the keloid sites and normal skin *in situ* and the line graph represents the associated microarray fold change in gene expression. In all cases the line graph follows the trend of the bar graph indicating the PCR reflects the microarray, thus validating the data. Data are presented as mean  $\pm$  SEM and are from at least three independent experiments.

ADAM, a disintegrin and metalloproteinase; ADAMTS, a disintegrin and metalloproteinase with thrombospondin motifs; BMP2, bone morphogenetic protein 2; CD36, cluster of differentiation 36; COMP, cartilage oligomeric protein; NOTCH4, notch 4; WDR66, WD repeat domain 66.

### Conclusions and perspectives

In this study we have combined LCM and microarray to examine KD by looking at the lesion as separate components; epidermis and dermis as well as centre, margin and extralesional sites. First, we showed this *in situ* approach was both more accurate and more sensitive than either whole tissue biopsy or monolayer cell culture methods in the dissection of the heterogeneous lesion that is keloid scar.

Through this strategy, we have distinguished several genes that are either novel or supportive of emerging literature with respect to KD pathobiology. In this study, expression patterns indicate the residence of a cancer-like stem cell population in KD, an area that is surprisingly under-researched in this field given the association with both EMT and drug resistance [171, 172]. The plausible presence of such a cell population in KD, which to date has been associated with inflammatory infiltrate [13, 34, 128], provides a reasonable explanation for the persistent growth, recurrence and multi-drug resistance that are characteristic of this disorder. The *in situ* strategy detailed in this study could benefit the isolation and characterisation of these cancer-like stem cells from within the keloid tissue and therefore constitutes an interesting focus for future work.

The multi-level ECM regulators, *ADAMTS14* and *ADAMTS2*, make attractive KD therapeutic targets. The potential redundancy of both these proteins with *ADAMTS3*, which we did not find to be upregulated in KD, indicates possible attenuation of their effect without the consequences of complete abrogation. *IL-37* overexpression *in vivo* in transgenic mice has resulted in dampened *IL-6*, *IL-1 $\beta$*  and *IL-17* [173], which are all previously shown to be upregulated in KD [13]. This suggests therapeutic induction of *IL-37* expression in KE, in order to dampen the pathologic inflammatory response, may be a prospective management strategy. Interestingly, there is differential gene expression between extralesional keloid and NS tissue. This may represent a field cancerisation effect whereby keloid tumour invasive growth is mediated by paracrine signalling with the adjacent NS and that within this extralesional perimeter the risk of keloid recurrence following treatment is greatest. Therefore, establishment of the extent of this extralesional expression divergence from that of NS may have clinical implications for KD management.

Given the clinically distinct keloid phenotypes and the morphological heterogeneity within the keloid scar, which is fully reflected here by the isolated gene expression profile of defined KD-associated lesion compartments, it is most likely a gene signature rather than a single biomarker that will prove valuable as a diagnostic tool when distinguishing KD from other cutaneous fibroses. Improved differential diagnosis prevents the morbidity and mortality associated with inappropriate management of clinically comparable conditions, some of which may have more serious consequences if improperly treated (for example; dermatofibrosarcoma protuberans and systemic sclerosis). The heterogeneity of KD has been addressed through the innovative *in situ* gene expression profiling approach in this study, which has provided a better-defined gene signature of distinct regions of keloid tissue pathobiology.

Therefore, there are differences evident between not only keloid and normal skin but also between each of these distinct keloid sites and normal skin. The use of IPA for data analysis as depicted in figures 2 and 4 of this paper highlight a number of upstream regulators of

proliferation and apoptosis as key differences between keloid and normal skin, which is in keeping with the literature [5, 8]. IPA analysis from both the epidermal and dermal compartments compared with normal skin identify *MYC*, *p53*, *EIF3E*, *DAB2* and several other regulators as key players in the centre and margin sites of the keloid scar, where the balance between proliferation and apoptosis is altered [5, 8, 264]. Particularly in the dermis, cell growth and proliferation were highlighted as important networks from the expression profiles where the centre and margin or centre and extralesional *in situ* dermis overlap.

It is likely that the complex nature of KD results from an interplay of simultaneously occurring processes, such that inflammation recruits factors that trigger EMT, which in turn can trigger cellular reversion to a stem cell-like state and thus exacerbate drug resistance [174]. While *TGFβ* is an attractive therapeutic target, the pleiotropic nature of this molecule makes a simplistic *TGFβ*-neutralisation strategy imprudent. Therefore, it would be useful if alternative molecular mechanisms that are important in KD pathobiology but more specific to it, could be selectively targeted therapeutically. Several novel, potentially important molecular targets and KD pathobiology candidate mechanisms have been dissected here that invite and facilitate further studies.

### **Acknowledgements**

The authors are grateful to Yaron Har-Shai and Guyan Arscott for their assistance with tissue sample provision and to Adam Taylor for his contribution to analysis. We thank Leo Zeef of the Bioinformatics and Genomic Technologies Core Facilities at the University of Manchester for providing support with regard to microarrays.

## References

1. Jumper N, Paus R, Bayat A. Functional histopathology of keloid disease. *Histol Histopathol.* 2015;30: 1033-57.
2. Berman B, Kaufman J. Pilot study of the effect of postoperative imiquimod 5% cream on the recurrence rate of excised keloids. *Journal of the American Academy of Dermatology.* 2002;47: S209-11.
3. Marttala J, Andrews JP, Rosenbloom J, Uitto J. Keloids: Animal models and pathologic equivalents to study tissue fibrosis. *Matrix Biol.* 2016.
4. Butler PD, Longaker MT, Yang GP. Current progress in keloid research and treatment. *J Am Coll Surg.* 2008;206: 731-41.
5. Seifert O, Bayat A, Geffers R, Dienus K, Buer J, Lofgren S, et al. Identification of unique gene expression patterns within different lesional sites of keloids. *Wound repair and regeneration : official publication of the Wound Healing Society [and] the European Tissue Repair Society.* 2008;16: 254-65.
6. Bagabir R, Byers RJ, Chaudhry IH, Muller W, Paus R, Bayat A. Site-specific immunophenotyping of keloid disease demonstrates immune upregulation and the presence of lymphoid aggregates. *Br J Dermatol.* 2012;167: 1053-66.
7. Syed F, Ahmadi E, Iqbal SA, Singh S, McGrouther DA, Bayat A. Fibroblasts from the growing margin of keloid scars produce higher levels of collagen I and III compared with intralesional and extralesional sites: clinical implications for lesional site-directed therapy. *Br J Dermatol.* 2011;164: 83-96.
8. Lu F, Gao J, Ogawa R, Hyakusoku H, Ou C. Biological differences between fibroblasts derived from peripheral and central areas of keloid tissues. *Plast Reconstr Surg.* 2007;120: 625-30.
9. Mitsui H, Suarez-Farinas M, Belkin DA, Levenkova N, Fuentes-Duculan J, Coats I, et al. Combined use of laser capture microdissection and cDNA microarray analysis identifies locally expressed disease-related genes in focal regions of psoriasis vulgaris skin lesions. *The Journal of investigative dermatology.* 2012;132: 1615-26.
10. Marmai C, Sutherland RE, Kim KK, Dolganov GM, Fang X, Kim SS, et al. Alveolar epithelial cells express mesenchymal proteins in patients with idiopathic pulmonary fibrosis. *Am J Physiol Lung Cell Mol Physiol.* 2011;301: L71-8.
11. Makhzami S, Rambow F, Delmas V, Larue L. Efficient gene expression profiling of laser-microdissected melanoma metastases. *Pigment Cell Melanoma Res.* 2012;25: 783-91.
12. Mabry KM, Payne SZ, Anseth KS. Microarray analyses to quantify advantages of 2D and 3D hydrogel culture systems in maintaining the native valvular interstitial cell phenotype. *Biomaterials.* 2016;74: 31-41.
13. Zhang Q, Yamaza T, Kelly AP, Shi S, Wang S, Brown J, et al. Tumor-like stem cells derived from human keloid are governed by the inflammatory niche driven by IL-17/IL-6 axis. *PLoS One.* 2009;4: e7798.
14. Lee JY, Yang CC, Chao SC, Wong TW. Histopathological differential diagnosis of keloid and hypertrophic scar. *Am J Dermatopathol.* 2004;26: 379-84.
15. Bayat A, Arscott G, Ollier WE, McGrouther DA, Ferguson MW. Keloid disease: clinical relevance of single versus multiple site scars. *British journal of plastic surgery.* 2005;58: 28-37.
16. Clement-Ziza M, Munnich A, Lyonnet S, Jaubert F, Besmond C. Stabilization of RNA during laser capture microdissection by performing experiments under argon atmosphere or using ethanol as a solvent in staining solutions. *RNA.* 2008;14: 2698-704.
17. Koliijn K, van Leenders GJ. Comparison of RNA extraction kits and histological stains for laser capture microdissected prostate tissue. *BMC research notes.* 2016;9: 1-6.

18. Harries MJ, Meyer K, Chaudhry I, J EK, Poblet E, Griffiths CE, et al. Lichen planopilaris is characterized by immune privilege collapse of the hair follicle's epithelial stem cell niche. *J Pathol.* 2013;231: 236-47.
19. Kameda T, Shide K, Yamaji T, Kamiunten A, Sekine M, Hidaka T, et al. Gene expression profiling of loss of TET2 and/or JAK2V617F mutant hematopoietic stem cells from mouse models of myeloproliferative neoplasms. *Genomics data.* 2015;4: 102-8.
20. Masuda A, Katoh N, Nakabayashi K, Kato K, Sonoda K, Kitade M, et al. An improved method for isolation of epithelial and stromal cells from the human endometrium. *The Journal of reproduction and development.* 2016;62: 213.
21. Leguen I, Le Cam A, Montfort J, Peron S, Fautrel A. Transcriptomic Analysis of Trout Gill Ionocytes in Fresh Water and Sea Water Using Laser Capture Microdissection Combined with Microarray Analysis. *PLoS one.* 2015;10: e0139938.
22. Ashcroft KJ, Syed F, Bayat A. Site-specific keloid fibroblasts alter the behaviour of normal skin and normal scar fibroblasts through paracrine signalling. *PLoS One.* 2013;8: e75600.
23. Jumper N, Hodgkinson T, Arscott G, Har-Shai Y, Paus R, Bayat A. The aldo-keto reductase AKR1B10 is upregulated in keloid epidermis, implicating retinoic acid pathway dysregulation in the pathogenesis of keloid disease. *The Journal of investigative dermatology.* 2016 Jul;136(7):1500-12.
24. Benjamini Y, Hochberg Y. Controlling the false discovery rate: a practical and powerful approach to multiple testing. *Journal of the royal statistical society Series B (Methodological).* 1995: 289-300.
25. Sidgwick GP, McGeorge D, Bayat A. Functional testing of topical skin formulations using an optimised ex vivo skin organ culture model. *Arch Dermatol Res.* 2016;308: 297-308.
26. Bolstad BM, Irizarry RA, Åstrand M, Speed TP. A comparison of normalization methods for high density oligonucleotide array data based on variance and bias. *Bioinformatics.* 2003;19: 185-93.
27. Ringnér M. What is principal component analysis? *Nature biotechnology.* 2008;26: 303-4.
28. Oliveros J. Venny. An interactive tool for comparing lists with Venn's diagrams.(2007–2015).
29. Baker BM, Chen CS. Deconstructing the third dimension: how 3D culture microenvironments alter cellular cues. *J Cell Sci.* 2012;125: 3015-24.
30. Lee WJ, Park JH, Shin JU, Noh H, Lew DH, Yang WI, et al. Endothelial-to-mesenchymal transition induced by Wnt 3a in keloid pathogenesis. *Wound repair and regeneration : official publication of the Wound Healing Society [and] the European Tissue Repair Society.* 2015;23: 435-42.
31. Lamouille S, Xu J, Derynck R. Molecular mechanisms of epithelial-mesenchymal transition. *Nat Rev Mol Cell Biol.* 2014;15: 178-96.
32. Yang YL, Ju HZ, Liu SF, Lee TC, Shih YW, Chuang LY, et al. BMP-2 suppresses renal interstitial fibrosis by regulating epithelial-mesenchymal transition. *J Cell Biochem.* 2011;112: 2558-65.
33. Pratap A, Singh S, Mundra V, Yang N, Panakanti R, Eason JD, et al. Attenuation of early liver fibrosis by pharmacological inhibition of smoothed receptor signaling. *J Drug Target.* 2012;20: 770-82.
34. Grant C, Chudakova DA, Itinteang T, Chibnall AM, Brasch HD, Davis PF, et al. Expression of embryonic stem cell markers in keloid-associated lymphoid tissue. *J Clin Pathol.* 2016.
35. Honda K, Yanai H, Negishi H, Asagiri M, Sato M, Mizutani T, et al. IRF-7 is the master regulator of type-I interferon-dependent immune responses. *Nature.* 2005;434: 772-7.
36. Lu P, Weaver VM, Werb Z. The extracellular matrix: a dynamic niche in cancer progression. *J Cell Biol.* 2012;196: 395-406.

37. Pan X, Hobbs RP, Coulombe PA. The expanding significance of keratin intermediate filaments in normal and diseased epithelia. *Curr Opin Cell Biol.* 2013;25: 47-56.
38. Rotty JD, Coulombe PA. A wound-induced keratin inhibits Src activity during keratinocyte migration and tissue repair. *J Cell Biol.* 2012;197: 381-9.
39. Luo S, Yufit T, Carson P, Fiore D, Falanga J, Lin X, et al. Differential keratin expression during epiboly in a wound model of bioengineered skin and in human chronic wounds. *Int J Low Extrem Wounds.* 2011;10: 122-9.
40. Leigh IM, Navsaria H, Purkis PE, McKay IA, Bowden PE, Riddle PN. Keratins (K16 and K17) as markers of keratinocyte hyperproliferation in psoriasis in vivo and in vitro. *Br J Dermatol.* 1995;133: 501-11.
41. Conley SJ, Bosco EE, Tice DA, Hollingsworth RE, Herbst R, Xiao Z. HER2 drives Mucin-like 1 to control proliferation in breast cancer cells. *Oncogene.* 2016.
42. Hakvoort TE, Altun V, Ramrattan RS, van der Kwast TH, Benner R, van Zuijlen PP, et al. Epidermal participation in post-burn hypertrophic scar development. *Virchows Arch.* 1999;434: 221-6.
43. Santucci M, Borgognoni L, Reali UM, Gabbiani G. Keloids and hypertrophic scars of Caucasians show distinctive morphologic and immunophenotypic profiles. *Virchows Arch.* 2001;438: 457-63.
44. Alessio M, Gruarin P, Castagnoli C, Trombotto C, Stella M. Primary ex vivo culture of keratinocytes isolated from hypertrophic scars as a means of biochemical characterization of CD36. *Int J Clin Lab Res.* 1998;28: 47-54.
45. Xiong W, Frasch SC, Thomas SM, Bratton DL, Henson PM. Induction of TGF-beta1 synthesis by macrophages in response to apoptotic cells requires activation of the scavenger receptor CD36. *PLoS One.* 2013;8: e72772.
46. He S, Liu X, Yang Y, Huang W, Xu S, Yang S, et al. Mechanisms of transforming growth factor beta(1)/Smad signalling mediated by mitogen-activated protein kinase pathways in keloid fibroblasts. *Br J Dermatol.* 2010;162: 538-46.
47. Zhou P, Shi L, Li Q, Lu D. Overexpression of RACK1 inhibits collagen synthesis in keloid fibroblasts via inhibition of transforming growth factor-beta1/Smad signaling pathway. *Int J Clin Exp Med.* 2015;8: 15262-8.
48. Zhong A, Xu W, Zhao J, Xie P, Jia S, Sun J, et al. S100A8 and S100A9 Are Induced by Decreased Hydration in the Epidermis and Promote Fibroblast Activation and Fibrosis in the Dermis. *Am J Pathol.* 2016;186: 109-22.
49. Ryckman C, Vandal K, Rouleau P, Talbot M, Tessier PA. Proinflammatory activities of S100: proteins S100A8, S100A9, and S100A8/A9 induce neutrophil chemotaxis and adhesion. *The Journal of Immunology.* 2003;170: 3233-42.
50. Ong C, Khoo Y, Mukhopadhyay A, Masilamani J, Do D, Lim I, et al. Comparative proteomic analysis between normal skin and keloid scar. *British Journal of Dermatology.* 2010;162: 1302-15.
51. Kerkhoff C, Voss A, Scholzen TE, Averill MM, Zänker KS, Bornfeldt KE. Novel insights into the role of S100A8/A9 in skin biology. *Experimental dermatology.* 2012;21: 822-6.
52. Wang Q, Ma C, Kemmner W. Wdr66 is a novel marker for risk stratification and involved in epithelial-mesenchymal transition of esophageal squamous cell carcinoma. *BMC Cancer.* 2013;13: 137.
53. Kalluri R, Neilson EG. Epithelial-mesenchymal transition and its implications for fibrosis. *J Clin Invest.* 2003;112: 1776-84.
54. Thiery JP, Sleeman JP. Complex networks orchestrate epithelial-mesenchymal transitions. *Nat Rev Mol Cell Biol.* 2006;7: 131-42.
55. Hahn JM, Glaser K, McFarland KL, Aronow BJ, Boyce ST, Supp DM. Keloid-derived keratinocytes exhibit an abnormal gene expression profile consistent with a distinct

- causal role in keloid pathology. *Wound repair and regeneration* : official publication of the Wound Healing Society [and] the European Tissue Repair Society. 2013;21: 530-44.
56. Do DV, Ong CT, Khoo YT, Carbone A, Lim CP, Wang S, et al. Interleukin-18 system plays an important role in keloid pathogenesis via epithelial-mesenchymal interactions. *Br J Dermatol*. 2012;166: 1275-88.
  57. Shang X, Lin X, Alvarez E, Manorek G, Howell SB. Tight junction proteins claudin-3 and claudin-4 control tumor growth and metastases. *Neoplasia*. 2012;14: 974-IN22.
  58. Lin X, Shang X, Manorek G, Howell SB. Regulation of the Epithelial-Mesenchymal Transition by Claudin-3 and Claudin-4. *PLoS One*. 2013;8: e67496.
  59. Michl P, Barth C, Buchholz M, Lerch MM, Rolke M, Holzmann KH, et al. Claudin-4 expression decreases invasiveness and metastatic potential of pancreatic cancer. *Cancer Res*. 2003;63: 6265-71.
  60. Bujko M, Kober P, Mikula M, Ligaj M, Ostrowski J, Siedlecki JA. Expression changes of cell-cell adhesion-related genes in colorectal tumors. *Oncol Lett*. 2015;9: 2463-70.
  61. Harrison H, Farnie G, Howell SJ, Rock RE, Stylianou S, Brennan KR, et al. Regulation of breast cancer stem cell activity by signaling through the Notch4 receptor. *Cancer Res*. 2010;70: 709-18.
  62. Bonyadi Rad E, Hammerlindl H, Wels C, Popper U, Ravindran Menon D, Breiteneder H, et al. Notch4 Signaling Induces a Mesenchymal-Epithelial-like Transition in Melanoma Cells to Suppress Malignant Behaviors. *Cancer Res*. 2016.
  63. Ma X, Chen J, Xu B, Long X, Qin H, Zhao RC, et al. Keloid-derived keratinocytes acquire a fibroblast-like appearance and an enhanced invasive capacity in a hypoxic microenvironment in vitro. *Int J Mol Med*. 2015;35: 1246-56.
  64. Yan L, Cao R, Wang L, Liu Y, Pan B, Yin Y, et al. Epithelial-mesenchymal transition in keloid tissues and TGF-beta1-induced hair follicle outer root sheath keratinocytes. *Wound repair and regeneration* : official publication of the Wound Healing Society [and] the European Tissue Repair Society. 2015;23: 601-10.
  65. Kalluri R, Weinberg RA. The basics of epithelial-mesenchymal transition. *The Journal of clinical investigation*. 2009;119: 1420-8.
  66. Verrecchia F, Mauviel A. Transforming growth factor-beta and fibrosis. *World J Gastroenterol*. 2007;13: 3056-62.
  67. Lan CC, Fang AH, Wu PH, Wu CS. Tacrolimus abrogates TGF-beta1-induced type I collagen production in normal human fibroblasts through suppressing p38MAPK signalling pathway: implications on treatment of chronic atopic dermatitis lesions. *J Eur Acad Dermatol Venereol*. 2014;28: 204-15.
  68. Steplewski A, Fertala A. Inhibition of collagen fibril formation. *Fibrogenesis Tissue Repair*. 2012;5: S29.
  69. Kelwick R, Desanlis I, Wheeler GN, Edwards DR. The ADAMTS (A Disintegrin and Metalloproteinase with Thrombospondin motifs) family. *Genome Biol*. 2015;16: 113.
  70. Bekhouche M, Colige A. The procollagen N-proteinases ADAMTS2, 3 and 14 in pathophysiology. *Matrix Biol*. 2015;44-46: 46-53.
  71. Colige A, Vandenberghe I, Thiry M, Lambert CA, Van Beeumen J, Li SW, et al. Cloning and characterization of ADAMTS-14, a novel ADAMTS displaying high homology with ADAMTS-2 and ADAMTS-3. *The Journal of biological chemistry*. 2002;277: 5756-66.
  72. Broder C, Arnold P, Vadon-Le Goff S, Konerding MA, Bahr K, Muller S, et al. Metalloproteases meprin alpha and meprin beta are C- and N-procollagen proteinases important for collagen assembly and tensile strength. *Proc Natl Acad Sci U S A*. 2013;110: 14219-24.
  73. Johnston P, Chojnowski AJ, Davidson RK, Riley GP, Donell ST, Clark IM. A complete expression profile of matrix-degrading metalloproteinases in Dupuytren's disease. *J Hand Surg Am*. 2007;32: 343-51.



74. Zhou SH, Yang WJ, Liu SW, Li J, Zhang CY, Zhu Y, et al. Gene expression profiling of craniofacial fibrous dysplasia reveals ADAMTS2 overexpression as a potential marker. *Int J Clin Exp Pathol.* 2014;7: 8532-41.
75. Colige A, Nuytinck L, Hausser I, van Essen AJ, Thiry M, Herens C, et al. Novel types of mutation responsible for the dermatosparactic type of Ehlers-Danlos syndrome (Type VIIC) and common polymorphisms in the ADAMTS2 gene. *The Journal of investigative dermatology.* 2004;123: 656-63.
76. Kumar S, Rao N, Ge R. Emerging Roles of ADAMTSs in Angiogenesis and Cancer. *Cancers (Basel).* 2012;4: 1252-99.
77. Cal S, Lopez-Otin C. ADAMTS proteases and cancer. *Matrix Biol.* 2015;44-46: 77-85.
78. Li SW, Arita M, Fertala A, Bao Y, Kopen GC, Langsjø TK, et al. Transgenic mice with inactive alleles for procollagen N-proteinase (ADAMTS-2) develop fragile skin and male sterility. *Biochem J.* 2001;355: 271-8.
79. Kesteloot F, Desmouliere A, Leclercq I, Thiry M, Arrese JE, Prockop DJ, et al. ADAM metalloproteinase with thrombospondin type 1 motif 2 inactivation reduces the extent and stability of carbon tetrachloride-induced hepatic fibrosis in mice. *Hepatology.* 2007;46: 1620-31.
80. Wang WM, Lee S, Steiglitiz BM, Scott IC, Lebares CC, Allen ML, et al. Transforming growth factor-beta induces secretion of activated ADAMTS-2. A procollagen III N-proteinase. *The Journal of biological chemistry.* 2003;278: 19549-57.
81. Bekhouche M, Leduc C, Dupont L, Janssen L, Delolme F, Vadon-Le Goff S, et al. Determination of the substrate repertoire of ADAMTS2, 3, and 14 significantly broadens their functions and identifies extracellular matrix organization and TGF-beta signaling as primary targets. *FASEB J.* 2016.
82. Jones GC, Riley GP. ADAMTS proteinases: a multi-domain, multi-functional family with roles in extracellular matrix turnover and arthritis. *Arthritis Res Ther.* 2005;7: 160-9.
83. Wang WM, Ge G, Lim NH, Nagase H, Greenspan DS. TIMP-3 inhibits the procollagen N-proteinase ADAMTS-2. *Biochem J.* 2006;398: 515-9.
84. Dulauroy S, Di Carlo SE, Langa F, Eberl G, Peduto L. Lineage tracing and genetic ablation of ADAM12(+) perivascular cells identify a major source of profibrotic cells during acute tissue injury. *Nat Med.* 2012;18: 1262-70.
85. Shih B, Wijeratne D, Armstrong DJ, Lindau T, Day P, Bayat A. Identification of biomarkers in Dupuytren's disease by comparative analysis of fibroblasts versus tissue biopsies in disease-specific phenotypes. *J Hand Surg Am.* 2009;34: 124-36.
86. Kveiborg M, Albrechtsen R, Couchman JR, Wewer UM. Cellular roles of ADAM12 in health and disease. *The international journal of biochemistry & cell biology.* 2008;40: 1685-702.
87. Ruff M, Leyme A, Le Cann F, Bonnier D, Le Seyec J, Chesnel F, et al. The Disintegrin and Metalloprotease ADAM12 Is Associated with TGF-beta-Induced Epithelial to Mesenchymal Transition. *PLoS One.* 2015;10: e0139179.
88. Naitoh M, Kubota H, Ikeda M, Tanaka T, Shirane H, Suzuki S, et al. Gene expression in human keloids is altered from dermal to chondrocytic and osteogenic lineage. *Genes Cells.* 2005;10: 1081-91.
89. Inui S, Shono F, Nakajima T, Hosokawa K, Itami S. Identification and characterization of cartilage oligomeric matrix protein as a novel pathogenic factor in keloids. *Am J Pathol.* 2011;179: 1951-60.
90. Agarwal P, Schulz JN, Blumbach K, Andreasson K, Heinegard D, Paulsson M, et al. Enhanced deposition of cartilage oligomeric matrix protein is a common feature in fibrotic skin pathologies. *Matrix Biol.* 2013;32: 325-31.
91. Li J, Cao J, Li M, Yu Y, Yang Y, Xiao X, et al. Collagen triple helix repeat containing-1 inhibits transforming growth factor-b1-induced collagen type I expression in keloid. *Br J Dermatol.* 2011;164: 1030-6.

92. Bauer Y, Tedrow J, de Bernard S, Birker-Robaczewska M, Gibson KF, Guardela BJ, et al. A novel genomic signature with translational significance for human idiopathic pulmonary fibrosis. *Am J Respir Cell Mol Biol*. 2015;52: 217-31.
93. LeClair R, Lindner V. The role of collagen triple helix repeat containing 1 in injured arteries, collagen expression, and transforming growth factor beta signaling. *Trends Cardiovasc Med*. 2007;17: 202-5.
94. Eriksson J, Le Joncour V, Nummela P, Jahkola T, Virolainen S, Laakkonen P, et al. Gene expression analyses of primary melanomas reveal CTHRC1 as an important player in melanoma progression. *Oncotarget*. 2016.
95. Wang CY, Zhang JJ, Hua L, Yao KH, Chen JT, Ren XQ. MicroRNA-98 suppresses cell proliferation, migration and invasion by targeting collagen triple helix repeat containing 1 in hepatocellular carcinoma. *Mol Med Rep*. 2016;13: 2639-44.
96. Ding Q, Zhang M, Liu C. Asporin participates in gastric cancer cell growth and migration by influencing EGF receptor signaling. *Oncol Rep*. 2015;33: 1783-90.
97. Hurley PJ, Sundi D, Shinder B, Simons BW, Hughes RM, Miller RM, et al. Germline Variants in Asporin Vary by Race, Modulate the Tumor Microenvironment, and Are Differentially Associated with Metastatic Prostate Cancer. *Clin Cancer Res*. 2016;22: 448-58.
98. Shih B, McGrouther DA, Bayat A. Identification of novel keloid biomarkers through profiling of tissue biopsies versus cell cultures in keloid margin specimens compared to adjacent normal skin. *Eplasty*. 2010;10: e24.
99. van Beuge MM, Ten Dam EJ, Werker PM, Bank RA. Wnt pathway in Dupuytren disease: connecting profibrotic signals. *Transl Res*. 2015;166: 762-71 e3.
100. Jian YC, Wang JJ, Dong S, Hu JW, Hu LJ, Yang GM, et al. Wnt-induced secreted protein 1/CCN4 in liver fibrosis both in vitro and in vivo. *Clin Lab*. 2014;60: 29-35.
101. Berschneider B, Ellwanger DC, Baarsma HA, Thiel C, Shimbori C, White ES, et al. miR-92a regulates TGF-beta1-induced WISP1 expression in pulmonary fibrosis. *The international journal of biochemistry & cell biology*. 2014;53: 432-41.
102. Andrews JP, Marttala J, Macarak E, Rosenbloom J, Uitto J. Keloids: The paradigm of skin fibrosis - Pathomechanisms and treatment. *Matrix Biol*. 2016.
103. Wu CS, Wu PH, Fang AH, Lan CC. FK506 inhibits the enhancing effects of transforming growth factor (TGF)-beta1 on collagen expression and TGF-beta/Smad signalling in keloid fibroblasts: implication for new therapeutic approach. *Br J Dermatol*. 2012;167: 532-41.
104. Katsuno Y, Lamouille S, Derynck R. TGF-beta signaling and epithelial-mesenchymal transition in cancer progression. *Curr Opin Oncol*. 2013;25: 76-84.
105. Derynck R, Muthusamy BP, Saeteurn KY. Signaling pathway cooperation in TGF-beta-induced epithelial-mesenchymal transition. *Curr Opin Cell Biol*. 2014;31: 56-66.
106. Strzyz P. Cancer biology: TGF [beta] and EMT as double agents. *Nature Reviews Molecular Cell Biology*. 2016.
107. David CJ, Huang Y-H, Chen M, Su J, Zou Y, Bardeesy N, et al. TGF- $\beta$  Tumor Suppression through a Lethal EMT. *Cell*. 2016;164: 1015-30.
108. Valcourt U, Carthy J, Okita Y, Alcaraz L, Kato M, Thuault S, et al. Analysis of Epithelial–Mesenchymal Transition Induced by Transforming Growth Factor  $\beta$ . *TGF- $\beta$  Signaling: Methods and Protocols*. 2016: 147-81.
109. Eming SA, Krieg T, Davidson JM. Inflammation in wound repair: molecular and cellular mechanisms. *The Journal of investigative dermatology*. 2007;127: 514-25.
110. Qian LW, Fourcaudot AB, Yamane K, You T, Chan RK, Leung KP. Exacerbated and prolonged inflammation impairs wound healing and increases scarring. Wound repair and regeneration : official publication of the Wound Healing Society [and] the European Tissue Repair Society. 2016;24: 26-34.

111. Zhang M, Xu Y, Liu Y, Cheng Y, Zhao P, Liu H, et al. Chemokine-Like Factor 1 (CKLF-1) is Overexpressed in Keloid Patients: A Potential Indicating Factor for Keloid-Predisposed Individuals. *Medicine (Baltimore)*. 2016;95: e3082.
112. Dong X, Mao S, Wen H. Upregulation of proinflammatory genes in skin lesions may be the cause of keloid formation (Review). *Biomed Rep*. 2013;1: 833-6.
113. Borthwick LA, Wynn TA. IL-13 and TGF- $\beta$ 1: Core Mediators of Fibrosis. *Current Pathobiology Reports*. 2015;3: 273-82.
114. Baraut J, Farge D, Jean-Louis F, Masse I, Grigore EI, Arruda LC, et al. Transforming growth factor-beta increases interleukin-13 synthesis via GATA-3 transcription factor in T-lymphocytes from patients with systemic sclerosis. *Arthritis Res Ther*. 2015;17: 196.
115. Oriente A, Fedarko NS, Pacocha SE, Huang SK, Lichtenstein LM, Essayan DM. Interleukin-13 modulates collagen homeostasis in human skin and keloid fibroblasts. *J Pharmacol Exp Ther*. 2000;292: 988-94.
116. McCormick SM, Heller NM. Commentary: IL-4 and IL-13 receptors and signaling. *Cytokine*. 2015;75: 38-50.
117. Granel B, Allanore Y, Chevillard C, Arnaud V, Marquet S, Weiller PJ, et al. IL13RA2 gene polymorphisms are associated with systemic sclerosis. *J Rheumatol*. 2006;33: 2015-9.
118. Chiaramonte MG, Mentink-Kane M, Jacobson BA, Cheever AW, Whitters MJ, Goad ME, et al. Regulation and function of the interleukin 13 receptor alpha 2 during a T helper cell type 2-dominant immune response. *J Exp Med*. 2003;197: 687-701.
119. Wood N, Whitters MJ, Jacobson BA, Witek J, Sypek JP, Kasaian M, et al. Enhanced interleukin (IL)-13 responses in mice lacking IL-13 receptor alpha 2. *J Exp Med*. 2003;197: 703-9.
120. Keane MP, Gomperts BN, Weigt S, Xue YY, Burdick MD, Nakamura H, et al. IL-13 is pivotal in the fibro-obliterative process of bronchiolitis obliterans syndrome. *J Immunol*. 2007;178: 511-9.
121. Kolodsick JE, Toews GB, Jakubzick C, Hogaboam C, Moore TA, McKenzie A, et al. Protection from fluorescein isothiocyanate-induced fibrosis in IL-13-deficient, but not IL-4-deficient, mice results from impaired collagen synthesis by fibroblasts. *J Immunol*. 2004;172: 4068-76.
122. Charrad R, Berraies A, Hamdi B, Ammar J, Hamzaoui K, Hamzaoui A. Anti-inflammatory activity of IL-37 in asthmatic children: Correlation with inflammatory cytokines TNF-alpha, IL-beta, IL-6 and IL-17A. *Immunobiology*. 2016;221: 182-7.
123. Imaeda H, Takahashi K, Fujimoto T, Kasumi E, Ban H, Bamba S, et al. Epithelial expression of interleukin-37b in inflammatory bowel disease. *Clin Exp Immunol*. 2013;172: 410-6.
124. Chen Z, O'Shea JJ. Regulation of IL-17 production in human lymphocytes. *Cytokine*. 2008;41: 71-8.
125. Benevides L, da Fonseca DM, Donate PB, Tiezzi DG, De Carvalho DD, de Andrade JM, et al. IL17 Promotes Mammary Tumor Progression by Changing the Behavior of Tumor Cells and Eliciting Tumorigenic Neutrophils Recruitment. *Cancer Res*. 2015;75: 3788-99.
126. Isailovic N, Daigo K, Mantovani A, Selmi C. Interleukin-17 and innate immunity in infections and chronic inflammation. *J Autoimmun*. 2015;60: 1-11.
127. Loubaki L, Hadj-Salem I, Fakhfakh R, Jacques E, Plante S, Boisvert M, et al. Co-culture of human bronchial fibroblasts and CD4+ T cells increases Th17 cytokine signature. *PloS one*. 2013;8: e81983.
128. Qu M, Song N, Chai G, Wu X, Liu W. Pathological niche environment transforms dermal stem cells to keloid stem cells: a hypothesis of keloid formation and development. *Med Hypotheses*. 2013;81: 807-12.
129. Gu FM, Li QL, Gao Q, Jiang JH, Zhu K, Huang XY, et al. IL-17 induces AKT-dependent IL-6/JAK2/STAT3 activation and tumor progression in hepatocellular carcinoma. *Mol Cancer*. 2011;10: 150.

130. Jadidi-Niaragh F, Ghalamfarsa G, Memarian A, Asgarian-Omran H, Razavi SM, Sarrafnejad A, et al. Downregulation of IL-17-producing T cells is associated with regulatory T cell expansion and disease progression in chronic lymphocytic leukemia. *Tumour Biol.* 2013;34: 929-40.
131. Francois A, Gombault A, Villeret B, Alsaleh G, Fanny M, Gasse P, et al. B cell activating factor is central to bleomycin- and IL-17-mediated experimental pulmonary fibrosis. *J Autoimmun.* 2015;56: 1-11.
132. Wang L, Chen S, Xu K. IL-17 expression is correlated with hepatitis B related liver diseases and fibrosis. *Int J Mol Med.* 2011;27: 385-92.
133. Okamoto Y, Hasegawa M, Matsushita T, Hamaguchi Y, Huu DL, Iwakura Y, et al. Potential roles of interleukin-17A in the development of skin fibrosis in mice. *Arthritis & Rheumatism.* 2012;64: 3726-35.
134. Nittka S, Gunther J, Ebisch C, Erbersdobler A, Neumaier M. The human tumor suppressor CEACAM1 modulates apoptosis and is implicated in early colorectal tumorigenesis. *Oncogene.* 2004;23: 9306-13.
135. Cruz PV, Wakai T, Shirai Y, Yokoyama N, Hatakeyama K. Loss of carcinoembryonic antigen-related cell adhesion molecule 1 expression is an adverse prognostic factor in hepatocellular carcinoma. *Cancer.* 2005;104: 354-60.
136. Busch C, Hanssen TA, Wagener C, B OB. Down-regulation of CEACAM1 in human prostate cancer: correlation with loss of cell polarity, increased proliferation rate, and Gleason grade 3 to 4 transition. *Hum Pathol.* 2002;33: 290-8.
137. Oliveira-Ferrer L, Tilki D, Ziegeler G, Hauschild J, Loges S, Irmak S, et al. Dual role of carcinoembryonic antigen-related cell adhesion molecule 1 in angiogenesis and invasion of human urinary bladder cancer. *Cancer Res.* 2004;64: 8932-8.
138. Ashkenazi S, Ortenberg R, Besser M, Schachter J, Markel G. SOX9 indirectly regulates CEACAM1 expression and immune resistance in melanoma cells. *Oncotarget.* 2016.
139. Zalzal H, Naudin C, Bastide P, Quittau-Prevostel C, Yaghi C, Poulat F, et al. CEACAM1, a SOX9 direct transcriptional target identified in the colon epithelium. *Oncogene.* 2008;27: 7131-8.
140. Roda G, Dahan S, Mezzanotte L, Caponi A, Roth-Walter F, Pinn D, et al. Defect in CEACAM family member expression in Crohn's disease IECs is regulated by the transcription factor SOX9. *Inflamm Bowel Dis.* 2009;15: 1775-83.
141. Yan C, Boyd DD. ATF3 regulates the stability of p53: a link to cancer. *Cell Cycle.* 2006;5: 926-9.
142. Hackl C, Lang SA, Moser C, Mori A, Fichtner-Feigl S, Hellerbrand C, et al. Activating transcription factor-3 (ATF3) functions as a tumor suppressor in colon cancer and is up-regulated upon heat-shock protein 90 (Hsp90) inhibition. *BMC Cancer.* 2010;10: 668.
143. Zhou H, Yuan Y, Ni J, Guo H, Deng W, Bian ZY, et al. Pleiotropic and puzzling effects of ATF3 in maladaptive cardiac remodeling. *Int J Cardiol.* 2016;206: 87-8.
144. Huang X, Li X, Guo B. KLF6 induces apoptosis in prostate cancer cells through up-regulation of ATF3. *The Journal of biological chemistry.* 2008;283: 29795-801.
145. Xie JJ, Xie YM, Chen B, Pan F, Guo JC, Zhao Q, et al. ATF3 functions as a novel tumor suppressor with prognostic significance in esophageal squamous cell carcinoma. *Oncotarget.* 2014;5: 8569-82.
146. Eo HJ, Kwon TH, Park GH, Song HM, Lee SJ, Park NH, et al. In Vitro Anticancer Activity of Phlorofuofuroeckol A via Upregulation of Activating Transcription Factor 3 against Human Colorectal Cancer Cells. *Mar Drugs.* 2016;14.
147. Jiliang S, Hui L, Gonghui L, Renan J, Liang S, Mingming C, et al. TR4 nuclear receptor enhances the cisplatin chemo-sensitivity via altering the ATF3 expression to better suppress HCC cell growth. *Oncotarget.* 2016.

148. Song HM, Park GH, Eo HJ, Jeong JB. Naringenin-Mediated ATF3 Expression Contributes to Apoptosis in Human Colon Cancer. *Biomol Ther (Seoul)*. 2016;24: 140-6.
149. Meech R, Rogers A, Zhuang L, Lewis BC, Miners JO, Mackenzie PI. Identification of residues that confer sugar selectivity to UDP-glycosyltransferase 3A (UGT3A) enzymes. *The Journal of biological chemistry*. 2012;287: 24122-30.
150. MacKenzie PI, Rogers A, Elliot DJ, Chau N, Hulin JA, Miners JO, et al. The novel UDP glycosyltransferase 3A2: cloning, catalytic properties, and tissue distribution. *Mol Pharmacol*. 2011;79: 472-8.
151. Morikawa Y, Kezuka C, Endo S, Ikari A, Soda M, Yamamura K, et al. Acquisition of doxorubicin resistance facilitates migrating and invasive potentials of gastric cancer MKN45 cells through up-regulating aldo-keto reductase 1B10. *Chem Biol Interact*. 2015;230: 30-9.
152. Januchowski R, Wojtowicz K, Zabel M. The role of aldehyde dehydrogenase (ALDH) in cancer drug resistance. *Biomed Pharmacother*. 2013;67: 669-80.
153. Nwabo Kamdje AH, Bassi G, Pacelli L, Malpeli G, Amati E, Nichele I, et al. Role of stromal cell-mediated Notch signaling in CLL resistance to chemotherapy. *Blood Cancer J*. 2012;2: e73.
154. Simoes BM, O'Brien CS, Eyre R, Silva A, Yu L, Sarmiento-Castro A, et al. Anti-estrogen Resistance in Human Breast Tumors Is Driven by JAG1-NOTCH4-Dependent Cancer Stem Cell Activity. *Cell Rep*. 2015;12: 1968-77.
155. Honoki K, Fujii H, Kubo A, Kido A, Mori T, Tanaka Y, et al. Possible involvement of stem-like populations with elevated ALDH1 in sarcomas for chemotherapeutic drug resistance. *Oncol Rep*. 2010;24: 501-5.
156. Whitman M, Hunter DG, Engle EC. Congenital Fibrosis of the Extraocular Muscles. In: Pagon RA, Adam MP, Ardinger HH, Wallace SE, Amemiya A, Bean LJH, et al., editors. *GeneReviews(R)*. Seattle (WA)1993.
157. Leandro-Garcia LJ, Leskela S, Landa I, Montero-Conde C, Lopez-Jimenez E, Leton R, et al. Tumoral and tissue-specific expression of the major human beta-tubulin isotypes. *Cytoskeleton (Hoboken)*. 2010;67: 214-23.
158. Lebok P, Ozturk M, Heilenkotter U, Jaenicke F, Muller V, Paluchowski P, et al. High levels of class III beta-tubulin expression are associated with aggressive tumor features in breast cancer. *Oncol Lett*. 2016;11: 1987-94.
159. Miyamoto A, Akasaka K, Oikawa H, Akasaka T, Masuda T, Maesawa C. Immunohistochemical study of HER2 and TUBB3 proteins in extramammary Paget disease. *Am J Dermatopathol*. 2010;32: 578-85.
160. McCarroll JA, Gan PP, Erlich RB, Liu M, Dwarte T, Sagnella SS, et al. TUBB3/betaIII-tubulin acts through the PTEN/AKT signaling axis to promote tumorigenesis and anoikis resistance in non-small cell lung cancer. *Cancer Res*. 2015;75: 415-25.
161. Tsourlakis MC, Weigand P, Grupp K, Kluth M, Steurer S, Schlomm T, et al. betaIII-tubulin overexpression is an independent predictor of prostate cancer progression tightly linked to ERG fusion status and PTEN deletion. *Am J Pathol*. 2014;184: 609-17.
162. Raspaglio G, Petrillo M, Martinelli E, Puma DDL, Mariani M, De Donato M, et al. Sox9 and Hif-2 $\alpha$  regulate TUBB3 gene expression and affect ovarian cancer aggressiveness. *Gene*. 2014;542: 173-81.
163. Duran GE, Wang YC, Francisco EB, Rose JC, Martinez FJ, Coller J, et al. Mechanisms of resistance to cabazitaxel. *Mol Cancer Ther*. 2015;14: 193-201.
164. Ferrandina G, Zannoni GF, Martinelli E, Paglia A, Gallotta V, Mozzetti S, et al. Class III beta-tubulin overexpression is a marker of poor clinical outcome in advanced ovarian cancer patients. *Clin Cancer Res*. 2006;12: 2774-9.
165. Mariani M, Shahabi S, Sieber S, Scambia G, Ferlini C. Class III  $\beta$ -tubulin (TUBB3): more than a biomarker in solid tumors? *Current molecular medicine*. 2011;11: 726-31.

166. Zhang Z, Nie F, Kang C, Chen B, Qin Z, Ma J, et al. Increased periostin expression affects the proliferation, collagen synthesis, migration and invasion of keloid fibroblasts under hypoxic conditions. *Int J Mol Med*. 2014;34: 253-61.
167. Touchi R, Ueda K, Kurokawa N, Tsuji M. Central regions of keloids are severely ischaemic. *Journal of plastic, reconstructive & aesthetic surgery : JPRAS*. 2016;69: e35-41.
168. Jones CD, Guiot L, Samy M, Gorman M, Tehrani H. The Use of Chemotherapeutics for the Treatment of Keloid Scars. *Dermatol Reports*. 2015;7: 5880.
169. van Leeuwen MC, Stokmans SC, Bulstra AE, Meijer OW, Heymans MW, Ket JC, et al. Surgical Excision with Adjuvant Irradiation for Treatment of Keloid Scars: A Systematic Review. *Plast Reconstr Surg Glob Open*. 2015;3: e440.
170. Arno AI, Gauglitz GG, Barret JP, Jeschke MG. Up-to-date approach to manage keloids and hypertrophic scars: a useful guide. *Burns*. 2014;40: 1255-66.
171. Song N, Wu X, Gao Z, Zhou G, Zhang WJ, Liu W. Enhanced expression of membrane transporter and drug resistance in keloid fibroblasts. *Hum Pathol*. 2012;43: 2024-32.
172. Moon J-H, Kwak SS, Park G, Jung H-Y, Yoon BS, Park J, et al. Isolation and characterization of multipotent human keloid-derived mesenchymal-like stem cells. *Stem cells and development*. 2008;17: 713-24.
173. Clavel G, Thiolat A, Boissier MC. Interleukin newcomers creating new numbers in rheumatology: IL-34 to IL-38. *Joint Bone Spine*. 2013;80: 449-53.
174. Singh A, Settleman J. EMT, cancer stem cells and drug resistance: an emerging axis of evil in the war on cancer. *Oncogene*. 2010;29: 4741-51.

## Supplementary Material to Chapter 4

Table S1 – Demographic data for the samples used in this study.

No.	Tissue type	Gender, Age	Ethnicity	Time present	Previous Treatment	Location of keloid
1	Keloid	F, 42yrs	Israeli	7-8 yrs	Nil	Left shoulder
2	Keloid	F, 25 yrs	Ethiopian	18 mnths	Nil	Right shoulder
3	Keloid	F, 19 yrs	Caucasian	2-3 yrs	Nil	Left ear helix
4	Keloid	F, 30 yrs	Caucasian	8 yrs	Nil	Central sternum
5	Keloid	F, 32 yrs	Caucasian	13 yrs	Radiation, steroid, silicone	Breasts bilaterally
6	Keloid	F, 41 yrs	Israeli	6 yrs	Steroid, silicone	Left deltoid
7	Keloid	F, 18yrs	Jamaican Afrocaribbean	1 yr	none	Bilateral ear lobes
8	Keloid	M, 23yrs	Jamaican Afrocaribbean	4 yrs	none	Bilateral ear lobes
9	Keloid	F, 27yrs	Jamaican Afrocaribbean	2 yrs	Surgery	Right ear lobe
10	Keloid	M, 20yrs	Jamaican Afrocaribbean	2 yrs	Surgery	Chin
11	Keloid	F, 19yrs	Jamaican Afrocaribbean	2 yrs	Surgery	Sternum
12	Keloid	F, 41yrs	Jamaican Afrocaribbean	6 yrs	None	Sternum
13	Keloid	M, 20yrs	Jamaican Afrocaribbean	15 yrs	None	Right ear lobe

14	Keloid	F, 22yrs	Jamaican Afrocarribean	3 yrs	None	Bilateral ear lobes
15	Normal skin	F, 57yrs	Caucasian	-	-	Facelift & blepharoplasty
16	Normal skin	M, 47yrs	Caucasian	-	-	Abdominoplasty
17	Normal skin	F, 19yrs	Caucasian	-	-	Bilateral breast reduction
18	Normal skin	F, 26yrs	Caucasian	-	-	Abdominoplasty
19	Normal skin	F, 41yrs	Caucasian	-	-	Abdominoplasty
20	Normal skin	F, 43yrs	Caucasian	-	-	Bilateral breast reduction
21	Normal skin	F, 43yrs	Caucasian	-	-	Bilateral breast reduction
22	Normal skin	F, 34yrs	Caucasian	-	-	Abdominoplasty
23	Normal skin	F, 47yrs	Caucasian	-	-	Mastopexy
24	Normal skin	F, 20yrs	Caucasian	-	-	Bilateral breast reduction
25	Normal skin	F, 42yrs	Caucasian	-	-	Bilateral breast reduction
26	Normal skin	F, 56yrs	Caucasian	-	-	Abdominoplasty
27	Normal skin	F, 51yrs	Caucasian	-	-	Abdominoplasty



**Table S2** – Expanded names for each of the gene symbols used throughout the manuscript text and figures.

<b>Gene symbol</b>	<b>Expansion</b>
<b>ACKR3</b>	atypical chemokine receptor 3
<b>ADAM</b>	a disintegrin and metalloproteinase
<b>ADAMTS</b>	a disintegrin and metalloproteinase with thrombospondin motifs
<b>AKR1B</b>	aldo-keto reductase family 1, member
<b>ALDH1A1</b>	aldehyde dehydrogenase 1 family member A1
<b>ANGPT</b>	angiopoietin
<b>AP-1</b>	activating protein 1
<b>ASPN</b>	asporin
<b>ATF3</b>	activating transcription factor 3
<b>ATM</b>	ataxia telangiectasia mutated
<b>BMP2</b>	bone morphogenetic protein 2
<b>BRD4</b>	bromodomain containing 4
<b>CCN</b>	Cyr61, CTGF, Nov (family of matricellular proteins)
<b>CD36</b>	cluster of differentiation 36
<b>CEACAM</b>	carcinoembryonic antigen-related cell adhesion molecule
<b>CLDN</b>	claudin
<b>CNTF</b>	ciliary neurotrophic factor
<b>COMP</b>	cartilage oligomeric protein
<b>CREB</b>	cAMP response element binding
<b>CTGF</b>	and connective tissue growth factor
<b>CTHRC1</b>	collagen triple helix repeat containing 1
<b>DAB2</b>	Dab, mitogen-responsive phosphoprotein, homolog 2 (drosophila)
<b>DACH1</b>	dachshund family transcription factor 1
<b>EIF3E</b>	eukaryotic translation initiation factor 3 subunit E
<b>EOMES</b>	eomesodermin
<b>EPHB4</b>	ephrin (EPH) receptor B4
<b>ErbB</b>	epidermal growth factor receptor family
<b>FBN1</b>	fibrillin 1
<b>FLT3</b>	fms related tyrosine kinase 3
<b>FN1</b>	fibronectin 1
<b>FOXF2</b>	forkhead box F2
<b>GNB1</b>	G protein subunit beta 1
<b>HIF-1<math>\alpha</math></b>	hypoxia-inducible factor-1 alpha
<b>HOXA13</b>	homeobox A13
<b>IFN</b>	interferon
<b>IGFBP4</b>	insulin-like growth factor binding protein 4
<b>IL</b>	interleukin
<b>ILC</b>	innate lymphoid cell
<b>IRAK4</b>	interleukin 1 receptor associated kinase 4
<b>IRF7</b>	interferon regulatory factor 7
<b>JAK</b>	janus kinase

<b>K</b>	keratin
<b>KLF6</b>	kruppel-like factor
<b>KMT2A</b>	lysine methyltransferase 2A
<b>LIMS2</b>	LIM zinc finger domain containing 2
<b>MAPK/ERK</b>	mitogen-activated protein kinase
<b>MEN1</b>	menin1
<b>MMP</b>	matrix metalloproteinase
<b>MUCL1</b>	mucin-like 1
<b>MYC</b>	c-Myc
<b>MYOCD</b>	myocardin
<b>NF-<math>\kappa</math>B</b>	nuclear factor kappa B
<b>NOTCH</b>	notch
<b>NRG1</b>	neuregulin-1
<b>OCT4</b>	octamer-binding transcription factor 4
<b>ORMDL3</b>	orosomucoid like 3
<b>OSM</b>	oncostatin M
<b>PAX8</b>	paired box 8
<b>PDGF</b>	platelet-derived growth factor
<b>PI3K</b>	phosphoinositide 3-kinase
<b>PKNOX1</b>	PBX/knotted 1 homeobox 1
<b>PRRX1</b>	paired related homeobox 1
<b>PTEN</b>	phosphatase and tensin homolog
<b>PXR</b>	pregnane X receptor
<b>RORc</b>	retinoic acid-related orphan receptor c
<b>RXR</b>	retinoid X receptor
<b>S100A8</b>	S100 calcium-binding protein A8
<b>SERPINE1/PAI-1</b>	serpin peptidase inhibitor. Clade E (plasminogen activator inhibitor 1)
<b>SMO</b>	smoothened
<b>SNAI1</b>	snail family zinc finger 1
<b>SNAI2</b>	snail family transcriptional repressor 2
<b>SOCS</b>	suppressor of cytokine signalling
<b>SOX9</b>	SRY (sex-determining region Y)-box 9
<b>SPHK1</b>	sphingosine kinase 1
<b>STAT</b>	signal transducer and activator of transcription
<b>TGF<math>\beta</math></b>	transforming growth factor beta
<b>TGM2</b>	transglutaminase 2
<b>TIMP3</b>	tissue inhibitor of metalloproteinases-3
<b>TLE1</b>	transducin like enhancer of split 1
<b>TNF</b>	tumour necrosis factor
<b>TNFR</b>	tumour necrosis factor receptor
<b>TP53</b>	tumor protein p53
<b>TSPYL5</b>	testis-specific protein Y encoded like 5
<b>TUBB3</b>	Tubulin $\beta$ 3, class III
<b>UGT3A2</b>	UDP glycosyltransferase family 3 member A2
<b>VEGF</b>	vascular endothelial growth factor
<b>WDR66</b>	WD repeat domain 66

<b>WISP1</b>	Wnt 1 inducible signaling pathway protein 1
<b>Wnt</b>	wingless-type MMTV integration site
<b>ZEB</b>	zinc finger E-box-binding proteins
<b><math>\alpha</math>-SMA/ACTA2</b>	alpha smooth muscle actin/actin, alpha 2, smooth muscle, aorta

**Table S3** – Details of primers used for qRT-PCR in this study.

<b>Gene</b>	<b>Forward primer</b> <b>Reverse primer</b>	<b>Accession number</b> <b>(Roche Diagnostics, UK)</b>	<b>Amplicon</b> <b>size (bp)</b>
ADAM12	Ggtaataagaacggtgactgctg gggactaggaagagcgtagtg	cat. no. 04685067001	78
ADAMTS2	Tggaagcctttggaagag cttcagcgaagacaggtg	cat. no. 04687663001	61
ADAMTS14	Ctttgggccctcaggtatg agaagccatcctcatggtg	cat. no. 04686900001	92
BMP2	Cagaccaccggttgaga cccactcgtttctgtagttct	cat. no. 04687647001	95
CD36	Gctcgggagactgaatctctt gagtcagtgacgcgatct	cat. no. 04687965001	71
COMP	Ccaagtgggctacatcagg gtccaagaccagttgctg	cat. no. 04688104001	73
NOTCH4	Gtttgaaggccccacct gtgtggcagtgatggaag	cat. no. 04685016001	62
WDR66	Ggtgcagtggaatacacct cagaccatagaatgggtcaa	cat. no. 04686896001	82
GAPDH	agccacatcgctcagacac gcccaatacgaccaaattcc	cat. no. 04688589001	66
RPL32	gaagttcctggtccacaacg gagcgatctcggcacagta	cat. no. 04686900001	77

**Figure S1** – qRT-PCR graphs showing differences in the degree of expression between LCM keloid and NS dermis and monolayer keloid and NS fibroblasts. FGF7, fibroblast growth factor 7; PDGFRA, platelet derived growth factor alpha.

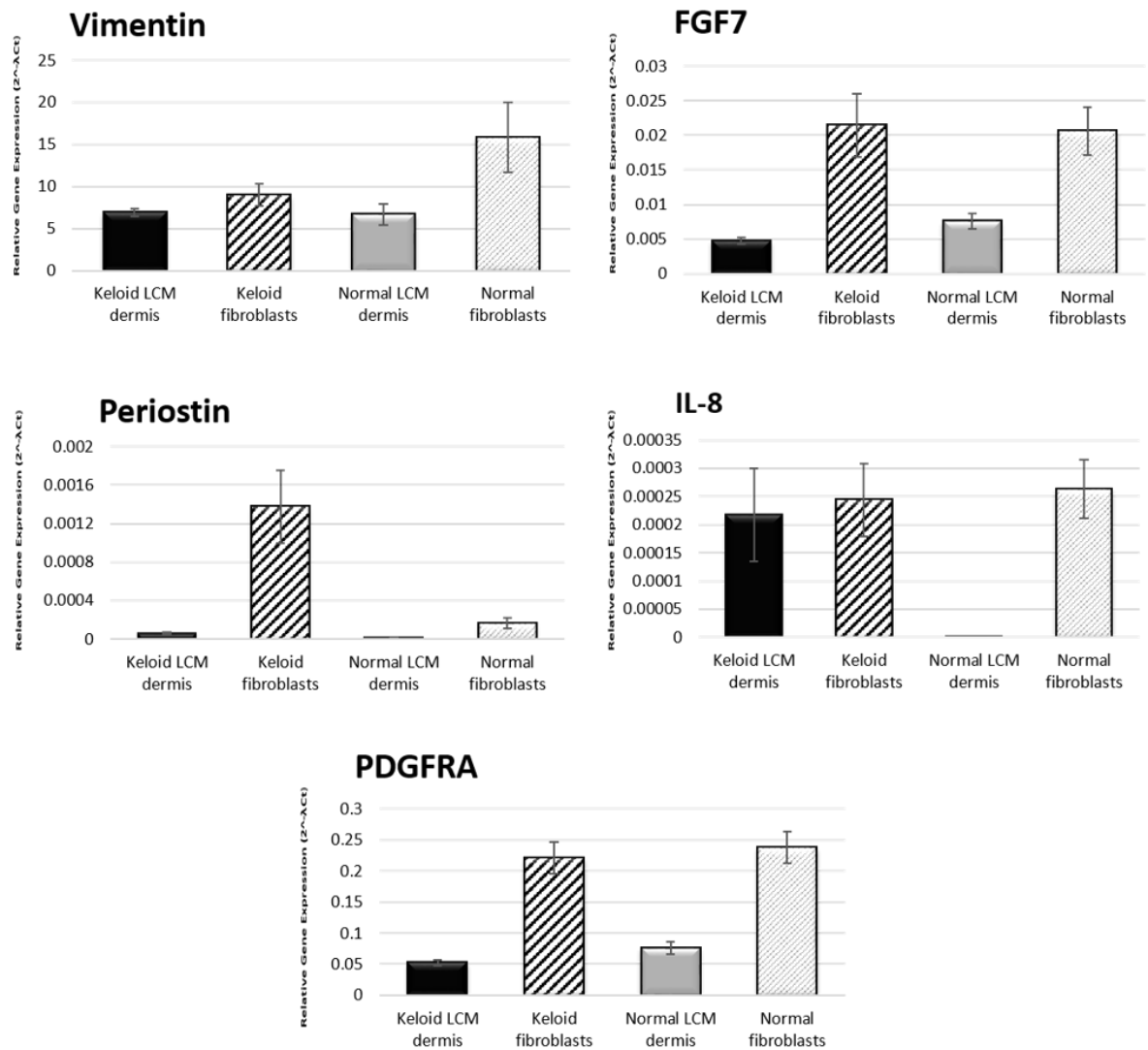


**Figure S2** – qRT-PCR graphs showing the *in situ* (LCM) contribution of both epidermis and dermis from keloid centre, margin and extralesional sites as well as normal skin to the overall gene expression of fibrosis-associated genes known to be dysregulated in KD. CTGF, connective tissue growth factor; FGF7, fibroblast growth factor 7; PDGFRA, platelet derived growth factor receptor A.

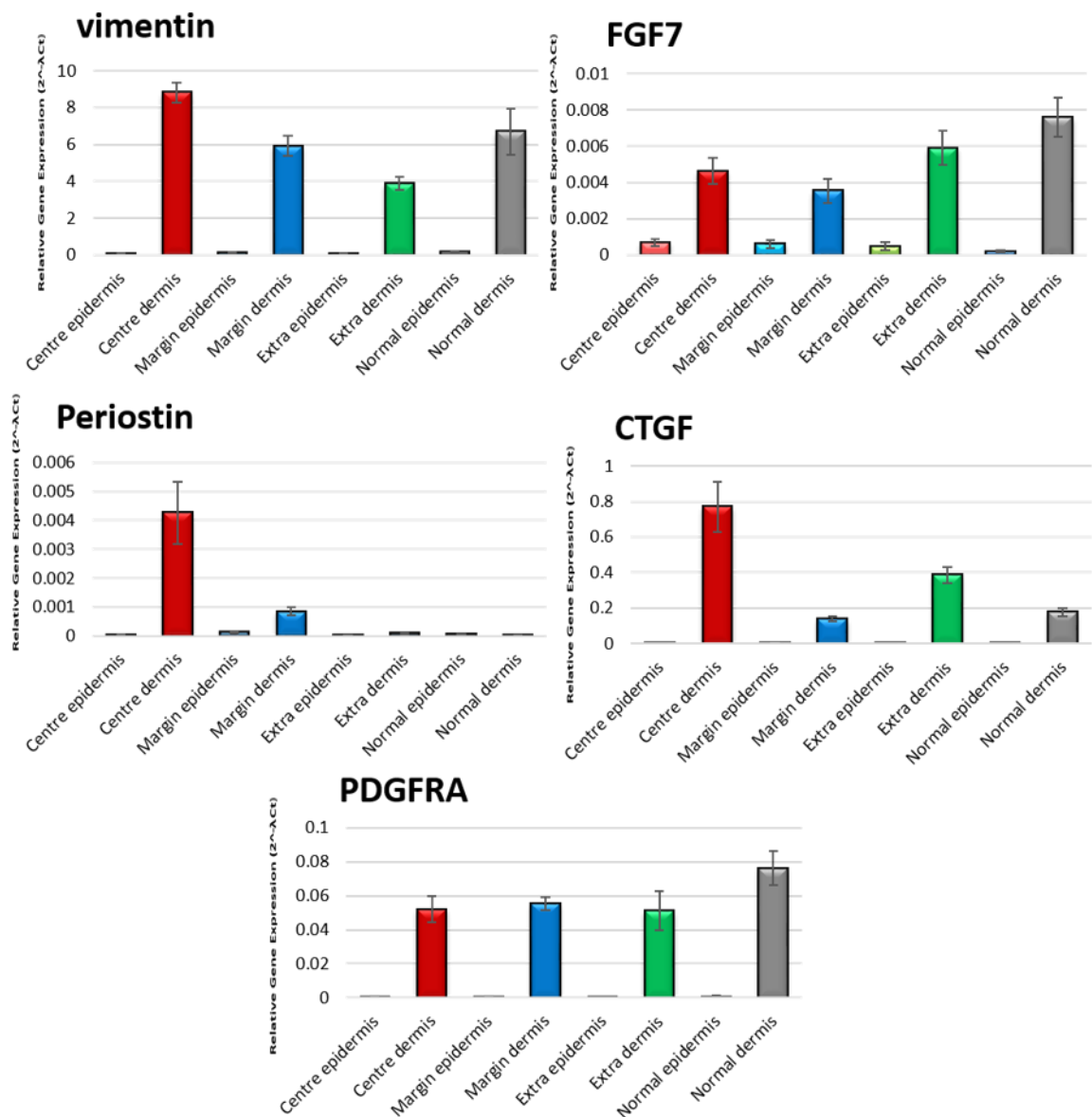


**Figure S3a** – Top upregulated genes in keloid vs NS epidermis, corrected for fold change >2, p value < 0.05 and q value < 0.05, where red indicates centre of the lesion, Blue the margin and green the extraslesional. Black indicates where all three overlap.

Site	Gene title	Gene symbol	Fold change	p-value	q-value	Same direction in (Fold change>2, p<0.05)
Epidermis	Aldo-keto reductase family 1, member B10	AKR1B10	75.56	1.19E-06	0.0156	
			64.69	5.85E-06	0.0264	
			86.03	2.14E-06	0.0097	
Epidermis	Von Willebrand factor C domain containing 2	VWC2	8.51	2.81E-07	0.0065	
			6.82	4.69E-06	0.0255	
			5.44	2.78E-05	0.0363	
Epidermis	GLIS family zinc finger 2	GLIS2	5.11	1.24E-05	0.031	
			5.72	1.25E-05	0.0406	
			5.34	2.2E-05	0.0314	
Epidermis	WC repeat domain 66	WDR66	86.49	1.73E-08	0.001	Margin, Extra
Epidermis	CD36 molecule (thrombospondin receptor)	CD36	42.56	2.97E-05	0.0459	Margin, Extra
Epidermis	Aldo-keto reductase family 1, member 15	AKR1B15	22.25	8.55E-06	0.0303	Margin, Extra
Epidermis	Leucine-rich repeat kinase 2	LRRK2	10.04	1.3E-05	0.031	Margin
Epidermis	Protease, serine, 53	PRSS53	9.82	2.66E-05	0.0434	
Epidermis	Protein phosphatase 1, regulatory subunit 3C	PPP1R3C	8.56	2.48E-06	0.0156	Margin
Epidermis	Lymphocyte antigen 96	LY96	7.77	5.93E-06	0.0232	Margin
Epidermis	C2 calcium-dependent domain containing 4B	C2CD4B	7.22	2.36E-06	0.0156	Margin, Extra
Epidermis	Notch 4	NOTCH4	7.15	1.18E-05	0.031	Margin, Extra
Epidermis	Zinc finger protein 354B	ZNF354B	3.58	1.02E-05	0.0351	Centre, Extra
Epidermis	Kinesin family member 12	KIF12	3.05	4.49E-07	0.0066	
Epidermis	GTPase activating protein and VPS9 domains 1	GAPVD1	10.3	1.21E-05	0.0209	
Epidermis	Deafness, autosomal recessive 31	DFNB31	10.02	1.14E-05	0.0209	
Epidermis	Zinc finger protein 275	ZNF275	9.24	2.72E-05	0.0363	Centre, Margin
Epidermis	Interferon, alpha-inducible protein 27	IFI27	7.91	2.86E-05	0.0363	Centre, Margin
Epidermis	Small Cajal body-specific RNA 14	SCARNA14	6.05	7.74E-06	0.0168	
Epidermis	Keratin 42 pseudogene	KRT42P	4.64	2.81E-06	0.0097	Margin

**Figure S3b** – Mean intensity and range for each group for representative genes from Table S3a. The intensity is the equivalent to absolute expression values for each sample and the range based on the 95% confidence interval.

Gene	Normal skin LCM epidermis	Keloid centre LCM epidermis	Keloid margin LCM epidermis	Keloid extralesional LCM epidermis
AKR1B10	5.7883 (4.2453, 7.3314)	12.0280 (10.6917, 13.3643)	11.8039 (10.2608, 13.3469)	12.2150 (10.6720, 13.7581)
VWC2	6.3249 (5.6248, 7.0251)	9.4145 (8.8082, 10.0209)	9.0951 (8.3950, 9.7953)	8.7680 (8.0678, 9.4681)
GLIS2	5.6115 (4.9312, 6.2917)	7.9659 (7.3768, 8.5550)	8.1279 (7.4477, 8.8081)	8.0270 (7.3468, 8.7073)
WDR66	6.9624 (5.7140, 8.2108)	13.3968 (12.3157, 14.4779)	13.1445 (11.8961, 14.3929)	9.9667 (8.7183, 11.2151)
CD36	8.1742 (6.5080, 9.8403)	13.5854 (12.1425, 15.0284)	13.0914 (11.4252, 14.7575)	12.7121 (11.0460, 14.3782)
NOTCH4	6.1833 (5.3667, 6.9999)	9.0209 (8.3137, 9.7281)	8.6960 (7.8794, 9.5126)	8.4458 (7.6292, 9.2624)
KRT42P	9.1876 (8.6465, 9.7288)	9.8140 (9.3454, 10.2826)	9.6174 (9.0763, 10.1586)	11.4023 (10.8612, 11.9434)



**Figure S4** – Top downregulated genes in keloid vs NS epidermis, corrected for fold change >2, p value < 0.05 and q value < 0.05, where red indicates centre of the lesion, Blue the margin and green the extralesional. Black indicates where all three overlap.

Site	Gene title	Gene symbol	Fold change	p-value	q-value	Same direction in (Fold change>2, p<0.05)
Epidermis	Anterior gradient 3 homolog ( <i>Xenopus laevis</i> )	AGR3	-11.24	1.59E-05	0.0334	Margin, Extra
Epidermis	Bone morphogenic protein 2	BMP2	-6.91	1.69E-05	0.0342	Margin, Extra
Epidermis	EPH receptor B1	EPHB1	-3.43	1.54E-05	0.0334	
Epidermis	Chromatin target of PRMT1	CHTOP	-3.05	1.32E-05	0.031	
Epidermis	Spermatogenesis and oogenesis specific basic helix-loop-helix 1	SOHLH1	-25.11	2.38E-06	0.0097	Centre, Margin
Epidermis	Docking protein 7	DOK7	-10.5	9.15E-06	0.0192	Centre, Margin
Epidermis	FSHD region gene 2	FRG2	-9.17	1.03E-05	0.0201	Centre, Margin
Epidermis	Abhydrolase domain containing 12B	ABHD12B	-7.25	4.25E-05	0.0462	Centre
Epidermis	Interleukin 20 receptor, alpha	IL20RA	-6.24	4.69E-06	0.0131	Margin

**Figure S5** – Top 100 upregulated genes in keloid centre vs normal skin epidermis. Corrected for fold change > 2 and p-value < 0.05 where blue indicates also significantly upregulated in the margin, green the extralesional and orange both.

Centre epidermis	Gene title	Gene symbol	Fold change	p-value
1	keratin 6B	KRT6B	146.02	0.0006
2	mucin-like 1	MUCL1	118.89	0.0013
3	WD repeat domain 66	WDR66	86.49	1.73E-08
4	aldo-keto reductase family 1, member B10 (aldose reductase)	AKR1B10	75.56	1.19E-06
5	S100 calcium binding protein A8	S100A8	51.58	0.0009
6	CD36 molecule (thrombospondin receptor)	CD36	42.56	2.97E-05
7	keratin 6A	KRT6A	30.79	0.0027
8	aldehyde dehydrogenase 1 family, member A1	ALDH1A1	22.96	0.0008
9	aldo-keto reductase family 1, member B15	AKR1B15	22.25	8.55E-06
10	NEL-like 2 (chicken)	NELL2	20.76	0.0011
11	family with sequence similarity 65, member C	FAM65C	17.76	0.0003
12	SRY (sex determining region Y)-box 9	SOX9	16.88	0.0008
13	trichohyalin	TCHH	15.07	0.0018
14	aldo-keto reductase family 1, member B1 (aldose reductase)	AKR1B1	14.30	0.0022
15	S100 calcium binding protein A12	S100A12	14.13	0.0453
16	E74-like factor 5 (ets domain transcription factor)	ELF5	13.20	0.0021
17	microsomal glutathione S-transferase 1	MGST1	12.63	0.0018
18	RAS-like, estrogen-regulated, growth inhibitor	RERG	11.48	0.0022
19	C-type lectin domain family 7, member A	CLEC7A	11.39	0.0007
20	hydroxysteroid (17-beta) dehydrogenase 2	HSD17B2	11.22	0.0013
21	S100 calcium binding protein A9	S100A9	11.12	0.0472
22	keratin 34	KRT34	10.94	0.0088
23	sulfatase 1	SULF1	10.70	0.0017
24	guanylate binding protein family, member 6	GBP6	10.50	0.0066
25	osteoglycin	OGN	10.49	0.0042
26	KIAA1462	KIAA1462	10.46	0.0095
27	ubiquitin carboxyl-terminal esterase L1 (ubiquitin thiolesterase)	UCHL1	10.41	0.0076
28	Fc fragment of IgG, low affinity IIIa, receptor (CD16a)	FCGR3A	10.37	0.0061
29	diacylglycerol kinase, gamma 90kDa	DGKG	10.23	0.0008
30	SLAM family member 7	SLAMF7	10.19	0.0018
31	leucine-rich repeat kinase 2	LRRK2	10.04	1.30E-05
32	protease, serine, 53	PRSS53	9.82	2.66E-05
33	gap junction protein, beta 2, 26kDa	GJB2	9.74	0.0077

Centre epidermis	Gene title	Gene symbol	Fold change	p-value
34	transmembrane protease, serine 11D	TMPRSS11D	9.49	0.001
35	caspase recruitment domain family, member 6	CARD6	9.44	0.0016
36	KIAA1609	KIAA1609	9.43	0.0043
37	v-myc myelocytomatosis viral related oncogene, neuroblastoma derived (avian)	MYCN	9.37	0.003
38	MORN repeat containing 4	MORN4	9.19	0.0187
39	Thy-1 cell surface antigen	THY1	9.19	0.0064
40	arachidonate 12-lipoxygenase pseudogene 2	ALOX12P2	9.14	0.0305
41	wingless-type MMTV integration site family, member 5A	WNT5A	8.84	0.0058
42	kelch repeat and BTB (POZ) domain containing 11	KBTBD11	8.64	0.0034
43	protein phosphatase 1, regulatory subunit 3C	PPP1R3C	8.56	2.48E-06
44	von Willebrand factor C domain containing 2	VWC2	8.51	2.81E-07
45	interleukin 13 receptor, alpha 1	IL13RA1	8.45	0.0002
46	eyes absent homolog 2 (Drosophila)	EYA2	8.23	0.0023
47	keratin 16	KRT16	8.11	0.012
48	tetra-peptide repeat homeobox-like	TPRXL	8.03	0.0003
49	histone demethylase UTY-like	DNATP3	7.80	0.0262
50	lymphocyte antigen 96	LY96	7.77	5.93E-06
51	collagen, type I, alpha 1	COL1A1	7.59	0.0089
52	internexin neuronal intermediate filament protein, alpha	INA	7.59	0.0065
53	sclerostin domain containing 1	SOSTDC1	7.55	0.0151
54	UDP glucuronosyltransferase 2 family, polypeptide A2	UGT2A2	7.54	0.003
55	EF-hand domain family, member B	EFHB	7.51	0.0009
56	integrin, beta-like 1 (with EGF-like repeat domains)	ITGBL1	7.49	0.0099
57	apolipoprotein L, 4	APOL4	7.46	0.0016
58	endogenous retrovirus group MER34, member 1	ERVMER34-1	7.38	0.0023
59	cysteine-rich secretory protein 2	CRISP2	7.34	0.0289
60	C2 calcium-dependent domain containing 4B	C2CD4B	7.22	2.36E-06
61	collagen, type V, alpha 1	COL5A1	7.18	0.0394
62	keratin 6C	KRT6C	7.17	0.0219
63	notch 4	NOTCH4	7.15	1.18E-05
64	signal-induced proliferation-associated 1 like 2	SIPA1L2	6.90	0.0018
65	homeobox C8	HOXC8	6.89	0.0183
66	endoplasmic reticulum protein 27	ERP27	6.86	0.0236

Centre epidermis	Gene title	Gene symbol	Fold change	p-value
67	sushi domain containing 4	SUSD4	6.82	0.0292
68	Rh family, C glycoprotein	RHCG	6.76	0.0453
69	insulin-like growth factor 2 (somatomedin A)	IGF2	6.71	0.0348
70	G protein-coupled receptor 12	GPR12	6.63	0.0433
71	glutathione peroxidase 2 (gastrointestinal)	GPX2	6.56	0.001
72	matrix Gla protein	MGP	6.56	0.0381
73	nucleoporin 210kDa	NUP210	6.55	0.0001
74	spindlin family, member 3	SPIN3	6.51	0.0048
75	inhibin, beta B	INHBB	6.51	0.0239
76	2'-5'-oligoadenylate synthetase 2, 69/71kDa	OAS2	6.37	0.0065
77	ADAM metallopeptidase domain 23	ADAM23	6.08	0.0122
78	family with sequence similarity 3, member B	FAM3B	6.08	0.0042
79	drebrin 1	DBN1	5.88	0.0027
80	Rho GTPase activating protein 28	ARHGAP28	5.86	0.0077
81	tryptase alpha/beta 1	TPSAB1	5.85	0.0136
82	chemokine (C-X-C motif) ligand 17	CXCL17	5.85	0.0137
83	FK506 binding protein 1A, 12kDa	FKBP1A	5.80	0.0063
84	transmembrane and coiled-coil domains 7	TMCO7	5.65	0.0016
85	protein kinase C, epsilon	PRKCE	5.60	0.0014
86	transmembrane protease, serine 4	TMPRSS4	5.57	0.007
87	CTAGE family, member 5	CTAGE5	5.55	0.0127
88	tryptase delta 1	TPSD1	5.55	0.0041
89	laminin, alpha 2	LAMA2	5.54	0.0331
90	ketoheokinase (fructokinase)	KHK	5.51	0.0094
91	PNMA-like 1	PNMAL1	5.42	0.0427
92	zinc finger, CCHC domain containing 24	ZCCHC24	5.41	0.0004
93	peptidyl arginine deiminase, type I	PADI1	5.33	0.0072
94	fatty acid binding protein 6, ileal	FABP6	5.30	0.0014
95	trichorhinophalangeal syndrome I	TRPS1	5.30	0.0048
96	interferon-induced protein with tetratricopeptide repeats 1	IFIT1	5.30	0.0024
97	transmembrane 4 L six family member 1	TM4SF1	5.29	0.0115
98	myosin, light chain 9, regulatory	MYL9	5.29	0.0066
99	melanoma cell adhesion molecule	MCAM	5.25	0.0049
100	protein C receptor, endothelial	PROCR	5.25	0.0037

**Figure S6** – Top 50 downregulated genes in keloid centre vs normal skin epidermis. Corrected for fold change > 2 and p-value < 0.05 where blue indicates also significantly downregulated in the margin, green the extralesional and orange both.

Centre epidermis	Gene title	Gene symbol	Fold change	p-value
1	UDP glycosyltransferase 3 family, polypeptide A2	UGT3A2	-42.55	0.0001
2	spermatogenesis and oogenesis specific basic helix-loop-helix 1	SOHLH1	-10.26	8.59E-05
3	collectin sub-family member 12	COLEC12	-10.01	0.0008
4	anterior gradient 3 homolog ( <i>Xenopus laevis</i> )	AGR3	-9.83	2.48E-05
5	N(alpha)-acetyltransferase 16, NatA auxiliary subunit	NAA16	-9.54	0.0004
6	protease, serine, 35	PRSS35	-8.77	0.031
7	methyltransferase like 6	METTL6	-8.76	0.0014
8	hyaluronan synthase 1	HAS1	-8.74	0.0068
9	HAUS augmin-like complex, subunit 5	HAUS5	-8.14	0.0018
10	ghrelin opposite strand RNA 2 (non-protein coding)	GHRLOS2	-8.08	0.0009
11	late cornified envelope 5A	LCE5A	-8.03	0.0069
12	MAM domain containing glycosylphosphatidylinositol anchor 1	MDGA1	-7.99	0.0044
13	activating transcription factor 3	ATF3	-7.86	0.0241
14	adrenergic, beta-2-, receptor, surface	ADRB2	-7.75	0.0063
15	RAB3B, member RAS oncogene family	RAB3B	-7.35	0.0003
16	tetraspanin 2	TSPAN2	-7.30	0.0158
17	insulin-like growth factor binding protein 3	IGFBP3	-7.16	0.0136
18	cellular retinoic acid binding protein 1	CRABP1	-7.16	0.0255
19	ST6 beta-galactosamide alpha-2,6-sialyltransferase 2	ST6GAL2	-7.07	0.0196
20	claudin 23	CLDN23	-7.00	0.0128
21	bone morphogenetic protein 2	BMP2	-6.91	1.69E-05
22	hemoglobin, alpha 2	HBA2	-6.85	0.0129
23	kinesin family member 4A	KIF4A	-6.84	0.0205
24	interleukin 37	IL37	-6.51	0.0013
25	ethanolamine kinase 2	ETNK2	-6.41	0.0006

Centre epidermis	Gene title	Gene symbol	Fold change	p-value
26	HLA complex group 4 (non-protein coding)	HCG4	-6.33	0.0065
27	centrosomal protein 68kDa	CEP68	-6.12	0.0056
28	six-twelve leukemia	STL	-5.87	0.0049
29	ORM1-like 1 ( <i>S. cerevisiae</i> )	ORMDL1	-5.83	6.56E-05
30	interferon regulatory factor 4	IRF4	-5.77	0.024
31	chromosome 6 open reading frame 164	C6orf164	-5.58	0.005
32	chromosome 21 open reading frame 116	C21orf116	-5.54	0.0053
33	outer dense fiber of sperm tails 3-like 1	ODF3L1	-5.41	0.0002
34	family with sequence similarity 70, member A	FAM70A	-5.40	0.0247
35	pleckstrin homology-like domain, family B, member 1	PHLDB1	-5.32	0.0014
36	pleckstrin homology domain containing, family A member 6	PLEKHA6	-5.29	0.0152
37	family with sequence similarity 153, member A	FAM153A	-5.27	0.0085
38	zinc finger protein 434	ZNF434	-5.26	0.0055
39	G protein-coupled receptor 18	GPR18	-5.24	0.006
40	PHD finger protein 15	PHF15	-5.21	0.0043
41	URB1 ribosome biogenesis 1 homolog ( <i>S. cerevisiae</i> )	URB1	-5.20	0.0004
42	SLAIN motif family, member 1	SLAIN1	-5.19	0.0001
43	keratin 77	KRT77	-5.17	0.0128
44	dispatched homolog 1 ( <i>Drosophila</i> )	DISP1	-5.17	0.0037
45	FBJ murine osteosarcoma viral oncogene homolog	FOS	-5.12	0.0309
46	dpy-19-like 2 ( <i>C. elegans</i> )	DPY19L2	-5.03	0.0047
47	abhydrolase domain containing 12B	ABHD12B	-4.96	0.0002
48	troponin I type 2 (skeletal, fast)	TNNI2	-4.93	0.0033
49	transmembrane protein 2	TMEM2	-4.91	0.0248
50	cytochrome P450, family 26, subfamily B, polypeptide 1	CYP26B1	-4.87	0.0092

**Figure S7** – Top 100 upregulated genes in keloid margin vs normal skin epidermis. Corrected for fold change > 2 and p-value < 0.05 where red indicates also significantly upregulated in the centre, green the extralesional and orange both

Margin epidermis	Gene title	Gene symbol	Fold change	p-value
1	WD repeat domain 66	WDR66	72.61	1.21E-07
2	aldo-keto reductase family 1, member B10 (aldose reductase)	AKR1B10	64.69	5.85E-06
3	mucin-like 1	MUCL1	44.26	0.0129
4	keratin 6B	KRT6B	42.92	0.0105
5	aldehyde dehydrogenase 1 family, member A1	ALDH1A1	31.49	0.0006
6	CD36 molecule (thrombospondin receptor)	CD36	30.28	0.0002
7	S100 calcium binding protein A8	S100A8	25.98	0.0077
8	v-myc myelocytomatosis viral related oncogene, neuroblastoma derived (avian)	MYCN	16.41	0.0007
9	aldo-keto reductase family 1, member B15	AKR1B15	16.02	9.22E-05
10	Fc fragment of IgG, low affinity IIIa, receptor (CD16a)	FCGR3A	14.67	0.0035
11	neuronal guanine nucleotide exchange factor	NGEF	13.69	0.0209
12	SRY (sex determining region Y)-box 9	SOX9	13.38	0.0031
13	pancreatic lipase-related protein 3	PNLIPRP3	13.28	0.0356
14	dachshund homolog 1 (Drosophila)	DACH1	13.03	0.0047
15	microsomal glutathione S-transferase 1	MGST1	12.99	0.0029
16	keratin 6A	KRT6A	12.88	0.0291
17	family with sequence similarity 65, member C	FAM65C	12.73	0.0021
18	XK, Kell blood group complex subunit-related family, member 6	XKR6	12.50	0.0002
19	sushi domain containing 4	SUSD4	12.45	0.0195
20	guanylate binding protein family, member 6	GBP6	12.05	0.0071
21	UDP-galactose-4-epimerase	GALE	11.89	0.0047
22	sclerostin domain containing 1	SOSTDC1	11.83	0.0063
23	leucine-rich repeat kinase 2	LRRK2	11.62	1.39E-05
24	carbohydrate (keratan sulfate Gal-6) sulfotransferase 1	CHST1	11.02	0.0161
25	methionine sulfoxide reductase B3	MSRB3	10.49	0.0036
26	protease, serine, 12 (neurotrypsin, motopsin)	PRSS12	10.48	0.0082
27	inhibin, beta B	INHBB	10.17	0.01
28	pleiotrophin	PTN	10.14	0.0082
29	PNMA-like 1	PNMAL1	9.84	0.0121
30	trichorhinophalangeal syndrome I	TRPS1	9.69	0.0311
31	C2 calcium-dependent domain containing 4B	C2CD4B	9.41	9.20E-07
32	wingless-type MMTV integration site family, member 5A	WNT5A	9.36	0.0078
33	KIAA1609	KIAA1609	9.32	0.0072

Margin epidermis	Gene title	Gene symbol	Fold change	p-value
34	aldo-keto reductase family 1, member B1 (aldose reductase)	AKR1B1	8.94	0.0148
35	2'-5'-oligoadenylate synthetase 2, 69/71kDa	OAS2	8.90	0.0031
36	Thy-1 cell surface antigen	THY1	8.90	0.0111
37	alcohol dehydrogenase 7 (class IV), mu or sigma polypeptide	ADH7	8.77	0.0011
38	UDP glucuronosyltransferase 2 family, polypeptide A2	UGT2A2	8.63	0.003
39	solute carrier family 29 (nucleoside transporters), member 3	SLC29A3	8.46	0.0049
40	forkhead box C1	FOXC1	8.36	0.0203
41	protein phosphatase 1, regulatory subunit 3C	PPP1R3C	8.35	8.01E-06
42	keratin 9	KRT9	8.18	0.0033
43	golgin A8 family, member A	GOLGA8A	7.93	0.0052
44	eyes absent homolog 2 (Drosophila)	EYA2	7.86	0.0048
45	protocadherin beta 5	PCDHB5	7.78	0.0048
46	trichorhinophalangeal syndrome I	TRPS1	7.54	0.0017
47	netrin 4	NTN4	7.50	0.0007
48	Leber congenital amaurosis 5	LCA5	7.49	0.021
49	Rho/Rac guanine nucleotide exchange factor (GEF) 2	ARHGEF2	7.40	0.0011
50	repetin	RPTN	7.32	0.0124
51	CTAGE family, member 5	CTAGE5	7.30	0.0074
52	osteoglycin	OGN	7.24	0.0204
53	E74-like factor 5 (ets domain transcription factor)	ELF5	7.23	0.0213
54	Rho GTPase activating protein 28	ARHGAP28	7.13	0.0058
55	FK506 binding protein 1A, 12kDa	FKBP1A	7.09	0.0046
56	drebrin 1	DBN1	6.97	0.0021
57	von Willebrand factor C domain containing 2	VWC2	6.82	4.69E-06
58	nitric oxide synthase 1 (neuronal)	NOS1	6.77	0.0006
59	ketohexokinase (fructokinase)	KHK	6.64	0.0072
60	EF-hand domain family, member B	EFHB	6.59	0.0031
61	brain and acute leukemia, cytoplasmic	BAALC	6.57	0.0366
62	guanine nucleotide binding protein (G protein), gamma transducing activity polypeptide 2	GNGT2	6.54	0.0051
63	methyl-CpG binding domain protein 5	MBD5	6.50	0.0233
64	kallikrein-related peptidase 14	KLK14	6.43	0.0228
65	mannosyl (alpha-1,3-)-glycoprotein beta-1,2-N-acetylglucosaminyltransferase	MGAT1	6.40	0.001
66	branched chain keto acid dehydrogenase E1, beta polypeptide	BCKDHB	6.38	0.0071



Margin epidermis	Gene title	Gene symbol	Fold change	p-value
67	B-cell linker	BLNK	6.32	0.026
68	chromosome 1 open reading frame 190	C1orf190	6.30	0.0002
69	hedgehog acyltransferase	HHAT	6.20	0.002
70	MARCKS-like 1	MARCKSL1	6.17	0.0037
71	chromosome 8 open reading frame 34	C8orf34	5.99	0.0051
72	IGF-like family member 4	IGFL4	5.95	0.0002
73	mal, T-cell differentiation protein	MAL	5.86	0.036
74	cell death-inducing DFFA-like effector a	CIDEA	5.80	0.0008
75	ets variant 5	ETV5	5.76	0.0424
76	interferon induced transmembrane protein 1 (9-27)	IFITM1	5.73	0.0008
77	GLIS family zinc finger 2	GLIS2	5.72	1.25E-05
78	neurofilament, light polypeptide	NEFL	5.71	0.0122
79	notch 4	NOTCH4	5.71	0.0001
80	chromosome 12 open reading frame 56	C12orf56	5.63	0.0013
81	Ellis van Creveld syndrome 2	EVC2	5.62	0.0292
82	glutathione peroxidase 2 (gastrointestinal)	GPX2	5.61	0.0037
83	TBCC domain containing 1	TBCCD1	5.60	0.0194
84	leucine rich repeat containing 8 family, member E	LRRC8E	5.58	0.0005
85	prickle homolog 1 (Drosophila)	PRICKLE1	5.50	0.0028
86	leucine rich repeat containing 69	LRRC69	5.48	0.0129
87	hydroxysteroid (17-beta) dehydrogenase 2	HSD17B2	5.45	0.0313
88	protection of telomeres 1 homolog (S. pombe)	POT1	5.44	0.0005
89	raftlin, lipid raft linker 1	RFTN1	5.41	0.0011
90	lysophosphatidylcholine acyltransferase 1	LPCAT1	5.38	0.012
91	doublecortin-like kinase 1	DCLK1	5.35	0.0098
92	Rho GTPase activating protein 28	ARHGAP28	5.33	0.0175
93	tetra-peptide repeat homeobox-like	TPRXL	5.30	0.0048
94	signal-induced proliferation-associated 1 like 2	SIPA1L2	5.25	0.0097
95	suppressor of cytokine signaling 2	SOCS2	5.25	0.0013
96	calnexin	CANX	5.25	0.0166
97	interleukin 17 receptor D	IL17RD	5.23	0.0008
98	arginine decarboxylase	ADC	5.18	0.0054
99	malic enzyme 3, NADP(+)-dependent, mitochondrial	ME3	5.18	0.002
100	serpin peptidase inhibitor, clade B (ovalbumin), member 10	SERPINB10	5.17	0.002

**Figure S8** – Top 50 downregulated genes in keloid margin vs normal skin epidermis. Corrected for fold change > 2 and p-value < 0.05 where red indicates also significantly downregulated in the centre, green the extralesional and orange both

Margin epidermis	Gene title	Gene symbol	Fold change	p-value
1	UDP glycosyltransferase 3 family, polypeptide A2	UGT3A2	-21.01	0.0018
2	cytochrome P450, family 26, subfamily B, polypeptide 1	CYP26B1	-13.21	0.0002
3	N(alpha)-acetyltransferase 16, NatA auxiliary subunit	NAA16	-9.58	0.0008
4	tetraspanin 2	TSPAN2	-9.55	0.0109
5	anterior gradient 3 homolog ( <i>Xenopus laevis</i> )	AGR3	-9.32	7.95E-05
6	FBJ murine osteosarcoma viral oncogene homolog	FOS	-9.00	0.008
7	protease, serine, 35	PRSS35	-8.93	0.0409
8	spermatogenesis and oogenesis specific basic helix-loop-helix 1	SOHLH1	-8.49	0.0005
9	ghrelin opposite strand RNA 2 (non-protein coding)	GHRLOS2	-8.22	0.0015
10	regulator of G-protein signaling 1	RGS1	-7.74	0.0351
11	activating transcription factor 3	ATF3	-7.49	0.0379
12	serpin peptidase inhibitor, clade E (nexin, plasminogen activator inhibitor type 1), member 1	SERPINE1	-7.39	0.0377
13	ST6 beta-galactosamide alpha-2,6-sialyltransferase 2	ST6GAL2	-7.24	0.0265
14	troponin I type 2 (skeletal, fast)	TNNI2	-6.94	0.0011
15	hornerin	HRNR	-6.77	0.0057
16	trafficking protein particle complex 2	TRAPPC2	-6.52	0.0014
17	nuclear receptor subfamily 4, group A, member 1	NR4A1	-6.22	0.0109
18	chromosome 11 open reading frame 65	C11orf65	-6.21	0.0011
19	cysteine-rich, angiogenic inducer, 61	CYR61	-6.21	0.0214
20	claudin 4	CLDN4	-6.16	0.0001
21	hyaluronan synthase 1	HAS1	-6.08	0.0304
22	dispatched homolog 1 ( <i>Drosophila</i> )	DISP1	-6.04	0.0031
23	ciliary rootlet coiled-coil, rootletin pseudogene 3	CROCCP3	-5.55	0.0029
24	myomesin (M-protein) 2, 165kDa	MYOM2	-5.49	0.0212
25	six-twelve leukemia	STL	-5.41	0.011

Margin epidermis	Gene title	Gene symbol	Fold change	p-value
26	forkhead box P2	FOXP2	-5.35	0.0087
27	GTPase, IMAP family member 2	GIMAP2	-5.32	0.0207
28	HAUS augmin-like complex, subunit 5	HAUS5	-5.26	0.016
29	collagen, type VI, alpha 5	COL6A5	-5.05	0.0249
30	Yip1 interacting factor homolog B ( <i>S. cerevisiae</i> )	YIF1B	-4.91	0.0284
31	chromosome 16 open reading frame 55	C16orf55	-4.89	0.0079
32	NMDA receptor regulated 2	NARG2	-4.87	0.0068
33	interleukin 37	IL37	-4.85	0.0088
34	FKSG29	FKSG29	-4.60	0.0153
35	MAM domain containing glycosylphosphatidylinositol anchor 1	MDGA1	-4.59	0.0417
36	CD69 molecule	CD69	-4.47	0.0045
37	microtubule associated monooxygenase, calponin and LIM domain containing 3	MICAL3	-4.46	0.0007
38	stearoyl-CoA desaturase 5	SCD5	-4.45	0.0039
39	synaptotagmin VIII	SYT8	-4.41	0.0067
40	chromosome 10 open reading frame 67	C10orf67	-4.37	8.76E-08
41	chromosome 1 open reading frame 226	C1orf226	-4.35	0.0011
42	FBJ murine osteosarcoma viral oncogene homolog B	FOSB	-4.34	0.0416
43	pleckstrin homology-like domain, family B, member 1	PHLDB1	-4.32	0.0069
44		Q93YZ4	-4.31	7.75E-06
45	phosphatase and actin regulator 3	PHACTR3	-4.27	0.0327
46	mucin 16, cell surface associated	MUC16	-4.25	0.0228
47	Rho GTPase activating protein 17	ARHGAP17	-4.20	0.0211
48	poliovirus receptor-related 3	PVRL3	-4.20	0.0006
49	GTP binding protein overexpressed in skeletal muscle	GEM	-4.11	0.0299
50	ankyrin repeat domain 20 family, member A4	ANKRD20A4	-4.09	2.85E-05

**Figure S9** – Top 100 upregulated genes in keloid extralesional vs normal skin epidermis. Corrected for fold change > 2 and p-value < 0.05 where red indicates also significantly upregulated in the centre, blue the margin and orange both.

Extra epidermis	Gene title	Gene symbol	Fold change	p-value
1	aldo-keto reductase family 1, member B10 (aldose reductase)	AKR1B10	86.03	2.14E-06
2	S100 calcium binding protein A8	S100A8	59.50	0.0012
3	mucin-like 1	MUCL1	45.41	0.0124
4	family with sequence similarity 65, member C	FAM65C	36.13	5.53E-05
5	chemokine (C-C motif) ligand 18 (pulmonary and activation-regulated)	CCL18	27.39	0.0002
6	CD36 molecule (thrombospondin receptor)	CD36	24.48	0.0004
7	S100 calcium binding protein A9	S100A9	23.45	0.0169
8	aldo-keto reductase family 1, member B15	AKR1B15	21.68	2.44E-05
9	phosphoserine phosphatase pseudogene 1	PSPHP1	19.29	0.0309
10	keratin 6B	KRT6B	18.67	0.0411
11	aldehyde dehydrogenase 1 family, member A1	ALDH1A1	15.12	0.0048
12	vault RNA 1-3	VTRNA1-3	14.78	0.0016
13	keratin 6A	KRT6A	14.20	0.024
14	sclerostin domain containing 1	SOSTDC1	11.82	0.0063
15	kallikrein-related peptidase 14	KLK14	11.43	0.0039
16	repetin	RPTN	10.59	0.0037
17	aldo-keto reductase family 1, member B1 (aldose reductase)	AKR1B1	10.57	0.0093
18	GTPase activating protein and VPS9 domains 1	GAPVD1	10.30	1.21E-05
19	deafness, autosomal recessive 31	DFNB31	10.02	1.14E-05
20	RNA, U11 small nuclear	RNU11	9.74	0.0002
21	Rh family, C glycoprotein	RHCG	9.35	0.0296
22	defensin, beta 4A	DEFB4A	8.83	0.0336
23	small proline-rich protein 2B	SPRR2B	8.50	0.0151
24	peptidase inhibitor 3, skin-derived	PI3	8.49	0.0184
25	pleckstrin homology-like domain, family A, member 2	PHLDA2	8.46	7.35E-05
26	tetra-peptide repeat homeobox-like	TPRXL	8.44	0.0005
27	tubulin, beta 3 class III	TUBB3	8.42	0.0011
28	OAF homolog (Drosophila)	OAF	8.30	0.001
29	Rho guanine nucleotide exchange factor (GEF) 7	ARHGEF7	8.26	4.94E-06
30	vault RNA 1-2	VTRNA1-2	8.12	0.0003
31	sodium channel, voltage-gated, type IV, beta	SCN4B	8.07	0.0008
32	vault RNA 2-1	VTRNA2-1	8.04	3.60E-05
33	WD repeat domain 66	WDR66	8.02	0.0017

Extra epidermis	Gene title	Gene symbol	Fold change	p-value
34	trichorhinophalangeal syndrome I	TRPS1	7.91	0.0481
35	interferon, alpha-inducible protein 27	IFI27	7.91	2.86E-05
36	small nucleolar RNA, C/D box 3B-1	SNORD3B-1	7.88	0.0008
37	RNA, U1 small nuclear 5	RNU1-5	7.77	3.41E-05
38	inhibitor of DNA binding 1, dominant negative helix-loop-helix protein	ID1	7.71	0.0011
39	apoptosis enhancing nuclease	AEN	7.63	0.0046
40	2'-5'-oligoadenylate synthetase 2, 69/71kDa	OAS2	7.47	0.0058
41	lipocalin 2	LCN2	7.29	0.0396
42	nitric oxide synthase 1 (neuronal)	NOS1	7.17	0.0004
43	double zinc ribbon and ankyrin repeat domains 1	DZANK1	7.03	0.0013
44	ubiquitin-like with PHD and ring finger domains 1	UHRF1	7.00	0.0109
45	dipeptidyl-peptidase 4	DPP4	6.97	0.0417
46	jun proto-oncogene	JUN	6.81	0.0006
47	G protein-coupled receptor, family C, group 5, member A	GPRC5A	6.78	0.0007
48	RNA, U4atac small nuclear (U12-dependent splicing)	RNU4ATAC	6.71	0.0004
49	transmembrane protein 198	TMEM198	6.68	0.0178
50	sperm acrosome associated 4	SPACA4	6.65	0.0003
51	nuclear receptor subfamily 1, group D, member 1	NR1D1	6.62	7.93E-05
52	jun B proto-oncogene	JUNB	6.58	0.0008
53	keratin 16 pseudogene 3	KRT16P3	6.48	0.0015
54	CTAGE family, member 5	CTAGE5	6.42	0.0116
55	FK506 binding protein 1A, 12kDa	FKBP1A	6.41	0.0068
56	SET domain containing (lysine methyltransferase) 7	SETD7	6.39	0.004
57	chitinase 3-like 2	CHI3L2	6.38	0.0026
58	integrin, alpha M (complement component 3 receptor 3 subunit)	ITGAM	6.24	0.0238
59	tribbles homolog 2 (Drosophila)	TRIB2	6.23	0.0019
60	v-myc myelocytomatosis viral related oncogene, neuroblastoma derived (avian)	MYCN	6.23	0.0189
61	HUS1 checkpoint homolog b (S. pombe)	HUS1B	6.14	0.0158
62	keratin 16	KRT16	6.14	0.0377
63	immediate early response 3	IER3	6.13	0.0033
64	small Cajal body-specific RNA 14	SCARNA14	6.05	7.74E-06
65	small nucleolar RNA, C/D box 82	SNORD82	5.90	0.0218
66	vault RNA 1-1	VTRNA1-1	5.80	0.001

Extra epidermis	Gene title	Gene symbol	Fold change	p-value
67	SH3-domain binding protein 4	SH3BP4	5.78	0.0224
68	transmembrane protein 63C	TMEM63C	5.74	0.0095
69	protease, serine 27	PRSS27	5.63	0.0014
70	interleukin 36, gamma	IL36G	5.59	0.0035
71	hydroxysteroid (17-beta) dehydrogenase 2	HSD17B2	5.51	0.0231
72	keratin 17 pseudogene	KRT17P	5.46	0.0002
73	von Willebrand factor C domain containing 2	VWC2	5.44	2.78E-05
74	wingless-type MMTV integration site family, member 5A	WNT5A	5.44	0.0382
75	potassium voltage-gated channel, subfamily G, member 3	KCNG3	5.42	0.0036
76	interferon induced transmembrane protein 1 (9-27)	IFITM1	5.40	0.0011
77	GLIS family zinc finger 2	GLIS2	5.34	2.20E-05
78	interleukin 32	IL32	5.20	0.0138
79	chondroitin sulfate proteoglycan 5 (neuroglycan C)	CSPG5	5.11	0.0009
80	MAX dimerization protein 3	MXD3	5.08	0.0031
81	chromosome 11 open reading frame 96	C11orf96	5.07	0.0062
82	protease, serine, 22	PRSS22	5.03	0.0011
83	SRY (sex determining region Y)-box 17	SOX17	5.03	0.007
84	glutathione peroxidase 3 (plasma)	GPX3	5.03	0.0455
85	MCF2L antisense RNA 1 (non-protein coding)	MCF2L-AS1	5.02	0.0159
86	DMRT-like family A1	DMRTA1	5.00	0.0263
87	replication protein A4, 30kDa	RPA4	4.93	0.0147
88	testis expressed 101	TEX101	4.92	0.0004
89	nuclear receptor subfamily 4, group A, member 1	NR4A1	4.91	0.0245
90	natriuretic peptide receptor C/guanylate cyclase C (atrionatriuretic peptide receptor C)	NPR3	4.91	0.0144
91	trafficking protein particle complex 6A	TRAPPC6A	4.88	0.0196
92	glutathione peroxidase 2 (gastrointestinal)	GPX2	4.83	0.0074
93	chromosome 9 open reading frame 68	C9orf68	4.82	0.0049
94	notch 4	NOTCH4	4.80	0.0004
95	cholinergic receptor, nicotinic, alpha 9	CHRNA9	4.79	0.0003
96	Pvt1 oncogene (non-protein coding)	PVT1	4.78	0.0004
97	tensin 1	TNS1	4.77	0.0004
98	Fanconi anemia, complementation group A	FANCA	4.77	0.0236
99	interferon-induced protein with tetratricopeptide repeats 1	IFIT1	4.76	0.0067
100	KRAB-A domain containing 1	KRBA1	4.75	0.0027

**Figure S10** – Top 50 downregulated genes in keloid extralesional vs normal skin epidermis. Corrected for fold change > 2 and p-value < 0.05, where red indicates also significantly downregulated in the centre, blue the margin and orange both.

Extra epidermis	Gene title	Gene symbol	Fold change	p-value
1	spermatogenesis and oogenesis specific basic helix-loop-helix 1	SOHLH1	-25.11	2.38E-06
2	UDP glycosyltransferase 3 family, polypeptide A2	UGT3A2	-21.89	0.0016
3	endoplasmic reticulum aminopeptidase 2	ERAP2	-12.86	0.0404
4	long intergenic non-protein coding RNA 173	LINC00173	-11.59	0.0066
5	ST6 beta-galactosamide alpha-2,6-sialyltransferase 2	ST6GAL2	-11.59	0.0073
6	coiled-coil domain containing 40	CCDC40	-10.72	0.0174
7	interleukin 37	IL37	-10.66	0.0002
8	docking protein 7	DOK7	-10.50	9.15E-06
9	tetraspanin 2	TSPAN2	-10.29	0.0088
10	ghrelin opposite strand RNA 2 (non-protein coding)	GHRLOS2	-9.85	0.0007
11	FSHD region gene 2	FRG2	-9.17	1.03E-05
12	anterior gradient 3 homolog (Xenopus laevis)	AGR3	-9.13	8.91E-05
13	HLA complex group 4 (non-protein coding)	HCG4	-8.70	0.0032
14	cellular retinoic acid binding protein 1	CRABP1	-8.25	0.025
15	v-kit Hardy-Zuckerman 4 feline sarcoma viral oncogene homolog	KIT	-8.23	0.0103
16	chromosome 14 open reading frame 132	C14orf132	-7.98	0.0007
17	betacellulin	BTC	-7.82	0.0018
18	aquaporin 7 pseudogene 1	AQP7P1	-7.63	0.0059
19	FSHD region gene 2 family, member C pseudogene	LOC146481	-7.55	1.15E-05
20	cyclin G2	CCNG2	-7.42	0.009
21	coiled-coil domain containing 73	CCDC73	-7.36	0.0007
22	abhydrolase domain containing 12B	ABHD12B	-7.25	4.25E-05
23	chromosome 9 open reading frame 40	C9orf40	-7.23	0.0038
24	homeobox A10	HOXA10	-6.94	0.038
25	centrosomal protein 68kDa	CEP68	-6.79	0.006

Extra epidermis	Gene title	Gene symbol	Fold change	p-value
26	claudin 23	CLDN23	-6.70	0.0217
27	myomesin (M-protein) 2, 165kDa	MYOM2	-6.58	0.0117
28	A kinase (PRKA) anchor protein 5	AKAP5	-6.56	0.0147
29	HAUS augmin-like complex, subunit 5	HAUS5	-6.52	0.0073
30	COBW domain containing 7	CBWD7	-6.45	0.0015
31	purinergic receptor P2Y, G-protein coupled, 13	P2RY13	-6.31	0.0178
32	CD59 molecule, complement regulatory protein	CD59	-6.25	0.001
33	interleukin 20 receptor, alpha	IL20RA	-6.24	4.69E-06
34	RAB3B, member RAS oncogene family	RAB3B	-6.21	0.0014
35	pregnancy specific beta-1-glycoprotein 8	PSG8	-6.20	0.0272
36	kelch repeat and BTB (POZ) domain containing 3	KBTBD3	-6.15	0.0342
37	nuclear casein kinase and cyclin-dependent kinase substrate 1	NUCKS1	-6.13	0.0012
38	family with sequence similarity 183, member A	FAM183A	-6.10	9.64E-07
39	proteasome (prosome, macropain) 26S subunit, non-ATPase, 5	PSMD5	-6.10	0.0478
40	HD domain containing 2	HDDC2	-6.09	0.0019
41	mitogen-activated protein kinase 8	MAPK8	-6.06	0.0002
42	testis specific, 10	TSGA10	-6.05	0.0011
43	URB1 ribosome biogenesis 1 homolog (S. cerevisiae)	URB1	-6.01	0.0003
44	ciliary rootlet coiled-coil, rootletin pseudogene 3	CROCCP3	-5.89	0.0022
45	family with sequence similarity 92, member A1	FAM92A1	-5.88	0.0005
46	transmembrane protein 14E	TMEM14E	-5.83	0.0257
47	resistance to inhibitors of cholinesterase 3 homolog (C. elegans)	RIC3	-5.76	0.0187
48	chemokine-like receptor 1	CMKLR1	-5.76	0.0241
49	abl-interactor 2	ABI2	-5.76	0.0025
50	keratin 77	KRT77	-5.72	0.0134



**Figure S11** – Top 100 upregulated genes in keloid centre vs NS dermis, corrected for fold change >2, p value < 0.05 and q value < 0.05, where blue indicates also significantly upregulated in the margin, green the extralesional and orange both.

Centre dermis	Gene title	Gene symbol	Fold change	p-value	q-value
1	ADAM metalloproteinase with thrombospondin type 1 motif, 14	ADAMTS14	60.94	8.69E-06	0.0026
2	asporin	ASPN	58.58	3.87E-05	0.006
3	tubulin, beta 3 class III	TUBB3	43.02	2.20E-07	0.0003
4	coiled-coil domain containing 102B	CCDC102B	40.83	3.65E-08	0.0002
5	synapse differentiation inducing 1	SYNDIG1	37.02	4.48E-05	0.0066
6	WNT1 inducible signaling pathway protein 1	WISP1	30.89	1.69E-07	0.0003
7	RAB15, member RAS oncogene family	RAB15	30.70	3.38E-07	0.0004
8	ADAM metalloproteinase with thrombospondin type 1 motif, 4	ADAMTS4	27.49	8.50E-06	0.0026
9	C1q and tumor necrosis factor related protein 6	C1QTNF6	25.24	7.61E-07	0.0006
10	matrix metalloproteinase 11 (stromelysin 3)	MMP11	24.79	7.37E-06	0.0024
11	KIAA1024	KIAA1024	24.22	3.40E-06	0.0014
12	aggrecan	ACAN	23.78	0.0014	0.0444
13	adenylate cyclase activating polypeptide 1 (pituitary)	ADCYAP1	22.62	0.0001	0.0109
14	chromosome 12 open reading frame 70	C12orf70	22.35	0.0006	0.0282
15	ST6 beta-galactosamide alpha-2,6-sialyltransferase 2	ST6GAL2	21.12	0.0006	0.0294
16	H19, imprinted maternally expressed transcript (non-protein coding)	H19	20.85	0.0003	0.0185
17	collagen triple helix repeat containing 1	CTHRC1	20.76	0.0012	0.0412
18	cartilage oligomeric matrix protein	COMP	20.64	0.0011	0.0387
19	SIX homeobox 1	SIX1	20.28	7.80E-06	0.0025
20	BEN domain containing 6	BEND6	20.02	4.31E-07	0.0004
21	paired-like homeodomain 2	PITX2	19.69	0.0011	0.0387
22	neuronal pentraxin II	NPTX2	19.46	1.15E-05	0.0031
23	ADAM metalloproteinase with thrombospondin type 1 motif, 2	ADAMTS2	18.79	0.0004	0.023
24	fibronectin type III domain containing 1	FNDC1	18.07	0.0007	0.0305
25	C-type lectin domain family 2, member A	CLEC2A	16.75	0.0017	0.0493
26	leucine rich repeat neuronal 3	LRRN3	16.59	3.84E-05	0.006
27	C-type lectin domain family 1, member B	CLEC1B	16.31	4.83E-05	0.0069
28	collagen, type X, alpha 1	COL10A1	16.20	0.0002	0.0158
29	collagen, type V, alpha 2	COL5A2	16.09	0.0001	0.0107
30	phosphatidic acid phosphatase type 2 domain containing 1A	PPAPDC1A	15.80	0.0013	0.043
31	piezo-type mechanosensitive ion channel component 2	PIEZO2	15.27	2.89E-07	0.0003
32	ADAM metalloproteinase with thrombospondin type 1 motif, 12	ADAMTS12	15.01	0.0013	0.0419
33	paired box 1	PAX1	14.66	0.0001	0.01

Centre dermis	Gene title	Gene symbol	Fold change	p-value	q-value
34	discs, large homolog 4 (Drosophila)	DLG4	14.64	2.87E-06	0.0013
35	cyclin-dependent kinase inhibitor 2A (melanoma, p16, inhibits CDK4)	CDKN2A	14.17	2.55E-07	0.0003
36	synaptosomal-associated protein, 25kDa	SNAP25	14.03	6.85E-05	0.0083
37	collagen, type V, alpha 3	COL5A3	13.95	7.11E-05	0.0085
38	leucine zipper, putative tumor suppressor 1	LZTS1	13.91	0.0006	0.0282
39	bone morphogenetic protein 1	BMP1	13.61	1.19E-05	0.0031
40	prion protein 2 (dublet)	PRND	13.38	3.15E-06	0.0014
41	flavin containing monooxygenase 3	FMO3	13.10	2.93E-07	0.0003
42	synaptotagmin-like 2	SYTL2	12.83	2.63E-05	0.0048
43	insulin-like growth factor 2 (somatomedin A)	IGF2	12.48	0.0009	0.0352
44	smoothelin-like 2	SMTNL2	11.81	0.0007	0.0309
45	carboxypeptidase X (M14 family), member 1	CPXM1	11.68	1.11E-06	0.0008
46	cell growth regulator with EF-hand domain 1	CGREF1	11.29	0.0006	0.0289
47	transforming growth factor, beta 3	TGFB3	11.20	0.0006	0.029
48	stonin 2	STON2	11.17	7.84E-06	0.0025
49	ADAM metallopeptidase with thrombospondin type 1 motif, 18	ADAMTS18	10.99	0.0006	0.0285
50	neuregulin 1	NRG1	10.71	0.0002	0.0155
51	transmembrane protein 132E	TMEM132E	10.50	0.0001	0.0117
52	proline rich 5 like	PRR5L	9.82	0.0005	0.0268
53	psoriasis susceptibility 1 candidate 1	PSORS1C1	9.73	4.76E-05	0.0068
54	opioid binding protein/cell adhesion molecule-like	OPCML	9.63	0.0016	0.0484
55	transmembrane protein 45A	TMEM45A	9.57	1.16E-05	0.0031
56	matrix metallopeptidase 23B	MMP23B	9.52	2.71E-06	0.0013
57	guanylate binding protein 3	GBP3	9.38	7.60E-05	0.0088
58	alpha-kinase 2	ALPK2	9.35	1.67E-05	0.0037
59	chromosome 18 open reading frame 34	C18orf34	9.33	1.49E-06	0.0009
60	short stature homeobox 2	SHOX2	9.23	2.27E-07	0.0003
61	chromosome 14 open reading frame 37	C14orf37	9.16	0.0002	0.0152
62	enabled homolog (Drosophila)	ENAH	9.11	1.82E-05	0.004
63	translocator protein 2	TSPO2	8.94	0.0002	0.015
64	methyltransferase like 11A	METTL11A	8.92	0.0001	0.0112
65	tweety homolog 3 (Drosophila)	TTYH3	8.91	1.69E-07	0.0003
66	GLIS family zinc finger 1	GLIS1	8.90	0.0003	0.02

Centre dermis	Gene title	Gene symbol	Fold change	p-value	q-value
67	tumor necrosis factor receptor superfamily, member 19	TNFRSF19	8.90	1.75E-05	0.0038
68	Zic family member 4	ZIC4	8.89	2.07E-06	0.0011
69	TAF11 RNA polymerase II, TATA box binding protein (TBP)-associated factor, 28kDa	TAF11	8.81	0.0002	0.0153
70	proprotein convertase subtilisin/kexin type 5	PCSK5	8.69	0.0007	0.0317
71	aldehyde dehydrogenase 1 family, member L2	ALDH1L2	8.68	6.29E-05	0.008
72	plexin C1	PLXNC1	8.46	2.68E-05	0.0048
73	leucine proline-enriched proteoglycan (leprecan) 1	LEPRE1	8.45	2.18E-09	3.20E-05
74	IKBKB interacting protein	IKBIP	8.26	0.0005	0.027
75	uncharacterized serine/threonine-protein kinase SgK494	SGK494	8.24	3.65E-05	0.0058
76	sortilin-related VPS10 domain containing receptor 2	SORCS2	8.22	1.96E-05	0.0041
77	small nucleolar RNA, C/D box 114-14	SNORD114-14	8.21	8.30E-05	0.009
78	midkine (neurite growth-promoting factor 2)	MDK	8.14	0.0012	0.0408
79	cholecystokinin A receptor	CCKAR	8.10	2.16E-05	0.0043
80	FK506 binding protein 10, 65 kDa	FKBP10	8.00	0.0011	0.0396
81	matrix metalloproteinase 14 (membrane-inserted)	MMP14	7.97	0.0003	0.0205
82	ceramide kinase	CERK	7.90	0.0002	0.016
83	RWD domain containing 2A	RWDD2A	7.86	0.0012	0.0414
84	C2 calcium-dependent domain containing 4B	C2CD4B	7.78	1.31E-06	0.0009
85	ArfGAP with RhoGAP domain, ankyrin repeat and PH domain 1	ARAP1	7.76	0.0001	0.01
86	collagen, type VI, alpha 6	COL6A6	7.64	3.27E-05	0.0053
87	hemicentin 1	HMCN1	7.62	0.0016	0.0473
88	prostaglandin E receptor 3 (subtype EP3)	PTGER3	7.52	0.0001	0.0103
89	tetratricopeptide repeat, ankyrin repeat and coiled-coil containing 2	TANC2	7.50	0.0002	0.0177
90	ADAM metalloproteinase with thrombospondin type 1 motif, 6	ADAMTS6	7.50	5.49E-05	0.0074
91	uncharacterized protein MGC16121	MGC16121	7.47	0.0001	0.011
92	ankyrin repeat and FYVE domain containing 1	ANKFY1	7.44	0.0011	0.0394
93	uncharacterized MGC4294	MGC4294	7.43	0.0005	0.0267
94	dynein, axonemal, heavy chain 12	DNAH12	7.40	0.0005	0.0247
95	ADAMTS-like 1	ADAMTSL1	7.39	5.16E-06	0.0019
96	glycosyltransferase 8 domain containing 2	GLT8D2	7.36	0.0009	0.0364
97	arylsulfatase B	ARSB	7.34	0.0006	0.0291
98	SLIT-ROBO Rho GTPase activating protein 2	SRGAP2	7.25	0.0001	0.0101
99	sushi-repeat containing protein, X-linked 2	SRPX2	7.23	0.0002	0.0171
100	small nucleolar RNA, C/D box 53	SNORD53	7.22	1.50E-06	0.0009

**Figure S12** – Top 50 downregulated genes in keloid centre vs normal skin dermis. Corrected for fold change > 2 and p-value < 0.05 q-value < 0.05 where blue indicates also significantly downregulated in the margin, green the extralesional and orange both.

Centre dermis	Gene title	Gene symbol	Fold change	p-value	q-value
1	mucin-like 1	MUCL1	-329.68	0.0002	0.0143
2	secretoglobin, family 1D, member 2	SCGB1D2	-161.77	0.0007	0.0316
3	secretoglobin, family 1D, member 1	SCGB1D1	-161.05	0.0005	0.0274
4	carcinoembryonic antigen-related cell adhesion molecule 3	CEACAM3	-160.13	1.43E-06	0.0009
5	Purkinje cell protein 4	PCP4	-92.40	2.18E-06	0.0012
6	SRY (sex determining region Y)-box 9	SOX9	-84.41	2.64E-06	0.0013
7	prolactin-induced protein	PIP	-81.14	0.0005	0.0254
8	secretoglobin, family 2A, member 1	SCGB2A1	-73.16	2.27E-07	0.0003
9	odorant binding protein 2A	OBP2A	-65.65	5.21E-08	0.0002
10	tetraspanin 8	TSPAN8	-60.57	0.0017	0.0485
11	gap junction protein, beta 6, 30kDa	GJB6	-59.93	4.67E-06	0.0018
12	creatine kinase, mitochondrial 2 (sarcomeric)	CKMT2	-57.27	3.37E-08	0.0002
13	G protein-coupled receptor 12	GPR12	-56.76	0.0001	0.0108
14	secretoglobin, family 1D, member 4	SCGB1D4	-55.52	0.0006	0.0284
15	matrix metalloproteinase 7 (matrilysin, uterine)	MMP7	-44.67	3.47E-05	0.0056
16	scavenger receptor class A, member 5 (putative)	SCARA5	-43.17	1.22E-05	0.0031
17	erythrocyte membrane protein band 4.1 like 4B	EPB41L4B	-39.29	2.92E-07	0.0003
18	ATPase, H+ transporting, lysosomal V0 subunit a4	ATP6V0A4	-38.59	7.86E-05	0.0089
19	epithelial cell adhesion molecule	EPCAM	-37.80	0.0002	0.0138
20	desmin	DES	-36.07	4.46E-06	0.0017
21	transcription factor CP2-like 1	TFCP2L1	-35.69	1.57E-06	0.001
22	transmembrane protein 213	TMEM213	-35.46	1.08E-10	6.35E-06
23	neuropeptide Y receptor Y1	NPY1R	-35.19	2.46E-05	0.0046
24	sodium channel, voltage-gated, type VII, alpha	SCN7A	-34.91	3.13E-08	0.0002
25	keratin 23 (histone deacetylase inducible)	KRT23	-32.52	8.54E-05	0.0092

Centre dermis	Gene title	Gene symbol	Fold change	p-value	q-value
26	carbonic anhydrase VI	CA6	-32.44	0.0003	0.0202
27	actin, gamma 2, smooth muscle, enteric	ACTG2	-31.90	0.0001	0.0119
28	RERG/RAS-like	RERGL	-31.87	0.0002	0.0164
29	annexin A3	ANXA3	-29.58	1.61E-05	0.0036
30	myocilin, trabecular meshwork inducible glucocorticoid response	MYOC	-29.19	2.01E-05	0.0042
31	brain expressed, X-linked 5	BEX5	-28.60	1.44E-05	0.0034
32	S100 calcium binding protein P	S100P	-28.13	0.0003	0.0187
33	peroxisome proliferator-activated receptor gamma, coactivator 1 alpha	PPARGC1A	-27.73	0.0005	0.0272
34	carcinoembryonic antigen-related cell adhesion molecule 5	CEACAM5	-26.60	0.0014	0.0445
35	tripartite motif containing 29	TRIM29	-26.22	0.0001	0.0107
36	WNT inhibitory factor 1	WIF1	-25.67	0.0002	0.0143
37	rhopilin, Rho GTPase binding protein 2	RHPN2	-24.58	2.97E-08	0.0002
38	serine palmitoyltransferase, small subunit B	SPTSSB	-24.19	0.0016	0.0472
39	creatine kinase, mitochondrial 1A	CKMT1A	-23.91	5.95E-06	0.0021
40	cytochrome P450, family 4, subfamily B, polypeptide 1	CYP4B1	-23.67	1.33E-05	0.0033
41	proline rich 15-like	PRR15L	-22.83	1.35E-07	0.0003
42	ATPase, H+ transporting, lysosomal 56/58kDa, V1 subunit B1	ATP6V1B1	-21.65	1.76E-05	0.0039
43	fatty acid 2-hydroxylase	FA2H	-21.25	0.0004	0.024
44	tandem C2 domains, nuclear	TC2N	-20.76	2.85E-06	0.0013
45	keratin 77	KRT77	-20.60	4.15E-05	0.0062
46	cystic fibrosis transmembrane conductance regulator (ATP-binding cassette sub-family C, member 7)	CFTR	-19.90	0.0001	0.0103
47	C1q and tumor necrosis factor related protein 9	C1QTNF9	-19.86	1.13E-06	0.0008
48	actin, alpha 1, skeletal muscle	ACTA1	-19.42	4.13E-05	0.0062
49	chromosome 2 open reading frame 54	C2orf54	-19.37	8.06E-05	0.0089
50	carcinoembryonic antigen-related cell adhesion molecule 1 (biliary glycoprotein)	CEACAM1	-19.34	4.21E-07	0.0004

**Figure S13** – Top 100 upregulated genes in keloid margin vs NS dermis, corrected for fold change >2, p value < 0.05 and q value < 0.05, where red indicates also significantly upregulated in the centre, green the extralesional and orange both.

Margin dermis	Gene title	Gene symbol	Fold change	p-value	q-value
1	ADAM metallopeptidase with thrombospondin type 1 motif, 14	ADAMTS14	75.06	1.11E-05	0.0049
2	coiled-coil domain containing 102B	CCDC102B	49.02	5.14E-08	0.0003
3	tubulin, beta 3 class III	TUBB3	41.92	7.59E-07	0.0016
4	synapse differentiation inducing 1	SYNDIG1	33.54	0.0001	0.0168
5	cyclin-dependent kinase inhibitor 3	CDKN3	29.54	0.0007	0.037
6	BEN domain containing 6	BEND6	29.48	1.70E-07	0.0006
7	synaptosomal-associated protein, 25kDa	SNAP25	26.03	1.00E-05	0.0047
8	RAB15, member RAS oncogene family	RAB15	25.03	2.69E-06	0.0024
9	cartilage oligomeric matrix protein	COMP	23.52	0.0014	0.0499
10	neuregulin 1	NRG1	22.24	1.59E-05	0.0059
11	C2 calcium-dependent domain containing 4B	C2CD4B	20.79	4.04E-09	5.93E-05
12	chromosome 2 open reading frame 43	C2orf43	20.59	9.48E-05	0.0137
13	C1q and tumor necrosis factor related protein 6	C1QTNF6	20.09	6.68E-06	0.0038
14	leucine zipper, putative tumor suppressor 1	LZTS1	19.79	0.0003	0.0249
15	ADAM metallopeptidase with thrombospondin type 1 motif, 2	ADAMTS2	19.72	0.0007	0.0354
16	BCL2-associated athanogene 3	BAG3	19.48	3.05E-06	0.0026
17	matrix metallopeptidase 11 (stromelysin 3)	MMP11	18.31	6.94E-05	0.0118
18	paired box 1	PAX1	18.23	8.83E-05	0.0134
19	EGF-like-domain, multiple 6	EGFL6	16.45	0.0007	0.0357
20	SIX homeobox 1	SIX1	16.13	5.67E-05	0.011
21	asporin	ASPN	16.06	0.0009	0.0407
22	chemokine (C-X-C motif) ligand 9	CXCL9	15.93	0.0003	0.0257
23	small nucleolar RNA, C/D box 114-14	SNORD114-14	15.87	5.08E-06	0.0034
24	KIAA1024	KIAA1024	15.43	7.08E-05	0.0119
25	piezo-type mechanosensitive ion channel component 2	PIEZO2	14.81	4.44E-06	0.0032
26	C-type lectin domain family 1, member B	CLEC1B	14.10	0.0002	0.0204
27	ankyrin repeat domain 16	ANKRD16	13.45	1.36E-06	0.0022
28	bone morphogenetic protein 1	BMP1	13.16	3.53E-05	0.0089
29	ceramide kinase	CERK	12.95	3.47E-05	0.0089
30	collagen, type VI, alpha 5	COL6A5	12.68	0.0009	0.042
31	transmembrane protein 132E	TMEM132E	12.42	0.0001	0.016
32	kelch-like 6 ( <i>Drosophila</i> )	KLHL6	12.36	0.0001	0.0166
33	kallikrein-related peptidase 4	KLK4	12.23	1.17E-05	0.005

Margin dermis	Gene title	Gene symbol	Fold change	p-value	q-value
34	sperm associated antigen 7	SPAG7	12.21	2.06E-07	0.0006
35	GRB2-associated binding protein 3	GAB3	11.64	0.0002	0.0209
36	interleukin 4 receptor	IL4R	11.41	0.0003	0.0226
37	WNT1 inducible signaling pathway protein 1	WISP1	11.02	9.16E-05	0.0136
38	selectin E	SELE	10.98	1.16E-06	0.0021
39	long intergenic non-protein coding RNA 478	LINC00478	10.91	1.12E-08	0.0001
40	collagen, type V, alpha 2	COL5A2	10.66	0.0013	0.0481
41	solute carrier family 7 (anionic amino acid transporter light chain, xc-system), member 11	SLC7A11	10.61	0.0007	0.036
42	ADAM metalloproteinase with thrombospondin type 1 motif, 4	ADAMTS4	10.56	0.0011	0.0452
43	EF-hand domain family, member B	EFHB	10.50	0.0004	0.0276
44	tubulin tyrosine ligase-like family, member 1	TTLL1	10.45	5.00E-05	0.0103
45	small nucleolar RNA, C/D box 113-4	SNORD113-4	10.19	0.0006	0.0337
46	guanylate binding protein 3	GBP3	10.14	0.0001	0.0153
47	matrix metalloproteinase 14 (membrane-inserted)	MMP14	10.06	0.0002	0.0206
48	cysteine/histidine-rich 1	CYHR1	9.80	2.16E-05	0.0069
49	selectin P (granule membrane protein 140kDa, antigen CD62)	SELP	9.68	8.09E-07	0.0016
50	carboxypeptidase X (M14 family), member 1	CPXM1	9.60	1.08E-05	0.0049
51	endogenous retrovirus group I, member 1	ERVI-1	9.57	6.30E-06	0.0036
52	long intergenic non-protein coding RNA 174	LINC00174	9.50	0.0003	0.0225
53	ADAM metalloproteinase with thrombospondin type 1 motif, 6	ADAMTS6	9.37	3.34E-05	0.0087
54	selectin L	SELL	9.09	8.30E-05	0.0129
55	chromosome 6 open reading frame 204	C6orf204	9.02	0.0007	0.0364
56	amyotrophic lateral sclerosis 2 (juvenile) chromosome region, candidate 11	ALS2CR11	8.96	8.57E-05	0.0132
57	synovial sarcoma, X breakpoint 3	SSX3	8.78	2.32E-08	0.0002
58	chromosome 18 open reading frame 34	C18orf34	8.55	7.49E-06	0.004
59	uncharacterized MGC4294	MGC4294	8.48	0.0005	0.0321
60	uncharacterized MGC24103	MGC24103	8.44	6.50E-05	0.0115
61	granzyme B (granzyme 2, cytotoxic T-lymphocyte-associated serine esterase 1)	GZMB	8.39	0.0006	0.0335
62	transmembrane protein 45A	TMEM45A	8.12	7.66E-05	0.0123
63	uncharacterized serine/threonine-protein kinase Sgk494	SGK494	8.10	9.40E-05	0.0137
64	SLIT-ROBO Rho GTPase activating protein 2	SRGAP2	8.08	0.0001	0.0158
65	matrix metalloproteinase 23B	MMP23B	8.05	2.19E-05	0.0069
66	retinitis pigmentosa 1 (autosomal dominant)	RP1	8.02	3.67E-05	0.0091



Margin dermis	Gene title	Gene symbol	Fold change	p-value	q-value
67	placenta-specific 8	PLAC8	7.96	0.0004	0.0286
68	mitogen-activated protein kinase kinase kinase 12	MAP3K12	7.93	1.36E-05	0.0053
69	long intergenic non-protein coding RNA 340	LINC00340	7.91	2.11E-05	0.0069
70	chromosome 15 open reading frame 5	C15orf5	7.76	0.0002	0.0182
71	asialoglycoprotein receptor 1	ASGR1	7.71	2.34E-05	0.0072
72	ribosomal protein S16 pseudogene 5	RPS16P5	7.68	0.0013	0.0485
73	psoriasis susceptibility 1 candidate 1	PSORS1C1	7.64	0.0004	0.0278
74	autism susceptibility candidate 2	AUTS2	7.53	0.0008	0.0386
75	phosphodiesterase 4D interacting protein	PDE4DIP	7.40	0.0006	0.035
76	nuclear receptor subfamily 5, group A, member 2	NR5A2	7.36	0.0012	0.0473
77	chromosome 14 open reading frame 183	C14orf183	7.32	7.23E-06	0.0039
78	microtubule associated monooxygenase, calponin and LIM domain containing 1	MICAL1	7.31	9.01E-05	0.0134
79	zinc finger protein 71	ZNF71	7.25	0.0013	0.0489
80	DAZ interacting protein 1-like	DZIP1L	7.25	1.11E-05	0.0049
81	PHD finger protein 8	PHF8	7.24	2.57E-06	0.0024
82	CD247 molecule	CD247	7.23	0.0012	0.0471
83	leucine proline-enriched proteoglycan (leprecan) 1	LEPRE1	7.14	3.78E-08	0.0002
84	flavin containing monooxygenase 3	FMO3	7.05	4.91E-05	0.0103
85	short stature homeobox 2	SHOX2	7.04	5.29E-06	0.0034
86	synaptotagmin-like 2	SYTL2	7.03	0.0012	0.0471
87	arachidonate 5-lipoxygenase	ALOX5	7.02	1.95E-05	0.0067
88	dynein, axonemal, heavy chain 12	DNAH12	6.93	0.0013	0.0481
89	zinc finger, DHHC-type containing 21	ZDHHC21	6.91	0.0002	0.0202
90	coiled-coil domain containing 88B	CCDC88B	6.88	8.87E-05	0.0134
91	NIMA (never in mitosis gene a)- related kinase 11	NEK11	6.86	0.0013	0.0489
92	troponin T type 3 (skeletal, fast)	TNNT3	6.81	0.0004	0.0281
93	hyaluronoglucosaminidase 3	HYAL3	6.75	3.22E-05	0.0086
94	guanylate cyclase 1, soluble, beta 3	GUCY1B3	6.74	0.0003	0.0246
95	transmembrane protein 39A	TMEM39A	6.61	0.0013	0.0489
96	LY6/PLAUR domain containing 1	LYPD1	6.59	0.001	0.0437
97	chemokine (C-X-C motif) ligand 10	CXCL10	6.58	7.32E-05	0.012
98	zinc finger protein 573	ZNF573	6.57	0.0002	0.02
99	sema domain, seven thrombospondin repeats (type 1 and type 1-like), transmembrane domain (TM) and short cytoplasmic domain, (semaphorin) 5B	SEMA5B	6.56	0.0007	0.0357
100	maternally expressed 8 (non-protein coding)	MEG8	6.53	0.0001	0.017



**Figure S14** – Top 50 downregulated genes in keloid margin vs normal skin dermis. Corrected for fold change > 2 and p-value < 0.05 q-value < 0.05 where red indicates also significantly downregulated in the centre, green the extralesional and orange both

Margin dermis	Gene title	Gene symbol	Fold change	p-value	q-value
1	rhopilin, Rho GTPase binding protein 2	RHPN2	-45.05	3.93E-09	5.93E-05
2	transmembrane protein 213	TMEM213	-40.54	2.03E-10	1.19E-05
3	myocilin, trabecular meshwork inducible glucocorticoid response	MYOC	-36.66	2.05E-05	0.0068
4	Purkinje cell protein 4	PCP4	-36.26	0.0001	0.0161
5	secretoglobin, family 2A, member 1	SCGB2A1	-36.16	1.09E-05	0.0049
6	carbonic anhydrase VI	CA6	-35.02	0.0005	0.0312
7	carcinoembryonic antigen-related cell adhesion molecule 3	CEACAM3	-33.07	0.0005	0.0296
8	actin, gamma 2, smooth muscle, enteric	ACTG2	-31.33	0.0003	0.0248
9	cytoplasmic polyadenylation element binding protein 3	CPEB3	-25.51	1.33E-06	0.0022
10	annexin A3	ANXA3	-25.00	5.31E-05	0.0108
11	epithelial cell adhesion molecule	EPCAM	-24.71	0.0012	0.048
12	SRY (sex determining region Y)-box 9	SOX9	-24.57	0.0004	0.0288
13	homer homolog 2 (Drosophila)	HOMER2	-23.25	5.45E-05	0.0109
14	sorbin and SH3 domain containing 1	SORBS1	-21.41	1.26E-05	0.0051
15	sodium channel, voltage-gated, type VII, alpha	SCN7A	-19.85	1.89E-06	0.0024
16	C1q and tumor necrosis factor related protein 9	C1QTNF9	-19.62	3.43E-06	0.0028
17	delta/notch-like EGF repeat containing	DNER	-18.85	6.45E-05	0.0115
18	brain expressed, X-linked 5	BEX5	-18.64	0.0002	0.0195
19	creatine kinase, mitochondrial 1A	CKMT1A	-17.90	5.54E-05	0.0109
20	ATPase, H <sup>+</sup> transporting, lysosomal 56/58kDa, V1 subunit B1	ATP6V1B1	-17.85	9.73E-05	0.0139
21	FBJ murine osteosarcoma viral oncogene homolog	FOS	-16.50	0.0011	0.0458
22	dystonin	DST	-16.22	2.51E-05	0.0073
23	desmin	DES	-15.70	0.0003	0.025
24	v-erb-b2 erythroblastic leukemia viral oncogene homolog 3 (avian)	ERBB3	-15.60	6.82E-07	0.0016
25	secreted frizzled-related protein 1	SFRP1	-15.19	6.21E-05	0.0114

Margin dermis	Gene title	Gene symbol	Fold change	p-value	q-value
26	hydroxysteroid (17-beta) dehydrogenase 6 homolog (mouse)	HSD17B6	-15.07	1.56E-07	0.0006
27	chromosome 2 open reading frame 40	C2orf40	-15.05	0.0009	0.0401
28	oxoglutarate (alpha-ketoglutarate) receptor 1	OXGR1	-14.92	2.23E-08	0.0002
29	mab-21-like 1 (C. elegans)	MAB21L1	-14.70	0.0002	0.0212
30	ankyrin 3, node of Ranvier (ankyrin G)	ANK3	-14.49	7.85E-05	0.0125
31	cytochrome P450, family 4, subfamily B, polypeptide 1	CYP4B1	-13.81	0.0003	0.0248
32	creatine kinase, mitochondrial 2 (sarcomeric)	CKMT2	-13.76	7.79E-05	0.0124
33	glypican 4	GPC4	-13.57	0.0006	0.034
34	grainyhead-like 1 (Drosophila)	GRHL1	-13.12	0.0002	0.0217
35	Kruppel-like factor 5 (intestinal)	KLF5	-12.94	0.0003	0.0233
36	Rap guanine nucleotide exchange factor (GEF)-like 1	RAPGEFL1	-12.54	0.0014	0.0499
37	protein phosphatase 1, regulatory subunit 12B	PPP1R12B	-12.46	0.0012	0.0473
38	carcinoembryonic antigen-related cell adhesion molecule 1 (biliary glycoprotein)	CEACAM1	-12.14	1.61E-05	0.006
39	chromosome 2 open reading frame 54	C2orf54	-12.13	0.0011	0.0451
40	carcinoembryonic antigen-related cell adhesion molecule 7	CEACAM7	-11.97	2.66E-05	0.0075
41	coagulation factor V (proaccelerin, labile factor)	F5	-11.97	0.001	0.0431
42	mucin 7, secreted	MUC7	-11.97	0.001	0.0442
43	Sin3A-associated protein, 18kDa	SAP18	-11.77	6.81E-05	0.0117
44	desmoglein 3	DSG3	-11.75	0.0002	0.0173
45	claudin 1	CLDN1	-11.75	0.0004	0.0282
46	nucleosome assembly protein 1-like 5	NAP1L5	-11.66	0.0005	0.0311
47	serine hydrolase-like 2	SERHL2	-11.66	0.0002	0.022
48	inositol(myo)-1(or 4)-monophosphatase 2	IMPA2	-11.64	0.0002	0.0195
49	mediator complex subunit 27	MED27	-11.59	0.0001	0.0166
50	coagulation factor III (thromboplastin, tissue factor)	F3	-11.49	7.18E-05	0.012

**Figure S15** – Top 100 upregulated genes in keloid extralesional vs NS dermis, corrected for fold change >2, p value < 0.05 and q value < 0.05, where red indicates also significantly upregulated in the centre, blue the margin and orange both.

Extra dermis	Gene title	Gene symbol	Fold change	p-value	q-value
1	keratin 79	KRT79	91.67	0.0002	0.0271
2	C2 calcium-dependent domain containing 4B	C2CD4B	59.46	8.31E-12	4.88E-07
3	small proline-rich protein 1B	SPRR1B	49.17	0.0005	0.0433
4	LIM homeobox 2	LHX2	31.14	1.51E-06	0.0035
5	peptidase inhibitor 3, skin-derived	PI3	28.28	0.0006	0.0457
6	acyl-CoA wax alcohol acyltransferase 2	AWAT2	27.55	2.55E-08	0.0003
7	RNA, U11 small nuclear	RNU11	25.85	1.69E-06	0.0037
8	coiled-coil domain containing 102B	CCDC102B	25.83	1.12E-06	0.0033
9	peptidase M20 domain containing 1	PM20D1	25.62	3.44E-05	0.0142
10	serum amyloid A2	SAA2	22.21	0.0004	0.0384
11	FBJ murine osteosarcoma viral oncogene homolog	FOS	19.43	0.0006	0.0494
12	galanin prepropeptide	GAL	19.30	3.71E-05	0.0144
13	zinc finger protein 36, C3H type-like 1	ZFP36L1	17.69	0.0002	0.028
14	hairless homolog (mouse)	HR	16.71	1.15E-06	0.0033
15	RAB15, member RAS oncogene family	RAB15	15.67	2.59E-05	0.0124
16	sulfotransferase family 1E, estrogen-preferring, member 1	SULT1E1	14.30	1.65E-05	0.01
17	cytokine receptor-like factor 1	CRLF1	13.59	0.0003	0.0361
18	ribosomal protein S16 pseudogene 5	RPS16P5	13.34	9.92E-05	0.0224
19	jun B proto-oncogene	JUNB	13.30	1.79E-05	0.0103
20	bradykinin receptor B1	BDKRB1	13.12	0.0002	0.0291
21	KIAA1683	KIAA1683	12.79	0.0002	0.027
22	chemokine (C-C motif) ligand 27	CCL27	12.47	0.0003	0.0356
23	death-associated protein kinase 2	DAPK2	11.90	2.49E-07	0.0014
24	small nucleolar RNA, C/D box 43	SNORD43	11.83	7.01E-06	0.0067
25	adenylate kinase 2	AK2	11.03	4.18E-05	0.015
26	selectin E	SELE	10.98	1.15E-06	0.0033
27	small nucleolar RNA, C/D box 3B-1	SNORD3B-1	10.79	0.0002	0.027
28	solute carrier family 16, member 7 (monocarboxylic acid transporter 2)	SLC16A7	10.60	1.78E-05	0.0103
29	RNA, U4atac small nuclear (U12-dependent splicing)	RNU4ATAC	10.07	4.10E-05	0.0149
30	vault RNA 2-1	VTRNA2-1	10.04	8.93E-06	0.0075
31	immediate early response 3	IER3	9.61	0.0004	0.0407
32	kelch-like 6 (Drosophila)	KLHL6	9.22	0.0005	0.0446
33	fatty acid desaturase 2	FADS2	9.15	0.0002	0.0275

Extra dermis	Gene title	Gene symbol	Fold change	p-value	q-value
34	cellular retinoic acid binding protein 1	CRABP1	9.15	0.0006	0.0453
35	vault RNA 1-1	VTRNA1-1	8.81	9.56E-05	0.0222
36	Hermansky-Pudlak syndrome 1	HPS1	8.38	1.49E-05	0.0096
37	deoxynucleotidyltransferase, terminal, interacting protein 1	DNTTIP1	8.31	0.0002	0.0304
38	FLJ45248 protein	FLJ45248	8.20	0.0002	0.0318
39	uncharacterized serine/threonine-protein kinase SgK494	SGK494	8.11	9.32E-05	0.0222
40	histone cluster 2, H2aa4	HIST2H2AA4	8.07	1.89E-05	0.0105
41	Rho GTPase activating protein 33	ARHGAP33	7.67	0.0004	0.0399
42	solute carrier family 6 (neurotransmitter transporter, taurine), member 6	SLC6A6	7.54	0.0001	0.0256
43	UBAC2 antisense RNA 1 (non-protein coding)	UBAC2-AS1	7.53	3.26E-05	0.0139
44	hydroxycarboxylic acid receptor 3	HCAR3	7.50	8.21E-06	0.0072
45	vault RNA 1-2	VTRNA1-2	7.49	0.0005	0.0424
46	melanocortin 5 receptor	MC5R	7.46	1.67E-05	0.01
47	fibronectin type III and ankyrin repeat domains 1	FANK1	7.39	0.0005	0.0437
48	immediate early response 2	IER2	7.33	4.00E-09	8.45E-05
49	regulator of G-protein signaling 16	RGS16	7.32	2.92E-06	0.0045
50	leucine zipper, putative tumor suppressor 1	LZTS1	7.31	0.0002	0.0276
51	leucine rich repeat containing 27	LRRC27	7.18	0.0004	0.0405
52	unc-51-like kinase 2 (C. elegans)	ULK2	7.18	0.0001	0.0228
53	RPA interacting protein	RPAIN	7.15	0.0003	0.0347
54	fatty acid synthase	FASN	7.12	3.57E-05	0.0143
55	tumor necrosis factor (ligand) superfamily, member 9	TNFSF9	7.11	6.18E-05	0.0184
56	sirtuin 5	SIRT5	7.10	0.0003	0.0361
57	NIPA-like domain containing 4	NIPAL4	7.02	0.0004	0.0413
58	prion protein 2 (duplet)	PRND	6.90	0.0003	0.0372
59	jun proto-oncogene	JUN	6.88	0.0006	0.0478
60	Kv channel interacting protein 4	KCNIP4	6.79	0.0006	0.0463
61	COMM domain containing 8	COMMD8	6.75	0.0006	0.0484
62	forkhead box F1	FOXF1	6.74	0.0001	0.0245
63	par-3 partitioning defective 3 homolog (C. elegans)	PARD3	6.69	7.72E-05	0.0201
64	nuclear factor of kappa light polypeptide gene enhancer in B-cells inhibitor, zeta	NFKBIZ	6.63	1.97E-05	0.0107
65	fer-1-like 4 (C. elegans) pseudogene	FER1L4	6.59	0.0003	0.0328
66	tripartite motif containing 32	TRIM32	6.57	8.56E-05	0.021

Extra dermis	Gene title	Gene symbol	Fold change	p-value	q-value
67	RNA, U1 small nuclear 5	RNU1-5	6.53	0.0001	0.0231
68	plakophilin 4	PKP4	6.33	0.0005	0.0434
69	vang-like 1 (van gogh, Drosophila)	VANGL1	6.33	3.48E-05	0.0142
70	inositol polyphosphate-1-phosphatase	INPP1	6.24	0.0002	0.0276
71	solute carrier family 24 (sodium/potassium/calcium exchanger), member 1	SLC24A1	6.07	0.0002	0.0283
72	ADP-dependent glucokinase	ADPGK	6.01	0.0001	0.0244
73	erythrocyte membrane protein band 4.1 like 4A	EPB41L4A	6.00	4.80E-05	0.0163
74	importin 4	IPO4	5.91	8.56E-05	0.021
75	keratin associated protein 5-8	KRTAP5-8	5.90	1.43E-06	0.0035
76	ring finger protein 126	RNF126	5.87	0.0004	0.0389
77	Ras-related GTP binding C	RRAGC	5.55	0.0002	0.0276
78	transmembrane protein with EGF-like and two follistatin-like domains 2	TMEFF2	5.53	6.19E-05	0.0184
79	staufen, RNA binding protein, homolog 2 (Drosophila)	STAU2	5.48	0.0001	0.0258
80	solute carrier family 3 (activators of dibasic and neutral amino acid transport), member 2	SLC3A2	5.44	4.30E-05	0.015
81	serrate RNA effector molecule homolog (Arabidopsis)	SRRT	5.39	0.0003	0.0365
82	deltex homolog 2 (Drosophila)	DTX2	5.36	0.0006	0.0453
83	endothelin converting enzyme 1	ECE1	5.28	0.0002	0.0309
84	POU class 3 homeobox 1	POU3F1	5.12	0.0006	0.0474
85	DEAD (Asp-Glu-Ala-Asp) box polypeptide 55	DDX55	5.05	0.0004	0.04
86	A1BG antisense RNA 1 (non-protein coding)	A1BG-AS1	4.99	4.67E-05	0.016
87	IWS1 homolog (S. cerevisiae)	IWS1	4.96	5.33E-05	0.0172
88	guanine nucleotide binding protein (G protein), beta polypeptide 1-like	GNB1L	4.85	7.24E-06	0.0067
89	sperm associated antigen 7	SPAG7	4.76	0.0002	0.0276
90	interleukin enhancer binding factor 3, 90kDa	ILF3	4.67	0.0004	0.0407
91	tumor necrosis factor	TNF	4.50	3.01E-06	0.0045
92	uncharacterized protein PRO2852	PRO2852	4.48	0.0005	0.0418
93	perilipin 3	PLIN3	4.42	7.38E-05	0.0196
94	testis-specific serine kinase 3	TSSK3	4.42	0.0001	0.0235
95	selectin P (granule membrane protein 140kDa, antigen CD62)	SELP	4.42	0.0003	0.0333
96	vitamin D (1,25- dihydroxyvitamin D3) receptor	VDR	4.37	7.17E-06	0.0067
97	ankyrin repeat domain 13B	ANKRD13B	4.34	1.33E-05	0.0089
98	cyclin L1	CCNL1	4.33	3.79E-05	0.0144
99	transmembrane protein 93	TMEM93	4.32	0.0001	0.0232
100	protein phosphatase 1, regulatory subunit 3F	PPP1R3F	4.31	0.0003	0.0365

**Figure S16** – Top 50 downregulated genes in keloid margin vs normal skin dermis. Corrected for fold change > 2 and p-value < 0.05 q-value < 0.05 where red indicates also significantly downregulated in the centre, blue the margin and orange both

Extra dermis	Gene title	Gene symbol	Fold change	p-value	q-value
1	interleukin 1 receptor-like 1	IL1RL1	-20.99	2.70E-05	0.0127
2	hydatidiform mole associated and imprinted (non-protein coding)	HYMAI	-19.87	0.0005	0.0437
3	C1q and tumor necrosis factor related protein 9	C1QTNF9	-18.44	4.71E-06	0.0053
4	G protein-coupled receptor 75	GPR75	-17.76	0.0005	0.0426
5	G protein-coupled receptor 64	GPR64	-17.55	0.0001	0.0257
6	creatine kinase, mitochondrial 2 (sarcomeric)	CKMT2	-16.99	2.88E-05	0.0131
7	proline rich 15-like	PRR15L	-15.90	6.17E-06	0.0064
8	desmin	DES	-14.93	0.0004	0.0389
9	lysine (K)-specific demethylase 5C	KDM5C	-14.58	3.73E-06	0.005
10	nuclear receptor subfamily 2, group F, member 1	NR2F1	-12.27	0.0001	0.0244
11	ATPase, H+ transporting, lysosomal 56/58kDa, V1 subunit B1	ATP6V1B1	-11.43	0.0006	0.0489
12	transmembrane protein 213	TMEM213	-11.43	5.42E-07	0.0021
13	Ras homolog enriched in brain	RHEB	-10.99	4.32E-09	8.45E-05
14	EPM2A (laforin) interacting protein 1	EPM2AIP1	-10.64	0.0001	0.026
15	small nucleolar RNA, C/D box 89	SNORD89	-10.60	0.0005	0.0416
16	MAP/microtubule affinity-regulating kinase 2 pseudogene 9	MARK2P9	-10.44	1.15E-05	0.0084
17	potassium channel regulator	KCNRG	-10.03	0.0002	0.0275
18	Scm-like with four mbt domains 2	SFMBT2	-9.98	2.64E-07	0.0014
19	glutaminase	GLS	-9.27	2.09E-06	0.0041
20	tRNA methyltransferase 11 homolog (S. cerevisiae)	TRMT11	-9.16	1.44E-06	0.0035
21	mediator complex subunit 27	MED27	-8.97	0.0005	0.0418
22	cold inducible RNA binding protein	CIRBP	-8.91	0.0002	0.0267
23	RAB GTPase activating protein 1-like	RABGAP1L	-8.90	0.0004	0.0407
24	synapsin II	SYN2	-8.83	6.43E-05	0.0187
25	SET and MYND domain containing 4	SMYD4	-8.76	2.54E-05	0.0123

Extra dermis	Gene title	Gene symbol	Fold change	p-value	q-value
26	FGF-2 activity-associated protein 3	GAFA3	-8.58	0.0002	0.0276
27	rhopilin, Rho GTPase binding protein 2	RHPN2	-8.45	5.00E-05	0.0166
28	forkhead box A1	FOXA1	-8.44	4.66E-06	0.0053
29	LysM, putative peptidoglycan-binding, domain containing 4	LYSMD4	-8.27	9.49E-06	0.0077
30	family with sequence similarity 69, member A	FAM69A	-8.08	0.0002	0.0267
31	fibroblast growth factor 1 (acidic)	FGF1	-8.03	1.72E-05	0.0102
32	glucosidase, beta (bile acid) 2	GBA2	-7.97	1.99E-05	0.0107
33	neuroligin 1	NLGN1	-7.67	0.0001	0.0235
34	activin A receptor, type IIB	ACVR2B	-7.66	0.0003	0.0338
35	FLJ46020 protein	FLJ46020	-7.55	3.51E-06	0.0049
36	senataxin	SETX	-7.51	2.32E-05	0.0116
37	transmembrane protein 181	TMEM181	-7.46	0.0004	0.0407
38	ankyrin repeat domain 62	ANKRD62	-7.44	6.50E-05	0.0187
39	UDP-N-acetyl-alpha-D-galactosamine:polypeptide N-acetylgalactosaminyltransferase 1 (GalNAc-T1)	GALNT1	-7.44	0.0006	0.0482
40	methyl CpG binding protein 2 (Rett syndrome)	MECP2	-7.44	0.0002	0.0276
41	GTF2I repeat domain containing 2	GTF2IRD2	-7.36	7.71E-05	0.0201
42	ectopic P-granules autophagy protein 5 homolog (C. elegans)	EPG5	-7.32	1.03E-05	0.0083
43	creatine kinase, brain	CKB	-7.26	0.0006	0.0475
44	otopetrin 1	OTOP1	-7.25	0.0003	0.0365
45	EF-hand calcium binding domain 4B	EFCAB4B	-7.24	7.82E-05	0.0202
46	SH3-domain binding protein 4	SH3BP4	-7.20	0.0002	0.0276
47	glucuronidase, beta pseudogene 1	GUSBP1	-7.16	1.68E-06	0.0037
48	zinc finger protein 280D	ZNF280D	-7.11	9.12E-06	0.0075
49	multiple EGF-like-domains 10	MEGF10	-6.98	9.45E-05	0.0222
50	thyroid adenoma associated	THADA	-6.96	2.85E-05	0.0131

# Chapter 5

---

## **The Aldo-Keto Reductase AKR1B10 Is Up-Regulated in Keloid Epidermis, Implicating Retinoic Acid Pathway Dysregulation in the Pathogenesis of Keloid Disease**

**Jumper N**, Hodgkinson T, Arscott G, Har-Shai Y, Paus R, Bayat A. The aldo-keto reductase AKR1B10 is upregulated in keloid epidermis, implicating retinoic acid pathway dysregulation in the pathogenesis of keloid disease. *The Journal of investigative dermatology*. 2016 Mar 26. pii: S0022-202X(16)30985-X. doi: 10.1016/j.jid.2016.03.022.

### **Declaration:**

Natalie Jumper, the first author, carried out all of the analysis, experimental work, interpretation of data, design and composition of the article and accompanying figures. The other authors provided human tissue samples, technical advice or assistance, guidance and final approval of the paper. This PDF version of the paper has been incorporated into the thesis in format in which it was published in the *Journal of Investigative Dermatology*. Supplementary material is included at the end of the article.





# The Aldo-Keto Reductase AKR1B10 Is Up-Regulated in Keloid Epidermis, Implicating Retinoic Acid Pathway Dysregulation in the Pathogenesis of Keloid Disease

Natalie Jumper<sup>1</sup>, Tom Hodgkinson<sup>1</sup>, Guyan Arcscott<sup>2</sup>, Yaron Har-Shai<sup>3</sup>, Ralf Paus<sup>4,5</sup> and Ardeshir Bayat<sup>1,4</sup>

Keloid disease is a recurrent fibroproliferative cutaneous tumor of unknown pathogenesis for which clinical management remains unsatisfactory. To obtain new insights into hitherto underappreciated aspects of keloid pathobiology, we took a laser capture microdissection-based, whole-genome microarray analysis approach to identify distinct keloid disease-associated gene expression patterns within defined keloid regions. Identification of the aldo-keto reductase enzyme AKR1B10 as highly up-regulated in keloid epidermis suggested that an imbalance of retinoic acid metabolism is likely associated with keloid disease. Here, we show that AKR1B10 transfection into normal human keratinocytes reproduced the abnormal retinoic acid pathway expression pattern we had identified in keloid epidermis. Cotransfection of AKR1B10 with a luciferase reporter plasmid showed reduced retinoic acid response element activity, supporting the hypothesis of retinoic acid synthesis deficiency in keloid epidermis. Paracrine signals released by AKR1B10-overexpressing keratinocytes into conditioned medium resulted in up-regulation of transforming growth factor- $\beta$ 1, transforming growth factor- $\beta$ 2, and collagens I and III in both keloid and normal skin fibroblasts, mimicking the typical profibrotic keloid profile. Our study results suggest that insufficient retinoic acid synthesis by keloid epidermal keratinocytes may contribute to the pathogenesis of keloid disease. We refocus attention on the role of injured epithelium in keloid disease and identify AKR1B10 as a potential new target in future management of keloid disease.

*Journal of Investigative Dermatology* (2016) 136, 1500–1512; doi:10.1016/j.jid.2016.03.022

## INTRODUCTION

Keloid disease (KD) is a benign, fibroproliferative cutaneous tumor of unknown pathogenesis, with a notoriously high rate of recurrence, for which clinical management remains decidedly unsatisfactory (Bijlard et al., 2015; Har-Shai et al., 2007; Ud-Din and Bayat, 2013), despite the description of a number of significantly dysregulated pathways (Jones et al., 2015; Shih et al., 2010; Trisliana Perdanasari et al., 2014). This failure of major therapeutic progress is compounded by

lack of a validated animal model for KD (Marttala et al., 2016).

These limitations have led many keloid researchers to rely on monolayer culture, co-culture, and whole-tissue biopsy studies that do not fully reflect the heterogeneity that exists both between and within keloid lesions (Syed et al., 2011) or the complex epithelial-mesenchymal tissue interactions likely to occur during KD development (Canady et al., 2013; Chua et al., 2011; Lim et al., 2009). Whole-tissue analysis of entire keloid lesions can result in “averaging out” of cellular signals (Crystal et al., 2002; El-Serag et al., 2009; Yazdi et al., 2010), thus missing functionally important differentially expressed genes. Monolayer culture has been shown to alter cell behavior, affecting both gene and protein expression (Baker and Chen, 2012; Pampaloni et al., 2007). Although two chamber co-culture studies have been invaluable in highlighting the significance of the epidermis and investigating the role of epithelial-mesenchymal interactions in KD (Lim et al., 2002; Lim et al., 2013; Xia et al., 2004), the lack of direct cell-cell contact is not representative of the three-dimensional architecture and in situ signaling occurring within this dynamic microenvironment (van den Broek et al., 2014; Zhang et al., 2006).

Clinically evident as variation between center and margin, keloid tumor sites differ on histological (Ashcroft et al., 2013; Jumper et al., 2015) and molecular levels with regard to collagen ratio, immune cell infiltrate, cell cycle phase, and apoptosis (Bagabir et al., 2012; Seifert et al., 2008; Syed et al., 2011). Recognizing discrepancies in gene and protein

<sup>1</sup>Plastic and Reconstructive Surgery Research, Manchester Institute of Biotechnology, University of Manchester, Manchester, UK; <sup>2</sup>Department of Plastic and Reconstructive Surgery, University of West Indies, Kingston, Jamaica; <sup>3</sup>Plastic Surgery Unit, Carmel Medical Center, Haifa, Israel; <sup>4</sup>Centre for Dermatology Research, Institute of Inflammation and Repair, University of Manchester, Manchester, UK; and <sup>5</sup>Department of Dermatology, University of Münster, D-48149, Münster, Germany

Correspondence: Ardeshir Bayat, Plastic and Reconstructive Surgery Research, Institute of Inflammation and Repair, University of Manchester, Stopford Building, Manchester M13 9PT, UK. E-mail: Ardeshir.Bayat@manchester.ac.uk

Abbreviations: AKR1B10, aldo-keto reductase family 1, member B10; ALDH, aldehyde dehydrogenase; CRABP, cellular retinoic acid binding protein; CYP26, cytochrome P450, family 26; KD, keloid disease; KE, keloid epidermis; KF, keloid fibroblast; LCM, laser capture microdissection; NSE, normal skin epidermis; NSF, normal skin fibroblast; NHEK, normal human epidermal keratinocytes; qRT-PCR, quantitative real-time PCR; RA, retinoic acid; TGF- $\beta$ , transforming growth factor-beta

Received 14 December 2015; revised 9 February 2016; accepted 7 March 2016; accepted manuscript published online 26 March 2016; corrected proof published online 14 May 2016

expression profiles between these sites, we chose a site-specific gene profiling approach for this study. Given previous evidence of changes surrounding the keloid lesion (Iqbal et al., 2010) we included the extralesional (adjacent normal skin) site to investigate potential field cancerization effects in this tumorigenic entity (Ud-Din et al., 2013). Specifically, we intended to identify distinct gene signature and candidate biomarkers in defined tissue compartments within and around keloid tumors. This was achieved using laser capture microdissection (LCM), which allowed isolation of epidermal versus dermal compartments within site-specific keloid tissue.

To our knowledge, this differential LCM and microarray profiling approach of the whole genome in distinct KD epidermal and dermal sites is previously unreported in the field. Through the combination of these techniques, the current study identified up-regulation of the aldo-keto reductase AKR1B10, a key enzyme in retinoic acid (RA) metabolism (Ruiz et al., 2012) (Figure 1a), in keloid epidermis (KE) when compared with normal skin epidermis (NSE). This highly efficient cytosolic enzyme has a specificity for retinaldehyde (Crosas et al., 2003; Ruiz et al., 2011), implicating it in the classical RA synthesis pathway, where it acts to convert retinal back to retinol in a rate-limiting step before the irreversible oxidation of retinal by aldehyde dehydrogenase (ALDH/retinaldehyde dehydrogenase) to RA (Ruiz et al., 2009). Because this suggested a potential role for RA in KD pathobiology, a further aim of our study was to explore this role through induced overexpression of AKR1B10 in primary normal human epidermal keratinocytes (NHEK), so as to reproduce the RA pathway dysregulation seen in KE.

RA is a physiologically active metabolite of retinol (vitamin A) acting both directly, through transcriptional regulation (retinoic acid receptors [RAR]- $\alpha$ , - $\beta$ , and - $\gamma$ /retinoid X receptor- $\alpha$ , - $\beta$ , and - $\gamma$ ) of retinoid responsive genes, and indirectly by influencing numerous cytokines and their signaling pathways (Dong et al., 2012; Napoli, 2012; Zhang, Kong, et al., 2014). Constitutive or iatrogenic abnormalities in RA metabolism are attracting interest in dermatology and skin disease models (Amann et al., 2014; Duncan et al., 2013; Everts et al., 2015; Regen et al., 2015), but this remains to be systematically investigated in KD pathobiology.

In view of this and on the basis of our microarray findings, we hypothesized that excess AKR1B10 expression and activity in KE may result in reduced RA levels, thus triggering profibrotic downstream effects that contribute to KD pathogenesis. This hypothesis was probed by overexpressing AKR1B10 in NHEK and examining paracrine signaling between AKR1B10-overexpressing human keratinocytes and dermal fibroblasts.

## RESULTS

### AKR1B10 messenger RNA expression is up-regulated in KE in situ

The site-specific gene profiling approach in this study was achieved by harvesting keloid biopsy samples from center (intralesional), margin (perilesional), and adjacent lesional (extralesional) sites (Figure 1b), which were then compared with normal skin. LCM was used to separate epidermis from dermis, after which expression of each of the KE sites was

compared with each other and with NSE. This yielded seven lists of comparisons that were filtered for *P*-value ( $<0.05$ ) and fold change ( $\geq 2$ ). AKR1B10 was found to be significantly up-regulated within all three sites of KE compared with NSE. The extralesional KE had the highest fold change at 86 ( $P = 2.14 \times 10^{-6}$ ), but intralesional KE (fold change = 75,  $P = 1.19 \times 10^{-6}$ ) and perilesional KE (fold change = 64,  $P = 5.85 \times 10^{-6}$ ) showed similar expression (see Supplementary Table S1 online).

Next, we aimed to validate these findings through quantitative real-time PCR (qRT-PCR) of laser-captured KE and NSE. qRT-PCR showed that AKR1B10 was most significantly up-regulated in adjacent extralesional KE ( $P = 0.00073$ ) but was also increased in intralesional ( $P = 0.0011$ ) and perilesional epidermis ( $P = 0.0037$ ), which correlated directly with expression differences seen in the microarray (Figure 1c).

Both AKR1B1 ( $P = 0.0022$ ) and AKR1B15 ( $P = 8.55 \times 10^{-6}$ ), which have a 71% and 91% amino acid identity, respectively, with AKR1B10 (Salabei et al., 2011), were also significantly up-regulated in all three KE sites on microarray (see Supplementary Table S1) and validated with qRT-PCR (see Supplementary Figure S1 online).

From within the aldo-keto reductase family of proteins, AKR1B10 has the highest catalytic efficiency ( $K_{cat}/K_m$ ) and specificity for retinaldehyde; therefore, we focused on this enzyme for subsequent studies (Gallego et al., 2007; Ruiz et al., 2012).

### AKR1B10 protein expression is increased in KE

To determine whether KE AKR1B10 protein levels were increased compared with NSE, immunohistochemistry was performed on tissue from NSE, keloid center, and keloid margin biopsy samples. Strong AKR1B10 expression was observed in 14 of 14 (100%) keloid samples, which showed diffuse granular cytoplasmic staining throughout the epidermis. There was no positive staining in NSE. When only center and margin sections were considered, AKR1B10 staining was positive in 6 of 6 examined patients, supporting the hypothesis that gene expression findings translated into protein expression changes (Figure 1d). This overexpression appears to be restricted to the KE, such that Western blot analysis of whole-tissue biopsy samples for AKR1B10 showed no difference between keloid and normal skin (not shown), highlighting the importance of the role of LCM in isolating signals that would otherwise be masked by whole-tissue extraction approaches.

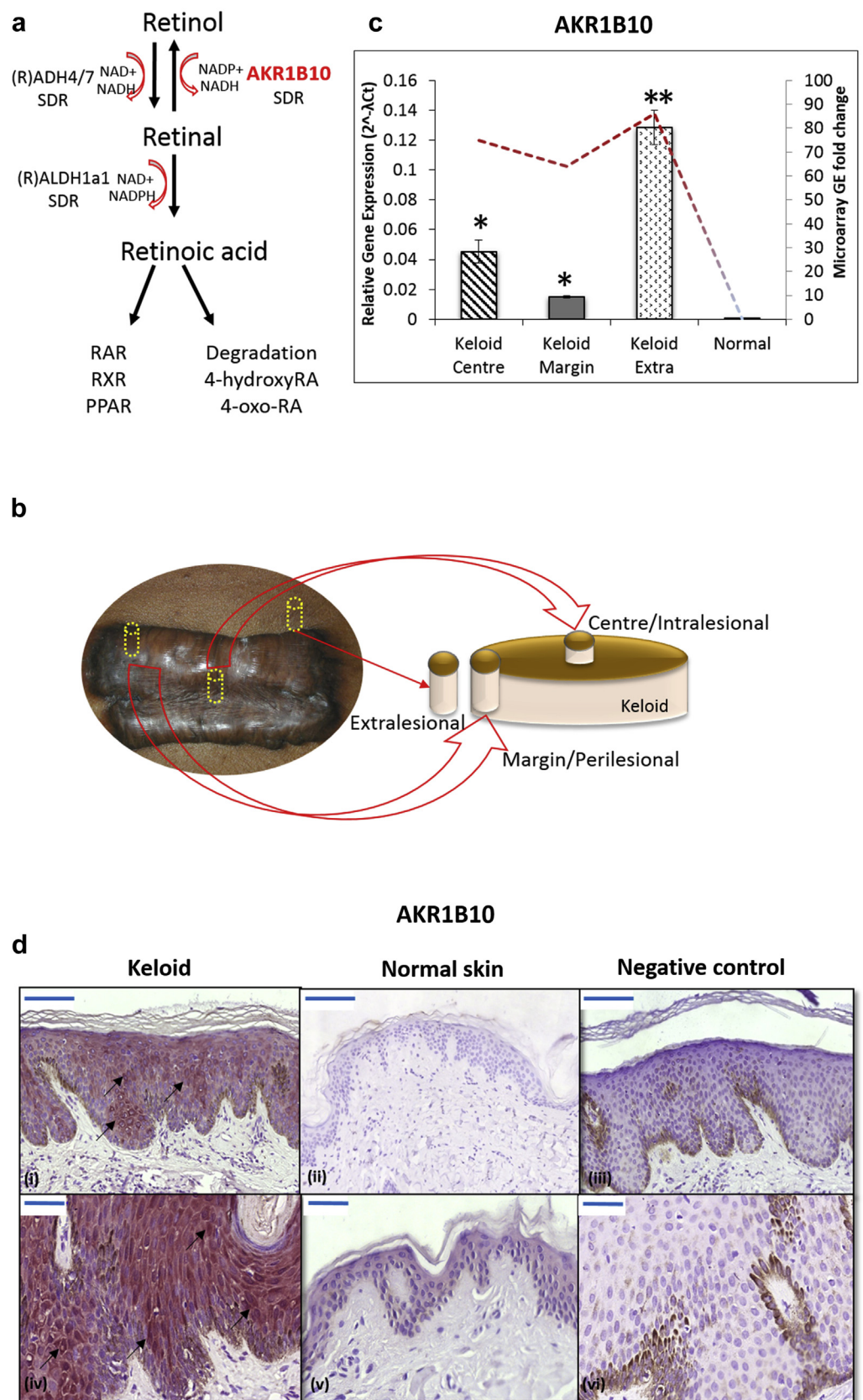
Prominent AKR1B10 overexpression on transcript and protein levels in KE led to our hypothesis that an abnormality in intraepidermal RA metabolism may generate signals contributing to KD pathogenesis.

### RA signaling is dysregulated in KE in situ

Having established AKR1B10 dysregulation in KE and postulated a resultant RA imbalance, we sought to identify any other related relevant classical RA synthesis pathway molecules that might also be dysregulated. RA concentrations are tightly controlled through autoregulatory enzyme feedback affecting retinoic acid response element promoter regions of other classical synthesis pathway members, including lecithin:retinol acetyltransferase, cellular retinoic acid binding

**Figure 1. AKR1B10 overexpression in keloid versus normal skin.**

**(a)** Classical retinoic acid biosynthesis pathway. **(b)** Keloid biopsy site diagram including intralesional (center), perilesional (margin), and extralesional (adjacent normal-appearing skin) sites. **(c)** AKR1B10 quantitative real-time PCR validation of microarray data. Bars represent quantitative real-time PCR of epidermal sites within keloid compared with normal skin. The line graph shows the corresponding microarray data. **(d)** AKR1B10 immunohistochemistry expression in keloid (n = 14) and normal skin tissue (n = 12). Keloid shows strong red suprabasal epidermal staining for AKR1B10 (black arrows). No expression was observed in normal skin or negative control. Micrographs i–iii, scale bar = 100 μm; iv–vi, scale bar = 50 μm. Data are represented as mean ± standard error of the mean from at least three independent experiments. \*P < 0.01, \*\*P < 0.005 using Student's t test. ADH, alcohol dehydrogenase; AKR1B10, aldo-keto reductase family 1 member B10; ALDH, aldehyde dehydrogenase; GE, gene expression; NAD, nicotinamide adenine dinucleotide (+ is oxidised form); NADH, hydroxylamine reductase; PPAR, peroxisome proliferator-activated receptor-α; RA, retinoic acid; RAR, retinoic acid receptor; (R)DH, retinol dehydrogenase; (R)ALDH, retinaldehyde dehydrogenase; RXR, retinoid X receptor; SDR, short-chain dehydrogenase.



protein 2 (CRABP2), cytochrome P450-26 enzymes (CYP26), and ALDH1a1 (Amann et al., 2015; Fisher and Voorhees, 1996; Pavez Lorie, Cools, et al., 2009). Therefore, we re-examined the microarray data for potential candidates.

We found significant up-regulation of both alcohol dehydrogenase 7 in margin KE (fold change = 8, P = 0.001) and ALDH1a1 in all three KE sites (fold change >15, P < 0.001), responsible for catalyzing the oxidation of retinol and retinal,



respectively (Duester, 2001; Xu et al., 2015). We also observed significant down-regulation of CRABP1 in center and extrasional KE ( $P = 0.025$ ) and CYP26B1 in center ( $P = 0.0092$ ) and margin ( $P = 0.0002$ ) KE, which together promote the catabolism and inactivation of RA by conversion to 4-hydroxyRA and 4-oxo-RA (Okano et al., 2012; Won et al., 2004). In KE, when compared with NSE using immunohistochemistry, increased expression of AKR1B10 was co-localized with the up-regulation of CRABP2, which transports RA to the nucleus for signaling (Budhu and Noy, 2002).

This co-localization suggests that these processes may be interdependent within KE keratinocytes, evident as intense yellow staining that indicates coexpression of AKR1B10 and CRABP2 in KE (Figure 2a and b). The position of these molecules within the pathway is shown graphically in Figure 2c, and relevant microarray data tabulated with fold change and  $P$ -values for these genes are shown in Supplementary Table S1. To validate these findings, we performed qRT-PCR for ALDH1a1 ( $P < 0.05$ ), CRABP2 ( $P < 0.05$ ), CRABP1, and CYP26B1 ( $P < 0.05$ ) (see Supplementary Figure S1). Altered expression of these enzymes and transporter proteins within the classical RA pathway indicates that RA signaling is dysregulated in KE.

#### Induced overexpression of AKR1B10 in normal skin keratinocytes mimics KE RA pathway expression

The short half-life and delicate nature of a light- and oxygen-sensitive polyene chain prevented the ideal scenario of direct quantification of specific RA metabolites in keloid tissue, particularly because the tissue was excised in an operating theater (Gundersen, 2006; Kane and Napoli, 2010). We therefore used a strategy using primary NHEK to examine whether the induced overexpression of AKR1B10 would produce the same changes as observed in the KE RA pathway. To achieve this, NHEK ( $n = 8$ ) were transiently transfected with an AKR1B10-containing cytomegalovirus vector. First, successful AKR1B10 expression was validated using qRT-PCR ( $P < 0.005$ ), Western blot analysis ( $P < 0.005$ ), and immunocytochemistry (Figure 3a–c). We then compared the gene expression of transfected and nontransfected NHEK.

This showed that CRABP2 ( $P < 0.01$ ) was significantly upregulated in AKR1B10-overexpressing primary NHEK, as was ALDH1a1 ( $P < 0.05$ ). CRABP1 showed only a trend toward down-regulation, but CYP26B1 ( $P < 0.05$ ) was significantly down-regulated, suggesting reduced RA degradation (Chen et al., 2003; Pavez Lorie, Li, et al., 2009) (Figure 3d). Thus, we were satisfied that this surrogate cell culture approach recreated the key elements of the RA metabolism-related abnormality we had observed in KE in situ.

#### AKR1B10-overexpressing keratinocytes show an abnormal secretion profile

To observe the effect of AKR1B10 up-regulation on retinol homeostasis, epidermal differentiation, and NHEK secretory profile, we compared messenger RNA and protein expressions of AKR1B10-transfected and nontransfected cells. qRT-PCR showed that the expression of lecithin:retinol acetyltransferase ( $P = 0.037$ ), an enzyme catalyzing retinyl ester synthesis to promote retinol storage (Amann et al., 2015; Kurlandsky et al., 1996), was significantly increased in AKR1B10-overexpressing keratinocytes, which is likely a

consequence of retinol excess (Figure 3e). Keratins 14 ( $P = 1.04 \times 10^{-5}$ ) and 6B ( $P = 8.2 \times 10^{-6}$ ), associated with basal layer epidermal proliferation and hyperproliferation/wound healing, respectively (Moll et al., 2008; Ramot et al., 2013), were also significantly up-regulated in AKR1B10-overexpressing keratinocytes (Figure 3f). Keratin 6B up-regulation is consistent with the persistence of activated keratinocytes in KE, suggested by our microarray-based observation that keratin 6b was also prominently overexpressed in KE (see Supplementary Table S1).

RA was previously shown to modulate transforming growth factor (TGF)- $\beta$  expression in keratinocytes, which in turn suppresses keratinocyte proliferation (Batova et al., 1992; Choi and Fuchs, 1990; Glick et al., 1989). Given this and the decreased expression of transforming growth factor receptor beta 2 and TGF $\beta$ 2 in KE microarray data (see Supplementary Table S1), we next investigated whether AKR1B10 overexpression in primary NHEK affects TGF- $\beta$  secretion. qRT-PCR of AKR1B10-transfected cells showed significantly decreased TGF- $\beta$ 1 ( $P = 0.0037$ ) and TGF- $\beta$ 2 ( $P = 0.0007$ ) compared with nontransfected keratinocytes (Figure 3e). Therefore, we further analyzed the microarray data and confirmed an inverse correlation between KE AKR1B10 expression and modules associated with profibrotic molecules, including TGF- $\beta$  (see Supplementary Figure S2 online). These findings are consistent with reduced RA pathway signaling activity, because RA mostly up-regulates TGF- $\beta$  secretion (Foitzik et al., 2005; Obinata et al., 2011). Furthermore, the cell culture data suggest that our microarray-based observation is clinically relevant in the context of KD.

AKR1B10-positive keratinocytes showed significantly decreased gene expression of E-cadherin ( $P = 0.034$ ) (Figure 3e). Although the epithelial-mesenchymal transition has been hypothesized to play a role in KD (Supp et al., 2014) and studies have shown E-cadherin loss in keloid (Ma et al., 2015; Yan et al., 2015), we have yet to identify a controlling factor for this change. RA has been previously associated with epithelial-mesenchymal plasticity (Werner et al., 2015) and shown to activate E-cadherin expression in other epithelial cell lines (von Gise et al., 2011; Woo and Jang, 2012). Furthermore, it has been shown that AKR1B10 knockdown results in significant up-regulation of E-cadherin and subsequent reduction of proliferation, migration, and invasion of pancreatic cancer cells (Chung et al., 2012; Zhang et al., 2014). However, we did not observe significant up-regulation of vimentin (see Supplementary Figure S3 online) (Yan et al., 2015), which may indicate that AKR1B10 contributes to but is not the driving force behind the epithelial-mesenchymal transition.

Overall, the altered expressions of lecithin:retinol acetyltransferase, keratin 14 (see Supplementary Figure S4 online), keratin 6B, TGF- $\beta$ 1 and 2, and E-cadherin reported here lend credence to the hypothesis of reduced RA levels resulting from excess AKR1B10.

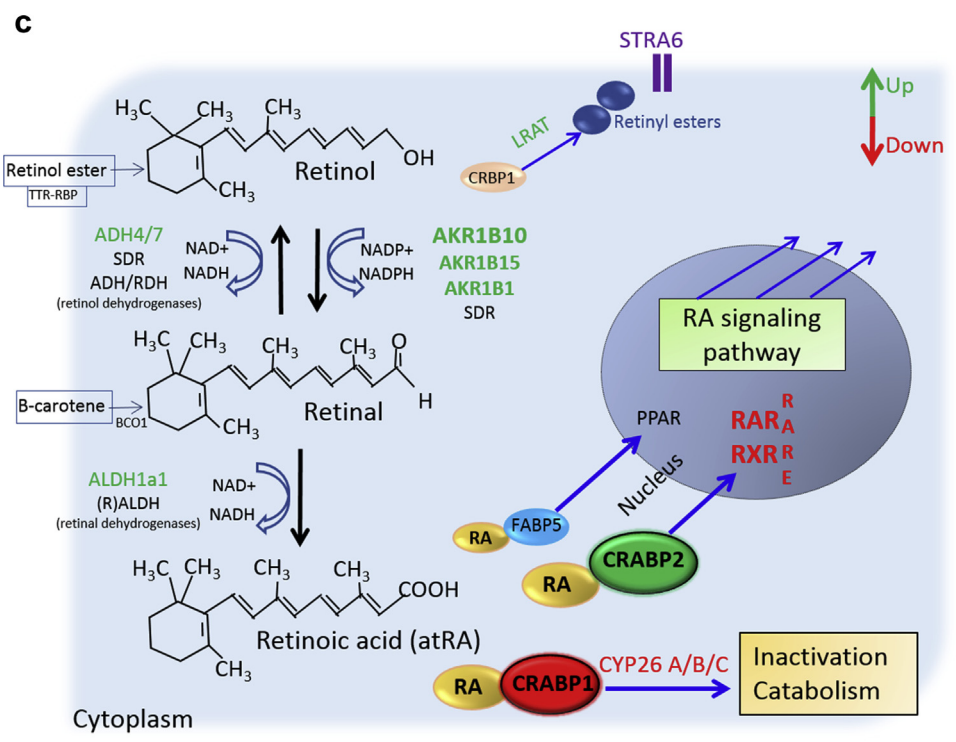
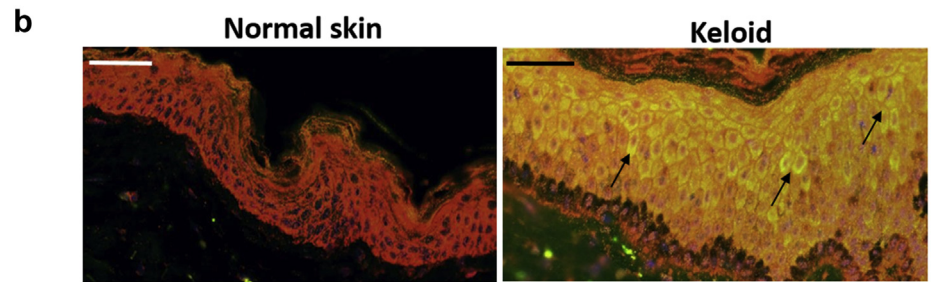
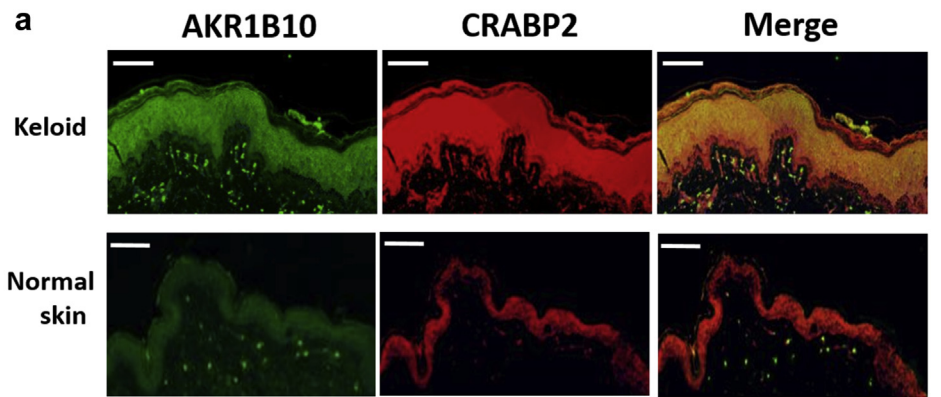
#### AKR1B10 overexpression in normal keratinocytes reduces RAR transactivation

RARs are thought to exert their effects through binding RA response elements located in the promoters of target genes (Al Tanoury et al., 2014; Germain et al., 2006; Samarut and

**Figure 2. Keloid tissue retinoic acid pathway dysregulation.** (a) Immunofluorescence showing increased epidermal staining intensity of AKR1B10 (green) and CRABP2 (red) for keloid (n = 5) (scale bar = 200 μm) compared with normal skin tissue (n = 6) (scale bar = 100 μm).

(b) Magnified images of merged AKR1B10 and CRABP2 for both keloid and normal skin tissue. Strong yellow staining in keloid epidermis, indicated by the black arrows, shows colocalization of AKR1B10 and CRABP2, particularly in the suprabasal layers. Normal skin epidermis, by contrast, remains red-orange. Scale bar = 50 μm.

(c) Detailed diagram of the classical retinoic acid biosynthesis pathway. Green represents up-regulation and red represents down-regulation of molecules identified from microarray data and confirmed on quantitative real-time PCR, which is available in [Supplementary Table S1](#). ADH, alcohol dehydrogenase; AKR1B10, aldo-keto reductase family 1 member B10; ALDH, aldehyde dehydrogenase; atRA, all-trans-retinoic acid; CRABP, cellular retinoic acid binding protein; CRBP1, cellular retinol binding protein 1; CYP26, cytochrome P450, family 26; FABP5, fatty acid binding protein 5; LRAT, lecithin:retinol acetyltransferase; NADP, nicotinamide adenine dinucleotide phosphate; NADPH, reduced NADP; PPAR, peroxisome proliferator-activated receptor; RA, retinoic acid; (R)ALDH, retinaldehyde dehydrogenase; RAR, retinoic acid receptor; RARE, retinoic acid response element; RDH, retinol dehydrogenase; RXR, retinoid X receptor; SDR, short-chain dehydrogenase; STRA6, stimulated by retinoic acid 6; TTR-RBP, transthyretin-retinol binding protein.



Rochette-Egly, 2012). Therefore, we also wished to ascertain the effect of AKR1B10 overexpression on RAR-activated signal transduction pathways in NHEK. To this end, NHEK were double transfected, first with AKR1B10 and then with a reporter plasmid expressing firefly luciferase under the control of RA response element. Resultant cell luminescence was compared with the negative control, giving a fold change in

activity (relative luciferase activity) for both AKR1B10-transfected and nontransfected NHEK.

Treatment with all-trans-retinoic acid was used to affirm the integrity of this assay, in which addition of 1 μmol/L all-trans-retinoic acid resulted in increased relative luciferase activity in transfected and nontransfected keratinocytes (Figure 3g). The addition of all-trans-retinol also resulted in

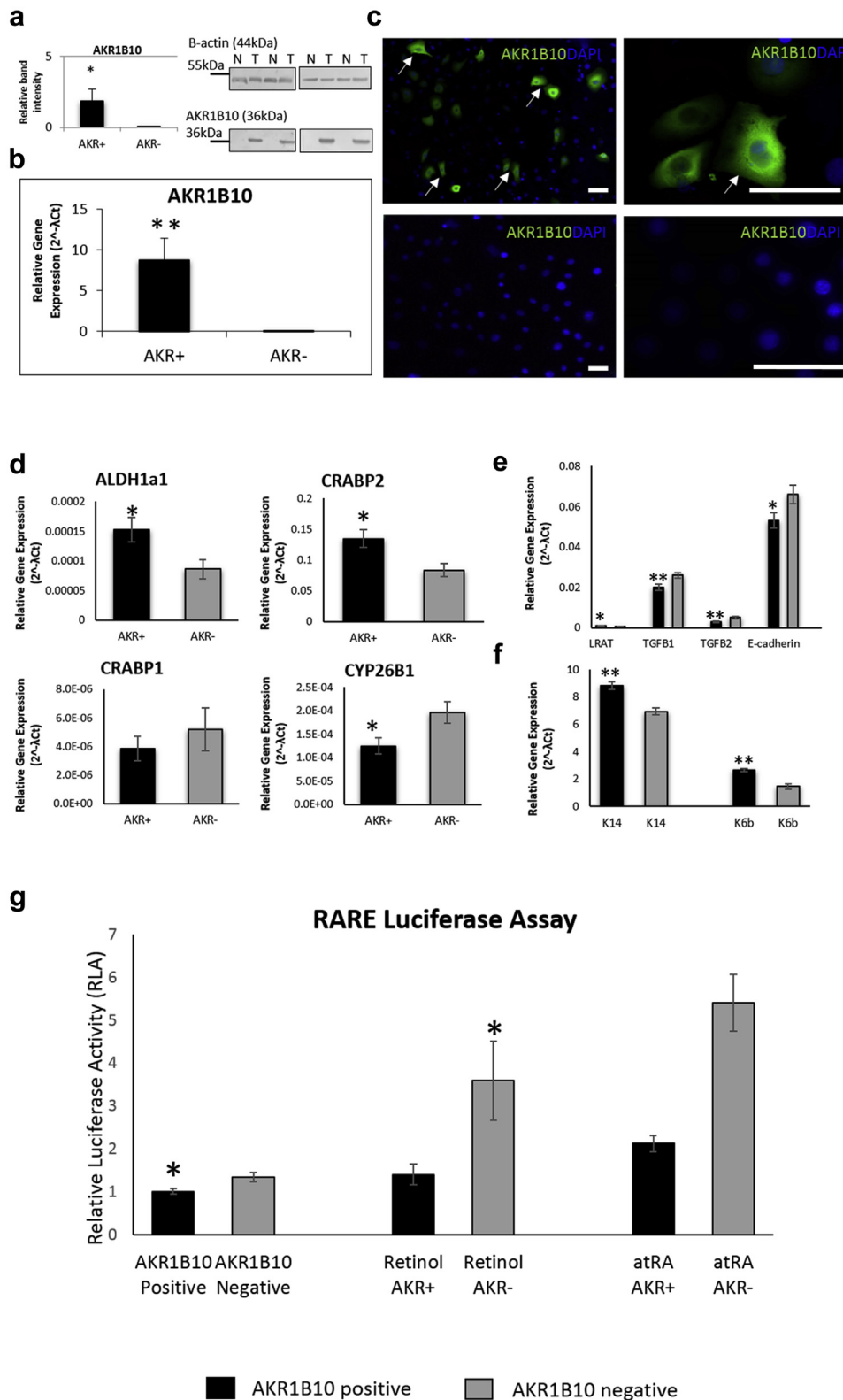


**Figure 3. AKR1B10 overexpression in normal skin keratinocytes.** (a) AKR1B10 expression quantified by Western blot test (n = 10). (b) Quantitative real-time PCR (n = 10). (c) Immunocytochemistry (n = 8). Arrows identify transfected keratinocytes. Scale bar = 50 μm. (d, e) Quantitative real-time PCR for retinoic acid pathway molecule expression and downstream signaling after AKR1B10 overexpression. (f) Keratin 14 and 6b quantitative real-time PCR in transfected versus nontransfected keratinocytes. (g) AKR1B10-transfected versus nontransfected relative luciferase activity, treated with 10 μmol/L retinol or 1 μmol/L all-*trans*-retinoic acid (n = 10). Data from at least three independent means ± standard error of the mean. \**P* < 0.05, \*\**P* < 0.005, Student's *t* test. AKR, aldo-keto reductase; AKR1B10, aldo-keto reductase 1, member B10; ALDH1a1, aldehyde dehydrogenase 1, member A1; atRA, all-*trans*-retinoic acid; CRABP, cellular retinoic acid binding protein; CYP26B1, cytochrome P450, family 26, subfamily B1; K, keratin; LRAT, lecithin:retinol acetyltransferase; N, not transfected with AKR1B10; RARE, retinoic acid response element; T, transfected with AKR1B10; TGF-β, transforming growth factor-beta.

increased activity in both transfected and nontransfected cells, confirming that NHEK are capable of baseline endogenous RA synthesis. There was a significant increase in the relative luciferase activity of nontransfected compared with transfected keratinocytes treated with retinol, indicating functioning AKR1B10 enzyme activity, whereby less RA

production resulted in comparatively reduced transactivation (Figure 3g). Overall, activity was shown to be significantly decreased in AKR1B10-overexpressing keratinocytes compared with nontransfected cells (Figure 3g), suggesting that reduced transactivation was attributable to the activity of this enzyme diminishing the generation of RA.



**AKR1B10-transfected keratinocytes secrete signals that enhance the profibrotic activity of human dermal fibroblasts**

Having investigated the effects of AKR1B10 overexpression on classical RA pathway and receptor transactivation, we next sought to analyze the downstream effects of NHEK AKR1B10 up-regulation. Keloid fibroblasts (KF) ( $n = 5$ ) and normal skin fibroblasts (NSF) ( $n = 5$ ) were subjected to conditioned media from AKR1B10-transfected and non-transfected NHEK ( $n = 6$ ). Both KF and NSF incubated in conditioned medium from transfected keratinocytes showed a trend toward increased expression of fibrotic factors, with TGF- $\beta$ 2 increased in both, TGF- $\beta$ 1 significantly increased in both ( $P < 0.01$ ), and TGF- $\beta$ 3 and fibroblast growth factor 7 significantly increased in NSF ( $P < 0.05$ ) (Figure 4a).

Connective tissue growth factor expression was significantly decreased in KF exposed to transfected keratinocyte medium ( $P < 0.01$ ) (Figure 4a). This correlates with previous findings in which NSF and KF showed reduced connective tissue growth factor when co-cultured with keloid keratinocytes, highlighting the importance of epithelial-mesenchymal interactions in keloid pathogenesis (Khoo et al., 2006).

In KF and NSF treated with conditioned medium from transfected keratinocytes, there was a significant increase in both collagen I and collagen III overall gene expression ( $P < 0.005$ ) compared with fibroblasts treated with medium from nontransfected keratinocytes (Figure 4b) (see Supplementary Figure S5 online for more detail). To assess whether this increased collagen messenger RNA expression produced a corresponding increase in protein, in-cell Western blot analysis was performed for both KF and NSF ( $n = 3$ ) using media from transfected and nontransfected keratinocytes ( $n = 3$ ). These results corresponded with the qRT-PCR results, in which 3 of 3 KF and 2 of 3 NSF showed significant increase in collagen I expression ( $P < 0.05$ ) and 2 of 3 KF and 3 of 3 NSF expressed increased collagen III protein ( $P < 0.05$ ) (Figure 4c) (see Supplementary Figure S5 for more detail). Furthermore, KF ( $n = 3$ ) treated with 24 hours of 1  $\mu$ mol/L all-trans-retinoic acid showed significantly decreased collagen III protein expression in only 2 of 3 patients and no significant TGF- $\beta$ 1 expression alteration, using in-cell Western blot analysis (see Supplementary Figure S6 online). This suggests that RA treatment of KF, although having some effect on collagen, does not completely abrogate the fibrotic signature of these cells.

Therefore, these results indicate that AKR1B10-overexpressing keratinocytes secrete paracrine signals that enhance the fibrogenic activity of dermal fibroblasts and may contribute to KD pathobiology but that RA application may not be selective enough to correct this abnormality.

**DISCUSSION**

In this study, we have shown that the highly efficient, retinaldehyde-specific aldo-keto reductase enzyme AKR1B10 is up-regulated in KE and that its induced overexpression in normal skin keratinocytes affects the classical RA pathway, recreating KE expression patterns. Additionally, AKR1B10 overexpression reduces RAR activity and produces paracrine effects downstream consistent with keloid fibrosis, thereby implicating RA in KD pathogenesis. To our knowledge,

AKR1B10 up-regulation in KD has not been previously reported, and the localization of its overexpression to the KE emphasizes the potentially critical role of the epithelium and epithelial-mesenchymal interactions in the pathogenesis of this fibrotic tumor and corroborates the LCM-based, site-specific targeted approach in this study.

Here, in an innovative approach to KD, we have combined LCM and whole-genome microarray to isolate separate in situ gene profiles of KE and keloid dermis for selected keloid sites and compared these with normal skin. Traditionally, the bulk of KD research has focused on the dermis, where fibroblasts are considered the culprits of pathological extracellular matrix deposition (Dohi et al., 2015; Kashiyaama et al., 2012; Schneider and Wickstrom, 2015). Therefore, despite the facts that the epidermis is invariably the first layer affected by the trauma that initiates keloid formation and that epidermal injury may well be a condition sine qua non for KD development, comparatively few studies have focused on the role of the epidermis and implications for epithelial-mesenchymal interactions in keloid pathogenesis (Hahn et al., 2013; Yan et al., 2015). Our focus on KE is especially relevant, because the epidermis is the site of wound closure, a driving force in immune cell recruitment and cytokine/chemokine production that is crucial to cutaneous wound healing, where it engages in intimate bidirectional communication with underlying mesenchyme (Achachi et al., 2015; Eming et al., 2014; Martin and Nunan, 2015).

Our identification of AKR1B10 up-regulation in all three KE sites compared with NSE compares with several other studies showing up-regulated AKR1B10 in early versus late wound healing (Nuutila et al., 2012), perhaps indicating a prolonged inflammatory phase in KD, several metaplastic conditions (Breton et al., 2008; Gomes et al., 2005; Li et al., 2008; Tsuzura et al., 2014), and cancers (Fukumoto et al., 2005; Ha et al., 2014; Kropotova et al., 2014). We validated significant up-regulation of AKR1B10 in extralesional KE, which may represent molecular transformation through paracrine signaling, that precedes the histological changes evident in KD. Because AKR1B10 has been previously associated with recurrence (Ma et al., 2012; Yoshitake et al., 2007), the overexpression in extralesional epidermis may have clinical implications in terms of determining excision margins (Tan et al., 2010). This dysregulation of AKR1B10 in KE has three major implications for KD pathogenesis. First, AKR1B10 mediates degradation of acetyl-CoA carboxylase  $\alpha$ , which is the rate-limiting step in de novo long-chain fatty acid synthesis (Davis et al., 2000; Zang et al., 2005), resulting in the stimulation of cell growth and survival (Cao et al., 1998; Ma et al., 2008), processes central to keloid tumorigenesis. Second, AKR1B10 catalyzes the reduction of carbonyls and xenobiotics (Shen et al., 2011), thereby moderating susceptibility to many chemotherapeutic agents (Balendiran et al., 2009; Jin and Penning, 2007; Morikawa et al., 2015; Zhong et al., 2011), which may explain the incomplete efficacy of these treatments when used in KD (Jones et al., 2015). Finally, through its effects on RA metabolism, AKR1B10 excess in KE provides not only mechanistic but also more concrete evidence for RA involvement in KD than previous studies in which supplementation of RA in vitro showed reduced KF proliferation and procollagen levels

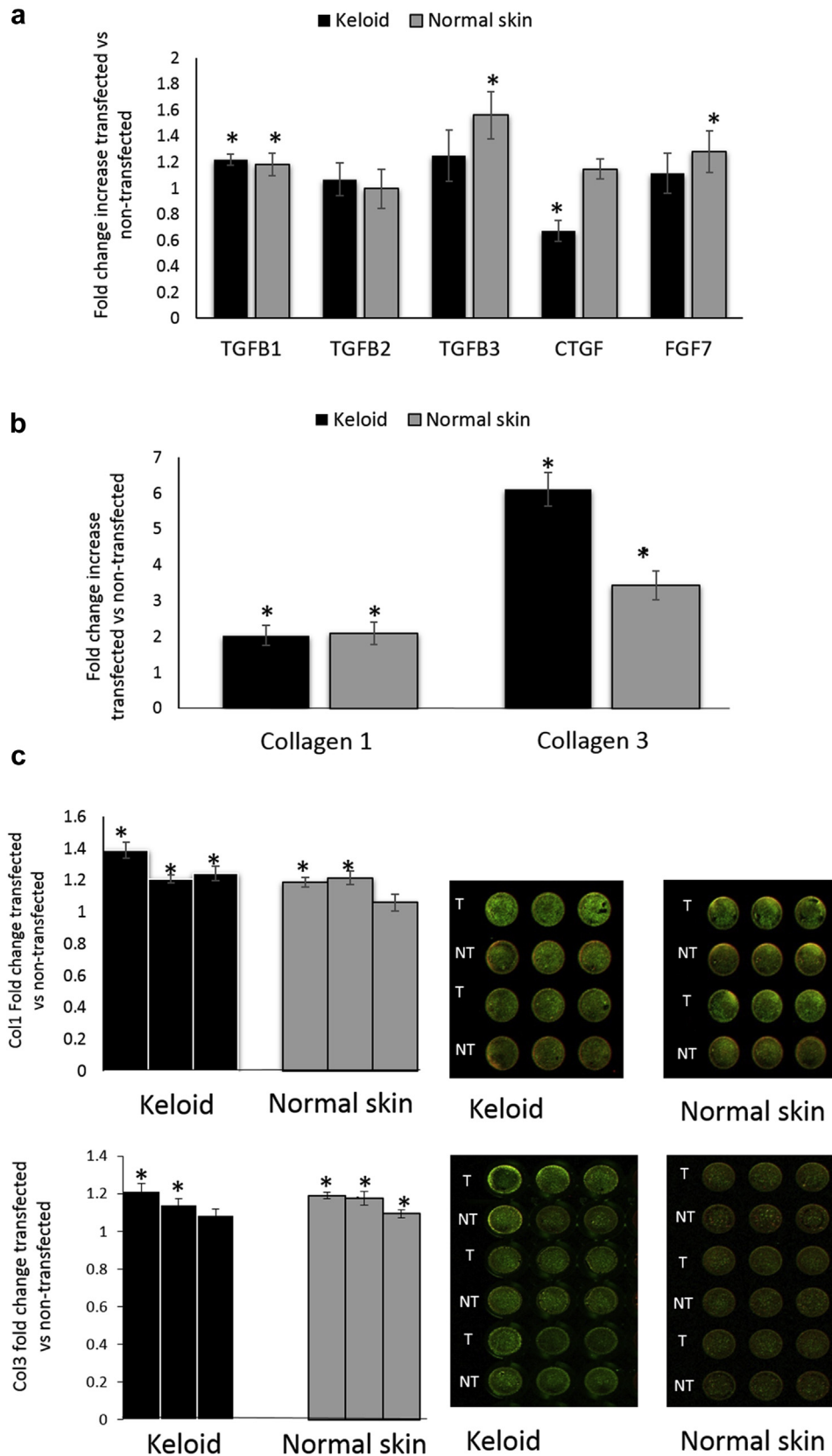


**Figure 4. Effect of conditioned media on keloid fibroblasts and normal skin fibroblasts.** (a) Fold change difference (quantitative real-time PCR) in the expression of profibrotic genes by keloid fibroblasts (n = 5) and normal skin fibroblasts (n = 5) treated with AKR1B10-transfected or nontransfected medium (n = 6). (b) Quantitative real-time PCR and (c) in-cell Western blot test for collagen I and III expression for fibroblasts treated with AKR1B10-transfected or nontransfected medium (n = 3). In-cell Western blot test fluorescence images accompany the graphs. Each bar on all graphs (a–c) represents fold change of fibroblasts treated with transfected versus nontransfected medium and associated significance with that fold change. Data are mean ± standard error of the mean from at least three independent experiments. \**P* < 0.05 using Student's *t* test. AKR1B10, aldo-keto reductase family 1, member B10; Col, collagen; CTGF, connective tissue growth factor; FGF, fibroblast growth factor; KF, keloid fibroblasts; NSF, normal skin fibroblasts; NT, treated with non-transfected keratinocyte medium; T, treated with transfected keratinocyte medium; TGFB1, transforming growth factor-β1; TGFB2, transforming growth factor-β2.

(Abergel et al., 1985; Cruz and Korchin, 1994; Oikarinen et al., 1985; Uchida et al., 2003), in addition to clinical improvement after topical and oral RA administration (Daly and Weston, 1986; Janssen de Limpens, 1980; Kwon

et al., 2014; Michaelis et al., 1975; Panabiere-Castaings, 1988).

We hypothesized a reduction in keloid intraepidermal RA levels because of dysregulation of the RA synthesis pathway.



We then showed this pathway dysregulation through qRT-PCR, confirming the altered expression of RA response element-regulated pathway molecules identified in our microarray data. This same altered expression of ALDH1a1, CRABP2, CRABP1, CYP26B1, and TGF- $\beta$ 2 in AKR1B10-transfected NHEK validated our use of cell culture data as clinically relevant in the context of KD. We supported our microarray-based hypothesis of deficient RA levels in KE using these AKR1B10-overexpressing transfected primary NHEKs, which indicated reduced transactivation at RAR nuclear receptors and a secretory profile expression that may contribute to hyperproliferation (keratin 14 and keratin 6b up-regulation), epithelial-mesenchymal transition (E-cadherin suppression), and TGF- $\beta$  dysregulation, all postulated to play a role in KD (Lee et al., 2015; Prathiba et al., 2001; Yan et al., 2015). We showed that the proposed reduction in epidermal RA had paracrine effects resulting in increased TGF- $\beta$ 1, TGF- $\beta$ 2, collagen I, and collagen III in KF, corresponding well to the dermal phenotype in KD patients, with abnormal extracellular matrix production and a profibrotic expression profile (Chen et al., 2013; Sidgwick and Bayat, 2012).

The clinical implications of our findings are 2-fold. First, the persistence of collagen and TGF- $\beta$  expression after all-*trans*-retinoic acid treatment of KF in our study suggests that blanket application of this metabolite to keloid tumors will not be consistently successful. Largely, RA has been postulated to abrogate factors that contribute to fibrosis and cancer by regulating immunity, extracellular matrix deposition, cell proliferation, and epidermal differentiation (Bidad et al., 2011; Ohata et al., 1997; Tabata et al., 2006; Zouboulis, 2001). Functioning optimally within a narrow, ill-defined concentration range, RA is a pleiotropic molecule with a bimodal effect on these processes, and when levels deviate outside this range in either direction, fibrosis (Zaitseva et al., 2008; Zhou et al., 2012) or cancer (Connolly et al., 2013; Tang and Gudas, 2011) can result. That is to say, both RA deficiency and excess can result in a similar phenotype, such that exogenous RA application may reinforce keloid formation. It is likely that previous topical RA treatment in KD was only partially successful because of its effect on multiple molecules and not classic pathway activation alone.

Second, our demonstration of a paracrine effect of the proposed RA-deficient keratinocytes on fibroblasts provides an argument for epidermal therapy that also affects the dermis. AKR1B10 represents an attractive, alternative, more-specific therapeutic target than RA, and the knock-down of this enzyme has been shown to be effective in reducing proliferation and enhancing sensitivity to carbonyl-containing compounds (Matkowskyj et al., 2014; Yan et al., 2007). In particular, the overexpression of this enzyme in the epidermis has beneficial therapeutic implications, in that topical application may circumvent requirement for invasive procedures, which themselves incur a risk of keloid recurrence. Current AKR1B10-selective inhibitors are under investigation and include nonsteroidal anti-inflammatory drugs such as sulindac and diclofenac (Cousido-Siah et al., 2015; Endo et al., 2010; Li et al., 2013), triterpenoids such as oleanolic acid (Takemura et al., 2011), steroidal derivatives (Zhang, Wang, et al., 2014), and novel synthetic compounds (Kumar et al., 2015; Porte et al., 2013).

Therefore, modulation of KE RA expression through topical application of AKR1B10 antagonists alone, after excision or as adjuvant treatment, holds promise for the future management of the complex disorder that is KD.

## MATERIALS AND METHODS

### Tissue procurement and processing

In line with North West Research Ethics Committee (Ref. 11/NW/0683) and Declaration of Helsinki protocols, both keloid and normal skin biopsy samples were harvested with full written informed consent. Keloid biopsy samples, fitting clinical criteria previously described (Suarez et al., 2014), were taken from center (intralesional), margin (perilesional), and adjacent normal skin (extralesional) of excised tissue, and normal skin biopsy samples were taken after routine elective surgical procedures (Supplementary Table S2 online). The biopsies were stored in RNA stabilization solution and then embedded in optimum cutting temperature before cryosection (Leica CM3050S, Leica Microsystems, Milton Keynes, UK) or were formalin fixed and paraffin embedded.

### LCM and microarray analysis

Laser microdissection pressure catapulting was performed using PALM MicroBeam 4.2 (Carl Zeiss, Munich, Germany), where a UV laser isolated epidermis from dermis. RNA extraction, amplification, and microarray are detailed in the Supplementary Materials and Methods online.

### Cell cultures

Primary fibroblast/keratinocyte cultures were established as previously described (Ashcroft et al., 2013), and conditioned media experiments are detailed in the Supplementary Materials and Methods.

### Keratinocyte transfection

Transfection of primary human normal skin keratinocytes with AKR1B10 (OriGene TrueClone, OriGene Technologies, MD) was performed using Turbofectin 8.0 (OriGene), and efficiency of transfection was determined by Western blot analysis with  $\beta$ -actin as the internal control. Further details are provided in the Supplementary Materials and Methods.

### Luciferase assay

RA response element receptor activity was performed using a luciferase signal reporter plasmid (SABioscience, Qiagen, Manchester, UK) and measured with Dual-Glo Luciferase Assay System (Promega, WI) according to the manufacturer's protocol. Data were normalized by *Renilla* luciferase luminescence intensity (see Supplementary Materials and Methods for details). The assay was repeated, cells were treated with either 10  $\mu$ mol/L all-*trans*-retinol or 1  $\mu$ mol/L all-*trans*-retinoic acid for 24 hours, and luminescence was quantified.

### qRT-PCR

qRT-PCR was performed as described previously (Ashcroft et al., 2013). Details and primer list (see Supplementary Table S3 online) can be found in Supplementary Material and Methods. Each reaction was performed in triplicate and normalized using ribosomal protein L32 and glyceraldehyde-3-phosphate dehydrogenase as house-keeping reference genes.

### Immunohistochemistry and immunocytochemistry

AKR1B10 tissue detection was performed using the Novolink peroxidase detection kit (Leica Biosystems, Milton Keynes, UK) and red chromogen counterstaining (Vector NovaRED, Vector Laboratories, Peterborough, UK). Combined AKR1B10/CRABP2

immunofluorescent staining was performed on keloid and normal skin tissue. AKR1B10 immunocytochemistry was done on transfected NHEK to confirm plasmid incorporation and protein expression. Further methodology is described in the [Supplementary Materials and Methods](#) and the antibody list in [Supplementary Table S4a](#) online.

### Western blot analysis

Western blot analyses of whole tissue and cell lysates are detailed in the [Supplementary Materials and Methods](#). In-cell Western blot analysis was performed for collagen I and III and for TGF- $\beta$ 1 according to manufacturer's instructions (LiCor, Cambridge, United Kingdom) (details are given in the [Supplementary Materials and Methods](#), with the antibodies listed in [Supplementary Tables S4b](#) and [c](#)).

### Statistical analysis

Microarray data analysis was completed using Array studio version 7.2 (Array Studio, OmicSoft, NC). Differentially expressed genes for keloid sites were compared with each other and with normal skin, then filtered by *P*-value less than 0.05 and fold change of greater than or equal to 2. For qRT-PCR, gene expression levels were normalized against internal controls, and  $\Delta\Delta C_T$  was calculated for fold change in target genes. Data are represented as mean  $\pm$  standard error of the mean. Statistical analysis was calculated using Student's *t* test, and a *P*-value less than 0.05 was considered statistically significant. The overall experimental flow is detailed in [Supplementary Figure S7](#) online.

### CONFLICT OF INTEREST

The authors state no conflict of interest.

### ACKNOWLEDGMENTS

This work was partly supported by GlaxoSmithKline. We thank Adam Taylor for his contribution to data analysis and Edward Mckenzie for his plasmid amplification expertise.

### SUPPLEMENTARY MATERIAL

Supplementary material is linked to the online version of the paper at [www.jidonline.org](http://www.jidonline.org), and at <http://dx.doi.org/10.1016/j.jid.2016.03.022>.

### REFERENCES

- Abergel RP, Meeker CA, Oikarinen H, Oikarinen AI, Uitto J. Retinoid modulation of connective tissue metabolism in keloid fibroblast cultures. *Arch Dermatol* 1985;121:632–5.
- Achachi A, Vocanson M, Bastien P, Peguet-Navarro J, Grande S, Goujon C, et al. UV radiation induces the epidermal recruitment of dendritic cells that compensate for the depletion of Langerhans cells in human skin. *J Invest Dermatol* 2015;135:2058–67.
- Al Tanoury Z, Piskunov A, Andriamoratsiresy D, Gaouar S, Lutzinger R, Ye T, et al. Genes involved in cell adhesion and signaling: a new repertoire of retinoic acid receptor target genes in mouse embryonic fibroblasts. *J Cell Sci* 2014;127:521–33.
- Amann PM, Czaja K, Bazhin AV, Ruhl R, Eichmuller SB, Merk HF, et al. LRAT overexpression diminishes intracellular levels of biologically active retinoids and reduces retinoid antitumor efficacy in the murine melanoma B16F10 cell line. *Skin Pharmacol Physiol* 2015;28:205–12.
- Amann PM, Czaja K, Bazhin AV, Ruhl R, Skazik C, Heise R, et al. Knockdown of lecithin retinol acyltransferase increases all-trans retinoic acid levels and restores retinoid sensitivity in malignant melanoma cells. *Exp Dermatol* 2014;23:832–7.
- Ashcroft KJ, Syed F, Bayat A. Site-specific keloid fibroblasts alter the behaviour of normal skin and normal scar fibroblasts through paracrine signalling. *PLoS One* 2013;8:e75600.
- Bagabir R, Byers RJ, Chaudhry IH, Muller W, Paus R, Bayat A. Site-specific immunophenotyping of keloid disease demonstrates immune upregulation and the presence of lymphoid aggregates. *Br J Dermatol* 2012;167:1053–66.
- Baker BM, Chen CS. Deconstructing the third dimension: how 3D culture microenvironments alter cellular cues. *J Cell Sci* 2012;125:3015–24.
- Balendiran GK, Martin HJ, El-Hawari Y, Maser E. Cancer biomarker AKR1B10 and carbonyl metabolism. *Chem Biol Interact* 2009;178:134–7.
- Batova A, Danielpour D, Pirisi L, Creek KE. Retinoic acid induces secretion of latent transforming growth factor beta 1 and beta 2 in normal and human papillomavirus type 16-immortalized human keratinocytes. *Cell Growth Differ* 1992;3:763–72.
- Bidad K, Salehi E, Oraei M, Saboor-Yaraghi AA, Nicknam MH. Effect of all-trans retinoic acid (ATRA) on viability, proliferation, activation and lineage-specific transcription factors of CD4+ T cells. *Iran J Allergy Asthma Immunol* 2011;10:243–9.
- Bijlard E, Steltenpool S, Niessen FB. Intralesional 5-fluorouracil in keloid treatment: a systematic review. *Acta Derm Venereol* 2015;95:778–2.
- Breton J, Gage MC, Hay AW, Keen JN, Wild CP, Donnellan C, et al. Proteomic screening of a cell line model of esophageal carcinogenesis identifies cathepsin D and aldo-keto reductase 1C2 and 1B10 dysregulation in Barrett's esophagus and esophageal adenocarcinoma. *J Proteome Res* 2008;7:1953–62.
- Budhu AS, Noy N. Direct channeling of retinoic acid between cellular retinoic acid-binding protein II and retinoic acid receptor sensitizes mammary carcinoma cells to retinoic acid-induced growth arrest. *Mol Cell Biol* 2002;22:2632–41.
- Canady J, Arndt S, Karrer S, Bosserhoff AK. Increased KGF expression promotes fibroblast activation in a double paracrine manner resulting in cutaneous fibrosis. *J Invest Dermatol* 2013;133:647–57.
- Cao D, Fan ST, Chung SS. Identification and characterization of a novel human aldose reductase-like gene. *J Biol Chem* 1998;273:11429–35.
- Chen AC, Yu K, Lane MA, Gudas LJ. Homozygous deletion of the CRABPI gene in AB1 embryonic stem cells results in increased CRABPII gene expression and decreased intracellular retinoic acid concentration. *Arch Biochem Biophys* 2003;411:159–73.
- Chen J, Zeng B, Yao H, Xu J. The effect of TLR4/7 on the TGF-beta-induced Smad signal transduction pathway in human keloid. *Burns* 2013;39:465–72.
- Choi Y, Fuchs E. TGF-beta and retinoic acid: regulators of growth and modifiers of differentiation in human epidermal cells. *Cell Regul* 1990;1:791–809.
- Chua AW, Ma D, Gan SU, Fu Z, Han HC, Song C, et al. The role of R-spondin2 in keratinocyte proliferation and epidermal thickening in keloid scarring. *J Invest Dermatol* 2011;131:644–54.
- Chung YT, Matkowskyj KA, Li H, Bai H, Zhang W, Tsao MS, et al. Overexpression and oncogenic function of aldo-keto reductase family 1B10 (AKR1B10) in pancreatic carcinoma. *Mod Pathol* 2012;25:758–66.
- Connolly RM, Nguyen NK, Sukumar S. Molecular pathways: current role and future directions of the retinoic acid pathway in cancer prevention and treatment. *Clin Cancer Res* 2013;19:1651–9.
- Cousido-Siah A, Ruiz FX, Crespo I, Porte S, Mitschler A, Pares X, et al. Structural analysis of sulindac as an inhibitor of aldose reductase and AKR1B10. *Chem Biol Interact* 2015;234:290–6.
- Crosas B, Hyndman DJ, Gallego O, Martras S, Pares X, Flynn TG, et al. Human aldose reductase and human small intestine aldose reductase are efficient retinal reductases: consequences for retinoid metabolism. *Biochem J* 2003;373:973–9.
- Cruz NI, Korchin L. Inhibition of human keloid fibroblast growth by isotretinoin and triamcinolone acetonide in vitro. *Ann Plast Surg* 1994;33:401–5.
- Crystal RG, Bitterman PB, Mossman B, Schwarz MI, Sheppard D, Almsy L, et al. Future research directions in idiopathic pulmonary fibrosis: summary of a National Heart, Lung, and Blood Institute working group. *Am J Respir Crit Care Med* 2002;166:236–46.
- Daly TJ, Weston WL. Retinoid effects on fibroblast proliferation and collagen synthesis in vitro and on fibrotic disease in vivo. *J Am Acad Dermatol* 1986;15:900–2.
- Davis MS, Solbiati J, Cronan JE Jr. Overproduction of acetyl-CoA carboxylase activity increases the rate of fatty acid biosynthesis in *Escherichia coli*. *J Biol Chem* 2000;275:28593–8.
- Dohi T, Miyake K, Aoki M, Ogawa R, Akaishi S, Shimada T, et al. Tissue inhibitor of metalloproteinase-2 suppresses collagen synthesis in cultured keloid fibroblasts. *Plast Reconstr Surg Glob Open* 2015;3:e520.
- Dong Z, Tai W, Yang Y, Zhang T, Li Y, Chai Y, et al. The role of all-trans retinoic acid in bleomycin-induced pulmonary fibrosis in mice. *Exp Lung Res* 2012;38:82–9.

- Duester G. Genetic dissection of retinoid dehydrogenases. *Chem Biol Interact* 2001;130–132:469–80.
- Duncan FJ, Silva KA, Johnson CJ, King BL, Szatkiewicz JP, Kamdar SP, et al. Endogenous retinoids in the pathogenesis of alopecia areata. *J Invest Dermatol* 2013;133:334–43.
- El-Serag HB, Nurgalieva ZZ, Mistretta TA, Finegold MJ, Souza R, Hilsenbeck S, et al. Gene expression in Barrett's esophagus: laser capture versus whole tissue. *Scand J Gastroenterol* 2009;44:787–95.
- Eming SA, Martin P, Tomic-Canic M. Wound repair and regeneration: mechanisms, signaling, and translation. *Sci Transl Med* 2014;6:265sr266.
- Endo S, Matsunaga T, Soda M, Tajima K, Zhao HT, El-Kabbani O, et al. Selective inhibition of the tumor marker AKR1B10 by antiinflammatory N-phenylanthranilic acids and glycyrrhetic acid. *Biol Pharm Bull* 2010;33:886–90.
- Everts HB, Suo L, Ghim S, Bennett Jenson A, Sundberg JP. Retinoic acid metabolism proteins are altered in trichoblastomas induced by mouse papillomavirus 1. *Exp Mol Pathol* 2015;99:546–51.
- Fisher GJ, Voorhees JJ. Molecular mechanisms of retinoid actions in skin. *FASEB J* 1996;10:1002–13.
- Foitzik K, Spexard T, Nakamura M, Halsner U, Paus R. Towards dissecting the pathogenesis of retinoid-induced hair loss: all-trans retinoic acid induces premature hair follicle regression (catagen) by upregulation of transforming growth factor-beta2 in the dermal papilla. *J Invest Dermatol* 2005;124:1119–26.
- Fukumoto S, Yamauchi N, Moriguchi H, Hippe Y, Watanabe A, Shibahara J, et al. Overexpression of the aldo-keto reductase family protein AKR1B10 is highly correlated with smokers' non-small cell lung carcinomas. *Clin Cancer Res* 2005;11:1776–85.
- Gallego O, Ruiz FX, Ardevol A, Dominguez M, Alvarez R, de Lera AR, et al. Structural basis for the high all-trans-retinaldehyde reductase activity of the tumor marker AKR1B10. *Proc Natl Acad Sci USA* 2007;104:20764–9.
- Germain P, Chambon P, Eichele G, Evans RM, Lazar MA, Leid M, et al. International Union of Pharmacology. LX. Retinoic acid receptors. *Pharmacol Rev* 2006;58:712–25.
- Glick AB, Flanders KC, Danielpour D, Yuspa SH, Sporn MB. (1989) Retinoic acid induces transforming growth factor-beta 2 in cultured keratinocytes and mouse epidermis. *Cell Regul* 1989;1:87–97.
- Gomes LJ, Esteves GH, Carvalho AF, Cristo EB, Hirata R Jr, Martins WK, et al. Expression profile of malignant and nonmalignant lesions of esophagus and stomach: differential activity of functional modules related to inflammation and lipid metabolism. *Cancer Res* 2005;65:7127–36.
- Gundersen TE. Methods for detecting and identifying retinoids in tissue. *J Neurobiol* 2006;66:631–44.
- Ha SY, Song DH, Lee JJ, Lee HW, Cho SY, Park CK. High expression of aldo-keto reductase 1B10 is an independent predictor of favorable prognosis in patients with hepatocellular carcinoma. *Gut Liver* 2014;8:648–54.
- Hahn JM, Glaser K, McFarland KL, Aronow BJ, Boyce ST, Supp DM. Keloid-derived keratinocytes exhibit an abnormal gene expression profile consistent with a distinct causal role in keloid pathology. *Wound Repair Regen* 2013;21:530–44.
- Har-Shai Y, Dujovny E, Rohde E, Zouboulis CC. Effect of skin surface temperature on skin pigmentation during contact and intralesional cryosurgery of keloids. *J Eur Acad Dermatol Venereol* 2007;21:191–8.
- Iqbal SA, Syed F, McGrouther DA, Paus R, Bayat A. Differential distribution of haematopoietic and nonhaematopoietic progenitor cells in intralesional and extralesional keloid: do keloid scars provide a niche for nonhaematopoietic mesenchymal stem cells? *Br J Dermatol* 2010;162:1377–83.
- Janssen de Limpens AM. The local treatment of hypertrophic scars and keloids with topical retinoic acid. *Br J Dermatol* 1980;103:319–23.
- Jin Y, Penning TM. Aldo-keto reductases and bioactivation/detoxication. *Annu Rev Pharmacol Toxicol* 2007;47:263–92.
- Jones CD, Guiot L, Samy M, Gorman M, Tehrani H. The use of chemotherapeutics for the treatment of keloid scars. *Dermatol Reports* 2015;7:5880.
- Jumper N, Paus R, Bayat A. Functional histopathology of keloid disease. *Histol Histopathol* 2015;30:1033–57.
- Kane MA, Napoli JL. Quantification of endogenous retinoids. *Methods Mol Biol* 2010;652:1–54.
- Kashiyama K, Mitsutake N, Matsuse M, Ogi T, Saenko VA, Ujifuku K, et al. miR-196a downregulation increases the expression of type I and III collagens in keloid fibroblasts. *J Invest Dermatol* 2012;132:1597–604.
- Khoo YT, Ong CT, Mukhopadhyay A, Han HC, Do DV, Lim JJ, et al. Upregulation of secretory connective tissue growth factor (CTGF) in keratinocyte-fibroblast coculture contributes to keloid pathogenesis. *J Cell Physiol* 2006;208:336–43.
- Kropotova ES, Zinovieva OL, Zyryanova AF, Dybovaya VI, Prasolov VS, Beresten SF, et al. Altered expression of multiple genes involved in retinoic acid biosynthesis in human colorectal cancer. *Pathol Oncol Res* 2014;20:707–17.
- Kumar R, Son M, Bavi R, Lee Y, Park C, Arulalapperumal V, et al. Novel chemical scaffolds of the tumor marker AKR1B10 inhibitors discovered by 3D QSAR pharmacophore modeling. *Acta Pharmacol Sin* 2015;36:998–1012.
- Kurlandsky SB, Duell EA, Kang S, Voorhees JJ, Fisher GJ. Auto-regulation of retinoic acid biosynthesis through regulation of retinol esterification in human keratinocytes. *J Biol Chem* 1996;271:15346–52.
- Kwon SY, Park SD, Park K. Comparative effect of topical silicone gel and topical tretinoin cream for the prevention of hypertrophic scar and keloid formation and the improvement of scars. *J Eur Acad Dermatol Venereol* 2014;28:1025–33.
- Lee WJ, Park JH, Shin JU, Noh H, Lew DH, Yang WI, et al. Endothelial-to-mesenchymal transition induced by Wnt 3a in keloid pathogenesis. *Wound Repair Regen* 2015;23:435–42.
- Li CP, Goto A, Watanabe A, Murata K, Ota S, Niki T, et al. AKR1B10 in usual interstitial pneumonia: expression in squamous metaplasia in association with smoking and lung cancer. *Pathol Res Pract* 2008;204:295–304.
- Li H, Yang AL, Chung YT, Zhang W, Liao J, Yang GY. Sulindac inhibits pancreatic carcinogenesis in LSL-KrasG12D-LSL-Trp53R172H-Pdx-1-Cre mice via suppressing aldo-keto reductase family 1B10 (AKR1B10). *Carcinogenesis* 2013;34:2090–8.
- Lim CK, Halim AS, Yaacob NS, Zainol I, Noorsal K. Keloid pathogenesis via Drosophila similar to mothers against decapentaplegic (SMAD) signaling in a primary epithelial-mesenchymal in vitro model treated with biomedical-grade chitosan porous skin regenerating template. *J Biosci Bioeng* 2013;115:453–8.
- Lim CP, Phan TT, Lim JJ, Cao X. Cytokine profiling and Stat3 phosphorylation in epithelial-mesenchymal interactions between keloid keratinocytes and fibroblasts. *J Invest Dermatol* 2009;129:851–61.
- Lim JJ, Phan TT, Bay BH, Qi R, Huynh H, Tan WT, et al. Fibroblasts cocultured with keloid keratinocytes: normal fibroblasts secrete collagen in a keloid-like manner. *Am J Physiol Cell Physiol* 2002;283:C212–22.
- Ma J, Luo DX, Huang C, Shen Y, Bu Y, Markwell S, et al. AKR1B10 overexpression in breast cancer: association with tumor size, lymph node metastasis and patient survival and its potential as a novel serum marker. *Int J Cancer* 2012;131:E862–71.
- Ma J, Yan R, Zu X, Cheng JM, Rao K, Liao DF, et al. Aldo-keto reductase family 1 B10 affects fatty acid synthesis by regulating the stability of acetyl-CoA carboxylase-alpha in breast cancer cells. *J Biol Chem* 2008;283:3418–23.
- Ma X, Chen J, Xu B, Long X, Qin H, Zhao RC, et al. Keloid-derived keratinocytes acquire a fibroblast-like appearance and an enhanced invasive capacity in a hypoxic microenvironment in vitro. *Int J Mol Med* 2015;35:1246–56.
- Martin P, Nunan R. Cellular and molecular mechanisms of repair in acute and chronic wound healing. *Br J Dermatol* 2015;173:370–8.
- Marttala J, Andrews JP, Rosenbloom J, Uitto J. Keloids: Animal models and pathologic equivalents to study tissue fibrosis [e-pub ahead of print]. *Matrix Biol* 2016; <http://dx.doi.org/10.1016/j.matbio.2016.01.014>.
- Matkowskyj KA, Bai H, Liao J, Zhang W, Li H, Rao S, et al. Aldoketoreductase family 1B10 (AKR1B10) as a biomarker to distinguish hepatocellular carcinoma from benign liver lesions. *Hum Pathol* 2014;45:834–43.
- Michaelis W, Dietrich F, Kohrlein H. Die perorale Vitamin A Behandlung hypertrophischer Narben. Stuttgart: Schattauer; 1975.
- Moll R, Divo M, Langbein L. The human keratins: biology and pathology. *Histochem Cell Biol* 2008;129:705–33.
- Morikawa Y, Kezuka C, Endo S, Ikari A, Soda M, Yamamura K, et al. Acquisition of doxorubicin resistance facilitates migrating and invasive potentials

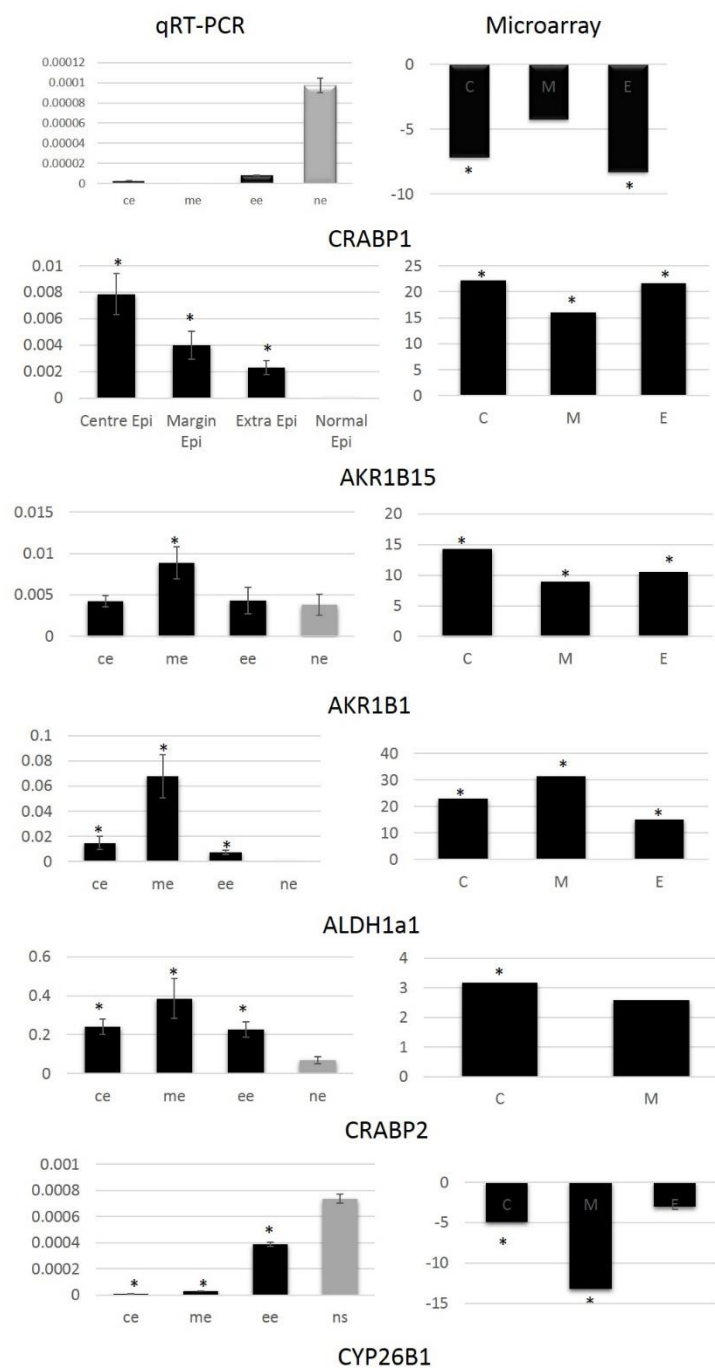


- of gastric cancer MKN45 cells through up-regulating aldo-keto reductase 1B10. *Chem Biol Interact* 2015;230:30–9.
- Napoli JL. Physiological insights into all-trans-retinoic acid biosynthesis. *Biochim Biophys Acta* 2012;1821:152–67.
- Nuutila K, Siltanen A, Peura M, Bizik J, Kaartinen I, Kuokkanen H, et al. Human skin transcriptome during superficial cutaneous wound healing. *Wound Repair Regen* 2012;20:830–9.
- Obinata A, Osakabe K, Yamaguchi M, Morimoto R, Akimoto Y. Tgm2/Gh, Gbx1 and TGF-beta are involved in retinoic acid-induced trans-differentiation from epidermis to mucosal epithelium. *Int J Dev Biol* 2011;55:933–43.
- Ohata M, Lin M, Satre M, Tsukamoto H. Diminished retinoic acid signaling in hepatic stellate cells in cholestatic liver fibrosis. *Am J Physiol* 1997;272:G589–96.
- Oikarinen H, Oikarinen AI, Tan EM, Abergel RP, Meeker CA, Chu ML, et al. Modulation of procollagen gene expression by retinoids. Inhibition of collagen production by retinoic acid accompanied by reduced type I procollagen messenger ribonucleic acid levels in human skin fibroblast cultures. *J Clin Invest* 1985;75:1545–53.
- Okano J, Lichti U, Mamiya S, Aronova M, Zhang G, Yuspa SH, et al. Increased retinoic acid levels through ablation of Cyp26b1 determine the processes of embryonic skin barrier formation and peridermal development. *J Cell Sci* 2012;125:1827–36.
- Pampaloni F, Reynaud EG, Stelzer EH. The third dimension bridges the gap between cell culture and live tissue. *Nat Rev Mol Cell Biol* 2007;8:839–45.
- Panabiere-Castaings MH. Retinoic acid in the treatment of keloids. *J Dermatol Surg Oncol* 1988;14:1275–6.
- Pavez Lorie E, Cools M, Borgers M, Wouters L, Shroot B, Hagforsen E, et al. Topical treatment with CYP26 inhibitor talarozole (R115866) dose dependently alters the expression of retinoid-regulated genes in normal human epidermis. *Br J Dermatol* 2009;160:26–36.
- Pavez Lorie E, Li H, Vahlquist A, Torma H. The involvement of cytochrome p450 (CYP) 26 in the retinoic acid metabolism of human epidermal keratinocytes. *Biochim Biophys Acta* 2009;1791:220–8.
- Porte S, Xavier Ruiz F, Gimenez J, Molist I, Alvarez S, Dominguez M, et al. Aldo-keto reductases in retinoid metabolism: search for substrate specificity and inhibitor selectivity. *Chem Biol Interact* 2013;202:186–94.
- Prathiba V, Rao KS, Gupta PD. Altered expression of keratins during abnormal wound healing in human skin. *Cytobios* 2001;104:43–51.
- Ramot Y, Sugawara K, Zakany N, Toth BI, Biro T, Paus R. A novel control of human keratin expression: cannabinoid receptor 1-mediated signaling down-regulates the expression of keratins K6 and K16 in human keratinocytes in vitro and in situ. *PeerJ* 2013;1:e40.
- Regen F, Hildebrand M, Le Bret N, Herzog I, Heuser I, Hellmann-Regen J. Inhibition of retinoic acid catabolism by minocycline: evidence for a novel mode of action? *Exp Dermatol* 2015;24:473–6.
- Ruiz FX, Gallego O, Ardevol A, Moro A, Dominguez M, Alvarez S, et al. Aldo-keto reductases from the AKR1B subfamily: retinoid specificity and control of cellular retinoic acid levels. *Chem Biol Interact* 2009;178:171–7.
- Ruiz FX, Moro A, Gallego O, Ardevol A, Rovira C, Petrash JM, et al. Human and rodent aldo-keto reductases from the AKR1B subfamily and their specificity with retinaldehyde. *Chem Biol Interact* 2011;191:199–205.
- Ruiz FX, Porte S, Pares X, Farres J. Biological role of aldo-keto reductases in retinoic Acid biosynthesis and signaling. *Front Pharmacol* 2012;3:58.
- Salabei JK, Li XP, Petrash JM, Bhatnagar A, Barski OA. Functional expression of novel human and murine AKR1B genes. *Chem Biol Interact* 2011;191:177–84.
- Samarut E, Rochette-Egly C. Nuclear retinoic acid receptors: conductors of the retinoic acid symphony during development. *Mol Cell Endocrinol* 2012;348:348–60.
- Schneider D, Wickstrom SA. Force generation and transmission in keloid fibroblasts: dissecting the role of mechanosensitive molecules in cell function. *Exp Dermatol* 2015;24:574–5.
- Seifert O, Bayat A, Geffers R, Dienus K, Buer J, Lofgren S, et al. Identification of unique gene expression patterns within different lesional sites of keloids. *Wound Repair Regen* 2008;16:254–65.
- Shen Y, Zhong L, Johnson S, Cao D. Human aldo-keto reductases 1B1 and 1B10: a comparative study on their enzyme activity toward electrophilic carbonyl compounds. *Chem Biol Interact* 2011;191:192–8.
- Shih B, Garside E, McGrouther DA, Bayat A. Molecular dissection of abnormal wound healing processes resulting in keloid disease. *Wound Repair Regen* 2010;18:139–53.
- Sidgwick GP, Bayat A. Extracellular matrix molecules implicated in hypertrophic and keloid scarring. *J Eur Acad Dermatol Venereol* 2012;26:141–52.
- Suarez E, Syed F, Rasgado TA, Walmsley A, Mandal P, Bayat A. Skin equivalent tensional force alters keloid fibroblast behavior and phenotype. *Wound Repair Regen* 2014;22:557–68.
- Supp DM, Hahn JM, McFarland KL, Glaser K. Inhibition of hyaluronan synthase 2 reduces the abnormal migration rate of keloid keratinocytes. *J Burn Care Res* 2014;35:84–92.
- Syed F, Ahmadi E, Iqbal SA, Singh S, McGrouther DA, Bayat A. Fibroblasts from the growing margin of keloid scars produce higher levels of collagen I and III compared with intralesional and extralesional sites: clinical implications for lesional site-directed therapy. *Br J Dermatol* 2011;164:83–96.
- Tabata C, Kadokawa Y, Tabata R, Takahashi M, Okoshi K, Sakai Y, et al. All-trans-retinoic acid prevents radiation- or bleomycin-induced pulmonary fibrosis. *Am J Respir Crit Care Med* 2006;174:1352–60.
- Takemura M, Endo S, Matsunaga T, Soda M, Zhao HT, El-Kabbani O, et al. Selective inhibition of the tumor marker aldo-keto reductase family member 1B10 by oleanolic acid. *J Nat Prod* 2011;74:1201–6.
- Tan KT, Shah N, Pritchard SA, McGrouther DA, Bayat A. The influence of surgical excision margins on keloid prognosis. *Ann Plast Surg* 2010;64:55–8.
- Tang XH, Gudas LJ. Retinoids, retinoic acid receptors, and cancer. *Annu Rev Pathol* 2011;6:345–64.
- Trisliana Perdanasari A, Lazzeri D, Su W, Xi W, Zheng Z, Ke L, et al. Recent developments in the use of intralesional injections keloid treatment. *Arch Plast Surg* 2014;41:620–9.
- Tsuzura H, Genda T, Sato S, Murata A, Kanemitsu Y, Narita Y, et al. Expression of aldo-keto reductase family 1 member b10 in the early stages of human hepatocarcinogenesis. *Int J Mol Sci* 2014;15:6556–68.
- Uchida G, Yoshimura K, Kitano Y, Okazaki M, Harii K. Tretinoin reverses upregulation of matrix metalloproteinase-13 in human keloid-derived fibroblasts. *Exp Dermatol* 2003;12(Suppl. 2):35–42.
- Ud-Din S, Bayat A. Strategic management of keloid disease in ethnic skin: a structured approach supported by the emerging literature. *Br J Dermatol* 2013;169(Suppl. 3):71–81.
- Ud-Din S, Thomas G, Morris J, Bayat A. Photodynamic therapy: an innovative approach to the treatment of keloid disease evaluated using subjective and objective non-invasive tools. *Arch Dermatol Res* 2013;305:205–14.
- van den Broek LJ, Limandjaja GC, Niessen FB, Gibbs S. Human hypertrophic and keloid scar models: principles, limitations and future challenges from a tissue engineering perspective. *Exp Dermatol* 2014;23:382–6.
- von Gise A, Zhou B, Honor LB, Ma Q, Petryk A, Pu WT. WT1 regulates epicardial epithelial to mesenchymal transition through beta-catenin and retinoic acid signaling pathways. *Dev Biol* 2011;356:421–31.
- Werner S, Brors B, Eick J, Marques E, Pogenberg V, Parret A, et al. Suppression of early hematogenous dissemination of human breast cancer cells to bone marrow by retinoic acid-induced 2. *Cancer Discov* 2015;5:506–19.
- Won JY, Nam EC, Yoo SJ, Kwon HJ, Um SJ, Han HS, et al. The effect of cellular retinoic acid binding protein-1 expression on the CYP26-mediated catabolism of all-trans retinoic acid and cell proliferation in head and neck squamous cell carcinoma. *Metabolism* 2004;53:1007–12.
- Woo YJ, Jang KL. All-trans retinoic acid activates E-cadherin expression via promoter hypomethylation in the human colon carcinoma HCT116 cells. *Biochem Biophys Res Commun* 2012;425:944–9.
- Xia W, Phan TT, Lim JJ, Longaker MT, Yang GP. Complex epithelial-mesenchymal interactions modulate transforming growth factor-beta expression in keloid-derived cells. *Wound Repair Regen* 2004;12:546–56.
- Xu X, Chai S, Wang P, Zhang C, Yang Y, Yang Y, et al. Aldehyde dehydrogenases and cancer stem cells. *Cancer Lett* 2015;369:50–7.
- Yan L, Cao R, Wang L, Liu Y, Pan B, Yin Y, et al. Epithelial-mesenchymal transition in keloid tissues and TGF-beta1-induced hair follicle outer root sheath keratinocytes. *Wound Repair Regen* 2015;23:601–10.

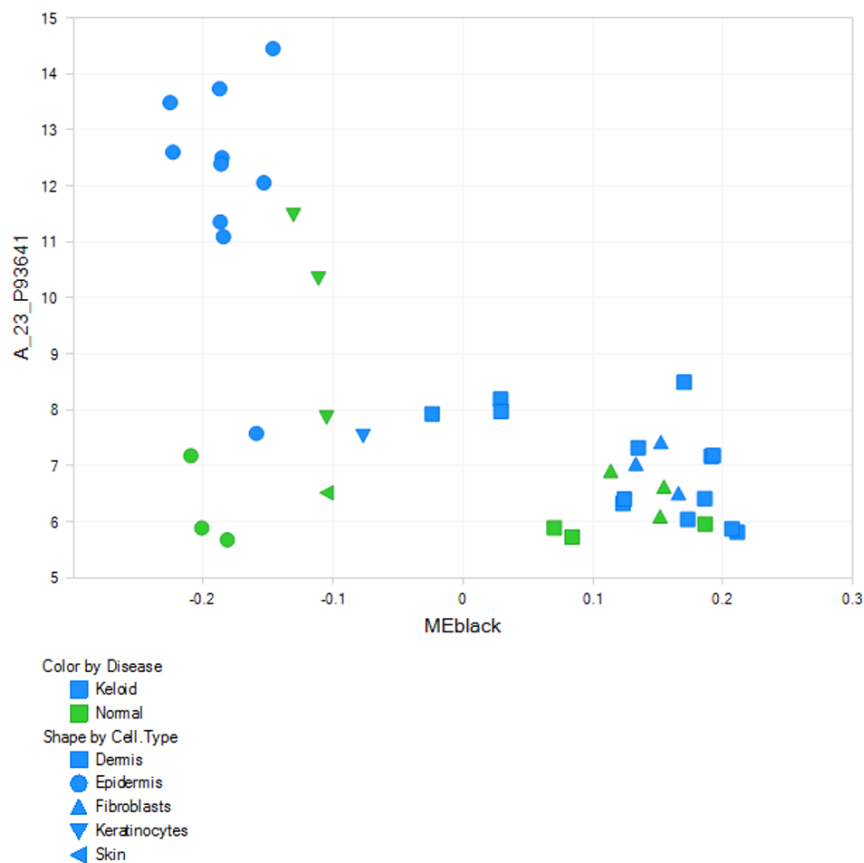
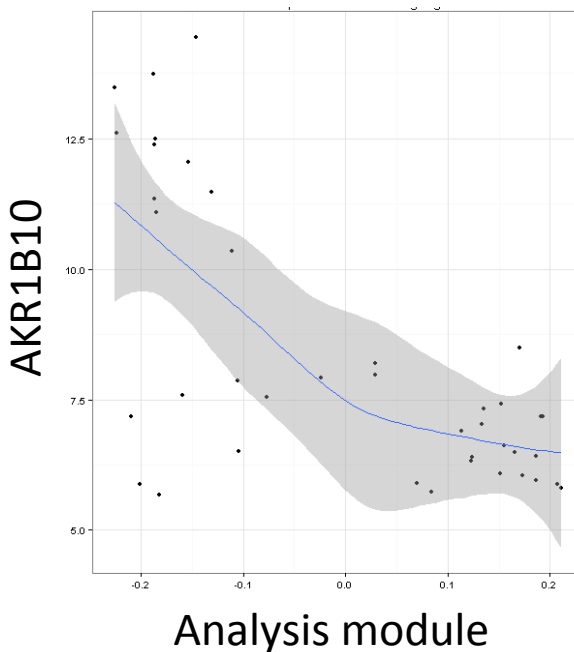
- Yan R, Zu X, Ma J, Liu Z, Adeyanju M, Cao D. Aldo-keto reductase family 1 B10 gene silencing results in growth inhibition of colorectal cancer cells: implication for cancer intervention. *Int J Cancer* 2007;121:2301–6.
- Yazdi AS, Ghoreschi K, Sander CA, Rocken M. Activation of the mitogen-activated protein kinase pathway in malignant melanoma can occur independently of the BRAF T1799A mutation. *Eur J Dermatol* 2010;20:575–9.
- Yoshitake H, Takahashi M, Ishikawa H, Nojima M, Iwanari H, Watanabe A, et al. Aldo-keto reductase family 1, member B10 in uterine carcinomas: a potential risk factor of recurrence after surgical therapy in cervical cancer. *Int J Gynecol Cancer* 2007;17:1300–6.
- Zaitseva M, Vollenhoven BJ, Rogers PA. Retinoids regulate genes involved in retinoic acid synthesis and transport in human myometrial and fibroid smooth muscle cells. *Hum Reprod* 2008;23:1076–86.
- Zang Y, Wang T, Xie W, Wang-Fischer YL, Getty L, Han J, et al. Regulation of acetyl CoA carboxylase and carnitine palmitoyl transferase-1 in rat adipocytes. *Obes Res* 2005;13:1530–9.
- Zhang C, Kong X, Ning G, Liang Z, Qu T, Chen F, et al. All-trans retinoic acid prevents epidural fibrosis through NF-kappaB signaling pathway in post-laminectomy rats. *Neuropharmacology* 2014;79:275–81.
- Zhang Q, Oh CK, Messadi DV, Duong HS, Kelly AP, Soo C, et al. Hypoxia-induced HIF-1 alpha accumulation is augmented in a co-culture of keloid fibroblasts and human mast cells: involvement of ERK1/2 and PI-3K/Akt. *Exp Cell Res* 2006;312:145–55.
- Zhang W, Li H, Yang Y, Liao J, Yang GY. Knockdown or inhibition of aldo-keto reductase 1B10 inhibits pancreatic carcinoma growth via modulating Kras-E-cadherin pathway. *Cancer Lett* 2014;355:273–80.
- Zhang W, Wang L, Zhang L, Chen W, Chen X, Xie M, et al. Synthesis and biological evaluation of steroidal derivatives as selective inhibitors of AKR1B10. *Steroids* 2014;86:39–44.
- Zhong L, Shen H, Huang C, Jing H, Cao D. AKR1B10 induces cell resistance to daunorubicin and idarubicin by reducing C13 ketonic group. *Toxicol Appl Pharmacol* 2011;255:40–7.
- Zhou TB, Drummen GP, Qin YH. The controversial role of retinoic acid in fibrotic diseases: analysis of involved signaling pathways. *Int J Mol Sci* 2012;14:226–43.
- Zouboulis CC. Retinoids—which dermatological indications will benefit in the near future? *Skin Pharmacol Appl Skin Physiol* 2001;14:303–15.

## Supplementary Material to Chapter 5

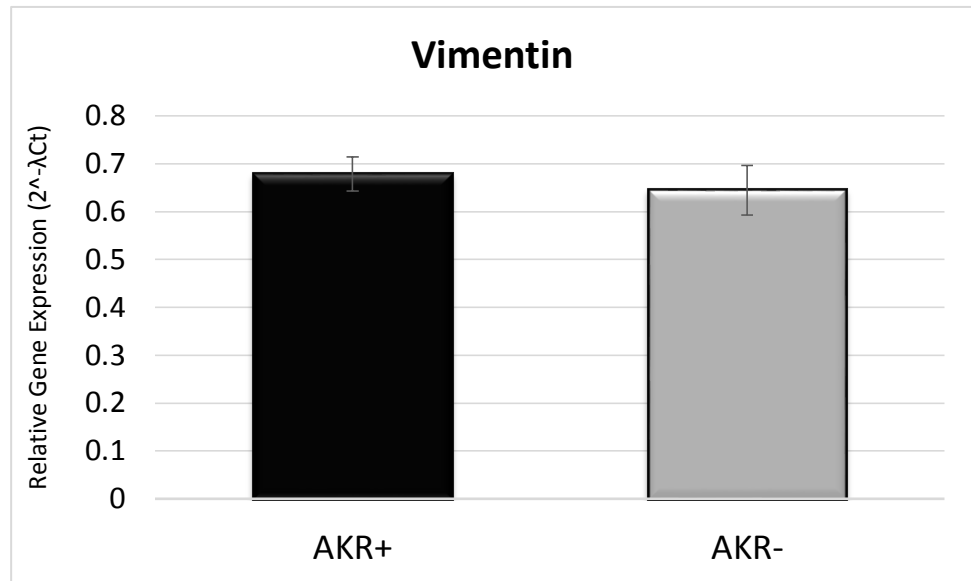
**Supplementary Figure S1** – qRT-PCR validation of relevant genes from the RA pathway found to be dysregulated in microarray data. The left column contains qRT-PCR data and the corresponding microarray graph is on the right. Data are the mean  $\pm$  SEM; \* $p$  < 0.05, students t-test analysis.



**Supplementary Figure S2** – Correlation plot showing negative correlation of AKR1B10 to analysis module with a strong remodelling component via TGF $\beta$  and Wnt signalling using MetaCore enrichment analysis output modules. The plot below illustrates the interpretation of the dots from the one above.



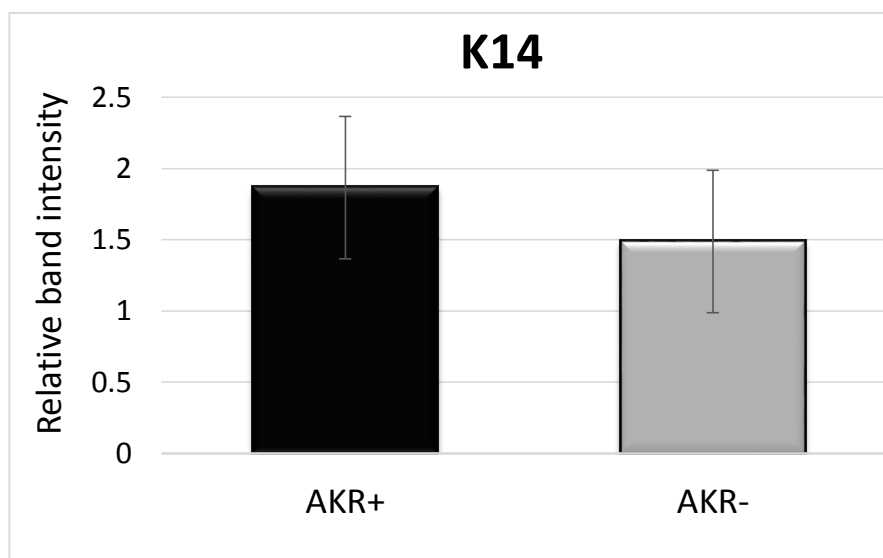
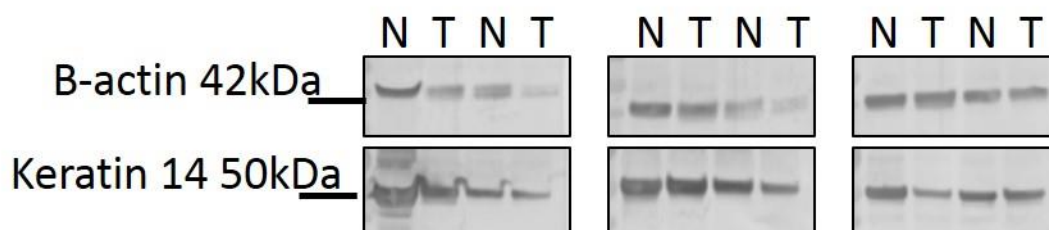
**Supplementary Figure S3** – qRT-PCR for vimentin in AKR1B10-transfected vs non-transfected keratinocytes ( $p = 0.5887$ ). Data are the mean  $\pm$  SEM;  $*p < 0.05$ , Students t-test analysis.



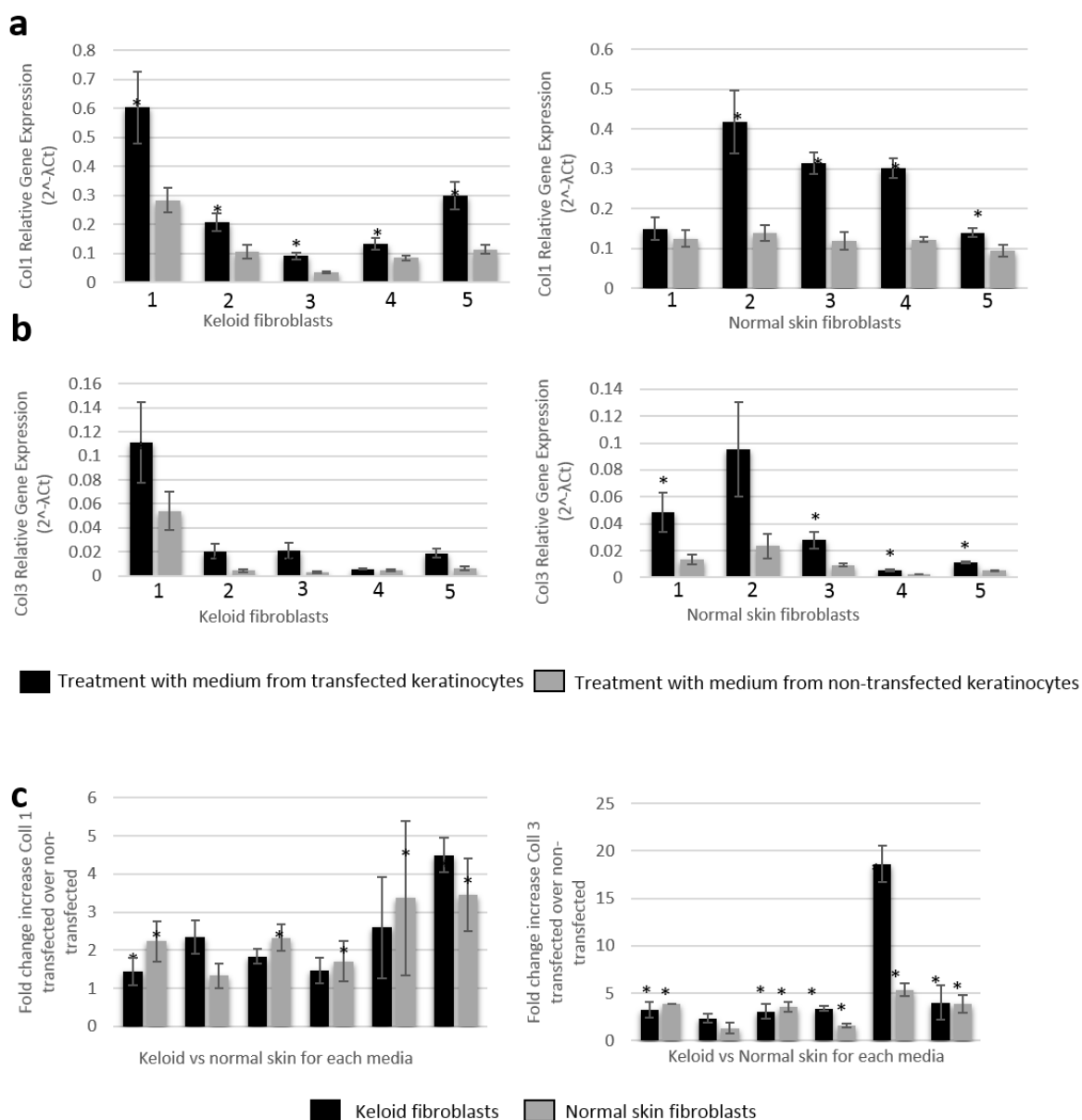
■ AKR1B10 positive    ■ AKR1B10 negative



**Supplementary Figure S4** – Western blot of keratin 14 in transfected and non-transfected samples, where **N** represents the non-transfected cell band and **T** represents the transfected cells protein band. The relative band intensity was quantified using Image J and is shown below ( $n = 4$ ).

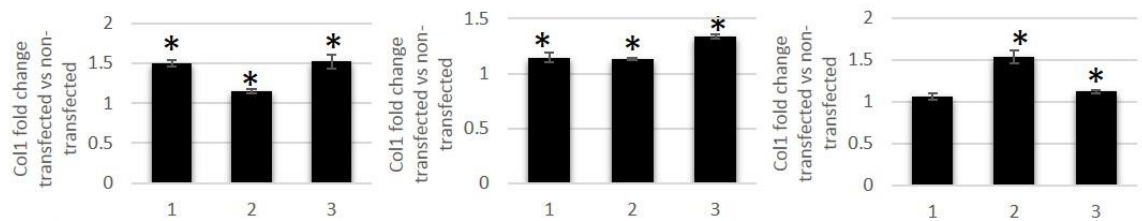


**Supplementary Figure S5 – Collagen I & III gene expression. A)** Relative gene expression of collagen I for keloid and normal skin fibroblasts treated with conditioned media of AKR1B10-transfected vs non-transfected keratinocytes. **B)** Relative gene expression of collagen III for keloid and normal skin fibroblasts treated with conditioned media of AKR1B10-transfected vs non-transfected keratinocytes. **C)** Fold change increase in keloid and normal skin fibroblast expression of collagens I & III for  $n = 6$  transfected vs non-transfected media. Data are the mean  $\pm$  SEM; \* $p < 0.05$ , Students t-test analysis.

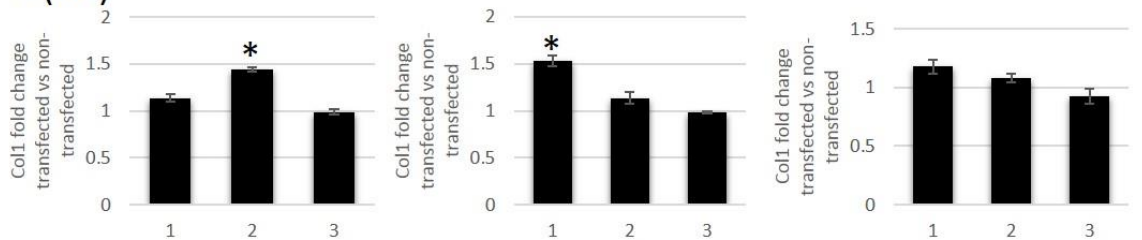


**Supplementary Figure S6** – In-cell western results for each keloid and normal skin fibroblast patient for collagen I & III. Graphs represent fold change for each patient treated with the medium of AKR1B10-transfected vs non-transfected keratinocytes. Data are the mean  $\pm$  SEM; \* $p < 0.05$ , Students t-test analysis.

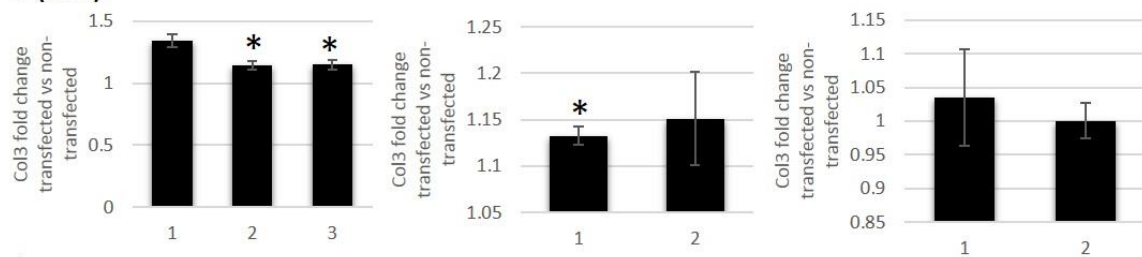
**a (KD)**



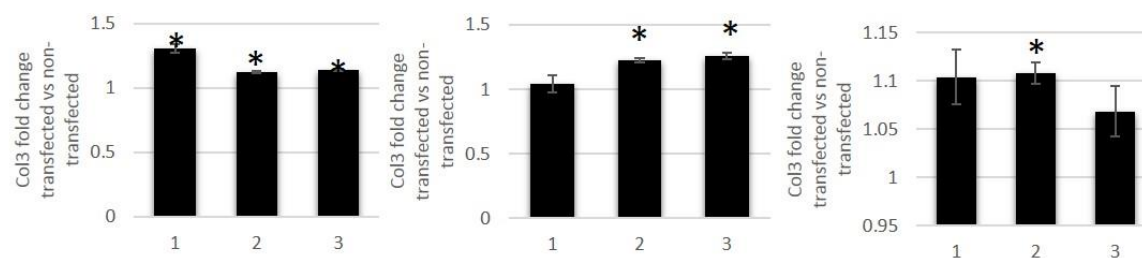
**b (NS)**



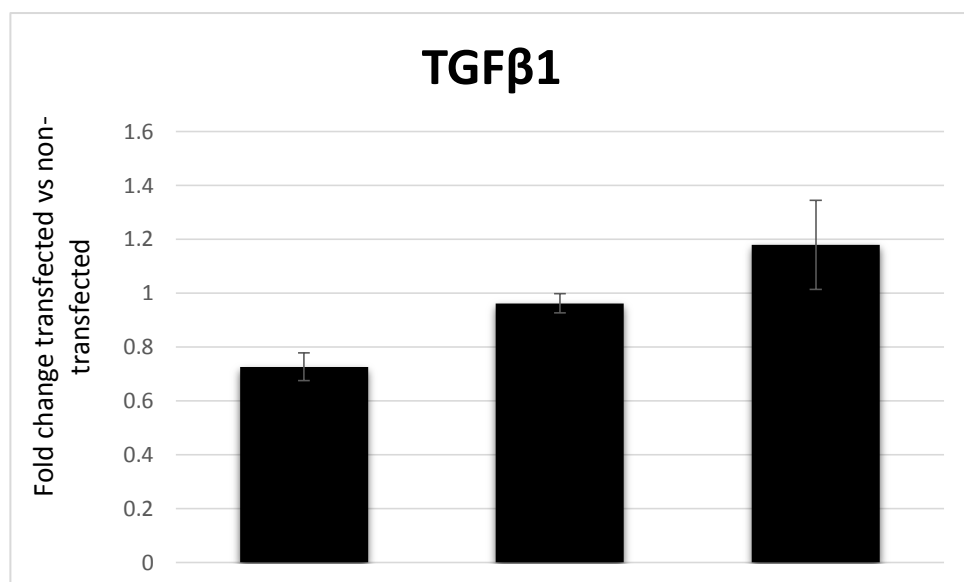
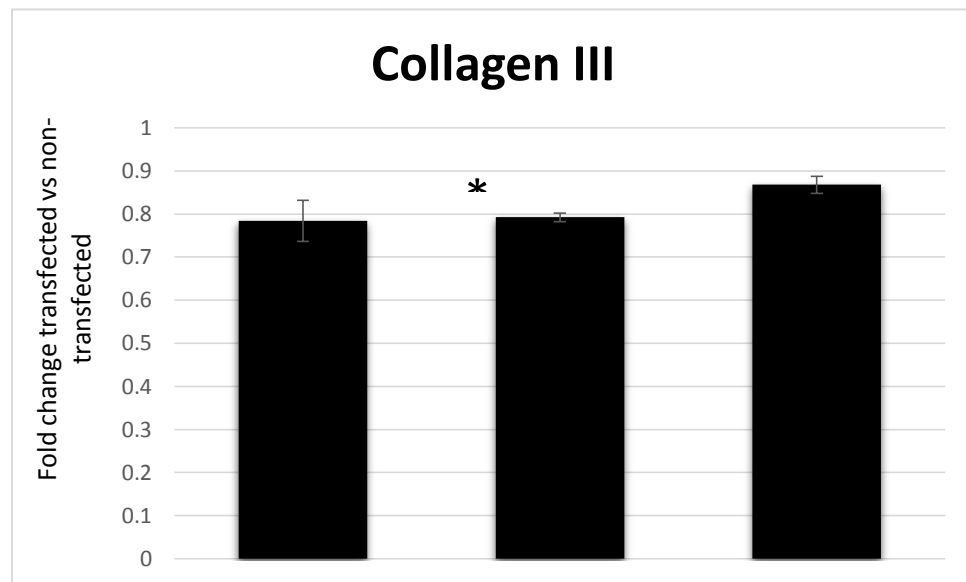
**c (KD)**



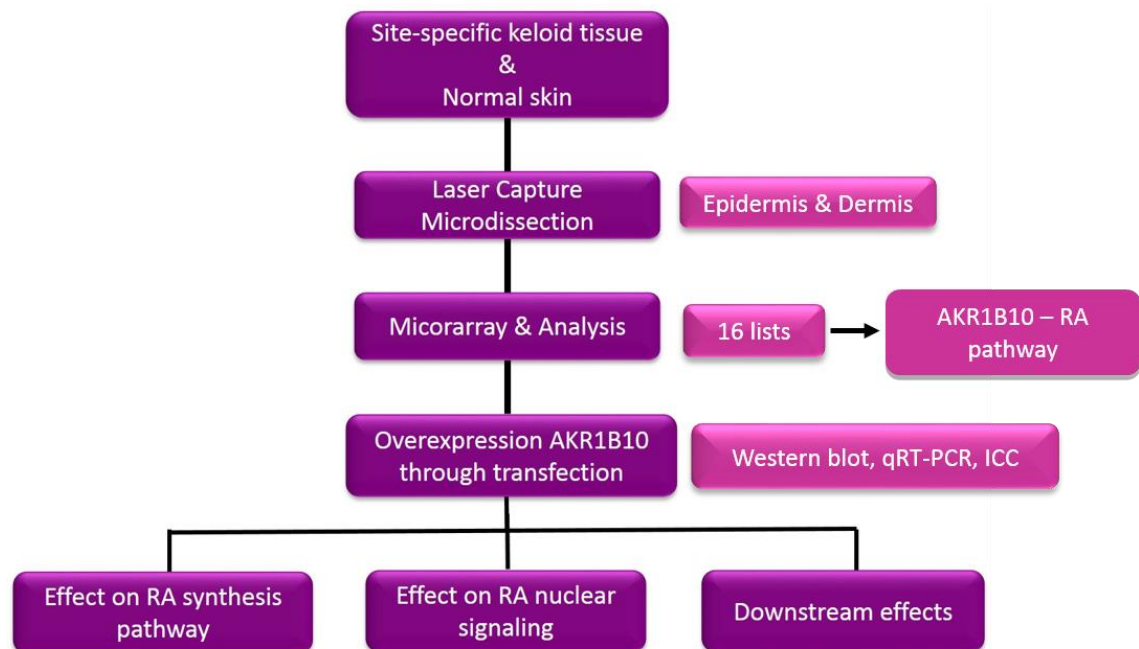
**d (NS)**



**Supplementary Figure S7** – Quantitative data graphs for in-cell western performed on keloid fibroblasts. The graphs show expression of collagen III and TGF $\beta$ 1 for keloid fibroblasts following 24hrs incubation in 1 $\mu$ M atRA. Graphs represent fold change of transfected vs non-transfected expression. Data are the mean  $\pm$  SEM; \* $p$  <0.05, Students t-test analysis.



**Supplementary Figure S8** – Flow chart depicting summary in chronological order of experimental process and results leading to identification of RA in keloid and how this was investigated.



## Supplementary Tables

Supplementary Table S1 – Microarray expression of genes relevant to this study.

Agilent Probe ID	Ref Sequence	Gene symbol	Site within lesion	Fold change	p-value
A_24_P129341	NM_020299.4	AKR1B10	Centre epidermis	75.56	1.19E-06
A_24_P129341	NM_020299.4	AKR1B10	Margin epidermis	64.69	5.85E-06
A_24_P129341	NM_020299.4	AKR1B10	Extralesional epidermis	86.03	2.14E-06
A_23_P258190	NM_001628.2	AKR1B1	Centre epidermis	14.3	0.0022
A_23_P258190	NM_001628.2	AKR1B1	Margin epidermis	8.94	0.0148
A_23_P258190	NM_001628.2	AKR1B1	Extralesional epidermis	10.57	0.0093
A_33_P3380992	NM_001080538.2	AKR1B15	Centre epidermis	22.25	8.55E-06
A_33_P3380992	NM_001080538.2	AKR1B15	Margin epidermis	16.02	9.22E-05
A_33_P3380992	NM_001080538.2	AKR1B15	Extralesional epidermis	21.68	2.44E-05
A_23_P92562	NM_001166504.1	ADH7	Margin epidermis	8.77	0.001
A_23_P83098	NM_000689.4	ALDH1a1	Centre epidermis	22.96	0.0008
A_23_P83098	NM_000689.4	ALDH1a1	Margin epidermis	31.49	0.0006
A_23_P83098	NM_000689.4	ALDH1a1	Extralesional epidermis	15.12	0.0048
A_23_P115064	NM_001878.3	CRABP2	Centre epidermis	3.17	0.0279
A_33_P3326483	NM_004378.2	CRABP1	Centre epidermis	-7.16	0.0255
A_33_P3326483	NM_004378.2	CRABP1	Extralesional epidermis	-8.25	0.025
A_23_P210109	NM_019885.3	CYP26B1	Centre epidermis	-4.87	0.0092
A_23_P210109	NM_019885.3	CYP26B1	Margin epidermis	-13.21	0.0002
A_23_P76249	NM_005555	KRT6B	Centre epidermis	146.02	0.0006
A_23_P76249	NM_005555	KRT6B	Margin epidermis	42.92	0.0105
A_23_P76249	NM_005555	KRT6B	Extralesional epidermis	18.67	0.0411
A_24_P402438	NM_001135599.2	TGFβ2	Centre epidermis	-2.57	0.1386

A_24_P402438	NM_001135599.2	TGF $\beta$ 2	Margin epidermis	-3.78	0.0542
A_24_P402438	NM_001135599.2	TGF $\beta$ 2	Extralesional epidermis	-2.42	0.1915
A_33_P3313825	NM_001024847.2	TGF $\beta$ R2	Centre epidermis	-1.99	0.05525
A_33_P3313825	NM_001024847.2	TGF $\beta$ R2	Margin epidermis	-2.58	0.0145
A_33_P3313825	NM_001024847.2	TGF $\beta$ R2	Extralesional epidermis	-1.76	0.1306

**Supplementary Table S2** – Demographic data of samples used in this study.

No.	Tissue type	Gender, Age	Ethnicity	Time present	Previous Treatment	Location of keloid
1	Keloid	F, 42yrs	Israeli	7-8 yrs	Nil	Left shoulder
2	Keloid	F, 25 yrs	Ethiopian	18 mnths	Nil	Right shoulder
3	Keloid	F, 19 yrs	Caucasian	2-3 yrs	Nil	Left ear helix
4	Keloid	F, 30 yrs	Caucasian	8 yrs	Nil	Central sternum
5	Keloid	F, 32 yrs	Caucasian	13 yrs	Radiation, steroid, silicone	Breasts bilaterally
6	Keloid	F, 41 yrs	Israeli	6 yrs	Steroid, silicone	Left deltoid
7	Keloid	F, 18yrs	Jamaican Afrocarribean	1 yr	none	Bilateral ear lobes
8	Keloid	M, 23yrs	Jamaican Afrocarribean	4 yrs	none	Bilateral ear lobes
9	Keloid	F, 27yrs	Jamaican Afrocarribean	2 yrs	Surgery	Right ear lobe
10	Keloid	M, 20yrs	Jamaican Afrocarribean	2 yrs	Surgery	Chin
11	Keloid	F, 19yrs	Jamaican Afrocarribean	2 yrs	Surgery	Sternum
12	Keloid	F, 41yrs	Jamaican Afrocarribean	6 yrs	None	Sternum
13	Keloid	M, 20yrs	Jamaican Afrocarribean	15 yrs	None	Right ear lobe
14	Keloid	F, 22yrs	Jamaican Afrocarribean	3 yrs	None	Bilateral ear lobes
15	Normal skin	F, 57yrs	Caucasian	-	-	Facelift & blepharoplasty



16	Normal skin	M, 47yrs	Caucasian	-	-	Abdominoplasty
17	Normal skin	F, 19yrs	Caucasian	-	-	Bilateral breast reduction
18	Normal skin	F, 26yrs	Caucasian	-	-	Abdominoplasty
19	Normal skin	F, 41yrs	Caucasian	-	-	Abdominoplasty
20	Normal skin	F, 43yrs	Caucasian	-	-	Bilateral breast reduction
21	Normal skin	F, 43yrs	Caucasian	-	-	Bilateral breast reduction
22	Normal skin	F, 34yrs	Caucasian	-	-	Abdominoplasty
23	Normal skin	F, 47yrs	Caucasian	-	-	Mastopexy
24	Normal skin	F, 20yrs	Caucasian	-	-	Bilateral breast reduction
25	Normal skin	F, 42yrs	Caucasian	-	-	Bilateral breast reduction
26	Normal skin	F, 56yrs	Caucasian	-	-	Abdominoplasty
27	Normal skin	F, 51yrs	Caucasian	-	-	Abdominoplasty

**Supplementary Table S3** – Details of primers used for qRT-PCR.

<b>Gene</b>	<b>Forward primer</b> <b>Reverse primer</b>	<b>Accession number</b> <b>(Roche Diagnostics, UK)</b>	<b>Amplicon</b> <b>size (bp)</b>
AKR1B10	aaagcaacgttcttgatgc tggaagtggtgaaattgg	cat. no. 04686900001	95
AKR1B1	ttttccattggatgagtcg ccttcatccaccagctctt	cat. no. 04688082001	91
AKR1B15	ggaaaaggaacgttcttggga cctctcgatctggaagtgg	cat. no. 04686993001	108
ALDH1a1	tgtagctgatgccgacttg ctggatcggctatacaaca	cat. no. 04689046001	91
CRABP2	tgcgaccacagagattaac tccatttcaccaggctct	cat. no. 04688678001	91
CRABP1	cagcgagaatttcgacgag tagaactgatccccgtcctg	cat. no. 04688961001	120
CYP26B1	acatccaccgcaacaagc ggatcttggcaggtactct	cat. no. 04688007001	78
RAR, gamma	cattggctccctgtgtctc gggtagaggggatgtaaac	cat. no. 04688538001	74
LRAT	tgctttagcactggtctcac tggggaatgagacggataag	cat. no. 04689062001	66
STRA6	ctatggcagctggtacatcg tatgctggtgtggcagga	cat. no. 04686926001	85
CRBP1	aggcatagatgaccgcaagt acccttctgcacacactgg	cat. no. 04687663001	73
TGFβ1	actgcaagtggacatcaacg ggccatgagaagcaggaa	cat. no. 04688104001	94
TGFβ2	gagagcgcaagtgaagagg tccctagaccgtcaggctaa	cat. no. 0468854001	62
TGFβ3	agtcagacacaaccacag ggtcctccaacatagtacagg	cat. no. 04684974001	129
Keratin 14	cctctcccagtctctct atgacctgggtcggattt	cat. no. 04686926001	79
Keratin 6B	tctcagtcccacagctctca gaggacaagcaacctgagga	cat. no. 04688970001	66
Involucrin	accatcaggagcaaatgaa agctcgacaggcaccttct	cat. no. 04686896001	68
Filaggrin	ggactctgagaggcatctg tgctcccgagaagatccat	cat. no. 04687965001	60
E-cadherin	cccgggacaacgtttattac gctggctcaagtcaagtcc	cat. no. 04687680001	72

FGF7	aagtctagcacacagcacttgg agcattgcttcaggctcttatt	cat. no. 04685067001	71
CTGF	ccgtactccaaaatctcca ttagctcggatgtcttcatgc	cat. no. 04688945001	75
Collagen Ia1	agggtcaccgtggcttct tccagaggaccttgttcac	cat. no. 04689020001	77
Collagen III	ctggaccccagggtcttc gaccatctgatccagggttc	cat. no. 04686934001	78
GAPDH	agccacatcgctcagacac gcccaatacgaccaaattcc	cat. no. 04688589001	66
RPL32	gaagttcctggtccacaacg gagcgatctcggcacagta	cat. no. 04686900001	77

**Supplementary Table S4a** – Concentration, incubation parameters and detection method of primary and secondary antibodies used in this study for immunohistochemistry.

<b>Primary antibody, product code &amp; company</b>	<b>Primary ab raised species, isotype, concentration</b>	<b>Incubation details</b>	<b>Secondary ab, company, concentration, incubation</b>	<b>Detection method</b>
AKR1B10, ab192865 [EPR14421], Abcam	Rabbit (monoclonal), IgG, 1:500 dilution	4°C overnight	Universal antibody by Novolink™ Leica Biosystems, Newcastle Ltd. 1 hour room temp	Peroxidase NovaRED™ Vector®
AKR1B10, ab57547, Abcam	Mouse (monoclonal), IgG2a, 3µg/ml	4°C overnight	Alexa Fluor®488 goat anti-mouse IgG (green), Life technologies, 1:250 dilution, 1hr room temp	Fluorescence 1:500 DAPI
CRABP2, ab74365, Abcam	Rabbit (polyclonal), IgG, 1:100 dilution	4°C overnight	Alexa Fluor®546 goat anti-rabbit IgG (red), Life technologies, 1:250 dilution, 1hr room temp	Fluorescence, DAPI 1:500
AKR1B10, ab192865 [EPR14421], Abcam	Rabbit (monoclonal), IgG, 1:50 dilution	4°C overnight	Alexa Fluor®488 goat anti-mouse IgG (green), Life technologies, 1:250 dilution, 1hr room temp	Fluorescence Immunocytochemistry

**Supplementary Table S4b** - Concentration, incubation parameters and detection method of primary and secondary antibodies used in this study for western blotting.

Primary antibody, product code & company	Primary ab raised species, isotype, concentration	Incubation details	Secondary ab, company, concentration, incubation	Detection method
B-actin, ab8227, Abcam	Rabbit (polyclonal), IgG, 1:800 dilution	4°C overnight	Goat IgG conjugated to alkaline phosphatase, ab97048, Abcam 1:2000 dilution 1hr room temp	NBT/BCIP
AKR1B10, ab192865 [EPR14421], Abcam	Rabbit (monoclonal), IgG, 1:5000 dilution	4°C overnight	Goat IgG conjugated to alkaline phosphatase, ab97048, Abcam 1:2000 dilution 1hr room temp	NBT/BCIP
Keratin 14, ab7800 [LL002], Abcam	Mouse (monoclonal), IgG3, 2µg/ml dilution	4°C overnight	Goat IgG conjugated to alkaline phosphatase, ab97048, Abcam 1:2000 dilution 1hr room temp	NBT/BCIP

**Supplementary Table S4c** - Concentration, incubation parameters and detection method of primary and secondary antibodies used in this study for in-cell western.

<b>Primary antibody, product code &amp; company</b>	<b>Primary ab raised species, isotype, concentration</b>	<b>Incubation details</b>	<b>Secondary ab, company, concentration, incubation</b>	<b>Detection method</b>
Collagen I, ab34710, Abcam	Rabbit (polyclonal), IgG, 1:500 dilution	4°C overnight	IRDye® 800CW goat anti- rabbit, Li-Cor, 1:800 dilution, 1hr room temp	In-cell western fluorescence
Collagen III, ab6310 [FH-7A], Abcam	Mouse (monoclonal), IgG1, 1:300 dilution	4°C overnight	IRDye® 800CW goat anti- mouse, 1:800 dilution, 1hr room temp	In-cell western fluorescence
TGFβ1, ab27969 [TB21], Abcam	Mouse (monoclonal), IgG1, 1: 200 dilution	4°C overnight	IRDye® 800CW goat anti- mouse, 1:800 dilution, 1hr room temp	In-cell western fluorescence

## Supplementary Materials and Methods

### Laser Capture Microdissection (LCM)

LCM is a platform combining an inverted light microscope to a high-precision ultraviolet laser enabling isolation of single cells or cell subpopulations from within a tissue section [1, 2]. Both keloid and normal skin biopsies were cryosectioned (Leica CM3050S) in 8µm thick sections onto polyethylene naphthalate (PEN) membrane slides (Carl Zeiss, UK) and stored at -80°C until the day of LCM. In order to preserve the RNA integrity the slides were stained immediately prior to capture using cresyl violet in an RNase-free class II safety cabinet. The slides were taken from frozen and placed into successive slide chambers using the following procedure:

1. 95% (v/v) ethanol (40 seconds)
2. 75% (v/v) ethanol (30 seconds)
3. 50% (v/v) ethanol (30 seconds)
4. 1 minute in 300µl cresyl violet (Ambion, UK)
5. 50% (v/v) ethanol (30 seconds)
6. 75% (v/v) ethanol (30 seconds)
7. 95% (v/v) ethanol (30 seconds)
8. 100% ethanol twice for one minute each.

The slides were air dried and taken for LCM using Carl Zeiss P.A.L.M MicroBeam LCM 4.2 fitted with an inverse microscope Axiovert 200 resp. 200M. Using the P.A.L.M. RoboSoftware the epidermis was easily discernible from the dermis and several elements from at least three epidermal sections of each biopsy were captured and pooled in an Eppendorf containing buffer 200ul RLT (Qiagen, UK) and 2-mercaptoethanol (Sigma-Aldrich, UK) in a ratio of 100:1. Images

were taken before and after each capture to confirm elements were present. These samples were RNA extracted and amplified before microarray.

### **RNA isolation of tissue and cells, cDNA synthesis and qRT-PCR**

#### *Tissue samples*

This took place in an RNase-free class II safety cabinet. The tissue sample was put in a 2ml round bottom Eppendorf containing trizol (Life technologies, UK) with a sterile ball bearing and homogenised in a Qiagen tissue lyser for three four minute cycles of 30 oscillations per second. Chloroform, at 0.2ml per 1ml of trizol, was added to the tube and shaken vigorously for 15 seconds before centrifugation at  $>10,000 \times g$  for 15 minutes. The upper aqueous layer, which contains the RNA, was pipetted off the surface and transferred to a new Eppendorf. An equal volume (1:1) of 70% (v/v) ethanol was added to the Eppendorf and mixed using a pipette. This mixture is then transferred to an RNeasy mini spin column (Qiagen, UK) and centrifuged at  $>10,000 \times g$  for 30 seconds. The elute was discarded from the collection tube, 700 $\mu$ l of buffer RW1 added to the spin column and centrifugation repeated. Following this a new collection tube was used for three cycles of 500 $\mu$ l buffer RPE at  $> 10,000 \times g$  for 30 seconds, 30 seconds and two minutes respectively. A one-minute dry cycle spin was conducted and the spin column transferred to a new tube for the collection of the RNA yield. 30 $\mu$ l of RNase-free water was added directly to the silica gel membrane and then centrifuged for one minute at  $>10,000 \times g$ . The yield was then quantified using a NanoDrop spectrophotometer (Thermo Scientific, UK).

#### *Monolayer cells*

The cells were trypsinised, pelleted and then resuspended in lysis buffer (RLT: 2-mercaptoethanol, 100:1). The volume was dependent on number of cells present. An equal volume (1:1) of 70% (v/v) ethanol was added to each tube and mixed thoroughly by pipetting



up and down. The mixture was then added to a Qiagen spin column and centrifuged at  $> 10,000$  x g for 30 seconds. The flow-through was discarded, 350 $\mu$ l of buffer RW1 added and centrifugation repeated. An intervening DNase step was performed with 80 $\mu$ l incubation over 15 minutes at room temperature. A further 350 $\mu$ l of RW1 was added and centrifugation repeated. Following this a new collection tube was used for three cycles of 500 $\mu$ l buffer RPE at  $> 10,000$  x g for 30 seconds, 30 seconds and two minutes respectively. A one minute dry cycle spin was conducted and the spin column transferred to a new tube for the collection of the RNA yield. 30 $\mu$ l of RNase-free water was added directly to the silica gel membrane and then centrifuged for one minute at  $>10,000$  x g. The yield was then quantified using a NanoDrop spectrophotometer (Thermo Scientific, UK).

*Note:* In cases where a low yield was predicted i.e for LCM captures the RNeasy Micro kit was used (Qiagen, UK).

#### *cDNA & qRT-PCR*

The RNA was normalised for all the samples and cDNA synthesis was performed using qScript™ cDNA SuperMix (Quanta Biosciences, MD, UK). Quantitative polymerase chain reactions were done in real time using the LightCycler®480 II platform (Roche Diagnostics, UK). Each reaction was carried out in a 96-well plate with a final volume of 10 $\mu$ l containing 4 $\mu$ l diluted normalised cDNA, 5 $\mu$ l LightCycler®480 probes master mix, 0.2 $\mu$ M forward and reverse primers, 0.1 $\mu$ l probe from Roche Universal Probe Library and 0.5 $\mu$ l nuclease-free water (Qiagen, UK). Each reaction was performed in triplicate and 2 housekeeping genes were used to allow relative quantification (GAPDH and RPL32). The cycle initiated at 95°C for 10 minutes to activate the Hot-Start Taq polymerase and then each of the 40 amplification cycles consisted of a 10 second denaturation step at 95°C followed by a 30 second annealing and elongations step at 60°C and finally a cooling step at 40°C. The fluorescence intensity is recorded prior to the cooling step. The amplified

targets were analysed using the LightCycler® 480 II software (1.5.0 SP3, Roche, UK). Details of primer sequences are in **Supplementary Table S3**.

### **RNA amplification and purification**

The instructions from Ovation® Pico WTA system v2 kit (NuGen Technologies) were adhered to exactly for RNA amplification and cDNA synthesis. In brief, samples were diluted to ensure concentrations were 500pg and 50ng using RNase-free water (Qiagen, UK). For primer annealing, 5µl of RNA from each sample was heated to 65°C for two minutes. Then for first strand cDNA synthesis the sample was added to the first strand buffer and enzyme mix (mixture of random and oligodT primers) before placing in a pre-cooled thermal cycler and then put through: 4°C – 2min, 25°C – 30min, 42°C – 15min, 70°C – 15min and returned to 4°C. The resulting sample was mixed with second strand buffer and enzyme mix (cDNA) to synthesise the second strand and placed in a thermal cycler: 4°C – 1min, 25°C – 10min, 50°C – 30min, 80°C – 20min and returned to 4°C. The resultant cDNA cleanup was then performed using a bead purification process (Agencourt® RNAClean® XP Purification Beads) prior to amplification. This was achieved using a magnet block and several 70% ethanol washes. The SPIA (single primer isothermal amplification) step elutes the cDNA from the beads using a DNA polymerase and RNase H in an isothermal assay put through thermal cycling: 4°C – 1min, 47°C – 75min, 95°C – 5min, return to 4°C. The final 100µl volume was then purified using QIAquick PCR purification kit (Qiagen, UK). The resultant elute was measured with NanoDrop (ThermoScientific, UK) using ssDNA setting.

### **Microarray**

This was done using SureTag DNA Labeling Kit, which forms part of Agilent Whole Genome (8 x 60K) Oligo Microarrays (Agilent Technologies, UK) containing 50,599 probes and is a one-colour

microarray-based gene expression analysis. Each sample was diluted to contain 1.8µg of cDNA in a final volume of 26µl. 5µl of random primer is added to the sample and incubated for 5 minutes at 95°C. They are then placed immediately in ice for 5 minutes and spun down in a centrifuge at 6000 x g for 1 minute. The cyanine 3 labeling master mix is prepared by mixing the sample with appropriate volumes of reaction buffer (10µl per reaction), 10 x dNTPs (5µl per reaction), cyanine 3-dUTP (3µl per reaction) and Exo (-) Klenow (1µl per reaction). This mix is then incubated at 37°C for 2 hours after which the samples are transferred to 65°C for 10 minutes to inactivate the enzyme. Samples are incubated on ice for 3 minutes and then centrifuged at 6000 x g for 1 minute.

The cDNA is purified following Cy3 labeling. 430µl of 1xTE (pH 8.0) is added to each sample in a purification column and spun for 10 minutes at 14,000 x g at room temperature. The flow-through is discarded and a further 480µl of 1xTE is added and again centrifuged at 14,000 x g for 10 minutes. The flow-through is discarded and the tube inverted into an Eppendorf and spun for 1 minute at 1,000 x g. The labelled cDNA sample is concentrated to dryness using a vacuum concentrator and resuspended in 21.5µl of 1xTE buffer. At this stage 1.5µl is placed in the NanoDrop (ThermoScientific, UK) to calculate the degree of labelling.

The labelled cDNA is prepared for hybridization by adding 10 x Gene Expression Blocking Agent (5µl per reaction) and 2 x Hi-RPM Hybridisation Buffer (25µl per reaction) then incubating at 95°C for 3 minutes before placing on ice. The samples were centrifuged briefly and 40µl of each sample was loaded onto a window of the 8-sample slide (SurePrint G3 Human GE 8x60K V2). The slides were hybridised at 65°C for 17 hours at 20 RPM before undergoing wash steps and storage in a cool dry ozone-free light-protected place. The slides were then scanned (Agilent DNA Microarray Scanner G2505c) and the data analysed following quantile normalisation.

### **Establishment of primary keratinocytes**

Tissue samples were washed first in PBS containing penicillin/streptomycin then cut into narrow strips approximately 1mm wide and 2cm long. This tissue was placed in a sterile falcon tube containing Dispase II (10mg/ml; Roche Diagnostics, UK) and incubated overnight in a 37°C water bath. Following incubation the epidermis was carefully separated from the dermis using a sterile scalpel and forceps. The epidermal strips were diced and carefully placed in TrypLE™Express (Invitrogen, UK) with serum-free keratinocyte media (Epilife®, Invitrogen Life Technologies, UK) for one hour in the water bath, with intermittent vigorous shaking to release the cells until the suspension was murky. Trypsin neutralising solution (Invitrogen, UK), equal in amount to the trypsin, was added and the cell-solution mixture and centrifuged at 1300 rpm for 8 minutes. The supernatant was discarded and the cells resuspended in complete defined SFKM using gentle, repeated pipetting to ensure a homogenised cell suspension. This was then seeded into T25 collagen1-coated CellBind (Corning, UK) culture flasks containing 4mls of SFKM. The flasks were then incubated undisturbed for 48 hours. Following this the cell culture media was changed every 48 hours until 80% confluent. Only keratinocytes from passage 2-4 were used in all experiments.

### **Keratinocyte Transfection**

In advance the AKR1B10-containing plasmid was transformed into a DH5a E. coli strain to scale up and the purified DNA NanoDrop checked for purity and gel-checked. The day prior to transfection primary normal skin keratinocytes were seeded in SFKM (Epilife®, Invitrogen Life Technologies, UK) at  $1 \times 10^6$  cells per well in a collagen-coated 6-well plate. This achieved a confluency of 80-90%, which is ideal for transfection using Turbofectin 8.0 (Origene, USA). Following an optimisation step, 3µg of the AKR1B10 cloned into pCMV6-XL5 vector (Origene TrueClone®, USA) was used per well. The Turbofectin 8.0 was added in a ratio of 1:2, at 6µl per well of a 6-well plate.

To 100µl of serum-free OptiMEM® (Life Technologies, UK) 6µl of transfection reagent (Turbofectin 8.0) was added and incubated at room temperature for 5 minutes. The plasmid was then added and gently pipette-mixed before incubating at room temperature for 20 minutes. The media in the 6-well plate was replaced with fresh SFKM and the transfection mixture added dropwise. The plate was gently rocked and left in the incubator at 37°C/5%CO<sub>2</sub> for 24 hours. For those keratinocytes used to determine effect of AKR1B10 overexpression on the RA pathway and downstream conditioned media experiments, the media was replaced with fresh SFKM at 24 hours for a further 24 hours. These cells were then harvested, under dimmed light, for western blot and qRT-PCR.

#### **Dual luciferase assay and analysis**

Similar to the forward transfection, primary normal skin keratinocytes were seeded at 5 x 10<sup>4</sup> cells per well of a 96-well opaque collagen-coated white plate the day before transfection. A clear 96-well plate was seeded simultaneously to allow assessment of cell confluence and viability following transfection. The following day the transfection mixture was prepared as above. Per well of a 96 well plate 0.3µl of transfection reagent (Turbofectin 8.0 (Origene, USA)) was added to 5µl of OptiMEM® and incubated for 5 minutes. 150ng/well of AKR1B10 plasmid was added to this and incubated at room temperature for a further 20 minutes. The mixture was added to freshly replaced 150µl SFKM in half of the wells for each patient. This was incubated at 37°C/5%CO<sub>2</sub> for 24 hours. At 24 hours the media was replaced with 125µ fresh SFKM and the RARE Signal dual luciferase reporter (SABioscience, Qiagen, UK) transfected using Attractene transfection reagent (Qiagen, UK). For each patient half of the wells are AKR1B10 positive and half negative. Of these each has RARE reporter transfected into 4 wells, negative control into 2 wells and positive control into one well. Per well 25µl of OptiMEM® is added to 0.6µl of Attractene and this is incubated for 5 minutes. 1µl of RARE reporter/negative control/positive control is then added and incubated for 20 minutes before being added to the

appropriate well of the 96-well plate. This is incubated at 37°C/5%CO<sub>2</sub> for 6 hours and then the media removed and replaced with 150µl fresh SFKM. After 24 hours the positive control well in the clear 96-well plate is checked for constitutive GFP fluorescence in the FITC channel of a phase contrast microscope (Olympus IX51 microscope; Olympus, UK). This confirms transfection is successful and the luciferase activity can be measured. Additional controls include non-transfected (with either plasmid) cells and empty wells.

The media is replaced with 75µl of SFKM and the Dual-Glo<sup>®</sup> Luciferase Assay System (Promega, UK) is used to measure luciferase *firefly* and *Renilla* activity. An equal volume (75µl) of Dual-Glo<sup>®</sup> Reagent is added to each well and left for 15 minutes to allow cell lysis. The *firefly* luminescence is then measured. (FLUOstar Optima, BMG Labtech)). Immediately afterwards 75µl of Dual-Glo<sup>®</sup> Stop&Glo<sup>®</sup> is added to each well and left for 15 minutes before reading *Renilla* luminescence.

For analysis the *firefly* reading is divided by *Renilla* readings to normalise for cell number. This is done for both RARE reporter cells and also the negative controls. The relative luciferase activity (RLA) is then measured by dividing the normalised RARE reporter value by the corresponding negative control to give a fold change increase over control.

### **Western blotting and analysis**

Keratinocytes were washed with phosphate buffered saline (PBS; Sigma-Aldrich) and then trypsinised using TrypLE™Express (Invitrogen, UK) and the corresponding neutraliser (Invitrogen, UK) added before pelleting at 1300 RPM for 8 minutes. The supernatant discarded and the pellet resuspended in radioimmunoprecipitation assay buffer (RIPA, Sigma-Aldrich), volume depending on number of cells. The RIPA buffer was supplemented with protease and phosphatase inhibitor cocktail (ThermoScientific, UK). The protein was then extracted using 5 freeze-thaw cycles including a 1.5 minute lysis step. The concentration was determined using

the bicinchoninic acid protein assay reagent kit (BCA; ThermoScientific, UK) and was plotted against a standard curve using bovine serum albumin (BSA).

An equal amount of protein (30 $\mu$ g) was denatured (NuPage sample buffer; ThermoScientific and 95°C heating x 5 minutes) and resolved on 4-12% Bis-Tris gels (Life Technologies) and electrophoresed according to the manufacturer's instructions. The protein was blotted onto polyvinylidene difluoride membranes (PVDF; Life Technologies) using iBlot Dry Blotting System (Life Technologies). Following transfer the PVDF membranes were incubated at room temperature in Odyssey® blocking buffer (LI-COR Biosciences, Cambridge, UK). Each membrane was then incubated in its respective primary antibody diluted in blocking buffer and rocked overnight at 4°C. The next day the membranes were washed in 1% tween (Fisher Bioreagents, UK) PBS before incubating in respective alkaline-phosphatase conjugated secondary antibodies at room temperature for 1 hour. Following washes the membrane was developed using one-step nitro blue tetrazolium/S-bromo-4-chloroindoxyl phosphate (NBT/BCIP; ThermoScientific). Each sample was blotted with its corresponding internal control ( $\beta$ -actin) each time. Antibodies are detailed in **Supplementary Table S4b**. To analyse the blots the percentage of band intensity was calculated by Image J (Fiji, 1.47t, NIH, USA). The band intensity for each target was divided by its own control and then compared with other samples using fold change.

### **In-cell western**

Both normal skin and keloid fibroblasts were seeded into a black opaque clear-bottom 96-well plate in 2%FBS DMEM the day before conditioned media addition. Media from both AKR1B10 transfected and non-transfected (6-well plates) keratinocytes was taken immediately after the first 24 hour incubation and added to a row each of the same fibroblast patient. This was repeated at 24 hours (48hour transfected). At 48 hours the plate was fixed for in-cell western blotting.

The media was removed and 150µl 4% formaldehyde (Sigma-Aldrich, UK) was added to each well for 20 minutes at room temperature. The cells were then permeabilised using 200µl of 0.1% Triton X-100 for 5 washes at 5 minutes each and subsequently blocked by adding 150µL Odyssey® (Li-Cor, Cambridge, UK) for 1.5 hours at room temperature with moderate shaking. 50µl of primary antibody in the listed concentration (**Supplementary Table S4c**) was added to each well and 50µl of blocking buffer to control wells. The plate was incubated at 4°C overnight and the next day washed with 1% tween PBS 5 times. All rabbit primary antibodies were stained with IRDye® 800CW goat anti-rabbit secondary antibody (1/800) (Li-Cor, UK) and the mouse with IRDye® 800CW goat anti-mouse (1/800). In addition, CellTag™ 700 stain was used to normalise for cell number. This was added to the diluted secondary antibody at 1/500 blocking buffer and the plate left at room temperature for 1 hour. The plate was protected from light from this point forward. Following a further wash with 0.1% tween PBS the plate was dried and scanned immediately.

For analysis the expression of each protein marker was normalised against the CellTag™ reading in the 700 channel (800/700nm ratio). The data was acquired with Odyssey software, exported and analysed in Excel (Microsoft, UK).

In-cell western was also completed for fibroblasts that had been treated with 1µM *all-trans* retinoic acid (atRA) (Sigma-Aldrich, UK) for 24 hours prior to fixation. The protocol was identical and the dilutions for atRA are described below.

#### **Reconstitution of *all-trans* retinoic (atRA) acid & *all-trans* retinol (vitamin A)**

For all experiments involving atRA and retinol the frozen aliquots from the following calculations were used and were kept in the dark:

atRA (Sigma-Aldrich 100mg) Molecular weight 300.4



*Stock solution*

100mg dissolved in 5ml 100% DMSO

$100/5 \times 300.4 = 0.0666M = 66,600\mu M$  (stored in aliquots at  $-20^{\circ}C$  light protected)

*Working solution 1 $\mu M$* 

$10,000 \times 1,000/66,600 = 150.15\mu l$  aliquots

Therefore, 150.15 $\mu l$  atRA stock dissolved in 849.85 $\mu l$  culture medium = 10,000 $\mu M$

Using a dilution factor of 10, 10,000 $\mu M$  diluted four times to get 1 $\mu M$ .

atRA was made fresh from stock each time and always kept protected from light.

Retinol (Sigma-Aldrich 100mg) Molecular weight 286.5

*Stock solution*

100mg dissolved in 5ml 100% DMSO

$100/5 \times 286.5 = 0.0698M = 69,800\mu M$  (stored at  $-70^{\circ}C$  in light protected aliquots)

*Working solution 10 $\mu M$* 

$10,000 \times 1,000/69,800 = 143.3\mu l$  aliquots

143.3 $\mu l$  stock dissolved in 856.7 $\mu l$  culture medium = 10,000 $\mu M$

Using a dilution factor of 10, 10,000 $\mu M$  diluted 3 times to get 10 $\mu M$

Retinol was made fresh from stock each time and always kept protected from light.

## **Immunohistochemistry (peroxidase detection), Immunofluorescence and Immunocytochemistry**

The paraffin slides were de-waxed by first putting them through three ten minute cycles of heated xylene. The subsequent steps all took place at room temperature, each lasting five minutes. This included a fourth xylene step followed by hydration through an ethanol gradient (100% x 3, 95%, 90%, 80%, 70% and 50% (v/v) ethanol) and two changes of distilled water prior to stain application. For antigen retrieval citrate buffer was used at either 95°C for 20 minutes or 60°C for 1 hour.

For immunohistochemistry the Novolink® polymer detection kit (Leica Biosystems, UK) was used from this point forward. This included endogenous peroxidase block 30 minutes, protein block 45 minutes, primary antibody (diluent 1%BSA or Odyssey® (Li-Cor, UK) blocking buffer) incubation 1hour at room temperature or overnight at 4°C, post primary block 30 minutes and Novolink® polymer incubation 30 minutes. Prior to the primary antibody tris buffered saline was used for washes and afterward tris buffered saline with 0.1% tween (Fisher, UK). After this sections were incubated with Vector® NovaRED™ substrate kit (Vector, CA, USA), which allowed positive staining detection in those with pigmented skin. Sections were counterstained with haematoxylin, rinsed in water and placed on a heat block at 55°C for 10 minutes to dry. They were then dipped in xylene twice for 2 minutes each and coverslipped.

For immunofluorescence staining, protein block using either Odyssey® blocking buffer or 10%human/10% donkey serum was done at room temperature for 1 hour following antigen retrieval. The primary antibodies were treated the same as above as were the wash steps. All steps involving secondary antibody were conducted in darkness. Sections were incubated in Alexa Fluor®-conjugated secondary antibodies for one hour at room temperature. 4',6-diamidino-2-phenylindole (DAPI; Invitrogen, UK) 1/500 was applied for 15 minutes before washing and mounting using hard-set Prolong® Gold reagent (Invitrogen, UK).

For immunocytochemistry experiments,  $2.5 \times 10^4$  normal skin keratinocytes were seeded onto collagen-coated 24 well plates with coverslips placed in the bottom. Half of these keratinocytes for each patient were transfected with AKR1B10 as above and incubated for 24 hours. The medium was then removed and the cells washed with PBS prior to fixation with 4% formaldehyde for 30 minutes at room temperature. Cells were then permeabilised with 0.1% Triton X-100 in PBS for 15 minutes and blocked in 10% human/10% donkey serum in PBS for 1 hour at room temperature. The primary antibody was diluted in Odyssey<sup>®</sup> blocking buffer and left overnight at 4°C. The next day following washes the cells were incubated in Alexa Fluor<sup>®</sup>-conjugated secondary antibody for 1 hour at room temperature and then DAPI for 10 minutes. The coverslips were then reverse mounted onto slides and dried before storing in the dark at 4°C.

All histology was analysed using a phase contrast microscope (Olympus IX51, Olympus, UK) and then scanned using a digital slide scanner (Panoramic 250 Flash III (3DHISTECH, Hungary)). All antibodies and incubation parameters re detailed in **Supplementary table S4a**.

**References**

1. Espina V, Wulfschlegel JD, Calvert VS, VanMeter A, Zhou W, Coukos G, et al. Laser-capture microdissection. *Nat Protoc.* 2006;1: 586-603.
2. Zhu KQ, Carragher GJ, Couture OP, Tuggle CK, Gibran NS, Engrav LH. Expression of collagen genes in the cones of skin in the Duroc/Yorkshire porcine model of fibroproliferative scarring. *J Burn Care Res.* 2008;29: 815-27.

# Chapter 6

---

## **A role for neuregulin-1 (NRG1) in promoting keloid fibroblast migration via ErbB2-mediated signaling**

### **Declaration:**

Natalie Jumper, the first author, carried out all of the analysis, interpretation of data, design and composition of the article and accompanying figures. All of the experimental work was carried out by Natalie Jumper except for the co-immunoprecipitation studies, with which she assisted but were performed by Dr. Tom Hodgkinson. The other authors provided guidance, final approval of the paper and significant instruction on revised paper. This paper appears in the thesis in the format in which it was submitted to *Acta Dermato-Venereologica*. Core figures have been incorporated into the text to facilitate data interpretation. Supplementary material is included at the end of the article.

**A role for neuregulin-1 (NRG1) in promoting keloid fibroblast migration via ErbB2-mediated signaling**

N. Jumper<sup>1</sup>, T. Hodgkinson<sup>1,2</sup>, R. Paus<sup>3,4</sup>, A. Bayat<sup>1,3</sup>

<sup>1</sup>*Plastic and Reconstructive Surgery Research, Stopford Building, Manchester M13 9PT*

<sup>2</sup>*Centre for Tissue Injury and Repair, Institute of Inflammation and Repair, University of Manchester, UK*

<sup>3</sup>*Centre for Dermatology Research, Institute of Inflammation and Repair, University of Manchester, Manchester, UK*

<sup>4</sup>*Department of Dermatology, University of Münster, D-48149, Münster, Germany*

*Correspondence to: Dr Ardeshir Bayat, Plastic & Reconstructive Surgery Research, Institute of Inflammation & Repair, University of Manchester, Stopford Building, Manchester M13 9PT.*

*Phone: 0161 306 0607 Email: Ardeshir.Bayat@manchester.ac.uk*

**ABSTRACT**

Keloid disease is a fibroproliferative tumour characterised by aggressive local invasion, evident from a clinically and histologically active migrating margin. During combined laser capture microdissection and microarray analysis-based *in situ* gene expression profiling, we identified upregulation of the polypeptide growth factor neuregulin-1 (NRG1) and ErbB2 oncogene in keloid margin dermis, leading to the hypothesis that NRG1 contributed to keloid margin migration through ErbB2-mediated signalling. The aim of this study was to probe this hypothesis through functional *in vitro* studies. Exogenous NRG1 addition to keloid and normal skin fibroblasts (KF/NSF) altered cytokine expression profiles, significantly increased *in vitro* migration and keloid fibroblast Src and protein tyrosine kinase 2 (PTK2/FAK) gene expression. ErbB2 siRNA knockdown attenuated both KF migration and Src/PTK2 expression, which were not recovered following NRG1 administration, suggesting the NRG1/ErbB2/Src/PTK2 signaling pathway may be a novel regulator of KF migration, thus promoting fibrosis and representing a potential new therapeutic target.

**Key words:** keloid disease, laser capture microdissection, neuregulin-1, ErbB2, migration

**Abbreviations**

CTGF, connective tissue growth factor; ECM, extracellular matrix; FAK/PTK2, focal adhesion kinase; IL, interleukin; KD, keloid disease; KF, keloid fibroblasts; KMD, keloid margin dermis; LCM, laser capture microdissection; NRG1, neuregulin-1; NS, normal skin; NSF, normal skin fibroblasts; qRT-PCR, quantitative real-time polymerase chain reaction; rhNRG1, recombinant human neuregulin-1; siRNA, small interfering RNA; STAT, signal transducer and activator of transcription; TGF $\beta$ , transforming growth factor receptor beta

## INTRODUCTION

Representing the extreme end of the cutaneous scarring spectrum, keloid disease (KD) is a fibroproliferative tumour characterised by excess extracellular matrix (ECM) deposition, increased inflammatory cytokine expression and aggressive local invasion (1). While KD is often referred to as benign, in that it does not metastasize, it behaves in a tumorigenic fashion by actively invading adjacent normal skin (NS) and spreading beyond the boundaries of the original wound (2, 3). To date, although significant progress has been made, the mechanisms underlying the migration required for keloid invasion have not been fully elucidated. The invasion and spread of keloid scars represent a significant clinical challenge not currently controlled with available therapies (4).

To embrace this challenge and address the concept of keloid migration, we pursued in-house microarray evidence from specific keloid tissue compartments demonstrating involvement of neuregulin-1 (NRG1) and ErbB2 (HER-2/*Neu*). The microarray data encompassed differential gene expression between intralesional (centre), perilesional (margin) and extralesional *in situ* keloid and NS dermis (**Figure 1a**), which was achieved using laser capture microdissection (LCM). Support for our focus on the margin as the active site of keloid migration arises from a clinically raised erythematous border, histological evidence of a hyper-cellular advancing tongue in the papillary keloid margin dermis (KMD) (5) and increased migration and collagen in fibroblasts from the growing margin of the keloid scar (6, 7). NRG1 is a polypeptide growth factor upregulated in several human cancers (8-10), is secreted from fibroblasts (11) and plays a role in skin pigmentation (12), keratinocyte migration in wound healing (13), hypertrophic scarring (14) and fibrosis (15). NRG1 binds either ErbB3 or ErbB4 resulting in recruitment and heterodimerisation with ErbB2, an orphan receptor with no affinity ligand of its own (16) but which is implicated in tumorigenesis (17, 18).

The functional association between NRG1 and ErbB2 on cell migration has been observed in cardiac myocytes, schwann cells and glioma tissue, indicating the NRG-1 $\beta$ /ErbB-dependent



activation of Src/FAK modulates cell-cell contact, cell motility and focal adhesion complex formation (19-21). Indeed protein tyrosine kinase 2 (PTK2/FAK), a non-receptor protein tyrosine kinase, was shown to be upregulated in KD, where it influences cell migration through alteration of the focal-complex assembly disassembly cycle (22-24). The aggressive invasion evident in KD supports the hypothesis of a mechanobiological aetiology (25, 26), where rapid focal adhesion turnover and modulation of tension actin filaments produce a “migration-related disease” (27). Our site-specific approach localised upregulation of NRG1 and ErbB2 to the isolated KMD, leading to our hypothesis that NRG1 overexpression promotes fibrosis and fibroblast migration into adjacent NS through ErbB2-mediated signaling.

In this study, we confirmed our microarray finding of NRG1 and ErbB2 overexpression in KMD compared with NS on both gene and protein levels. We then sought to demonstrate the pro-fibrotic and pro-migratory effects of NRG1 and to establish whether these effects are dependent on ErbB2 upregulation. We showed that keloid fibroblast (KF) expression reflects that of the KMD, supporting the use of functional *in vitro* assays to test our hypothesis. Exogenous NRG1 administration resulted in upregulation of pro-fibrotic factors, Src and PTK2 as well as increased fibroblast migration on *in vitro* scratch assay. The use of ErbB2 siRNA attenuated this migration and the expression of Src and PTK2 in KF. Failure to recover this expression with re-introduction of NRG1 suggested the effects were mediated through ErbB2.

## METHODS

### *Sample preparation*

Keloid (centre, margin and extralesional) (**Figure 1a**) and NS biopsies were harvested according to Declaration of Helsinki protocols with full written consent (North West Research Ethics Committee Ref. 11/NW/0683). Biopsies were stored in RNA stabilisation solution then OCT-embedded for serial cryosection or formalin-fixed and paraffin-embedded (FFPE). Demographic

data detailed in **Supplementary Table S2**, which indicates that some of the keloid and NS samples differ in terms of ethnicity and prior treatment.

#### *Laser Capture Microdissection and Microarray analysis*

To preserve RNA integrity a rapid staining protocol was used (LCM Staining Kit, Ambion, USA) prior to laser capture microdissection (PALM, Carl Zeiss, MicroBeam 4.2, Germany). The LCM, mRNA extraction, amplification and microarray analysis were performed as described previously (28).

#### *Quantitative real-time polymerase chain reaction (qRT-PCR)*

Performed on mRNA from laser-captured elements and cultured fibroblasts, as previously described (28). Primer lists detailed in **Supplementary Table S3**. Reactions were performed in triplicate and normalised against two house-keeping genes, RPL32 and GAPDH.

#### *Cell culture*

Primary fibroblast culture was established using standard techniques as described (7). In brief, tissue was minced, incubated in collagenase, combined with complete DMEM for 3 hours at 37°C. Cells were pelleted and grown in tissue culture flasks with medium changes every 48-72hrs until confluent. Passages 1-3 were used.

#### *Fibroblast treatment with neuregulin*

NSF and KF were seeded into 6-well plates in complete DMEM. Once confluent, cells were serum-starved for 24 hours before adding 50ng/ml recombinant human neuregulin- $\beta$ 1 (rhNRG1-

β1) (PeproTech, UK) for 24 hours. Control cells were treated with serum-free medium for a total of 48 hours. Cells were harvested using Trizol (Life Technologies, UK) for RNA extraction (RNeasy Mini Kit, Qiagen) or radioimmunoprecipitation assay buffer (RIPA, Sigma-Aldrich) for western blot analysis.

#### *Co-immunoprecipitation and western blot analysis*

To determine ErbB dimerisation, co-immunoprecipitation of ErbB receptor complexes was performed according to the manufacturer's protocol (Pierce co-immunoprecipitation (Co-IP) kit, ThermoFisher Scientific, UK). This is discussed in detail in **Supplementary Material** and the antibody list detailed in **Supplementary table S4**. Blots were developed using nitro blue tetrazolium/S-bromo-4-chloroindoxyl phosphate (NBT/BCIP, 34042, ThermoFisher Scientific, UK).

#### *Immunostaining*

FFPE sections (5µm) were stained for ErbB2 using manufacturer's instructions for Novolink® peroxidase detection kit (Leica Biosystems, UK) and red chromogen Vector® NovaRED™ substrate kit (Vector, CA, USA) to differentiate from melanin then counterstained with haematoxylin. Combined ErbB2/NRG1 immunofluorescence was performed using citrate buffer (pH 6) antigen retrieval for 20min at 90°C. A negative control was performed in each without primary antibody. (Antibody incubation details **Supplementary Table S5**).

#### *siRNA gene knockdown of ErbB2*

Following optimisation, 5nM ErbB2 siRNA (*Silencer*® select s613 validated, ThermoFisher scientific UK) or control siRNA (*Silencer*® Select Negative Control No. 1, ThermoFisher scientific

UK) was introduced to KF using Lipofectamine® RNAiMAX (Life Technologies, UK) according to manufacturer's instructions. Culture medium (Opti-MEM I, ThermoFisher Scientific, UK) for RNAi transfection was antibiotic and serum-free. Cells were harvested for RNA extraction or protein analysis by western blot.

#### *In vitro scratch migration assay*

This is described in detail in the **Supplementary Material**. In brief, fibroblasts were seeded into six well plates and a scratch introduced with a 10 $\mu$ l pipette tip. Cells were then treated with either rhNRG1, ErbB2 siRNA or both rhNRG1 and ErbB2 siRNA together. Images were taken at time 0 and 48 hours and compared to quantify the number of migrated cells which were then presented as mean  $\pm$  SEM.

#### *Cell viability assay*

1x10<sup>4</sup> KF and NSF seeded per well into 96-well plates and serum-starved for experiment duration. Cells were treated with 50ng/ml rhNRG1 for 72 hours, 5nM ErbB2 siRNA or control siRNA as indicated. Controls were treated with serum-free medium alone. Metabolically active cell number was assessed using MTT assay as described previously (29). Absorbance (550nm-690nm) was measured (FLUOstar Optima, BMG Labtech, UK) and expressed as mean  $\pm$  SEM from three independent experiments.

#### *Statistics*

For qRT-PCR, gene expression levels were normalised against two internal controls and  $\Delta\Delta C_T$  calculated. All data are represented as mean  $\pm$  SEM. Statistical analysis was calculated using

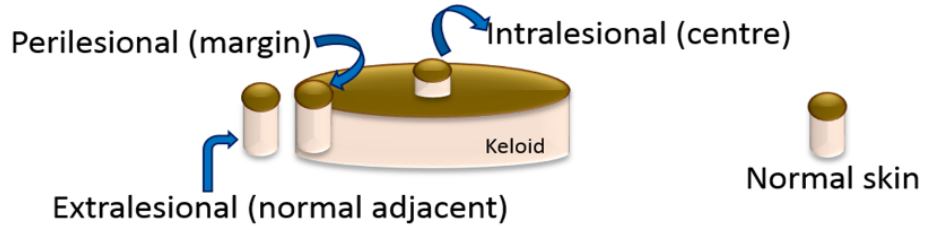
Student's *t* test and one way ANOVA with Tukey post-hoc correction (SPSS, IBM), where p-value < 0.05 considered statistically significant.

## RESULTS

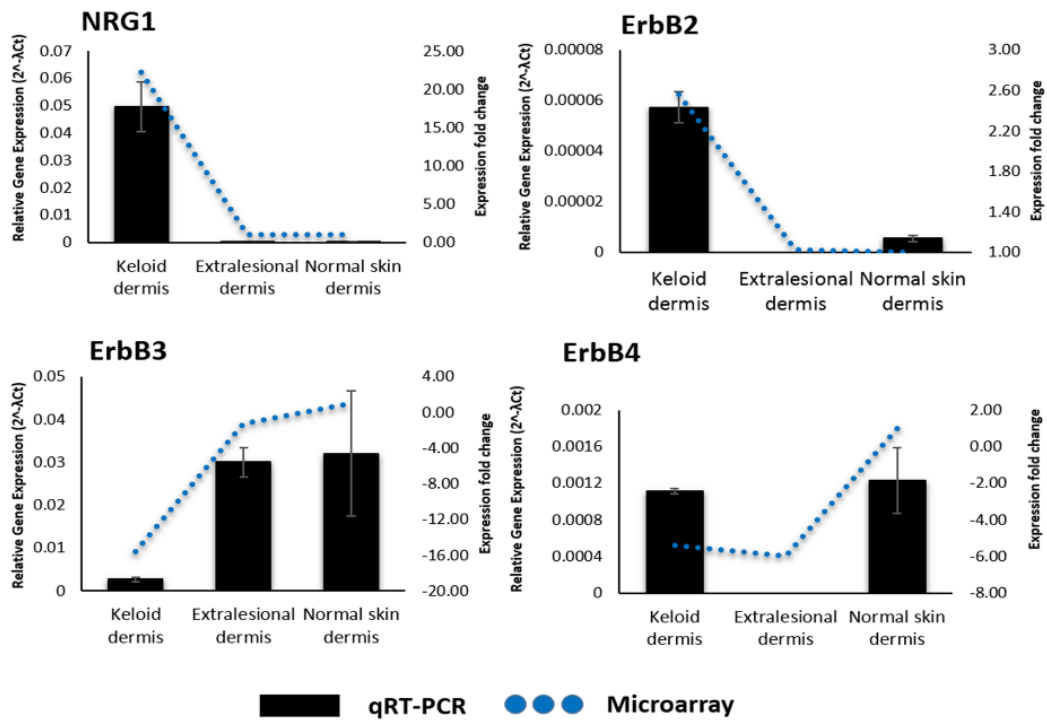
*In situ keloid dermis and cultured keloid fibroblasts showed increased NRG1 and Erbb2 mRNA expression but Erbb3 & Erbb4 downregulation compared with normal skin*

Combined LCM and microarray allowed site-specific comparison of keloid centre, margin and adjacent lesional sites with NS for epidermis and dermis (**Figure 1a**). NRG1 was identified as most significantly upregulated in KMD (fold change 22.24, p-value 1.59E-05) but was also upregulated in keloid centre dermis (fold change 10.71, p-value 0.0002). Given the upregulation of NRG1, we examined the microarray data for potential interaction candidates using criteria of fold change >2 and p-value < 0.05. ErbB2 was identified as most significantly upregulated in KMD (fold change 2.56, p-value 0.0031). ErbB3 (fold change 15.6, p-value 6.82E-07) and ErbB4 (fold change 5.42, p-value 0.0145), however, were significantly downregulated in KMD. Findings were validated using qRT-PCR, which reflected the microarray expression pattern (**Figure 1b**). Full expression data is detailed in **Supplementary Table S1**. Additionally, qRT-PCR (*n*=5) confirmed KF expressed increased NRG1 $\alpha$  (*p*=0.044) and NRG1 $\beta$  (*p*=2.7E-05) as well as ErbB2 (*p*=0.011) with reduced expression of ErbB3 (*p*=0.009) and ErbB4 (*p*=0.034) compared with NSF (**Figure 1c**). Therefore, KF in culture maintain the NRG1/ErbB gene expression of *in situ* keloid dermis, which is the presumed site leading keloid migration (30, 31). Given the complex nature of KD and the fact that there is no validated animal model for KD (32), the *in vitro* experiments are essential to confirm *in situ* observations made in human KD tissue in order to progress towards mechanistic understanding of the pathogenesis.

(a)



(b)



(c)

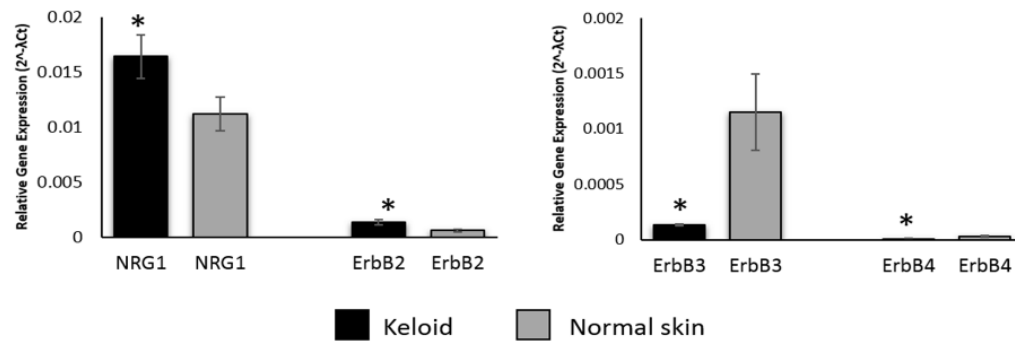


**Figure 1. Neuregulin-1 (NRG1) and ErbB2 gene expression for *in situ* keloid tissue and keloid fibroblasts (KF) compared with normal skin.** (A) Schematic diagram of keloid biopsy sites for combined laser capture microdissection and microarray approach. (B) qRT-PCR (bar graph) validation of microarray data (line graph represents fold change) for NRG1, ErbB2, ErbB3 and ErbB4 for *in situ* keloid vs normal skin. (C) qRT-PCR of KF and normal skin fibroblasts (NSF) ( $n=5$ ) for NRG1, ErbB2, ErbB3 and ErbB4. This downregulation of ErbB3 and ErbB4 may discourage homodimerisation thus promoting heterodimerisation with upregulated ErbB2 and generating the most efficient signalling. Data are mean  $\pm$  SEM from three independent experiments (\* $p < 0.05$ ).

*Keloid dermis and keloid fibroblasts show increased NRG1 and ErbB2 protein expression compared with normal skin*

To assess whether gene expression findings translated into protein changes, we performed immunohistochemistry for ErbB2 (**Figure 2a, b**) and immunofluorescence for combined NRG1 and ErbB2 (**Figure 2a**). 89% of keloid dermis samples showed increased ErbB2 expression ( $n=9$ ) compared with NS ( $n=5$ ), where there was no dermal expression. Interestingly, positive ErbB2 expression in keloid dermis was associated with histological features considered to be pathognomonic of KD (5), including dermal nodule (**Figure 2bi**), horizontal fibrous band (**Figure 2bii**), obliteration of papillary/reticular border (**Figure 2biii**) and papillary dermal inflammatory infiltrate (**Figure 2biv**). Combined NRG1/ErbB2 immunofluorescent staining (yellow stain) demonstrated co-localisation within the dermis (**Figure 2a**), which was increased in KD ( $n=13$ ) compared with NS ( $n=6$ ). Similar to ErbB2 immunohistochemistry, this co-localised expression in keloid dermis was more frequently in areas of inflammatory infiltrate. When only KMD sections were considered, both NRG1 and ErbB2 were positive in 6/6 examined patients, supporting microarray data.

Protein expression, determined by western blot ( $n=5$ ), showed a trend toward increased expression of both NRG1 and ErbB2 (**Figure 2c**) with decreased ErbB3 and ErbB4 expression in KF compared with NSF (**Supplementary figure S1**). Overall, our results show increased NRG1 and ErbB2 protein expression in keloid dermis compared with NS, supporting gene expression findings.



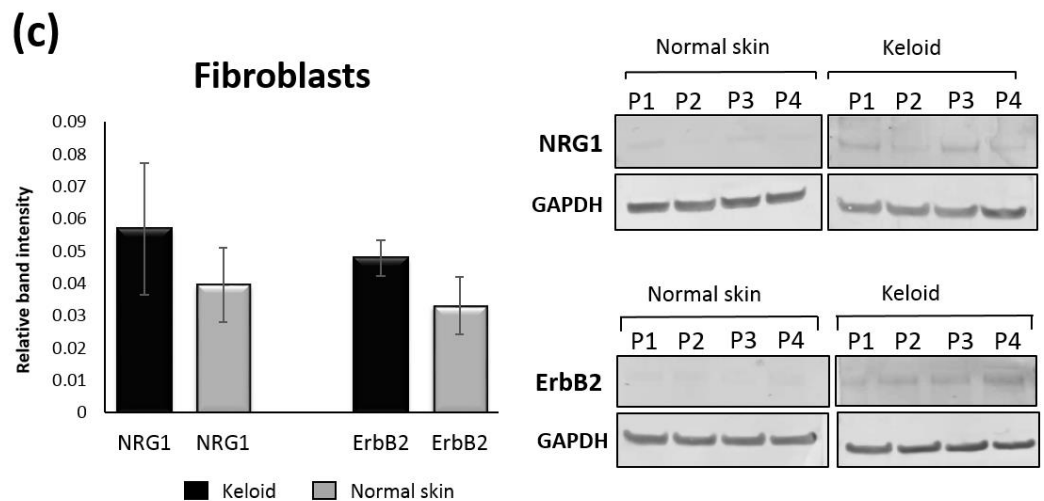
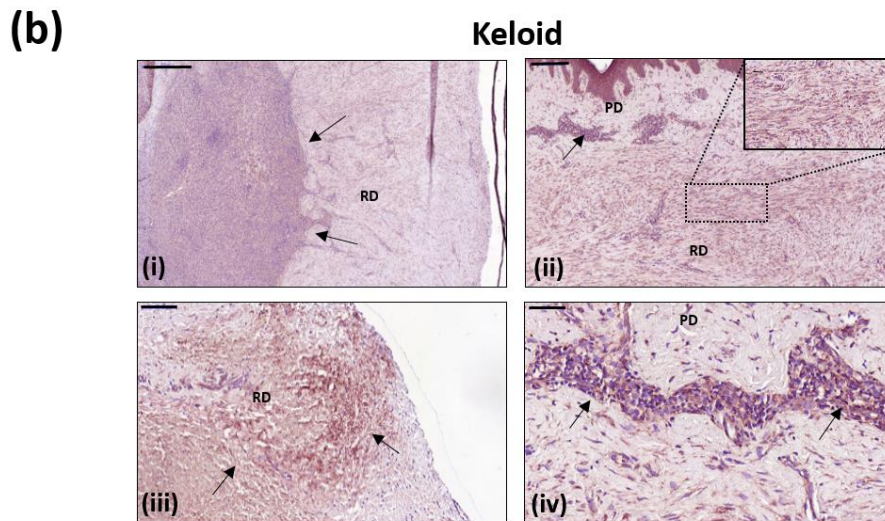
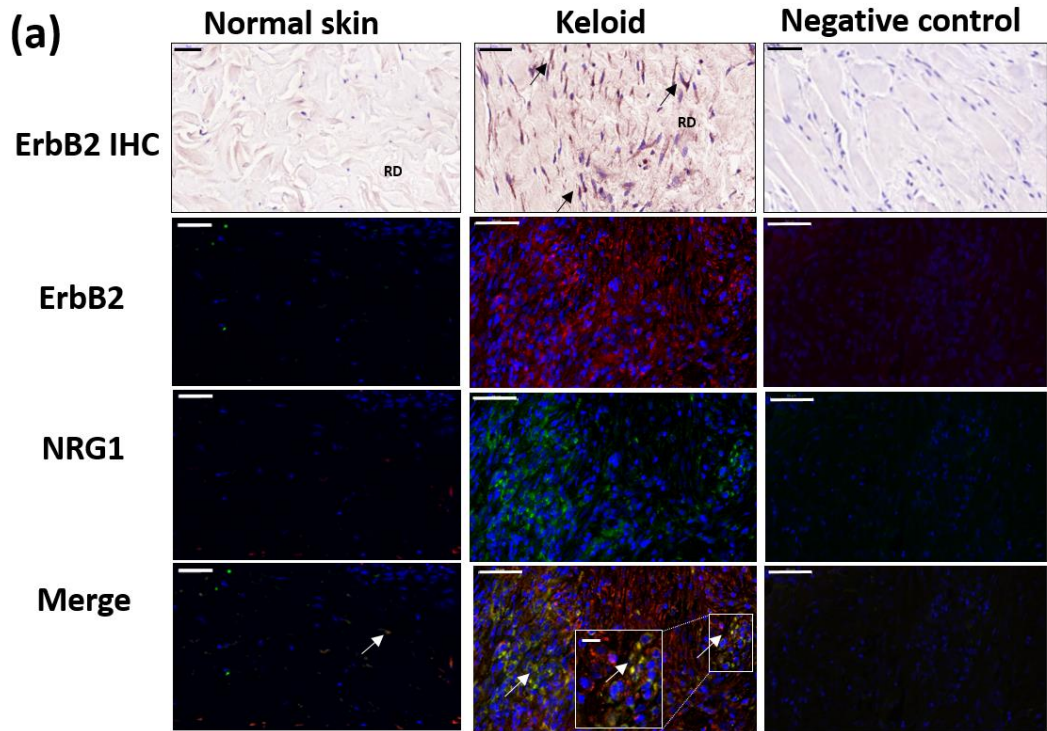


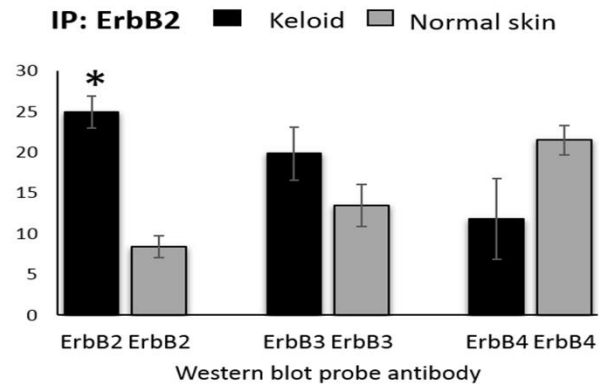
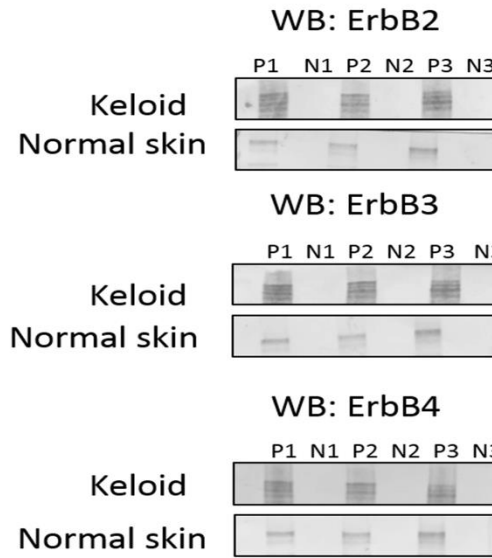
**Figure 2. Neuregulin-1 (NRG1) and ErbB2 protein expression in keloid versus normal skin (NS).**

(A) ErbB2 immunohistochemistry for KD ( $n=9$ ) and NS ( $n=5$ ) show ErbB2 (black arrows) in KD sections only. Combined NRG1 (green/FITC) ERbB2 (red/TRITC) immunofluorescence for KD ( $n=13$ ) and NS ( $n=6$ ). Dermal co-localisation (white arrows indicating yellow stain) increased in KD vs NS. Negative control with no primary antibody treatment shown also. (B) ErbB2 immunohistochemistry of keloid margin ( $n=6$ ). Positive staining associated with i) hyper-cellular dermal nodule ii) horizontal fibrous band iii) papillary-reticular border obliteration iv) Papillary dermis (PD) inflammatory infiltrate. (C) Western blot and mean fold change quantification for NRG1 and ErbB2 in keloid fibroblasts and NS fibroblasts. Scale bar = 50 $\mu$ m. Scale bar of inset magnification = 10 $\mu$ m. RD, reticular dermis.

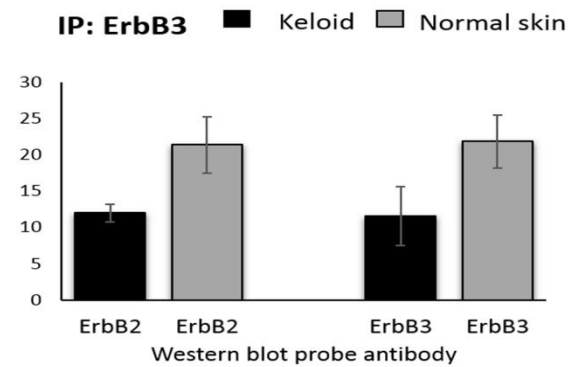
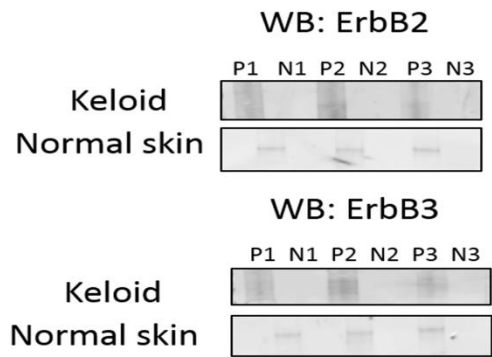
*Increased levels of Erbb2/Erbb2 homodimers and Erbb2/Erbb3 heterodimers in keloid fibroblasts compared with normal skin*

To evaluate ErbB dimerisation status, co-immunoprecipitation was performed using KF and NSF lysates ( $n=3$ ) and the immunoprecipitate subjected to western blot analysis (**Figure 3**). KF immunoprecipitation of ErbB2 led to increased co-precipitation of ErBB2 ( $p=0.003$ ) and ErbB3 when compared with NSF. Additionally, ErbB3 and ErbB4 homodimers preferentially occurred in NSF versus KF. Assay specificity was demonstrated by absence of immunoreactivity in negative controls. These results suggest KF express higher levels of ErbB2/ErbB2 homodimers and ErbB2/ErbB3 heterodimers than NSF.

**Immunoprecipitate pull down: ErbB2**



**Immunoprecipitate pull down: ErbB3**



**Immunoprecipitate pull down: ErbB4**

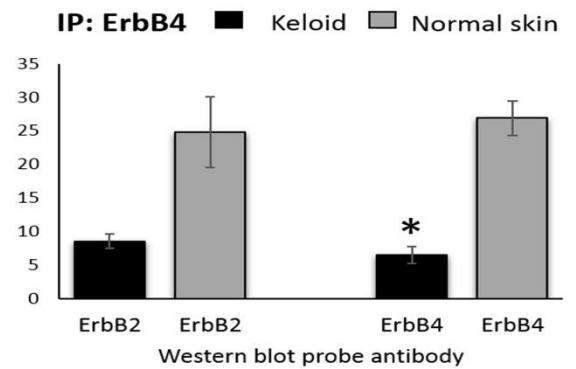
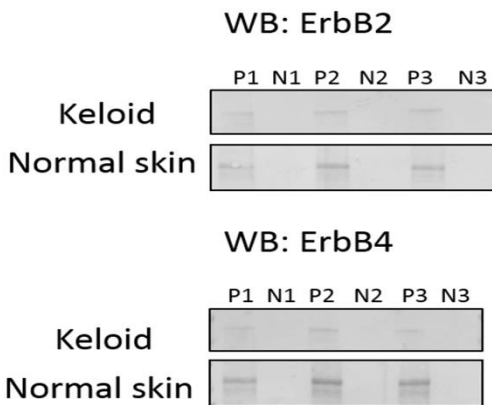


**Figure 3.** Co-immunoprecipitation of total keloid and normal skin fibroblast protein lysate ( $n=3$ ) and western blot analysis with antibody against ERbb2, ErbB3 and ErbB4. The immunoprecipitate (IP) pull down and associated western blot (WB) for each specific antibody probed shown with the accompanying quantification graph under the relevant headings. Quantification was performed with ImageJ analysis and this was repeated three times. Data are represented as mean  $\pm$  SEM where  $*p<0.05$  using Student's  $t$  test. The western blots show each sample for  $n=3$  for both KF and NSF. The patient lanes are marked with "P" and the negative control lanes for that same patient marked with "N". KF, keloid fibroblasts; NSF, normal skin fibroblasts.

*Treatment of normal skin fibroblasts with rhNRG1 produced keloid-like release of pro-fibrotic cytokines*

As the more active isoform, exogenous rhNRG1-  $\beta 1$  was added to NSF at 50ng/ml for 24 hours and compared with untreated (serum-free medium) NSF ( $n=5$ ). qRT-PCR was performed for a number of pro-fibrotic genes known to be dysregulated in KD (1, 33-35) (**Figure 4a, b**). NSF treatment with rhNRG1 resulted in significant upregulation of collagen I ( $p=0.0016$ ), collagen III ( $p=0.001$ ) and fibronectin ( $p=0.007$ ) as well as pro-inflammatory cytokines transforming growth factor receptor (TGF $\beta$ 1) ( $p=0.04$ ), IL-6 ( $p=0.0059$ ) and IL-8 ( $p=0.0019$ ). These results indicate exposure to NRG1 produces a pro-fibrotic response in NSF that reflects the keloid expression profile.

*Treatment of keloid fibroblasts with rhNRG1 reinforces pro-fibrotic cytokine release*

**Figure 4b** shows KF treatment with 50ng/ml rhNRG1 for 24 hours ( $n=5$ ) stimulated significant upregulation of TGF $\beta$ 1 ( $p=3.97E-07$ ). There was also upregulation of fibroblast growth factor

(FGF7) (40) ( $p=0.0086$ ) (**Supplementary figure S2**) as well as a trend toward increased expression of collagen I, collagen III, fibronectin and IL-6 (**Supplementary figure S3 & S4**).

*Treatment with rhNRG1 enhanced migration in both keloid and normal skin fibroblasts*

*In vitro* scratch assay was used to assess migration capacity of KF and NSF (**Figure 4c**). Untreated fibroblasts were compared to those stimulated with 50ng/ml rhNRG1 over 48 hours. Untreated KF showed significantly more migration than NSF. Additionally, rhNRG1 treatment resulted in significantly increased migration for KF ( $p=0.02$ ) and NSF ( $p=5.0E-05$ ) over untreated cells (**Figure 4d**). A 72-hour MTT assay ( $n=4$ ) on all fibroblasts confirmed cell numbers remained constant for experimental duration and were equal between KF and NSF (**Figure 4e**).

Given that NRG1 is known to affect cell migration and motility through effects on Src/FAK and signal transducer and activator of transcription (STAT3) (20, 36-38), here we investigated the effect of rhNRG1 on these molecules in KF and NSF. **Figure 4f** demonstrates qRT-PCR of KF ( $n=5$ ) treated with rhNRG1 showed significant upregulation of Src ( $p=0.006$ ), PTK2/FAK ( $p=0.04$ ) and STAT3 ( $p=0.005$ ). NSF ( $n=5$ ) also showed significant upregulation of Src ( $p=0.016$ ) and STAT3 ( $p=0.004$ ) but not PTK2.

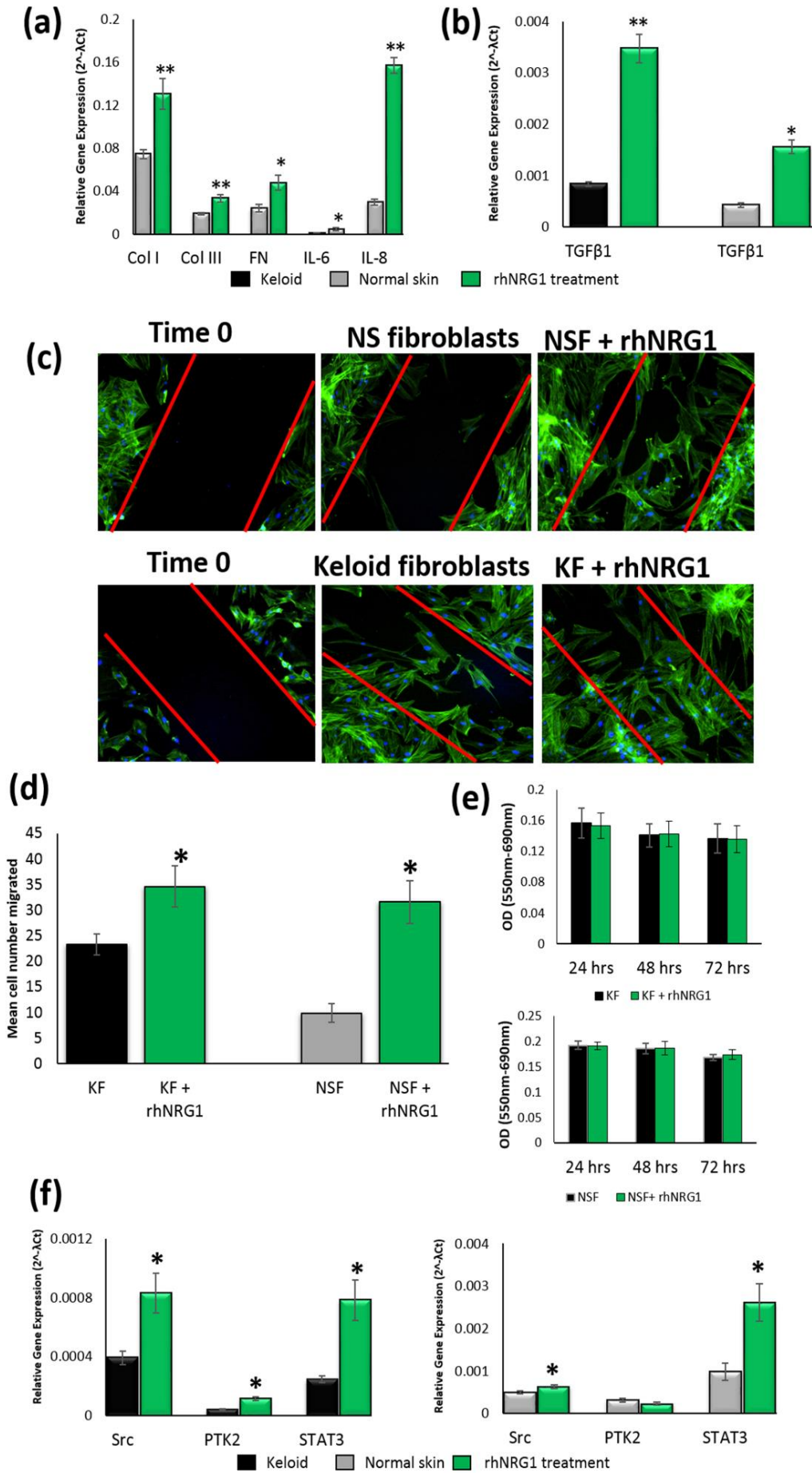


**Figure 4. Fibroblast ( $n=5$ ) treatment with recombinant human neuregulin-1 (rhNRG1).** (A) qRT-PCR showing significantly increased collagen I, collagen III, fibronectin (FN), IL-6 and IL-8 expression in rhNRG1-treated normal skin fibroblasts (NSF) and (B) significantly increased transforming growth factor (TGF $\beta$ 1) in keloid fibroblasts (KF) and NSF. (C) Representative micrographs of *in vitro* scratch migration assay ( $n=3$ ) showing KF/NSF response towards injury at 0hrs and 48hrs with/without rhNRG1 treatment. (D) Average number of migrated KF and NSF based on time 0 were plotted on the graph. (E) 72hr MTT assay on rhNRG1-treated and untreated fibroblasts ( $n=4$ ). (F) qRT-PCR for Src, FAK/PTK2 and signal transducer and activator of transcription (STAT3) of rhNRG1-treated vs untreated KF or NSF. Data are mean  $\pm$  SEM from at least three independent experiments (\* $p<0.05$ , \*\* $p<0.005$ ).

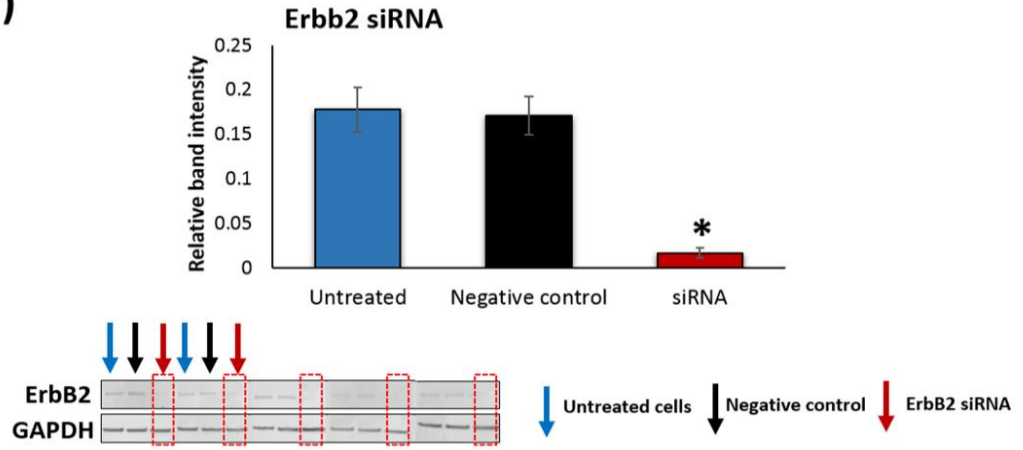
*ErbB2 knockdown in keloid fibroblasts attenuates pro-fibrotic cytokine expression and reduces cell migration*

To clarify ErbB2 involvement in keloid fibrosis and migration, KF ( $n=5$ ) were treated with 5nM ErbB2 siRNA or scrambled siRNA negative control for 48 hours and successful knockdown confirmed by western blot (**Figure 5a**). qRT-PCR of ErbB2 knockdown KF showed significantly less expression of collagen I ( $p=1E-05$ ), collagen III ( $p=0.019$ ), fibronectin ( $p=0.012$ ) and TGF $\beta$ 1 ( $p=0.04$ ) than negative control (**Supplementary figure S5 & S6**).

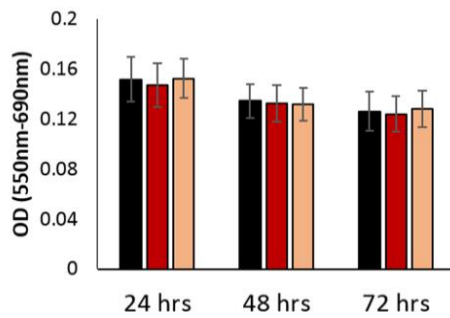
The MTT assay ( $n=4$ ) of siRNA-treated KF confirmed viability was maintained over the 72 hour experimental period with minimal cell proliferation in serum-free environment, as expected (**Figure 5b**). Therefore, the significantly reduced cell migration seen in ErbB2 knockdown KF ( $p=0.005$ ) was not due to apoptosis (**Figure 5c, d**). Reduced migration of ErbB2 siRNA-transfected KF, seen with *in vitro* scratch assay, is supported by significantly reduced gene expression of PTK2 ( $p=0.0002$ ) and Src ( $p=0.003$ ) compared with negative control (**Figure 5e**).



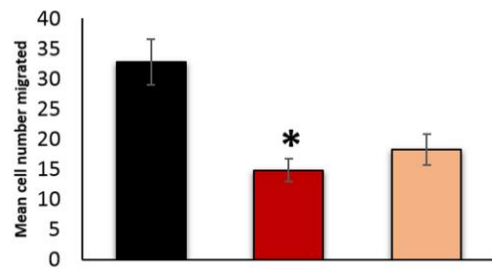
(a)



(b)

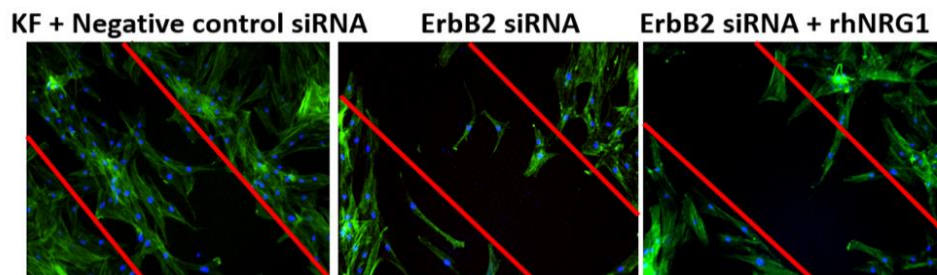


(c)



■ KF + Negative control siRNA    ■ ErbB2 siRNA    ■ ErbB2 siRNA + rhNRG1

(d)



(e)

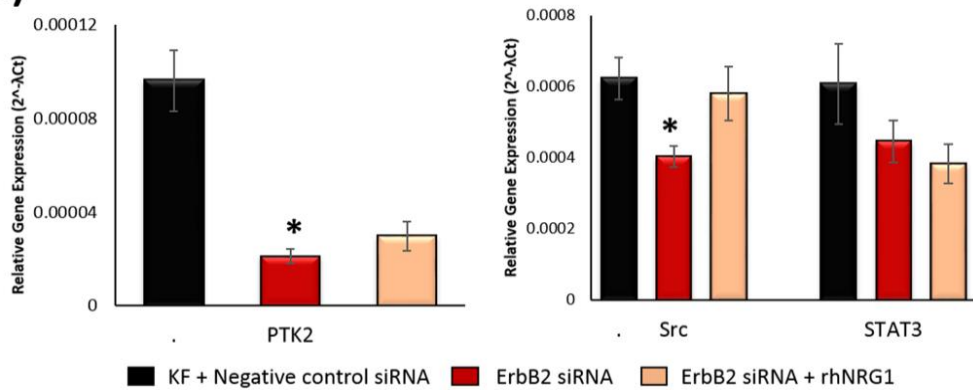




**Figure 5. ErbB2 siRNA-transfected keloid fibroblasts (KF).** (A) Quantification ( $n=5$ ) and blot showing significant (~90%) ErbB2 protein (30 $\mu$ g) expression reduction in siRNA-transfected (red arrow) vs untreated (blue arrow) and negative control (black arrow) KF. (B) 72hr MTT of keloid fibroblasts (KF). (C) Average number of migrated KF plotted on the graph. (D) Representative micrographs of *in vitro* scratch migration assay ( $n=3$ ). Fibroblast migration response towards injury at time 0 and 48hrs following treatment: negative control, ErbB2 siRNA or both ErbB2 siRNA and neuregulin (NRG1) together. (E) qRT-PCR for PTK2, Src and STAT3 expression of KF treated with negative control, ErbB2 siRNA or both ErbB2 siRNA and rhNRG1 together. Data are mean  $\pm$  SEM from at least three independent experiments (\* $p<0.05$ , \*\* $p<0.005$ ).

*ErbB2 knockdown keloid fibroblasts do not recover cell migration with rhNRG1 treatment*

Having demonstrated the effect of ErbB2 knockdown on KF migration, we next sought to determine whether the observed pro-migratory effects of NRG1 on KF were mediated through ErbB2. Addition of rhNRG1 to KF transfected with ErbB2 siRNA did not result in a significant increase in migration ( $p=0.29$ ) on *in vitro* scratch assay (**Figure 5c, d**). Nor did addition of rhNRG1 to ErbB2 knockdown KF restore the expression of PTK2 or Src (**Figure 5e**), suggesting effects of NRG1 in KD are mediated by ErbB2 overexpression and other ErbB members are unable to compensate for ErbB2 loss or they may use alternate signaling mechanisms.

## DISCUSSION

Keloid disease is a quasineoplastic cutaneous tumour characterised by migration into surrounding skin beyond the original wound borders, failure to regress and high recurrence rates following excision (1). Our identification of NRG1 and ErbB2 upregulation in the clinically and histologically active (5, 39) KMD *in situ*, suggested a heretofore unexamined mechanism underlying invasive migration contributing to KD pathogenesis.

Here, we have demonstrated KF reflect *in situ* KMD tissue, with increased NRG1 and ErbB2 but decreased ErbB3 and ErbB4 expression compared to NS. ErbB2 overexpression leads to homodimerisation and constitutive activity through autophosphorylation, leading to ligand-independent signaling (40, 41). Alternatively, ErbB2 is the preferred dimerization partner of both ErbB4 and kinase-impaired ErbB3 (42, 43), which even at low levels can produce potent signal transduction through ErbB2/ErbB3 heterodimerisation (44). Given heterodimerisation with ErbB2 generates the most robust signaling downstream, we hypothesised the downregulation of ErbB3 and ErbB4 discouraged their homodimerisation in favour of ErbB2 (45), achieving maximal signaling activity with NRG1 affinity (46) (**Supplementary figure S7**). This is supported by our finding of increased ErbB2 homodimers and ErbB2/ErbB3 heterodimers in the co-immunoprecipitation of KF versus NSF. Although ErbB3 and ErbB4 serve as the NRG1 receptors, we have shown that ErbB2 ablation hinders keloid cell's ability to respond to NRG1 (17).

This study has shown that rhNRG1 treatment elicited a keloid-like pro-fibrotic cytokine expression profile in NSF, with significant upregulation of collagen I, collagen III, TGF $\beta$ 1, fibronectin, IL-6 and IL-8. These observations led us to hypothesise a possible mechanism whereby paracrine NRG1 signals from migrating/advancing KF may alter the expression profile of adjacent NSF, thereby driving keloid expansion at the margin into extralesional/normal skin (**Supplementary figure S8**) (11). NRG1 was recently found to be upregulated in hypertrophic scar fibroblasts, where it regulated ECM expression through connective tissue growth factor (CTGF) (14). Here, although we found exogenous rhNRG1 treatment resulted in decreased CTGF expression in KF (**Supplementary Figure S9 & S10**), this does not detract from previous findings in hypertrophic scarring. Indeed, these differences may have clinical implications given the continued difficulties with differential diagnosis between keloid and hypertrophic scars. However, further studies are required to explore the mechanisms underlying these divergent responses to rhNRG1 *in vitro*.

We demonstrated reinforcement of TGF $\beta$ 1 overexpression in rhNRG1-treated KF. TGF $\beta$ 1, a pleiotropic growth factor already known to be upregulated in KD (1, 35), has been postulated to facilitate scar expansion through pro-inflammatory and pro-migratory effects (47, 48). Interestingly, our finding of NRG1 and ErbB2 co-localisation in keloid dermis was frequently observed within previously described areas of keloid inflammatory infiltrate (49). TGF $\beta$ 1 is known to influence cell migration through MMP regulation (50) and its effect on single cell motility is thought to require synergy with the EGFR family of tyrosine kinase receptors (51, 52), such as ErbB2 (53-55). Both ErbB2 and TGF $\beta$  also independently activate PI3K/Akt (56, 57) and MAPK/Erk (58, 59) pathways, which are regulators of migration and are both known to be dysregulated in KD (60, 61).

Our finding of TGF $\beta$ 1 upregulation and CTGF downregulation following rhNRG1 treatment of KF is curious, especially as TGF $\beta$  is well known to induce CTGF in KF (57). Thus, NRG1 upregulation may only be one contributing element in the regulatory systems that underlie increased TGF $\beta$ 1 in KD (3); in combination with other factors inducing TGF $\beta$ 1 overexpression, this may override the negative effects of NRG1 on the CTGF expression seen here. Alternatively, the incompletely understood complexity of Smad/non-Smad signaling, as well as the other signaling regulators that are known to affect CTGF expression and to be dysregulated in KD including mechanical stress/tension (1, 62-64), may drive the overall expression of CTGF in KD *in vivo*. While this is an interesting finding and represents a focus for future research, further investigation into this relationship was beyond the scope of the current study.

NRG1 adheres to ECM *in vivo*, thereby activating ErbB2 receptors on invading cells and contributing to cell migration (19). Here, we show rhNRG1 stimulation promoted significant cell migration in both NSF and KF. Additionally, we demonstrated rhNRG1 treatment resulted in significant upregulation of Src in NSF and both Src and PTK2 in KF. Importantly, the small but significant upregulation of PTK2 in concert with Src, seen only in KF and which is considered essential to the establishment of an invasive cell phenotype (65, 66), may contribute to the

migratory fibroblast phenotype that differentiates keloids from normal scars. We established the role of ErbB2 in this study through ErbB2 siRNA studies, which resulted in significant reduction in both cell migration *in vitro* and also downregulation of Src and PTK2 gene expression in KF. PTK2 facilitates migration through ECM-integrin junction signaling (67), also playing a role in inflammation and fibrosis (68). The site-specific approach in our study highlights identification of ErbB2 and NRG1 dysregulation in keloid dermis as opposed to epidermis and interestingly, dermal PTK2 has been suggested as more vital to cutaneous healing than epidermal (68).

To determine whether the effects of NRG1 and ErbB2 on migration were co-dependent, we treated the ErbB2 knockdown KF with rhNRG1. This treatment failed to significantly increase *in vitro* migration or gene expression of Src and PTK2 in KF, indicating NRG1 requires ErbB2 for its pro-migratory effects in KF. STAT3 has been previously implicated in keloid migration (69) and it has been suggested that increased ErbB2 can activate STAT3 via Src (70, 71). Interestingly, our results revealed a significant STAT3 increase ( $p < 0.01$ ) in both NSF and KF treated with rhNRG1. However, ErbB2 knockdown in KF did not significantly reduce STAT3 or known STAT3 modulator IL-6 when compared with untreated KF controls (72-74). Additionally, STAT3 in KMD in our microarray data was marginally downregulated (fold change 2.02, p-value 0.0051), suggesting NRG1 is not the dominant regulator of STAT3 and any stimulation of these molecules may contribute to fibroblast migration through alternative mechanisms (75). Although STAT3 has been shown to play a significant role in keloid pathogenesis, the site-specific nature of this study may account for differences in observed expression (76).

One of the limitations of our study was the availability of optimal keloid tissue samples with few of the keloid samples having previous treatment and only some of the keloid patients were Caucasian, whereas all of the NS samples were from Caucasian patients. Given the ethical implications of excising normal skin tissue from keloid-prone patients distant to the scar, we matched the samples to the maximum degree within our control. Although not ideal, the

extralesional tissue may be interpreted as a type-matched control and in the extralesional dermis, NRG1, ErbB2 and ErbB3 were not dysregulated (**Supplementary Table S1**).

In summary, we have shown NRG1 and ErbB2 upregulation in KMD and that suppression of ErbB2 expression in KF neutralises the pro-fibrotic cytokine expression profile and pro-migratory effects of NRG1. This study examines the molecular mechanisms underlying keloid migration, which is an essential component of the invasion that is pathognomonic of KD. Confirmation of the functional importance of these findings through keloid organ culture may provide further evidence supporting the exposure in this study of a potential role for NRG1/ErbB2/FAK/Src signaling localised to KMD, which presents an intriguing aspect of keloid migration not previously investigated. The potential future clinical implications include current availability of targeted therapies for ErbB2, which with site-specific application may be a novel strategy in the management of KD.

#### **Conflicts of interest**

The authors report no conflict of interest

#### **Acknowledgments**

The authors are grateful to Yaron Har-Shai and Guyan Arscott for their assistance with sample provision and to Adam Taylor (GSK) for his technical assistance with analysis.

## References

1. Andrews JP, Marttala J, Macarak E, Rosenbloom J, Uitto J. Keloids: The paradigm of skin fibrosis - Pathomechanisms and treatment. *Matrix Biol* 2016.
2. Dong X, Mao S, Wen H. Upregulation of proinflammatory genes in skin lesions may be the cause of keloid formation (Review). *Biomed Rep* 2013; 1: 833-6.
3. Unahabhokha T, Sucontphunt A, Nimmannit U, Chanvorachote P, Yongsanguanchai N, Pongrakhananon V. Molecular signalings in keloid disease and current therapeutic approaches from natural based compounds. *Pharm Biol* 2015; 53: 457-63.
4. Bijlard E, Steltenpool S, Niessen FB. Intralesional 5-Fluorouracil in Keloid Treatment: A Systematic Review. *Acta Derm Venereol* 2015; 95: 778-82.
5. Jumper N, Paus R, Bayat A. Functional histopathology of keloid disease. *Histol Histopathol* 2015; 30: 1033-57.
6. Syed F, Ahmadi E, Iqbal SA, Singh S, McGrouther DA, Bayat A. Fibroblasts from the growing margin of keloid scars produce higher levels of collagen I and III compared with intralesional and extralesional sites: clinical implications for lesional site-directed therapy. *Br J Dermatol* 2011; 164: 83-96.
7. Ashcroft KJ, Syed F, Bayat A. Site-specific keloid fibroblasts alter the behaviour of normal skin and normal scar fibroblasts through paracrine signalling. *PLoS One* 2013; 8: e75600.
8. Montero JC, Rodriguez-Barrueco R, Ocana A, Diaz-Rodriguez E, Esparis-Ogando A, Pandiella A. Neuregulins and cancer. *Clin Cancer Res* 2008; 14: 3237-41.
9. Okazaki S, Nakatani F, Masuko K, Tsuchihashi K, Ueda S, Masuko T, et al. Development of an ErbB4 monoclonal antibody that blocks neuregulin-1-induced ErbB4 activation in cancer cells. *Biochem Biophys Res Commun* 2016.
10. Han M-E, Kim H-J, Shin DH, Hwang S-H, Kang C-D, Oh S-O. Overexpression of NRG1 promotes progression of gastric cancer by regulating the self-renewal of cancer stem cells. *Journal of gastroenterology* 2015; 50: 645-56.
11. Capparelli C, Rosenbaum S, Berger AC, Aplin AE. Fibroblast-derived neuregulin 1 promotes compensatory ErbB3 receptor signaling in mutant BRAF melanoma. *The Journal of biological chemistry* 2015; 290: 24267-77.
12. Choi W, Wolber R, Gerwat W, Mann T, Batzer J, Smuda C, et al. The fibroblast-derived paracrine factor neuregulin-1 has a novel role in regulating the constitutive color and melanocyte function in human skin. *J Cell Sci* 2010; 123: 3102-11.
13. Kim JS, Bak EJ, Lee BC, Kim YS, Park JB, Choi IG. Neuregulin induces HaCaT keratinocyte migration via Rac1-mediated NADPH-oxidase activation. *J Cell Physiol* 2011; 226: 3014-21.
14. Kim JS, Choi IG, Lee BC, Park JB, Kim JH, Jeong JH, et al. Neuregulin induces CTGF expression in hypertrophic scarring fibroblasts. *Mol Cell Biochem* 2012; 365: 181-9.
15. Nethery D, Bonfield T, Chmiel J, Konstan M, Kern J, Finigan J, et al. Her2-Neuregulin Mediated IL-8 Release In Cystic Fibrosis. *Am J Respir Crit Care Med* 2011; 183: A1112.
16. Xu Y, Li X, Zhou M. Neuregulin-1/ErbB signaling: a druggable target for treating heart failure. *Curr Opin Pharmacol* 2009; 9: 214-9.
17. Zhang K, Wong P, Duan J, Jacobs B, Borden EC, Bedogni B. An ERBB3/ERBB2 oncogenic unit plays a key role in NRG1 signaling and melanoma cell growth and survival. *Pigment Cell Melanoma Res* 2013; 26: 408-14.
18. Meng Y, Zheng L, Yang Y, Wang H, Dong J, Wang C, et al. A monoclonal antibody targeting ErbB2 domain III inhibits ErbB2 signaling and suppresses the growth of ErbB2-overexpressing breast tumors. *Oncogenesis* 2016; 5: e211.
19. Ritch PA, Carroll SL, Sontheimer H. Neuregulin-1 enhances motility and migration of human astrocytic glioma cells. *The Journal of biological chemistry* 2003; 278: 20971-8.
20. Kuramochi Y, Guo X, Sawyer DB. Neuregulin activates erbB2-dependent src/FAK signaling and cytoskeletal remodeling in isolated adult rat cardiac myocytes. *J Mol Cell Cardiol* 2006; 41: 228-35.

21. Wakatsuki S, Araki T, Sehara-Fujisawa A. Neuregulin-1/glial growth factor stimulates Schwann cell migration by inducing  $\alpha 5 \beta 1$  integrin–ErbB2–focal adhesion kinase complex formation. *Genes to Cells* 2014; 19: 66-77.
22. Wang Z, Fong KD, Phan TT, Lim IJ, Longaker MT, Yang GP. Increased transcriptional response to mechanical strain in keloid fibroblasts due to increased focal adhesion complex formation. *J Cell Physiol* 2006; 206: 510-7.
23. Schneider D, Wickstrom SA. Force generation and transmission in keloid fibroblasts: dissecting the role of mechanosensitive molecules in cell function. *Exp Dermatol* 2015; 24: 574-5.
24. Zhang Z, Nie F, Chen X, Qin Z, Kang C, Chen B, et al. Upregulated periostin promotes angiogenesis in keloids through activation of the ERK 1/2 and focal adhesion kinase pathways, as well as the upregulated expression of VEGF and angiopoietin1. *Mol Med Rep* 2015; 11: 857-64.
25. Ogawa R, Okai K, Tokumura F, Mori K, Ohmori Y, Huang C, et al. The relationship between skin stretching/contraction and pathologic scarring: the important role of mechanical forces in keloid generation. *Wound repair and regeneration : official publication of the Wound Healing Society [and] the European Tissue Repair Society* 2012; 20: 149-57.
26. Suarez E, Syed F, Rasgado TA, Walmsley A, Mandal P, Bayat A. Skin equivalent tensional force alters keloid fibroblast behavior and phenotype. *Wound repair and regeneration : official publication of the Wound Healing Society [and] the European Tissue Repair Society* 2014; 22: 557-68.
27. Harn HI, Wang YK, Hsu CK, Ho YT, Huang YW, Chiu WT, et al. Mechanical coupling of cytoskeletal elasticity and force generation is crucial for understanding the migrating nature of keloid fibroblasts. *Experimental dermatology* 2015; 24: 579-84.
28. Jumper N, Hodgkinson T, Arscott G, Har-Shai Y, Paus R, Bayat A. The aldo-keto reductase AKR1B10 is upregulated in keloid epidermis, implicating retinoic acid pathway dysregulation in the pathogenesis of keloid disease. *The Journal of investigative dermatology* 2016.
29. Bagabir R, Syed F, Paus R, Bayat A. Long-term organ culture of keloid disease tissue. *Exp Dermatol* 2012; 21: 376-81.
30. Shih B, McGrouther DA, Bayat A. Identification of novel keloid biomarkers through profiling of tissue biopsies versus cell cultures in keloid margin specimens compared to adjacent normal skin. *Eplasty* 2010; 10: e24.
31. Bond JE, Bergeron A, Thurlow P, Selim MA, Bowers EV, Kuang A, et al. Angiotensin-II mediates nonmuscle myosin II activation and expression and contributes to human keloid disease progression. *Mol Med* 2011; 17: 1196-203.
32. Marttala J, Andrews JP, Rosenbloom J, Uitto J. Keloids: Animal models and pathologic equivalents to study tissue fibrosis. *Matrix Biology* 2016; 51: 47-54.
33. Canady J, Arndt S, Karrer S, Bosserhoff AK. Increased KGF expression promotes fibroblast activation in a double paracrine manner resulting in cutaneous fibrosis. *Journal of Investigative Dermatology* 2013; 133: 647-57.
34. Kelsh RM, McKeown-Longo PJ, Clark RA. EDA Fibronectin in Keloids Create a Vicious Cycle of Fibrotic Tumor Formation. *The Journal of investigative dermatology* 2015; 135: 1714-8.
35. Berman B, Maderal A, Raphael B. Keloids and Hypertrophic Scars: Pathophysiology, Classification, and Treatment. *Dermatol Surg* 2016.
36. Liu J, Kern JA. Neuregulin-1 activates the JAK-STAT pathway and regulates lung epithelial cell proliferation. *Am J Respir Cell Mol Biol* 2002; 27: 306-13.
37. Chang HM, Shyu MK, Tseng GF, Liu CH, Chang HS, Lan CT, et al. Neuregulin facilitates nerve regeneration by speeding Schwann cell migration via ErbB2/3-dependent FAK pathway. *PLoS One* 2013; 8: e53444.
38. Pentassuglia L, Sawyer DB. ErbB/integrin signaling interactions in regulation of myocardial cell-cell and cell-matrix interactions. *Biochim Biophys Acta* 2013; 1833: 909-16.

39. Rees PA, Greaves NS, Baguneid M, Bayat A. Chemokines in Wound Healing and as Potential Therapeutic Targets for Reducing Cutaneous Scarring. *Adv Wound Care (New Rochelle)* 2015; 4: 687-703.
40. Brix DM, Clemmensen KK, Kallunki T. When Good Turns Bad: Regulation of Invasion and Metastasis by ErbB2 Receptor Tyrosine Kinase. *Cells* 2014; 3: 53-78.
41. Hu S, Sun Y, Meng Y, Wang X, Yang W, Fu W, et al. Molecular architecture of the ErbB2 extracellular domain homodimer. *Oncotarget* 2015; 6: 1695-706.
42. Hynes NE, Lane HA. ERBB receptors and cancer: the complexity of targeted inhibitors. *Nat Rev Cancer* 2005; 5: 341-54.
43. Berger MB, Mendrola JM, Lemmon MA. ErbB3/HER3 does not homodimerize upon neuregulin binding at the cell surface. *FEBS letters* 2004; 569: 332-6.
44. Stortelers C, van der Woning SP, Jacobs-Oomen S, Wingens M, van Zoelen EJ. Selective formation of ErbB-2/ErbB-3 heterodimers depends on the ErbB-3 affinity of epidermal growth factor-like ligands. *The Journal of biological chemistry* 2003; 278: 12055-63.
45. Birtwistle MR, Hatakeyama M, Yumoto N, Ogunnaike BA, Hoek JB, Kholodenko BN. Ligand-dependent responses of the ErbB signaling network: experimental and modeling analyses. *Mol Syst Biol* 2007; 3: 144.
46. Li Z, Mei Y, Liu X, Zhou M. Neuregulin-1 only induces trans-phosphorylation between ErbB receptor heterodimer partners. *Cell Signal* 2007; 19: 466-71.
47. Fujiwara M, Muragaki Y, Ooshima A. Keloid-derived fibroblasts show increased secretion of factors involved in collagen turnover and depend on matrix metalloproteinase for migration. *Br J Dermatol* 2005; 153: 295-300.
48. Lee CH, Hong CH, Chen YT, Chen YC, Shen MR. TGF-beta1 increases cell rigidity by enhancing expression of smooth muscle actin: keloid-derived fibroblasts as a model for cellular mechanics. *Journal of dermatological science* 2012; 67: 173-80.
49. Bagabir R, Byers RJ, Chaudhry IH, Muller W, Paus R, Bayat A. Site-specific immunophenotyping of keloid disease demonstrates immune upregulation and the presence of lymphoid aggregates. *Br J Dermatol* 2012; 167: 1053-66.
50. Leivonen SK, Kahari VM. Transforming growth factor-beta signaling in cancer invasion and metastasis. *Int J Cancer* 2007; 121: 2119-24.
51. Giampieri S, Manning C, Hooper S, Jones L, Hill CS, Sahai E. Localized and reversible TGFbeta signalling switches breast cancer cells from cohesive to single cell motility. *Nat Cell Biol* 2009; 11: 1287-96.
52. Wang SE, Xiang B, Zent R, Quaranta V, Pozzi A, Arteaga CL. Transforming growth factor  $\beta$  induces clustering of HER2 and integrins by activating Src-focal adhesion kinase and receptor association to the cytoskeleton. *Cancer Res* 2009; 69: 475-82.
53. Seton-Rogers SE, Lu Y, Hines LM, Koundinya M, LaBaer J, Muthuswamy SK, et al. Cooperation of the ErbB2 receptor and transforming growth factor beta in induction of migration and invasion in mammary epithelial cells. *Proc Natl Acad Sci U S A* 2004; 101: 1257-62.
54. Landis MD, Seachrist DD, Montanez-Wiscovich ME, Danielpour D, Keri RA. Gene expression profiling of cancer progression reveals intrinsic regulation of transforming growth factor-beta signaling in ErbB2/Neu-induced tumors from transgenic mice. *Oncogene* 2005; 24: 5173-90.
55. Chow A, Arteaga CL, Wang SE. When tumor suppressor TGFbeta meets the HER2 (ERBB2) oncogene. *J Mammary Gland Biol Neoplasia* 2011; 16: 81-8.
56. Carmona FJ, Montemurro F, Kannan S, Rossi V, Verma C, Baselga J, et al. AKT signaling in ERBB2-amplified breast cancer. *Pharmacol Ther* 2015.
57. Song R, Li G, Li S, Aspidin PB, a novel natural anti-fibrotic compound, inhibited fibrogenesis in TGF-beta1-stimulated keloid fibroblasts via PI-3K/Akt and Smad signaling pathways. *Chem Biol Interact* 2015; 238: 66-73.
58. Zhang YE. Non-Smad pathways in TGF-beta signaling. *Cell Res* 2009; 19: 128-39.



59. Lyu H, Huang J, Edgerton SM, Thor AD, He Z, Liu B. Increased erbB3 promotes erbB2/neu-driven mammary tumor proliferation and co-targeting of erbB2/erbB3 receptors exhibits potent inhibitory effects on breast cancer cells. *Int J Clin Exp Pathol* 2015; 8: 6143-56.
60. Lim IJ, Phan TT, Tan EK, Nguyen TT, Tran E, Longaker MT, et al. Synchronous activation of ERK and phosphatidylinositol 3-kinase pathways is required for collagen and extracellular matrix production in keloids. *The Journal of biological chemistry* 2003; 278: 40851-8.
61. Huang C, Akaishi S, Ogawa R. Mechanosignaling pathways in cutaneous scarring. *Arch Dermatol Res* 2012; 304: 589-97.
62. Blom IE, Goldschmeding R, Leask A. Gene regulation of connective tissue growth factor: new targets for antifibrotic therapy? *Matrix Biol* 2002; 21: 473-82.
63. Chaqour B, Goppelt-Struebe M. Mechanical regulation of the Cyr61/CCN1 and CTGF/CCN2 proteins. *FEBS J* 2006; 273: 3639-49.
64. Mu S, Kang B, Zeng W, Sun Y, Yang F. MicroRNA-143-3p inhibits hyperplastic scar formation by targeting connective tissue growth factor CTGF/CCN2 via the Akt/mTOR pathway. *Mol Cell Biochem* 2016.
65. Mitra SK, Schlaepfer DD. Integrin-regulated FAK-Src signaling in normal and cancer cells. *Curr Opin Cell Biol* 2006; 18: 516-23.
66. Kolli-Bouhafs K, Sick E, Noulet F, Gies J, De Mey J, Rondé P. FAK competes for Src to promote migration against invasion in melanoma cells. *Cell death & disease* 2014; 5: e1379.
67. Mitra SK, Hanson DA, Schlaepfer DD. Focal adhesion kinase: in command and control of cell motility. *Nat Rev Mol Cell Biol* 2005; 6: 56-68.
68. Wong VW, Rustad KC, Akaishi S, Sorkin M, Glotzbach JP, Januszyk M, et al. Focal adhesion kinase links mechanical force to skin fibrosis via inflammatory signaling. *Nat Med* 2012; 18: 148-52.
69. Canady J, Karrer S, Fleck M, Bosserhoff AK. Fibrosing connective tissue disorders of the skin: molecular similarities and distinctions. *Journal of dermatological science* 2013; 70: 151-8.
70. DeArmond D, Brattain MG, Jessup JM, Kreisberg J, Malik S, Zhao S, et al. Autocrine-mediated ErbB-2 kinase activation of STAT3 is required for growth factor independence of pancreatic cancer cell lines. *Oncogene* 2003; 22: 7781-95.
71. Hawthorne VS, Huang WC, Neal CL, Tseng LM, Hung MC, Yu D. ErbB2-mediated Src and signal transducer and activator of transcription 3 activation leads to transcriptional up-regulation of p21Cip1 and chemoresistance in breast cancer cells. *Mol Cancer Res* 2009; 7: 592-600.
72. Banerjee K, Resat H. Constitutive activation of STAT3 in breast cancer cells: A review. *Int J Cancer* 2015.
73. Zou M, Zhang X, Xu C. IL6-induced metastasis modulators p-STAT3, MMP-2 and MMP-9 are targets of 3,3'-diindolylmethane in ovarian cancer cells. *Cell Oncol (Dordr)* 2015.
74. Ray S, Ju X, Sun H, Finnerty CC, Herndon DN, Brasier AR. The IL-6 trans-signaling-STAT3 pathway mediates ECM and cellular proliferation in fibroblasts from hypertrophic scar. *The Journal of investigative dermatology* 2013; 133: 1212-20.
75. Zhang B, Xie S, Su Z, Song S, Xu H, Chen G, et al. Heme oxygenase-1 induction attenuates imiquimod-induced psoriasiform inflammation by negative regulation of Stat3 signaling. *Sci Rep* 2016; 6: 21132.
76. Lim CP, Phan TT, Lim IJ, Cao X. Stat3 contributes to keloid pathogenesis via promoting collagen production, cell proliferation and migration. *Oncogene* 2006; 25: 5416-25.

## Supplementary Material to Chapter 6

### Methods

#### *Co-Immunoprecipitation and western blot*

This was performed according to the manufacturer's protocol (Pierce co-immunoprecipitation (Co-IP) kit, ThermoFisher Scientific, UK). Normal skin fibroblasts and keloid fibroblasts were lysed in Co-IP Lysis Buffer, the cell debris was pelleted and the protein quantified through the bicinchoninic acid protein assay reagent kit (BCA; ThermoScientific, UK). 1 mg of each cell population lysate was pre-cleared by 1 hour incubation with non-specific agarose resin. For each receptor subunit, the primary antibody was covalently bound to an amine-reactive resin and incubated with cleared cell lysate over-night at 4°C. Input lysate was also incubated with negative control resin as per the manufacturer's protocol. Non-bound protein was removed, control and specifically bound complex-resin washed and proteins eluted. Immunoprecipitate was subjected to western blot. Blots from each Co-IP reaction were probed with anti-ErbB2, 3 and 4 antibodies and developed using nitro blue tetrazolium/S-bromo-4-chloroindoxyl phosphate (NBT/BCIP, 34042, ThermoFisher Scientific, UK). The western blots were analysed using ImageJ software, including only the area where the protein band was located and each quantification repeated three times to ensure accuracy.

For western blot alone, each sample was run on the same blot as its own internal control using GAPDH. In order to compare samples the fold change over control was used and the mean of these fold changes quantified and presented on the bar graphs.

#### *In vitro scratch assay*

Both normal skin and keloid fibroblasts were seeded into 6-well plates ( $3 \times 10^5$ ) and grown to confluence (~90%). Normal skin fibroblasts were treated with 50ng/ml rhNRG1 for 24hrs. Keloid

fibroblasts were treated with 50ng/ml rhNRG1 alone, 5nM ErbB2 siRNA alone or combined rhNRG1 and ErbB2 siRNA. Control wells treated with serum-free medium alone or negative control siRNA and were performed in tandem. Scratch wounds were introduced using a sterile 10 $\mu$ l pipette tip, cells were washed to remove cell debris and then treated as described above. Six scratch wound were introduced into each well and experiments performed in duplicate. Images were taken at time 0 and marks made adjacent to the scratch beneath the plate surface as reference points. Final images were taken at 48 hrs and this image compared with the original scratch wound at time 0. Fibroblasts were fixed with 4% formaldehyde for 30 minutes, permeabilised with 0.1% triton X-100 (Sigma-Aldrich, UK) and stained with F-actin using rhodamine isothiocyanate 1:250 (Sigma-Aldrich, UK) and nuclei stained with 1:500 DAPI. Three non-overlapping fields were captured at 10x (inverted Olympus IX71) for each scratch, equating to a total of 54 measurements for each experimental condition ( $n=3$ ) for each of keloid and normal skin fibroblasts. The number of cells (defined as cells with nuclei) migrated into the wound site counted and presented as mean  $\pm$  SEM.

**Table S1** – Microarray expression of genes relevant to this study

<b>Agilent Probe ID</b>	<b>Ref Sequence</b>	<b>Gene symbol</b>	<b>Site within lesion</b>	<b>Fold change</b>	<b>p-value</b>
A_33_P3284345	NM_013956.3	NRG1	Centre dermis	10.71	0.0002
A_33_P3284345	NM_013956.3	NRG1	Margin dermis	22.24	1.59E-05
A_33_P3284345	NM_013956.3	NRG1	Extralesional dermis	-2	0.42
A_33_P3292596	NM_004448.3	ErbB2	Margin dermis	2.56	0.0031
A_33_P3292596	NM_004448.3	ErbB2	Extralesional dermis	1.03	0.927
A_23_P349416	NM_001982.3	ErbB3	Centre dermis	-10.14	3.53E-06
A_23_P349416	NM_001982.3	ErbB3	Margin dermis	-15.6	6.82E-07
A_23_P349416	NM_001982.3	ErbB3	Extralesional dermis	-1.25	0.6075
A_32_P183765	NM_005235.2	ErbB4	Centre dermis	-6.83	0.0038
A_32_P183765	NM_005235.2	ErbB4	Margin dermis	-5.42	0.0145
A_32_P183765	NM_005235.2	ErbB4	Extralesional dermis	-5.96	0.013

**Table S2** – Demographic data of samples used in this study

<b>No.</b>	<b>Tissue type</b>	<b>Gender, Age</b>	<b>Ethnicity</b>	<b>Time present</b>	<b>Previous Treatment</b>	<b>Location of keloid</b>
1	Keloid	F, 42yrs	Israeli	7-8 yrs	Nil	Left shoulder
2	Keloid	F, 25 yrs	Ethiopian	18 mnths	Nil	Right shoulder
3	Keloid	F, 19 yrs	Caucasian	2-3 yrs	Nil	Left ear helix
4	Keloid	F, 30 yrs	Caucasian	8 yrs	Nil	Central sternum
5	Keloid	F, 32 yrs	Caucasian	13 yrs	Radiation, steroid, silicone	Breasts bilaterally
6	Keloid	F, 41 yrs	Israeli	6 yrs	Steroid, silicone	Left deltoid
7	Keloid	F, 18yrs	Jamaican Afrocarribean	1 yr	none	Bilateral ear lobes
8	Keloid	M, 23yrs	Jamaican Afrocarribean	4 yrs	none	Bilateral ear lobes
9	Keloid	F, 27yrs	Jamaican Afrocarribean	2 yrs	Surgery	Right ear lobe
10	Keloid	M, 20yrs	Jamaican Afrocarribean	2 yrs	Surgery	Chin
11	Keloid	F, 19yrs	Jamaican Afrocarribean	2 yrs	Surgery	Sternum
12	Keloid	F, 41yrs	Jamaican Afrocarribean	6 yrs	None	Sternum
13	Keloid	M, 20yrs	Jamaican Afrocarribean	15 yrs	None	Right ear lobe
14	Keloid	F, 22yrs	Jamaican Afrocarribean	3 yrs	None	Bilateral ear lobes

15	Normal skin	F, 57yrs	Caucasian	-	-	Facelift & blepharoplasty
16	Normal skin	M, 47yrs	Caucasian	-	-	Abdominoplasty
17	Normal skin	F, 19yrs	Caucasian	-	-	Bilateral breast reduction
18	Normal skin	F, 26yrs	Caucasian	-	-	Abdominoplasty
19	Normal skin	F, 41yrs	Caucasian	-	-	Abdominoplasty
20	Normal skin	F, 43yrs	Caucasian	-	-	Bilateral breast reduction
21	Normal skin	F, 43yrs	Caucasian	-	-	Bilateral breast reduction
22	Normal skin	F, 34yrs	Caucasian	-	-	Abdominoplasty
23	Normal skin	F, 47yrs	Caucasian	-	-	Mastopexy
24	Normal skin	F, 20yrs	Caucasian	-	-	Bilateral breast reduction
25	Normal skin	F, 42yrs	Caucasian	-	-	Bilateral breast reduction
26	Normal skin	F, 56yrs	Caucasian	-	-	Abdominoplasty
27	Normal skin	F, 51yrs	Caucasian	-	-	Abdominoplasty

Table S3 – Details of primers used for qRT-PCR

Gene	Forward primer Reverse primer	Accession number (Roche Diagnostics, UK)	Amplicon size (bp)
NRG1	Cccatgaaagtccaaaacca ccggttatggcagcactct	cat. no. 04686900001	68
NRG1	Tgtcaccagactcctagcc acgattacagagtggttcg	cat. no. 04689011001	78
ErbB2	Ttgctccaatcacaggag ggggaatctcagcttcaaa	cat. no. 04685091001	88
ErbB3	Aatcaagttaacccaacagc ccaccaccacttctgagat	cat. no. 04689135001	68
ErbB4	Aggagtgaaattggacacagc caaactggtttctgacatgg	cat. no. 04688481001	61
PTK2/FAK	gtctgccttcgcttcacg gccgagatcatgccactc	cat. no. 04686926001	92
Src	ggagacagacctgtccttcaa ccaccagtctcctctgtgt	cat. no. 04688112001	70
STAT3	Cccttgattgagagtcaaga aagcggctatactgctggc	cat. no. 04685130001	108
IL-6	Caggagcccagctatgaact gaaggcagcaggcaaac	cat. no. 04685059001	91
IL-8	Aaaaccaggtgagagtga tctgagatcccgtcagagc	cat. no. 04688678001	65
FN	Gcgagagtgccctactaca gttggatgaatcgaggatca	cat. no. 04688490001)	71
TGFβ1	actgcaagtggacatcaacg ggccatgagaagcaggaa	cat. no. 04688104001	94
FGF7	aagtctagcacacagcacttgg agcattgcttcaggctcttatt	cat. no. 04685067001	71
CTGF	ccgtactccaaaatctcca ttagctcggatgtcttcatgc	cat. no. 04688945001	75
Collagen Ia1	agggtcaccgtggcttct tccagaggaccttgttcac	cat. no. 04689020001	77
Collagen III	ctggaccccagggtcttc gaccatctgatccagggttc	cat. no. 04686934001	78
GAPDH	agccacatcgctcagacac gcccaatacgaccaaattcc	cat. no. 04688589001	66
RPL32	gaagttcctgtccacaacg gagcgatctcggcacagta	cat. no. 04686900001	77

**Table S4** – Concentration, incubation parameters and detection method of primary and secondary antibodies used in this study for co-immunoprecipitation and western blot

<b>Primary antibody, product code &amp; company</b>	<b>Primary ab raised species, isotype, concentration</b>	<b>Incubation details</b>	<b>Secondary ab, company, concentration, incubation</b>	<b>Detection method</b>
ErbB2, ab16901 [3B5]	Mouse(monoclonal), IgG fraction, 2.5µg/ml dilution	4°C overnight	Goat IgG conjugated to alkaline phosphatase, ab97048, Abcam 1:2000 dilution 1hr room temp	NBT/BCIP
ErbB2, mAb#4290 (D8F12)XP®	Rabbit (monoclonal), IgG, 1:1000 dilution	4°C overnight	Goat IgG conjugated to alkaline phosphatase, ab97048, Abcam 1:2000 dilution 1hr room temp	NBT/BCIP
ErbB3, ab20161 [RTJ2]	Mouse (monoclonal) IgG1 2.5µg/ml dilution	4°C overnight	Goat IgG conjugated to alkaline phosphatase, ab97048, Abcam 1:2000 dilution 1hr room temp	NBT/BCIP
ErbB4, ab19391 [HFR-1]	Mouse (monoclonal) IgG2b 3µg/ml dilution	4°C overnight	Goat IgG conjugated to alkaline phosphatase, ab97048, Abcam 1:2000 dilution 1hr room temp	NBT/BCIP

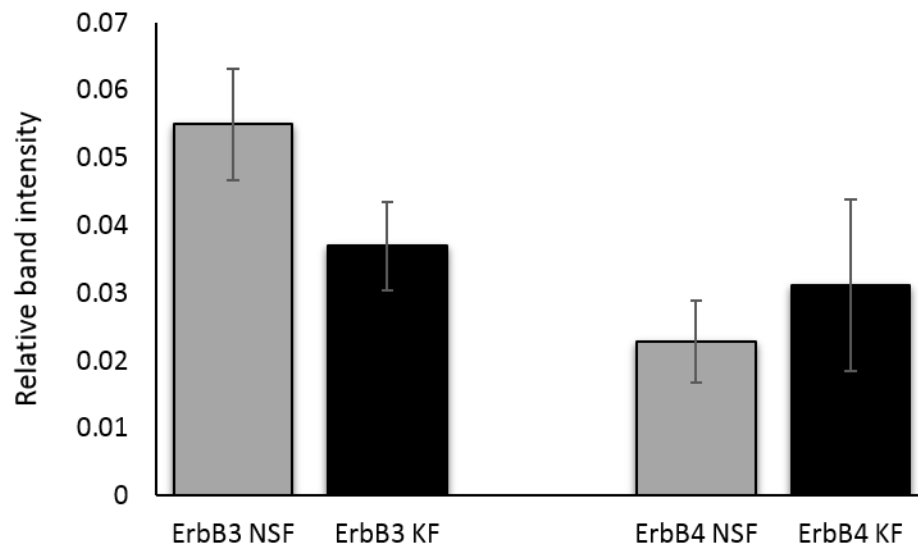


**Table S5** – Concentration, incubation parameters and detection method of primary and secondary antibodies used in this study for immunohistochemistry

<b>Primary antibody, product code &amp; company</b>	<b>Primary ab raised species, isotype, concentration</b>	<b>Incubation details</b>	<b>Secondary ab, company, concentration, incubation</b>	<b>Detection method</b>
ErbB2, ab16901 [3B5]	Mouse(monoclonal), IgG fraction, 2.5µg/ml dilution	4°C overnight	Universal antibody by Novolink™ Leica Biosystems, Newcastle Ltd. 1 hour room temp	Peroxidase NovaRED™ Vector®
NRG1-1α/β1/2 (c-20): sc-348	Rabbit (polyclonal), IgG, 1:100 dilution	4°C overnight	Alexa Fluor®488 goat anti-mouse IgG (green), Life technologies, 1:250 dilution, 1hr room temp	Fluorescence 1:500 DAPI
ErbB2, ab16901 [3B5]	Mouse(monoclonal), IgG fraction, 2.5µg/ml dilution	4°C overnight	Alexa Fluor®546 goat anti-rabbit IgG (red), Life technologies, 1:250 dilution, 1hr room temp	Fluorescence 1:500 DAPI

**Figure S1 – Western blot for ErbB3 and ErbB4 in fibroblasts**

While there is a trend toward increased ErbB3 in NSF and ErbB4 in KF neither is significant.

**Figure S2 – qRT-PCR gene expression of fibroblast growth factor 7 (FGF7) in keloid fibroblasts**

was significantly upregulated following addition of 50ng/ml rhNRG1.

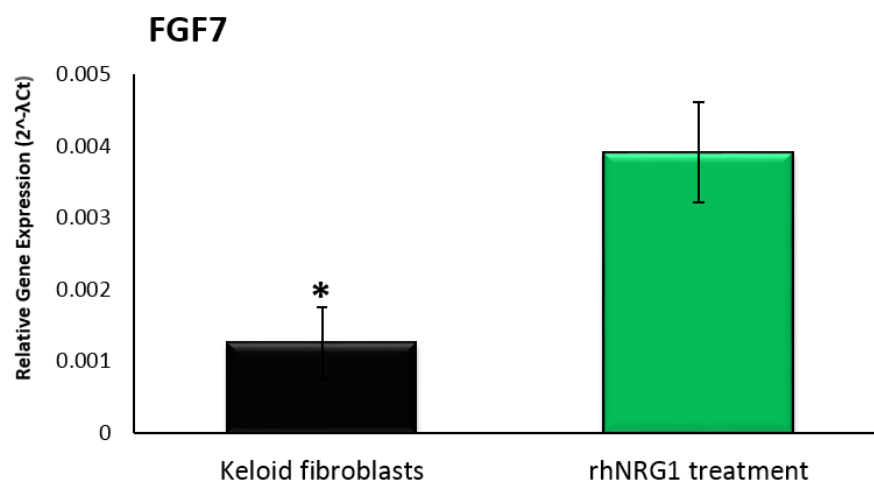


**Figure S3** – qRT-PCR gene expression of collagen I (col I), collagen III (col III) and fibronectin (FN) in keloid fibroblasts. Following addition of 50ng/ml rhNRG1 there was a trend toward increased expression of these genes but the results were not statistically significant.

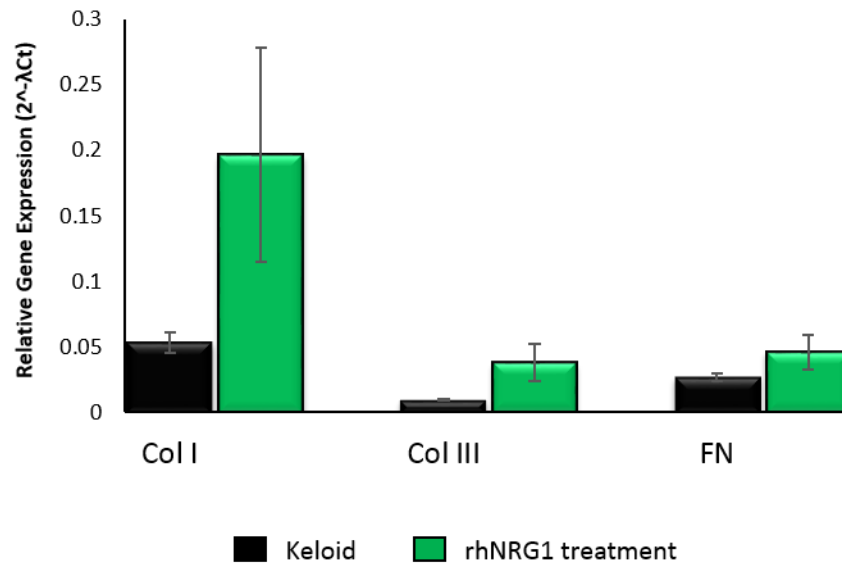


**Figure S4**– qRT-PCR gene expression of IL-6 in keloid fibroblasts. Following addition of 50ng/ml rhNRG1 there was a trend toward increased expression but the results were not statistically significant.

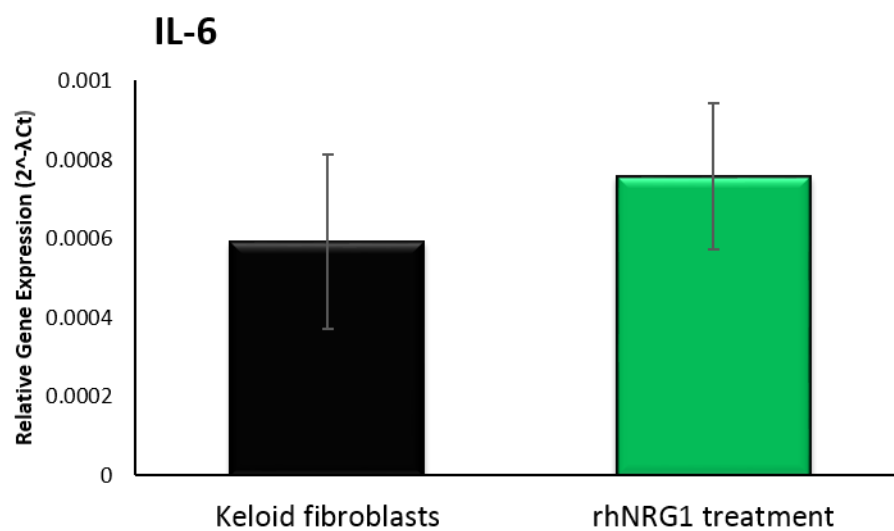


**Figure S5**— qRT-PCR gene expression in keloid fibroblasts treated with negative control siRNA or treated with ErbB2siRNA. This graph shows significant downregulation of collagen I, collagen III and fibronectin following treatment with ErbB2 siRNA

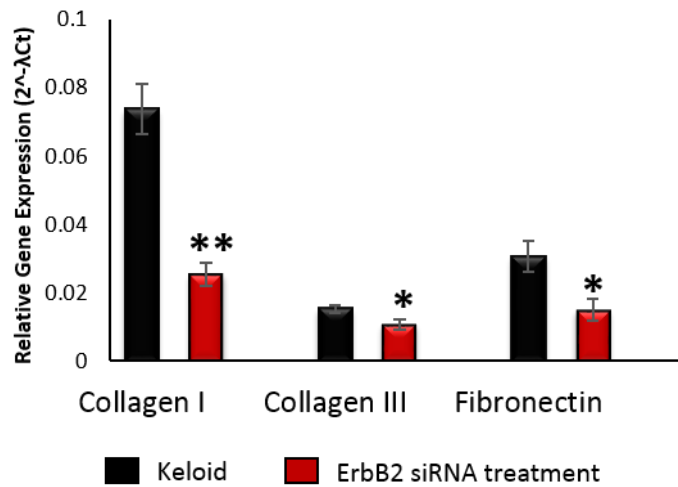


**Figure S6**— qRT-PCR gene expression in keloid fibroblasts treated with negative control siRNA or treated with ErbB2siRNA. This graph shows significant downregulation of TGFβ1 following treatment with ErbB2 siRNA.

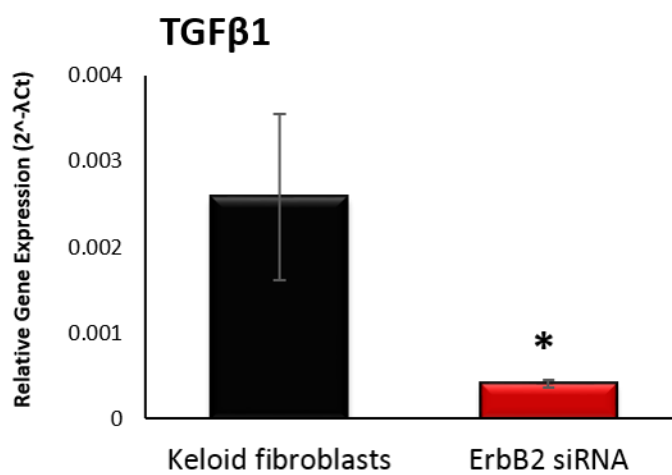


**Figure S7** - Schematic diagram representing possible ErbB signalling permutations with NRG1 ligand. EGFR/ErbB1 doesn't interact with NRG1. ErbB2 heterodimerisation results in the most potent signalling, particularly with ErbB3. NRG1 doesn't interact with ErbB2 directly but overexpression can result in homodimerisation and constitutive activation.

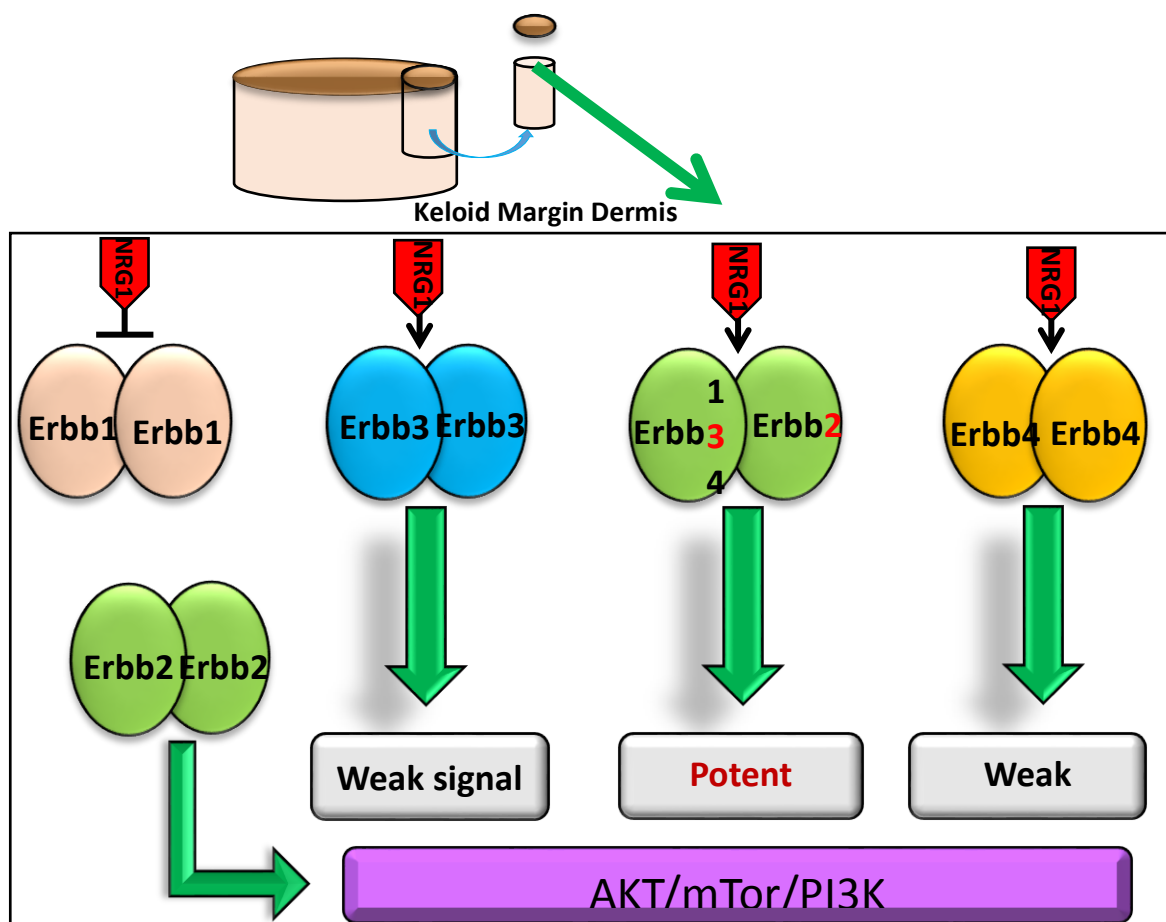


**Figure S8-** Conceptual illustration of the proposed mechanism underlying keloid margin dermis migration. KF NRG1/ErbB2 overexpression promotes migration and through paracrine signalling induces migration and fibrosis in adjacent NSF resulting in a continuous cycle of migration and expansion.

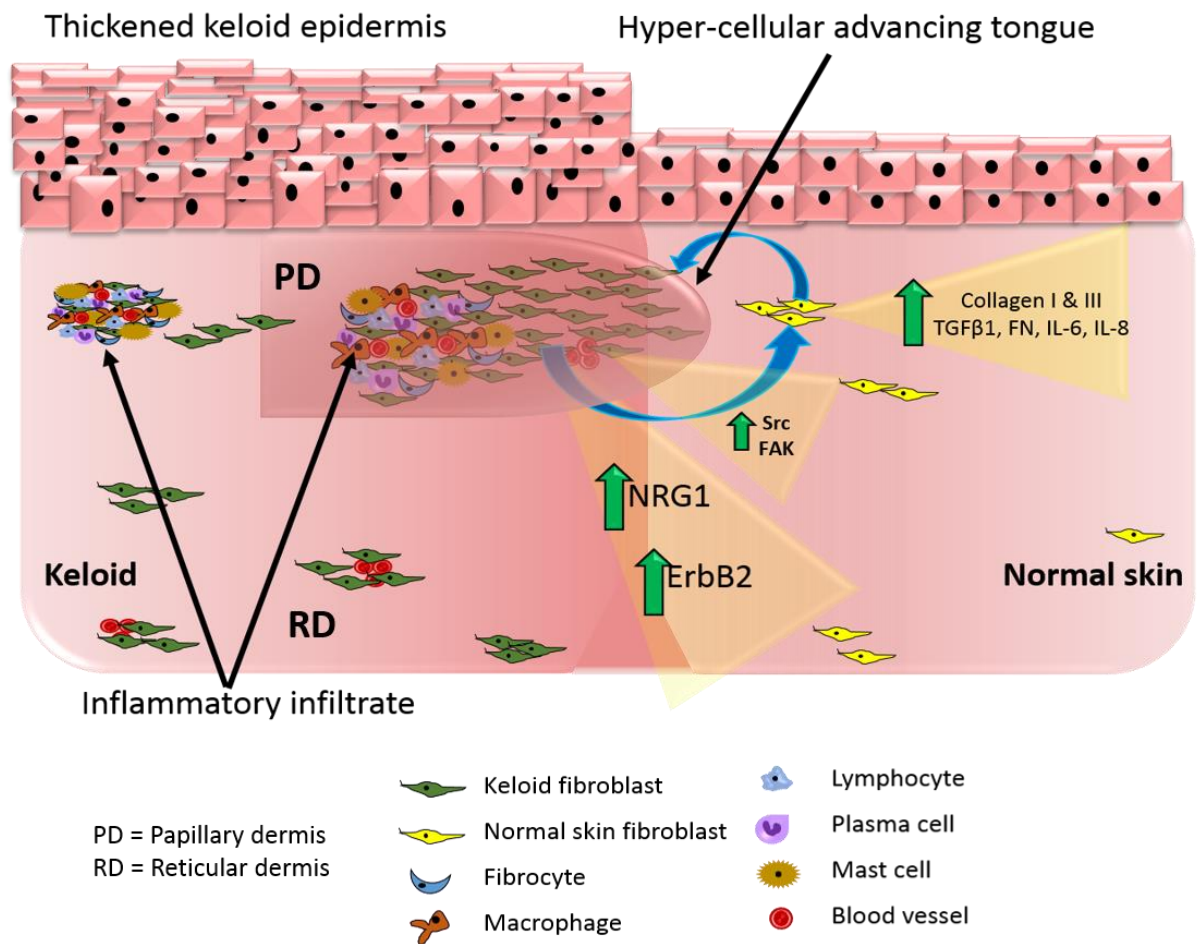


**Figure S9** - qRT-PCR gene expression in keloid and normal skin fibroblasts for CTGF, untreated and treated with 50ng/ml rhNRG1. There was a small decrease in CTGF expression in keloid fibroblasts and increase in CTGF expression in normal skin fibroblasts but neither of these was statistically significant.

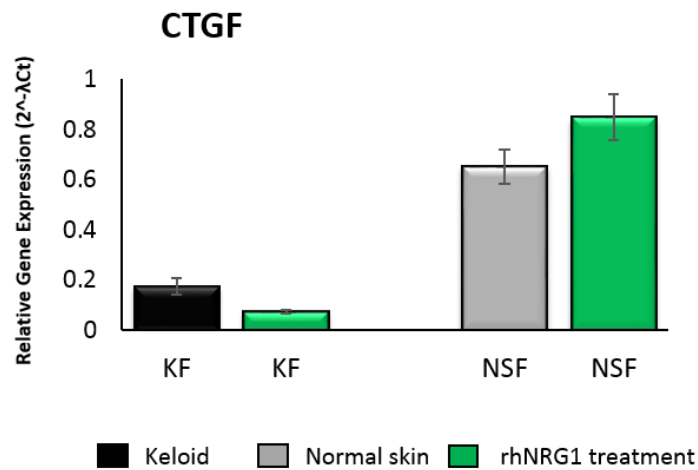
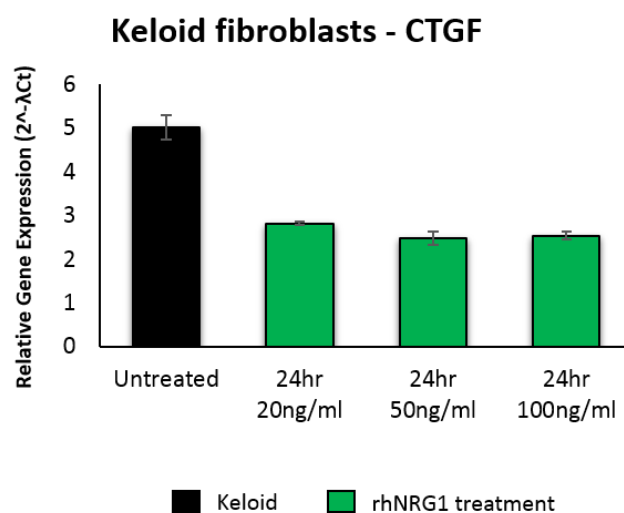


**Figure S10** – qRT-PCR expression of CTGF in keloid fibroblasts following treatment with exogenous rhNRG1 at 20, 50 and 100ng/ml over a period of 24 hours. These are compared with untreated fibroblasts. There is a decrease in CTGF expression with rhNRG1 treatment at all time points.



# Chapter 7

---

## Discussion



## **7.1 Discussion layout**

This chapter has been structured so as to begin with a brief description of the challenges facing KD research, which first established the focus of this thesis. Second, the specific questions arising out of the four aims of this project are addressed and finally, an overarching discussion of the findings from this thesis, in the context of the current literature and the implications for keloid disease is provided. To finish, the strengths and limitations of this thesis as well as the potential for future work that may arise from this project are considered.

## **7.2 Contributions of this thesis to keloid disease research**

### **7.2.1 The challenges**

This thesis has attempted to shed light on the complex pathobiology of keloid disease (KD) and in doing so, address some of the many challenges facing keloid research including overcoming existing experimental limitations and proposing new management strategies. To date, the elucidation of the mechanisms underlying keloid pathogenesis has been hindered by the heterogeneity that exists between patients, between keloid scars and within this fibroproliferative scar itself [1-3]. This lesional heterogeneity has been evidenced on a macroscopic, microscopic and molecular level, resulting in varied descriptions and reports in the literature that complicate the diagnosis and management of KD. Recent studies have endeavoured to address these differences within the keloid scar by separating the lesion into component parts and examining the gene and protein expression of each of these sites individually [4, 5]. This advance has brought to light not only the disparity between centre and margin regions within the keloid scar but also the variation in expression between the different strata: epidermis, papillary and reticular dermis [6]. In the past, KD was accepted as a dermal disorder, embracing fibroblasts as the culprits of its formation [7]. More recently, this focus has

shifted and the role of the epidermis explored for its potential contribution to the aberrant wound healing processes that result in abnormal scarring [8, 9].

Although keloid scars have been examined through site-specific analysis in recent years, to date there are no comprehensive studies combining this approach with an *in situ* technique such as laser capture microdissection (LCM). Traditional methods of investigation, including whole tissue analysis and monolayer cell culture, fail to fully reflect the natural architecture of the tissue optimal for the experimental dissection of these keloid sites [10-12]. Lack of a validated animal model for KD limits investigative options and complicates gene/molecular pathway manipulation, leaving researchers heavily reliant on exploring alternative methods [2, 13]. Previous research using monolayer culture and whole tissue has greatly added to the field in identifying differences in expression between keloid sites but it is the interactions between these sites that was hypothesised here to contribute to keloid formation and that have not been recreated in the lab with traditional methods. The precision and accuracy of LCM has provided an *in situ* setting with which to examine the relationships between these sites within the keloid scar and further KD research [14, 15]. Given previous success in the fields of both cutaneous disease and fibrosis, LCM offered an ideal platform for the investigation of heterogeneous tissues, such as KD [12, 16, 17].

### **7.2.2 Aims and specific questions addressed**

The first aim of this research was to investigate the *in situ* site-specific expression of KD by pairing LCM with whole genome microarray and subsequently comparing this approach with traditional methods of keloid research, including whole tissue biopsy analysis and 2D monolayer cell culture.

*Is a site-specific in situ approach the optimal strategy to investigate the pathogenesis of keloid disease and identify potentially significant differential gene expression?*

The work in this thesis has demonstrated that an *in situ* site-specific approach is both more accurate and more sensitive than either whole tissue or monolayer culture methods of dissection (**Chapter 4**). The reason this strategy is optimal lies in the heterogeneous nature of keloid scars, whereby better-defined expression profiles of distinct lesional sites facilitates improved understanding of KD pathobiology, the potential for enhanced differential diagnosis and targeted therapies. Although LCM is more technically challenging than traditional methods, requiring specialised equipment and time-consuming experimental optimisation, this *in situ* approach incorporated the expression profiles of both alternative methods of dissection, leading to a global picture for each keloid region, with a large number of genes from which to identify potentially significant differential expression.

The second aim of this project was to compare the genomic expression between well-defined distinct keloid sites and normal skin.

*Is there differential gene expression between different sites within the keloid epidermis and dermis?*

The data analysis from this *in situ* site-specific approach identified a number of differentially expressed genes (DEG) not only between keloid and normal skin but also between the three chosen sites (centre, margin and extralesional) within the keloid epidermis and dermis (**Chapter 4**). A combination of Ingenuity Pathway Analysis (IPA) gene ontology investigation and a thorough search of the current literature for individual top significant DEG of interest, demonstrated the variation in molecular processes specific to the different sites and highlighted

the contribution of the epidermis as a separate entity to the dermis in KD pathobiology. Through understanding the different mechanisms ongoing in different compartments of the keloid lesion, for example migration and angiogenesis at the invading margin, it may be possible to target therapies to specific sites and improve the efficacy of treatment.

The third aim of this thesis was to develop and explore hypotheses arising from the site-specific gene profiling approach so as to enhance understanding of KD pathobiology and promote new strategies for diagnosis and management.

*Do the DEG and expression patterns identified between keloid sites within the epidermis and dermis offer new insight to KD pathobiology from which novel hypotheses can be developed?*

The success of this strategy led to the development of a number of hypotheses for potential mechanisms underlying keloid pathobiology, two of which were then explored in detail, forming the latter two results chapters of this thesis. There were several intriguing lines of potential investigation outlined in **chapter 4**, which could also have been developed into full hypotheses. The existence of EMT in keloid scars, the role of ADAMTS in keloid dermal collagen deposition, the loss of epidermal IL-37 in the keloid inflammatory process and the contribution of gene dysregulation to the therapeutic resistance associated with KD, all form the basis of novel hypotheses relevant to KD research. These findings offer new insight into KD pathobiology that through further studies may prove to benefit the future management of KD.

The fourth and final aim of this thesis was to probe hypotheses arising out of the data analysis using functional *in vitro* studies.

As the first comprehensive study to combine a site-specific and *in situ* approach to KD, this thesis is unique in its exploration of retinoic acid pathway dysregulation and the contribution of neuregulin-1 to keloid pathology. Both of the hypotheses outlined below were probed in detail forming **chapter 5** and **chapter 6** of this thesis.

*Hypothesis I: Upregulation of AKR1B10 in keloid epidermis in situ implicates dysregulated retinoic acid metabolism in the pathogenesis of keloid disease*

*Hypothesis II: Neuregulin-1 (NRG1) upregulation in keloid margin dermis promotes keloid fibroblast migration through ErbB2 mediated signalling*

The importance of the findings resulting from the pursuit of both of these hypotheses is discussed below, where in combination with the findings from **chapter 4**, the significance of interrupted retinoic acid metabolism and NRG1/ErbB2 signaling are put into context with regard to the current literature and relevance to KD.

### **7.2.3 General discussion**

As demonstrated in **chapter 4**, combined LCM and whole genome microarray presents an *in situ* approach to dissecting KD that is more sensitive and more accurate than traditional methods of investigation. Whole tissue analysis can be diluted by the heterogeneity of multi-component transcriptomes causing reduced sensitivity and here it was shown that monolayer cell culture resulted in distorted magnitudes of differential gene expression, masking the significance of keloid and normal skin divergence. The uniquely applied *in situ* technique to KD described in this thesis incorporated the expression patterns of both of whole tissue and monolayer methods, giving a more complete and spatially resolved overall picture of relative keloid gene expression. Therefore, subsequent analysis performed in this thesis focussed on the *in situ*

expression to perform both gene enrichment using Ingenuity Pathway Analysis (IPA) and specific filtering criteria (fold change > 2, p-value < 0.05 and for DEG q-value < 0.05). The potential importance of this approach to KD was highlighted by the exposure of several DEG in the epidermis, previously overlooked with traditional methods of dissection. Analysis revealed an activated pro-inflammatory epidermis with dysregulation of S100A8, WDR66 and AKR1B10, supporting a role for EMT in keloid pathogenesis [8, 18]. As one of the most significantly upregulated genes common to all three sites of the keloid epidermis with fold changes over sixty times that of the normal skin epidermis and not previously identified in KD, AKR1B10 was further explored (**Chapter 5**).

The role of this highly efficient aldo-keto reductase enzyme in KD may be multi-factorial, making the novel identification of its dysregulation in KD one of the cornerstones of this thesis. As a rate-limiting enzyme in *de novo* synthesis of long chain fatty acids, AKR1B10 contributes to tumour cell growth and knockdown of this enzyme has shown this is achieved through acetyl-coA carboxylase- $\alpha$  (ACCA) stability [19]. AKR1B10 is also associated with recurrence and therapeutic resistance, both of which are significant obstacles in the management of KD [20, 21]. Perhaps most significantly, AKR1B10 has a specificity for retinaldehyde that implicates it in the retinoic acid (RA) biosynthesis pathway, which may be the governing link between many of the processes contributing to KD [22]. The combination of upregulated AKR1B10, ADH7, ALDH1A1, CRABP2 and downregulation of CRABP1 and CYP26B1, led to the hypothesis that there was an overall deficiency of RA in keloid epidermis *in situ*. As a pleiotropic metabolite acting through both direct transcriptional regulation and indirect influence of numerous cytokines and their signaling pathways, the dysregulation of RA has far-reaching effects in terms proliferation, apoptosis, differentiation, inflammation, immune regulation, metabolism and angiogenesis [23-25]. In the current work, identification of this altered epidermal RA

metabolism emphasises the potentially critical role of the epidermis in keloid pathobiology and the downstream effects of its communication with the underlying dermis. By recreating the keloid epidermal expression pattern through induced overexpression of AKR1B10, the resultant reduction of RARE transactivation produced pro-fibrotic responses in keloid fibroblasts with increased TGF $\beta$ 1, collagen I and collagen III. These paracrine signals may be an essential component in the development and maintenance of KD and the revelation of the potential regulation of these processes by RA described in this thesis not only enriches our knowledge on the mechanisms underlying keloid pathobiology but also delivers alternative therapeutic options to address the existing management conundrums [26]. This is particularly interesting as RA has been used for the management of KD in the past, where topical, oral and *in vitro* administration have shown both clinical improvement and reduced collagen production and cell proliferation [27-29].

Despite this success, the molecular and mechanistic role of RA was never fully explored in KD until this current work and over the last 20 years the investigation of RA in KD and use of RA, its isomeric forms and its derivatives in management, had largely fallen out of favour in the literature. This is especially curious as the constitutive abnormalities in RA metabolism in dermatology in general are attracting increasing interest [30, 31]. One reason for this may be the mixed reports regarding the effects of RA on fibrosis in the literature and the report of keloid and hypertrophic scar formation following isotretinoin treatment [32]. The pleiotropy of RA combined with the narrow ill-defined target range within which it optimally functions, results in a bi-modal effect of this metabolite on significant processes, including those responsible for the production and maintenance of keloid scars [33, 34]. The failure of RA to abrogate the expression of TGF $\beta$  and collagen in **chapter 5**, demonstrated the utility of mechanistic investigation whereby previous clinical treatment with RA likely triggered simultaneous

uncontrolled signaling activation/inhibition and not just classical pathway activation alone. This thesis affirms the importance of targeted therapies in a heterogeneous condition such as KD, where manipulation of significant modulators like TGF $\beta$  and RA cannot restrain the tide of multiple concurrent effects. Therefore, with further studies AKR1B10 presents an ideal candidate for focussed interference in KD. From the continued discussion below it is evident that RA pervades many of the other aspects of keloid pathology discussed in this thesis, lending increased significance to the findings presented here.

Retinoic acid is a well-established immune modulator and regulator of inflammation [35, 36]. Given the evidence in the literature to date of the significant role of immune responses and presence of inflammation in KD [37, 38], the identification of AKR1B10 overexpression and the postulated dysregulation of RA metabolism put forward in this thesis, presents intriguing potential for elucidation of keloid immune mechanisms. RA is also known to interact with TGF $\beta$ , itself firmly established to be dysregulated in KD, to direct immune function [39]. In the context of this thesis, the complex alteration in the expression of IL-1 $\beta$ , IL-2, IL-4, IL-6, IL-13 and IL-17 receptors as well as STAT3 indicated in **chapters 4** and **6**, may be intricately connected with the identified RA metabolism dysregulation identified in **chapter 4**. In the gut, RA has been shown to regulate the functional differentiation of T cells, mediate the TGF $\beta$ -dependent expression of Foxp3 (transcription factor for regulatory T cells that serves to inhibit immune responses) and modulate T<sub>H</sub>1, T<sub>H</sub>2 and T<sub>H</sub>17 cell generation [40, 41]. This same study on mesenteric lymph node-dendritic cells, showed that RA inhibits T<sub>H</sub>2 cell-induced IL-13 [42], however, there are several studies that contend RA promotes inflammatory T<sub>H</sub>2 [23]. Stimulation of murine T cells with exogenous RA *in vitro* resulted in the inhibition of T<sub>H</sub>1, T<sub>H</sub>2 and T<sub>H</sub>17 polarisation with resultant reduction in pro-inflammatory IL-17, IFN- $\gamma$  and IL-4 as well as the enhancement of anti-inflammatory Foxp3<sup>+</sup> cells [43]. Through a SOCS3-dependent mechanism, RA has been



shown to inhibit the expression of IL-6, which itself influences T<sub>H</sub>17 generation and acts in concert with TGF $\beta$  via STAT3 to induce ROR $\gamma$ c in T cells, a transcription factor related to retinoic acid receptors (RAR) and retinoid X receptors (RXR) [42-44]. Furthermore, RA has been shown to suppress the expression of IL-1 family of cytokines in dermatological diseases [45]. By regulating the fate of dendritic cells, RA influences the expression of numerous cytokines and chemokines involved in immunological function and control of inflammation, including the modulation of innate lymphoid cells (ILC) [42]. The existence of contradictory reports in the literature regarding the exact role of RA in various aspects of immune modulation and ILC regulation highlights the fact that this is still a nascent field of research and as previously noted, deviation of RA concentrations outside a restricted range may affect different molecules in different ways. The direction of change in expression of many of the inflammatory markers (IL-1 $\beta$ , IL-4R, IL-6R, IL-13R and IL-17R as well as STAT3) described in **chapter 4** of this thesis correlate with the hypothesised deficiency in RA demonstrated in **chapter 5**. Therefore, RA is an ideal therapeutic target to modulate inflammation in KD, however, given the aforementioned pleiotropy and lack of consistency within the literature as well as the incomplete mechanistic understanding of the immunological role in KD, further studies and a deeper insight is required before altering significant members of the immune system.

Altered RA metabolism is likely to play a significant role in stem cell biology and therefore may have effects in KD beyond those identified here [46]. The theory of cancer-like stem cells, as compared with mesenchymal stem cells, has been previously alluded to in keloid pathobiology [47] but considering the association of these cells with several other heterogeneous solid tumours it is a surprisingly under-investigated topic in keloid research [48]. Keloid scars are often described as tumorigenic or quasineoplastic, given the propensity for continued growth and invasion [49, 50]. This theory suggests the majority of tumour-like mesenchymal cells in

keloid scars are derived from a much smaller population of multipotent cancer-like stem cells that allow unlimited self-renewal and exponential growth [51]. The designation of OCT4 as an upstream regulator in the analysis presented in this work (**Chapter 4**) supports a recent study that identified embryonic stem cell (ESC) markers within the specialised keloid-associated lymphoid tissue (KALT) [52]. It may be that the described ESC-like population and the cancer-like stem cell niche are linked, whereby environmental stressors, such as hypoxia, induce de-differentiation of fibroblasts to a stem cell-like state, a process thought to partially depend on Notch signaling [51].

Several of the genes discussed throughout the current work have been connected with therapeutic resistance including ALDH1A1 and AKR1B10, which metabolises carbonyl compounds, xenobiotics and may mediate chemoresistance of cancer cells [21, 53]. Also detected were UGT3A2, which plays a role in drug metabolism and TUBB3, which in particular has been connected with taxane resistance [54, 55]. Additionally, some chemotherapeutic resistance has been reported in ErbB2 positive breast tumours [56]. While the description of the significant upregulation of both NOTCH4 and ALDH1A1 in this thesis are only two of the molecules that have been linked with these types of cells in the literature [57-59], the well-reported therapeutic resistance associated with KD also lends itself to the existence of a cancer-like stem cell population or niche within the scar. Given the plasticity of these cells and their dynamic adaptive nature to different signals, it may be that the variation in keloid phenotypes arises as a result of this subpopulation of cells responding to alternative environments. Hypoxia, a frequently proposed aetiological factor in keloid development, is a well-established factor in the cancer microenvironment and along with modulators including IL-6, Wnt and Notch (**Chapter 4**), may participate in a positive feedback loop promoting the maintenance of these cancer-like stem cells. Further support for the presence of these cells lies in the consistent

records of keloid recurrence [60]. Most treatments are associated with partial resolution and frequent relapse, with the secondary keloid worse than the original [61]. If cancer-like stem cells reside within keloid scars and are not eliminated with surgery or treatment, it is a reasonable assumption that they would contribute to re-growth. Additionally, individual significant DEG discussed throughout this thesis have independently been associated with tumour return and thus may contribute to keloid recurrence in a similar fashion. AKR1B10 was overexpressed in 87.5% of recurrent breast tumours and is subsequently being investigated in a clinical trial as a potential marker for recurrence [20], ALDH1A1 was found to correlate with tumour recurrence in bladder cancer [62] and both ErbB2 and NOTCH4 have been associated with recurrence in breast and salivary adenoma cancers [63, 64]. COMP and CTHRC1 as well as ADADM12 have all been associated with recurrence and investigated for markers of relapse in various cancers [65, 66], with the latter showing positivity in desmoid tumours which bear some similarity to keloid scars in terms of heterogeneity, local aggressive invasion without metastasis and high recurrence rates [67, 68]. The persistence and recapitulation of keloid scars following treatment has been well established but to date been incompletely understood. This thesis highlights the multi-factorial nature of this recurrence and underlines the benefits of a site-specific and targeted approach, most likely requiring polytherapy.

Epithelial-mesenchymal transition (EMT) is also a relatively under-investigated topic in KD [8, 69]. Therefore, although the evidence supporting this concept in keloid pathology is minimal to date [9], the findings in this thesis support the likelihood of this phenomenon or indeed a “partial EMT” process contributing to KD. Enrichment studies using IPA produced a number of upstream regulators (Wnt, MAPK, HOX, ZEB, PRXX1 etc) previously linked with EMT in other pathologies (**Chapter 4**). Downregulation of BMP2, CLDN4 and CLDN23 as well as upregulation of WDR66 and  $\alpha$ -SMA in the keloid epidermis *in situ* (**Chapter 4**) indicate an epithelium

undergoing cell-cell junction dissolution and adoption of mesenchymal markers. A possible role for RA in this process is supported here primarily by the downregulation of E-cadherin in AKR1B10-overexpressing keratinocytes (**Chapter 5**) but also RA has been associated with reciprocal activation of BMP2 [70-72], whose loss may therefore result from the hypothesised RA deficiency in the keloid epidermis. The presence of EMT in KD is additionally supported by the prominence of TGF $\beta$  throughout this thesis (**Chapters 4, 5 & 6**). Long considered the master regulator of fibrosis [73, 74], TGF $\beta$  has been implicated in multiple aspects of keloid pathobiology, including inflammation, differentiation, proliferation, EMT, collagen deposition, migration and invasion [61, 75, 76]. As the histological hallmark of KD, collagen excess has been a therapeutic target for some time and although its production has been abrogated through therapies mediating TGF $\beta$  expression, the definitive interruption of its formation has not been achieved. To this end, the identification of enzymes crucial to collagen assembly and production in **chapter 4**, including ADAMTS14, ADAMTS2, COMP, CTHRC1 and ADAM12 may represent alternative targets, especially as a number of them are thought to be locked in a positive feedback loop with TGF $\beta$ 1 [77, 78].

ADAMTS2 and ADAMTS14 in particular are interesting targets; not previously investigated in KD and possibly associated with a degree of redundancy with ADAMTS3 [79], which was not found to be dysregulated in this study, modulation of these enzymes could be a useful adjuvant therapy to reduce keloid tumour bulk, but this would need follow-up investigation. TGF $\beta$ , previously inculpatated in keloid migration in the literature [80], was also found in this current work to be induced by neuregulin-1 (NRG1), a peptide significantly upregulated in keloid margin dermis and not previously associated with KD (**Chapter 6**). Cell migration is a necessary component of the invasion that is pathognomonic of KD and the exposure of NRG1/ErbB2/FAK/Src signaling as contributory to this process in the keloid margin, represents

an appealing hypothesis. In addition to migration at the margin dermis of the keloid scar, the overexpression of NRG1 and ErbB2 may also have paracrine effects on the epidermis, cooperating with other factors to produce hyper-proliferation and keratinocyte migration [81, 82]. ErbB2, one of the four EGF receptor tyrosine kinase family members is a well-known oncogene associated with breast cancer [83]. Interestingly, in a cohort of ductal carcinoma in situ (DCIS) samples there was a strong correlation between AKR1B10 and ErbB2 [84]. This reciprocity is further supported by ability of RA to decrease the duration of signaling at EGF receptors in breast cancer, thereby decreasing cell proliferation [85].

Given the incidence of KD in darker-skinned individuals it was interesting to note that NRG1 is highly expressed in individuals with Fitzpatrick type IV skin (darker) and that treatment with rhNRG1 resulted in melanocyte proliferation and pigmentation [86]. Further to this, TUBB3 and RA are also associated with melanogenesis. TUBB3 is considered to be a novel biomarker of melanocytes [87] and may play a role in the pigmentation response of the skin through interaction with MC1R [88]. Widely used as a topical treatment for melasma and photoaged skin, the mechanism by which RA affects pigmentation remains undistinguished but is thought to involve ALDH1A1 [89]. Similar to other effects of RA, there is some discrepancy in the literature with regard to the influence of RA on skin pigment and the inability to replicate the clinically observed depigmentation using *in vitro* experiments [90]. That said, when the ethnic differences in gene expression were examined for women with uterine leiomyoma (benign fibrotic tumours of the myometrium) it was observed that the expression of RAR $\alpha$  and RXR $\alpha$  differed significantly in black women [91]. Determination of the differences in RA metabolism between ethnicities in KD may reveal similarly intriguing results.

A further field of interest in keloid disease but significantly under-investigated is the role of epigenetics, which is the alteration of gene expression without changing the DNA sequence. A recent publication postulated the keloid methylome is hypomethylated, suggesting an activated state, as methylation generally represses gene transcription [92]. This study also described the dysregulation of genes involved in histone degradation in keloid disease, which may play a role in the pathogenesis of this condition. Of further interest is the potential link with retinoic acid, which has also been associated with methylation and is often given as treatment in combination with epigenome-altering drugs [93]. The suggestion that retinoic acid receptors (RAR) interact with co-repressors to affect HDAC (histone deacetylase) expression and maintain chromatin in a condensed state [94] ties in with the findings in this thesis, such that loss of RA results in an activated state in keloid disease. This would be an interesting focus for future work in keloid disease research.

In summary, this thesis successfully addresses the challenges of overcoming keloid heterogeneity while maintaining the existing pathological microenvironment by combining site-specific and *in situ* approaches. The comprehensive work presented here is unique in its achievement of looking at both of these major variables at once. The management of KD is notoriously difficult with both clinicians and patients frustrated by lack of an effective treatment. Through the identification of RA metabolism dysregulation in KD and the exploration of this in relation to the underlying pathobiology, this work not only adds a significant contribution to our fundamental understanding of KD but also carries clinical implications.

### 7.3 Thesis strengths and limitations

There are several strengths of the research presented in this thesis. Foremost, the use of human tissue samples for *in situ* analysis and further experimentation with human tissue and primary cells, allows for parallels to be drawn in terms of translational research. In both the retinoic acid and neuregulin-1 studies, the expression pattern of the transfected keratinocytes and keloid fibroblasts respectively, reflected that of the *in situ* tissue expression, supporting the use of the *in vitro* work for functional studies.

The comprehensive study of KD from both a site-specific and *in situ* LCM approach had not been previously described and proved more sensitive and accurate when compared with traditional methods of investigation, including whole tissue biopsy and monolayer cell culture analysis. Results were consistent and there were a number of significant and novel findings from this work. The identification of so many relevant differentially expressed genes provides a firm basis for future hypotheses and potential studies that may prove fundamental in the pathogenesis of KD and the wider study of fibrosis. Exploration of two central hypotheses using multiple, corroborating investigative methodologies, revealed previously uninvestigated mechanisms contributing keloid scarring. Additionally, the work in this thesis has been peer reviewed or is under review as part of submission to scientific journals, thereby supporting its strengths and value in presenting it to the wider academic community.

The major, yet unavoidable, weakness of this study lies in the ethnic divergence of keloid from control tissue samples. All of the normal skin control biopsies were harvested from Caucasian patients whereas only 3 of the keloid scar samples were from Caucasian patients. Therefore, while there was some variation between keloid and normal skin, there were also some age-matched, location-matched and type-matched skin samples. Given the nature of KD, the limited

availability of samples and the ethical considerations of obtaining normal skin from keloid-prone patients, these differences were controlled for as far as was possible. The extralesional tissue, while not wholly representative of patient-matched normal skin given the field cancerisation effect, generally shows an opposing pattern of expression than keloid centre and margin, suggesting this unique dataset may also serve as a patient-matched control.

A further limitation of the work concerns the exposure of the potential role of NRG1/ErbB2/FAK/Src in keloid migration in the margin dermis. Further analysis of the effects of exogenous rhNRG1 supplementation and ErbB2 siRNA on both PTK2 and Src expression should be conducted on a protein level. This could be achieved through the implementation of western blot and would add further weight to the conclusions drawn regarding the role of this signaling mechanism in keloid migration and invasion.

As with all scientific research it is only through repeated studies with large sample numbers can true patterns be established and progress confirmed.

#### **7.4 Future work**

The current work contributes significantly to the understanding of keloid pathobiology and consequent to offering new insight and perspectives on a complex disorder such as KD, raises a number of interesting targets for future research (**Figure 7.1**). The overall analysis of the extensive microarray data described in **chapter 4** revealed several concepts that should form the basis of future studies in KD.



As a disorder characterised primarily by collagen excess, the exposure of the overexpression of key enzymes in the regulation of collagen production offers new targets for an unresolved burden in KD. ADAMTS14 and ADAMTS2 have not been previously investigated in KD and given the association with other fibroses [95, 96] as well as the evidence of the effect of their knockout on fibrosis [95], these molecules represent ideal candidates for targeted studies. Furthermore, the likely involvement of ADAMTS2 in a positive feedback loop with TGF $\beta$ 1 offers an attractive alternative to the manipulation of such a pleiotropic molecule as TGF $\beta$ , especially as there may be some redundancy between ADAMTS2 and ADAMTS14 with ADAMTS3 [79]. A follow-up study interrogating the role of these three metalloproteinases in KD would involve first confirming their expression patterns in a sufficient number of tissue samples compared with normal skin. Additional *in vitro* studies to corroborate these findings and support the use of cell culture for functional studies would be recommended. Pending the results of this validation, further work would entail siRNA studies to evaluate the significance of these enzymes in collagen synthesis in KD and establish any redundancy between them so as to balance their knockdown and allow for appropriate ECM regulation.

Now largely accepted as partially the result of a prolonged inflammation, the literature describes not only inflammatory infiltrate and specialised keloid-associated lymphoid tissue (KALT) but also significant disturbance of immune regulation in KD, thus far evidenced by dysregulation of several chemokines and cytokines [37, 97, 98]. Indeed, inflammation is considered an essential process in fibrosis and thought to involve elements of both innate and adaptive immune responses [99]. **Chapter 4** exposes dysregulated IL-13, IL-4 and IL-17 receptors as well as IL-37 downregulation in keloid epidermis *in-situ*, unveiling yet more pieces of the complex puzzle that constitutes the inflammatory mechanisms underlying keloid pathogenesis. The plausible presence of innate lymphoid cells (ILCs) alluded to in **chapter 4**, has not been previously examined in KD and given the correlation with not only cytokine dysregulation (IL-13, IL-17 and RORc) but also retinoic acid [100], would constitute a fascinating subject for

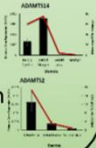


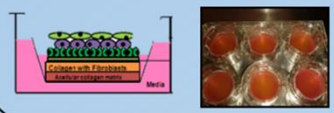

further work in keloid research. ILCs have been implicated in wound healing and fibrosis but the exploration of these cells in humans is still in the nascent stages and some of the groups remain to be precisely defined [101-103]. Initial experiments would involve locating the different subgroups of ILCs within keloid tissue through immunostaining for the appropriate characteristic markers [104]. Following localisation, LCM could be used to isolate these cells and determine their expression profiles, thus advancing our understanding of their role in KD. If these cells prove to contribute to keloid fibrosis they may represent a novel therapeutic target.

Similarly, alluded to in **chapter 4** and broached in the discussion, is the existence of cancer-like stem cells in KD. Keloid derived precursor cells (KPCs) have previously been identified, demonstrating characteristic self-renewal, clonogenicity and multipotency [47]. Indeed these cells may even arise as a result of EMT [105]. LCM could significantly advance the study of these cells in KD, by allowing accurate isolation from the tissue and focussed analysis of their expression profile. The molecular distinction from tumour bulk cells would allow directed therapies or as in other studies, treatments to differentiate the stem cell niche back to an epithelial-like state [105, 106].

Alongside this thesis, some preliminary work was done on the development of an organotypic keloid model. Given that there is no validated animal model for KD, heavy reliance on *in vitro* techniques necessitates the development of reliable and reproducible model that recapitulates the *in vivo* environment as closely as possible. An organotypic culture model entails combining cells of different lineages in experimentally defined ratios to recreate an organ, in this case the skin [107, 108]. The substitution of keloid keratinocytes and fibroblasts into this direct cell-cell contact model would reflect the 3D architecture of keloid scars more closely than monolayer

cells. In addition to dimensionality, this model would allow for manipulation of various parameters including cell signaling, gene expression modification and constituent alteration such as inhibitors or treatments. More so than 2-chamber co-culture models, the organotypic models have *in vivo* relevance, strengthened by direct contact of epidermal and dermal layers and the formation of a dermo-epidermal junction [109], allowing for maintenance of EMI, which in this thesis were established to play a role in KD. With improving technology and the evolution of composite scaffolds, the ability to develop increasingly complex 3D models that incorporate multiple cell types, blood vessels and nerves, will be essential in conditions for which there are no alternatives, such as KD. The establishment of a working organotypic model for KD is a fundamental step in this process and would form the basis of relevant future work.

In this work, the significant upregulation of AKR1B10 led to the implication of RA metabolism dysregulation in keloid pathogenesis. There is a lot of scope for the continuation of this work, which would include targeting AKR1B10 in keloid as well as examining the effect of RA on keloid inflammation and EMT. It has been shown in this thesis that AKR1B10 overexpression in keratinocytes has pro-fibrotic effects on the underlying fibroblasts. The first aim would be to use *in vitro* siRNA studies to knock down AKR1B10 in keloid keratinocytes and analyse the effect of this on RA metabolism pathway, transactivation and epithelial-mesenchymal interactions. This work would be greatly aided by the development of an organotypic model, in which AKR1B10-negative keloid keratinocytes could be combined with keloid fibroblasts. These models would also benefit investigation of topical treatments, especially given the overexpression of AKR1B10 in the keloid epidermis. The effects of AKR1B10 and RA on both EMT markers and inflammatory markers is justified by the involvement of RA in these processes in the literature as well as the support provided in this thesis.

	Unanswered questions	Aims	Methods
Topic 1	<p>What role do ADAMTS2 and ADAMTS14 play in keloid collagen deposition?</p> <p>Is there redundancy between ADAMTS2, ADAMTS3 &amp; ADAMTS14?</p>	<ul style="list-style-type: none"> <li>Establish the gene &amp; protein expression of ADAMTS2,3,14 for keloid vs normal skin <i>in vivo</i> &amp; <i>in vitro</i></li> <li>Determine the effects of ADAMTS2,3,14 knockdown on collagen formation in KD</li> </ul>	<p>mRNA western blot for keloid and normal skin tissue and fibroblasts. IHC for both tissues</p> <p>siRNA studies of each ADAMTS2,3,14 in keloid fibroblasts combined with collagen quantification</p> 
Topic 2	<p>Are ILCs present in keloid scars?</p> <p>Do ILCs contribute to keloid pathogenesis?</p>	<ul style="list-style-type: none"> <li>Localisation of ILCs within KD tissue</li> <li>Isolate keloid ILC &amp; examine expression profiles</li> <li>Identify cellular effects produced by released factors</li> </ul>	<p>Immunostaining for characteristic ILC markers</p> <p>LCM to isolate identified cells from tissue</p>  <p>Microarray panel to establish expression of isolated cells</p>
Topic 3	<p>Is there a cancer-like stem cell (CSC) niche in KD</p> <p>What role does this niche have in keloid pathogenesis?</p>	<ul style="list-style-type: none"> <li>Isolation of CSC within keloid tissue</li> <li>Examine the expression profile of CSC in KD</li> <li>Deplete CSC using combination therapy and evaluate impact</li> </ul>	<p>Stain keloid tissue for OCT4, Nanog, CD133, ALDH1A1 etc to localise CSC</p> <p>LCM to isolate CSC from within tissue</p>  <p>Combine with microarray</p>
Topic 4	<p>Would a 3D organotypic model for KD be suitable for both investigation of pathogenesis and therapeutic testing?</p>	<ul style="list-style-type: none"> <li>Establish a 3D cell-cell model using keloid-derived primary cultured cells</li> </ul> 	<p>Compare the established model with keloid tissue expression: mRNA, IHC and western blot for comparative studies</p> <p>Exogenous administration of compounds or siRNA for functional studies</p>
Topic 5	<p>Does AKR1B10 attenuation alter RA metabolism in keloid?</p> <p>Does AKR1B10 attenuation affect fibrosis within keloid dermis?</p> <p>In KD, does RA influence EMT and inflammation?</p>	<ul style="list-style-type: none"> <li>Analyse the effect of AKR1B10 on RA pathway in keloid keratinocytes (KK)</li> <li>Analyse AKR1B10 attenuation in KK on keloid fibroblasts</li> <li>Assess RA administration vs AKR1B10 knockdown on EMT &amp; inflammatory markers</li> </ul>	<p>AKR1B10 siRNA in KK</p> <p>Use of siRNA KK in organotypic model to analyse effect on dermal layer</p>  <p>Exogenous RA and/or AKR1B10 siRNA on organotypic model and mRNA for EMT/inflamm markers</p>

ADAMTS, A disintegrin and metalloproteinase with thrombospondin motif; AKR1B10, aldo-keto reductase family 1, member B10; CSC, cancer-like stem cell; EMT, epithelial-mesenchymal transition; IHC, immunohistochemistry; KK, keloid keratinocyte; ILC, innate lymphoid cell; RA, retinoic acid

**Figure 7.1 Proposed future work.** The diagram addresses questions raised from the thesis and suggests techniques to approach the aims established from these questions.

## 7.5 Concluding remarks

This thesis has demonstrated that combined site-specific and *in situ* techniques with whole genome microarray represents a robust approach to elucidating the mechanisms underlying the pathogenesis of KD. Although technically challenging, through careful optimisation the application of LCM methodology to KD is one of the major contributions in this thesis. It is through the employment of LCM that novel hypotheses concerning the pathobiology of KD were formed. The localisation of previously unexplored migration pathways in keloid margin dermis exemplifies the utility of this approach and represents a potential target to control the invasion of keloid into normal skin, a hallmark of tumorigenic behaviour. The LCM-facilitated exposure of altered retinoic acid metabolism in keloid epidermis was not only shown to contribute to dermal fibrosis through EMI but given the pleiotropic nature of RA, this metabolite may represent the nexus in a network of dysregulated mechanisms underlying KD. RA has been shown to be intertwined with several of the characteristic aberrations of KD, including immune responses, inflammation, EMT, cancer-like stem cells, collagen deposition, pigmentation, therapeutic resistance and keloid recurrence. RA is also linked with some of the aetiological hypotheses underlying keloid formation such as hypoxia, the sebum theory and cell cycle control. Given the altered metabolism of RA was identified in keloid epidermis, further studies into the effect of targeted AKR1B10 knockdown may reveal a treatment strategy that can be topically applied, facilitating patient compliance and reducing the risk of recurrence. Overall, the application of a site-specific *in situ* approach to keloid disease research has provided a competitive alternative to traditional methods of dissection and produced novel hypotheses on the mechanisms underlying KD pathobiology that may instruct future research and benefit both diagnostic and management strategies.

## References

1. Taylor A, Budd DC, Shih B, Seifert O, Beaton A, Wright T, et al. Transforming Growth Factor beta Gene Signatures are Spatially Enriched in Keloid Tissue Biopsies and In vitro-Cultured Keloid Fibroblasts. *Acta Derm Venereol*. 2016.
2. Marttala J, Andrews JP, Rosenbloom J, Uitto J. Keloids: Animal models and pathologic equivalents to study tissue fibrosis. *Matrix Biology*. 2016;51: 47-54.
3. Bella H, Heise M, Yagi KI, Black G, McGrouther DA, Bayat A. A clinical characterization of familial keloid disease in unique African tribes reveals distinct keloid phenotypes. *Plast Reconstr Surg*. 2011;127: 689-702.
4. Seifert O, Bayat A, Geffers R, Dienus K, Buer J, Lofgren S, et al. Identification of unique gene expression patterns within different lesional sites of keloids. *Wound repair and regeneration : official publication of the Wound Healing Society [and] the European Tissue Repair Society*. 2008;16: 254-65.
5. Syed F, Ahmadi E, Iqbal SA, Singh S, McGrouther DA, Bayat A. Fibroblasts from the growing margin of keloid scars produce higher levels of collagen I and III compared with intralesional and extralesional sites: clinical implications for lesional site-directed therapy. *Br J Dermatol*. 2011;164: 83-96.
6. Supp DM, Hahn JM, Glaser K, McFarland KL, Boyce ST. Deep and superficial keloid fibroblasts contribute differentially to tissue phenotype in a novel in vivo model of keloid scar. *Plast Reconstr Surg*. 2012;129: 1259-71.
7. Datubo-Brown DD. Keloids: a review of the literature. *British journal of plastic surgery*. 1990;43: 70-7.
8. Hahn JM, Glaser K, McFarland KL, Aronow BJ, Boyce ST, Supp DM. Keloid-derived keratinocytes exhibit an abnormal gene expression profile consistent with a distinct causal role in keloid pathology. *Wound repair and regeneration : official publication of the Wound Healing Society [and] the European Tissue Repair Society*. 2013;21: 530-44.
9. Yan L, Cao R, Wang L, Liu Y, Pan B, Yin Y, et al. Epithelial-mesenchymal transition in keloid tissues and TGF-beta1-induced hair follicle outer root sheath keratinocytes. *Wound repair and regeneration : official publication of the Wound Healing Society [and] the European Tissue Repair Society*. 2015;23: 601-10.
10. Baker BM, Chen CS. Deconstructing the third dimension: how 3D culture microenvironments alter cellular cues. *J Cell Sci*. 2012;125: 3015-24.
11. Mabry KM, Payne SZ, Anseth KS. Microarray analyses to quantify advantages of 2D and 3D hydrogel culture systems in maintaining the native valvular interstitial cell phenotype. *Biomaterials*. 2016;74: 31-41.
12. Lovendorf MB, Mitsui H, Zibert JR, Ropke MA, Hafner M, Dyring-Andersen B, et al. Laser capture microdissection followed by next-generation sequencing identifies disease-related microRNAs in psoriatic skin that reflect systemic microRNA changes in psoriasis. *Exp Dermatol*. 2015;24: 187-93.
13. Williams FN, Herndon DN, Branski LK. Where we stand with human hypertrophic and keloid scar models. *Exp Dermatol*. 2014;23: 811-2.
14. Datta S, Malhotra L, Dickerson R, Chaffee S, Sen CK, Roy S. Laser capture microdissection: Big data from small samples. *Histol Histopathol*. 2015;30: 1255-69.
15. Espina V, Wulfkuhle JD, Calvert VS, VanMeter A, Zhou W, Coukos G, et al. Laser-capture microdissection. *Nat Protoc*. 2006;1: 586-603.
16. Zhu KQ, Carrougher GJ, Couture OP, Tuggle CK, Gibran NS, Engrav LH. Expression of collagen genes in the cones of skin in the Duroc/Yorkshire porcine model of fibroproliferative scarring. *J Burn Care Res*. 2008;29: 815-27.
17. Sabo-Attwood T, Ramos-Nino ME, Eugenia-Ariza M, Macpherson MB, Butnor KJ, Vacek PC, et al. Osteopontin modulates inflammation, mucin production, and gene expression signatures after inhalation of asbestos in a murine model of fibrosis. *Am J Pathol*. 2011;178: 1975-85.

18. Do DV, Ong CT, Khoo YT, Carbone A, Lim CP, Wang S, et al. Interleukin-18 system plays an important role in keloid pathogenesis via epithelial-mesenchymal interactions. *Br J Dermatol.* 2012;166: 1275-88.
19. Ma J, Yan R, Zu X, Cheng JM, Rao K, Liao DF, et al. Aldo-keto reductase family 1 B10 affects fatty acid synthesis by regulating the stability of acetyl-CoA carboxylase- $\alpha$  in breast cancer cells. *The Journal of biological chemistry.* 2008;283: 3418-23.
20. Ma J, Luo DX, Huang C, Shen Y, Bu Y, Markwell S, et al. AKR1B10 overexpression in breast cancer: association with tumor size, lymph node metastasis and patient survival and its potential as a novel serum marker. *Int J Cancer.* 2012;131: E862-71.
21. Morikawa Y, Kezuka C, Endo S, Ikari A, Soda M, Yamamura K, et al. Acquisition of doxorubicin resistance facilitates migrating and invasive potentials of gastric cancer MKN45 cells through up-regulating aldo-keto reductase 1B10. *Chem Biol Interact.* 2015;230: 30-9.
22. Ruiz FX, Moro A, Gallego O, Ardevol A, Rovira C, Petrash JM, et al. Human and rodent aldo-keto reductases from the AKR1B subfamily and their specificity with retinaldehyde. *Chem Biol Interact.* 2011;191: 199-205.
23. Tavakolpour S, Daneshpazhooh M, Mahmoudi HR, Balighi K. The dual nature of retinoic acid in pemphigus and its therapeutic potential: Special focus on all-trans Retinoic Acid. *Int Immunopharmacol.* 2016;36: 180-6.
24. Zhang R, Wang Y, Li R, Chen G. Transcriptional Factors Mediating Retinoic Acid Signals in the Control of Energy Metabolism. *Int J Mol Sci.* 2015;16: 14210-44.
25. Liang C, Guo S, Yang L. Effects of all-trans retinoic acid on VEGF and HIF-1 $\alpha$  expression in glioma cells under normoxia and hypoxia and its anti-angiogenic effect in an intracerebral glioma model. *Molecular medicine reports.* 2014;10: 2713-9.
26. Arno AI, Gauglitz GG, Barret JP, Jeschke MG. Up-to-date approach to manage keloids and hypertrophic scars: a useful guide. *Burns.* 2014;40: 1255-66.
27. Panabiere-Castaings MH. Retinoic acid in the treatment of keloids. *The Journal of dermatologic surgery and oncology.* 1988;14: 1275-6.
28. Abergel RP, Meeker CA, Oikarinen H, Oikarinen AI, Uitto J. Retinoid modulation of connective tissue metabolism in keloid fibroblast cultures. *Archives of dermatology.* 1985;121: 632-5.
29. Cruz NI, Korchin L. Inhibition of human keloid fibroblast growth by isotretinoin and triamcinolone acetonide in vitro. *Ann Plast Surg.* 1994;33: 401-5.
30. Amann PM, Czaja K, Bazhin AV, Ruhl R, Eichmuller SB, Merk HF, et al. LRAT overexpression diminishes intracellular levels of biologically active retinoids and reduces retinoid antitumor efficacy in the murine melanoma B16F10 cell line. *Skin Pharmacol Physiol.* 2015;28: 205-12.
31. Everts HB, Suo L, Ghim S, Bennett Jenson A, Sundberg JP. Retinoic acid metabolism proteins are altered in trichoblastomas induced by mouse papillomavirus 1. *Exp Mol Pathol.* 2015;99: 546-51.
32. Rubenstein R, Roenigk HH, Stegman SJ, Hanke CW. Atypical keloids after dermabrasion of patients taking isotretinoin. *Journal of the American Academy of Dermatology.* 1986;15: 280-5.
33. Zaitseva M, Vollenhoven BJ, Rogers PA. Retinoids regulate genes involved in retinoic acid synthesis and transport in human myometrial and fibroid smooth muscle cells. *Hum Reprod.* 2008;23: 1076-86.
34. Zhou TB, Drummen GP, Qin YH. The controversial role of retinoic acid in fibrotic diseases: analysis of involved signaling pathways. *Int J Mol Sci.* 2012;14: 226-43.
35. Jones LH, Cook PC, Ivens AC, Thomas GD, Phythian-Adams AT, Allen JE, et al. Modulation of dendritic cell alternative activation and function by the vitamin A metabolite retinoic acid. *Int Immunol.* 2015;27: 589-96.
36. Kim CH. Retinoic acid, immunity, and inflammation. *Vitam Horm.* 2011;86: 83-101.

37. Bagabir R, Byers RJ, Chaudhry IH, Muller W, Paus R, Bayat A. Site-specific immunophenotyping of keloid disease demonstrates immune upregulation and the presence of lymphoid aggregates. *Br J Dermatol.* 2012;167: 1053-66.
38. Jiao H, Fan J, Cai J, Pan B, Yan L, Dong P, et al. Analysis of Characteristics Similar to Autoimmune Disease in Keloid Patients. *Aesthetic Plast Surg.* 2015;39: 818-25.
39. Mucida D, Cheroutre H. TGFbeta and retinoic acid intersect in immune-regulation. *Cell Adh Migr.* 2007;1: 142-4.
40. Yokota-Nakatsuma A, Takeuchi H, Ohoka Y, Kato C, Song SY, Hoshino T, et al. Retinoic acid prevents mesenteric lymph node dendritic cells from inducing IL-13-producing inflammatory Th2 cells. *Mucosal Immunol.* 2014;7: 786-801.
41. Yokota A, Takeuchi H, Maeda N, Ohoka Y, Kato C, Song SY, et al. GM-CSF and IL-4 synergistically trigger dendritic cells to acquire retinoic acid-producing capacity. *Int Immunol.* 2009;21: 361-77.
42. Raverdeau M, Mills KH. Modulation of T cell and innate immune responses by retinoic Acid. *J Immunol.* 2014;192: 2953-8.
43. Elias KM, Laurence A, Davidson TS, Stephens G, Kanno Y, Shevach EM, et al. Retinoic acid inhibits Th17 polarization and enhances FoxP3 expression through a Stat-3/Stat-5 independent signaling pathway. *Blood.* 2008;111: 1013-20.
44. Xiao S, Jin H, Korn T, Liu SM, Oukka M, Lim B, et al. Retinoic acid increases Foxp3+ regulatory T cells and inhibits development of Th17 cells by enhancing TGF-β-driven Smad3 signaling and inhibiting IL-6 and IL-23 receptor expression. *The Journal of Immunology.* 2008;181: 2277-84.
45. Balato A, Schiattarella M, Lembo S, Mattii M, Prevete N, Balato N, et al. Interleukin-1 family members are enhanced in psoriasis and suppressed by vitamin D and retinoic acid. *Arch Dermatol Res.* 2013;305: 255-62.
46. Chute JP, Muramoto GG, Whitesides J, Colvin M, Safi R, Chao NJ, et al. Inhibition of aldehyde dehydrogenase and retinoid signaling induces the expansion of human hematopoietic stem cells. *Proc Natl Acad Sci U S A.* 2006;103: 11707-12.
47. Zhang Q, Yamaza T, Kelly AP, Shi S, Wang S, Brown J, et al. Tumor-like stem cells derived from human keloid are governed by the inflammatory niche driven by IL-17/IL-6 axis. *PLoS One.* 2009;4: e7798.
48. Visvader JE, Lindeman GJ. Cancer stem cells in solid tumours: accumulating evidence and unresolved questions. *Nature reviews cancer.* 2008;8: 755-68.
49. Iqbal S, Syed F, McGrouther D, Paus R, Bayat A. Differential distribution of haematopoietic and nonhaematopoietic progenitor cells in intralesional and extralesional keloid: do keloid scars provide a niche for nonhaematopoietic mesenchymal stem cells? *British Journal of Dermatology.* 2010;162: 1377-83.
50. Fong CY, Biswas A, Subramanian A, Srinivasan A, Choolani M, Bongso A. Human keloid cell characterization and inhibition of growth with human Wharton's jelly stem cell extracts. *Journal of cellular biochemistry.* 2014;115: 826-38.
51. Lopez-Bertoni H, Li Y, Laterra J. Cancer Stem Cells: Dynamic Entities in an Ever-Evolving Paradigm. *Biol Med (Aligarh).* 2015;7.
52. Grant C, Chudakova DA, Itinteang T, Chibnall AM, Brasch HD, Davis PF, et al. Expression of embryonic stem cell markers in keloid-associated lymphoid tissue. *J Clin Pathol.* 2016.
53. Januchowski R, Wojtowicz K, Zabel M. The role of aldehyde dehydrogenase (ALDH) in cancer drug resistance. *Biomed Pharmacother.* 2013;67: 669-80.
54. Ferlini C, Raspaglio G, Cicchillitti L, Mozzetti S, Prislei S, Bartollino S, et al. Looking at drug resistance mechanisms for microtubule interacting drugs: does TUBB3 work? *Current cancer drug targets.* 2007;7: 704-12.
55. MacKenzie PI, Rogers A, Elliot DJ, Chau N, Hulin JA, Miners JO, et al. The novel UDP glycosyltransferase 3A2: cloning, catalytic properties, and tissue distribution. *Mol Pharmacol.* 2011;79: 472-8.



56. Yokoyama G, Fujii T, Ogo E, Yanaga H, Toh U, Yamaguchi M, et al. Advanced chemoresistant breast cancer responding to multidisciplinary treatment with hyperthermia, radiotherapy, and intraarterial infusion. *Int J Clin Oncol*. 2005;10: 139-43.
57. Yassin Fel Z. Aldehyde dehydrogenase (ALDH1A1) delineating the normal and cancer stem cells in spectral lung lesions: An immunohistochemical appraisal. *Pathol Res Pract*. 2016;212: 398-409.
58. D'Angelo RC, Ouzounova M, Davis A, Choi D, Tchienkam SM, Kim G, et al. Notch reporter activity in breast cancer cell lines identifies a subset of cells with stem cell activity. *Mol Cancer Ther*. 2015;14: 779-87.
59. Simoes BM, O'Brien CS, Eyre R, Silva A, Yu L, Sarmiento-Castro A, et al. Anti-estrogen Resistance in Human Breast Tumors Is Driven by JAG1-NOTCH4-Dependent Cancer Stem Cell Activity. *Cell Rep*. 2015;12: 1968-77.
60. Viera MH, Vivas AC, Berman B. Update on Keloid Management: Clinical and Basic Science Advances. *Adv Wound Care (New Rochelle)*. 2012;1: 200-6.
61. Andrews JP, Marttala J, Macarak E, Rosenbloom J, Uitto J. Keloids: The paradigm of skin fibrosis - Pathomechanisms and treatment. *Matrix Biol*. 2016.
62. Su Y, Qiu Q, Zhang X, Jiang Z, Leng Q, Liu Z, et al. Aldehyde dehydrogenase 1 A1-positive cell population is enriched in tumor-initiating cells and associated with progression of bladder cancer. *Cancer Epidemiol Biomarkers Prev*. 2010;19: 327-37.
63. Pandya K, Meeke K, Clementz AG, Rogowski A, Roberts J, Miele L, et al. Targeting both Notch and ErbB-2 signalling pathways is required for prevention of ErbB-2-positive breast tumour recurrence. *Br J Cancer*. 2011;105: 796-806.
64. Ding LC, She L, Zheng DL, Huang QL, Wang JF, Zheng FF, et al. Notch-4 contributes to the metastasis of salivary adenoid cystic carcinoma. *Oncol Rep*. 2010;24: 363-8.
65. Englund E, Bartoschek M, Reitsma B, Jacobsson L, Escudero-Esparza A, Orimo A, et al. Cartilage oligomeric matrix protein contributes to the development and metastasis of breast cancer. *Oncogene*. 2016.
66. Ma MZ, Zhuang C, Yang XM, Zhang ZZ, Ma H, Zhang WM, et al. CTHRC1 acts as a prognostic factor and promotes invasiveness of gastrointestinal stromal tumors by activating Wnt/PCP-Rho signaling. *Neoplasia*. 2014;16: 265-78, 78 e1-13.
67. Colombo C, Creighton CJ, Ghadimi MP, Bolshakov S, Warneke CL, Zhang Y, et al. Increased midkine expression correlates with desmoid tumour recurrence: a potential biomarker and therapeutic target. *J Pathol*. 2011;225: 574-82.
68. Misemer BS, Skubitz AP, Carlos Manivel J, Schmechel SC, Cheng EY, Henriksen JC, et al. Expression of FAP, ADAM12, WISP1, and SOX11 is heterogeneous in aggressive fibromatosis and spatially relates to the histologic features of tumor activity. *Cancer Med*. 2014;3: 81-90.
69. Sato M. Upregulation of the Wnt/  $\beta$ -catenin Pathway Induced by Transforming Growth Factor-  $\alpha$  in Hypertrophic Scars and Keloids. *Acta dermato-venereologica*. 2006;86: 300-7.
70. Rogers M, Rosen V, Wozney J, Gudas L. Bone morphogenetic proteins-2 and-4 are involved in the retinoic acid-induced differentiation of embryonal carcinoma cells. *Mol Biol Cell*. 1992;3: 189-96.
71. Glozak MA, Rogers MB. Specific induction of apoptosis in P19 embryonal carcinoma cells by retinoic acid and BMP2 or BMP4. *Developmental biology*. 1996;179: 458-70.
72. Bi W, Gu Z, Zheng Y, Wang L, Guo J, Wu G. Antagonistic and synergistic effects of bone morphogenetic protein 2/7 and all-trans retinoic acid on the osteogenic differentiation of rat bone marrow stromal cells. *Dev Growth Differ*. 2013;55: 744-54.
73. Prud'Homme GJ. Pathobiology of transforming growth factor  $\beta$  in cancer, fibrosis and immunologic disease, and therapeutic considerations. *Laboratory investigation*. 2007;87: 1077-91.
74. Meng XM, Nikolic-Paterson DJ, Lan HY. TGF-beta: the master regulator of fibrosis. *Nat Rev Nephrol*. 2016.

75. Zhou P, Shi L, Li Q, Lu D. Overexpression of RACK1 inhibits collagen synthesis in keloid fibroblasts via inhibition of transforming growth factor-beta1/Smad signaling pathway. *Int J Clin Exp Med*. 2015;8: 15262-8.
76. He S, Yang Y, Liu X, Huang W, Zhang X, Yang S. Compound Astragalus and Salvia miltiorrhiza extract inhibits cell proliferation, invasion and collagen synthesis in keloid fibroblasts by mediating transforming growth factor- $\beta$ /Smad pathway. *British Journal of Dermatology*. 2012;166: 564-74.
77. Bekhouche M, Leduc C, Dupont L, Janssen L, Delolme F, Vadon-Le Goff S, et al. Determination of the substrate repertoire of ADAMTS2, 3, and 14 significantly broadens their functions and identifies extracellular matrix organization and TGF-beta signaling as primary targets. *FASEB J*. 2016.
78. Dulauroy S, Di Carlo SE, Langa F, Eberl G, Peduto L. Lineage tracing and genetic ablation of ADAM12(+) perivascular cells identify a major source of profibrotic cells during acute tissue injury. *Nat Med*. 2012;18: 1262-70.
79. Bekhouche M, Colige A. The procollagen N-proteinases ADAMTS2, 3 and 14 in pathophysiology. *Matrix Biology*. 2015;44: 46-53.
80. Fujiwara M, Muragaki Y, Ooshima A. Keloid-derived fibroblasts show increased secretion of factors involved in collagen turnover and depend on matrix metalloproteinase for migration. *Br J Dermatol*. 2005;153: 295-300.
81. Kiguchi K, Bol D, Carbajal S, Beltrán L, Moats S, Chan K, et al. Constitutive expression of erbB2 in epidermis of transgenic mice results in epidermal hyperproliferation and spontaneous skin tumor development. *Oncogene*. 2000;19.
82. Kim JS, Bak EJ, Lee BC, Kim YS, Park JB, Choi IG. Neuregulin induces HaCaT keratinocyte migration via Rac1-mediated NADPH-oxidase activation. *Journal of cellular physiology*. 2011;226: 3014-21.
83. Huszno J, Nowara E. Current therapeutic strategies of anti-HER2 treatment in advanced breast cancer patients. *Contemp Oncol (Pozn)*. 2016;20: 1-7.
84. Li Z, He X, Xing S, Ni J, Zhang W, Xu X, et al. Overexpression of Aldo-keto reductase family 1 B10 protein in ductal carcinoma in situ of the breast correlates with HER2 positivity. *Cancer Biomark*. 2013;13: 181-92.
85. Tighe AP, Talmage DA. Retinoids arrest breast cancer cell proliferation: retinoic acid selectively reduces the duration of receptor tyrosine kinase signaling. *Exp Cell Res*. 2004;301: 147-57.
86. Choi W, Kolbe L, Hearing VJ. Characterization of the bioactive motif of neuregulin-1, a fibroblast-derived paracrine factor that regulates the constitutive color and the function of melanocytes in human skin. *Pigment Cell Melanoma Res*. 2012;25: 477-81.
87. Locher H, de Rooij KE, de Groot JC, van Doorn R, Gruis NA, Lowik CW, et al. Class III beta-tubulin, a novel biomarker in the human melanocyte lineage. *Differentiation*. 2013;85: 173-81.
88. Dalziel M, Kolesnichenko M, das Neves RP, Iborra F, Goding C, Furger A. Alpha-MSH regulates intergenic splicing of MC1R and TUBB3 in human melanocytes. *Nucleic Acids Res*. 2011;39: 2378-92.
89. Kleszczynski K, Slominski AT. Targeting ALDH1A1 to treat pigmentary disorders. *Exp Dermatol*. 2013;22: 316-7.
90. Yoshimura K, Tsukamoto K, Okazaki M, Virador VM, Lei TC, Suzuki Y, et al. Effects of all-trans retinoic acid on melanogenesis in pigmented skin equivalents and monolayer culture of melanocytes. *Journal of dermatological science*. 2001;27 Suppl 1: S68-75.
91. Othman E-ER, Al-Hendy A. Molecular genetics and racial disparities of uterine leiomyomas. *Best Practice & Research Clinical Obstetrics & Gynaecology*. 2008;22: 589-601.
92. Jones LR, Greene J, Chen KM, Divine G, Chitale D, Shah V, et al. Biological significance of genome-wide DNA methylation profiles in keloids. *Laryngoscope*. 2016.

93. Mongan NP, Gudas LJ. Valproic acid, in combination with all-trans retinoic acid and 5-aza-2'-deoxycytidine, restores expression of silenced RARbeta2 in breast cancer cells. *Mol Cancer Ther.* 2005;4: 477-86.
94. Ginestier C, Wicinski J, Cervera N, Monville F, Finetti P, Bertucci F, et al. Retinoid signaling regulates breast cancer stem cell differentiation. *Cell cycle.* 2009;8: 3297-302.
95. Kesteloot F, Desmoulière A, Leclercq I, Thiry M, Arrese JE, Prockop DJ, et al. ADAM metalloproteinase with thrombospondin type 1 motif 2 inactivation reduces the extent and stability of carbon tetrachloride-induced hepatic fibrosis in mice. *Hepatology.* 2007;46: 1620-31.
96. Johnston P, Chojnowski AJ, Davidson RK, Riley GP, Donell ST, Clark IM. A complete expression profile of matrix-degrading metalloproteinases in Dupuytren's disease. *The Journal of hand surgery.* 2007;32: 343-51.
97. Rees PA, Greaves NS, Baguneid M, Bayat A. Chemokines in wound healing and as potential therapeutic targets for reducing cutaneous scarring. *Advances in wound care.* 2015;4: 687-703.
98. Ghazizadeh M, Tosa M, Shimizu H, Hyakusoku H, Kawanami O. Functional implications of the IL-6 signaling pathway in keloid pathogenesis. *Journal of investigative Dermatology.* 2007;127: 98-105.
99. Wick G, Grundtman C, Mayerl C, Wimpissinger T-F, Feichtinger J, Zelger B, et al. The immunology of fibrosis. *Annual review of immunology.* 2013;31: 107-35.
100. Kim MH, Taparowsky EJ, Kim CH. Retinoic Acid Differentially Regulates the Migration of Innate Lymphoid Cell Subsets to the Gut. *Immunity.* 2015;43: 107-19.
101. Hwang YY, McKenzie AN. Innate lymphoid cells in immunity and disease. *Crossroads Between Innate and Adaptive Immunity IV: Springer;* 2013. p. 9-26.
102. Spits H, Di Santo JP. The expanding family of innate lymphoid cells: regulators and effectors of immunity and tissue remodeling. *Nat Immunol.* 2011;12: 21-7.
103. Wohlfahrt T, Usherenko S, Englbrecht M, Dees C, Weber S, Beyer C, et al. Type 2 innate lymphoid cell counts are increased in patients with systemic sclerosis and correlate with the extent of fibrosis. *Ann Rheum Dis.* 2016;75: 623-6.
104. Spits H, Artis D, Colonna M, Diefenbach A, Di Santo JP, Eberl G, et al. Innate lymphoid cells—a proposal for uniform nomenclature. *Nature Reviews Immunology.* 2013;13: 145-9.
105. Singh A, Settleman J. EMT, cancer stem cells and drug resistance: an emerging axis of evil in the war on cancer. *Oncogene.* 2010;29: 4741-51.
106. Duscher D, Barrera J, Wong VW, Maan ZN, Whittam AJ, Januszyk M, et al. Stem Cells in Wound Healing: The Future of Regenerative Medicine? A Mini-Review. *Gerontology.* 2016;62: 216-25.
107. Butler PD, Ly DP, Longaker MT, Yang GP. Use of organotypic coculture to study keloid biology. *The American Journal of Surgery.* 2008;195: 144-8.
108. Carlson MW, Alt-Holland A, Egles C, Garlick JA. Three-dimensional tissue models of normal and diseased skin. *Curr Protoc Cell Biol.* 2008;Chapter 19: Unit 19 9.
109. Shamir ER, Ewald AJ. Three-dimensional organotypic culture: experimental models of mammalian biology and disease. *Nature reviews Molecular cell biology.* 2014;15: 647-64.

## Review

# Functional histopathology of keloid disease

N. Jumper<sup>1</sup>, R. Paus<sup>2,3</sup> and A. Bayat<sup>1,3</sup>

<sup>1</sup>Plastic and Reconstructive Surgery Research, Manchester Institute of Biotechnology, University of Manchester, Manchester, UK,

<sup>2</sup>Department of Dermatology, University of Münster, Münster, Germany and <sup>3</sup>Centre for Dermatology Research, Institute of Inflammation and Repair, University of Manchester, Manchester, UK

**Summary.** Keloid disease is a benign, yet locally aggressive and recurrent cutaneous fibroproliferative condition characterised by excessive scarring. Unique to humans, keloids represent the end-point of a spectrum of abnormal wound healing, are aesthetically disfiguring and can cause major functional impairment. Its heterogeneous phenotype can confound clinical diagnosis leading to mismanagement. This review examines the histological morphology of keloid disease relative to the underlying pathobiology, places it in the context of other cutaneous fibroses and highlights gaps within the literature that hinder differential diagnosis. The pathological similarity to hypertrophic scarring, dermatofibrosarcoma protuberans, dermatofibroma and scleroderma emphasise the importance of detailing the architectural and cellular components of this unique entity. In the papillary dermis keloid tumours show a tongue-like advancing edge that resembles invasive tumour growth. A thickened but flattened epidermis, hyalinised haphazardly arranged collagen bundles that dominate the dermis with subsequent obliteration of the papillary-reticular boundary along with displacement and eventually destruction of skin appendages, exemplify additional hallmark findings associated with keloid disease. Compared to healthy skin, keloid scars show an increased type I/III collagen ratio, decreased fibrillin-1 and decorin expression, increased dermal cellularity and increased expression of fibronectin,

versican, elastin and tenascin in the reticular dermis and hyaluronan and osteopontin in the epidermis. We illustrate these “pathognomonic” features of keloid disease by representative micrographs and discuss them in the context of inflammation, hypoxia and tension - as key elements of keloid disease. Finally, we highlight deficits within the keloid research literature as well as discuss important areas for future research in keloid histology.

**Key words:** Keloid, Histopathology, ECM, Cutaneous fibroses

## Introduction

Keloid scars invariably arise following skin trauma that entails damage to both epidermis and dermis. While the pathogenesis of keloid disease (KD) remains incompletely elucidated, it does represent an abnormality of normal wound healing mechanisms (Butler et al., 2008; Gauglitz et al., 2011). Despite an

**Abbreviations.** BMZ, Basement membrane zone; DEJ, Dermo-epidermal junction; DFSP, Dermatofibrosarcoma protuberans; ECM, Extracellular matrix; EMI, Epithelial-mesenchymal interactions; EMT, Epithelial-mesenchymal transition; HA, Hyaluronic acid; HTS, Hypertrophic scar; IHC, Immunohistochemistry; KALT, Keloid associated lymphoid tissue; KD, Keloid disease; KF, Keloid fibroblasts; KK, Keloid keratinocytes; MC, Mast cell; NSF, Normal skin fibroblasts; NSK, Normal skin keratinocytes; PD, Papillary dermis; RD, Reticular dermis; SLRP, Small leucine rich protein; TGF $\beta$ , Transforming growth factor;  $\alpha$ SMA, alpha smooth muscle actin

increased incidence in the third decade (Seifert and Mrowietz, 2009) and a higher preponderance among dark-skinned individuals (Sun et al., 2014), there are case reports describing keloid in different anatomical locations affecting humans of both genders, all ages (Tirgan et al., 2013) and ethnicities (Shih and Bayat 2012). KD has been described as an inability to restrain the wound healing process, resulting in an excess of scar tissue (Gauglitz et al., 2011). An imbalance between the phases of inflammation, proliferation and remodelling is thought to contribute to the distinguishing histological features associated with KD and other cutaneous fibroses, such as hypertrophic scars, dermatofibrosarcoma protuberans (DFSP) and dermatofibroma. Despite significant recent progress in the pathobiology of KD (see for recent literature: (Suarez et al., 2013; Ogawa et al., 2014; Spiekman et al., 2014; Chen et al., 2015)) we have yet to identify the one pivotal pathway that determines keloid development, the course of KD and/or its response to therapy. The histological features associated with KD likely reflect a combination of distinct pathobiological elements, whose relative importance is likely to differ between affected individuals and which may underlie the heterogeneity that exists not only between and within keloid lesions but also between patients.

Much of keloid research to date has focussed on identifying potential biomarkers for KD associated with the classical four phases of wound healing (haemostasis, inflammation, proliferation and remodelling). These integrated phases of wound healing are regulated by numerous transcription factors, cytokines and growth factors, which are beyond the scope of this review (see: (Gurtner et al., 2008; Muller et al., 2012; Ding and Tredget, 2014; Haertel et al., 2014; Olczyk et al., 2014)). By approaching the histology from a pathobiological angle that compares KD with normal wound healing one can attempt to understand the dynamic histological features of KD and can correlate them with the emerging advances in molecular keloid research (Arbi et al., 2015).

Written from a pathobiological perspective, this review focuses on the histology of KD, emphasising its cellular and extracellular matrix (ECM) components and how these allow one to distinguish KD from similar fibrotic cutaneous conditions. Whilst this review attempts to facilitate differential diagnosis, we also highlight gaps within the KD literature and delineate promising areas for future research in this field.

### **Haemostasis (Day 1)**

As the first phase of wound healing, the initial formation of a haemostatic clot may not be considered histologically relevant in KD, where the clinical criteria for diagnosis require lesions to be present for at least a year. However, the cytokine release from de-granulated platelets e.g. platelet-derived growth factor, stimulate surrounding fibroblasts to lay down early ECM and

through chemotaxis, are responsible for much of the inflammatory infiltrate seen in histological sections (Weyrich et al., 2009). Additionally, it has been hypothesised that inadequate removal of the fibrin clot in keloid, secondary to PAI-1 excess, may lead to sustained fibroblastic release of collagen and result in fibrosis (Simone et al., 2014).

### **Inflammation**

“Appropriate inflammation” is an essential part of the normal wound healing mechanism (Guo and Dipietro, 2010) but persistence of this process can lead to many of the features observed in KD. It has been hypothesised that the sustained release of cytokines and growth factors from immune cells results in continued cell proliferation and ECM deposition (Reinke and Sorg, 2012). The presence, even in mature keloid scars, of an inflammatory infiltrate (Fig. 1A), keloid-associated lymphoid tissue (KALT) and excess matrix, supports this theory. Immunohistochemistry has demonstrated the persistence of a number of pro-inflammatory immune cells, primarily macrophages and lymphocytes, known to be involved in chronic inflammation. Also discussed here, as well as schematically depicted in Fig. 5, are cells with an immune role shown to be present in keloid tissue when compared with normal skin, including mast cells, Langerhans cells and fibrocytes (antigen presenting function).

### *Macrophages*

These cells, derived from circulating monocytes, are a heterogeneous population dependent on their mode of activation. Macrophages can be classically (M1, CD68+) or alternatively (M2, CD163+) activated and both of these are present within the keloid PD and RD. At both intralesional and perilesional sites, these cells were increased in comparison with normal skin and normal skin scars (Bagabir et al., 2012). The classically activated macrophages are degradative and therefore are responsible for much of the destruction of the ECM. Additionally, macrophages can produce collagen (usually collagen VII) and may also secrete perlecan and versican (Schnoor et al., 2008). These cells have been found to lie in close contact with both other immune cells and fibroblasts suggesting that, through their release of cytokines, these immune cells may be engaged in a paracrine loop resulting in the evident histological changes (Shaker et al., 2011).

### *Lymphocytes*

Immune cell infiltrate in keloid tissue was shown by Martin and Muir to demonstrate that T-cell lymphocytes were present in higher numbers over a longer period of time when compared with normal scar tissue. Additionally, a more abundant T-cell population, particularly Th cells, was noted at the margin of the



## Keloid disease

## Normal skin

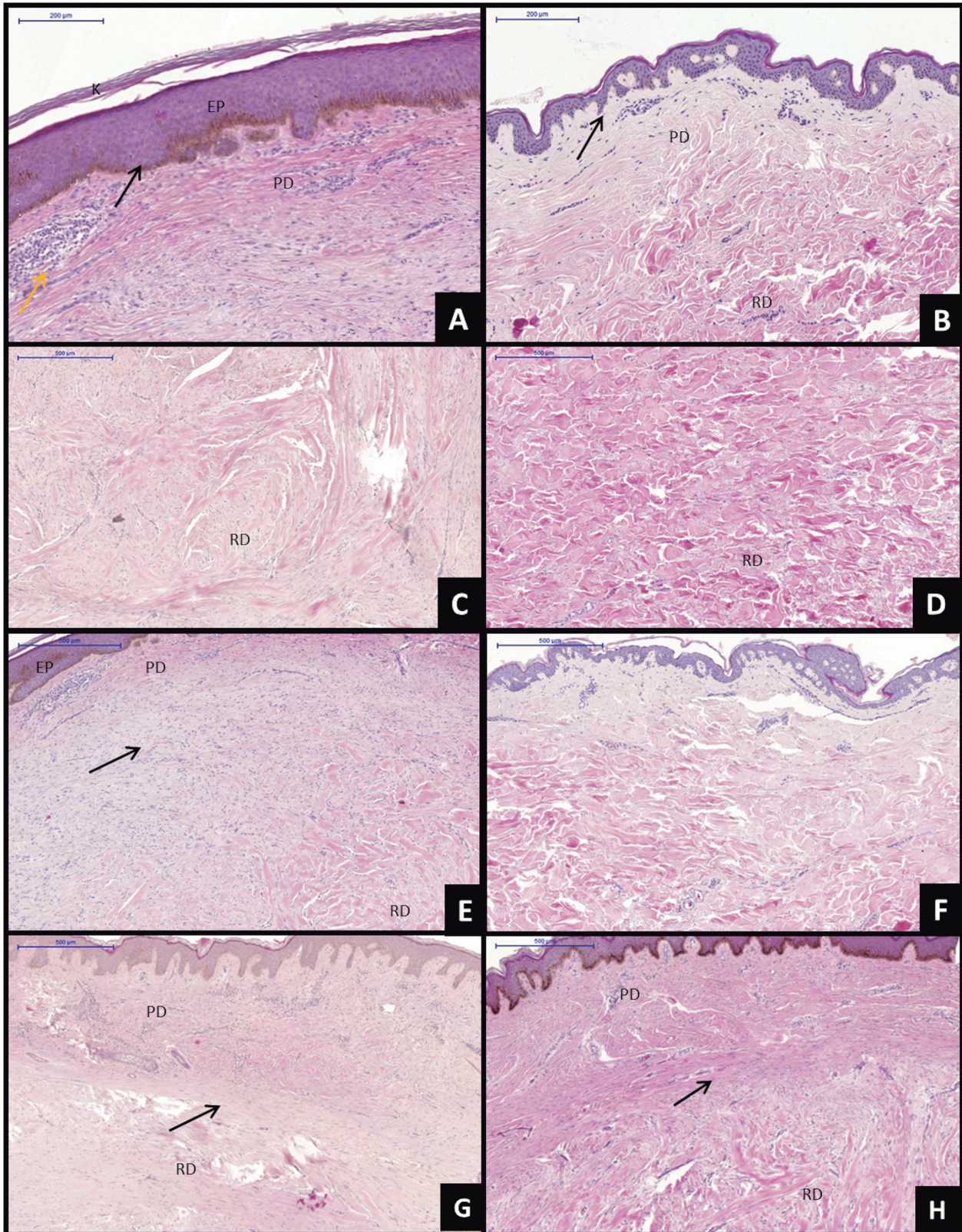


**Fig. 1.** Morphological analysis of keloid and normal skin using haematoxylin and eosin (H&E). The tissue was formalin-fixed and paraffin-embedded before cutting 5µm sections and stained using a standard protocol. **A.** Thickened flattened epidermis of keloid (black arrow) with inflammation (orange arrow). Evidence of hyperkeratosis (K). **B.** Normal skin with thin epidermis and rete ridges. **C.** Whorls of haphazard hyalinised thickened collagen in keloid. **D.** Organised fine collagen of normal skin. **E.** Increased cellularity in keloid (black arrow). **F.** Reduced cellularity in normal skin. **G and H.** Horizontal fibrous band in upper dermis of keloid (black arrow).



keloid tissue when compared with the less active centre (Martin and Muir, 1990). Lymphocytes are morphologically identified as small round cells with round nuclei but immunohistochemistry is required to

reliably differentiate between B and T cells. T-cell lymphocytes, typically those that are CD3+, are consistently found to be increased in keloid tissue, mostly perivascularly, but also dispersed between

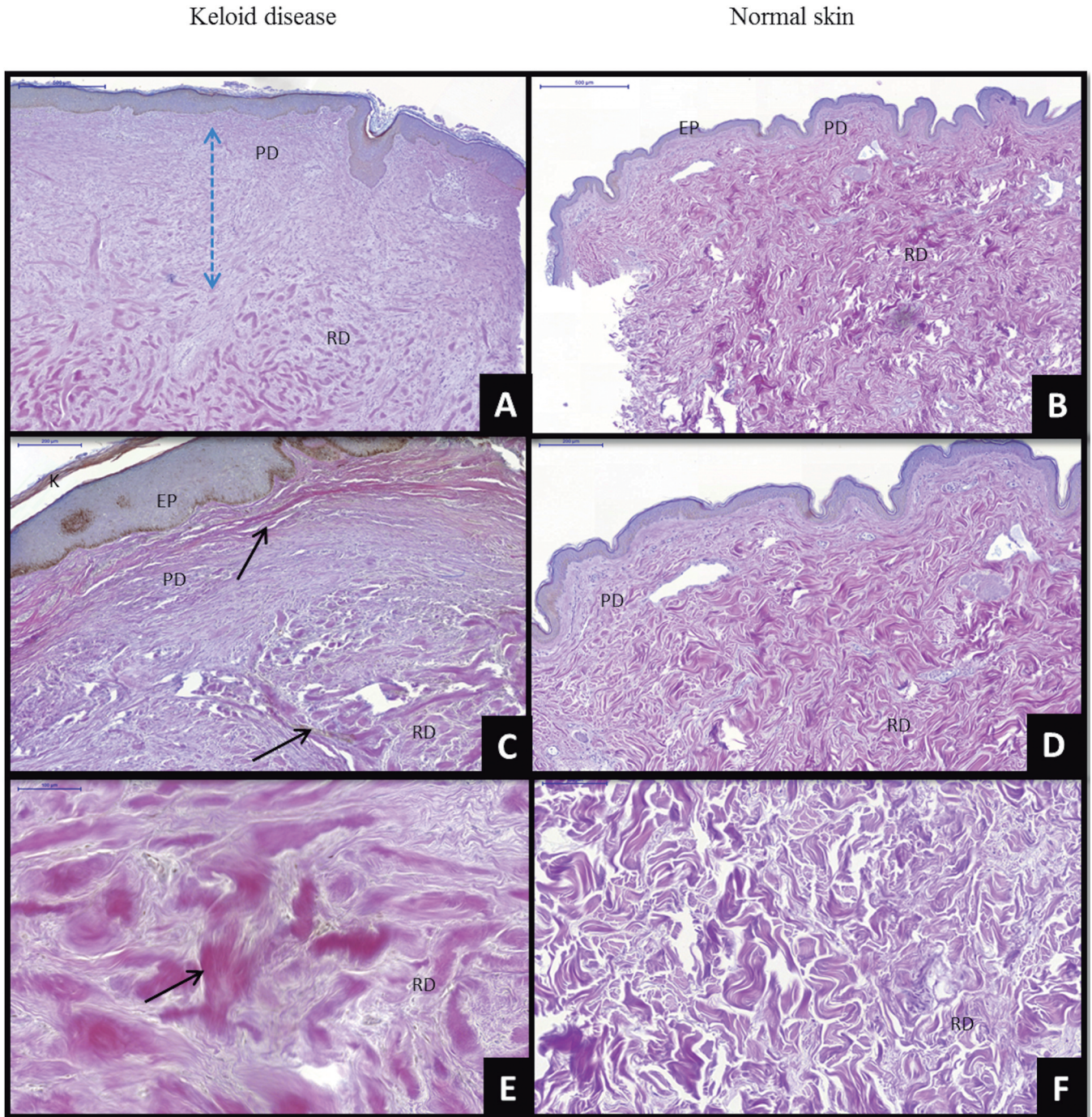


**Fig. 2.** Morphological analysis of keloid and normal skin using Herovici staining. **A and B.** Larger volume of sub-epidermal area with increased Collagen III:I ratio vs normal skin (blue arrows). **C and D.** Transition from thin sub-epidermal Collagen I to thick coarse Collagen I with intervening collagen III vs normal skin. **E and F.** Thickened haphazard collagen I:III ratio vs normal skin.



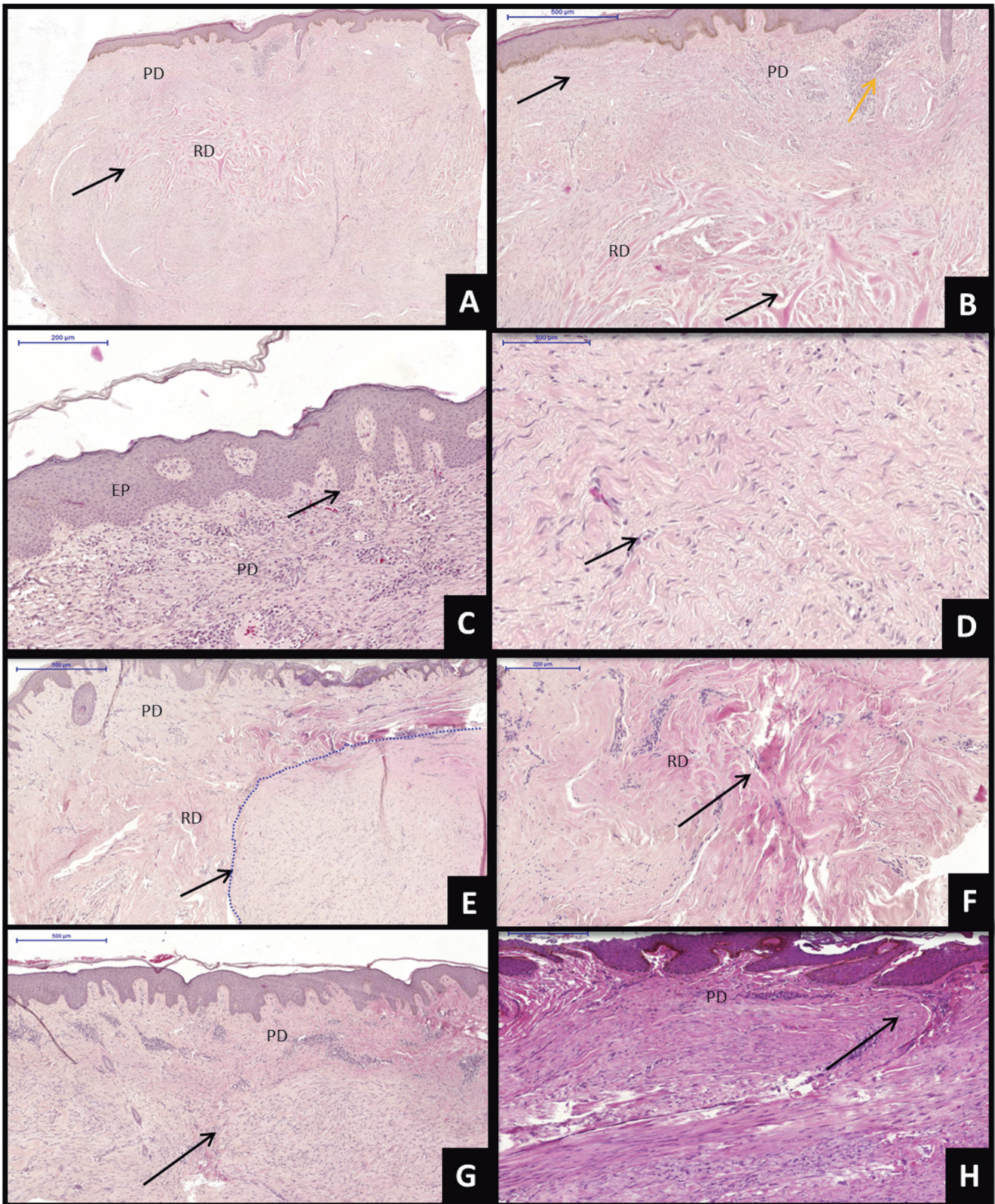


**Fig. 3.** H&E staining of keloid tissue demonstrating specified features. **A.** Obliteration of the papillary-reticular boundary. **B.** Combination of multiple features including inflammation (orange arrow) fine to coarse collagen fibres (black arrows), hyper-cellularity and thickened flattened epidermis. **C.** Thickened epidermis but not flattened. **D.** Finer collagen but remains hyper-cellular. **E.** Nodule within dermis. **F.** Focal point of collagen explosion. **G and H.** Advancing edge within papillary dermis as shown by black arrows.



collagen bundles (Moshref and Mufti, 2010; Shaker et al., 2011). There has also been a reported increase in the CD4+:CD8+ ratio within T lymphocytes in keloid samples, however the significance of this remains undetermined (Boyce, 1994; Bagabir et al., 2012). One study looked at 28 hypertrophic and 26 keloid samples, determining there was a delayed-type immune reaction that seemed to be age-dependent in hypertrophic scars, maintaining the possibility to differentially diagnose these lesions (Santucci et al., 2001). While T lymphocytes invariably showed increased numbers in keloid tissue when compared with normal skin or normal scar, the distribution of B-cell lymphocytes was more erratic. Many of the earlier studies reported few B lymphocytes in either normal or scarred dermis (Martin and Muir, 1990; Boyce, 1994), however more contemporary works, using the pan-B cell marker CD20, have identified a higher number at both central and marginal sites when compared with controls (Shaker et al., 2011; Bagabir et al., 2012). Interestingly, a recent

study identified novel patterns of KD-associated inflammatory infiltrates that resemble tertiary lymphoid follicles and has coined this “keloid-associated lymphoid tissue” (KALT). Despite being present in only some of the KD samples examined, the presence of aggregates emphasises the importance of an immune role in KD and supports the need for further investigation (Bagabir et al., 2012). Perhaps this phenomenon shows some similarities to the most recently described perivascular clustering of leukocytes that may be essential for the elicitation of effective contact hypersensitivity responses in murine skin (Natsuaki et al., 2014).

#### Mast cells (MC)

Found in large numbers in a study including 44 keloid samples, MC were evidenced to be in close contact with fibroblasts, a term referred to as “cell talk” (Shaker et al., 2011). These cells release histamine when de-granulated, which may be responsible for the pruritus

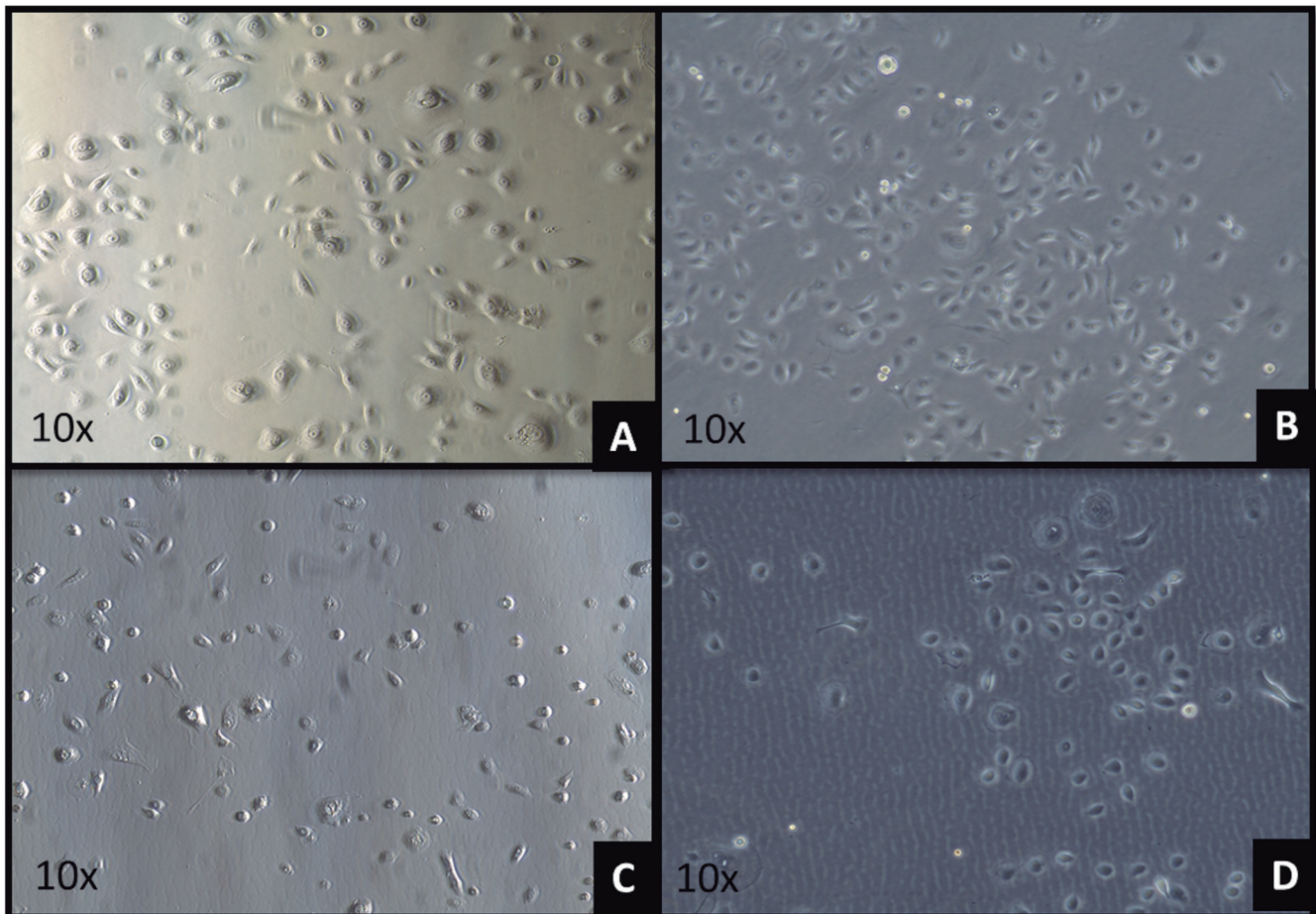


**Fig. 4.** Keloid and normal keratinocytes in monolayer *in vitro* culture P0. **A and C.** keloid keratinocytes form looser colonies than their normal skin counterparts (**B and D**).

## Histopathology of keloid disease

and erythema associated with keloids, explaining why these symptoms are attenuated with the application of corticosteroid and/or compression (Lavker and Schechter, 1985; Hassel et al., 2007; Schneider et al., 2013). When normal scar and hypertrophic scar tissue were analysed, it was found that the MC numbers increased with increasing scar age, although it was highlighted that the activation of these cells and not just the number of cells was of significance (Niessen et al., 2004). Several studies have shown that MC are increased in keloid tissue (Kamath et al., 2002; Ammendola et al., 2013; Dong et al., 2014). A recent study showed an increased number of mature and activated MC, both intralesionally and perilesionally in keloid tissue when compared with normal skin and normal scars (Bagabir et al., 2012). Direct cell-cell contact between MC and KF has recently been shown using transmission electron microscopy and was hypothesised to be responsible for KF proliferation through the MC release of cytokines and growth factors. This group also postulated that increased collagen may attract MC, which then reduce collagen bulk through phagocytosis (Arbi et al., 2015).

### Langerhans cells

Despite the finding that the release of IL-1 $\alpha$  and attraction of T lymphocytes by activated Langerhans cells can influence collagen levels, there is limited evidence in the literature on their abnormal presence in keloid tissue (Niessen et al., 2004). One study, using

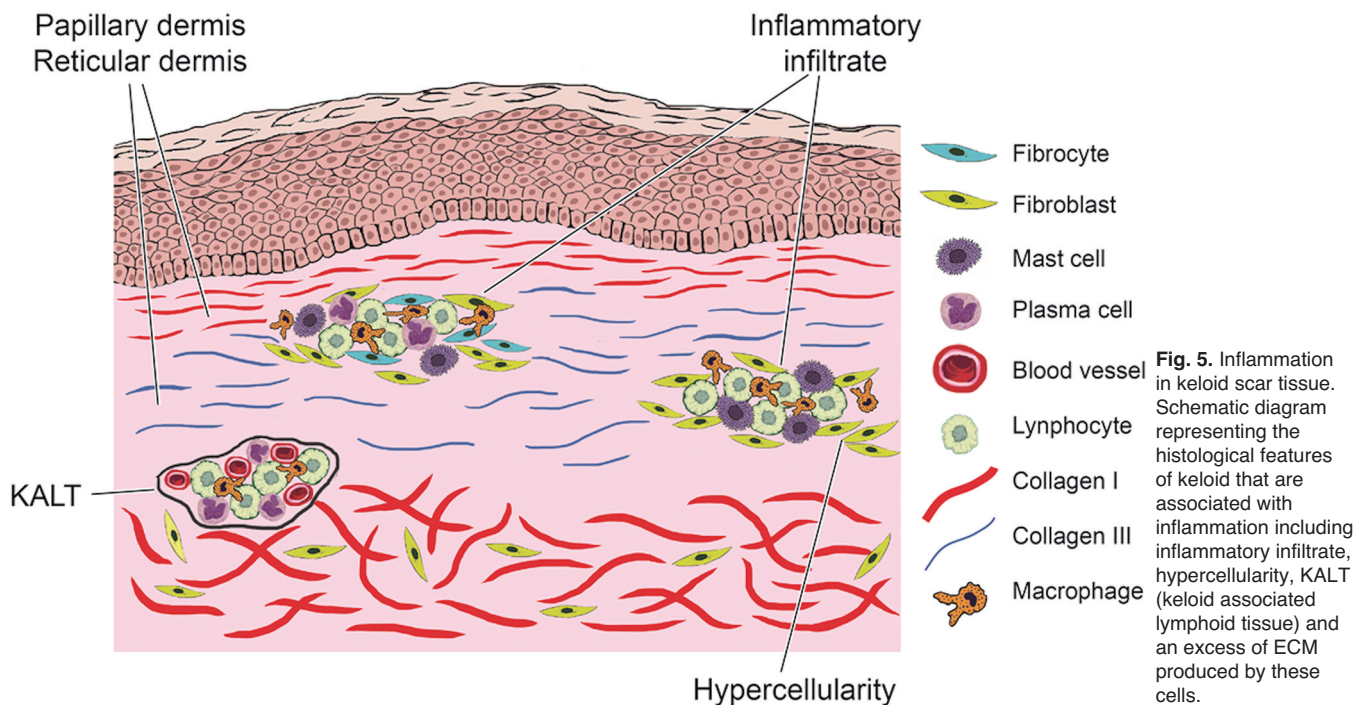
CD207 staining, found no difference in numbers between keloid and normal skin or normal scars (Bagabir et al., 2012). A separate group using anti-CD1a showed the presence of these cells in hypertrophic scars diminished over time finding reduced cells positive in old hypertrophic scars but did show positive staining present in approximately 40% of keloid tissue samples (Santucci et al., 2001).

### Fibrocytes

Fibrocytes are mesenchymal precursor cells expressing myeloid (CD45RO) and haematopoietic (CD34) antigens, as well as structural proteins including collagen I, collagen III, fibronectin and vimentin (Abe et al., 2001; Bucala, 2012). Morphologically distinguishable by their spindle shape and mid-length fibre-like projections, these cells may account for up to 10% of cells infiltrating wound sites (Bucala et al., 1994).

Fibrocytes have been shown to be a population distinct from MSC (mesenchymal stem cells), identified by a double positive CD34/collagen I and/or CD45/collagen I stain (Iqbal et al., 2012). Discussed here because of their their pro-angiogenic and immune role (Reilkoff et al., 2011), acting as antigen-presenting cells, fibrocytes also contribute to both the proliferation and remodelling phases of wound healing through differentiation into fibroblast and myofibroblast populations (Bellini and Mattoli, 2007).

Although less dense than normal fibroblasts within keloid tissue (0.4 versus 4.8 per area (Ueda et al.,





1999)), fibrocytes are thought to contribute to excess scarring through collagen production, both themselves and by induction of fibroblasts, as well as by differentiation into  $\alpha$ SMA-expressing myofibroblasts, which exert contractile forces on the healing wound (Iqbal et al., 2012). Fibrocytes have been shown to affect keratinocyte proliferation and impact the re-epithelialisation process (Kao et al., 2011) and are postulated to be the source of scarring in burn wounds, where it may be difficult for fibroblasts to migrate from the healthy wound edge (Mathangi Ramakrishnan et al., 2012).

This, in addition to their increased prolyl-4-hydroxylase (Aiba and Tagami, 1997) release, an enzyme responsible for the stabilisation of the collagen triple helix, is thought to result in the excess ECM deposition that is the hallmark of KD (McCoy et al., 1980; Ala-Kokko et al., 1987). As fibrocytes are derived from CD14+ cells in the peripheral blood (Curran and Ghahary 2013), these have been used as an upstream target for therapeutics. Serum amyloid P (SAP) inhibits fibrocyte differentiation thereby decreasing the myofibroblast population in the wound and reducing scarring (Naik-Mathuria et al., 2008; Blakaj and Bucala, 2012). Although not the primary source of collagen, it may be that targeting fibrocytes is an important strategy for targeting the scar tissue volume in KD.

**Proliferation**

This wound healing phase is marked by the formation of granulation tissue, re-epithelialisation, neo-angiogenesis and new ECM deposition (Baum and Arpey, 2005). While the features associated with these

processes are discussed under proliferation, there is significant overlap with both the inflammatory and remodelling phases whereby cells, cytokines and growth factors from all three stages contribute to the dysregulation leading to keloid histology (Shih et al., 2010).

It is postulated that a prolonged proliferation phase is responsible for the majority of features considered characteristic of KD (Young et al., 2013) and these are schematically depicted in Fig. 6. While an overproduction of collagen is the subject of much focus in the literature, it is the microscopic changes in the non-collagenous ECM elements that distinguish keloid from other cutaneous fibroses and are therefore discussed in further detail.

*Epidermal proliferation*

The majority of literature to-date has described the keloid epidermis as thickened with flattened rete ridges (Fig. 1A,B), presumably secondary to pressure from the large collagen bundles occupying the dermis that impinge upon the epidermis (Lee et al., 2004; Kose and Waseem, 2008). The normal epidermis, composed mostly of keratinocytes in distinct stages of differentiation is also populated by Merkel cells, Langerhans cells, T lymphocytes (CD4+, CD8+ or  $\gamma\delta$ -T cell receptor+) and melanocytes, complemented by intraepidermal nerve fibres arising from distally located, extracutaneous sensory neurons arising from spinal dorsal root ganglia (Kanitakis, 2002; Fradette et al., 2003; Di Meglio et al., 2011).

Although not extensively studied, keloid epidermis exhibits an increased immune cell infiltrate (discussed

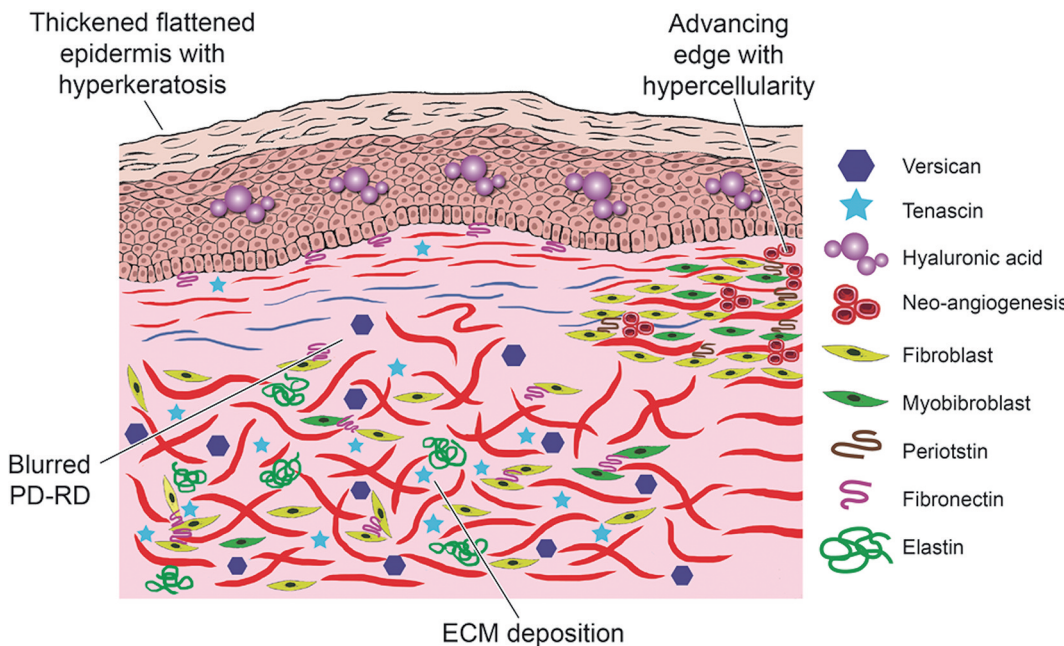


**Fig. 6.** Proliferation in keloid scar tissue. Schematic diagram representing the histological features of keloid disease associated with proliferative stage of wound healing. Hypercellularity resulting in both thickened epidermis and an advancing edge in the dermis. Increased ECM deposition resulting in blurring of the papillary-reticular boundary. ECM molecules known to show increased staining in keloid tissue are depicted here.

## Histopathology of keloid disease

below) at both the lesion centre and margin (Bagabir et al., 2012) as well as positively expressing immune cell mediators, COX-1 and COX-2 (Abdou et al., 2014). The keloid epidermis expresses osteopontin, although this was not compared with normal skin (Miragliotta et al., 2014), positively stained compared with normal skin for TGF $\beta$ -1 (Abdou et al., 2011) and no difference was shown between KD, HTS and normal skin with regard to epidermal insulin-like growth factor-1 receptor staining (Hu et al., 2014). There is however, a noticeable paucity of information in the literature on melanocytes and Merkel cells in keloid epidermis and any abnormalities in these cell types compared to the epidermis of healthy skin or normal scars.

### Keratinocytes

Keratinocytes change their morphology with differentiation status, allowing formation of a stratified epithelium that generates a protective barrier (Eckert, 1989). Under certain pathological conditions, epidermal keratinocytes express alternate keratins to those found in normal skin. This is also seen in KD, where hyper-proliferation marker keratin 16 has been shown to be expressed as well as keratin 2e, normally found in the cornified envelope but in keloid, it is expressed in the basal epidermis (Bloor et al., 2003; Ong et al., 2010). Histochemically this goes along with epidermal hypergranulosis and hyperkeratosis (Figs. 1A, 2C) (Moshref and Mufti, 2010).

This keloid keratinocyte (KK) hyper-proliferation is thought to account for the consistently thickened epidermis observed in keloid histology and may contribute to BMZ changes. With most of the histological disorganisation occurring below the DEJ, the basal cells in keloid tissue appear regular with minimal disarray, albeit showing some vacuolar changes (Moshref and Mufti, 2010). Whilst previously thought only to be a result of aberrations in dermal tissue, namely fibroblasts, the effect of local paracrine loops

involving keratinocytes and the epidermis has now been realised in the context of cutaneous wound healing and scar formation (Garner, 1998; Machesney et al., 1998).

3D models and co-cultures have been employed to demonstrate dysregulation of EMI in keloid formation (Lim et al., 2001, 2002) and investigate keloid pathology (Supp et al., 2012; van den Broek et al., 2014). Additionally, KF expression was shown to be altered when in direct cell-cell contact with keratinocytes when compared with exposure only to keratinocyte medium (Funayama et al., 2003). As well as their autocrine and paracrine roles in initiating inflammatory responses (Pasparakis et al., 2014), keratinocytes participate in regulation of fibroblast proliferation, apoptosis and collagen production, thus participating in ECM synthesis (Kose and Waseem, 2008; Wang et al., 2015).

While KK have been compared to normal skin keratinocytes (NSK) on a transcriptional level (Xia et al., 2006) there is limited evidence in the literature comparing their monolayer cell morphologies. One study implicates this cell's role in EMT by showing immunohistochemical evidence of desmosomal discontinuity impacting keratinocyte adhesion. They also describe KK displaying detached, more widely disbanded colonies when compared with NSK and showed evidence of faster migration using a scratch assay (Hahn et al., 2013). We also found that NSK formed tighter, more compact colonies when compared with KK in monolayer culture as shown in Fig. 4.

### Melanocytes

While there are a few studies that investigated the expression of melanocytic factors in KF, including melanocortin-1 receptor (Luo et al., 2013) and proopiomelanocortin (Teofoli et al., 1997), the only reference to keloid tissue pigmentation was from that of one grafted into a hamster cheek pouch, where they hypothesised that grafted keloid tissue must contain melanoblasts that differentiated into melanocytes in the

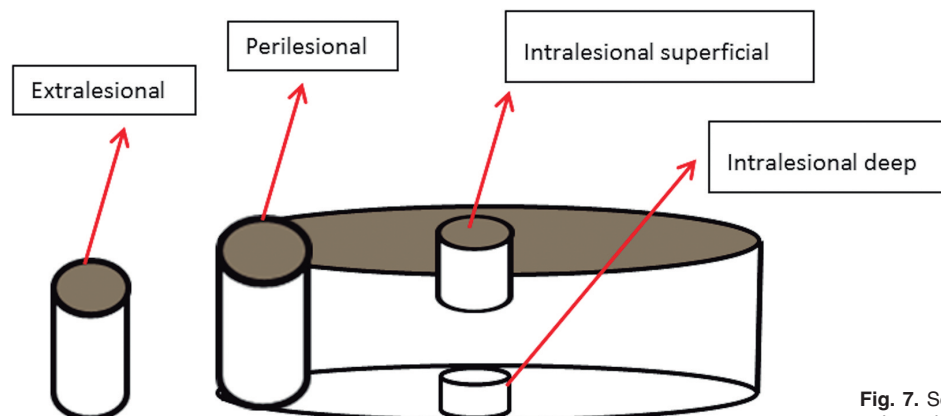


Fig. 7. Schematic representation of defined sites used to investigate site-specific keloid disease pathobiology.

hamster environment, something that does not occur in the human samples (Hochman et al., 2005). There is some evidence that melanocytes induce fibroblast proliferation resulting in increased ECM deposition (Gao et al., 2013) and that reduction in melanocytes may be responsible for the relative success of current therapies (Har-Shai et al., 2006). A recent study investigating the effect of melanocytes and fibroblasts on the contractile behaviour of keratinocytes suggested that the balance of melanocytes rather than the presence or absence is more significant (Rakar et al., 2014). Given the recent experimental findings in mice, that wounding or UV trauma of the epidermis recruits melanocyte stem cells from the hair follicle epithelium into the epidermis (Chou et al., 2013) and the concept that melanocytes may play a more active role in damage response and tissue remodelling than widely appreciated (Paus, 2013), there is clearly a lot of scope for further research for defining the role of the melanocyte in keloid pathobiology.

#### Dermal proliferation

##### Extracellular matrix deposition

The dermis of human skin is composed of two distinct layers: papillary and reticular. It has been noted in several histological keloid specimens that, as a result of matrix overproduction, the distinction between the papillary and reticular dermis becomes blurred (Fig. 3A) (Huang et al., 2012).

##### Collagen

Collagen, an abundant triple helix protein (Mienaltowski and Birk, 2014), is the main ECM constituent and is found in abundance in KD. It is generally accepted that keloids contain surplus amounts of collagen within the dermis, accounting for most of the bulk of the scar tissue. Lee et al. in 2004 referred to this haphazard collagen pattern (Fig. 1C) as “keloidal collagen”, identifying it as a histological hallmark of KD, albeit with a low sensitivity (Lee et al., 2004). The discord regarding the exact quantity, type, morphology and location of this collagen is due to much of the literature being based on individual findings, often using small sample numbers or lacking comparisons to normal and hypertrophic scars.

These factors, compounded by the inherent heterogeneity of keloid fibrosis, have led to confusion in diagnosis and inappropriate management strategies (Atiyeh et al., 2005). There is little disagreement over the “keloidal collagen” being thickened, hyalinised and eosinophilic with a distinct glassy appearance. Whether confined to a particular zone (Bux and Madaree, 2010) or diffusely distributed throughout the dermis (Moshref, 2010), the collagen bundles have been described as organised parallel to the surface (Ehrlich et al., 1994) but more frequently haphazardly arranged (Knapp et al.,

1977; Da Costa et al., 2008). These bundles occur with higher frequency and increased thickness in the perilesional sub-papillary (Bux and Madaree, 2010) or RD when compared with intralesional and extralesional sites (Syed et al., 2011).

Furthermore, it has been described that the ratio of the two primary collagens involved in wound healing, types I and III, is altered in keloids (Abergel et al., 1985) with more recent studies supporting an elevated collagen I/III ratio (Fig. 2) based on raised collagen I and unaltered collagen III levels (Uitto et al., 1985; Peltonen et al., 1991). This ratio may vary between different sites within the keloid tissue as demonstrated in a recent study revealing increased collagen I and III production within perilesional sites of the keloid, both *in vitro* and *in vivo*, when it is compared with intralesional and extralesional sites (Syed et al., 2011).

In addition to “keloidal collagen” several other features allow one to distinguish keloid from hypertrophic scarring (Lee et al., 2004). These are summarised in Table 4. The most significant of these was the presence of a PD tongue-like advancing edge, which has also been described in relation to keloid histology previously and may be a point of differentiation from hypertrophic scars (Fig. 3G,H) (Cosman and Wolff, 1972; Moshref and Mufti, 2010).

The expression of other collagens in keloid tissue, such as collagen V, collagen VI and collagen VII, remains to be systematically analysed. Additionally the absence of collagen nodules, originally believed to be a diagnostic marker of KD (Linares and Larson, 1974; Ehrlich et al., 1994), cannot be safely used to exclude KD, as several studies have identified their presence in both keloid (Fig. 3E) and hypertrophic scars (Kischer and Brody, 1981; Lee et al., 2004).

##### Non-collagenous matrix

The role of the ECM is both structural and regulatory, requiring a balanced composition to maintain optimal structure and function (Mitts et al., 2010). Composed of varying amounts of glycosaminoglycans, proteoglycans and elastic fibres, a disturbance in the proportions of these molecules can result in excess matrix, consistent with the formation of raised dermal scarring. Microfibrillar proteins constitute the bulk of the non-collagenous ECM, along with hyaluronan and fibronectin. Deposited in early natal life, microfibrillar proteins, consisting of an elastin core and surrounding fibrillin microfibrils, extend from the DEJ through the papillary dermis (PD), where they are thin, to the reticular dermis (RD), where they form thick bands (Kielty, 2006; Kadoya et al., 2015). Microfibrillar proteins also influence cell migration and adhesion through sequestration and presentation of wound healing cytokines such as TGF $\beta$  (Ramirez and Rifkin, 2009; Massam-Wu et al., 2010).

In KD, immunohistochemistry, stereology and multiphoton microscopy have shown that elastin and



fibrillin are disorganised when compared with normal skin and normal scar tissue. Fibrillin-1 deposition is decreased throughout the tissue (Amadeu et al., 2004) whereas elastin is almost absent in the PD yet significantly increased in the RD, where it forms nodes (Chen et al., 2011). It has been speculated that this may result from an initial overproduction of both collagen and elastin by KF, followed by the continued presence of collagen without elastin.

Hyaluronan (HA), a glycosaminoglycan thought to be of central importance to scarless fetal wound healing (Namazi et al., 2011), is a significant ECM component. Hyaluronan has structural and regulatory roles as well as implications in angiogenesis and inflammation (Frenkel, 2014). It has been postulated to be important in effective epithelialisation and may influence fibroblast morphology (Tan et al., 2011), thus securing itself and the molecules involved in its synthesis and degradation as potential targets in keloid therapeutics (Sidgwick et al., 2013).

In keloids, HA has been shown to exhibit a different expression pattern from that of normal and hypertrophic scarring: using biotinylated hyaluronic acid binding protein (HABP), normal skin, normal scar tissue and to a lesser degree hypertrophic scars showed HA to be principally concentrated in the PD and yet scanty in the epidermis (Bertheim and Hellstrom, 1994). In contrast, keloids consistently demonstrated the opposite phenomenon, with staining reduced in the PD and being maximal in the intercellular space between keratinocytes in the suprabasal layers of the epidermis (Meyer et al., 2000; Tan et al., 2011). On this basis, HA alone has been used to classify scar types for the purpose of experimentation (Hellstrom et al., 2014).

Fibronectin, a linking glycoprotein that binds to integrins and other matrix molecules, forming an early component of granulation tissue (Martino et al., 2011; To and Midwood 2011), is more strongly expressed in keloid than normal tissue (Kischer and Hendrix, 1983; Ashcroft et al., 2013) and can be further enhanced by TGF $\beta$ 1 and abrogated by triamcinolone acetonide treatment (Lee et al., 2013). While some studies describe diffuse fibronectin staining in both normal skin and keloid (Knaggs et al., 1994), those that yielded more intense staining in keloid tissue describe it as increased at the DEJ and co-localised with fibroblasts between collagen bundles in the dermis (Sible et al., 1994). KF also produce more fibronectin in culture than normal dermal fibroblasts (Babu et al., 1989). During normal wound healing with respect to the above, keloid fibronectin is gradually replaced by neo-dermis; notably however its expression is maintained in abnormal scarring (Santucci et al., 2001). This continued presence may result in prolonged interaction with other matrix proteins or cells forming the bulky growth that is typical of KD. If the keloid lesion can be confirmed to stain positive for fibronectin, reducing fibronectin expression might be therapeutically beneficial (different ways of reducing fibronectin expression have already been

reported) (Lee et al., 2011; Liang et al., 2013).

Besides these larger and better-investigated molecules, little is known in the literature on the histology of ECM in KD, such as dermatopontin, periostin, small leucine-rich proteoglycans (SLRP) and tenascin (Sidgwick and Bayat, 2012). The latter, a hexameric glycoprotein involved in fibrosis, has been shown to have some homology with fibronectin and potentially influence its biologic activity, similarly disappearing from the wound with the replacement of granulation tissue during normal wound healing (Shrestha et al., 1996; Halper and Kjaer, 2014). Having been previously associated with scleroderma (Lacour et al., 1992), hyper-proliferative skin conditions (Schalkwijk et al., 1991) and acne-associated KD (Knaggs et al., 1994), the role of tenascin was investigated in KD. This protein was diffusely expressed in keloid tissue, especially the RD, when compared with normal skin where it formed a linear band at the DEJ but failed to show any deeper positive staining (Dalkowski et al., 1999). This was supported in a more recent study where reduction in the overexpression of tenascin was seen using cryotherapy (Abdel-Meguid et al., 2014).

The ECM component dermatopontin has been implicated in wound re-epithelialisation (Krishnaswamy and Korrapati, 2014), delayed healing (Krishnaswamy et al., 2014) and fibrosis (Kuroda et al., 1999), although little is known on its role in KD. Due to the decreased expression of dermatopontin in KF (Russell et al., 2010), it was directly compared to leiomyomas, which also showed reduced dermatopontin mRNA expression in microarray analysis; the authors further reported that dermatopontin protein expression is also reduced in keloid tissue compared to healthy skin (Catherino et al., 2004).

As the most abundant glycoprotein in normal skin dermis, the SLRP decorin binds to other matrix proteins including collagen, fibronectin and thrombospondin, playing a role in ECM assembly and therefore an attractive protein to investigate in wound healing (Tracy et al., 2014). Decorin is thought to interact with dermatopontin to alter TGF $\beta$  expression, thereby affecting collagen fibrillogenesis (Zhang et al., 2006) and has been implicated in the inflammatory process of wound healing, involving toll-like receptors 2 and 4 (Merline et al., 2011), which have also been investigated in pathological scarring (Wang et al., 2011; Chen et al., 2013). Decorin has been shown to be comparable in normal skin and mature scars but reduced in early wound healing and delayed in abnormal wound healing such as post-burn hypertrophic scars (Scott et al., 1995; Sayani et al., 2000). Keloid immunohistochemistry showed no difference when compared with normal skin (Tan et al., 1993; Hunzelmann et al., 1996), although proteoglycan composition analysis by a more recent study reported decreased decorin expression in keloid versus normal skin (Carrino et al., 2012). This finding is supported by two recent studies that showed up-regulation of decorin in treated versus untreated keloid

samples (Trisliana Perdanasari et al., 2014; Chen et al., 2015). Interestingly, this molecule has recently been shown to be reduced in the tumour microenvironment when compared with normal tissue controls and therefore of potentially significant importance in a tumour suppression role (Neill et al., 2012; Bozoky et al., 2014). Decorin's postulated role (namely, to control TGF $\beta$ 1 activity, thus manipulating collagen bundle formation) (Okamoto et al., 1999) along with the delayed appearance of decorin in hypertrophic scarring (Sayani et al., 2000) suggests there is a period in early keloid formation, where decorin administration or up-regulation could be therapeutically beneficial.

Analysis of biglycan, another SLRP, has generated contradictory results in the literature. In normal skin, biglycan descriptions range from no presence at all

(Scott et al., 1995) to a linear band adjacent to the BMZ. In comparison, keloid tissue reportedly showed either indistinguishable staining from normal skin (Tan et al., 1993) or positive expression in the collagen nodules of the dermis, encouraging the theory that biglycan is associated with collagen deposition (Hunzelmann et al., 1996).

Periostin has been investigated in KD with regard to its role in promoting angiogenesis (Zhang et al., 2015), a histological feature associated with this scar (Huang et al., 2012). Keloid tissue shows increased staining in both epidermis and dermis when compared with normal skin (Zhou et al., 2010) and significant co-localisation with CD31, suggesting a correlation with blood vessel density (Zhang et al., 2015). In hypertrophic scarring, periostin has been shown to increase dermal fibroblast

**Table 1.** Summary of the ECM molecules previously investigated in keloid disease tissue.

ECM molecule	Location within keloid tissue	Technique	Ref.
Collagen I	Abundant expression throughout dermis	Histochemistry (Masson's trichome)	Kauh et al., 1997
	$\uparrow$ thicker bundles at margin, especially reticular dermis	Histochemistry (Herovici)	Syed et al., 2011
Collagen III	Thinner vs collagen I, $\uparrow$ in papillary dermis of keloid margin	Herovici	Syed et al., 2011
	Strongly $\uparrow$ in keloid vs normal skin	IHC	Naitoh et al., 2001
Collagen IV	Along BMZ and $\uparrow$ proximal to small blood vessels	IHC	Naitoh et al., 2001
Collagen VI	Co-localised with col I proximal to small blood vessels Also $\uparrow$ papillary dermis	IHC	Peltonen et al., 1991
Fibronectin	$\uparrow$ at dermo-epidermal junction Co-localised with cells in deep dermis between collagen bundles	IHC	Sible et al., 1994
	Intense localisation with fibroblasts upper reticular	IHC	Kischer and Hendrix, 1983
	Diffuse positivity in keloid tissue	IHC	Knaggs et al., 1994; Santucci et al., 2001; Liang et al., 2013
Hyaluronan (HA)	Gross HA stain in upper layers epidermis PD- mesh-like staining, RD- Intense staining	HABP	Bertheim and Hellstrom, 1994
	$\uparrow$ Interstitial in spinous & granular layers $\downarrow$ HA in keloid dermis	HABP	Meyer et al., 2000
	$\downarrow$ intensity stain in papillary dermis	HABP	Tan et al., 2011
Elastin	$\downarrow$ superficial dermis $\uparrow$ deep dermis, parallel to collagen	IHC Histomorphometric	Amadeu et al., 2004
	$\downarrow$ elastic fibres all scar types	Verhoeff van Giesson stain	Kamath et al., 2002
	$\downarrow$ elastic fibres, due to impaired fibrillin-1	IHC	Ikeda et al., 2009
	$\uparrow$ elastin deep dermis, node structure	Multiphoton microscopy	Chen et al., 2011
Fibrillin	$\downarrow$ superficial and deep dermis Thin fibres, no candelabra pattern	IHC Histomorphometric	Amadeu et al., 2004
	Altered distribution, thick irregular bundles	IHC	Ikeda et al., 2009
	Altered fibrillin distribution, related to TGF $\beta$	IHC	Nie et al., 2008
Tenascin	Diffusely expressed in dermis Associated with $\uparrow$ collagen bundles in reticular dermis	IHC	Dalkowski et al., 1999
Dermatopontin	$\downarrow$ stain compared with normal skin	IHC	Catherino et al., 2004
Decorin	Indistinguishable from normal skin, strong stain in dermis, weaker in epidermis	IHC	Tan et al., 1993; Hunzelmann et al., 1996; Catherino et al., 2004
Biglycan	$\uparrow$ in nodular areas of keloid	IHC	Hunzelmann et al., 1996
	Indistinguishable from normal skin	IHC	Tan et al., 1993
Periostin	$\uparrow$ in epidermis and dermis vs normal skin Co-localisation with CD31	IHC	Zhang et al., 2015
	$\uparrow$ especially in acellular node region of deep dermis	IHC	Zhou et al., 2010
Versican	Intense deposition in keloid but not normal skin	IHC	Yagi et al., 2012

## Histopathology of keloid disease

proliferation and differentiation into myofibroblasts (Crawford et al., 2015), but this has yet to be investigated in KD.

Finally, versican is a large proteoglycan capable of sequestering large amounts of water through its glycosaminoglycans and therefore, similar to HA, is theorised to be responsible for some of the volume in keloid scars (Yagi et al., 2013). Moreover, in the hair follicle mesenchyme, versican expression is correlated with inductive properties of specialised fibroblasts that engage in intimate EMI with the adjacent epithelium (Kishimoto et al., 1999; Soma et al., 2005; Ohyama et al., 2010). Versican immunostaining has revealed intense deposition in keloid tissue when compared with normal skin (Yagi et al., 2012) and this was confirmed in a separate protein study using composite gels (Carrino et al., 2012).

### Fibroblasts

Fibroblasts are elongated spindle-shaped cells, defined by their ability to secrete ECM. They are a heterogeneous cell type, differing in function and morphology even within an organ (Sorrell and Caplan, 2009). Although identified morphologically, the varied fibroblast subtypes or derivatives express specific proteins that can be used to differentiate them within tissues. It has been shown that KF differ from NSF in ECM production, especially collagen, which is produced in excess in keloid scars (Lim et al., 2002). While there

has been some debate in the past over the degree of cellularity in keloid tissue, the consensus is in favour of a high cellularity, with the predominance of those cells being fibroblasts (Shaker et al., 2011).

It has been noted that in addition to the haphazard collagen deposition, the fibroblasts themselves also lie in a disorganised fashion (Lee et al., 2004) and are frequently degenerate or necrotic (Bux and Madaree, 2010). Further to this, the cell phenotype can be heterogeneous within the scar itself as well as between scar types. It has been shown that the superficial (papillary) and deep (reticular) fibroblasts within keloid exhibit differential expression and are postulated to result in alternative keloid phenotypes clinically (Supp et al., 2012). These altered phenotypic KF respond differently to the NSF, not only in relation to cytokines and growth factors but also to immunomodulatory treatments (Russell et al., 1995). Other than phenotype, a key factor in the production of excess matrix appears to be the interaction of fibroblasts with both keratinocytes and the immune cell infiltrate (Martin and Muir, 1990; Shaker et al., 2011). Additionally, the fibroblasts of non-keloid tissue have been shown to respond in a keloid-like manner to the media taken from KF (Ashcroft et al., 2013).

### Vascularity

Opinion diverges with regard to the vascularity of keloid scars. Studies have been conducted using

**Table 2.** Summary of the cells identified in keloid disease, their morphology and stain used to identify them within the tissue.

Cell type	Morphology	Stain	Present/Absent in KD	Sample no.	Ref.
Keratinocyte	Differentiation status dependent	Cytokeratins	K2e/K16 Present in epidermis (K6/K16 also present in HTS)	n=14	Machesney et al., 1996
				n=10	Bloor et al., 2003
				n=10	Ong et al., 2010
Langerhans cell	Dendritic suprabasal cells, 2% epidermis	CD1a, S-100, Langerin (CD207)	Present within epidermis	n=26	Santucci et al., 2001
				n=25	Bagabir et al., 2012
Melanocyte	Highly dendritic, basal epidermal	Fontana-masson, Mel-5	Present/increased within epidermis	n=1 into fragments	Hochman et al., 2005
Fibrocyte	Spindled, mid-length fibre-like projections	CD34/Coll I; CD45/Coll I; CD86	Present within dermis	n=11	Iqbal et al., 2012
Fibroblast	Spindle-shaped	TE-7, Fibronectin, vimentin	Increased activity within dermis	n=12	Theoret et al., 2013;
				n=39	Chong et al., 2015
Myofibroblast	Spindled, fusiform indented nuclei	αSMA, transgelin, cytoglobin, P4Hβ	Present within dermis	n=40	Lee et al., 2004
				n=26	Santucci et al., 2001
Mast cell	Large, mononuclear, Metachromatic granules	CD117, anti-chymase, anti-tryptase, c-kit	Increased in dermis	n=5	Dong et al., 2014
				n=25	Bagabir et al., 2012
Lymphocyte	Spherical/ovoid, densely packed nuclear chromatin dominating cytoplasm	Giemsa/wright, CD45 T: CD3, CD4&8, TCR B: CD20, CD38, CD79a	Present in epidermis & dermis, ?increased in both	n=25	Bagabir et al., 2012
				n=8	Boyce et al., 2001
Macrophage	Large with granules & vacuoles vs monocytes	CD68 (M1) CD163 (M2)	Increased in reticular & papillary dermis	n=25	Bagabir et al., 2012
				n=44	Shaker et al., 2011
Endothelial cell	Elongated, flat & aligned in direction blood flow	CD31, VEGF, vWf	Present in epidermis & dermis	n=15	Zhang et al., 2015
				n=9	Kischer et al., 1982



stereological analysis of dermal vessels (Amadeu et al., 2003), transmission electron microscopy (Ueda et al., 2004), doppler assessment and quantitative microscopic examination in combination with CD31, CD34, CD105,  $\alpha$ SMA and VEGF immunostaining. While some of the literature favours hypervascularity associated with long and dilated vessels (Amadeu et al., 2003), the bulk of studies investigating keloid blood supply found limited microvasculature associated with luminal occlusion (Beer et al., 1998; Bux and Madaree, 2010; Har-Shai et al., 2011), most frequently attributed to obstruction by endothelial cells (Kischer et al., 1982; Kischer, 1992). The impaired blood supply within the keloid tissue has encouraged the hypothesis that hypoxia is a key element in the pathogenesis of KD (Butler et al., 2011). Bux and Madaree proposed that the impaired vasculature explains the features of degeneration and necrosis evident in keloid tissue and that the capillary occlusion results from chronic inflammation, occurring predominantly at the level of the subpapillary plexus (Bux and Madaree, 2010).

Due to the site-specific differences observed clinically (Syed et al., 2011), between keloid centre and margin, a more recent paper examined the differences in vascular density between these sites of the keloid lesion. Whilst there was no significant vascular density differences, it was noted that the vessels located centrally were more flattened, based on major and minor axes (Kurokawa et al., 2010). This correlated with the histological finding of an advancing edge with increased cellularity and microvasculature compared with the occluded vessels of the centre.

### Remodelling

This phase of wound healing, in contrast to the relatively short preceding phases, can last for months to years and is thought to be delayed in keloid. The ultimate role of this phase is to increase the tensile strength within the wound, decrease the thickness of the newly formed tissue and promote terminal differentiation of the epidermis, thereby restoring a functional barrier (Carlson and Longaker, 2004). The role of the myofibroblast, which begins with contraction

during the phase of proliferation, is instrumental in this phase and the failure to undergo apoptosis likely to be causative in keloid scar formation.

### Myofibroblasts

Myofibroblasts are mesenchymal cells expressing characteristics of both fibroblasts and smooth muscle cells. The origin of this hybrid cell has long been under debate, with reports of differentiation from pericytes, fibroblasts, smooth muscle cells and most recently from fibrocytes (Hinz et al., 2012). Myofibroblasts, like their predecessors, are spindle-shaped cells but have fusiform indented nuclei, a fibronectin-rich but laminin-deplete layer at their surface and, in addition to expressing fibronectin and vimentin, express  $\alpha$  smooth muscle actin ( $\alpha$ SMA) (Eyden et al., 2009). It is these non-muscle myosin microfilaments in combination with gap junctions that allow participation in wound closure and may cause the contracture postulated to be causative in hypertrophic and keloid scarring (Van De Water et al., 2013; Tholpady et al., 2014).

There has been much controversy over whether there are myofibroblasts in KD (Matsuoka et al., 1988) and whether there is  $\alpha$ SMA positive staining (Sarrazy et al., 2011). It had been suggested that  $\alpha$ SMA is used as a differentiation marker between keloid and hypertrophic scars (Ehrlich et al., 1994), however it was confirmed that keloid cells do express  $\alpha$ SMA (Lee et al., 2012) and due to the variability in expression in both forms of scarring (45% of keloid and 70% hypertrophic), this cannot be a reliable method of distinction (Lee et al., 2004).

Other markers have been used to detect myofibroblasts in keloid including transgelin, cytoglobin and prolyl-4-hydroxylase  $\beta$ , interestingly all of which are controlled by hypoxia, theorised to be one of the driving forces in keloid pathogenesis (Har-Shai et al., 2011). In fact, it has been reported that myofibroblasts are the predominant cell type present in keloid tissue regardless of the age of the lesion and that the collagen nodules in particular stain positive for  $\alpha$ SMA (Santucci et al., 2001; Hunasgi et al., 2013). It may be that the  $\alpha$ SMA expression of hypertrophic scars declines over

**Table 3.** Summary of the features of other skin-related fibrotic disorders in common with and different from keloid disease as well as the stains most commonly used in the diagnosis.

Condition	Histological features in common with KD	Histological features different from KD	Stain
Hypertrophic scar	Raised scar; Thickened collagen Nodules Increased cellularity	Non-flattened epidermis; Organised collagen fibres No recurrence	H&E $\alpha$ SMA
DFSP	Slow-growing; Raised, pigmented skin Recurrence	Increased nodularity; Honeycomb pattern Non-polarizing collagen	Vimentin; $\alpha$ SMA CD34+; XVIIIa-; S100-
Dermatofibroma	Thickened epidermis; Hyperkeratosis Hyalinised collagen	Scaly lesions; No recurrence Reduced cellularity; Grenz zone	XVIII+ CD34-
Scleroderma/ morphea	Pigmented Lack of adnexal appendages Nodules	Reduced cellularity; Collagen arranged parallel Systemic features	CD34-; CD1a; CD3; CD8; CD20+; CD25, CD57+

## Histopathology of keloid disease

time whereas that of keloids remains constant, allowing for distinction of older lesions (Santucci et al., 2001; Sarrazy et al., 2011). This failure to quiesce or apoptose may account for the continued growth observed in keloids as myofibroblasts in normal wound healing disappear when re-epithelialisation is complete (Hinz, 2007; Darby et al., 2014; Li-Tsang et al., 2015).

### Differential diagnose: KD versus other cutaneous fibroses

Since there is not one reliable and definitive keloid biomarker available, one needs to rely on both clinical appearance and histopathology in order to distinguish KD from other forms of cutaneous fibrosis (Table 3).

#### Hypertrophic scarring

The condition most commonly confused with keloid and a source of much contention is hypertrophic scarring. For the purposes of diagnosis and indeed research, several macroscopic criteria are generally applied to distinguish these two entities. Keloid scars extend beyond the margins of the original wound to invade the surrounding normal skin, whereas hypertrophic scars remain confined to the boundaries of the initial injury but push them out by expansion. This invasion is described histologically, by the advancing edge dominating the papillary dermis (Fong et al., 1999; Lee et al., 2004) but also as a clinically evident advancing edge (Cosman and Wolff, 1972). Unlike keloids, hypertrophic scars tend to regress with time and do not usually recur after excision but are more associated with contractures than their counterparts, due

to a higher rate of fibrin matrix gel contraction (Mustoe et al., 2002). Keloid scars are more likely to be erythematous and pruritic compared to hypertrophic scars but both can present with these symptoms and indeed it happens that there may be a mixture of the two processes occurring within the one wound. This clinical pattern led to the description of keloids as having an inflammatory zone, at the lesion base, a raised pale central area and a regressing portion where it resembles normal scarring (Seifert and Mrowietz, 2009).

#### Dermatofibrosarcoma protuberans

Dermatofibrosarcoma protuberans (DFSP), more commonly confused with dermatofibroma, can also pose a diagnostic dilemma when considering keloid, especially in its early stages. Similar to keloid, this cutaneous sarcoma is slow-growing, absent from the hands and feet, has a higher incidence in darker skin (Criscione and Weinstock, 2007), occurs most frequently between 20-50 years of age and may recur on excision (Sabater-Marco et al., 2006). It differs macroscopically in that it is often larger and more nodular and in some instances has been shown to metastasize (Liang et al., 2014). Microscopically DFSP is discernible by a characteristic storiform pattern of spindle cells surrounded by fibrous stroma that causes a honeycomb pattern when it extends into adipose tissue (Sabater-Marco et al., 2006). Similar to keloid and several other fibroses, it has been shown to stain positive for both vimentin (Tsai et al., 2014) and occasionally positive, although more routinely negative, for  $\alpha$ SMA (De Pasquale et al., 2009; Sundram, 2009; Kim et al., 2012).

Two markers have been used to specifically

**Table 4.** Summary of the characteristic features of keloid disease and their frequency, including data based on the images shown in Figs. 1-3.

Ref	Sample no.	Epidermis	Advancing edge	Collagen	Cellularity	Horizontal fibrous band	Inflammation	$\alpha$ SMA(+)	Vascularity
Moshref and Mufti, 2010	15	10/15 rete	-	15/15 haphazard	10/15	14/15	-	5/15	Sub-epidermal
Bux and Madaree, 2010	58	-	-	Thick bundles	Between collagen bundles. Fibroblastic. Immune	-	Chronic	-	Impaired angiogenesis
Santucci et al., 2001	26	Flattened. Adnexae displaced.	-	25/26 Thick; Hyalinised Haphazard	24/26 Diffuse, myofibroblasts	-	Persistent immune cell infiltrate	21/26	-
Lee et al., 2004	40	37/40 flattened	14/14 marginal sections	24/40 Thick hyalinised bundles	33/40	10/40	39/40 Lymphocytes 8/40 sinus tract/ ruptured follicle	18/40 (>10% +)	Disarray
Ong et al., 2010	10	Thickened	Lined with BM	-	-	-	-	-	-
Bayat et al., 2014 (unpublished)	13	Thickened & flattened 11/13 Thickened not flattened 2/13 Hyperkeratotic 12/13	3/13	Whorls, thickened Haphazard 11/13 Nodule 1/13 Fine, organised 1/13 Obliteration PD-RD 11/13	Diffuse 13/13 Including between collagen bundles	5/13 Upper dermis	10/13 most commonly sub-epidermally	-	10/13 occlusion PD-RD between collagen fibres, Neoangiogenesis deeper dermis

discriminate DFSP from other cutaneous pathologies: non-polarizable collagen (Barr et al., 1986) and positive CD34<sup>+</sup> staining (Aiba et al., 1992). There is a single reference to the polarization of keloid collagen that suggests that it is polarizable (Barr and Stegman, 1984), which may make it a potential point of differential diagnosis but this requires more studies before being reliably diagnostic. While the literature suggests consistent positive staining for CD34 in DFSP, the consensus in keloid seems to be that the perilesional and extralesional dermal sites are positive relative to the inflammatory process (Iqbal et al., 2010; Bakry et al., 2014). The CD34 immuno-staining in KD may show an inverse correlation with collagen I production (Aiba and Tagami, 1997).

#### *Dermatofibroma*

Like keloid, dermatofibroma often occurs at sites of previous trauma and microscopically appears ill-defined and frequently characterised by a hyperkeratotic, hyperplastic epidermis. Indeed, there is a keloid variant of this lesion that contains hyalinised collagen at the periphery leading to dependence on the presence of other features associated with dermatofibroma to rule out keloid (Alves et al., 2014). Dermatofibroma can be a scaly lesion more frequently occurring on the limbs, it tends not to recur following excision and in combination with microscopic features of a grenz zone (spared PD), elongated rete ridges and increased hair follicle structures, it should be distinguishable from keloid (Luzar and Calonje, 2010). The differences in PD at the margin of both lesions may be the diagnostic crux, where in keloid, it is the active site with increased cellularity and contrastingly in dermatofibroma, the PD is spared and the margin RD is the site of collagen bundles. Unlike DFSP, dermatofibroma (fibrous histiocytoma) is more easily differentiated by immunohistochemistry from DFSP than from keloid. A lesion that is CD34<sup>+</sup> and factor XVIIIa negative is likely to be DFSP, however CD34<sup>-</sup> and XVIIIa positive is more likely to be dermatofibroma (Altman et al., 1993) although the jury is out with regard to keloid. Similar to CD34, there is a lack of uniformity within the literature with respect to factor XVIIIa staining in keloid, with studies claiming both absence and augmentation (Kamath et al., 2002; Onodera et al., 2007).

#### *Morphea*

Another condition frequently misdiagnosed is cutaneous scleroderma or morphea, which similar to dermatofibroma has a keloid variant, making it more difficult to distinguish from the classic keloid scar. Macroscopically, sclerosis is characterised by thickened dermis and occasionally nodules or keloid-like lesions that are hyper-pigmented and lack appendages. Microscopically these nodules consist of collagen bundles lying parallel to the dermis and reduced

fibroblasts (Rencic et al., 2003). The presence of myofibroblasts has been suggested as a method to determine the stage of differentiation along a hypothetical continuum from morpheiform nodule to hypertrophic scar and finally keloid (Barzilai et al., 2003). These nodules can resemble keloid with flattened rete ridges, increased collagen and immune infiltrate (Buechner et al., 1993), diffuse tenascin staining (Lacour et al., 1992) and recently identified increased cartilage oligomeric matrix protein (COMP) staining (Moinzadeh et al., 2013). Due to the impact of systemic disease, it is essential to correctly diagnose these nodules and rule out any other signs of systemic sclerosis.

### **Perspectives for future, histopathology-based research into KD pathobiology**

#### *Site-specific disease*

Based originally on the clinical differences observed between the margin and centre of keloid scars, site-specific variations have only recently been exploited as a way to potentially target the active site of disease. Macroscopically, the centre (intralesional) is often pale, soft and involuted when compared with the margin (perilesional), where there is frequently a raised erythematous edge considered to be the aggressive site of activity. It has also been shown that fibroblasts from the PD and RD behave differently (Supp et al., 2012), leading to division of the upper and lower centre of the lesion as two separate sites.

This novel approach has already shown altered behaviour on a molecular level with regard to apoptosis (Lu et al., 2007; Seifert et al., 2008), collagen expression (Syed et al., 2011) and also on a protein level (Javad and Day, 2012). While there are some histological studies that analysed these areas separately (Bagabir et al., 2012) the benefits of site-specific staining to aid diagnosis and allow targeted therapy has yet to be fully explored. The standardised dissection of each keloid lesion into defined sites (see, for example Fig. 7) and the examination of ECM component histology for each site would abrogate the risk of incorrect diagnosis based on sampling site.

#### *Morphological classification*

Despite the disparity between different studies in the literature with regard to keloid histopathology, there is consistent reference to the heterogeneity that exists concerning this entity. Macroscopically, the keloid scar varies from a flat, claw-like invading lesion to a polypoid pedunculated lesion, both with varying degrees of central regression and marginal erythema and firmness. As these details are often not recorded and correlated with the histological findings, it is difficult to confidently identify effective treatments or judge accurate prognoses. Although keloid is usually the end-point in scar scale classification (Mustoe et al., 2002), it

would be beneficial to draw up a classification within keloid disease itself, delineating specific features found in each category based on morphology, enabling easier diagnosis and management.

#### *Basement membrane zone*

The basement membrane zone (BMZ) at the dermo-epidermal junction, whilst described as thickened in KD with random discontinuities when compared to normal skin (Mogili et al., 2012), has not been comprehensively examined in the keloid research literature. The BMZ provides not only structural support but also crucially contributes to cell signalling, the regulation of cell trafficking and EMI (LeBleu et al., 2007; Breitzkreutz et al., 2013; Bruckner-Tuderman and Has, 2014). One recent publication, using hyaluronan (HA) staining to classify scar types, describes the keloid BMZ as having shorter more cuboidal desmosomes when compared with normal skin and theorises that this may represent impaired epidermal barrier function (Hellstrom et al., 2014). There is very limited information on the expression of collagen IV (Ala-Kokko et al., 1987), collagen VII, perlecan, laminin, integrins and dystroglycans in relation to KD. With the recognition of the importance of EMI in wound healing and the likely demonstration of paracrine loops between keratinocytes and fibroblasts (Barton et al., 2010; Sobel et al., 2014), these BMZ components are likely to be altered in KD and may provide additional immunohistological and molecular markers for differentiating KD from other scarring entities.

#### *Tissue microarray (TMA) and Next generation sequencing (NGS)*

Originally referred to as the “sausage block” method, TMA allows high throughput screening, experimental uniformity and large sample number simultaneous analysis (Jawhar, 2009). Primarily used in tumour research the processing of multiple histological tissue sections under identical conditions is efficient and cost-effective (Kononen et al., 1998). Tissue-based assays including histochemistry, immunohistochemistry and in situ hybridisation can be performed on up to 1000 re-planted paraffin embedded core biopsies in a single block visualised on one slide. Application to heterogeneous tissue is not recommended, as the core biopsy may not be representative of the lesion as a whole (Barrette et al., 2014). Although keloid is heterogeneous it may be possible to use this technique to assess multiple areas of the same lesion at one time, similar to including multiple tumour progression stages on the one block. In this way, site-specific disease can be analysed and compared between keloid lesions and emerging patterns applied to differential diagnosis.

The advent of NGS (Hedegaard et al., 2014) may be of benefit to KD, especially as it has recently been shown to be applicable to formalin-fixed paraffin-

embedded (FFPE) tissue sections (Corless and Spellman, 2012). While this technology is currently largely applied to oncology (Dander et al., 2014), the paucity of available fresh keloid tissue and potential numbers of archived FFPE samples that could be pooled, means NGS would be an ideal platform to apply to KD, also enabling comparison to other similar scarring entities (Sweeney and van de Rijn, 2012).

#### **Summary and conclusions**

KD is characterised clinically by patient and lesion heterogeneity resulting in inconsistent histological findings with mixed reports in the literature as well as varied response to therapy. The majority of recent focus in keloid has been on identifying genetic biomarkers to diagnose and target keloid scars, leaving histological descriptions incomplete.

Based on our literature search, we found the discerning features of keloid to be the epidermis and non-collagenous matrix molecules, altered by an imbalance in the phases of wound healing. The significant changes in these ECM molecules, attributed to prolonged proliferation and delayed remodelling phase, are summarised in Table 1 and the most common “pathognomonic” changes in Table 4. In some cases, it is the persistence of staining (decorin) or cellularity (myofibroblasts) that contributes to the interpretation rather than its definite presence or absence, highlighting the necessity of taking the age of the lesion into account. In addition to diagnostic value, these findings may help explain the aetiology of certain keloids. The evidence of reduced or occluded vascularity, particularly in the lesion centre, supports the hypoxic theory that has been put forward as a contributor to this disease. Similarly, the structure of keloid collagen has been described as tendon-like, suggesting it was thickened to deal with increased mechanical stress, another postulation for keloid aetiology (Bux and Madaree, 2012). Normally populated by a number of adnexae including pilosebaceous units and sweat glands, the observations of keloid dermis have demonstrated a scarcity of these structures (Tan et al., 2011). Indeed, studies have alluded to some specimens containing draining sinus tracts and/or inflamed ruptured hair follicles, suggesting a chronic inflammatory role in keloid pathogenesis (Lee et al., 2004).

The histology panels in Figs. 1-3, showing keloid and normal skin histochemistry stained in our own laboratory, depict many of the characteristic features associated with keloid disease. The thickened, flattened epidermis with associated hyperkeratosis (Fig. 1A), whorls of haphazard hyalinised collagen (Fig. 1C), hyper-cellularity (Fig. 1D) and horizontal fibrous bands (Fig. 1G,H) are shown. Fig. 2 compares keloid and normal skin using Herovici staining (Fitzgerald et al., 1996; Turner et al., 2013), where immature collagen III stains blue and mature collagen I stains red. There is a striking difference in the size of the sub-epidermal and



PD between keloid and normal skin. This increased distance in keloid is dominated by purplish staining, suggesting a mixture of types I and III collagen compared to the dominance of collagen I in the RD. This transition occurs much more quickly in the normal skin where it fades to a fine wavy regular type I collagen pattern. This difference in ratio of collagen I:III between the papillary and reticular dermis has been alluded to previously in reference to keloid (Syed et al., 2011).

Fig. 3 emphasises the significance of using a combination of features to aid diagnosis. The blurring of the papillary-reticular boundary (Fig. 3A) and evolution from fine collagen fibres sub-epidermally to coarser thickened fibres in the deeper dermis (Fig. 3B) are easily identified in samples with a complete profile of tissue present. Frequently the signs are more subtle, in that the epidermis is thickened but not necessarily flattened (Fig. 3C) or perhaps the collagen may not be the thickened coarser collagen expected of keloid but the associated cellularity and hyper-proliferative epidermis still support the diagnosis. Many of the samples show signs of inflammation, particularly sub-epidermally. Occasionally, the microscopic elements less routinely associated with keloid, including the presence of nodules (Fig. 3E) and a focal point of eruptive collagen (Fig. 3F), which depend on the area of the keloid biopsied and can lead to confusion with other entities. Any residual overlap with histological features of other cutaneous fibroses could potentially be laid to rest by closing the gap in knowledge with regard to BMZ features, unstudied ECM molecules and cellular confirmation. Further research into these histological components forms just part of the future work that should be undertaken to better understand KD. From the comparisons of keloid with hypertrophic scar to date, it is apparent that age-related findings play an important part in differential diagnosis with many of the similar findings between these two diverging with increasing age.

Approaching KD from a pathobiological perspective enables histological discrimination, improved differential diagnosis and correlation with molecular analysis. Amidst the continued search for a target biomarker, the histomorphology of keloid scars remains the mainstay of diagnosis. The inherent heterogeneity within fibrosis and limited availability of keloid samples has resulted in a widely variable and conflicting description of the morphology and tissue architecture. This review clarifies and emphasises the “pathognomonic” features that allow critical but undervalued distinction from other conditions and also highlights the gaps within the literature that may form the basis of future work. Improved differential diagnosis serves not only to prevent misdiagnosis of sinister disease but also allows targeting with appropriate therapy. While keloid therapeutic options are not the focus of this review and are discussed in detail elsewhere in the literature (Viera et al., 2012; Gold et al., 2014), we have highlighted a number of histological

markers that may be of therapeutic interest. This is especially important in KD, where despite a plethora of available therapies, there is no one effective treatment.

## References

- Abdel-Meguid A.M., Weshahy A.H., Sayed D.S., Refaiy A.E. and Awad S.M. (2014). Intralesional vs. contact cryosurgery in treatment of keloids: a clinical and immunohistochemical study. *Int. J. Dermatol.* 54, 468-475.
- Abdou A.G., Maraee A.H., Al-Bara A.M. and Diab W.M. (2011). Immunohistochemical expression of TGF-beta1 in keloids and hypertrophic scars. *Am. J. Dermatopathol.* 33, 84-91.
- Abdou A.G., Maraee A.H. and Saif H.F. (2014). Immunohistochemical evaluation of COX-1 and COX-2 expression in keloid and hypertrophic scar. *Am. J. Dermatopathol.* 36, 311-317.
- Abe R., Donnelly S.C., Peng T., Bucala R. and Metz C.N. (2001). Peripheral blood fibrocytes: differentiation pathway and migration to wound sites. *J. Immunol.* 166, 7556-7562.
- Abergel R.P., Pizzurro D., Meeker C.A., Lask G., Matsuoka L.Y., Minor R.R., Chu M.L. and Uitto J. (1985). Biochemical composition of the connective tissue in keloids and analysis of collagen metabolism in keloid fibroblast cultures. *J. Invest. Dermatol.* 84, 384-390.
- Aiba S. and Tagami H. (1997). Inverse correlation between CD34 expression and proline-4-hydroxylase immunoreactivity on spindle cells noted in hypertrophic scars and keloids. *J. Cutan. Pathol.* 24, 65-69.
- Aiba S., Tabata N., Ishii H., Ootani H. and Tagami H. (1992). Dermatofibrosarcoma protuberans is a unique fibrohistiocytic tumour expressing CD34. *Br. J. Dermatol.* 127, 79-84.
- Ala-Kokko L., Rintala A. and Savolainen E.R. (1987). Collagen gene expression in keloids: analysis of collagen metabolism and type I, III, IV, and V procollagen mRNAs in keloid tissue and keloid fibroblast cultures. *J. Invest. Dermatol.* 89, 238-244.
- Altman D.A., Nickoloff B.J. and Fivenson D.P. (1993). Differential expression of factor XIIIa and CD34 in cutaneous mesenchymal tumors. *J. Cutan. Pathol.* 20, 154-158.
- Alves J.V., Matos D.M., Barreiros H.F. and Bartolo E.A. (2014). Variants of dermatofibroma—a histopathological study. *Anais brasileiros de dermatologia.* 89, 472-477.
- Amadeu T., Braune A., Mandarim-de-Lacerda C., Porto L.C., Desmouliere A. and Costa A. (2003). Vascularization pattern in hypertrophic scars and keloids: a stereological analysis. *Pathol. Res. Pract.* 199, 469-473.
- Amadeu T.P., Braune A.S., Porto L.C., Desmouliere A. and Costa A.M. (2004). Fibrillin-1 and elastin are differentially expressed in hypertrophic scars and keloids. *Wound. Repair. Regen.* 12, 169-174.
- Ammendola M., Zuccala V., Patruno R., Russo E., Luposella M., Amorosi A., Vescio G., Sammarco G., Montemurro S., De Sarro G., Sacco R. and Ranieri G. (2013). Tryptase-positive mast cells and angiogenesis in keloids: a new possible post-surgical target for prevention. *Updates Surg.* 65, 53-57.
- Arbi S., Eksteen E.C., Oberholzer H.M., Taute H. and Bester M.J. (2015). Premature collagen fibril formation, fibroblast-mast cell interactions and mast cell-mediated phagocytosis of collagen in keloids. *Ultrastruct. Pathol.* 39, 95-103.
- Ashcroft K.J., Syed F. and Bayat A. (2013). Site-specific keloid fibroblasts alter the behaviour of normal skin and normal scar

## *Histopathology of keloid disease*

- fibroblasts through paracrine signalling. *PLoS One*. 8, e75600.
- Atiyeh B.S., Costagliola M. and Hayek S.N. (2005). Keloid or hypertrophic scar: the controversy: review of the literature. *Ann. Plast. Surg.* 54, 676-680.
- Babu M., Diegelmann R. and Oliver N. (1989). Fibronectin is overproduced by keloid fibroblasts during abnormal wound healing. *Mol. Cell. Biol.* 9, 1642-1650.
- Bagabir R., Byers R.J., Chaudhry I.H., Muller W., Paus R. and Bayat A. (2012). Site-specific immunophenotyping of keloid disease demonstrates immune upregulation and the presence of lymphoid aggregates. *Br. J. Dermatol.* 167, 1053-1066.
- Bakry O.A., Samaka R.M., Basha M.A., Tharwat A. and El Meadawy I. (2014). Hematopoietic stem cells: do they have a role in keloid pathogenesis? *Ultrastruct. Pathol.* 38, 55-65.
- Barr R.J. and Stegman S.J. (1984). Delayed skin test reaction to injectable collagen implant (Zyderm). The histopathologic comparative study. *J. Am. Acad. Dermatol.* 10, 652-658.
- Barr R.J., Young E.M. Jr. and King D.F. (1986). Non-polarizable collagen in dermatofibrosarcoma protuberans: a useful diagnostic aid. *J. Cutan. Pathol.* 13, 339-346.
- Barrette K., van den Oord J.J. and Garmyn M. (2014). Tissue microarray. *J. Invest. Dermatol.* 134, e24.
- Barton C.E., Johnson K.N., Mays D.M., Boehnke K., Shyr Y., Boukamp P. and Pietenpol J.A. (2010). Novel p63 target genes involved in paracrine signaling and keratinocyte differentiation. *Cell Death Dis.* 1, e74.
- Barzilai A., Lyakhovitsky A., Horowitz A. and Trau H. (2003). Keloid-like scleroderma. *Am. J. Dermatopath.* 25, 327-330.
- Baum C.L. and Arpey C.J. (2005). Normal cutaneous wound healing: clinical correlation with cellular and molecular events. *Dermatol. Surg.* 31, 674-686; discussion 686.
- Beer W., Baldwin H.C., Goddard J.R., Gallagher P.J. and Wright D.H. (1998). Angiogenesis in pathological and surgical scars. *Hum. Path.* 29, 1273-1278.
- Bellini A. and Mattoli S. (2007). The role of the fibrocyte, a bone marrow-derived mesenchymal progenitor, in reactive and reparative fibroses. *Lab. Invest.* 87, 858-870.
- Bertheim U. and Hellstrom S. (1994). The distribution of hyaluronan in human skin and mature, hypertrophic and keloid scars. *Br. J. Plast. Surg.* 47, 483-489.
- Blakaj A. and Bucala R. (2012). Fibrocytes in health and disease. *Fibrogenesis Tissue Repair* 5, S6.
- Bloor B.K., Tidman N., Leigh I.M., Odell E., Dogan B., Wollina U., Ghali L. and Waseem A. (2003). Expression of keratin K2e in cutaneous and oral lesions: association with keratinocyte activation, proliferation, and keratinization. *Am. J. Pathol.* 162, 963-975.
- Boyce S.T. (1994). Epidermis as a secretory tissue. *J. Invest. Dermatol.* 102, 8-10.
- Boyce D.E., Ciampolini J., Ruge F., Murison M.S. and Harding K.G. (2001). Inflammatory-cell subpopulations in keloid scars. *Br. J. Plast. Surg.* 54, 511-516.
- Bozoky B., Savchenko A., Guven H., Ponten F., Klein G. and Szekely L. (2014). Decreased decorin expression in the tumor microenvironment. *Cancer Med.* 3, 485-491.
- Breitkreutz D., Koxholt I., Thiemann K. and Nischt R. (2013). Skin basement membrane: the foundation of epidermal integrity--BM functions and diverse roles of bridging molecules nidogen and perlecan. *Biomed. Res. Int.* 2013 179784.
- Bruckner-Tuderman L. and Has C. (2014). Disorders of the cutaneous basement membrane zone--the paradigm of epidermolysis bullosa. *Matrix Biol.* 33, 29-34.
- Bucala R. (2012). Review Series--Inflammation & fibrosis. Fibrocytes and fibrosis. *QJM* 105, 505-508.
- Bucala R., Spiegel L.A., Chesney J., Hogan M. and Cerami A. (1994). Circulating fibrocytes define a new leukocyte subpopulation that mediates tissue repair. *Mol. Med.* 1, 71-81.
- Buechner S.A., Winkelmann R.K., Lautenschlager S., Gilli L. and Ruffli T. (1993). Localized scleroderma associated with *Borrelia burgdorferi* infection. Clinical, histologic, and immunohistochemical observations. *J. Am. Acad. Dermatol.* 29 190-196.
- Butler P.D., Longaker M.T. and Yang G.P. (2008). Current progress in keloid research and treatment. *J. Am. Coll. Surg.* 206, 731-741.
- Butler P.D., Wang Z., Ly D.P., Longaker M.T., Koong A.C. and Yang G.P. (2011). Unfolded protein response regulation in keloid cells. *J. Surg. Res.* 167, 151-157.
- Bux S. and Madaree A. (2010). Keloids show regional distribution of proliferative and degenerate connective tissue elements. *Cells Tissues Organs* 191, 213-234.
- Bux S. and Madaree A. (2012). Involvement of upper torso stress amplification, tissue compression and distortion in the pathogenesis of keloids. *Med. Hypoth.* 78, 356-363.
- Carlson M.A. and Longaker M.T. (2004). The fibroblast-populated collagen matrix as a model of wound healing: a review of the evidence. *Wound Repair Regen.* 12, 134-147.
- Carrino D.A., Mesiano S., Barker N.M., Hurd W.W. and Caplan A.I. (2012). Proteoglycans of uterine fibroids and keloid scars: similarity in their proteoglycan composition. *Biochem. J.* 443, 361-368.
- Catherino W.H., Leppert P.C., Stenmark M.H., Payson M., Potlog-Nahari C., Nieman L.K. and Segars J.H. (2004). Reduced dermatopontin expression is a molecular link between uterine leiomyomas and keloids. *Genes Chromosom. Cancer* 40, 204-217.
- Chen J., Zhuo S., Jiang X., Zhu X., Zheng L., Xie S., Lin B. and Zeng H. (2011). Multiphoton microscopy study of the morphological and quantity changes of collagen and elastic fiber components in keloid disease. *J. Biomed. Optics* 16, 051305.
- Chen J., Zeng B., Yao H. and Xu J. (2013). The effect of TLR4/7 on the TGF-beta-induced Smad signal transduction pathway in human keloid. *Burns* 39, 465-472.
- Chen R., Zhang Z., Xue Z., Wang L., Fu M., Lu Y., Bai L., Zhang P. and Fan Z. (2015). Protein-protein interaction network of gene expression in the hydrocortisone-treated keloid. *Int. J. Dermatol.* 54, 549-554.
- Chong Y., Park T.H., Seo S.W. and Chang C.H. (2015). Histomorphometric analysis of collagen architecture of auricular keloids in an asian population. *Dermatol. Surg.* 41, 415-422.
- Chou W.C., Takeo M., Rabbani P., Hu H., Lee W., Chung Y.R., Carucci J., Overbeek P. and Ito M. (2013). Direct migration of follicular melanocyte stem cells to the epidermis after wounding or UVB irradiation is dependent on Mc1r signaling. *Nat. Med.* 19, 924-929.
- Corless C.L. and Spellman P.T. (2012). Tackling formalin-fixed, paraffin-embedded tumor tissue with next-generation sequencing. *Cancer. Discov.* 2, 23-24.
- Cosman B. and Wolff M. (1972). Acne keloidalis. *Plast. Reconstr. Surg.* 50(1), 25-30.
- Crawford J., Nygard K., Gan B.S. and O'Gorman D.B. (2015). Periostin induces fibroblast proliferation and myofibroblast persistence in hypertrophic scarring. *Exp. Dermatol.* 24(2), 120-126.
- Criscione V.D. and Weinstock M.A. (2007). Descriptive epidemiology of

- dermatofibrosarcoma protuberans in the United States, 1973 to 2002. *J. Am. Acad. Dermatol.* 56(6), 968-973.
- Curran T.A. and Ghahary A. (2013). Evidence of a role for fibrocyte and keratinocyte-like cells in the formation of hypertrophic scars. *J. Burn Care Res.* 34(2), 227-231.
- Da Costa V., Wei R., Lim R., Sun C.H., Brown J.J. and Wong B.J. (2008). Nondestructive imaging of live human keloid and facial tissue using multiphoton microscopy. *Arch. Facial Plast. Surg.* 10, 38-43.
- Dalkowski A., Schuppan D., Orfanos C.E. and Zouboulis C.C. (1999). Increased expression of tenascin C by keloids *in vivo* and *in vitro*. *Br. J. Dermatol.* 141, 50-56.
- Dander A., Baldauf M., Sperk M., Pabinger S., Hiltbold B. and Trajanoski Z. (2014). Personalized Oncology Suite: integrating next-generation sequencing data and whole-slide bioimages. *BMC Bioinform.* 15, 306.
- Darby I.A., Laverdet B., Bonte F. and Desmouliere A. (2014). Fibroblasts and myofibroblasts in wound healing. *Clin. Cosmet. Investig. Dermatol.* 7, 301-311.
- De Pasquale R., Dinotta F., Scuderi L., Musumeci M.L. and Micali G. (2009). Dermatofibrosarcoma protuberans. *Giornale italiano di dermatologia e venereologia.* 144, 199-203.
- Di Meglio P., Perera G.K. and Nestle F.O. (2011). The multitasking organ: recent insights into skin immune function. *Immunity.* 35, 857-869.
- Ding J. and Tredget E.E. (2014). The role of chemokines in fibrotic wound healing. *Adv. Wound. Care* (in press).
- Dong X., Zhang C., Ma S. and Wen H. (2014). Mast cell chymase in keloid induces profibrotic response via transforming growth factor-beta1/Smad activation in keloid fibroblasts. *Int. J. Clin. Exp. Pathol.* 7, 3596-3607.
- Eckert R.L. (1989). Structure, function, and differentiation of the keratinocyte. *Physiol. Rev.* 69, 1316-1346.
- Ehrlich H.P., Desmouliere A., Diegelmann R.F., Cohen I.K., Compton C.C., Garner W.L., Kapanci Y. and Gabbiani G. (1994). Morphological and immunochemical differences between keloid and hypertrophic scar. *Am. J. Pathol.* 145, 105-113.
- Eyden B., Banerjee S.S., Shenjere P. and Fisher C. (2009). The myofibroblast and its tumours. *J. Clin. Pathol.* 62, 236-249.
- Fitzgerald A.M., Kirkpatrick J.J., Foo I.T. and Naylor I.L. (1996). Human skin histology as demonstrated by Herovici's stain: a guide for the improvement of dermal substitutes for use with cultured keratinocytes? *Burns* 22, 200-202.
- Fong E.P., Chye L.T. and Tan W.T. (1999). Keloids: time to dispel the myths? *Plast. Reconstr. Surg.* 104, 1199-1202.
- Fradette J., Larouche D., Fugere C., Guignard R., Beauparlant A., Couture V., Caouette-Laberge L., Roy A. and Germain L. (2003). Normal human Merkel cells are present in epidermal cell populations isolated and cultured from glabrous and hairy skin sites. *J. Invest. Dermatol.* 120, 313-317.
- Frenkel J.S. (2014). The role of hyaluronan in wound healing. *Int. Wound J.* 11, 159-163.
- Funayama E., Chodon T., Oyama A. and Sugihara T. (2003). Keratinocytes promote proliferation and inhibit apoptosis of the underlying fibroblasts: an important role in the pathogenesis of keloid. *J. Invest. Dermatol.* 121, 1326-1331.
- Gao F.L., Jin R., Zhang L. and Zhang Y.G. (2013). The contribution of melanocytes to pathological scar formation during wound healing. *Int. J. Clin. Exp. Med.* 6, 609-613.
- Garner W.L. (1998). Epidermal regulation of dermal fibroblast activity. *Plast. Reconstr. Surg.* 102, 135-139.
- Gauglitz G.G., Korting H.C., Pavicic T., Ruzicka T. and Jeschke M.G. (2011). Hypertrophic scarring and keloids: pathomechanisms and current and emerging treatment strategies. *Mol. Med.* 17, 113-125.
- Gold M.H., McGuire M., Mustoe T.A., Pusic A., Sachdev M., Waibel J. and Murcia C. (2014). Updated international clinical recommendations on scar management: Part 2—algorithms for scar prevention and treatment. *Derm. Surg.* 40, 825-831.
- Guo S. and Dipietro L.A. (2010). Factors affecting wound healing. *J. Dent. Res.* 89, 219-229.
- Gurtner G.C., Werner S., Barrandon Y. and Longaker M.T. (2008). Wound repair and regeneration. *Nature* 453, 314-321.
- Haertel E., Werner S. and Schafer M. (2014). Transcriptional regulation of wound inflammation. *Semin. Immunol.* 26, 321-328.
- Hahn J.M., Glaser K., McFarland K.L., Aronow B.J., Boyce S.T. and Supp D.M. (2013). Keloid-derived keratinocytes exhibit an abnormal gene expression profile consistent with a distinct causal role in keloid pathology. *Wound Repair Regen.* 21, 530-544.
- Halper J. and Kjaer M. (2014). Basic components of connective tissues and extracellular matrix: elastin, fibrillin, fibulins, fibrinogen, fibronectin, laminin, tenascins and thrombospondins. *Adv. Exp. Med. Biol.* 802, 31-47.
- Har-Shai Y., Mettanes I., Zilberstein Y., Genin O., Spector I. and Pines M. (2011). Keloid histopathology after intralesional cryosurgery treatment. *J. Eur. Acad. Dermatol. Venereol.* 25, 1027-1036.
- Har-Shai Y., Sabo E., Rohde E., Hyams M., Assaf C. and Zouboulis C.C. (2006). Intralesional cryosurgery enhances the involution of recalcitrant auricular keloids: a new clinical approach supported by experimental studies. *Wound Repair Regen.* 14, 18-27.
- Hassel J.C., Roberg B., Kreuter A., Voigtlander V., Rammelsberg P. and Hassel A.J. (2007). Treatment of ear keloids by compression, using a modified oyster-splint technique. *Dermatol. Surg.* 33, 208-212.
- Hedegaard J., Thorsen K., Lund M.K., Hein A.M., Hamilton-Dutoit S.J., Vang S., Nordentoft I., Birkenkamp-Demtroder K., Kruhoffer M., Hager H., Knudsen B., Andersen C.L., Sorensen K.D., Pedersen J.S., Orntoft T.F. and Dyrskjot L. (2014). Next-generation sequencing of RNA and DNA isolated from paired fresh-frozen and formalin-fixed paraffin-embedded samples of human cancer and normal tissue. *PLoS One* 9, e98187.
- Hellstrom M., Hellstrom S., Engstrom-Laurent A. and Berthelm U. (2014). The structure of the basement membrane zone differs between keloids, hypertrophic scars and normal skin: A possible background to an impaired function. *J. Plast. Reconstr. Aesthet. Surg.* 67, 1564-1572.
- Hinz B. (2007). Formation and function of the myofibroblast during tissue repair. *J. Invest. Dermatol.* 127, 526-537.
- Hinz B., Phan S.H., Thannickal V.J., Prunotto M., Desmouliere A., Varga J., De Wever O., Mareel M. and Gabbiani G. (2012). Recent developments in myofibroblast biology: paradigms for connective tissue remodeling. *Am. J. Pathol.* 180, 1340-1355.
- Hochman B., Vilas Boas F.C., Mariano M. and Ferreiras L.M. (2005). Keloid heterograft in the hamster (*Mesocricetus auratus*) cheek pouch, Brazil. *Acta Cirurgica Brasileira* 20, 200-212.
- Hu Z.C., Tang B., Guo D., Zhang J., Liang Y.Y., Ma D. and Zhu J.Y. (2014). Expression of insulin-like growth factor-1 receptor in keloid and hypertrophic scar. *Clin. Exp. Dermatol.* 39, 822-828.
- Huang C., Akaiishi S., Hyakusoku H. and Ogawa R. (2012). Are keloid and hypertrophic scar different forms of the same disorder? A

## *Histopathology of keloid disease*

- fibroproliferative skin disorder hypothesis based on keloid findings. *Int. Wound. J.* 11, 517-522.
- Hunasgi S., Koneru A., Vanishree M. and Shamala R. (2013). Keloid: A case report and review of pathophysiology and differences between keloid and hypertrophic scars. *J. Oral. Maxillofac. Pathol.* 17, 116-120.
- Hunzelmann N., Anders S., Sollberg S., Schonherr E. and Krieg T. (1996). Co-ordinate induction of collagen type I and biglycan expression in keloids. *Br. J. Dermatol.* 135, 394-399.
- Ikeda M., Naitoh M., Kubota H., Ishiko T., Yoshikawa K., Yamawaki S., Kurokawa M., Utani A., Nakamura T., Nagata K. and Suzuki S. (2009). Elastic fiber assembly is disrupted by excessive accumulation of chondroitin sulfate in the human dermal fibrotic disease, keloid. *Biochem. Biophys. Res. Commun.* 390, 1221-1228.
- Iqbal S.A., Syed F., McGrouther D.A., Paus R. and Bayat A. (2010). Differential distribution of haematopoietic and nonhaematopoietic progenitor cells in intralesional and extralesional keloid: do keloid scars provide a niche for nonhaematopoietic mesenchymal stem cells? *Br. J. Dermatol.* 162, 1377-1383.
- Iqbal S.A., Sidgwick G.P. and Bayat A. (2012). Identification of fibrocytes from mesenchymal stem cells in keloid tissue: a potential source of abnormal fibroblasts in keloid scarring. *Arch. Dermatol. Res.* 304, 665-671.
- Javad F. and Day P.J. (2012). Protein profiling of keloidal scar tissue. *Arch. Dermatol. Res.* 304, 533-540.
- Jawhar N.M. (2009). Tissue microarray: A rapidly evolving diagnostic and research tool. *Ann. Saudi Med.* 29, 123-127.
- Kadoya K., Amano S., Nishiyama T., Inomata S., Tsunenaga M., Kumagai N. and Matsuzaki K. (2015). Changes in fibrillin-1 expression, elastin expression and skin surface texture at sites of cultured epithelial autograft transplantation onto wounds from burn scar excision. *Int. Wound. J.* (in press).
- Kamath N.V., Ormsby A., Bergfeld W.F. and House N.S. (2002). A light microscopic and immunohistochemical evaluation of scars. *J. Cutan. Pathol.* 29, 27-32.
- Kanitakis J. (2002). Anatomy, histology and immunohistochemistry of normal human skin. *Eur. J. Dermatol.* 12, 390-399.
- Kao H.K., Chen B., Murphy G.F., Li Q., Orgill D.P. and Guo L. (2011). Peripheral blood fibrocytes: enhancement of wound healing by cell proliferation, re-epithelialization, contraction, and angiogenesis. *Ann. Surg.* 254, 1066-1074.
- Kauh Y.C., Rouda S., Mondragon G., Tokarek R., diLeonardo M., Tuan R.S. and Tan E.M. (1997). Major suppression of pro-alpha1(I) type I collagen gene expression in the dermis after keloid excision and immediate intrawound injection of triamcinolone acetonide. *J. Am. Acad. Dermatol.* 37, 586-589.
- Kielty C.M. (2006). Elastic fibres in health and disease. *Expert. Rev. Mol. Med.* 8, 1-23.
- Kim M., Cho K.H., Lee J.H., Chang M.S. and Cho S. (2012). Intratumoral mast cell number is negatively correlated with tumor size and mitosis in dermatofibrosarcoma protuberans. *Exp. Dermatol.* 21, 559-561.
- Kischer C.W. (1992). The microvessels in hypertrophic scars, keloids and related lesions: a review. *J. Submicrosc. Cytol. Pathol.* 24, 281-296.
- Kischer C.W. and Brody G.S. (1981). Structure of the collagen nodule from hypertrophic scars and keloids. *Scan. Electron. Microsc.* (Pt 3), 371-376.
- Kischer C.W. and Hendrix M.J. (1983). Fibronectin (FN) in hypertrophic scars and keloids. *Cell. Tissue Res.* 231, 29-37.
- Kischer C.W., Thies A.C. and Chvapil M. (1982). Perivascular myofibroblasts and microvascular occlusion in hypertrophic scars and keloids. *Hum. Pathol.* 13, 819-824.
- Kishimoto J., Ehama R., Wu L., Jiang S., Jian N. and Burgeson R.E. (1999). Selective activation of the versican promoter by epithelial-mesenchymal interactions during hair follicle development. *Proc. Natl. Acad. Sci. USA* 96, 7336-7341.
- Knaggs H.E., Layton A.M., Morris C., Wood E.J., Holland D.B. and Cunliffe W.J. (1994). Investigation of the expression of the extracellular matrix glycoproteins tenascin and fibronectin during acne vulgaris. *Br. J. Dermatol.* 130, 576-582.
- Knapp T.R., Daniels R.J. and Kaplan E.N. (1977). Pathologic scar formation. Morphologic and biochemical correlates. *Am. J. Pathol.* 86, 47-70.
- Kononen J., Bubendorf L., Kallionimi A., Bärnlund, M., Schraml P., Leighton S., Torhorst J., Mihatsch M.J., Sauter G. and Kallionimi O.-P. (1998). Tissue microarrays for high-throughput molecular profiling of tumor specimens. *Nature Med.* 4, 844-847.
- Kose O. and Waseem A. (2008). Keloids and hypertrophic scars: are they two different sides of the same coin? *Dermatol. Surg.* 34, 336-346.
- Krishnaswamy V.R. and Korrapati P.S. (2014). Role of dermatopontin in re-epithelialization: implications on keratinocyte migration and proliferation. *Sci. Rep.* 4, 7385.
- Krishnaswamy V.R., Manikandan M., Munirajan A.K., Vijayaraghavan D. and Korrapati P.S. (2014). Expression and integrity of dermatopontin in chronic cutaneous wounds: a crucial factor in impaired wound healing. *Cell. Tissue. Res.* 358, 833-841.
- Kuroda K., Okamoto O. and Shinkai H. (1999). Dermatopontin expression is decreased in hypertrophic scar and systemic sclerosis skin fibroblasts and is regulated by transforming growth factor-beta1, interleukin-4, and matrix collagen. *J. Invest. Dermatol.* 112, 706-710.
- Kurokawa N., Ueda K. and Tsuji M. (2010). Study of microvascular structure in keloid and hypertrophic scars: density of microvessels and the efficacy of three-dimensional vascular imaging. *J. Plast. Surg. Hand. Surg.* 44, 272-277.
- Lacour J.P., Vitetta A., Chiquet-Ehrismann R., Pisani A. and Ortonne J.P. (1992). Increased expression of tenascin in the dermis in scleroderma. *Br. J. Dermatol.* 127, 328-334.
- Lavker R.M. and Schechter N.M. (1985). Cutaneous mast cell depletion results from topical corticosteroid usage. *J. Immunol.* 135, 2368-2373.
- LeBleu V.S., Macdonald B. and Kalluri R. (2007). Structure and function of basement membranes. *Exp. Biol. Med.* 232, 1121-1129.
- Lee J.Y., Yang C.C., Chao S.C. and Wong T.W. (2004). Histopathological differential diagnosis of keloid and hypertrophic scar. *Am. J. Dermatopathol.* 26, 379-384.
- Lee W.J., Kim Y.O., Choi I.K., Rah D.K. and Yun C.O. (2011). Adenovirus-relaxin gene therapy for keloids: implication for reversing pathological fibrosis. *Br. J. Dermatol.* 165, 673-677.
- Lee C.H., Hong C.H., Chen Y.T., Chen Y.C. and Shen M.R. (2012). TGF-beta1 increases cell rigidity by enhancing expression of smooth muscle actin: keloid-derived fibroblasts as a model for cellular mechanics. *J. Dermatol. Sci.* 67, 173-180.
- Lee W.J., Choi I.K., Lee J.H., Kim Y.O. and Yun C.O. (2013). A novel three-dimensional model system for keloid study: Organotypic multicellular scar model. *Wound Repair Regen.* 21, 155-165.
- Li-Tsang C.W., Feng B., Huang L., Liu X., Shu B., Chan Y.T. and



- Cheung K.K. (2015). A histological study on the effect of pressure therapy on the activities of myofibroblasts and keratinocytes in hypertrophic scar tissues after burn. *Burns*. (in press).
- Liang C.J., Yen Y.H., Hung L.Y., Wang S.H., Pu C. M., Chien H.F., Tsai J.S., Lee C.W., Yen F.L. and Chen Y.L. (2013). Thalidomide inhibits fibronectin production in TGF-beta1-treated normal and keloid fibroblasts via inhibition of the p38/Smad3 pathway. *Biochem. Pharmacol.* 85, 1594-1602.
- Liang C.A., Jambusaria-Pahlajani A., Karia P.S., Elenitsas R., Zhang P.D. and Schmults C.D. (2014). A systematic review of outcome data for dermatofibrosarcoma protuberans with and without fibrosarcomatous change. *J. Am. Acad. Dermatol.* 71, 781-786.
- Lim I.J., Phan T.T., Song C., Tan W.T. and Longaker M.T. (2001). Investigation of the influence of keloid-derived keratinocytes on fibroblast growth and proliferation *in vitro*. *Plast. Reconstr. Surg.* 107, 797-808.
- Lim I.J., Phan T.T., Bay B.H., Qi R., Huynh H., Tan W.T., Lee S.T. and Longaker M.T. (2002). Fibroblasts cocultured with keloid keratinocytes: normal fibroblasts secrete collagen in a keloidlike manner. *American journal of physiology. Cell. Physiol.* 283, C212-222.
- Linares H.A. and Larson D.L. (1974). Early differential diagnosis between hypertrophic and nonhypertrophic healing. *J. Invest. Dermatol.* 62, 514-516.
- Lu F., Gao J., Ogawa R., Hyakusoku H. and Ou C. (2007). Biological differences between fibroblasts derived from peripheral and central areas of keloid tissues. *Plast. Reconstr. Surg.* 120, 625-630.
- Luo L.F., Shi Y., Zhou Q., Xu S.Z. and Lei T.C. (2013). Insufficient expression of the melanocortin-1 receptor by human dermal fibroblasts contributes to excess collagen synthesis in keloid scars. *Exp. Dermatol.* 22, 764-766.
- Luzar B. and Calonje E. (2010). Cutaneous fibrohistiocytic tumours - an update. *Histopathology* 56, 148-165.
- Machesney M., Tidman N., Waseem A., Kirby L. and Leigh I. (1998). Activated keratinocytes in the epidermis of hypertrophic scars. *Am. J. Pathol.* 152, 1133-1141.
- Martin C.W. and Muir I.F. (1990). The role of lymphocytes in wound healing. *Br. J. Plast. Surg.* 43, 655-662.
- Martino M.M., Tortelli F., Mochizuki M., Traub S., Ben-David D., Kuhn G.A., Müller R., Livne E., Eming S.A. and Hubbell J.A. (2011). Engineering the growth factor microenvironment with fibronectin domains to promote wound and bone tissue healing. *Sci. Translat. Med.* 3, 100ra189-100ra189.
- Massam-Wu T., Chiu M., Choudhury R., Chaudhry S.S., Baldwin A.K., McGovern A., Baldock C., Shuttleworth C.A. and Kietly C.M. (2010). Assembly of fibrillin microfibrils governs extracellular deposition of latent TGF beta. *J. Cell. Sci.* 123, 3006-3018.
- Mathangi Ramakrishnan K., Meenakshi Janakiraman M. and Babu M. (2012). Expression of fibrocyte markers by keloid fibroblasts: an insight into fibrosis during burn wound healing - a preliminary study. *Ann. Burns Fire Disasters* 25, 148-151.
- Matsuoka L.Y., Uitto J., Wortsman J., Abergel R.P. and Dietrich J. (1988). Ultrastructural characteristics of keloid fibroblasts. *Am. J. Dermatopathol.* 10, 505-508.
- McCoy B.J., Diegelmann R.F. and Cohen I.K. (1980). *In vitro* inhibition of cell growth, collagen synthesis, and prolyl hydroxylase activity by triamcinolone acetonide. *Exp. Biol. Med.* 163, 216-222.
- Merline R., Moreth K., Beckmann J., Nastase M.V., Zeng-Brouwers J., Tralhao J.G., Lemarchand P., Pfeilschifter J., Schaefer R.M., Iozzo R.V. and Schaefer L. (2011). Signaling by the matrix proteoglycan decorin controls inflammation and cancer through PDCD4 and MicroRNA-21. *Sci. Signal.* 4, ra75.
- Meyer L.J., Russell S.B., Russell J.D., Trupin J.S., Egbert B.M., Shuster S. and Stern R. (2000). Reduced hyaluronan in keloid tissue and cultured keloid fibroblasts. *J. Invest. Dermatol.* 114, 953-959.
- Mienaltowski M.J. and Birk D.E. (2014). Structure, physiology, and biochemistry of collagens. *Adv. Exp. Med. Biol.* 802 5-29.
- Miragliotta V., Pirone A., Donadio E., Abramo F., Ricciardi M.P. and Theoret C.L. (2014). Osteopontin expression in healing wounds of horses and in human keloids. *Equine Vet. J.* (in press).
- Mitts T.F., Bunda S., Wang Y. and Hinek A. (2010). Aldosterone and mineralocorticoid receptor antagonists modulate elastin and collagen deposition in human skin. *J. Invest. Dermatol.* 130, 2396-2406.
- Mogili N.S., Krishnaswamy V.R., Jayaraman M., Rajaram R., Venkatraman A. and Korrapati P.S. (2012). Altered angiogenic balance in keloids: a key to therapeutic intervention. *Translat. Res.* 159, 182-189.
- Moinzadeh P., Agarwal P., Bloch W., Orteu C., Hunzelmann N., Eckes B. and Krieg T. (2013). Systemic sclerosis with multiple nodules: characterization of the extracellular matrix. *Arch. Dermatol. Res.* 305, 645-652.
- Moshref S.S. and Mufti S.T. (2010). Keloid and Hypertrophic scars: Comparative Histopathological and Immunohistochemical Study. *J. King Abdulaziz Univ. Med. Sc.* 17, 3-22.
- Muller A.K., Meyer M. and Werner S. (2012). The roles of receptor tyrosine kinases and their ligands in the wound repair process. *Semin. Cell Dev. Biol.* 23, 963-970.
- Mustoe T.A., Cooter R.D., Gold M.H., Hobbs F.D., Ramelet A.A., Shakespeare P.G., Stella M., Teot L., Wood F.M. and Ziegler U.E. (2002). International clinical recommendations on scar management. *Plast. Reconstr. Surg.* 110, 560-571.
- Naik-Mathuria B., Pilling D., Crawford J.R., Gay A.N., Smith C.W., Gomer R.H. and Olutoye O.O. (2008). Serum amyloid P inhibits dermal wound healing. *Wound Repair. Regen.* 16, 266-273.
- Naitoh M., Hosokawa N., Kubota H., Tanaka T., Shirane H., Sawada M., Nishimura Y. and Nagata K. (2001). Upregulation of HSP47 and collagen type III in the dermal fibrotic disease, keloid. *Biochem. Biophys. Res. Commun.* 280, 1316-1322.
- Namazi M.R., Fallahzadeh M.K. and Schwartz R.A. (2011). Strategies for prevention of scars: what can we learn from fetal skin? *Int. J. Dermatol.* 50, 85-93.
- Natsuaki Y., Egawa G., Nakamizo S., Ono S., Hanakawa S., Okada T., Kusuba N., Otsuka A., Kitoh A., Honda T., Nakajima S., Tsuchiya S., Sugimoto Y., Ishii K.J., Tsutsui H., Yagita H., Iwakura, Y., Kubo M., Ng L., Hashimoto T., Fuentes J., Guttman-Yassky E., Miyachi Y. and Kabashima K. (2014). Perivascular leukocyte clusters are essential for efficient activation of effector T cells in the skin. *Nat. Immunol.* 15, 1064-1069.
- Neill T., Schaefer L. and Iozzo R.V. (2012). Decorin: a guardian from the matrix. *Am. J. Pathol.* 181, 380-387.
- Nie F.F., Wang Q. and Qin Z.L. (2008). The expression of fibrillin 1 in pathologic scars and its significance. *Zhonghua Zheng Xing Wai Ke Za Zhi J. Plast. Surg.* 24, 339-342. (in chinese).
- Niessen F.B., Schalkwijk J., Vos H. and Timens W. (2004). Hypertrophic scar formation is associated with an increased number of epidermal Langerhans cells. *J. Pathol.* 202, 121-129.
- Ogawa R., Watanabe A., Than Naing B., Sasaki M., Fujita A., Akaishi

## Histopathology of keloid disease

- S., Hyakusoku H. and Shimada T. (2014). Associations between keloid severity and single-nucleotide polymorphisms: importance of rs8032158 as a biomarker of keloid severity. *J. Invest. Dermatol.* 134, 2041-2043.
- Ohyama M., Zheng Y., Paus R. and Stenn K.S. (2010). The mesenchymal component of hair follicle neogenesis: background, methods and molecular characterization. *Exp. Dermatol.* 19, 89-99.
- Okamoto O., Fujiwara S., Abe M. and Sato Y. (1999). Dermopontin interacts with transforming growth factor beta and enhances its biological activity. *Biochem. J.* 337, 537-541.
- Olczyk P., Mencner L. and Komosinska-Vassev K. (2014). The role of the extracellular matrix components in cutaneous wound healing. *Biomed. Res. Int.* 2014, 747584.
- Ong C.T., Khoo Y.T., Mukhopadhyay A., Masilamani J., Do D.V., Lim I.J. and Phan T.T. (2010). Comparative proteomic analysis between normal skin and keloid scar. *Br. J. Dermatol.* 162, 1302-1315.
- Onodera M., Ueno M., Ito O., Suzuki S., Igawa H.H. and Sakamoto H. (2007). Factor XIIIa-positive dermal dendritic cells in keloids and hypertrophic and mature scars. *Pathol. Int.* 57, 337-342.
- Pasparakis M., Haase I. and Nestle F.O. (2014). Mechanisms regulating skin immunity and inflammation. *Nat. Rev. Immunol.* 14, 289-301.
- Paus R. (2013). Migrating melanocyte stem cells: masters of disaster? *Nat. Med.* 19, 818-819.
- Peltonen J., Hsiao L.L., Jaakkola S., Sollberg S., Aumailley M., Timpl R., Chu M.L. and Uitto J. (1991). Activation of collagen gene expression in keloids: co-localization of type I and VI collagen and transforming growth factor-beta 1 mRNA. *J. Invest. Dermatol.* 97, 240-248.
- Rakar J., Krammer M.P. and Kratz G. (2014). Human melanocytes mitigate keratinocyte-dependent contraction in an *in vitro* collagen contraction assay. *Burns.* (in press).
- Ramirez F. and Rifkin D.B. (2009). Extracellular microfibrils: contextual platforms for TGFbeta and BMP signaling. *Curr. Opin. Cell. Biol.* 21, 616-622.
- Reilkoff R.A., Bucala R. and Herzog E.L. (2011). Fibrocytes: emerging effector cells in chronic inflammation. *Nat. Rev. Immunol.* 11, 427-435.
- Reinke J.M. and Sorg H. (2012). Wound repair and regeneration. *Eur. Surg. Res.* 49, 35-43.
- Rencic A., Brinster N. and Nousari C.H. (2003). Keloid morphea and nodular scleroderma: two distinct clinical variants of scleroderma? *J. Cutan. Med. Surg.* 7, 20-24.
- Russell S.B., Trupin J.S., Kennedy R.Z., Russell J.D. and Davidson J.M. (1995). Glucocorticoid regulation of elastin synthesis in human fibroblasts: down-regulation in fibroblasts from normal dermis but not from keloids. *J. Invest. Dermatol.* 104, 241-245.
- Russell S.B., Russell J.D., Trupin K.M., Gayden A.E., Opalenik S.R., Nanney L.B., Broquist A.H., Raju L. and Williams S.M. (2010). Epigenetically altered wound healing in keloid fibroblasts. *J. Invest. Dermatol.* 130, 2489-2496.
- Sabater-Marco V., Perez-Valles A., Berzal-Cantalejo F., Rodriguez-Serna M., Martinez-Diaz F. and Martorell-Cebollada M. (2006). Sclerosing dermatofibrosarcoma protuberans (DFSP): an unusual variant with focus on the histopathologic differential diagnosis. *Int. J. Dermatol.* 45, 59-62.
- Santucci M., Borgognoni L., Reali U.M. and Gabbiani, G. (2001). Keloids and hypertrophic scars of Caucasians show distinctive morphologic and immunophenotypic profiles. *Virchows Arch.* 438, 457-463.
- Sarrazy V., Billet F., Micallef L., Coulomb B. and Desmouliere A. (2011). Mechanisms of pathological scarring: role of myofibroblasts and current developments. *Wound Repair Regen.* 19 (Suppl 1) s10-15.
- Sayani K., Dodd C.M., Nedelec B., Shen Y.J., Ghahary A., Tredget E.E. and Scott P.G. (2000). Delayed appearance of decorin in healing burn scars. *Histopathology* 36, 262-272.
- Schalkwijk J., Van Vlijmen I., Oosterling B., Perret C., Koopman R., Van den Born J. and Mackie E.J. (1991). Tenascin expression in hyperproliferative skin diseases. *Br. J. Dermatol.* 124, 13-20.
- Schneider M., Meites E. and Daane S.P. (2013). Keloids: Which treatment is best for your patient? *J. Fam. Prac.* 62, 227-233.
- Schnoor M., Cullen P., Lorkowski J., Stolle K., Robenek H., Troyer D., Rauterberg J. and Lorkowski S. (2008). Production of type VI collagen by human macrophages: a new dimension in macrophage functional heterogeneity. *J. Immunol.* 180, 5707-5719.
- Scott P.G., Dodd C.M., Tredget E.E., Ghahary A. and Rahemtulla F. (1995). Immunohistochemical localization of the proteoglycans decorin, biglycan and versican and transforming growth factor-beta in human post-burn hypertrophic and mature scars. *Histopathology* 26, 423-431.
- Seifert O. and Mrowietz U. (2009). Keloid scarring: bench and bedside. *Arch. Dermatol. Res.* 301, 259-272.
- Seifert O., Bayat A., Geffers R., Dienus K., Buer J., Lofgren S. and Matussek A. (2008). Identification of unique gene expression patterns within different lesional sites of keloids. *Wound Repair. Regen.* 16, 254-265.
- Shaker S.A., Ayuob N.N. and Hajrah N.H. (2011). Cell talk: a phenomenon observed in the keloid scar by immunohistochemical study. *Appl. Immunohistochem. Mol. Morphol.* 19, 153-159.
- Shih B. and Bayat A. (2012). Comparative genomic hybridisation analysis of keloid tissue in Caucasians suggests possible involvement of HLA-DRB5 in disease pathogenesis. *Arch. Dermatol. Res.* 304, 241-249.
- Shih B., Garside E., McGrouther D.A. and Bayat A. (2010). Molecular dissection of abnormal wound healing processes resulting in keloid disease. *Wound Repair Regen.* 18, 139-153.
- Shrestha P., Sumitomo S., Lee C.H., Nagahara K., Kamegai A., Yamanaka T., Takeuchi H., Kusakabe M. and Mori M. (1996). Tenascin: growth and adhesion modulation--extracellular matrix degrading function: an *in vitro* study. *Eur. J. Cancer. B. Oral. Oncol.* 32B, 106-113.
- Sible J.C., Eriksson E., Smith S.P. and Smith N. (1994). Fibronectin gene expression differs in normal and abnormal human wound healing. *Wound Repair Regen.* 2, 3-19.
- Sidgwick G.P. and Bayat A. (2012). Extracellular matrix molecules implicated in hypertrophic and keloid scarring. *J. Eur. Acad. Dermatol. Venerol.* 26, 141-152.
- Sidgwick G.P., Iqbal S.A. and Bayat A. (2013). Altered expression of hyaluronan synthase and hyaluronidase mRNA may affect hyaluronic acid distribution in keloid disease compared with normal skin. *Exp. Dermatol.* 22, 377-379.
- Simone T.M., Longmate W.M., Law B.K. and Higgins P.J. (2014). Targeted inhibition of PAI-1 activity impairs epithelial migration and wound closure following cutaneous injury. *Adv. Wound Care* (in press).
- Sobel K., Tham M., Stark H.J., Stammer H., Pratzel-Wunder S., Bickenbach J.R. and Boukamp P. (2014). Wnt-3a-activated human fibroblasts promote human keratinocyte proliferation and matrix destruction. *International journal of cancer. J. Int. Cancer* 136, 27,

- 86-98.
- Soma T., Tajima M. and Kishimoto J. (2005). Hair cycle-specific expression of versican in human hair follicles. *J. Dermatol. Sci.* 39, 147-154.
- Sorrell J.M. and Caplan A.I. (2009). Fibroblasts-a diverse population at the center of it all. *Int. Rev. Cell. Mol. Biol.* 276, 161-214.
- Spiekman M., Przybyt E., Plantinga J.A., Gibbs S., van der Lei B. and Harmsen M.C. (2014). Adipose tissue-derived stromal cells inhibit TGF-beta1-induced differentiation of human dermal fibroblasts and keloid scar-derived fibroblasts in a paracrine fashion. *Plast. Reconstr. Surg.* 134, 699-712.
- Suarez E., Syed F., Alonso-Rasgado T., Mandal, P. and Bayat, A. (2013). Up-regulation of tension-related proteins in keloids: knockdown of Hsp27, alpha2beta1-integrin, and PAI-2 shows convincing reduction of extracellular matrix production. *Plast. Reconstr. Surg.* 131, 158e-173e.
- Sun L.M., Wang K.H. and Lee Y.C. (2014). Keloid incidence in Asian people and its comorbidity with other fibrosis-related diseases: a nationwide population-based study. *Arch. Dermatol. Res.* 306, 803-808.
- Sundram U.N. (2009). Review: Dermatofibrosarcoma protuberans: histologic approach and updated treatment recommendations. *Clin. Adv. Hematol. Oncol.* 7, 406-408.
- Supp D.M., Hahn J.M., Glaser K., McFarland K.L. and Boyce S.T. (2012). Deep and superficial keloid fibroblasts contribute differentially to tissue phenotype in a novel *in vivo* model of keloid scar. *Plast. Reconstr. Surg.* 129, 1259-1271.
- Sweeney R.T. and van de Rijn M. (2012). Microarrays and high-throughput sequencing in desmoid-type fibromatosis and scar. *Desmoid Tumors 2012*, 181-193.
- Syed F., Ahmadi E., Iqbal S.A., Singh S., McGrouther D.A. and Bayat A. (2011). Fibroblasts from the growing margin of keloid scars produce higher levels of collagen I and III compared with intralesional and extralesional sites: clinical implications for lesional site-directed therapy. *Br. J. Dermatol.* 164, 83-96.
- Tan E.M., Hoffren J., Rouda S., Greenbaum S., Fox J. 4th, Moore J.H. Jr and Dodge G.R. (1993). Decorin, versican, and biglycan gene expression by keloid and normal dermal fibroblasts: differential regulation by basic fibroblast growth factor. *Exp. Cell Res.* 209, 200-207.
- Tan K.T., McGrouther D.A., Day A.J., Milner C.M. and Bayat A. (2011). Characterization of hyaluronan and TSG-6 in skin scarring: differential distribution in keloid scars, normal scars and unscarred skin. *J. Eur. Acad. Dermatol. Venereol.* 25, 317-327.
- Teofoli P., Motoki K., Lotti T.M., Uitto J. and Mauviel A. (1997). Proopiomelanocortin (POMC) gene expression by normal skin and keloid fibroblasts in culture: modulation by cytokines. *Exp. Dermatol.* 6, 111-115.
- Theoret C.L., Olutoye O.O., Parnell L.K. and Hicks J. (2013). Equine exuberant granulation tissue and human keloids: a comparative histopathologic study. *Vet. Surg.* 42, 783-789.
- Tholpady S.S., DeGeorge B.R. Jr, and Campbell C.A. (2014). The effect of local Rho-kinase inhibition on murine wound healing. *Ann. Plast. Surg.* 72, S213-S219.
- Tirgan M.H., Shutty C.M. and Park T.H. (2013). Nine-month-old patient with bilateral earlobe keloids. *Pediatrics* 131, e313-317.
- To W.S. and Midwood K.S. (2011). Plasma and cellular fibronectin: distinct and independent functions during tissue repair. *Fibrogenesis Tissue Repair* 4, 21.
- Tracy L.E., Minasian R.A. and Caterson E. (2014). Extracellular matrix and dermal fibroblast function in the healing wound. *Adv. Wound. Care* (in press).
- Trisliana Perdanasari A., Lazzeri D., Su W., Xi W., Zheng Z., Ke L., Min P., Feng S., Zhang Y.X. and Persichetti P. (2014). Recent developments in the use of intralesional injections keloid treatment. *Arch. Plast. Surg.* 41, 620-629.
- Tsai Y.J., Lin P.Y., Chew K.Y. and Chiang Y.C. (2014). Dermatofibrosarcoma protuberans in children and adolescents: Clinical presentation, histology, treatment, and review of the literature. *J. Plast. Reconstr. Aesthet. Surg.* 67, 1222-1229.
- Turner N.J., Pezzone M.A., Brown B.N. and Badylak S.F. (2013). Quantitative multispectral imaging of Herovici's polychrome for the assessment of collagen content and tissue remodelling. *J. Tissue Eng. Regen. Med.* 7, 139-148.
- Ueda K., Furuya E., Yasuda Y., Oba S. and Tajima S. (1999). Keloids have continuous high metabolic activity. *Plast. Reconstr. Surg.* 104, 694-698.
- Ueda K., Yasuda Y., Furuya E. and Oba S. (2004). Inadequate blood supply persists in keloids. *Scand. J. Plast. Reconstr. Hand Surg.* 38, 267-271.
- Uitto J., Perejda A.J., Abergel R.P., Chu M.L. and Ramirez F. (1985). Altered steady-state ratio of type I/III procollagen mRNAs correlates with selectively increased type I procollagen biosynthesis in cultured keloid fibroblasts. *Proc. Natl. Acad. Sci. USA* 82, 5935-5939.
- Van De Water, L., Varney, S. and Tomasek J.J. (2013). Mechanoregulation of the myofibroblast in wound contraction, scarring, and fibrosis: Opportunities for new therapeutic intervention. *Adv. Wound. Care.* 2, 122-141.
- van den Broek L.J., Limandjaja G.C., Niessen F.B. and Gibbs S. (2014). Human hypertrophic and keloid scar models: principles, limitations and future challenges from a tissue engineering perspective. *Exp. Dermatol.* 23, 382-386.
- Viera M.H., Vivas A.C. and Berman B. (2012). Update on keloid management: Clinical and basic science advances. *Adv. Wound. Care.* 1, 200-206.
- Wang J., Hori K., Ding J., Huang Y., Kwan P., Ladak A. and Tredget E. E. (2011). Toll-like receptors expressed by dermal fibroblasts contribute to hypertrophic scarring. *J. Cell. Physiol.* 226, 1265-1273.
- Wang Z., Liu X., Zhang D., Wang X., Zhao F., Shi P. and Pang X. (2015). Coculture with human fetal epidermal keratinocytes promotes proliferation and migration of human fetal and adult dermal fibroblasts. *Mol. Med. Rep.* 11, 1105-1110.
- Weyrich A.S., Schwertz H., Kraiss L.W. and Zimmerman G.A. (2009). Protein synthesis by platelets: historical and new perspectives. *J. Thromb. Haemost.* 7, 241-246.
- Xia W., Phan T.T., Lim I.J., Longaker M.T. and Yang G.P. (2006). Differential transcriptional responses of keloid and normal keratinocytes to serum stimulation. *J. Surg. Res.* 135, 156-163.
- Yagi Y., Muroga E., Naitoh M., Isogai Z., Matsui S., Ikehara Y., Suzuki S., Miyachi Y. and Utani A. (2012). An ex vivo model employing keloid-derived cell-seeded collagen sponges for therapy development. *J. Invest. Dermatol.* 133, 386-393.
- Yagi Y., Muroga E., Naitoh M., Isogai Z., Matsui S., Ikehara S., Suzuki S., Miyachi Y. and Utani A. (2013). An ex vivo model employing keloid-derived cell-seeded collagen sponges for therapy development. *J. Invest. Dermatol.* 133, 386-393.
- Young P., Fisher M., Segel J., Stucker F., Becker A. and Chen A.

*Histopathology of keloid disease*

- (2013). Treatment of Large Keloids With Secondary-Intention Healing. *Am. J. Cosmetic. Surg.* 30, 193-199.
- Zhang G., Ezura Y., Chervoneva I., Robinson P.S., Beason D.P., Carine E.T., Soslowsky L.J., Iozzo R.V. and Birk D.E. (2006). Decorin regulates assembly of collagen fibrils and acquisition of biomechanical properties during tendon development. *J. Cell. Biochem.* 98, 1436-1449.
- Zhang Z., Nie F., Chen X., Qin Z., Kang C., Chen B., Ma J., Pan B. and Ma Y. (2015). Upregulated periostin promotes angiogenesis in keloids through activation of the ERK 1/2 and focal adhesion kinase pathways, as well as the upregulated expression of VEGF and angiopoietin-1. *Mol. Med. Rep.* 11, 857-864.
- Zhou H.M., Wang J., Elliott C., Wen W., Hamilton D.W. and Conway, S.J. (2010). Spatiotemporal expression of periostin during skin development and incisional wound healing: lessons for human fibrotic scar formation. *J. Cell. Commun. Signal.* 4, 99-107.

Accepted April 22, 2015